Institut de Génétique et de Biologie Moléculaire et Cellulaire

CNRS-INSERM-Université de Strasbourg

Thèse

Présentée en vue de l'obtention du grade de

Docteur de l'Université de Strasbourg

par

Roberto SILVA ROJAS

Physiopathology of Tubular Aggregate Myopathy (TAM) and Therapeutic Approaches

Soutenue le 22 Octobre 2021 à Strasbourg

Discipline : Sciences du Vivant

Aspects moléculaires et cellulaires de la biologie

Thèse dirigée par :

M. Johann BOHM	DR, INSERM, IGBMC

Rapporteurs externes et examinateur interne :

Mme. Maud FRIEDEN (externe)	MCF, Université de Genève
M. Marc BARTOLI (externe)	DR, CNRS, Université Aix-Marseille
M. Fabien ALPY (interne)	DR, INSERM, IGBMC

"There are a lot of little reasons why the big things in our lives happen."

Ted Mosby, *How I Met Your Mother*

ACKNOWLEDGMENTS

names 😊. I would like to thank particularly **Arielle** because I am aware of how difficult was the starts of TAM project and I know that most of my scientific luck was to be in the right place at the right time.

Science without collaborations is like politics without politicians but the difference is that I was lucky to work with diligent people that I would like to thank. **Susan Treves** for the help with all the calcium experiments, advice and professionalisms you've always had. **Anne-Laure Charles** et **Bernard Geny** pour la simplicité et efficacité de notre collaboration. **Alexandru Parlog** et **Daniel Moulaert** pour leur enthousiasme et temps d'analyser le phénotype des os des souris. **Nadia Messaddeq** pour rendre visible l'invisible et **Hugues Jacobs** pour son temps et expérience dans les études histologiques. Et surtout, un grand merci à **Nadine Banquart** et **Chadia Nahy** pour être des animalières tellement efficaces et professionnelles. De même je remercie à **Isabelle Gonçalves** car je n'ai jamais rencontré une autre personne tellement résolutive et efficace. Pour des mêmes raisons j'aimerais remercier **Pascale Koebel** pour sa rapidité et intérêt dans la production des virus AAV.

I would like to write some words to the master trainees I had the opportunity to work with. **Lisa**, j'ai vraiment été chanceux de travailler avec toi. J'aimerais te remercier pour ton effort, enthousiasme et patience avec moi. **Emma**, tu es tellement intelligente et organisée que tu pourras arriver à tout ce que tu veux. Ça a été hyper simple de travailler avec toi et c'est grâce à toi qu'une partie de ma thèse a pu aboutir à terme. **Laura**, tú que aprendiste a medir pH conmigo, la Pili de mis días en el trabajo y la que se convirtió en la "drama queen" de los informes, me has hecho el trabajo más fácil y la tesis menos científica. Gracias por tu entusiasmo en el trabajo y los buenos momentos que hemos pasado en el laboratorio. Si hoy puedo presentar mi tesis es en gran parte a tu trabajo y dedicación. A great part of my success has been to work with you three because you made my days easier and my life longer 😊.

Gracias a los embajadores de España en Estrasburgo por todas las viajes, cenas y noches que hemos pasado juntos. **Arantxa, Bea, Pau, Rafa, Laia, Jordi y Xènia** habéis hecho que tenga menos morriña y me sienta menos lejos de donde quiero estar. Gracias a vosotros quitasteis carga a mi familia que tanto he echado de menos estos 6 años fuera de casa. A mi familia quiero agradecer la cercanía en la distancia y el apoyo cuando lo necesitaba. Estar tanto tiempo alejado de vosotros

me he hecho ver aún más cuánto os quiero **mamá, papá** y **hermano**. Pronto estaré de vuelva en casa para dar por c*** pero con amor ☺.

And last but not least, I would like to thank the acquired family during these years, and particularly those supported me in the distance and the proximity. **Jaime,** porque, aunque haya habido 1695 km entre nosotros, nunca has dejado de mantener el contacto y siempre estás ahí. **Alba** y **Rubén,** por haberos convertido en el primer cachito que me llevo de Estrasburgo y que, como los buenos Pomar de Burgos, sólo puede mejorar con el tiempo. **Sarah,** the new Harvard woman, for all the good moments spent together and your personal and scientific input in my projects. **Xènia** i **Jordi,** per tots els moments que hem compartit aquests anys I els que ens queden per viure. Habéis sido nuestra vida en Estrasburgo y lo seguiréis siendo cuando estemos cerca de nuevo. Y cuando digo nosotros es porque la otra parte eres TÚ. **Raquel**, no estaría donde estoy, ni sería quien soy, si no fuese por tí. Me has dado el apoyo cuando lo he necesitado y me has guiado en todo lo bueno que he hecho. Espero que el siguiente capítulo de mi vida lo escriba contigo. Te quiero.

Contents

ABBREVIATIONS

AAV	Adeno-associated virus
ASO	antisense oligonucleotide
Ca^{2+}	Calcium
CASQ	Calsequestrin
CC	Coiled-coil
CCD	Central core disease
CDI	Calcium-dependent inactivation
cDNA	Complementary DNA
CEUs	Calcium entry units
CK	Creatine kinase
CNM	Centronuclear myopathy
CRAC	Calcium release activated channel
DHPR	Diphyropiridine receptor
DMD	Duchenne's muscular distrophy
DNA	Deoxyribonucleic acid
EC	Excitation-contraction
EDL	Extensor digitorum longus
EDTA	Ethylenediaminetetraacetic acid
EMA	European Medecines Agency
ER	Endoplasmic reticulum
FCS	Fetal calf serum
FDA	Food and Drugs Administration
GO	Gene Ontology
GoF	Gain-of-function
H&E	Hematoxylin and eosin
HRP	Horseradish peroxidase
ID	Inactivation domain
IP_3R	1,4,5-inositol triphosphate receptor
LGMD	Limb girdle muscle dystrophy
LoF	Loss-of-function
MH	Malignant hyperthermia

Na$^+$	Sodium
NCX	Sodium/calcium exchangers
PCR	Polymerase chain reaction
PM	Plasma membrane
PMCA	Plasma membrane calcium ATPase
PMSF	Phenylmethylsulfonyl fluoride
qPCR	Quantitative polymerase chain reaction
RIPA	Radio immunoprecipitation
RNA	Ribonucleic acid
RNAi	Interference ribonucleic acid
RT	Reverse transcriptase
RyR	Ryanodine receptor
SAM	Sterile α motif
SCID	Severe combined immunodeficiency
SDH	Succinate dehydrogenase
SEM	Standard error of the mean
SERCA	Sarcoplasmic/endoplasmic reticulum calcium-ATPase
shRNA	Short hairpin ribonucleic acid
siRNA	Small interference ribonucleic acid
SOAR	Stromal interactor molecule 1-ORAI1 activating region
SOCE	Store-operated calcium entry
SR	Sarcoplasmic reticulum
STIM1	Stromal interactor molecule 1
STRMK	Stormorken
TA	Tibialis anterior
TAM	Tubular aggregate myopathy
TM	Transmembrane domain
TRPC	Transient receptor potential channels
UPR	Unfolded protein respone
WT	Wild type

FIGURES AND TABLES

Page

INTRODUCTION

1. MUSCLE

1.1. General overview

Muscles are specialized organs with contractile properties classified into 3 types. Smooth muscles, responsible for proper arterial pressure and digestion, are formed of small spindle-shaped mononuclear fibers disposed in layers where contraction is stimulated by hormones, the autonomous nervous system and local factors. Cardiac muscles, required for blood circulation, are composed of branched cylinders with one to three nuclei where contraction is timed by the autonomous nervous system. Skeletal muscle, attached to bones by tendons and responsible for voluntary movement, are composed of multinucleated fibers forming bundles where contraction is activated by the somatic nervous system. The latest, as well as the cardiac muscle, are formed of striated fibers characterized by their highly ordered organization of actin and myosin filaments (Sweeney and Hammers, 2018) (Figure 1).
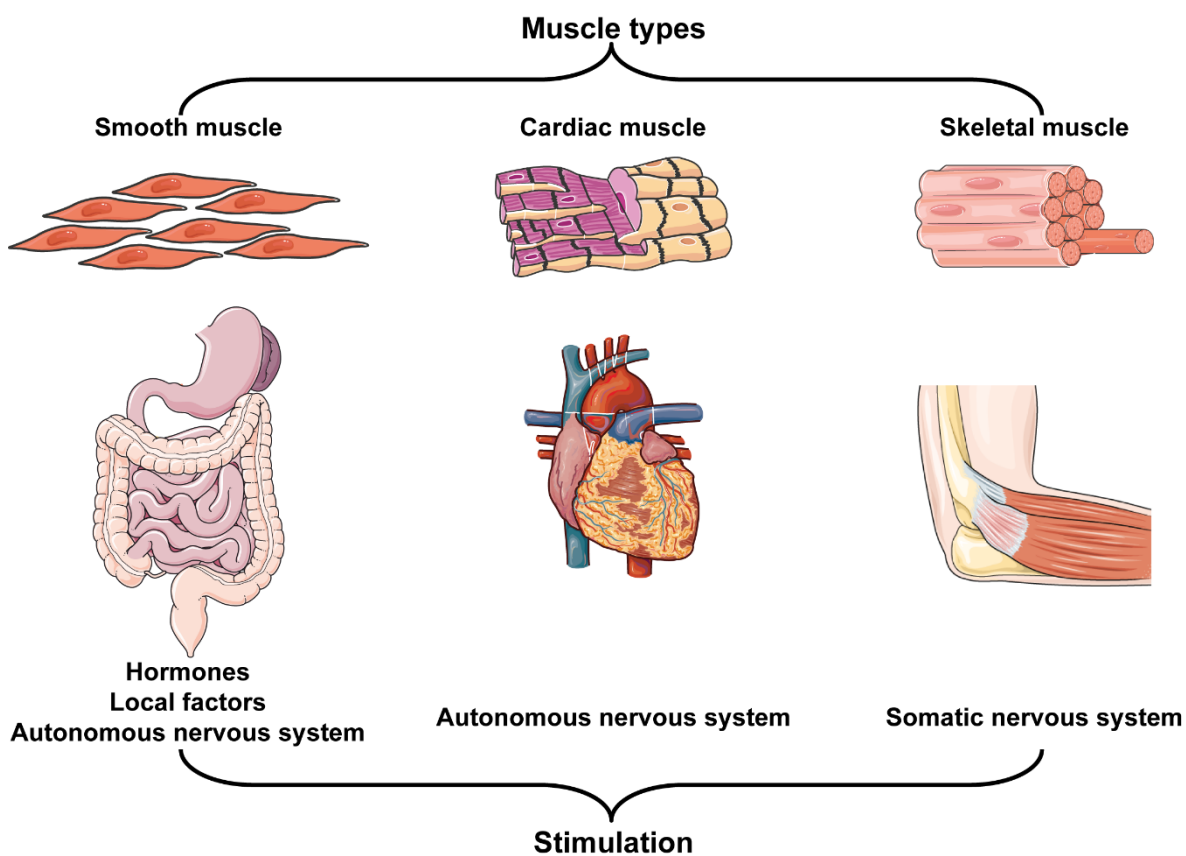
Figure 1. **Types of muscle organization, distribution and activation.**

Representation of myofiber organization in smooth, cardiac and skeletal muscle. Smooth muscle mediates the peristaltic movements and is stimulated by hormones, local factors and autonomous nervous system. Cardiac muscle is restrained to the heart and stimulated by the autonomous nervous system, and skeletal muscle is attached to the bones by tendons and is activated by the somatic nervous system. The figure uses modified images from Servier Medical Art Commons Attribution 3.0 Unported License (https://smart.servier.com).

Skeletal muscle represents 40% of total body weight and 50-75% of all body protein (Frontera and Ochala, 2015). Any individual skeletal muscle is composed of muscle fascicles separated by a connective tissue known as epimysium and the whole muscle delimitated by the outermost perimysial layer of connective tissue. The smallest unit are the muscle fibers, large multinucleated cells with high sarcoplasmic organization. 70-80% of their protein content are actin and myosin, the two main proteins of the myofilaments. In a precise and characteristic assembly pattern, these myofilaments form the sarcomeres, the basic contractile unit (Figure 2). Sarcomeres are composed of longitudinal stacks of actin (thin filament) and myosin (thick filament), and transversal scaffolds in the Z-line where actin filaments are attached, and the M-band where the myosin tails converge (Schiaffino and Reggiani, 2011) (Figure 2). The sarcomere length is defined from Z-line to Z-line and contains some of the largest proteins of the body as titin and nebulin that stabilize the sarcomeric structure by binding myosin and actin respectively and enabling sarcomere organization to act as a mechanical spring and restore sarcomere length following contraction (Frontera and Ochala, 2015; Schiaffino and Reggiani, 2011; Sweeney and Hammers, 2018).

Muscle contraction is an ATP-dependent process where myosin heads bind actin in the absence of ATP, the ATP binding and hydrolysis release the myosin-actin binding and allows the myosin head to bind an adjacent actin molecule. The Pi release triggers the myosin head movement and displace the actin filament towards the M-line. ADP is released at this point and the cycle can restart again with ATP binding (Figure 2). These contractile forces are finally transmitted across the muscle through the connections of the sarcomeres with the sarcolemma and external matrix to finally reach force production through the tendon junction with the bones (Frontera and Ochala, 2015).
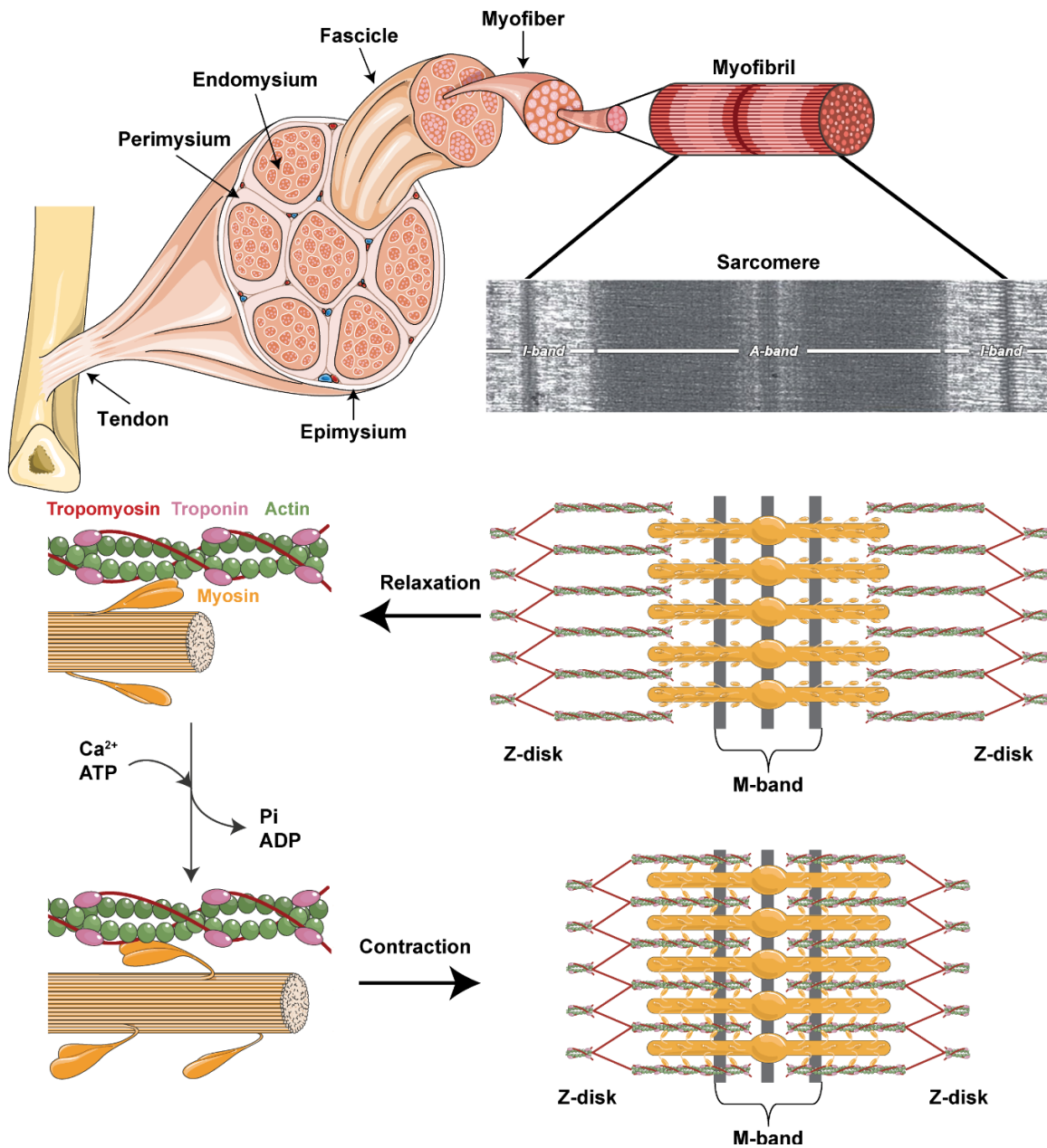
Figure 2. Skeletal muscle organization, sarcomere structure at rest and during contraction.

Skeletal muscles are connected to bones by tendons, contain myofiber fascicles interconnected and surrounded by connective tissue (endomysium and perimysium), and the entire muscle is enlaced by the outermost epimysial layer. The minimal unit is the myofiber and contains parallel organization of sarcomeres interconnected by transversal Z disks and M-bands. Ca^{2+} binding to troponin triggers tropomyosin sliding and the accessibility of actin to myosin heads. ATP binding and hydrolysis in the myosin head provides the energy for actin displacement towards the M-band in the contraction process. The figure uses modified images from Servier Medical Art Commons Attribution 3.0 Unported License (https://smart.servier.com) and electron micrograph is adapted from Schiaffino and Reggiani, 2011.

1.2. Energy source and fiber types

The skeletal muscle requires ATP as energy fuel to produce and maintain contraction and its source depend on the duration and intensity: 1) ATP stores are the first source to be used; 2) creatine phosphate generated by muscle creatine kinase are the second ATP source; 3) anaerobic glycolysis sustain ATP for an exercise lasting several minutes; and 4) mitochondrial oxidative phosphorylation provide ATP for long-lasting exercises (Schiaffino and Reggiani, 2011).

The myofibers originate from fusion of immature myoblasts into myotubes that will further differentiate until the formation of mature myofibers with nuclei in the periphery. These mature myofibers can be classified according to: 1) contraction speed, 2) fatigability, 4) mitochondrial amount and 5) myosin isoform composition (Augusto et al., 2004; Frontera and Ochala, 2015; Schiaffino and Reggiani, 2011):

- Type I fibers are slow fibers with the highest fatigue resistance and present a rich mitochondrial network. They express mainly myosin isoform *MYH7* and are primarily found in slow muscles as soleus and diaphragm.
- Type IIa fibers present a mixed I/II pattern with relatively fast contraction and fatigue resistance and present a moderate amount of mitochondria. They predominantly express *MYH2* and are particularly found in vastus lateralis and soleus.
- Type IIx/IId fibers are fast fibers that present moderated fatigue resistance and low mitochondrial amount. They predominantly express *MYH1* and are found in gastrocnemius and diaphragm.
- Type IIb fibers are fast fibers with low fatigue resistance and very low mitochondrial amount. They express *MYH4* and are found in fast muscles like EDL and TA.

1.3. Neuromuscular disorders

Skeletal muscle activation requires the connection of the muscle fibers with the peripheral nervous system. The connection is referred to as the motor unit and is composed of a motor neuron that innervates the myofibers in the contact sites known as neuromuscular junctions. Neuromuscular

disorders are severe and potentially lethal disorders with a strong impact on the quality of life. They mostly involve general muscle weakness associated with respiratory insufficiency, and can be accompanied by skeletal deformities. Depending on the affected part of the motor unit, they are classified as neuropathies in case of defects in motor neurons, myasthenic syndromes in case of anomalies in the neuromuscular junction, and myopathies if the primary problem results from proteins of the myofibers or the extracellular matrix (Dowling et al., 2018; Dowling et al., 2021) (Figure 3). Myopathies can result from mutations in genes implicated in:

- Plasma membrane integrity
- Structural sarcomeric stability
- Nuclear envelope
- Protein turnover
- Membrane repair
- Ca^{2+} handling
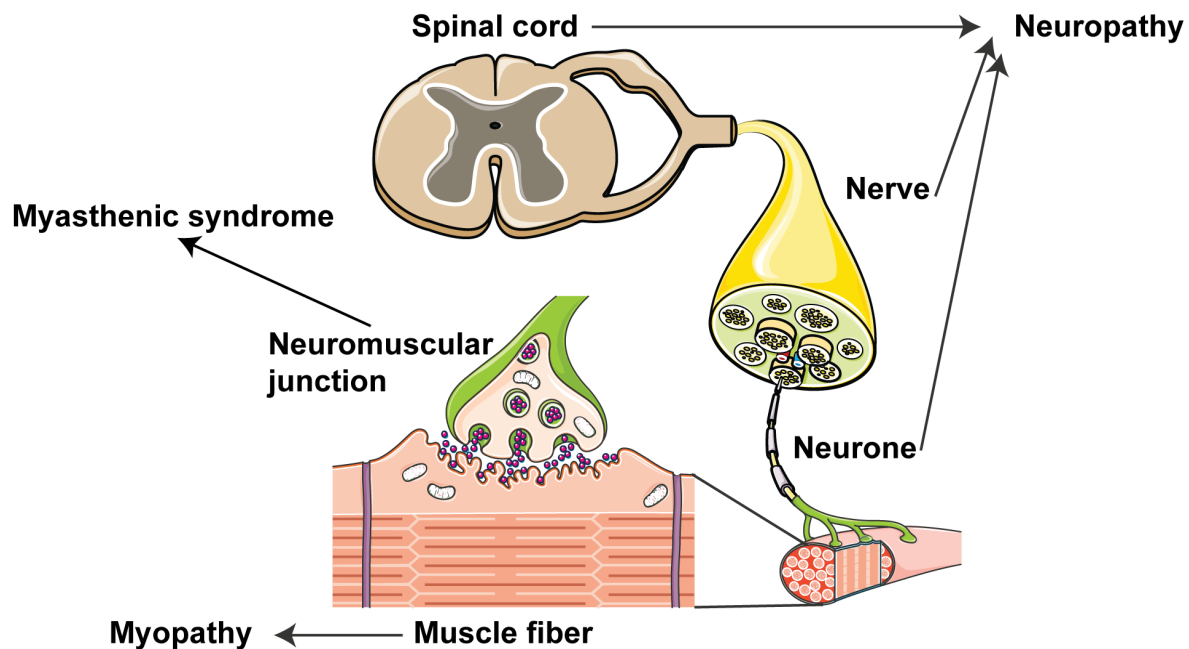
Figure 3. Different parts of motor unit and associated diseases.

The motor unit is composed of the motor neuron connecting the spinal cord and the myofiber via a neuromuscular junction. Nerve defects can cause neuropathies, defective neuromuscular junctions cause myasthenic syndromes and primary defects in the myofibers result in myopathies. The figure uses modified images from Servier Medical Art Commons Attribution 3.0 Unported License (https://smart.servier.com).

2. Ca^{2+} HANDLING IN SKELETAL MUSCLE

The contraction of skeletal muscle is a voluntary process mediated by somatic neuronal connections that reach the muscle through the neuromuscular junctions. The action potential activates voltage-dependent Ca^{2+} channels in the presynaptic neuron and triggers the release of the neurotransmitter acetylcholine that will activate nicotinic acetylcholine receptors (nAChR) in the sarcolemma of the postsynaptic myofiber. nAChR activation induces Na$^+$ entry and membrane depolarization to finally activate the voltage-sensing subunit of diphyropiridine receptors (DHPR), enabling the excitation-contraction (EC) coupling and mobilization of intracellular Ca^{2+} stores (Schiaffino and Reggiani, 2011). Troponin C binds Ca^{2+}, moving tropomyosin and enabling actin-myosin binding and sliding, and muscle contraction (Sweeney and Hammers, 2018) (Figure 2). Here, I describe the major mechanisms regulating Ca^{2+} handling in skeletal muscle.

2.1. Excitation-contraction coupling

In skeletal and cardiac muscles, the fibers present sarcolemmal membrane invaginations named T-tubules. These structures are found in close proximity to sarcoplasmic reticulum stacks forming the triads in skeletal muscle and diads in cardiac muscle (Schartner et al., 2019). They are membrane contact sites between the sarcoplasmic reticulum and the plasma membrane (SR-PM) and are shaped by the concerted action of membrane remodeling proteins and the SR-PM bridging junctophilins (Al-Qusairi and Laporte, 2011; Chen et al., 2019). (Figure 4). T-tubules contain dihydropyridine receptors (DHPR), a type of voltage-operated Ca^{2+} channels. Voltage-operated Ca^{2+} channels are present in excitable cells and are composed of 5 subunits differentiated by their α1 subunit and their voltage dependence (Catterall, 2011).
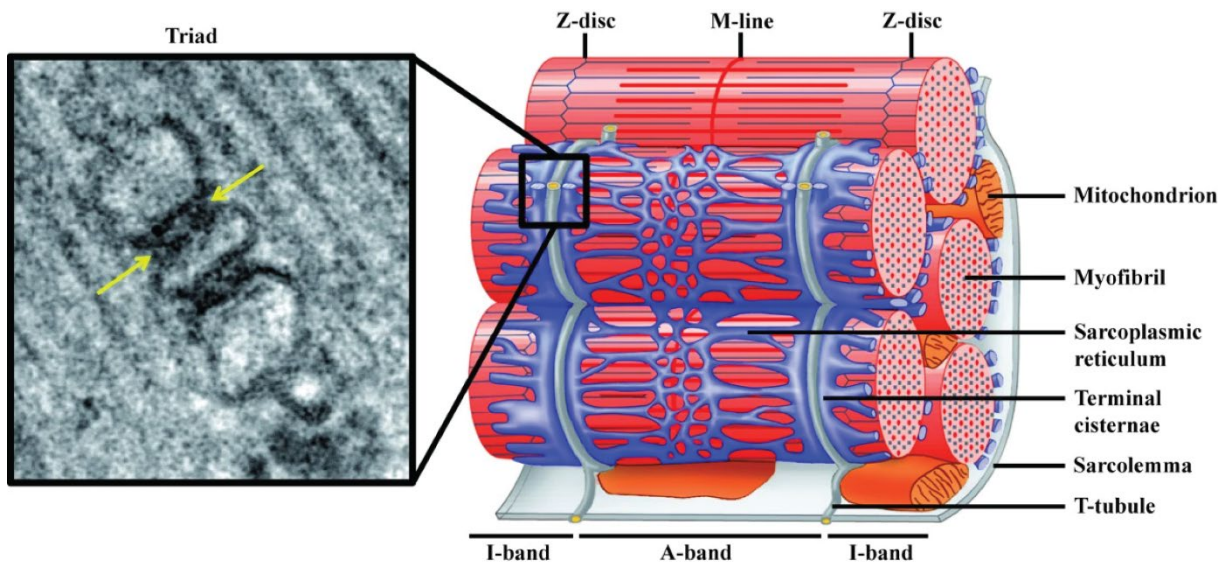
Figure 4. Sarcoplasmic reticulum and membrane invaginations in myofibers.

Myofibers are composed of myofibrils surrounded by sarcoplasmic reticulum and contained within the sarcolemma (plasma membrane). Sarcolemma invaginations known as T-tubules are in close contact with sarcoplasmic reticulum stacks forming the triads (highlighted electron microscopy) where the players of EC coupling concentrate. Ca^{2+} movement near the triads are required for muscle contraction and energy production in mitochondria. Yellow arrows indicate the contact sites between SR and T-tubule within the triad. Adapted from Al-Qusairi and Laporte, 2011.

The membrane depolarization in the sarcolemma triggers conformational changes of DHPR with different effects depending on the muscle type. In cardiac muscle, extracellular Ca^{2+} enters via DHPR and activates the Ca^{2+} channel RyR2 channel in the sarcoplasmic reticulum to release reticular Ca^{2+}. In the skeletal muscle, DHPR conformational change enables a physical interaction with RyR1 channel and permits the liberation of reticular Ca^{2+} (Dayal et al., 2017; Lamb, 2000) (Figure 5). In both cases, the interaction is facilitated by the close proximity of T-tubules and the SR, and the depletion of the reticular Ca^{2+} stores permits the increase of free cytosolic Ca^{2+} and contraction.

Mutations in the genes encoding the α1 subunit of skeletal DHPR (*CACNA1S*) and RyR1 (*RYR1*) are associated with different muscle diseases depending on the mutation effect. Loss-of-function (LoF) mutations in *CACNA1S* are found in patients with hypokalemic periodic paralysis (HOKPP), characterized by muscle weakness and paralysis episodes. LoF mutations in *RYR1* are associated with different congenital myopathies including central core disease (CCD), multi-minicore disease

(MmD), congenital fiber type disproportion (CFTD), centronuclear myopathy (CNM) and Samaritan myopathy. Gain-of-function (GoF) mutations in *CACNA1S* and *RYR1* induce malignant hyperthermia (MH), a susceptibility to volatile anesthetics that results in uncontrolled contractures, muscle rigidity and hyperthermia (Schartner et al., 2019).

2.2. Store-operated Ca^{2+} entry

Endoplasmic/sarcoplasmic reticulum (ER/SR) represents the main Ca^{2+} store of the cell and its depletion via 1,4,5-inositol triphosphate receptor (IP_3R) or the ryanodine receptors (RyR) is required to activate a large range of cellular functions including T cell activation, growth and differentiation, and muscle contraction. In any case, reticular Ca^{2+} depletion activates a ubiquitous Ca^{2+} handling mechanism known as store-operated Ca^{2+} entry (SOCE) where STIM1 and ORAI1 form the main players. STIM1 is a transmembrane protein with a luminal Ca^{2+} sensing part and a cytosolic part implicated in self-oligomerization and binding to ORAI1. When the reticular Ca^{2+} store decreases (e.g. EC coupling), the luminal part of STIM1 undergoes a conformational change that results in STIM1 oligomerization and activation of the plasma membrane Ca^{2+} channel ORAI1 triggering extracellular Ca^{2+} entry (more details in Molecular basis of SOCE section). The reticular Ca^{2+} content is later refilled by the action of SERCA pumps as will be described in the reticular Ca^{2+} store refilling section (Manjarres et al., 2010; Park et al., 2009; Stathopulos et al., 2008) (Figure 5).

Other STIM and ORAI paralogues have been described but their contribution to SOCE is less studied and the first experiments reveal a rather negative regulation of SOCE. STIM2 has higher affinity for Ca^{2+} than STIM1 (Kd STIM1 = 0.2 mM; Kd STIM2 = 0.4 mM) and activates after small fluctuations in reticular Ca^{2+}. Several STIM2 isoforms exist and overexpression or silencing of the ubiquitous *STIM2.1* isoform respectively inhibited or activated SOCE, revealing its role as negative regulator of SOCE (Miederer et al., 2015; Rosado et al., 2015). Silencing of *ORAI2* and *ORAI3* in human myoblasts had low impact on SOCE and their expression is consequently reduced compared to *ORAI1*, indicating lesser importance of the *ORAI1* paralogues in skeletal muscle (https://www.gtexportal.org) (Darbellay et al., 2009). In murine T cells, where *Orai1*, *Orai2* and *Orai3* are similarly expressed, *Orai2* silencing resulted in increased Ca^{2+} entry via SOCE and

pointed to ORAI2 as a negative regulator of SOCE in lymphocytes (Vaeth et al., 2017). Other less selective Ca^{2+} channels exist and transient receptor potential channels (TRPC) also contribute to SOCE. In particular, TRPC1, TRPC3, TRPC4 and TRPC6 participate, together with STIM1 and ORAI1, in the Ca^{2+} entry following ER store depletion (Choi et al., 2020; Gailly, 2012; Lopez et al., 2020).

In skeletal muscle, SOCE is essential to counteract the effects of fatigue by sustaining muscle contraction during periods of repetitive muscle stimulation. Repetitive activations of EC coupling reduce the reticular Ca^{2+} content and activate SOCE to allow a constant level of cytosolic and reticular Ca^{2+} (Michelucci et al., 2018). The activation of SOCE in skeletal muscle is also faster than in other cells and tissues (milliseconds versus seconds and minutes), and this is due to the presence of a muscle-specific STIM1 isoform (STIM1L) constantly anchored in the plasma membrane allowing fast ORAI1 activation and Ca^{2+} entry (Darbellay et al., 2011).

Mutations in *STIM1* and *ORAI1* lead to severe life-threatening conditions in humans and mice. The effects of LoF and GoF mutations in these genes have mirror-like effects and will be presented later in a [review](#).

2.3. Reticular Ca^{2+} store refilling

After SR Ca^{2+} depletion and SOCE, cytosolic Ca^{2+} needs to be reincorporated into the ER/SR to permit muscle relaxation and prepare the luminal Ca^{2+} store for future EC coupling trains (Schiaffino and Reggiani, 2011). Ca^{2+} reuptake into the ER/SR is mediated by Sarcoplasmic/endoplasmic reticulum Ca^{2+}-ATPase (SERCA) pumps accounting for almost 70% of the free Ca^{2+} reoriented after EC coupling (Schiaffino and Reggiani, 2011). Three SERCA paralogues and a total of 10 isoforms are found in different organs and tissues (Periasamy and Kalyanasundaram, 2007):

- SERCA1 is found in skeletal muscle during adult (SERCA1a) and fetal (SERCA1b) stages.
- SERCA2 is found in cardiac and slow muscles (SERCA2a), all tissues (SERCA2b) and cardiac muscle only (SERCA2c).
- SERCA3 and its three isoforms are principally expressed in hematopoietic cells.

SERCA proteins are composed of 10 transmembrane helixes and 3 cytosolic domains to anchor, phosphorylate and bind ATP. The Ca^{2+} binding sites lie near the TM4, TM5, TM6 and TM8 transmembrane helixes (Periasamy and Kalyanasundaram, 2007). All SERCA isoforms share a high degree of identity and can be efficiently inhibited by thapsigargin. Endogenous modulators of SERCA1a and SERCA2a are phospholamban and sarcolipin, small peptides that inhibit SERCA pumping activity and regulate SR Ca^{2+} refilling (Periasamy and Kalyanasundaram, 2007) (Figure 5).
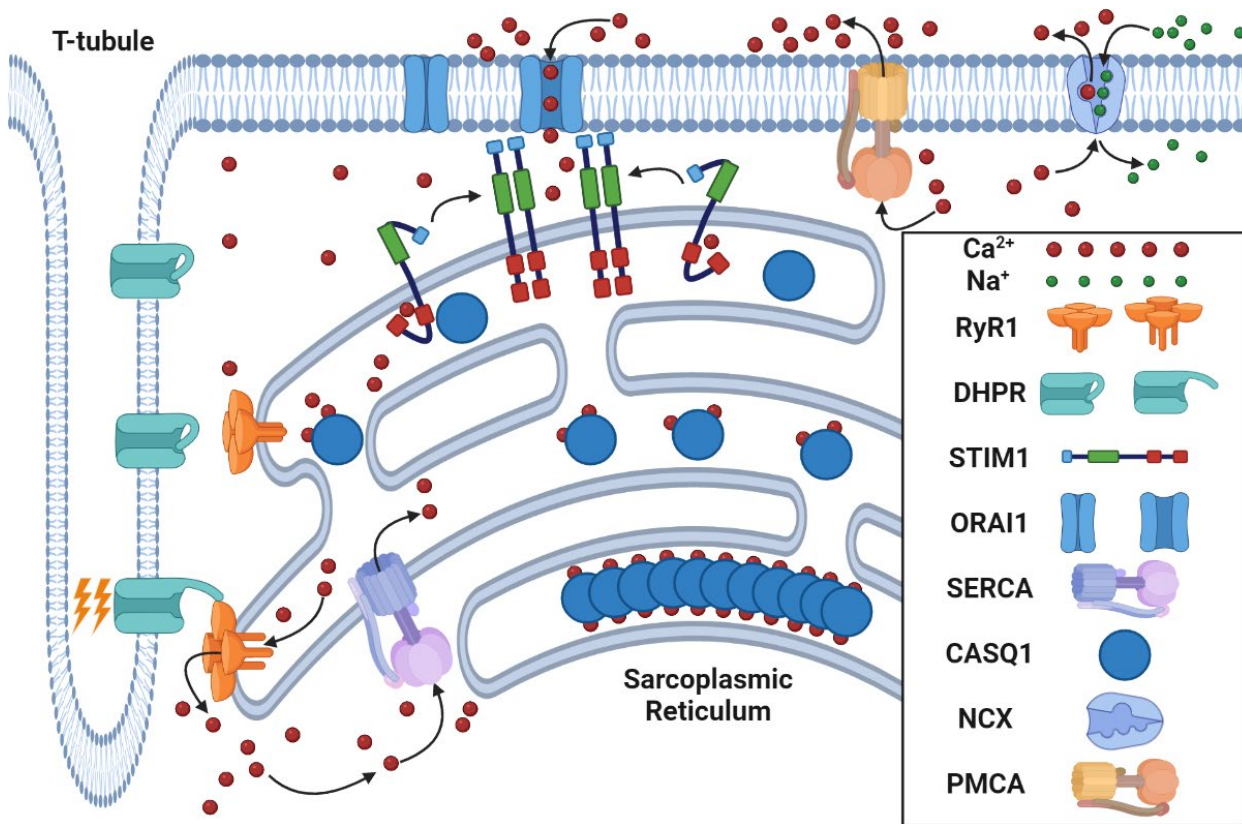
Figure 5. Ca^{2+} handling mechanisms in skeletal muscle.

Membrane depolarization triggers DHPR conformational change, RyR1 interaction and Ca^{2+} release from the sarcoplasmic reticulum. Following a decrease in Ca^{2+} store, STIM1 loses the interaction to Ca^{2+}, oligomerizes and activates ORAI1 enabling extracellular Ca^{2+} entry. Reticular Ca^{2+} stores are refilled by the action of SERCA pumps and Ca^{2+} is retained and stored through binding to the CASQ1 polymers. Other mechanisms to decrease the cytosolic Ca^{2+} content rely on ATP-dependent plasma membrane Ca^{2+} pumps (PMCA), and Na^+/Ca^{2+} exchangers (NCX), incorporating three Na^+ ions per Ca^{2+} ejected to the extracellular matrix. This image was created with BioRender (https://biorender.com/).

Fast muscle fibers, mostly expressing SERCA1a, have higher SR Ca^{2+} uptake rates than slow muscle fibers expressing SERCA2a (Schiaffino and Reggiani, 2011). However, functional analysis in COS-1 cells revealed similar Ca^{2+} kinetics and capacities of SERCA1a and SERCA2a when expressed at similar levels (Lytton et al., 1992). Therefore, the elevated SR refilling rate observed in fast fibers is explained by 1) increased pump density in the SR of fast fibers; 2) reduced presence of phospholamban or sarcolipin in fast muscle fibers; and 3) higher Ca^{2+} storage capacities of the SR in fast fibers (Schiaffino and Reggiani, 2011; Vangheluwe et al., 2005). The last point arises from the different expression of calsequestrin, the major luminal Ca^{2+} buffering protein. Calsequestrin monomers binds Ca^{2+} and form oligomeric structures with high Ca^{2+} capacity (Wang and Michalak, 2020) (Figure 5). The polymerization rate varies depending on the calsequestrin paralogue. CASQ1 is exclusively expressed in fast-twitch muscle fibers and has higher polymerization rates and Ca^{2+} storage capacities than CASQ2, found in slow-twitch fibers and cardiac muscle (Bal et al., 2015; Wang and Michalak, 2020).

Mutations in genes encoding SERCA are found in several conditions. Autosomal recessive GoF mutations in *ATP2A1,* encoding SERCA1a, cause Brody's disease, characterized by severe cramps and exercise-induced impairment of relaxation consistent with abnormal SR replenishment after contraction (Periasamy and Kalyanasundaram, 2007; Vattemi et al., 2010). Autosomal dominant mutations in *ATP2A2* encoding SERCA2a cause Darier's disease, a rare skin disorder with defective keratinocyte adhesion and abnormal keratinization, while no cardiac involvement is observed despite its prominent expression in heart (Periasamy and Kalyanasundaram, 2007; Ruiz-Perez et al., 1999). Following heart failure, SERCA2a expression is reduced and phospholamban inactivation is increased leading to reduced SR Ca^{2+} reuptake and deficient cardiac contraction (Lipskaia et al., 2010). In this line, several clinical trials have tested the efficiency of restoring SERCA2a expression with AAVs in the context of heart failure (Lyon et al., 2020) (NCT00534703, NCT01966887, NCT04703842). Thyroid hormone (T4) has been shown to impact on the expression of SERCA isoforms and inhibitors. Indeed, hypothyroidism results in decreased SR Ca^{2+} uptake, slower heartbeat and impairment in skeletal muscle relaxation similar to Brody's patients with reduced SERCA1 expression. Hyperthyroidism has opposite effects in SR uptake with increased SR uptake rates and faster heartbeat by increased SERCA2a expression (Periasamy and Kalyanasundaram, 2007).

2.4. Na$^+$/Ca^{2+} exchangers

Na$^+$/Ca^{2+} exchangers (NCX) allow the equilibration of Na$^+$ and Ca^{2+} concentrations inside and outside the cell. Topology modeling with canine NCX1 sequence suggest an organization in 9 transmembrane domains (TM) with a cytosolic loop region between TM5 and TM6 for Ca^{2+} binding and NCX1 regulation, and 2 α repeats connecting TM2 with TM3 and TM7 with TM8 involved in extracellular ion binding and transport (Brini and Carafoli, 2011; Nicoll et al., 2006). Of the three NCX homologues present in mammals, only NCX1 and NCX3 are present in protein lysates from rat skeletal muscle (Fraysse et al., 2001). NCX1 is in close proximity to the T-tubules (Sacchetto et al., 1996), enabling Ca^{2+} extrusion after contraction (Schiaffino and Reggiani, 2011). In normal conditions, NCX internalize three Na$^+$ ions per ion of expulsed Ca^{2+}, while, in conditions where sarcoplasmic Na$^+$ raises (e.g. exercise, hypoxia), NCX has the reversible action and three molecules of Na$^+$ exit for one of Ca^{2+} that enters (Wirth and Scheibenbogen, 2021) (Figure 5). Myalgic encephalomyelitis/chronic fatigue syndrome is an autoimmune disorder where β2-adrenergic signaling is over-activated and results in increased cellular Na$^+$ levels (Wirth and Scheibenbogen, 2021). The increased Ca^{2+} entry alters mitochondrial function, cell metabolism and energetics resulting in exercise intolerance. NCX activity also participates in the disease progression of animal models for other stroke and neurodegenerative disorders, pointing to the modulation of the exchanger activity as a promising strategy for future preclinical trials (Annunziato et al., 2020).

2.5. Plasma membrane Ca^{2+} ATPases

Plasma membrane Ca^{2+} ATPase (PMCA), alike SERCA pumps, are P-type ATPases composed of 10 transmembrane domains. The N-terminal and C-terminal regions of PMCA are cytosolic and the latest contains a calmodulin binding domain that regulates PMCA activity. In a calmodulin-bound status, the autoinhibitory loop formed between TM2-3 and TM4-5 domains is destabilized and the catalytic activity of PMCA enables Ca^{2+} transport to the extracellular matrix (Stafford et al., 2017) (Figure 5). There are four PMCA homologues. PMCA1 and PMCA4 are ubiquitously expressed and PMCA2 and PMCA3 are mostly expressed in neuronal tissues (Stafford et al.,

2017). In comparison with NCX, PMCA pumps may have smaller contribution to Ca^{2+} extrusion and mutations in PMCA homologues have not been associated to any muscle disease yet. Genome-wide association studies revealed single nucleotide polymorphisms in *ATP2B1* (PMCA1) and *ATP2B4* (PMCA4) associated with hypertension and familiar spastic paraplegia, probably resulting from altered Ca^{2+} homeostasis (Stafford et al., 2017). In line with their neuron-restricted expression, mutations in *ATP2B2* (PMCA2) and *ATP2B3* (PMCA3) are associated with neurological disorders like ataxia or autism (Boczek et al., 2021; Stafford et al., 2017).

3. MOLECULAR BASIS OF SOCE

SOCE is a mechanism regulating extracellular Ca^{2+} entry in response to the depletion of reticular Ca^{2+} stores. Its concept was firstly proposed in 1986 by James Putney (Putney, 1986) and small interference RNA (siRNA) screenings evidenced the role of STIM1 as reticular Ca^{2+} sensor in 2005 (Liou et al., 2005; Roos et al., 2005) and of ORAI1 as the plasma membrane Ca^{2+} channel in 2006 (Feske et al., 2006; Vig et al., 2006b; Zhang et al., 2006). While not present in yeast, SOCE is conserved in nearly all metazoans and is even present in unicellular *Monosiga brevicollis* (Collins and Meyer, 2011; Lewis, 2011; Prakriya and Lewis, 2015). Anomalies of SOCE can severely impact the physiology and function of several cells and tissues (Lacruz and Feske, 2015).

3.1. STIM1 structure

STIM1 is a single-pass transmembrane protein residing in the ER/SR and contains a luminal and a cytosolic part. The luminal part encompasses a N-terminal peptide signal ensuring the anchoring into the ER/SR membrane, a canonical EF hand binding Ca^{2+}, a non-canonical EF hand that does not bind Ca^{2+}, and a sterile α motif (SAM). The cytosolic part is composed of three coiled-coil domains (CC1-3), an inactivation domain, a proline/serine rich region and a lysine rich region (Lewis, 2011; Stathopulos et al., 2008) (Figure 6A, left).

The Ca^{2+} sensing ability of STIM1 relies on its canonical EF hand and more specifically on the Asp76 and Asp78 residues that keep STIM1 in a resting state upon Ca^{2+} binding (Schober et al., 2019; Stathopulos et al., 2008). In a Ca^{2+}-bound status, the adjacent non-canonical EF hand and the SAM domain form a hydrophobic cleft and remain in a packed conformation. Ca^{2+} unbinding weakens the EF-SAM interaction, and the luminal part unfolds (Novello et al., 2018; Schober et al., 2019; Stathopulos et al., 2008). The propagation of the conformational switch requires molecular rearrangements in the transmembrane domain (Ma et al., 2015; Ma et al., 2017) that finally result in unfolding and oligomerization of the cytosolic part (Ma et al., 2017; Novello et al., 2018). The clamp formed between the cytosolic CC1 and CC3 domains in the resting state is then released, resulting in the exposure of the SOAR (STIM1-ORAI1 activating region) and the polybasic lysine rich region (Lys) to bind ORAI1 and the phosphoinositides at the plasma membrane (Lunz et al., 2019; Ma et al., 2015; Ma et al., 2017) (Figure 6B). The inactivation domain (ID) is required for fast Ca^{2+}-dependent inactivation (CDI) of ORAI1 as will be described in the next ORAI1 structure text passage (Lunz et al., 2019; Prakriya and Lewis, 2015). Regarding the STIM1 stoichiometry, it is widely accepted that STIM1 forms dimers stabilized by intermolecular CC interactions in the resting state and higher oligomeric structures in the activated state (Lunz et al., 2019; Yen and Lewis, 2019).

3.2. ORAI1 structure

ORAI1 is a transmembrane protein in the plasma membrane with 4 transmembrane domains connected by 2 extracellular (TM1-TM2 and TM3-TM4) and 1 intracellular (TM2-TM3) loops, and flanked by N and C-terminal cytosolic strands essential for STIM1 binding, activation and inactivation (Lewis, 2011; Lunz et al., 2019; Tiffner et al., 2021) (Figure 6A, right). ORAI1 assembles as hexamers with the TM1 domains forming the pore and TM2-4 shaping concentric rings surrounding the pore (Hou et al., 2012). ORAI1 is a highly Ca^{2+}-selective channel with a 3.8 Å pore diameter, almost half of the diameter observed in DHPR or TRPCs (Prakriya and Lewis, 2015), reflecting the low ion conductance of the channel and challenging electrophysiological study of endogenous ORAI1 (Prakriya et al., 2006). ORAI1 is 1000 times more selective to Ca^{2+} than Na^+ and this selectivity resides in the outermost segment of TM1 where acidic Glu106 residue

binds Ca^{2+} and acts channel selectivity filter (Prakriya and Lewis, 2015). Other TM1 residues are lined in inner part of the pore and form a first hydrophobic stretch with Val102 and Gly98 acting as channel hinge, and an innermost basic region with Arg91, together with the formation of a water layer, act as channel gate (Lunz et al., 2019) (Figure 6A, right).

The interaction of ORAI1 with the STIM1 SOAR requires both N and C-terminal cytosolic termini of ORAI1 (Lunz et al., 2019). Ca^{2+} modulates ORAI1 activity in two temporally spaced inactivation processes referred as fast and slow Ca^{2+}-dependent inactivation (CDI). Fast CDI occurs with a delay of milliseconds after ORAI1 activation and results from the local increase of Ca^{2+} content and binding of Ca^{2+} molecules intracellular face of the pore reducing the channel conductance (Prakriya and Lewis, 2015). STIM1 also participates in the fast CDI via its negatively charged inactivation domain (ID) that may act as a Ca^{2+} sensor in the proximity of the plasma membrane and interacts with the C-terminal cytosolic tail of ORAI1 to reduce channel conductance (Prakriya and Lewis, 2015). The STIM1-dependent fast CDI, as well as ORAI1 activation, require a stoichiometric STIM1:ORAI1 ratio higher than 2, highlighting the relevance of STIM1:ORAI1 equilibrium for proper SOCE regulation (Yen and Lewis, 2019). Slow CDI is the final attenuation of SOCE after ER/SR store replenishment by the action of SERCA pumps, resulting in Ca^{2+} binding to the canonical EF hand of STIM1, return to the STIM1 resting state and STIM1-ORAI1 uncoupling (Prakriya and Lewis, 2015).
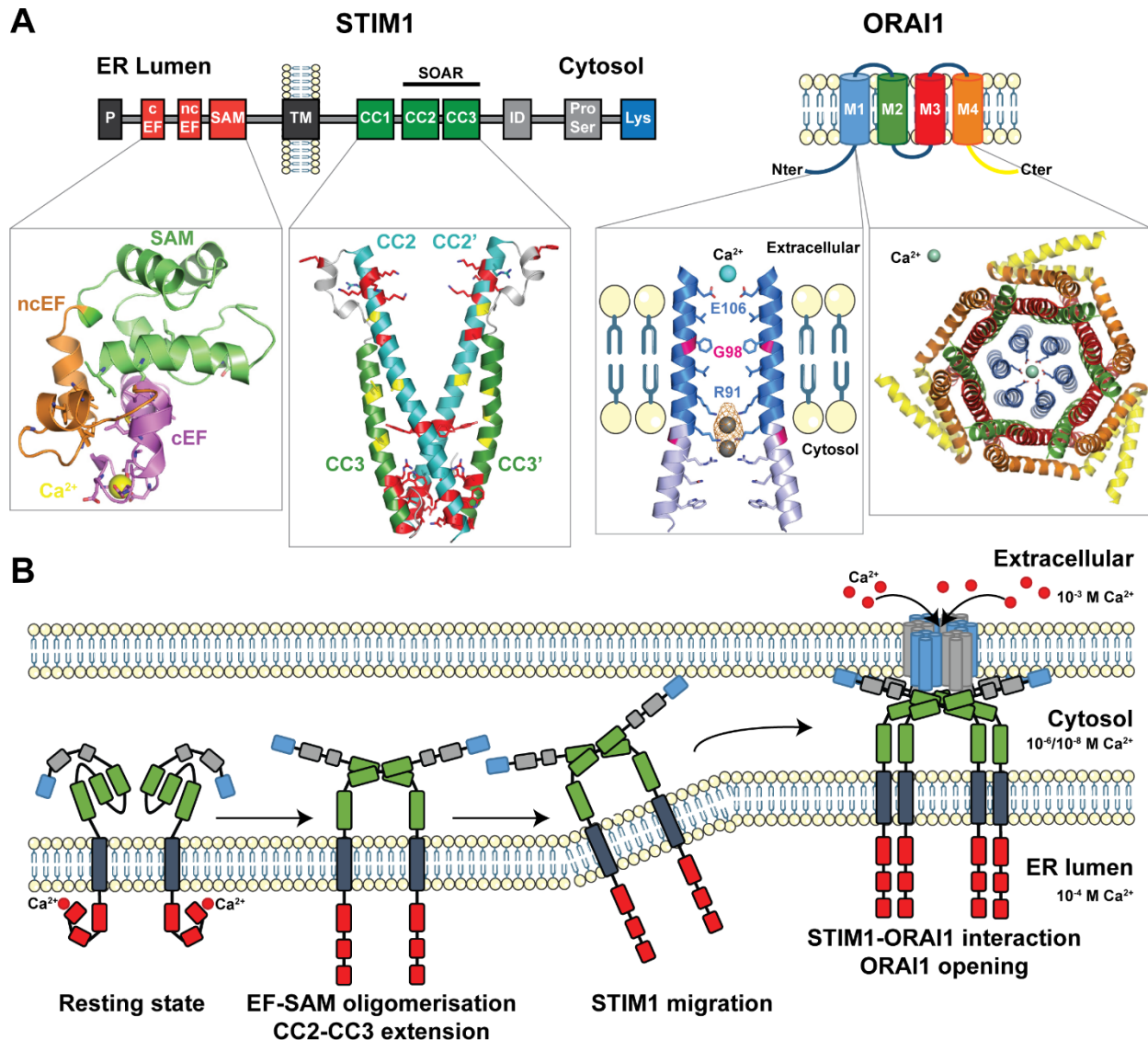
Figure 6. STIM1/ORAI1 structure and SOCE molecular arrangements.

(A) STIM1 is composed of an addressing-terminal reticular signal peptide signal (P) followed by canonical and non-canonical EF hands (cEF and ncEF). The cytosolic part has 3 coiled coil domains (CC1-CC3) with CC2 and CC3 containing the STIM1-ORAI1 activating region (SOAR), an inactivation domain (ID), a proline/serine rich region (Pro/Ser), and a C-terminal lysine rich (Lys) region to bind the negatively charged phospholipids in the plasma membrane. The ORAI1 channel is a hexamer, and each monomer consists of four transmembrane domains arranged as concentric rings with the M1 transmembrane domain forming the pore and controlling Ca^{2+} inflow. (B) In a Ca^{2+}-bound configuration, STIM1 is folded and inactive. Ca^{2+} detachment results in conformational changes of both luminal and cytosolic parts. STIM1 migration and the final interaction with the plasma membrane and ORAI1 triggers the opening of the channel and the entry of extracellular Ca^{2+}. The figure uses modified images from Servier Medical Art Commons

3.3. *STIM1* and *ORAI1* isoforms

STIM1 is composed of 12 exons encoding the conventional STIM1 isoform with 685 amino acids but other splice variants have also been described. Alternative splicing of exon 11 generates a 106 amino acid expansion near the inactivation domain of STIM1, and this longer isoform is referred to as STIM1L. This expansion has shown actin-binding properties facilitating anchoring near the ORAI1 contact sites. Indeed, STIM1L is predominantly expressed in skeletal muscle where SOCE activation takes less than 1 second and is significantly faster than in other tissues (Darbellay et al., 2011; Rosado et al., 2015). In addition, it has been shown that STIM1L could bind TRPC1, TRPC3, TRPC4 and TRPC6, all TRPCs with known contribution to SOCE (Antigny et al., 2017; Dyrda et al., 2020; Horinouchi et al., 2012; Lopez et al., 2020). Recently discovered splice variants have been described as a neuron-specific shorter STIM1 isoform lacking the C-terminal part or a longer and ubiquitous STIM1 isoform characterized by the insertion of a new exon between exons 10 and 11, both reducing SOCE activity (Knapp et al., 2020; Ramesh et al., 2021). We also found this exon insertion in a skeletal muscle-specific isoform whose transcription starts in a shorter exon 10 and contains the long exon 11 (unpublished) (Figure 7A). As a result of the absence of the luminal part, this new skeletal muscle splice variant is predicted to be cytosolic and possibly remains in the vicinity of ORAI1 contact sites similarly to STIM1L. Its precise role as SOCE modulator remains to be determined.

ORAI1 is composed of 2 exons and alternative translational start results in a longer ORAI1 α and a smaller ORAI1β isoform lacking the first 64-70 amino acids (Figure 7B). Both variants are ubiquitously expressed and participate in SOCE, but the absence of the N-terminal part in the ORAI1β isoform removes the proline/serine rich and arginine rich regions and presumably impact on STIM1 binding and the interaction with plasma membrane phosphoinositides (Rosado et al., 2015).
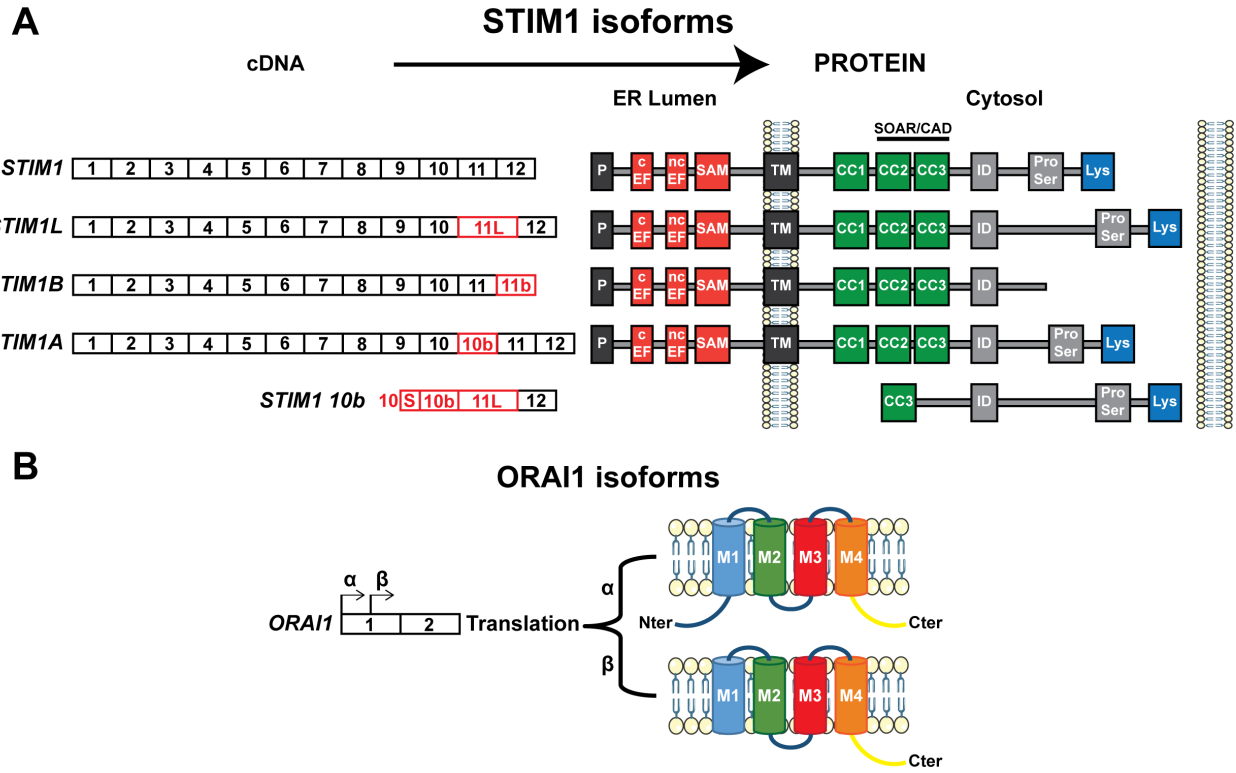
Figure 7. Splice variants of *STIM1* and *ORAI1*.

(A) The canonical STIM1 splice variant contains 12 exons encoding the different protein domains described in Figure 6A. STIM1L contains a longer exon 11 resulting from alternative splicing and producing a 106 amino acid extension of the protein between inactivation domain (ID) and proline/serine rich region (Pro/Ser), bringing the lysine rich region (Lys) closer to the plasma membrane. The STIM1B isoform terminates with the new exon 11b and lacks exon 12, which results in the absence of proline/serine and lysine rich regions. The STIM1A splice variant has a new small exon 10b between exons 10 and 11, increasing the space between inactivation domain and proline/serine rich domain by 31 amino acids. The STIM110b splice variant starts with a smaller version of exon 10, contains the new exon 10b, the long exon 11 and exon 12, resulting in a predicted cytosolic isoform of STIM1. (B) ORAI1 has 2 exons and the alternative translational start results in a full length ORAI1 (α) and a smaller ORAI1 lacking the first 64-71 amino acids (β). The figure uses modified images from Servier Medical Art Commons Attribution 3.0 Unported License (https://smart.servier.com).

3.4. Post-translational modifications

As previously mentioned, the first 22 amino acids of STIM1 form an ER signal peptide and its cleavage represents the first post-translational modification of STIM1. STIM1 phosphorylation at Ser486 and Ser668 by cyclin dependent kinase 1 (CDK1) suppresses SOCE during mitosis (Smyth et al., 2009). In contrast, STIM1 phosphorylation at Ser575, Ser608 and Ser621 by extracellular-signal-regulated kinases 1 and 2 (ERK1/2) facilitate STIM1-ORAI1 interactions and SOCE (Pozo-Guisado et al., 2010). Similar effects are observed when the tyrosines are phosphorylated by Butron's tyrosine kinase (Btk) or proline-rich kinase 2 (Pyk2) (Lopez et al., 2012; Yazbeck et al., 2017). ORAI1 phosphorylation at Ser27 and Ser30 by protein kinase C (PKC) has negative effects on SOCE (Kawasaki et al., 2010). Similarly, Ser34 phosphorylation by protein kinase A (PKA) stimulates fast CDI (Zhang et al., 2019).

Glycosylation represents another mechanism regulating SOCE activity. STIM1 glycosylation has a substantial role on the oligomerization process in response to ER Ca^{2+} depletion. Substitution of the Asn131 and Asn171 residues within the EF-SAM core affected the luminal destabilization required for STIM1 activation and oligomerization resulting in SOCE abolishment (Choi et al., 2017; Kilch et al., 2013). The enzymes driving STIM1 glycosylation have not been identified yet, but deficiency of the DPAGT1 glycosyltransferase in patients with limb-girdle myasthenic syndrome generate a double band for STIM1 (Selcen et al., 2014). This disease is characterized by anomalies in the neuromuscular junction associated with muscle weakness, and muscle biopsies from affected individuals showed tubular aggregates as in TAM/STRMK patients (more details in appendix section TUBULAR AGGREGATES IN AGING AND DISEASE). ORAI1 glycosylation on residue Asn223 was shown as a negative regulator of SOCE and N223A substitution or knockdown of sialyltransferase ST6GAL1 avoided or reduced ORAI1 glycosylation and increased Ca^{2+} entry in Jurkat T cells (Dorr et al., 2016).

ORAI1 S-acetylation at position Cys143 is required for ORAI1 mobility and activation particularly in the context of T cell activation. Alanine substitution decreased ORAI1 localization near the STIM1 puncta in ER-PM and consequently reduced in SOCE showing ORAI1 acetylation as a positive regulator of SOCE (Carreras-Sureda et al., 2021; West et al., 2022).

4. DISEASES CAUSED BY MUTATIONS IN *STIM1* AND *ORAI1*

STIM1 and ORAI1 are ubiquitously expressed proteins whose expression and activity needs to be tightly regulated to ensure normal physiology. Consistently, dysfunction of STIM1 or ORAI1 results in severe human disorders with multi-systemic phenotype. Recessive LoF mutations in *STIM1* or *ORAI1* cause CRAC channelopathy, a disorder encompassing immune deficiency and recurrent infections with low muscle tone (muscle hypotonia), defects in ectoderm-derived tissues (ectodermal dysplasia), sweat retention (anhydrosis) and reduced pupil contraction (mydriasis) (Lacruz and Feske, 2015). In opposition, GoF mutations in *STIM1* or *ORAI1* cause Tubular Aggregate Myopathy and Stormorken syndrome (TAM/STRMK) a clinical continuum characterized by muscle weakness, cramps and myalgia, together with short stature, small/absent spleen (hyposplenism/asplenia), low platelet counts associated with bleeding diathesis (thrombocytopenia), hypercontracted pupils (miosis), and dyslexia (Bohm and Laporte, 2018; Morin et al., 2020). Both human disorders arise from defective or over-activated SOCE, highlighting its role in Ca^{2+} homeostasis and in the physiological balance of different cells and tissues in health and disease.

In the following review, we describe the mirror-like effects of SOCE-deficiency or over-activation in different cells and tissues. To this aim, we compared the phenotypes observed in patients and mouse models of CRAC channelopathy and TAM/STRMK with a focus on the eye, skin, enamel, bone, spleen, immune system, platelets and skeletal muscle. We also updated the roles of STIM1 and ORAI1 interactors in the modulation of SOCE and the potential implications of SOCE in other diseases. This literature review revealed mirror phenotypes affecting different cells and tissues correlating with the SOCE levels and points to potentially underdiagnosed clinical signs in patients relevant for the evaluation of disease severity, patient management and the development of therapeutic strategies.

STIM1/ORAI1 Loss-of-Function and Gain-of-Function Mutations Inversely Impact on SOCE and Calcium Homeostasis and Cause Multi-Systemic Mirror Diseases

Roberto Silva-Rojas, Jocelyn Laporte and Johann Böhm

STIM1/ORAI1 Loss-of-Function and Gain-of-Function Mutations Inversely Impact on SOCE and Calcium Homeostasis and Cause Multi-Systemic Mirror Diseases

OPEN ACCESS

Roberto Silva-Rojas†, Jocelyn Laporte*† and Johann Böhm*†

Institut de Génétique et de Biologie Moléculaire et Cellulaire (IGBMC), Inserm U1258, CNRS UMR 7104, Université de Strasbourg, Illkirch, France

Edited by:
Enrique Jaimovich,
University of Chile, Chile

Reviewed by:
Vincenzo Sorrentino,
University of Siena, Italy
D. George Stephenson,
La Trobe University, Australia

*Correspondence:
Jocelyn Laporte
jocelyn@igbmc.fr
Johann Böhm
johann@igbmc.fr

†ORCID:
Roberto Silva-Rojas
orcid.org/0000-0002-0349-4283
Jocelyn Laporte
orcid.org/0000-0001-8256-5862
Johann Böhm
orcid.org/0000-0001-8019-9504

Store-operated Ca^{2+} entry (SOCE) is a ubiquitous and essential mechanism regulating Ca^{2+} homeostasis in all tissues, and controls a wide range of cellular functions including keratinocyte differentiation, osteoblastogenesis and osteoclastogenesis, T cell proliferation, platelet activation, and muscle contraction. The main SOCE actors are STIM1 and ORAI1. Depletion of the reticular Ca^{2+} stores induces oligomerization of the luminal Ca^{2+} sensor STIM1, and the oligomers activate the plasma membrane Ca^{2+} channel ORAI1 to trigger extracellular Ca^{2+} entry. Mutations in *STIM1* and *ORAI1* result in abnormal SOCE and lead to multi-systemic disorders. Recessive loss-of-function mutations are associated with CRAC (Ca^{2+} release-activated Ca^{2+}) channelopathy, involving immunodeficiency and autoimmunity, muscular hypotonia, ectodermal dysplasia, and mydriasis. In contrast, dominant *STIM1* and *ORAI1* gain-of-function mutations give rise to tubular aggregate myopathy and Stormorken syndrome (TAM/STRMK), forming a clinical spectrum encompassing muscle weakness, thrombocytopenia, ichthyosis, hyposplenism, short stature, and miosis. Functional studies on patient-derived cells revealed that CRAC channelopathy mutations impair SOCE and extracellular Ca^{2+} influx, while TAM/STRMK mutations induce excessive Ca^{2+} entry through SOCE over-activation. In accordance with the opposite pathomechanisms underlying both disorders, CRAC channelopathy and TAM/STRMK patients show mirror phenotypes at the clinical and molecular levels, and the respective animal models recapitulate the skin, bones, immune system, platelet, and muscle anomalies. Here we review and compare the clinical presentations of CRAC channelopathy and TAM/STRMK patients and the histological and molecular findings obtained on human samples and murine models to highlight the mirror phenotypes in different tissues, and to point out potentially undiagnosed anomalies in patients, which may be relevant for disease management and prospective therapeutic approaches.

Keywords: SOCE, calcium, STIM1, ORAI1, CRAC channelopathy, tubular aggregate myopathy, Stormorken syndrome

22

INTRODUCTION

Calcium (Ca^{2+}) is an elemental factor regulating a multitude of metabolic processes, signaling pathways, and cellular functions in all tissues, and mediates muscle contraction, nerve conduction, hormone release, and blood coagulation. Consistently, normal tissue and organ physiology strictly depends on the precise control of Ca^{2+} entry, storage, and release, while abnormal Ca^{2+} homeostasis induces various rare and common disorders affecting skeletal muscle, heart, bones, brain, skin, or the immune and hormonal systems (Peacock, 2010; Gattineni, 2014).

Ca^{2+} is mainly stored in the endoplasmic/sarcoplasmic reticulum (ER/SR), and refilling of the stocks is initiated by store-operated Ca^{2+} entry (SOCE), a ubiquitous mechanism driven by the concerted action of STIM1 and ORAI1 (Zhang et al., 2005; Feske et al., 2006). STIM1 contains an intraluminal region with EF hands sensing the reticular Ca^{2+} concentration, and a cytosolic part interacting with the plasma membrane CRAC (Ca^{2+} release-activated Ca^{2+}) channel ORAI1 (Stathopulos et al., 2006, 2008). Ca^{2+} store depletion induces STIM1 unfolding and oligomerization, and the STIM1 oligomers hence activate ORAI1 to trigger extracellular Ca^{2+} entry (Stathopulos et al., 2008; Prakriya and Lewis, 2015; Stathopulos and Ikura, 2017).

Abnormal SOCE has been associated with different human disorders. Recessive *STIM1* and *ORAI1* loss-of-function (LoF) mutations resulting in insufficient SOCE cause CRAC channelopathies characterized by severe combined immunodeficiency (SCID) involving recurrent and chronic infections, autoimmunity, muscular hypotonia, ectodermal dysplasia, anhidrosis, and mydriasis (Feske et al., 2006; Picard et al., 2009; Lacruz and Feske, 2015). The majority of the LoF mutations involve a total loss of STIM1 or ORAI1 (Lacruz and Feske, 2015), but single point mutations disrupting the STIM1 function and interfering with the STIM1-ORAI1 interaction (R426C, R429C) (Fuchs et al., 2012; Wang et al., 2014) or generating an obstructed ORAI1 channel (R91W) (Feske et al., 2006) have also been described (**Figure 1**). In contrast, dominant *STIM1* and *ORAI1* gain-of-function (GoF) mutations inducing excessive Ca^{2+} entry through SOCE over-activation were found in patients with tubular aggregate myopathy (TAM) and Stormorken syndrome (STRMK) (Bohm et al., 2013; Misceo et al., 2014; Morin et al., 2014; Nesin et al., 2014). TAM and STRMK form a clinical continuum characterized by progressive muscle weakness and myalgia predominantly affecting the lower limbs (Chevessier et al., 2005), and most patients manifest a varying degree of additional multi-systemic signs as miosis, ichthyosis, short stature, hyposplenism, thrombocytopenia, and dyslexia (Endo et al., 2015; Markello et al., 2015; Walter et al., 2015; Bohm et al., 2017; Garibaldi et al., 2017; Noury et al., 2017; Bohm and Laporte, 2018; Morin et al., 2020). All GoF mutations are missense mutations affecting highly conserved amino acids in the Ca^{2+}-binding EF hands (H72Q, N80T, G81D, D84G, D84E, S88G, L92V, L96V, Y98C, F108I, F108L; H109N, H109R, H109Y, I115F) (Bohm et al., 2013, 2014; Hedberg et al., 2014; Markello et al., 2015; Walter et al., 2015; Harris et al., 2017; Noury et al., 2017; Li et al., 2019; Claeys et al., 2020; Morin et al., 2020) or in the luminal coiled-coil domains of STIM1 (R304W,

R304Q) (Misceo et al., 2014; Morin et al., 2014; Nesin et al., 2014; Markello et al., 2015; Harris et al., 2017; Alonso-Jimenez et al., 2018; Borsani et al., 2018; Sura et al., 2020), or in the ORAI1 transmembrane domains forming the channel pore or concentric rings surrounding the pore (G97C, G98S, V107M, L138F, T184M, P245L) (Nesin et al., 2014; Endo et al., 2015; Bohm et al., 2017; Garibaldi et al., 2017; **Figure 1**). Missense mutations in the muscle-specific SR Ca^{2+} buffer calsequestrin (*CASQ1*) have moreover been reported in patients with late-onset muscle weakness and myalgia, forming the mild end of the TAM/STRMK spectrum (Barone et al., 2017; Bohm et al., 2018; **Figure 1**).

Animal models for CRAC channelopathy and TAM/STRMK exist and widely recapitulate the clinical signs of the human disorders. Mice lacking STIM1 or ORAI1 die perinatally (Baba et al., 2008; Oh-Hora et al., 2008), and the tissue-specific deletion of *Stim1* or *Orai1* or the generation of chimeras through transplantation of hematopoietic $Stim1^{-/-}$ or $Orai1^{-/-}$ stem cells results in defective T cell activation and Treg suppression (Gwack et al., 2008; Oh-Hora et al., 2008, 2013; McCarl et al., 2010), splenomegaly (Oh-Hora et al., 2008, 2013), autoimmunity (Oh-Hora et al., 2008, 2013), reduced platelet activation and thrombus formation (Varga-Szabo et al., 2008; Bergmeier et al., 2009; Braun et al., 2009; Ahmad et al., 2011), anhidrosis (Concepcion et al., 2016), amelogenesis imperfecta (Gwack et al., 2008), and muscle weakness with reduced resistance to fatigue (Stiber et al., 2008; Srikanth et al., 2010; Li et al., 2012; Wei-Lapierre et al., 2013; Carrell et al., 2016; Sampieri et al., 2018). Mice harboring the *Stim1* GoF mutations D84G, I115F, or R304W show a varying degree of multi-systemic disease signs including small size (Cordero-Sanchez et al., 2019; Silva-Rojas et al., 2019), eye movement defects (Silva-Rojas et al., 2019), skin and spleen anomalies (Grosse et al., 2007; Cordero-Sanchez et al., 2019; Silva-Rojas et al., 2019), bleeding diathesis with thrombocytopenia (Grosse et al., 2007; Cordero-Sanchez et al., 2019; Silva-Rojas et al., 2019), and muscle weakness (Cordero-Sanchez et al., 2019; Silva-Rojas et al., 2019). SOCE deficiency in drosophila resulting from *Stim* or *Orai* downregulation impairs the flight capacities (Venkiteswaran and Hasan, 2009; Agrawal et al., 2010), and zebrafish embryos injected with mRNA containing *STIM1* or *ORAI1* GoF mutations display thrombocytopenia (Nesin et al., 2014), highlighting the conservation of SOCE in specific tissues.

The present review aims to provide an update on the current knowledge of CRAC channelopathy and TAM/STRMK, to highlight the molecular and/or clinical mirror phenotypes caused by either LoF or GoF mutations in the SOCE key players, and to provide an overview of the available animal models recapitulating the human disorders. We thoroughly and stepwise compare the eye, skin, bone, enamel, spleen, immune, platelet, and muscle phenotypes in human and mouse, and we detail the inverse mutational effects and pathomechanisms underlying CRAC channelopathy and TAM/STRMK, and their impact on the sequence of events leading to the diverging clinical manifestations and mirror-image anomalies in most affected tissues. We also point to clinical signs that are potentially underdiagnosed in patients, and may be relevant

23
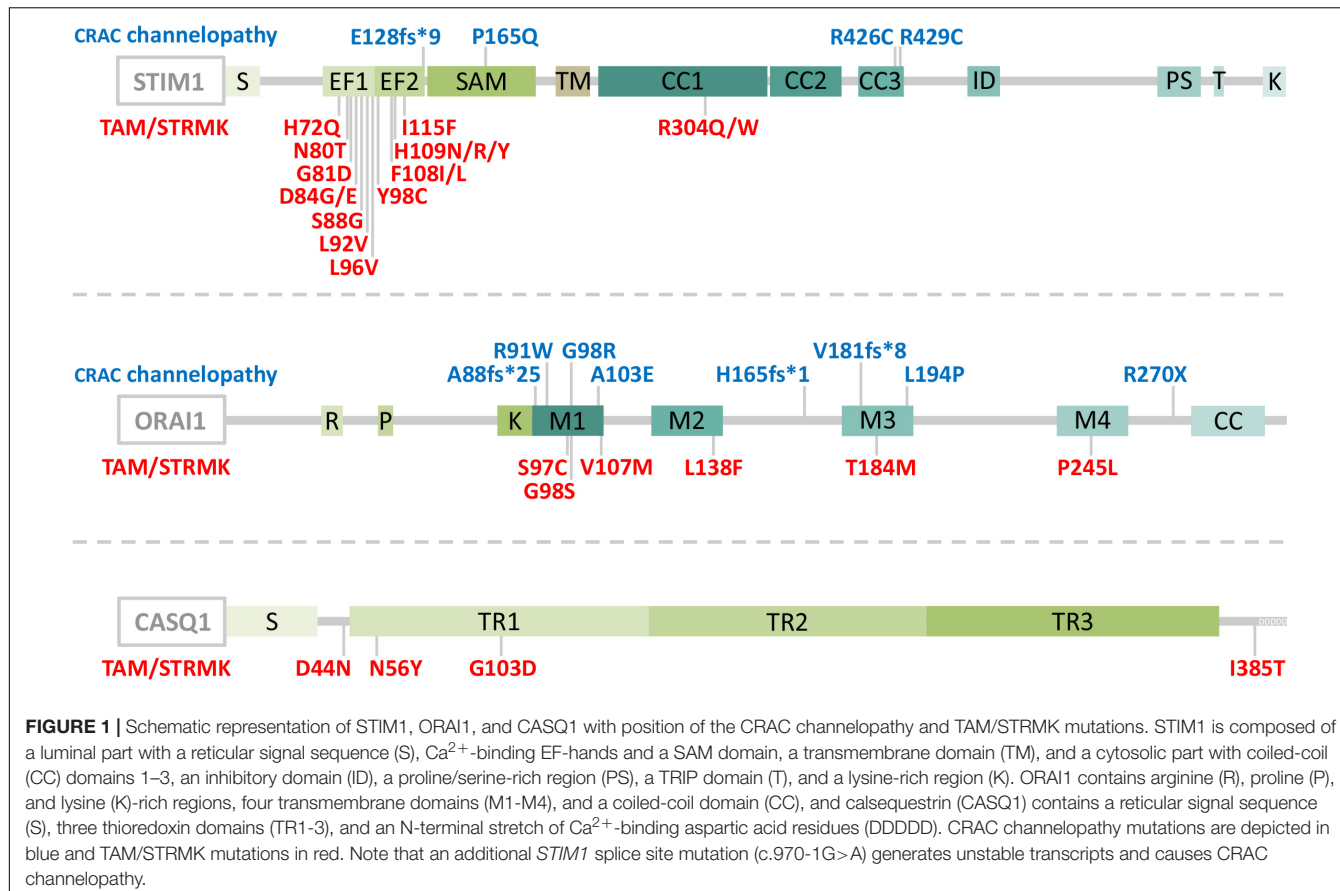
FIGURE 1 | Schematic representation of STIM1, ORAI1, and CASQ1 with position of the CRAC channelopathy and TAM/STRMK mutations. STIM1 is composed of a luminal part with a reticular signal sequence (S), Ca^{2+}-binding EF-hands and a SAM domain, a transmembrane domain (TM), and a cytosolic part with coiled-coil (CC) domains 1–3, an inhibitory domain (ID), a proline/serine-rich region (PS), a TRIP domain (T), and a lysine-rich region (K). ORAI1 contains arginine (R), proline (P), and lysine (K)-rich regions, four transmembrane domains (M1-M4), and a coiled-coil domain (CC), and calsequestrin (CASQ1) contains a reticular signal sequence (S), three thioredoxin domains (TR1-3), and an N-terminal stretch of Ca^{2+}-binding aspartic acid residues (DDDDD). CRAC channelopathy mutations are depicted in blue and TAM/STRMK mutations in red. Note that an additional *STIM1* splice site mutation (c.970-1G>A) generates unstable transcripts and causes CRAC channelopathy.

for diagnosis and disease management, and disclose treatment options. A schematic illustration opposing the clinical pictures of CRAC channelopathy versus TAM/STRMK is shown in **Figure 2**, and is supported by a detailed description in **Table 1**.

PHENOTYPIC TRAITS IN CRAC CHANNELOPATHY AND TAM/STRMK PATIENTS AND MICE

CRAC channelopathy and TAM/STRMK are multi-systemic disorders, and patients with either disease can manifest impairments of pupillary function, eye movement, skin, enamel, bones, immune system, spleen, coagulation, and skeletal muscle. The following chapter provides a comparative overview of the clinical anomalies and the molecular and mechanistic causes, and also refers to the phenotypic traits of diverse CRAC channelopathy and TAM/STRMK mouse models.

Pupillary Dysfunction and Eye Movement Limitations

Vision is primarily a photochemical process, and can be adapted to the lighting conditions through iris constriction/dilatation and eye movement, both governed by Ca^{2+}-dependent muscle contraction. Ca^{2+} release from the reticulum activates the contractile apparatus, which generates force, causing the shortening of the muscle cells (Ebashi, 1974). The iris acts as a diaphragm controlling the amount of light entering the eye through the pupil, and SOCE substantially sustains the muscle tonus for the steady contraction of the smooth sphincter and dilator muscles for an appropriate view in brightness and obscurity (Eckstein et al., 2017; Feldman et al., 2017).

Pupillary dysfunction is a main clinical sign of CRAC channelopathy and TAM/STRMK. While CRAC channelopathy patients typically show iris dilatation (mydriasis) (Feske et al., 2006; Picard et al., 2009; Fuchs et al., 2012; Lian et al., 2018), the inverse phenotype of light-insensitive iris hypercontraction (miosis) is a hallmark of TAM/STRMK, and results in migraine and reduced night vision (Misceo et al., 2014; Morin et al., 2014, 2020; Nesin et al., 2014; Markello et al., 2015; Bohm et al., 2017; Garibaldi et al., 2017; Harris et al., 2017; Alonso-Jimenez et al., 2018; Borsani et al., 2018; Claeys et al., 2020; Sura et al., 2020). Mydriasis and miosis have, however, not been described in murine models for CRAC channelopathy or TAM/STRMK. They may have been missed, or may reflect physiological differences between the species. Indeed, mice are nocturnal animals, and murine pupil constriction is essentially triggered by a light-dependent mechanism known as local pupillary reflex that is absent in humans (Xue et al., 2011).

Eye movement relies on the rapid and concerted contraction of six striated extraocular muscles, and ophthalmoplegia
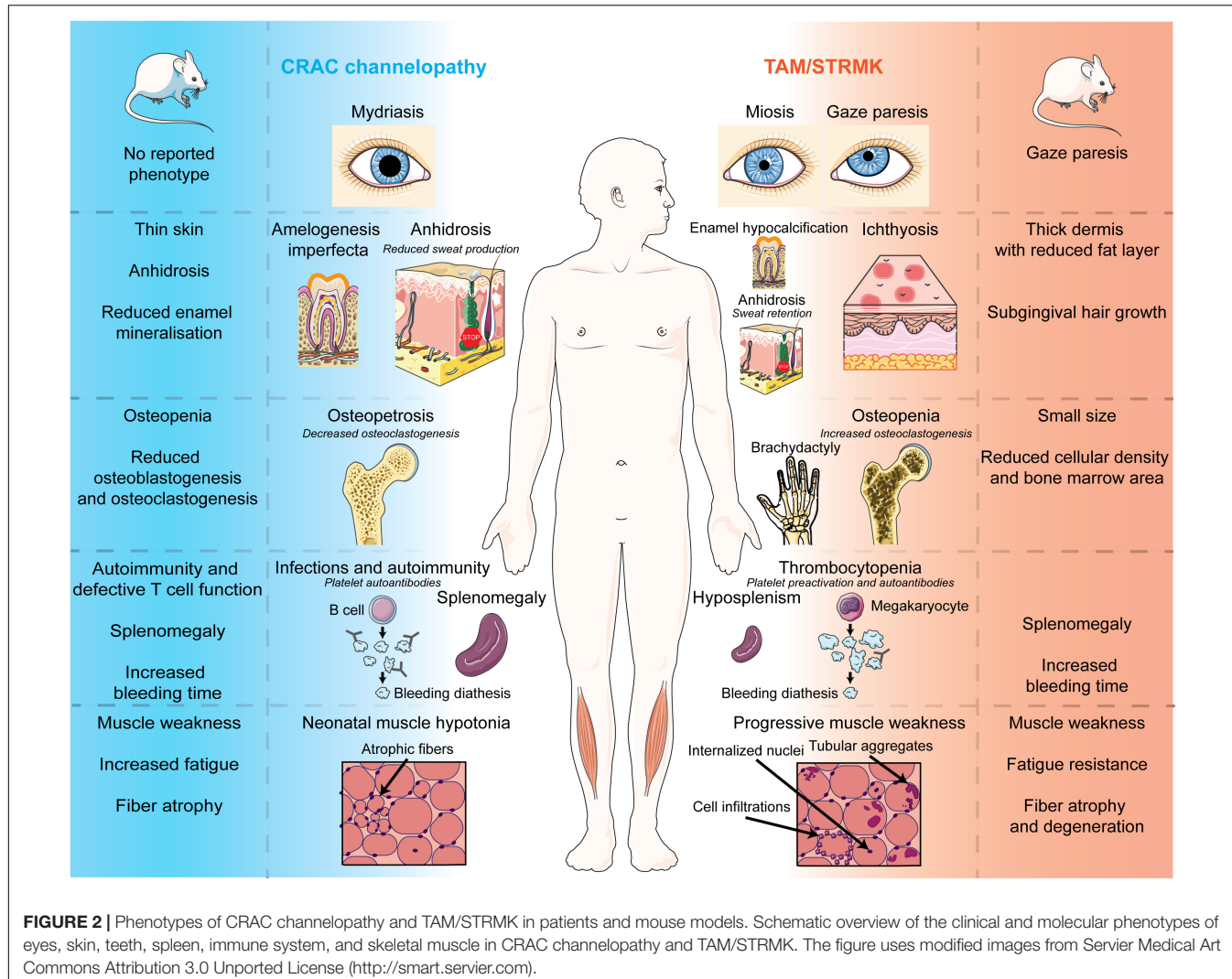
FIGURE 2 | Phenotypes of CRAC channelopathy and TAM/STRMK in patients and mouse models. Schematic overview of the clinical and molecular phenotypes of eyes, skin, teeth, spleen, immune system, and skeletal muscle in CRAC channelopathy and TAM/STRMK. The figure uses modified images from Servier Medical Art Commons Attribution 3.0 Unported License (http://smart.servier.com).

including upward gaze paresis (Bohm et al., 2013; Noury et al., 2017), lateral gaze paresis (Morin et al., 2020), or reduced lateral and/or upward gaze (Bohm et al., 2014; Hedberg et al., 2014; Markello et al., 2015; Walter et al., 2015; Harris et al., 2017; Noury et al., 2017) is commonly seen in TAM/STRMK patients. In accordance, the TAM/STRMK mouse model harboring the most common STIM1 GoF mutation R304W also features an upward gaze paresis (Silva-Rojas et al., 2019).

Skin Anomalies and Enamel Defects

Skin forms the first defense barrier to protect from external agents, and also plays a pivotal role in thermoregulation by sweat production. Keratinocytes are the principal components of the outermost skin layer, the epidermis, and their growth, differentiation, and migration is driven by SOCE in both humans and mice (Numaga-Tomita and Putney, 2013; Vandenberghe et al., 2013). SOCE also triggers the opening of the Ca^{2+}-activated chloride channel TMEM16A in the sweat glands, and thereby enables chloride secretion and sweat production (Concepcion et al., 2016). In the absence of SOCE, CRAC

channelopathy patients present with thermoregulatory instability and anhidrosis accompanied by heat intolerance, dry skin, and eczema (Feske et al., 2006; Fuchs et al., 2012; Schaballie et al., 2015; Lian et al., 2018). Skin anomalies including eczema and ichthyosis are also commonly seen in TAM/STRMK patients (Misceo et al., 2014; Morin et al., 2014, 2020; Bohm et al., 2017; Harris et al., 2017; Claeys et al., 2020), and one patient additionally manifested anhidrosis (Ishitsuka et al., 2019). Histological examinations of the skin biopsy revealed an obstruction of the spiral duct in the eccrine gland, the acrosyringia, resulting in sweat retention. This is different from CRAC channelopathy patients, where the sweat glands display a reduced lumen due the lack of sweat production (Lian et al., 2018). Noteworthy, the ectodermal barrier protein proflaggrin was found to be aggregated in the acrosyringia of the TAM/STRMK patient. Loss of proflaggrin is a major predisposing factor of idiopathic ichthyosis (Palmer et al., 2006), indicating that the skin phenotype in TAM/STRMK patients may be a direct consequence of the abnormal proflaggrin accumulation in the sweat glands.

TABLE 1 | Descriptive comparison of the clinical signs and physiological defects in CRAC channelopathy and TAM/STRMK patients and mouse models.

		CRAC channelopathy Reduced SOCE		TAM/STRMK Increased SOCE	
		Mouse models	Patients	Patients	Mouse models
Eye	Pupils	Not reported	Mydriasis	Miosis	Not reported
	Eye movement	Not reported	Not reported	Upward/lateral gaze paresis	Upward gaze paresis ($Stim1^{R304W/+}$)
Ectodermal tissues	Skin	Thin skin ($Orai1^{-/-}$), anhidrosis ($Orai1^{-/-}$, $Stim1^{-/-}$ $Stim2^{-/-}$)	Anhidrosis	Anhidrosis, ichthyosis	Thick dermis, reduced subcutaneous fat layer ($Stim1^{R304W/+}$)
	Teeth	Reduced enamel mineralization ($Orai1^{-/-}$)	Amelogenesis imperfecta	Enamel hypocalcification	Subgingival hair growth ($Stim1^{R304W/+}$)
Bones	Clinical signs	Not reported	Facial dysmorphism	Short stature brachydactyly, syndactyly, Klippel-Feil anomaly	Small size ($Stim1^{R304W/+}$), reduced number of ribs ($Stim1^{R304W/R304W}$), thin and compact bones ($Stim1^{R304W/R304W}$)
	Molecular findings	Reduced osteoblastogenesis and osteoclastogenesis, osteopenia ($Orai1^{-/-}$)	Osteopetrosis, reduced osteoclasteogenesis	Osteopenia, increased osteoclasteogenesis	Reduced cellular density, reduced bone marrow area ($Stim1^{R304W/+}$)
Immune system	Clinical signs	Autoimmunity, splenomegaly ($Stim1^{-/-}$ $Stim2^{-/-}$, $Orai1^{R93W/R93W}$)	Recurrent and chronic infections, autoimmunity, splenomegaly	Hyposplenism	Splenomegaly ($Stim1^{D84G/+}$, $Stim1^{I115F/+}$ and $Stim1^{R304W/+}$)
	Molecular findings	Reduced cytokine expression ($Stim1^{-/-}$, $Orai1i^{-/-}$, $Stim1^{-/-}$ $Stim2^{-/-}$, $Orai1^{R93W/R93W}$), reduced suppressive function of NKT and Treg cells ($Stim1^{-/-}$ $Stim2^{-/-}$, $Orai1^{R93W/R93W}$)	Reduced T cell proliferation, cytokine expression, immunoglobulin production, iNKT and Treg cells, presence of anti-platelet autoantibodies	Lymphoproliferation, presence of anti-platelet autoantibodies	Reduced Treg and NK cells, increased neutrophils and monocytes ($Stim1^{R304W/+}$)
Coagulation	Clinical signs	Slightly increased bleeding time ($Stim1^{-/-}$, $Orai1^{-/-}$)	Mild bleeding diathesis	Bleeding diathesis	Increased bleeding time ($Stim1^{D84G/+}$)
	Molecular findings	Reduced platelet activation ($Stim1^{-/-}$, $Orai1^{-/-}$, $Stim1^{-/-}$ $Orai1^{-/-}$, $Orai1^{R93W/R93W}$), reduced thrombus formation ($Stim1^{-/-}$ $Orai1^{-/-}$, $Orai1^{-/-}$, $Stim1^{-/-}$ $Orai1^{-/-}$)	Reduced platelet activation, reduced thrombus formation	Thrombocytopenia, Platelet pre-activation, aberrant size and morphology, reduced platelet-platelet adhesion	Thrombocytopenia ($Stim1^{D84G/+}$, $Stim1^{I115F/+}$, $Stim1^{R304W/+}$), platelet pre-activation, increased platelet clearance ($Stim1^{D84G/+}$)
Skeletal muscle	Clinical signs	Muscle weakness ($Stim1^{-/-}$, $Orai1^{-/-}$), increased fatigue ($Stim1^{-/-}$, $Orai1^{-/-}$)	Neonatal hypotonia, muscle weakness	Muscle weakness, cramps, myalgia	Muscle weakness, increased resistance to fatigue ($Stim1^{I115F/+}$, $Stim1^{R304W/+}$)
	Molecular findings	Fiber atrophy, swollen mitochondria ($Stim1^{-/-}$, $Orai1^{-/-}$)	Type I predominance, type II fiber atrophy	Tubular aggregates, type I fiber predominance, type II fiber atrophy, internalized nuclei, vacuoles, fibrosis, elevated serum CK	Fiber atrophy and degeneration, type I fiber predominance, swollen mitochondria, elevated serum CK ($Stim1^{I115F/+}$, $Stim1^{R304W/+}$)

26

Alike skin and sweat glands, teeth derive from the ectoderm, and CRAC channelopathy patients also manifest dental maturation defects including major enamel loss, discoloration and poor mineralization of both deciduous and permanent teeth (Feske et al., 2006; McCarl et al., 2009; Picard et al., 2009; Fuchs et al., 2012; Wang et al., 2014; Schaballie et al., 2015; Lian et al., 2018), highlighting the importance of SOCE in ameloblast formation and mineralization (Wang et al., 2014). In contrast, amelogenesis imperfecta is not a typical feature of TAM/STRMK, and enamel hypocalcification was only noted in a single patient (Noury et al., 2017).

CRAC channelopathy and TAM/STRMK animal models partially recapitulate the human enamel and skin phenotypes. Mice lacking ORAI1 manifest reduced enamel mineralization (Robinson et al., 2012) and thinner skin with elongated keratinocytes and smaller vibrissae follicles (Gwack et al., 2008), and the ectodermal-specific knockout of *Orai1*/*Stim1*/*Stim2* impairs SOCE and results in anhidrosis and a reduced sweat gland lumen (Concepcion et al., 2016). The TAM/STRMK mouse harboring the STIM1 R304W mutation shows a thickened dermis and a reduction of the subcutaneous fat layer (Silva-Rojas et al., 2019), and a subset of the animals additionally exhibit subgingival hair growth on the lower incisors (Gamage et al., 2020).

Bone Anomalies

Bones represent 15% of the total body weight and are essential for motion, mineral storage, and hematopoiesis. Bone deposition and resorption are dynamic and balanced processes driven by bone-forming osteoblasts and bone-resorbing osteoclasts (Florencio-Silva et al., 2015), and their growth and differentiation is regulated by SOCE-dependent Ca^{2+} homeostasis (Eapen et al., 2010; Blair et al., 2011; Chen et al., 2018). Bone resorption by osteoclasts generates a local increment of extracellular Ca^{2+}, inducing the activation of the calcineurin/NFAT signaling pathway, and resulting in osteoblastogenesis (Zayzafoon, 2006). Calcineurin/NFAT signaling is also essential for osteoclastogenesis and T cell activation, and the inhibition of this pathway with cyclosporine A to prevent transplant rejection is associated with an increased incidence of bone fractures (Zayzafoon, 2006).

Overt bone anomalies are largely absent in CRAC channelopathy and TAM/STRMK patients with exception of individual cases with facial dysmorphism (McCarl et al., 2009), fusion of the cervical vertebrae (Klippel-Feil anomaly) (Morin et al., 2020), brachydactyly (Morin et al., 2020), or syndactyly of the second and third toes (Borsani et al., 2018). Bone mineralization was found to be increased in two CRAC channelopathy patients (osteopetrosis) and decreased in a single TAM/STRMK patient (osteopenia), and accordingly, functional studies demonstrated a decreased osteoclastogenesis in bone marrow mononuclear macrophages from the CRAC channelopathy patients, and an increased osteoclastogenesis in cells derived from the TAM/STRMK patient (Huang et al., 2020). Of note, a number of TAM/STRMK patients exhibit a short stature (Misceo et al., 2014; Morin et al., 2014, 2020; Noury et al., 2017; Borsani et al., 2018), and other more subtle or late-onset bone disorders might have been overlooked in CRAC

channelopathy and TAM/STRMK patients. This is supported by the impaired differentiation and function of osteoblasts and osteoclasts leading to osteopenia with decreased bone density and trabecular bone volume in ORAI1-deficient mice (Hwang et al., 2012; Robinson et al., 2012). Alike patients, TAM/STRMK mice are smaller than their littermates, and micro-CT analyses revealed a decreased cellular density and a reduced bone marrow area in femur and tibia, potentially affecting bone strength and stiffness (Silva-Rojas et al., 2019). Surviving mice carrying the STIM1 R304W mutation at the homozygous state show a more severe skeletal phenotype with thinner and more compact bones, and also feature a reduced number of ribs (Gamage et al., 2020).

Immune System and Spleen Anomalies

The immune system is an essential and complex defense network, and SOCE directs the fate and function of diverse cells of the innate and adaptive immune system, including dendritic cell maturation (Felix et al., 2013), neutrophil activation (Zhang et al., 2014), lymphocyte cytotoxicity and cytokine production (Maul-Pavicic et al., 2011), as well as T cell proliferation, differentiation, and metabolism (Vaeth et al., 2017; Vaeth and Feske, 2018). T cells play a pivotal role in the adaptive immune system and act as effector, memory, suppressor, or helper cells in response to external agents. The antigen recognition by the T cell receptors activates a signaling cascade resulting in the continuous depletion of the reticular Ca^{2+} stores and a durable extracellular Ca^{2+} entry via SOCE to initiate the Ca^{2+}-dependent transcriptional program necessary for T cell function (Feske, 2007).

Recurrent infections and autoimmunity are the predominant clinical traits of CRAC channelopathy (Feske et al., 2006; McCarl et al., 2009; Picard et al., 2009; Byun et al., 2010; Fuchs et al., 2012; Wang et al., 2014; Chou et al., 2015; Lacruz and Feske, 2015; Schaballie et al., 2015; Badran et al., 2016; Lian et al., 2018), and hematological examinations of affected individuals revealed normal levels of T cells, while functional investigations detected a reduced T cell proliferation and cytokine expression, and an impaired production of immunoglobulins in response to antigens (Feske et al., 1996, 2006; Fuchs et al., 2012; Lian et al., 2018). Invariant natural killer T cells (iNKT) and/or regulatory T cells (Treg) were reduced (Schaballie et al., 2015; Badran et al., 2016; Lian et al., 2018), suggesting a defect in self-tolerance as in autoimmune disorders (Dejaco et al., 2006; Novak and Lehuen, 2011; Josefowicz et al., 2012). In accordance with the immune cell dysregulation in patients, cytokine expression is impaired in mice with T CD4+ cell-specific deletion of *Stim1* or *Orai1*, and chimeric *Orai1*$^{R93W/R93W}$ animals (corresponding to R91W in humans) and *Stim1* and *Stim2* double knockout mice additionally show a reduced suppressive function of Treg and NKT cells and an associated autoimmunity and splenomegaly (Gwack et al., 2008; Oh-Hora et al., 2008, 2013; McCarl et al., 2010).

The spleen is the largest lymphoid organ and functions as a blood filter, and ensures the biogenesis and storage of white and red blood cells, as well as the phagocytosis of circulating microorganisms (de Porto et al., 2010). CRAC channelopathy patients develop hepatosplenomegaly (Picard et al., 2009; Byun et al., 2010; Schaballie et al., 2015; Lian et al., 2018), while asplenia or hyposplenia is a clinical hallmark of TAM/STRMK (Morin

et al., 2020). As an indication of abnormal spleen function, Howell-Jolly bodies have moreover been found on peripheral blood film in several affected individuals (Misceo et al., 2014; Morin et al., 2014; Markello et al., 2015; Harris et al., 2017; Noury et al., 2017), but an increased rate of infections has nevertheless not been reported. Contrasting the patients, the TAM/STRMK mouse models present with splenomegaly, and histological investigations of the spleen revealed megakaryocyte hypoplasia (Grosse et al., 2007; Silva-Rojas et al., 2019). This is possibly related to a physiological difference between both species, as hematopoiesis lowers with age in humans, while it is maintained throughout life in mice (Bronte and Pittet, 2013). Of note, hematological analyses disclosed abnormal B, NK, and Treg counts in the STIM1 R304W mouse (Silva-Rojas et al., 2019), indicating that disturbances of the immune system may also occur in TAM/STRMK patients and potentially contribute to the spleen, platelet, and skin anomalies. This is sustained by the detection of lymphoproliferation and circulating antibodies against platelets in a single patient with STIM1 R304W mutation (Sura et al., 2020).

Coagulation Defects

Hemostasis prevents and stops bleeding through the formation of a thrombus, which is ultimately resolved in the process of wound healing. Platelets play an essential role in thrombus formation, and the activation of platelets is induced by the presence of the subcortical component collagen in the blood flow following vessel wall damage (Bye et al., 2016). The collagen fragments bind to glycoprotein VI (GPVI) at the surface of the platelets and trigger a signaling cascade involving SOCE and leading to the Ca^{2+}-dependent exposure of phosphatidylserine (PS) and the secretion of alpha granules containing thrombotic factors (Berna-Erro et al., 2016; van der Meijden and Heemskerk, 2019), which will then prompt the coagulation process and modulate inflammation and angiogenesis in the injured area (Blair and Flaumenhaft, 2009).

As a result of SOCE deficiency, PS exposure and alpha granule secretion is reduced in platelets from CRAC channelopathy patients, impeding platelet aggregation and thrombus formation (Nakamura et al., 2013). In consequence of the overall reduction of Treg cells, high titers of anti-platelet autoantibodies are detectable in the serum of the patients, lead to hemolytic anemia, and contribute to mild or intermittent susceptibility to bleed in several affected individuals (Picard et al., 2009; Byun et al., 2010; Fuchs et al., 2012; Lian et al., 2018). Bleeding diathesis associated with thrombocytopenia is a major clinical feature of TAM/STRMK (Misceo et al., 2014; Morin et al., 2014, 2020; Nesin et al., 2014; Markello et al., 2015; Bohm et al., 2017; Harris et al., 2017; Noury et al., 2017; Alonso-Jimenez et al., 2018; Borsani et al., 2018; Li et al., 2019; Claeys et al., 2020; Sura et al., 2020), and the analysis of blood samples from patients revealed increased platelet activation markers and enhanced secretion of alpha granules in unstimulated platelets (Misceo et al., 2014). Despite this pre-activation state caused by elevated resting Ca^{2+}, the platelet-platelet adhesion is impaired, and platelets often appeared with aberrant size and morphology (Markello et al., 2015), suggesting that the coagulation defect in

TAM/STRMK patients results from a combination of platelet loss and platelet dysfunction.

In analogy to CRAC channelopathy patients, PS exposure and secretion of alpha granules is diminished in mice with platelet-specific deletion of *Stim1* and in chimeric $Orai1^{R93W/R93W}$ animals (Bergmeier et al., 2009; Ahmad et al., 2011). Chimeric $Stim1^{-/-}$ and $Orai1^{-/-}$ mice additionally show impaired platelet aggregation and thrombus formation, leading to a slight increase in bleeding time (Varga-Szabo et al., 2008; Braun et al., 2009; Gilio et al., 2010). The murine TAM/STRMK models similarly recapitulate the coagulation defects seen in the patients, as thrombocytopenia is evident in all three STIM1 D84G, I115F, and R304W models (Grosse et al., 2007; Cordero-Sanchez et al., 2019; Silva-Rojas et al., 2019). Further analyses on the STIM1 D84G mice uncovered that the pre-activation state of the platelets increases platelet clearance, and thereby prevents efficient platelet aggregation (Grosse et al., 2007). If and to what extent the bleeding diathesis is exacerbated by the immune system defects in TAM/STRMK mice and potentially in patients remains to be determined.

Muscle Weakness

Skeletal muscles maintain posture and allow movements under the voluntary control of the somatic nervous system, and also regulate body temperature and nutrition storage. SOCE activation and extracellular Ca^{2+} entry is significantly faster in myofibers compared with other cell types, occurring within milliseconds after each action potential (Launikonis et al., 2009; Edwards et al., 2010). This is believed to be related to the presence of the muscle-specific STIM1L isoform forming pre-activated Ca^{2+} entry units with ORAI1 at the SR/plasma membrane junction (Darbellay et al., 2011). Refilling of the Ca^{2+} stores is mediated by the ATP-dependent SERCA pumps to maintain high Ca^{2+} gradients across the SR membrane, thus limiting the SR depletion of Ca^{2+} during repetitive tetanic stimulations (Pan et al., 2002; Zhao et al., 2005).

CRAC channelopathy patients manifest neonatal hypotonia and generalized muscle weakness, and show delayed motor milestones and reduced walking distance in infancy, with additional respiratory insufficiency in individual cases (Feske et al., 2006; McCarl et al., 2009; Picard et al., 2009; Fuchs et al., 2012; Chou et al., 2015; Schaballie et al., 2015; Badran et al., 2016; Lian et al., 2018). Histological investigations were performed on muscle biopsies from two patients, and revealed fiber type I fiber predominance and type II atrophy (McCarl et al., 2009; Lian et al., 2018). Muscle weakness and exercise intolerance are primary clinical features of TAM/STRMK, and the onset and severity depend on the causative gene and correlate with the position of the mutation (Morin et al., 2020). In most cases, disease onset is during infancy or childhood, and first and foremost affects the proximal muscles of the lower limbs. Muscle weakness is generally accompanied by elevated serum creatine kinase (CK) levels, indicating moderate fiber degeneration, and myalgia and cramps are often observed as secondary features, but can also occur as isolated signs (Bohm et al., 2013; Bohm et al., 2014, 2017, 2018; Hedberg et al., 2014; Misceo et al., 2014; Morin et al., 2014, 2020; Nesin et al., 2014;

Endo et al., 2015; Markello et al., 2015; Walter et al., 2015; Barone et al., 2017; Garibaldi et al., 2017; Harris et al., 2017; Noury et al., 2017; Alonso-Jimenez et al., 2018; Borsani et al., 2018; Li et al., 2019; Claeys et al., 2020). Noteworthy, Ca^{2+} overload in skeletal muscle fibers has been shown to disrupt excitation-contraction coupling (ECC) (Lamb et al., 1995), which possibly contributes to the reduced muscle force in TAM/STRMK patients. Muscle sections from affected individuals typically show tubular aggregates appearing in red on Gomori trichrome staining, and adopting a honeycomb structure of densely packed tubules on electron microscopy (Chevessier et al., 2004, 2005; Bohm and Laporte, 2018). The tubular aggregates are highly Ca^{2+}-rich, and immunofluorescence studies have shown that they essentially contain SR proteins such as STIM1, calsequestrin, triadin, or RyR1, indicating that they are of reticular origin (Chevessier et al., 2004, 2005; Bohm et al., 2013, 2017; Endo et al., 2015). It has been suggested that the abundance of Ca^{2+} in muscle fibers may cause SR protein misfolding and aggregation, leading to the formation of membrane stacks as precursors of tubular aggregates (Morin et al., 2020). Alternatively, the occurrence of tubular aggregates may reflect the attempt to regenerate a functional triad, a specialized membrane complex in skeletal muscle hosting the ECC machinery. This is supported by the observation that Ca^{2+} excess induces the proteolysis of junctophilins, which tether the SR membrane to deep plasma membrane invaginations known as T-tubules to form the triad (Murphy et al., 2013). Further histopathological signs on TAM/STRMK biopsies encompass fiber size variability, type I fiber predominance, type II fiber atrophy, internalized nuclei, vacuoles, and fibrosis (Bohm et al., 2013, 2014, 2017, 2018; Hedberg et al., 2014; Morin et al., 2014, 2020; Nesin et al., 2014; Endo et al., 2015; Markello et al., 2015; Walter et al., 2015; Harris et al., 2017; Noury et al., 2017; Borsani et al., 2018; Li et al., 2019; Claeys et al., 2020).

Stim1 KO and *Orai1* KO Mice die perinatally (Baba et al., 2008; Gwack et al., 2008; Oh-Hora et al., 2008), and the muscle-specific invalidation of either gene results in diminished cellular Ca^{2+} transients following stimulation, and interferes with muscle contractility and the production of force (Stiber et al., 2008; Li et al., 2012; Wei-Lapierre et al., 2013; Carrell et al., 2016). The mice also show an increased susceptibility to fatigue (Stiber et al., 2008; Wei-Lapierre et al., 2013; Carrell et al., 2016), and histological and ultrastructural investigations of muscle samples uncovered a reduction in fiber size and overall muscle mass, and swollen mitochondria (Stiber et al., 2008; Li et al., 2012; Wei-Lapierre et al., 2013; Carrell et al., 2016). The STIM1 I115F and R304W TAM/STRMK mouse models exhibit reduced muscle force (Cordero-Sanchez et al., 2019; Silva-Rojas et al., 2019), and continuous muscle stimulation evidenced a slower force decay compared with WT littermates, presumably reflecting an increased resistance to fatigue (Silva-Rojas et al., 2019). The animals exhibit elevated serum CK levels, and histological examinations of muscle samples revealed an increased proportion of type I fibers, an overall reduction of fiber diameter with signs of muscle fiber degeneration and regeneration, and electron microscopy uncovered swollen mitochondria (Cordero-Sanchez et al., 2019; Silva-Rojas et al.,

2019). Most strikingly, tubular aggregates are absent from muscles in both murine TAM/STRMK models, highlighting a major structural difference between human and mouse muscle pathologies despite the concordance of the overall clinical picture. Considering the observation that dystrophic signs are more prominent in TAM/STRMK mice than in patients, the tubular aggregates may protect the human muscle fibers from degeneration by bundling excessive free Ca^{2+}. Another STIM1 R304W mouse model does not show functional or structural skeletal muscle aberrations (Gamage et al., 2018), and a potential muscle phenotype of the STIM1 D84G mouse was not assessed (Grosse et al., 2007).

SOCE REGULATORS, ASSOCIATED DISEASES AND ANIMAL MODELS

Ca^{2+} controls a multitude of metabolic processes, signaling pathways, and cellular functions including transcription, proliferation, differentiation, and exocytosis. As a major regulator of Ca^{2+} homeostasis, SOCE takes a central role in the physiology of all tissues and organs, and needs to be adaptable to the Ca^{2+} sensitivity and Ca^{2+} balance of the individual cell types forming an organism.

The STIM1 homologue STIM2 has been shown to modulate SOCE activity (Darbellay et al., 2011; Miederer et al., 2015), and several additional regulators either promoting or restricting extracellular Ca^{2+} entry are known. Positive effectors encompass CRACR2A and septins, facilitating STIM1-ORAI1 coupling (Srikanth et al., 2010; Sharma et al., 2013), STIMATE, favoring STIM1 clustering (Jing et al., 2015), and the inositol triphosphate receptor (IP$_3$R), lowering the local Ca^{2+} levels in proximity to the STIM1 EF hands (Sampieri et al., 2018). Negative regulators include SARAF and calsequestrin, both hampering STIM1 oligomerization (Palty et al., 2012; Jha et al., 2013; Wang et al., 2015), Golli-MBP, binding and dispersing the STIM1-ORAI1 complex (Feng et al., 2006; Walsh et al., 2010), ORMLD3, fostering STIM1-ORAI1 uncoupling following Ca^{2+} influx (Carreras-Sureda et al., 2013), and ALG2, ALG14, DPAGT1, GFPT1, and GMPPB, all mediating post-translational modifications repressing the activity of STIM1 and ORAI1 (Belaya et al., 2012, 2015; Guergueltcheva et al., 2012; Cossins et al., 2013). To date, IP$_3$R, calsequestrin, ALG2, ALG14, DPAGT1, GFPT1, and GMPPB have been associated with human pathologies, suggesting that mutations in the other SOCE regulators may similarly impact on Ca^{2+} homeostasis and cause CRAC channelopathy, TAM/STRMK, or related disorders. It is, however, possible that potential physiological anomalies remain within the normal range of tissue and organ functionality due to a marginal effect on the intracellular Ca^{2+} balance, and are therefore hardly detectable.

LoF mutations in *ITPR1*, encoding IP$_3$R type 1, cause Gillespie syndrome (GLSP), characterized by muscular hypotonia, mydriasis, ataxia, and intellectual disability (Gerber et al., 2016), and *Itpr1*-null mice manifest severe ataxia and epileptic seizures (Matsumoto et al., 1996). Mutations in *ITPR2* and *ITRP3*, respectively, encoding IP$_3$R types 2 and 3, are associated with

29

anhidrosis in patients (Klar et al., 2014; Kerkhofs et al., 2018), and the same phenotype is also observed in *Itpr2* and *Itpr3* double knockout mice (Futatsugi et al., 2005). This is in accordance with the idea that the reduction of SOCE through the loss of the positive effector IP$_3$R results in a clinical phenotype resembling CRAC channelopathy. In the same line, *STING* GoF mutations are found in patients with systemic inflammatory syndrome and autoimmunity (Jeremiah et al., 2014), and a mouse model carrying a patient mutation recapitulates the clinical signs (Bouis et al., 2019). STING is a signaling adaptor residing in the ER, and is retained in an inactive state through direct interaction with STIM1. In response to DNA pathogens, STING translocates to the ER-Golgi intermediate compartment to trigger an interferon response through the STING-TBK1-IRF3 pathway (Ishikawa and Barber, 2008, 2011). Loss of STIM1 in mouse and human CRAC channelopathy cell lines induces a spontaneous activation of STING and an enhanced expression of type 1 interferons under sterile conditions, thereby stimulating the immune system even in the absence of pathogens (Srikanth et al., 2019).

Calsequestrin (CASQ1) is the major Ca^{2+} buffering protein in the sarcoplasmic reticulum in skeletal muscle, and polymerizes with increasing luminal Ca^{2+} concentrations (Manno et al., 2017). In turn, Ca^{2+} store depletion promotes depolymerization, and the calsequestrin monomers sequester STIM1 and hence negatively regulate SOCE (Wang et al., 2015). Specific missense mutations in *CASQ1* interfere with the polymerization and depolymerization dynamics of calsequestrin, lower the Ca^{2+} buffer capacities of the reticulum and impair calsequestrin monomerization, leading to an increase in SOCE activity (Barone et al., 2017; Bohm et al., 2018). As calsequestrin expression is restricted to skeletal muscle, patients with *CASQ1* mutations show a mild form of TAM/STRMK with late-onset muscle weakness, myalgia, and abundant tubular aggregates, but without additional multi-systemic signs (Bohm and Laporte, 2018; Bohm et al., 2018). A murine model harboring a *CASQ1* mutation found in patients does not exist, and the total loss of calsequestrin generates a malignant hyperthermia phenotype with an increased risk of sudden death in mice (Protasi et al., 2009). Noteworthy, CASQ1 null mice show an increased expression of STIM1 and ORAI1 associated with enhanced SOCE activity, possibly reflecting a compensatory mechanism to ensure the maintenance of contractile force despite the reduction of bound and releasable Ca^{2+} in the SR (Michelucci et al., 2020). Tubular aggregates containing STIM1 and calsequestrin are also seen on muscle biopsies from patients with limb-girdle congenital myasthenic syndrome (LG-CMS), marked by fluctuating muscle weakness and fatigability (Evangelista et al., 2015). LG-CMS is caused by the impaired transmission at the neuromuscular junction, the relay between motor neuron and muscle fiber, and results from LoF mutations in *ALG2*, *ALG14*, *DPAGT1*, *GFPT1*, or *GMPP8* (Belaya et al., 2012, 2015; Guergueltcheva et al., 2012; Cossins et al., 2013). All five genes code for proteins of the glycosylation pathway and procure posttranslational modifications to a wide variety of proteins including STIM1 and ORAI1. Hypoglycosylation of STIM1 and ORAI1 stimulates SOCE and extracellular Ca^{2+} influx (Selcen et al., 2014), and the muscle-specific deletion of *Gfpt1* in mice causes myasthenia and

the occurrence of tubular aggregates in muscle fibers (Issop et al., 2018). These examples show that the dysfunction of proteins directly or indirectly associated with STIM1 and ORAI1 can cause human pathologies overlapping with TAM/STRMK at the clinical and histological level.

CONCLUSION AND PERSPECTIVES

LoF mutations in *STIM1* and *ORAI1* impair SOCE and cause CRAC channelopathy, while GoF mutations in both genes involve SOCE over-activation and result in TAM/STRMK (Lacruz and Feske, 2015; Bohm and Laporte, 2018). In agreement with the opposite mutational effects and pathomechanisms leading to either CRAC channelopathy or TAM/STRMK, both disorders by and large show clinical mirror phenotypes affecting the eyes, bones, immune system, platelets, and skeletal muscle. While CRAC channelopathy is characterized by mydriasis, increased bone mineralization, immunodeficiency, splenomegaly, impaired platelet activation, and muscle hypotonia, TAM/STRMK patients typically present with miosis, decreased bone mineralization, hyposplenism, platelet pre-activation, and muscle cramping. A single TAM/STRMK patient was additionally diagnosed with lymphoproliferation (Sura et al., 2020), indicating an over-active immune system. Investigations on TAM/STRMK mouse models confirmed a dysregulation of various immune system cells, which may account for the skin phenotype in humans and mice (Silva-Rojas et al., 2019). It is interesting to note that the clinical anomalies of platelets and skeletal muscle are similar in CRAC channelopathy and TAM/STRMK patients despite the inverse pathogenic effect of *STIM1* and *ORAI1* LoF and GoF mutations at the molecular level, highlighting the importance of strict SOCE regulation for normal tissue physiology. Thrombus formation is impaired in both disorders and enhances the tendency to bleed following injury. This is due to the reduced activation of platelets in CRAC channelopathy (Nakamura et al., 2013), and results from the impaired adhesion between platelets in TAM/STRMK (Markello et al., 2015). Similarly, muscle weakness either arises from the incapacity to sustain a sufficient muscle tonus in the absence of Ca^{2+} store refill in CRAC channelopathy, or from cytosolic Ca^{2+} excess disrupting excitation-contraction coupling and/or restraining proper muscle relaxation in TAM/STRMK.

CRAC channelopathy and TAM/STRMK mouse models recapitulate the main clinical signs of the human disorders, and are valuable and powerful tools to understand the importance of Ca^{2+} balance and the impact of Ca^{2+} imbalance on eye, bones, enamel, skin, platelets, spleen, immune system, and skeletal muscle physiology. Patients are usually examined by specialized physicians with a major focus on the principal handicap, and additional phenotypic anomalies might be overlooked, especially in the context of multi-systemic disorders with mild to moderate involvement of specific tissues. In contrast, murine models generally undergo unbiased phenotyping and offer the possibility for a detailed analysis of all organs to provide an overview of the disease. As an example, the complete characterization

of the STIM1 R304W TAM/STRMK mouse model unveiled anomalies of the glucose metabolism, hepatic function, and the immune system (Silva-Rojas et al., 2019), which have not been described in patients yet, but might be of medical importance. Conversely, psychiatric diseases including confusion (Misceo et al., 2014; Harris et al., 2017), Capgras syndrome (Harris et al., 2017), and manic psychosis (Harris et al., 2017) have only been reported in individual TAM/STRMK cases, and thorough investigations on the mouse model might help to determine if these anomalies are disease-related or unrelated. Lastly, the mouse models faithfully recapitulating CRAC channelopathy and TAM/STRMK can serve for the assessment of therapeutic approaches, which may also be relevant for other Ca^{2+}-related disorders affecting the bones, platelets, spleen, immune system, or skeletal muscle.

REFERENCES

Agrawal, N., Venkiteswaran, G., Sadaf, S., Padmanabhan, N., Banerjee, S., and Hasan, G. (2010). Inositol 1,4,5-trisphosphate receptor and dSTIM function in *Drosophila* insulin-producing neurons regulates systemic intracellular calcium homeostasis and flight. *J. Neurosci.* 30, 1301–1313. doi: 10.1523/JNEUROSCI.3668-09.2010

Ahmad, F., Boulaftali, Y., Greene, T. K., Ouellette, T. D., Poncz, M., Feske, S., et al. (2011). Relative contributions of stromal interaction molecule 1 and CalDAG-GEFI to calcium-dependent platelet activation and thrombosis. *J. Thromb. Haemost.* 9, 2077–2086. doi: 10.1111/j.1538-7836.2011.04474.x

Alonso-Jimenez, A., Ramon, C., Dols-Icardo, O., Roig, C., Gallardo, E., Clarimon, J., et al. (2018). Corpus callosum agenesis, myopathy and pinpoint pupils: consider Stormorken syndrome. *Eur. J. Neurol.* 25, e25–e26. doi: 10.1111/ene.13545

Baba, Y., Nishida, K., Fujii, Y., Hirano, T., Hikida, M., and Kurosaki, T. (2008). Essential function for the calcium sensor STIM1 in mast cell activation and anaphylactic responses. *Nat. Immunol.* 9, 81–88. doi: 10.1038/ni1546

Badran, Y. R., Massaad, M. J., Bainter, W., Cangemi, B., Naseem, S. U., Javad, H., et al. (2016). Combined immunodeficiency due to a homozygous mutation in ORAI1 that deletes the C-terminus that interacts with STIM 1. *Clin. Immunol.* 166-167, 100–102. doi: 10.1016/j.clim.2016.03.012

Barone, V., Del, Re, V., Gamberucci, A., Polverino, V., Galli, L., et al. (2017). Identification and characterization of three novel mutations in the CASQ1 gene in four patients with tubular aggregate myopathy. *Hum. Mutat.* 38, 1761–1773. doi: 10.1002/humu.23338

Belaya, K., Finlayson, S., Slater, C. R., Cossins, J., Liu, W. W., Maxwell, S., et al. (2012). Mutations in DPAGT1 cause a limb-girdle congenital myasthenic syndrome with tubular aggregates. *Am. J. Hum. Genet.* 91, 193–201. doi: 10.1016/j.ajhg.2012.05.022

Belaya, K., Rodriguez Cruz, P. M., Liu, W. W., Maxwell, S., McGowan, S., Farrugia, M. E., et al. (2015). Mutations in GMPPB cause congenital myasthenic syndrome and bridge myasthenic disorders with dystroglycanopathies. *Brain* 138(Pt 9), 2493–2504. doi: 10.1093/brain/awv185

Bergmeier, W., Oh-Hora, M., McCarl, C. A., Roden, R. C., Bray, P. F., and Feske, S. (2009). R93W mutation in Orai1 causes impaired calcium influx in platelets. *Blood* 113, 675–678. doi: 10.1182/blood-2008-08-174516

Berna-Erro, A., Jardin, I., Smani, T., and Rosado, J. A. (2016). Regulation of platelet function by Orai, STIM and TRP. *Adv. Exp. Med. Biol.* 898, 157–181. doi: 10.1007/978-3-319-26974-0_8

Blair, H. C., Robinson, L. J., Huang, C. L., Sun, L., Friedman, P. A., Schlesinger, P. H., et al. (2011). Calcium and bone disease. *Biofactors* 37, 159–167. doi: 10.1002/biof.143

Blair, P., and Flaumenhaft, R. (2009). Platelet alpha-granules: basic biology and clinical correlates. *Blood Rev.* 23, 177–189. doi: 10.1016/j.blre.2009.04.001

Bohm, J., Bulla, M., Urquhart, J. E., Malfatti, E., Williams, S. G., O'Sullivan, J., et al. (2017). ORAI1 mutations with distinct channel gating defects in tubular aggregate myopathy. *Hum. Mutat.* 38, 426–438. doi: 10.1002/humu.23172

Bohm, J., Chevessier, F., Koch, C., Peche, G. A., Mora, M., Morandi, L., et al. (2014). Clinical, histological and genetic characterisation of patients with tubular aggregate myopathy caused by mutations in STIM1. *J. Med. Genet.* 51, 824–833. doi: 10.1136/jmedgenet-2014-102623

Bohm, J., Chevessier, F., Maues, De Paula, A., Koch, C., Attarian, S., et al. (2013). Constitutive activation of the calcium sensor STIM1 causes tubular-aggregate myopathy. *Am. J. Hum. Genet.* 92, 271–278. doi: 10.1016/j.ajhg.2012.12.007

Bohm, J., and Laporte, J. (2018). Gain-of-function mutations in STIM1 and ORAI1 causing tubular aggregate myopathy and Stormorken syndrome. *Cell Calc.* 76, 1–9. doi: 10.1016/j.ceca.2018.07.008

Bohm, J., Lornage, X., Chevessier, F., Birck, C., Zanotti, S., Cudia, P., et al. (2018). CASQ1 mutations impair calsequestrin polymerization and cause tubular aggregate myopathy. *Acta Neuropathol.* 135, 149–151. doi: 10.1007/s00401-017-1775-x

Borsani, O., Piga, D., Costa, S., Govoni, A., Magri, F., Artoni, A., et al. (2018). Stormorken syndrome caused by a p.R304W STIM1 mutation: the first italian patient and a review of the literature. *Front. Neurol.* 9:859. doi: 10.3389/fneur.2018.00859

Bouis, D., Kirstetter, P., Arbogast, F., Lamon, D., Delgado, V., Jung, S., et al. (2019). Severe combined immunodeficiency in stimulator of interferon genes (STING) V154M/wild-type mice. *J. Allergy Clin. Immunol.* 143, 712.e5–725.e5. doi: 10.1016/j.jaci.2018.04.034

Braun, A., Varga-Szabo, D., Kleinschnitz, C., Pleines, I., Bender, M., Austinat, M., et al. (2009). Orai1 (CRACM1) is the platelet SOC channel and essential for pathological thrombus formation. *Blood* 113, 2056–2063. doi: 10.1182/blood-2008-07-171611

Bronte, V., and Pittet, M. J. (2013). The spleen in local and systemic regulation of immunity. *Immunity* 39, 806–818. doi: 10.1016/j.immuni.2013.10.010

Bye, A. P., Unsworth, A. J., and Gibbins, J. M. (2016). Platelet signaling: a complex interplay between inhibitory and activatory networks. *J. Thromb. Haemost.* 14, 918–930. doi: 10.1111/jth.13302

Byun, M., Abhyankar, A., Lelarge, V., Plancoulaine, S., Palanduz, A., Telhan, L., et al. (2010). Whole-exome sequencing-based discovery of STIM1 deficiency in a child with fatal classic Kaposi sarcoma. *J. Exp. Med.* 207, 2307–2312. doi: 10.1084/jem.20101597

Carrell, E. M., Coppola, A. R., McBride, H. J., and Dirksen, R. T. (2016). Orai1 enhances muscle endurance by promoting fatigue-resistant type I fiber content but not through acute store-operated Ca2+ entry. *FASEB J.* 30, 4109–4119. doi: 10.1096/fj.201600621R

Carreras-Sureda, A., Cantero-Recasens, G., Rubio-Moscardo, F., Kiefer, K., Peinelt, C., Niemeyer, B. A., et al. (2013). ORMDL3 modulates store-operated calcium entry and lymphocyte activation. *Hum. Mol. Genet.* 22, 519–530. doi: 10.1093/hmg/dds450

Chen, Y., Ramachandran, A., Zhang, Y., Koshy, R., and George, A. (2018). The ER Ca(2+) sensor STIM1 can activate osteoblast and odontoblast differentiation in mineralized tissues. *Connect Tissue Res.* 59(Suppl. 1), 6–12. doi: 10.1080/03008207.2017.1408601

AUTHOR CONTRIBUTIONS

FUNDING

31

Chevessier, F., Bauche-Godard, S., Leroy, J. P., Koenig, J., Paturneau-Jouas, M., Eymard, B., et al. (2005). The origin of tubular aggregates in human myopathies. *J. Pathol.* 207, 313–323. doi: 10.1002/path.1832

Chevessier, F., Marty, I., Paturneau-Jouas, M., Hantai, D., and Verdiere-Sahuque, M. (2004). Tubular aggregates are from whole sarcoplasmic reticulum origin: alterations in calcium binding protein expression in mouse skeletal muscle during aging. *Neuromuscul. Disord.* 14, 208–216. doi: 10.1016/j.nmd.2003.11.007

Chou, J., Badran, Y. R., Yee, C. S., Bainter, W., Ohsumi, T. K., Al-Hammadi, S., et al. (2015). A novel mutation in ORAI1 presenting with combined immunodeficiency and residual T-cell function. *J. Allergy Clin. Immunol.* 136, 479.e1–482.e1. doi: 10.1016/j.jaci.2015.03.050

Claeys, T., Goosens, V., Race, V., Theys, T., Thal, D. R., Depuydt, C. E., et al. (2020). Clinical and muscle MRI features in a family with tubular aggregate myopathy and novel STIM1 mutation. *Neuromuscul. Disord.* 30, 709–718. doi: 10.1016/j.nmd.2020.07.010

Concepcion, A. R., Vaeth, M., Wagner, L. E. II, Eckstein, M., Hecht, L., Yang, J., et al. (2016). Store-operated Ca2+ entry regulates Ca2+-activated chloride channels and eccrine sweat gland function. *J. Clin. Invest.* 126, 4303–4318. doi: 10.1172/JCI89056

Cordero-Sanchez, C., Riva, B., Reano, S., Clemente, N., Zaggia, I., Ruffinatti, F. A., et al. (2019). A luminal EF-hand mutation in STIM1 in mice causes the clinical hallmarks of tubular aggregate myopathy. *Dis. Model Mech.* 13:dmm041111. doi: 10.1242/dmm.041111

Cossins, J., Belaya, K., Hicks, D., Salih, M. A., Finlayson, S., Carboni, N., et al. (2013). Congenital myasthenic syndromes due to mutations in ALG2 and ALG14. *Brain* 136(Pt 3), 944–956. doi: 10.1093/brain/awt010

Darbellay, B., Arnaudeau, S., Bader, C. R., Konig, S., and Bernheim, L. (2011). STIM1L is a new actin-binding splice variant involved in fast repetitive Ca2+ release. *J. Cell Biol.* 194, 335–346. doi: 10.1083/jcb.201012157

de Porto, A. P., Lammers, A. J., Bennink, R. J., ten Berge, I. J., Speelman, P., and Hoekstra, J. B. (2010). Assessment of splenic function. *Eur. J. Clin. Microbiol. Infect. Dis.* 29, 1465–1473. doi: 10.1007/s10096-010-1049-1

Dejaco, C., Duftner, C., Grubeck-Loebenstein, B., and Schirmer, M. (2006). Imbalance of regulatory T cells in human autoimmune diseases. *Immunology* 117, 289–300. doi: 10.1111/j.1365-2567.2005.02317.x

Eapen, A., Sundivakkam, P., Song, Y., Ravindran, S., Ramachandran, A., Tiruppathi, C., et al. (2010). Calcium-mediated stress kinase activation by DMP1 promotes osteoblast differentiation. *J. Biol. Chem.* 285, 36339–36351. doi: 10.1074/jbc.M110.145607

Ebashi, S. (1974). Regulatory mechanism of muscle contraction with special reference to the Ca-troponin-tropomyosin system. *Essays Biochem.* 10, 1–36.

Eckstein, M. K., Guerra-Carrillo, B., Miller Singley, A. T., and Bunge, S. A. (2017). Beyond eye gaze: what else can eyetracking reveal about cognition and cognitive development? *Dev. Cogn. Neurosci.* 25, 69–91. doi: 10.1016/j.dcn.2016.11.001

Edwards, J. N., Murphy, R. M., Cully, T. R., von Wegner, F., Friedrich, O., and Launikonis, B. S. (2010). Ultra-rapid activation and deactivation of store-operated Ca(2+) entry in skeletal muscle. *Cell Calc.* 47, 458–467. doi: 10.1016/j.ceca.2010.04.001

Endo, Y., Noguchi, S., Hara, Y., Hayashi, Y. K., Motomura, K., Miyatake, S., et al. (2015). Dominant mutations in ORAI1 cause tubular aggregate myopathy with hypocalcemia via constitutive activation of store-operated Ca(2)(+) channels. *Hum. Mol. Genet.* 24, 637–648. doi: 10.1093/hmg/ddu477

Evangelista, T., Hanna, M., and Lochmuller, H. (2015). Congenital myasthenic syndromes with predominant limb girdle weakness. *J. Neuromuscul. Dis.* 2(Suppl. 2), S21–S29. doi: 10.3233/JND-150098

Feldman, C. H., Grotegut, C. A., and Rosenberg, P. B. (2017). The role of STIM1 and SOCE in smooth muscle contractility. *Cell Calc.* 63, 60–65. doi: 10.1016/j.ceca.2017.02.007

Felix, R., Crottes, D., Delalande, A., Fauconnier, J., Lebranchu, Y., Le Guennec, J. Y., et al. (2013). The Orai-1 and STIM-1 complex controls human dendritic cell maturation. *PLoS One* 8:e61595. doi: 10.1371/journal.pone.0061595

Feng, J. M., Hu, Y. K., Xie, L. H., Colwell, C. S., Shao, X. M., Sun, X. P., et al. (2006). Golli protein negatively regulates store depletion-induced calcium influx in T cells. *Immunity* 24, 717–727. doi: 10.1016/j.immuni.2006.04.007

Feske, S. (2007). Calcium signalling in lymphocyte activation and disease. *Nat. Rev. Immunol.* 7, 690–702. doi: 10.1038/nri2152

Feske, S., Gwack, Y., Prakriya, M., Srikanth, S., Puppel, S. H., Tanasa, B., et al. (2006). A mutation in Orai1 causes immune deficiency by abrogating CRAC channel function. *Nature* 441, 179–185. doi: 10.1038/nature04702

Feske, S., Muller, J. M., Graf, D., Kroczek, R. A., Drager, R., Niemeyer, C., et al. (1996). Severe combined immunodeficiency due to defective binding of the nuclear factor of activated T cells in T lymphocytes of two male siblings. *Eur. J. Immunol.* 26, 2119–2126. doi: 10.1002/eji.1830260924

Florencio-Silva, R., Sasso, G. R., Sasso-Cerri, E., Simoes, M. J., and Cerri, P. S. (2015). Biology of bone tissue: structure, function, and factors that influence bone cells. *Biomed. Res. Int.* 2015:421746. doi: 10.1155/2015/421746

Fuchs, S., Rensing-Ehl, A., Speckmann, C., Bengsch, B., Schmitt-Graeff, A., Bondzio, I., et al. (2012). Antiviral and regulatory T cell immunity in a patient with stromal interaction molecule 1 deficiency. *J. Immunol.* 188, 1523–1533. doi: 10.4049/jimmunol.1102507

Futatsugi, A., Nakamura, T., Yamada, M. K., Ebisui, E., Nakamura, K., Uchida, K., et al. (2005). IP3 receptor types 2 and 3 mediate exocrine secretion underlying energy metabolism. *Science* 309, 2232–2234. doi: 10.1126/science.1114110

Gamage, T. H., Gunnes, G., Lee, R. H., Louch, W. E., Holmgren, A., Bruton, J. D., et al. (2018). STIM1 R304W causes muscle degeneration and impaired platelet activation in mice. *Cell Calc.* 76, 87–100. doi: 10.1016/j.ceca.2018.10.001

Gamage, T. H., Lengle, E., Gunnes, G., Pullisaar, H., Holmgren, A., Reseland, J. E., et al. (2020). STIM1 R304W in mice causes subgingival hair growth and an increased fraction of trabecular bone. *Cell Calc.* 85:102110. doi: 10.1016/j.ceca.2019.102110

Garibaldi, M., Fattori, F., Riva, B., Labasse, C., Brochier, G., Ottaviani, P., et al. (2017). A novel gain-of-function mutation in ORAI1 causes late-onset tubular aggregate myopathy and congenital miosis. *Clin. Genet.* 91, 780–786. doi: 10.1111/cge.12888

Gattineni, J. (2014). Inherited disorders of calcium and phosphate metabolism. *Curr. Opin. Pediatr.* 26, 215–222. doi: 10.1097/MOP.0000000000000064

Gerber, S., Alzayady, K. J., Burglen, L., Bremond-Gignac, D., Marchesin, V., Roche, O., et al. (2016). Recessive and dominant De Novo ITPR1 mutations cause gillespie syndrome. *Am. J. Hum. Genet.* 98, 971–980. doi: 10.1016/j.ajhg.2016.03.004

Gilio, K., van Kruchten, R., Braun, A., Berna-Erro, A., Feijge, M. A., Stegner, D., et al. (2010). Roles of platelet STIM1 and Orai1 in glycoprotein VI- and thrombin-dependent procoagulant activity and thrombus formation. *J. Biol. Chem.* 285, 23629–23638. doi: 10.1074/jbc.M110.108696

Grosse, J., Braun, A., Varga-Szabo, D., Beyersdorf, N., Schneider, B., Zeitlmann, L., et al. (2007). An EF hand mutation in Stim1 causes premature platelet activation and bleeding in mice. *J. Clin. Invest.* 117, 3540–3550. doi: 10.1172/JCI32312

Guergueltcheva, V., Muller, J. S., Dusl, M., Senderek, J., Oldfors, A., Lindbergh, C., et al. (2012). Congenital myasthenic syndrome with tubular aggregates caused by GFPT1 mutations. *J. Neurol.* 259, 838–850. doi: 10.1007/s00415-011-6262-z

Gwack, Y., Srikanth, S., Oh-Hora, M., Hogan, P. G., Lamperti, E. D., Yamashita, M., et al. (2008). Hair loss and defective T- and B-cell function in mice lacking ORAI1. *Mol. Cell Biol.* 28, 5209–5222. doi: 10.1128/MCB.00360-08

Harris, E., Burki, U., Marini-Bettolo, C., Neri, M., Scotton, C., Hudson, J., et al. (2017). Complex phenotypes associated with STIM1 mutations in both coiled coil and EF-hand domains. *Neuromuscul. Disord.* 27, 861–872. doi: 10.1016/j.nmd.2017.05.002

Hedberg, C., Niceta, M., Fattori, F., Lindvall, B., Ciolfi, A., D'Amico, A., et al. (2014). Childhood onset tubular aggregate myopathy associated with de novo STIM1 mutations. *J. Neurol.* 261, 870–876. doi: 10.1007/s00415-014-7287-x

Huang, Y., Li, Q., Feng, Z., and Zheng, L. (2020). STIM1 controls calcineurin/Akt/mTOR/NFATC2-mediated osteoclastogenesis induced by RANKL/M-CSF. *Exp. Therap. Med.* 20, 736–747. doi: 10.3892/etm.2020.8774

Hwang, S. Y., Foley, J., Numaga-Tomita, T., Petranka, J. G., Bird, G. S., and Putney, J. W. Jr. (2012). Deletion of Orai1 alters expression of multiple genes during osteoclast and osteoblast maturation. *Cell Calc.* 52, 488–500. doi: 10.1016/j.ceca.2012.10.001

Ishikawa, H., and Barber, G. N. (2008). STING is an endoplasmic reticulum adaptor that facilitates innate immune signalling. *Nature* 455, 674–678. doi: 10.1038/nature07317

Ishikawa, H., and Barber, G. N. (2011). The STING pathway and regulation of innate immune signaling in response to DNA pathogens. *Cell. Mol. Life Sci.* 68, 1157–1165. doi: 10.1007/s00018-010-0605-2

32

Ishitsuka, Y., Inoue, S., Furuta, J., Koguchi-Yoshioka, H., Nakamura, Y., Watanabe, R., et al. (2019). Sweat retention anhidrosis associated with tubular aggregate myopathy. *Br. J. Dermatol.* 181, 1104–1106. doi: 10.1111/bjd.18175

Issop, Y., Hathazi, D., Khan, M. M., Rudolf, R., Weis, J., Spendiff, S., et al. (2018). GFPT1 deficiency in muscle leads to myasthenia and myopathy in mice. *Hum. Mol. Genet.* 27, 3218–3232. doi: 10.1093/hmg/ddy225

Jeremiah, N., Neven, B., Gentili, M., Callebaut, I., Maschalidi, S., Stolzenberg, M. C., et al. (2014). Inherited STING-activating mutation underlies a familial inflammatory syndrome with lupus-like manifestations. *J. Clin. Invest.* 124, 5516–5520. doi: 10.1172/JCI79100

Jha, A., Ahuja, M., Maleth, J., Moreno, C. M., Yuan, J. P., Kim, M. S., et al. (2013). The STIM1 CTID domain determines access of SARAF to SOAR to regulate Orai1 channel function. *J. Cell Biol.* 202, 71–79. doi: 10.1083/jcb.201301148

Jing, J., He, L., Sun, A., Quintana, A., Ding, Y., Ma, G., et al. (2015). Proteomic mapping of ER-PM junctions identifies STIMATE as a regulator of Ca(2)(+) influx. *Nat. Cell Biol.* 17, 1339–1347. doi: 10.1038/ncb3234

Josefowicz, S. Z., Lu, L. F., and Rudensky, A. Y. (2012). Regulatory T cells: mechanisms of differentiation and function. *Annu. Rev. Immunol.* 30, 531–564. doi: 10.1146/annurev.immunol.25.022106.141623

Kerkhofs, M., Seitaj, B., Ivanova, H., Monaco, G., Bultynck, G., and Parys, J. B. (2018). Pathophysiological consequences of isoform-specific IP3 receptor mutations. *Biochim. Biophys. Acta Mol. Cell Res.* 1865(11 Pt B), 1707–1717. doi: 10.1016/j.bbamcr.2018.06.004

Klar, J., Hisatsune, C., Baig, S. M., Tariq, M., Johansson, A. C., Rasool, M., et al. (2014). Abolished InsP3R2 function inhibits sweat secretion in both humans and mice. *J. Clin. Invest.* 124, 4773–4780. doi: 10.1172/JCI70720

Lacruz, R. S., and Feske, S. (2015). Diseases caused by mutations in ORAI1 and STIM1. *Ann. N. Y. Acad. Sci.* 1356, 45–79. doi: 10.1111/nyas.12938

Lamb, G. D., Junankar, P. R., and Stephenson, D. G. (1995). Raised intracellular [Ca2+] abolishes excitation-contraction coupling in skeletal muscle fibres of rat and toad. *J. Physiol.* 489(Pt 2), 349–362. doi: 10.1113/jphysiol.1995.sp021056

Launikonis, B. S., Stephenson, D. G., and Friedrich, O. (2009). Rapid Ca2+ flux through the transverse tubular membrane, activated by individual action potentials in mammalian skeletal muscle. *J. Physiol.* 587(Pt 10), 2299–2312. doi: 10.1113/jphysiol.2009.168682

Li, A., Kang, X., Edelman, F., and Waclawik, A. J. (2019). Stormorken syndrome: a rare cause of myopathy with tubular aggregates and dystrophic features. *J. Child Neurol.* 34, 321–324. doi: 10.1177/0883073819829389

Li, T., Finch, E. A., Graham, V., Zhang, Z. S., Ding, J. D., Burch, J., et al. (2012). STIM1-Ca(2+) signaling is required for the hypertrophic growth of skeletal muscle in mice. *Mol. Cell Biol.* 32, 3009–3017. doi: 10.1128/MCB.06599-11

Lian, J., Cuk, M., Kahlfuss, S., Kozhaya, L., Vaeth, M., Rieux-Laucat, F., et al. (2018). ORAI1 mutations abolishing store-operated Ca(2+) entry cause anhidrotic ectodermal dysplasia with immunodeficiency. *J. Allergy Clin. Immunol.* 142, 1297.e11–1310.e11. doi: 10.1016/j.jaci.2017.10.031

Manno, C., Figueroa, L. C., Gillespie, D., Fitts, R., Kang, C., Franzini-Armstrong, C., et al. (2017). Calsequestrin depolymerizes when calcium is depleted in the sarcoplasmic reticulum of working muscle. *Proc. Natl. Acad. Sci. U.S.A.* 114, E638–E647. doi: 10.1073/pnas.1620265114

Markello, T., Chen, D., Kwan, J. Y., Horkayne-Szakaly, I., Morrison, A., Simakova, O., et al. (2015). York platelet syndrome is a CRAC channelopathy due to gain-of-function mutations in STIM1. *Mol. Genet. Metab.* 114, 474–482. doi: 10.1016/j.ymgme.2014.12.307

Matsumoto, M., Nakagawa, T., Inoue, T., Nagata, E., Tanaka, K., Takano, H., et al. (1996). Ataxia and epileptic seizures in mice lacking type 1 inositol 1,4,5-trisphosphate receptor. *Nature* 379, 168–171. doi: 10.1038/379168a0

Maul-Pavicic, A., Chiang, S. C., Rensing-Ehl, A., Jessen, B., Fauriat, C., Wood, S. M., et al. (2011). ORAI1-mediated calcium influx is required for human cytotoxic lymphocyte degranulation and target cell lysis. *Proc. Natl. Acad. Sci. U.S.A.* 108, 3324–3329. doi: 10.1073/pnas.1013285108

McCarl, C. A., Khalil, S., Ma, J., Oh-hora, M., Yamashita, M., Roether, J., et al. (2010). Store-operated Ca2+ entry through ORAI1 is critical for T cell-mediated autoimmunity and allograft rejection. *J. Immunol.* 185, 5845–5858. doi: 10.4049/jimmunol.1001796

McCarl, C. A., Picard, C., Khalil, S., Kawasaki, T., Rother, J., Papolos, A., et al. (2009). ORAI1 deficiency and lack of store-operated Ca2+ entry cause immunodeficiency, myopathy, and ectodermal dysplasia. *J. Allergy Clin. Immunol.* 124, 1311.e7–1318.e7. doi: 10.1016/j.jaci.2009.10.007

Michelucci, A., Boncompagni, S., Pietrangelo, L., Takano, T., Protasi, F., and Dirksen, R. T. (2020). Pre-assembled Ca2+ entry units and constitutively active Ca2+ entry in skeletal muscle of calsequestrin-1 knockout mice. *J. Gen. Physiol.* 152:e202012617. doi: 10.1085/jgp.202012617

Miederer, A. M., Alansary, D., Schwar, G., Lee, P. H., Jung, M., Helms, V., et al. (2015). A STIM2 splice variant negatively regulates store-operated calcium entry. *Nat. Commun.* 6:6899. doi: 10.1038/ncomms7899

Misceo, D., Holmgren, A., Louch, W. E., Holme, P. A., Mizobuchi, M., Morales, R. J., et al. (2014). A dominant STIM1 mutation causes Stormorken syndrome. *Hum. Mutat.* 35, 556–564. doi: 10.1002/humu.22544

Morin, G., Biancalana, V., Echaniz-Laguna, A., Noury, J. B., Lornage, X., Moggio, M., et al. (2020). Tubular aggregate myopathy and Stormorken syndrome: mutation spectrum and genotype/phenotype correlation. *Hum. Mutat.* 41, 17–37. doi: 10.1002/humu.23899

Morin, G., Bruechle, N. O., Singh, A. R., Knopp, C., Jedraszak, G., Elbracht, M., et al. (2014). Gain-of-function mutation in STIM1 (P.R304W) is associated with Stormorken Syndrome. *Hum. Mutat.* 35, 1221–1232. doi: 10.1002/humu.22621

Murphy, R. M., Dutka, T. L., Horvath, D., Bell, J. R., Delbridge, L. M., and Lamb, G. D. (2013). Ca2+-dependent proteolysis of junctophilin-1 and junctophilin-2 in skeletal and cardiac muscle. *J. Physiol.* 591, 719–729. doi: 10.1113/jphysiol.2012.243279

Nakamura, L., Sandrock-Lang, K., Speckmann, C., Vraetz, T., Buhrlen, M., Ehl, S., et al. (2013). Platelet secretion defect in a patient with stromal interaction molecule 1 deficiency. *Blood* 122, 3696–3698. doi: 10.1182/blood-2013-08-522037

Nesin, V., Wiley, G., Kousi, M., Ong, E. C., Lehmann, T., Nicholl, D. J., et al. (2014). Activating mutations in STIM1 and ORAI1 cause overlapping syndromes of tubular myopathy and congenital miosis. *Proc. Natl. Acad. Sci. U.S.A.* 111, 4197–4202. doi: 10.1073/pnas.1312520111

Noury, J. B., Bohm, J., Peche, G. A., Guyant-Marechal, L., Bedat-Millet, A. L., Chiche, L., et al. (2017). Tubular aggregate myopathy with features of Stormorken disease due to a new STIM1 mutation. *Neuromuscul. Disord.* 27, 78–82. doi: 10.1016/j.nmd.2016.10.006

Novak, P., and Lehuen, A. (2011). Mechanism of regulation of autoimmunity by iNKT cells. *Cytokine* 53, 263–270. doi: 10.1016/j.cyto.2010.11.001

Numaga-Tomita, T., and Putney, J. W. (2013). Role of STIM1- and Orai1-mediated Ca2+ entry in Ca2+-induced epidermal keratinocyte differentiation. *J. Cell Sci.* 126(Pt 2), 605–612. doi: 10.1242/jcs.115980

Oh-Hora, M., Komatsu, N., Pishyareh, M., Feske, S., Hori, S., Taniguchi, M., et al. (2013). Agonist-selected T cell development requires strong T cell receptor signaling and store-operated calcium entry. *Immunity* 38, 881–895. doi: 10.1016/j.immuni.2013.02.008

Oh-Hora, M., Yamashita, M., Hogan, P. G., Sharma, S., Lamperti, E., Chung, W., et al. (2008). Dual functions for the endoplasmic reticulum calcium sensors STIM1 and STIM2 in T cell activation and tolerance. *Nat. Immunol.* 9, 432–443. doi: 10.1038/ni1574

Palmer, C. N., Irvine, A. D., Terron-Kwiatkowski, A., Zhao, Y., Liao, H., Lee, S. P., et al. (2006). Common loss-of-function variants of the epidermal barrier protein filaggrin are a major predisposing factor for atopic dermatitis. *Nat. Genet.* 38, 441–446. doi: 10.1038/ng1767

Palty, R., Raveh, A., Kaminsky, I., Meller, R., and Reuveny, E. (2012). SARAF inactivates the store operated calcium entry machinery to prevent excess calcium refilling. *Cell* 149, 425–438. doi: 10.1016/j.cell.2012.01.055

Pan, Z., Yang, D., Nagaraj, R. Y., Nosek, T. A., Nishi, M., Takeshima, H., et al. (2002). Dysfunction of store-operated calcium channel in muscle cells lacking mg29. *Nat. Cell Biol.* 4, 379–383. doi: 10.1038/ncb788

Peacock, M. (2010). Calcium metabolism in health and disease. *Clin. J. Am. Soc. Nephrol.* 5(Suppl. 1), S23–S30. doi: 10.2215/CJN.05910809

Picard, C., McCarl, C. A., Papolos, A., Khalil, S., Luthy, K., Hivroz, C., et al. (2009). STIM1 mutation associated with a syndrome of immunodeficiency and autoimmunity. *N. Engl. J. Med.* 360, 1971–1980. doi: 10.1056/NEJMoa0900082

Prakriya, M., and Lewis, R. S. (2015). Store-operated calcium channels. *Physiol. Rev.* 95, 1383–1436. doi: 10.1152/physrev.00020.2014

Protasi, F., Paolini, C., and Dainese, M. (2009). Calsequestrin-1: a new candidate gene for malignant hyperthermia and exertional/environmental heat stroke. *J. Physiol.* 587(Pt 13), 3095–3100. doi: 10.1113/jphysiol.2009.171967

Robinson, L. J., Mancarella, S., Songsawad, D., Tourkova, I. L., Barnett, J. B., Gill, D. L., et al. (2012). Gene disruption of the calcium channel Orai1 results

33

in inhibition of osteoclast and osteoblast differentiation and impairs skeletal development. *Lab. Invest.* 92, 1071–1083. doi: 10.1038/labinvest.2012.72

Sampieri, A., Santoyo, K., Asanov, A., and Vaca, L. (2018). Association of the IP3R to STIM1 provides a reduced intraluminal calcium microenvironment, resulting in enhanced store-operated calcium entry. *Sci. Rep.* 8:13252. doi: 10.1038/s41598-018-31621-0

Schaballie, H., Rodriguez, R., Martin, E., Moens, L., Frans, G., Lenoir, C., et al. (2015). A novel hypomorphic mutation in STIM1 results in a late-onset immunodeficiency. *J. Allergy Clin. Immunol.* 136, 816.e4–819.e4. doi: 10.1016/j.jaci.2015.03.009

Selcen, D., Shen, X. M., Brengman, J., Li, Y., Stans, A. A., Wieben, E., et al. (2014). DPAGT1 myasthenia and myopathy: genetic, phenotypic, and expression studies. *Neurology* 82, 1822–1830. doi: 10.1212/WNL.0000000000000435

Sharma, S., Quintana, A., Findlay, G. M., Mettlen, M., Baust, B., Jain, M., et al. (2013). An siRNA screen for NFAT activation identifies septins as coordinators of store-operated Ca2+ entry. *Nature* 499, 238–242. doi: 10.1038/nature12229

Silva-Rojas, R., Treves, S., Jacobs, H., Kessler, P., Messaddeq, N., Laporte, J., et al. (2019). STIM1 over-activation generates a multi-systemic phenotype affecting the skeletal muscle, spleen, eye, skin, bones and immune system in mice. *Hum. Mol. Genet.* 28, 1579–1593. doi: 10.1093/hmg/ddy446

Srikanth, S., Jung, H. J., Kim, K. D., Souda, P., Whitelegge, J., and Gwack, Y. (2010). A novel EF-hand protein, CRACR2A, is a cytosolic Ca2+ sensor that stabilizes CRAC channels in T cells. *Nat. Cell Biol.* 12, 436–446. doi: 10.1038/ncb2045

Srikanth, S., Woo, J. S., Wu, B., El-Sherbiny, Y. M., Leung, J., Chupradit, K., et al. (2019). The Ca(2+) sensor STIM1 regulates the type I interferon response by retaining the signaling adaptor STING at the endoplasmic reticulum. *Nat. Immunol.* 20, 152–162. doi: 10.1038/s41590-018-0287-8

Stathopulos, P. B., and Ikura, M. (2017). Store operated calcium entry: from concept to structural mechanisms. *Cell Calc.* 63, 3–7. doi: 10.1016/j.ceca.2016.11.005

Stathopulos, P. B., Li, G. Y., Plevin, M. J., Ames, J. B., and Ikura, M. (2006). Stored Ca2+ depletion-induced oligomerization of stromal interaction molecule 1 (STIM1) via the EF-SAM region: an initiation mechanism for capacitive Ca2+ entry. *J. Biol. Chem.* 281, 35855–35862. doi: 10.1074/jbc.M608247200

Stathopulos, P. B., Zheng, L., Li, G. Y., Plevin, M. J., and Ikura, M. (2008). Structural and mechanistic insights into STIM1-mediated initiation of store-operated calcium entry. *Cell* 135, 110–122. doi: 10.1016/j.cell.2008.08.006

Stiber, J., Hawkins, A., Zhang, Z. S., Wang, S., Burch, J., Graham, V., et al. (2008). STIM1 signalling controls store-operated calcium entry required for development and contractile function in skeletal muscle. *Nat. Cell Biol.* 10, 688–697. doi: 10.1038/ncb1731

Sura, A., Jacher, J., Neil, E., McFadden, K., Walkovich, K., and Hannibal, M. (2020). Chronic thrombocytopenia as the initial manifestation of STIM1-related disorders. *Pediatrics* 145:e20192081. doi: 10.1542/peds.2019-2081

Vaeth, M., and Feske, S. (2018). NFAT control of immune function: new frontiers for an abiding trooper. *F1000Res* 7:260. doi: 10.12688/f1000research.13426.1

Vaeth, M., Maus, M., Klein-Hessling, S., Freinkman, E., Yang, J., Eckstein, M., et al. (2017). Store-Operated Ca(2+) entry controls clonal expansion of t cells through metabolic reprogramming. *Immunity* 47, 664.e6–679.e6. doi: 10.1016/j.immuni.2017.09.003

van der Meijden, P. E. J., and Heemskerk, J. W. M. (2019). Platelet biology and functions: new concepts and clinical perspectives. *Nat. Rev. Cardiol.* 16, 166–179. doi: 10.1038/s41569-018-0110-0

Vandenberghe, M., Raphael, M., Lehen'kyi, V., Gordienko, D., Hastie, R., Oddos, T., et al. (2013). ORAI1 calcium channel orchestrates skin homeostasis. *Proc. Natl. Acad. Sci. U.S.A.* 110, E4839–E4848. doi: 10.1073/pnas.1310394110

Varga-Szabo, D., Braun, A., Kleinschnitz, C., Bender, M., Pleines, I., Pham, M., et al. (2008). The calcium sensor STIM1 is an essential mediator of arterial thrombosis and ischemic brain infarction. *J. Exp. Med.* 205, 1583–1591. doi: 10.1084/jem.20080302

Venkiteswaran, G., and Hasan, G. (2009). Intracellular Ca2+ signaling and store-operated Ca2+ entry are required in Drosophila neurons for flight. *Proc. Natl. Acad. Sci. U.S.A.* 106, 10326–10331. doi: 10.1073/pnas.0902982106

Walsh, C. M., Doherty, M. K., Tepikin, A. V., and Burgoyne, R. D. (2010). Evidence for an interaction between Golli and STIM1 in store-operated calcium entry. *Biochem. J.* 430, 453–460. doi: 10.1042/BJ20100650

Walter, M. C., Rossius, M., Zitzelsberger, M., Vorgerd, M., Muller-Felber, W., Ertl-Wagner, B., et al. (2015). 50 years to diagnosis: autosomal dominant tubular aggregate myopathy caused by a novel STIM1 mutation. *Neuromuscl. Disord.* 25, 577–584. doi: 10.1016/j.nmd.2015.04.005

Wang, L., Zhang, L., Li, S., Zheng, Y., Yan, X., Chen, M., et al. (2015). Retrograde regulation of STIM1-Orai1 interaction and store-operated Ca2+ entry by calsequestrin. *Sci. Rep.* 5:11349. doi: 10.1038/srep11349

Wang, S., Choi, M., Richardson, A. S., Reid, B. M., Seymen, F., Yildirim, M., et al. (2014). STIM1 and SLC24A4 are critical for enamel maturation. *J. Dent. Res.* 93(7 Suppl), 94S–100S. doi: 10.1177/0022034514527971

Wei-Lapierre, L., Carrell, E. M., Boncompagni, S., Protasi, F., and Dirksen, R. T. (2013). Orai1-dependent calcium entry promotes skeletal muscle growth and limits fatigue. *Nat. Commun.* 4:2805. doi: 10.1038/ncomms3805

Xue, T., Do, M. T., Riccio, A., Jiang, Z., Hsieh, J., Wang, H. C., et al. (2011). Melanopsin signalling in mammalian iris and retina. *Nature* 479, 67–73. doi: 10.1038/nature10567

Zayzafoon, M. (2006). Calcium/calmodulin signaling controls osteoblast growth and differentiation. *J. Cell Biochem.* 97, 56–70. doi: 10.1002/jcb.20675

Zhang, H., Clemens, R. A., Liu, F., Hu, Y., Baba, Y., Theodore, P., et al. (2014). STIM1 calcium sensor is required for activation of the phagocyte oxidase during inflammation and host defense. *Blood* 123, 2238–2249. doi: 10.1182/blood-2012-08-450403

Zhang, S. L., Yu, Y., Roos, J., Kozak, J. A., Deerinck, T. J., Ellisman, M. H., et al. (2005). STIM1 is a Ca2+ sensor that activates CRAC channels and migrates from the Ca2+ store to the plasma membrane. *Nature* 437, 902–905. doi: 10.1038/nature04147

Zhao, X., Yoshida, M., Brotto, L., Takeshima, H., Weisleder, N., Hirata, Y., et al. (2005). Enhanced resistance to fatigue and altered calcium handling properties of sarcalumenin knockout mice. *Physiol. Genomics* 23, 72–78. doi: 10.1152/physiolgenomics.00020.2005

34

5. CURRENT STATE IN THE TREATMENT OF MUSCLE DISEASES

Neuromuscular diseases were poorly studied human pathologies until 1987 when mutations in the Dystrophin gene *DMD* were shown to be causative of Duchenne's muscular dystrophy (DMD). The advances in the molecular biology within the past 34 years allowed the identification and characterization of 500 genes associated with neuromuscular disorders. The understanding of the physiological implications of the mutations enabled the development of straightforward therapeutic approaches based on gene replacement, gene downregulation or more indirect drug repurposing (Dowling et al., 2018; Dowling et al., 2021). Currently, a large panel of therapeutic approaches are being tested on clinical trials or are already approved and commercially distributed, particularly for DMD (Table 1).

5.1. Protein therapies

The first enzyme replacement therapy approved in humans consisted in intravenous injection of β-glucocerebrosidase in Gaucher's disease where the deficiency of the protein results in accumulation of sphingolipids in certain organs and tissues (Neufeld, 2006). In the same line, Pompe disease is caused by α-glucosidase deficiency with the consequent accumulation of glycogen in several tissues and resulting in heart defects, hepatomegaly and muscle weakness and hypotonia. Currently, an enzyme replacement approach is commercially distributed and consists of intravenous injection of recombinant α-glucosidase every 2 weeks (Table 1).

Table 1. Clinical trials and commercial therapeutic approaches for myopathies.

DMD, Duchenne's muscular dystrophy; BMD, Becker muscular dystrophy; DM1, type 1 myotonic dystrophy;

CNM, centronuclear myopathy; LGMD, limb girdle muscle dystrophy; FSHD, fascioscapulohumeral muscular dystrophy

Therapeutic approach	Disease	Mutated gene	Physiological impact	Strategy	Clinical stage	Commercial name or clinical trial	Clinical trial sponsor / Manufacturer
Protein therapies	Pompe disease	*GAA*	α-glucosidase deficiency and defect in glycogen breakdown	Enzyme replacement	Commercial	Lumizyme®	Sanofi Genzyme
Antisense oligonucleotides	DMD	*DMD*	Dystrophin deficiency and fragile sarcolemma	Exon skipping to produce small dystrophin	Commercial	Amondys 45 (casimersen), Exondys 51 (eteplirsen), and Vyondys 53 (golodirsen)	SAREPTA and IONIS
	DM1	*DMPK*	CTG expansion and chromatin condensation	Exon skipping for premature degradation	I/II discontinued	NCT02312011	IONIS
	CNM	*MTM1/ DNM2*	Dynamin 2 over-activation	*DNM2* knockdown	I/II	NCT04743557/NCT04033159	Dynacure
Adeno-associated viruses	DMD	*DMD*	Dystrophin deficiency and fragile sarcolemma	Expression of smaller dystrophin (minigene)	I/II, I/II and III	NCT03375164 / NCT03769116, NCT03368742, NCT04281485 / NCT03362502	SAREPTA (2), Solid Biosciences, Pfizer (2)
	DMD	*DMD*	Dystrophin deficiency and fragile sarcolemma	Exon 2 skipping	I/II	NCT04240314	ASTELLAS
	DMD	*DMD*	Dystrophin deficiency and fragile sarcolemma	Skipping of exon 51 and exon 53	Preclinical	-	ASTELLAS

Table 1. (Continued)

Therapeutic approach	Disease	Mutated gene	Physiological impact	Strategy	Clinical stage	Commercial name or clinical trial	Clinical trial sponsor / Manufacturer
	DMD	*GALGT2*	Dystrophin deficiency and fragile sarcolemma	*GALTGT2* over-expression increases utrophin expression	I/II	NCT03333590	SAREPTA
	DM1	*DMPK*	CTG expansion and chromatin condensation	*DMPK* shRNA	Preclinical	-	ASTELLAS
	LGMD2B	*DYSF*	Dysferlin deficiency and fragile sarcolemma	Gene replacement	I	NCT02710500	SAREPTA
Adeno-associated viruses	LGMD2D	*SGCA*	α-sarcoglycan deficiency and fragile sarcolemma	Gene replacement	I/II	NCT01976091	SAREPTA
	LGMD2E	*SGCB*	β-sarcoglycan deficiency and fragile sarcolemma	Gene replacement	I/II	NCT03652259	SAREPTA
	Pompe disease	*GAA*	α-glucosidase deficiency and defect in glycogen breakdown	Gene replacement	I/II	NCT04174105, NCT03533673	ASTELLAS, AskBio
	XL-CNM	*MTM1*	Myotubularin 1 deficiency	Gene replacement	I/II	NCT03199469	ASTELLAS
Cell therapy	DMD	*DMD*	Dystrophin deficiency and fragile sarcolemma	Allogenic transplant of cardiosphere-derived cells	II completed	NCT03406780	Capricor Therapeutics

37

Table 1. (Continued)

Therapeutic approach	Disease	Mutated gene	Physiological impact	Strategy	Clinical stage	Commercial name or clinical trial	Clinical trial sponsor / Manufacturer
Cell therapy	DMD	*DMD*	Dystrophin deficiency and fragile sarcolemma	Allogenic transplant and autologous transplant of cells modified *in vitro*	I/II	NCT03067831	Stem Cells Arabia
	DMD	*DMD*	Dystrophin deficiency and fragile sarcolemma	Allogenic transplant of myoblasts	I/II	NCT02196467	CHU de Quebec-Universite Laval
	DMD	*DMD*	Ribosome inhibitor	Inhibit premature Translation termination	Commercial	Translarna™ (ataluren)	PTC Therapeutics
	DMD	*DMD*	Dissociative steroids	Anti-inflammatory	Commercial	EMFLAZA® (deflazacort)	PTC Therapeutics
Small molecules	DMD	*DMD*	Dissociative steroids	Anti-inflammatory	II	NCT02760264/ NCT02760277/ NCT03038399/ NCT02439216/ NCT02858362	ReveraGen BioPharma, Inc./Catabasis Pharmaceuticals/ Summit Therapeutics
	DMD	*DMD*	Givinostat	HDAC inhibitor acts on inflammation and regeneration	III	NCT02851797	Italfarmaco
	BMD	*DMD*	Givinostat	HDAC inhibitor acts on inflammation and regeneration	II	NCT03238235	Italfarmaco

Table 1. (Continued)

Therapeutic approach	Disease	Mutated gene	Physiological impact	Strategy	Clinical stage	Commercial name or clinical trial	Clinical trial sponsor / Manufacturer
	DMD	*DMD*	Rimeporide	Reduces cytosolic Na⁺ and Ca²⁺	I completed	NCT02710591	EspeRare Foundation
	DMD	*DMD*	Tamoxifen	Unknown	III	NCT03354039	University of Basel
	CNM	*MTM1*	Tamoxifen	Unknown	I/II	NCT04915846	The Hospital for Sick Children
Small molecules	DM1	*DMPK*	Mexiletine	Non-selective voltage-gated sodium channel blocker	II completed and III ongoing	NCT01406873 and NCT04624750/NCT04622553	University of Rochester and Lupin Ltd. (2)
	FSHD	*DUX4*	Resolaris™ (ATYR1940)	Anti-inflammatory	I/II completed	NCT02603562/NCT02239224/NCT02836418/NCT02579239/NCT02531217	aTyr Pharma
	FSHD	*DUX4*	Losmapimod	p38/MAPK inhibition to inhibit DUX4 and anti-inflammatory	II completed (short term) and II ongoing (long term)	NCT04003974/NCT04004000/NCT04264442	Fulcrum Therapeutics

5.2. Antisense oligonucleotides

RNA interference (RNAi) and antisense oligonucleotides (ASOs) are used to modulate gene and protein expression by binding the target RNA in a sequence-specific manner. For RNA interference, short hairpin RNA (shRNA) are produced by RNA polymerase III and consist of a double stranded RNA sequence connected by a loop. The short hairpin RNA is processed by Dicer eliminating the loop and generating the small interference RNA (siRNA). One strand of the siRNA will be loaded into RISC complexes and will serve as the prey to bind the target mRNA ultimately cleaved by the RISC complex (Sheng et al., 2020; Watts and Corey, 2012). If the complementarity to the target mRNA is not complete, protein translation can also be inhibited (Figure 8). To mimic this biological process, vectors containing shRNA under the control of a U6 promoter can be used and will be described in the adeno-associated viruses section (Figure 8). Also, double stranded siRNAs can be directly produced and delivered. siRNAs have been widely used in cell experiments for its simplicity and accessibility in research, and several clinical trials are ongoing for a wide range of diseases but not yet for skeletal myopathies (Saw and Song, 2020), probably due to the lack of tissue-targeted siRNA complexes in the past (Biscans et al., 2021).

In contrast to siRNAs, antisense oligonucleotides (ASOs) are small and single-stranded 18-30 DNA base pair sequences (Figure 8). They can carry modifications in: 1) bases to enhance RNA affinity and modulate base-pairing specificity; 2) phosphodiester backbone to increase nuclease resistance; 3) sugar to increase the binding affinity and nuclease resistance; and 4) ASO extremities to modulate ASO distribution and cell targeting (Goyenvalle et al., 2016; Wan and Seth, 2016) (Figure 9A-B). ASOs are more versatile than siRNAs as they can be used to generate a knockdown of a gene, block its protein expression or induce exon skipping. Gene knockdown is achieved by the association of ASOs and RNAse H1 that will degrade the mRNA while splice skipping and protein translation inhibition is achieved by steric blocking of ASO to the splicing machinery and ribosome, respectively (Scoles et al., 2019) (Figure 8).
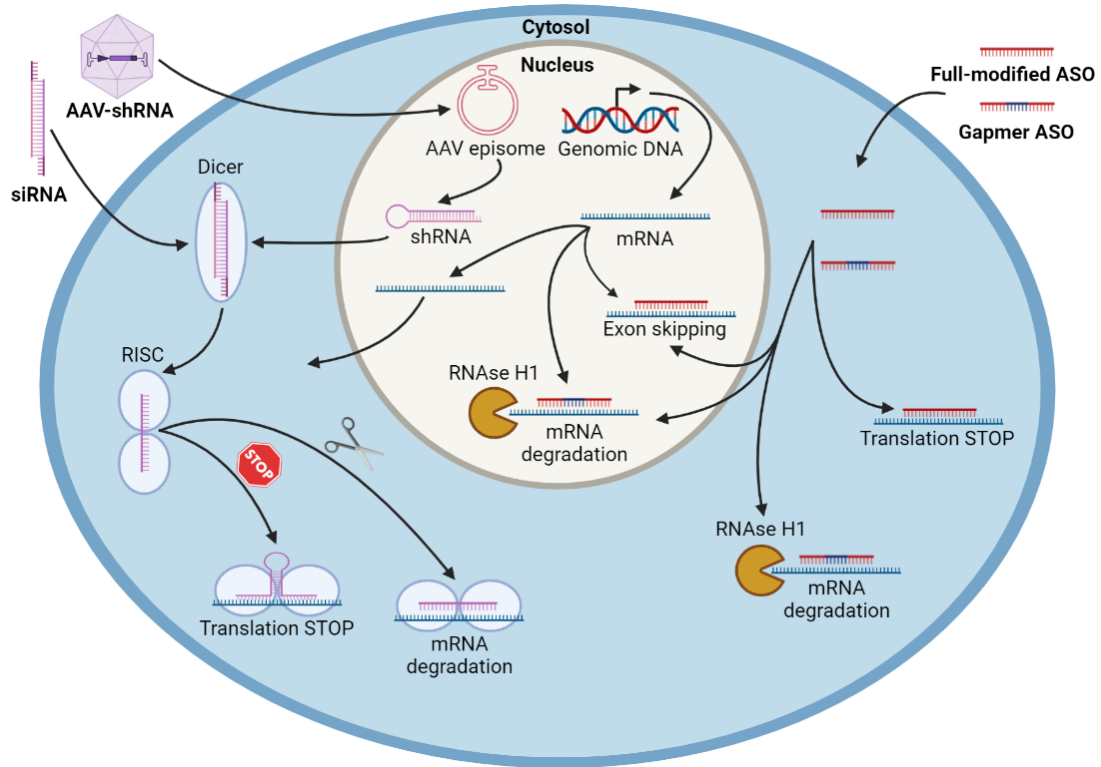
Figure 8. shRNA and ASO mechanisms.

Adeno-associated viruses (AAVs) containing shRNAs are internalized in the nuclei of the host cells and the AAV genome remains stable as episome. Host DNA polymerases transcribe the shRNA later processed by Dicer and RISC complex, generating single stranded RNA sequences that will bind the target mRNA. Full complementarity to the target mRNA results in mRNA degradation while incomplete complementarity blocks mRNA translation by the ribosome. Artificial siRNAs can be engineered and delivered to the cell with identical effects to encoded shRNA but with lower durability.

Antisense oligonucleotides (ASOs) can be fully modified or have a gapmer structure with a central non-modified DNA structure and modified external wings. The first will enter the nuclei and generate exon skipping during splicing or stay in the cytosol where the strong and steric interaction with the target mRNA will block ribosomal mRNA translation. Gapmer ASOs will bind and allow RNAse H1 degradation of the target pre-mRNA in the nuclei or the mature mRNA in the cytosol.

This image was created with BioRender (https://biorender.com/).
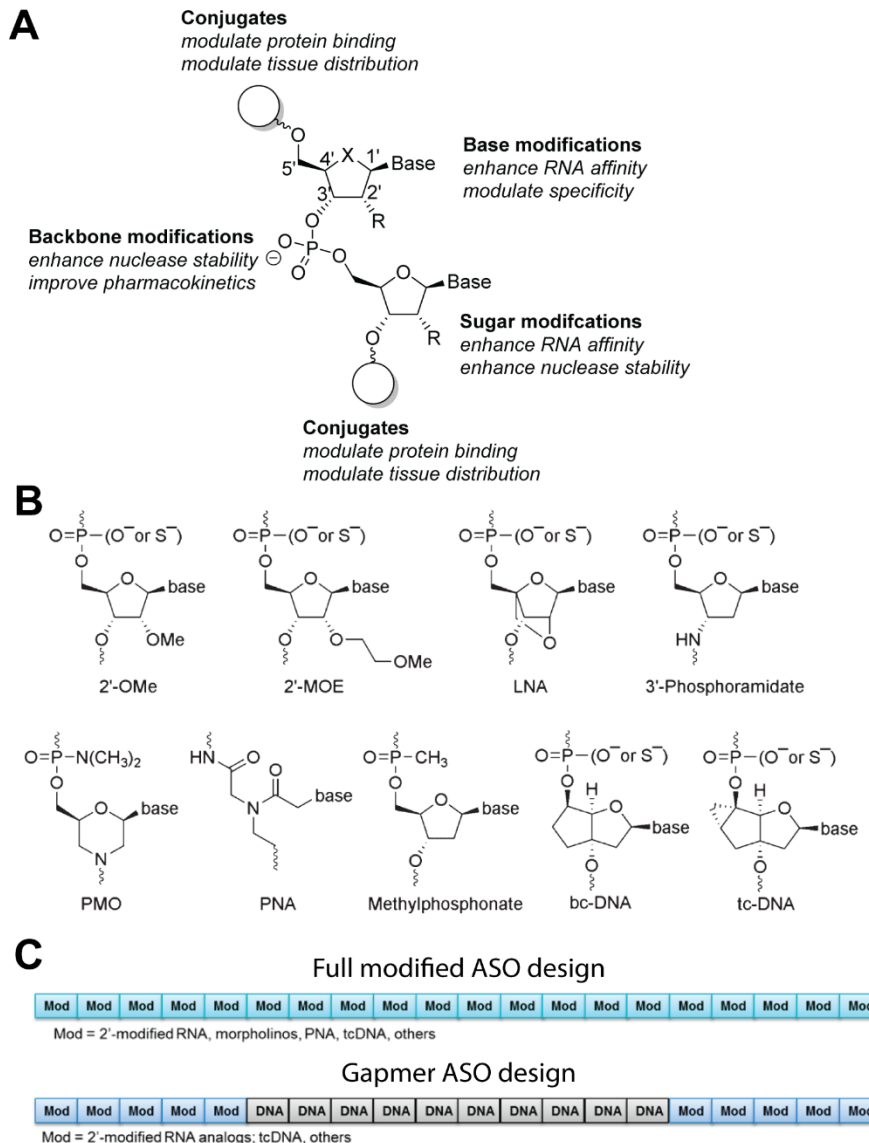
Figure 9. ASO modifications and design.

(A) Antisense oligonucleotides (ASOs) modification sites and effects. (B) Most common modifications of ASOs. (C) Structures of fully modified ASOs and gapmer ASOs. Adapted from Wan and Seth, 2016 and Goyenvalle et al., 2016.

ASO chemistry and structure can impact the access of mRNA to RNAseH1, spliceosome and ribosome. Fully modified ASOs impede the access of RNAse H1 to mRNA and block splicing and translation. They are thus used for exon skipping and translation inhibition (Figure 8 and 9C). This

ASO chemistry has been approved commercially to treat Duchenne's muscular dystrophy (DMD) by targeting *DMD* exon 45 (Amondys 45, casimersen), exon 51 (Exondys 51, eteplirsen) exon 53 (Vyondys, golodirsen), and has been tested to treat myotonic dystrophy type 1 targeting *DMPK*, but the phase I/II clinical trial was discontinued due to low muscle biodistribution of the ASO (Table 1). To achieve gene knockdown, the current strategy is based on ASO gapmers which consist on modified wings to avoid nuclease degradation and an unmodified central ASO part to ensure RNAse H1 action (Figure 8 and 9C). Such ASO structure is currently been tested in phase I/II clinical trials to target *DNM2* in centronuclear myopathy (Table 1).

5.3. Adeno-associated viruses

Adeno-associated virus (AAV) are envelop-free viruses with a small single stranded DNA genome of 4.7 kb composed of flanking palindromic ITR sequences, *rep* genes for virus replication and *cap* genes encoding the proteins that will form the capsid. They belong to the genus *Dependoparvovirus* by their need for auxiliary viruses such as adenovirus to replicate because, due to its small genome size, they lack factors required for virus replication like the viral DNA polymerase (Goncalves, 2005). AAVs bind cell receptors in the plasma membrane and are endocytosed and transported to the nucleus where the AAV loses the capsid and releases the viral genome. Ultimately, the DNA polymerization machinery of the host cell produces the complementary strand and circular DNA episomes are formed. These viral genome structures remain in the nucleus of the host cell while a small percentage has been observed to integrate into the host genome (Wang et al., 2019) (Figure 10A). Indeed, the major advantage of AAV-derived therapies is that, owing to their episomal resting state, a single injection in the childhood-adolescence possibly confers a life-long therapeutic effect. This is of particular interest for dystrophies where other techniques like ASOs implicate weekly intravenous injections.
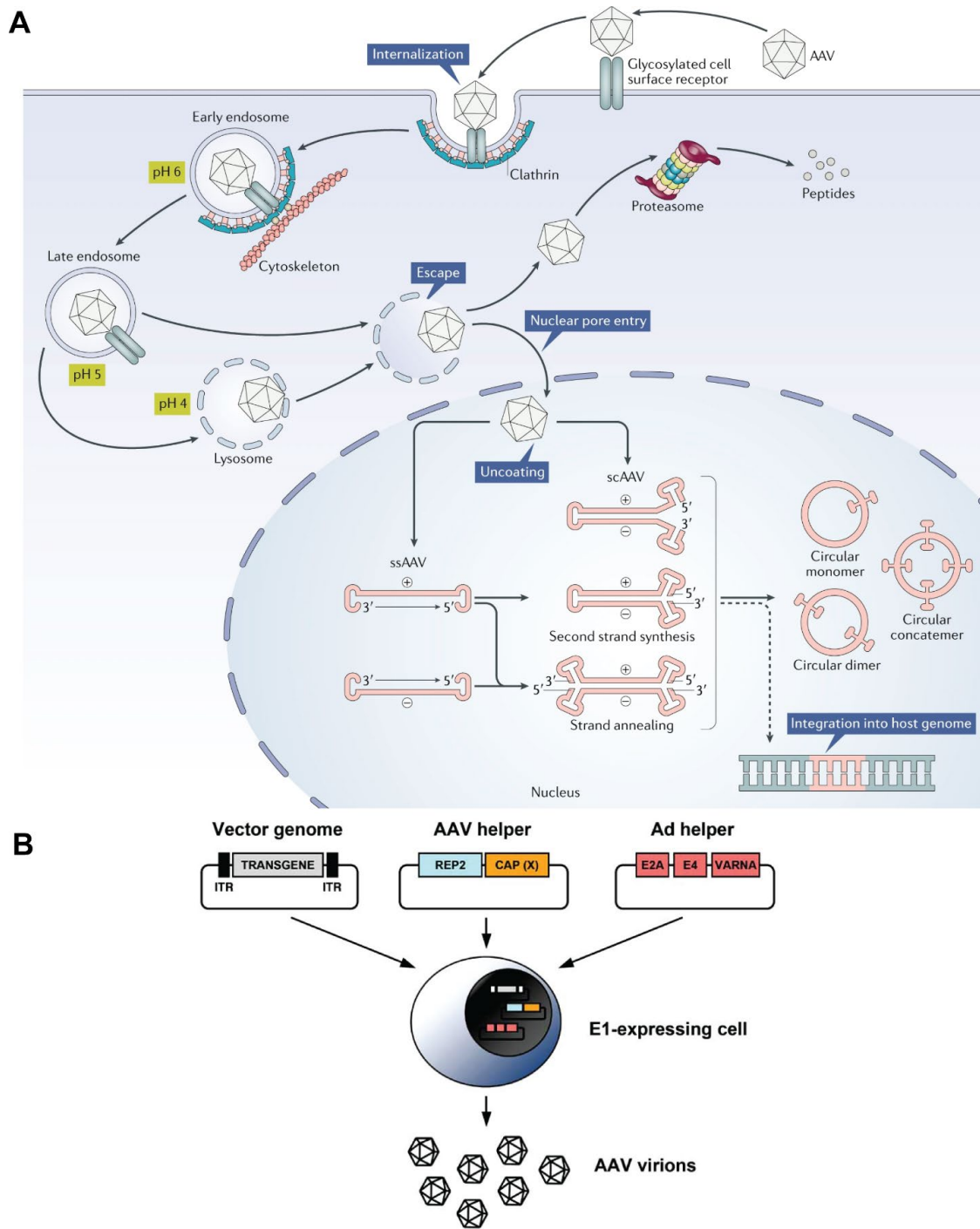
Figure 10. AAV cell infection and strategy to produce recombinant AAVs.

(A) Adeno-associated viruses (AAVs) enter the cell by endocytosis and escape the lysosomes to internalize into the nuclei where they lose the capsid and their genome circularizes and remain stable as episome, while a small percentage integrates into the host genome. (B) Recombinant AAVs are produced by triple transfection of cells with plasmids containing: 1) the transgene

flanked by ITR AAV sequences, 2) Rep and Cap AAV genes, and 3) adenoviral factors required for virus replication. Adapted from Wang et al., 2019 and Ayuso et al., 2010.

Cell tropism is determined by the capsid proteins and differs between the AAVs (Colon-Thillet et al., 2021). Currently, cell tropism is known for 12 AAVs and some of them are widely used *in vivo* to target liver, the central nervous system and skeletal muscle (Table 2) (Colon-Thillet et al., 2021; Wang et al., 2019). To produce recombinant AAVs, cells are transfected with 3 different plasmids: 1) one containing *rep* and *cap* genes that will determine the AAV serotype and tropism; 2) a second plasmid containing the minimal adenoviral genes required for AAV replication; and 3) a plasmid containing the promoter and transgene of interest flanked by inverted terminal repeats (ITR) (Figure 10B) (Ayuso et al., 2010). AAV particles are produced by the cells and the supernatant is harvested to concentrate the virus.

Table 2. AAV serotypes and tropism.

Bold refers to tropism widely targeted in vivo. Adapted from Colon-Thillet et al et al., 2021.

AAV capsid	Natural origin	Likely species origin	In vivo tropism
AAV1	yes	Non-human primate	**Skeletal muscle**, central nervous system, airway, retina, heart, liver
AAV2	yes	Human	Skeletal muscle, central nervous system retina, liver
AAV3	yes	Human	Skeletal muscle, liver
AAV4	yes	African green monkey	Central nervous system, retina, kidney, lung
AAV5	yes	Human	Skeletal muscle, **central nervous system**, airway, retina
AAV6	yes	Human	**Skeletal muscle**, airway, heart
AAV7	yes	Rhesus macaque	Skeletal muscle, central nervous system, retina, liver
AAV8	yes	Rhesus macaque	**Skeletal muscle**, central nervous system, airway, retina, heart, **liver**
AAV9	yes	Human	**Skeletal muscle**, **central nervous system**, airway, retina, heart, **liver**
AAV.rh10	yes	Rhesus macaque	Skeletal muscle, **central nervous system**, airway, retina, heart, **liver**
AAV.DJ	no	-	Central nervous system, retina, **liver**
AAV.LK03	no	-	Human liver

The first AAV-based therapeutic approach was approved by the European Medicines Agency (EMA) in 2012 and consisted of gene replacement for lipoprotein lipase deficiency (Yla-Herttuala, 2012). In 2019, at least 60 clinical trials used AAV vectors to treat diseases affecting the brain, spinal cord, eye, liver and skeletal muscle, and the therapeutic strategy of most of them was gene replacement (Wang et al., 2019). In the field of neuromuscular disorders, the more advanced clinical trials (phase III) aim to express small mini dystrophin in DMD patients (Table 1). There are is also one clinical trial based on a surrogate gene strategy targeting *GALGT2* (Table 1). Overexpression of *Galgt2* in a murine model for DMD was shown to increase the expression of utrophin, the embryonic dystrophin homologue, and was accompanied by improved heart and skeletal muscle function (Xu et al., 2019). Other clinical trials involving AAVs are ongoing for limb girdle muscle dystrophies (LGMD) types 2B, 2D and 2E and aim to restore the expression of *DYSF*, *SGCA* and *SGCB*, respectively (Table 1). Gene replacement is also being tested for X-linked centronuclear myopathy (CNM) caused by *MTM1* LoF mutations and for Pompe disease involving α-glucosidase deficiency (Table 1).

While gene replacement has been the major interest of AAVs, they can also be used for exon skipping and gene knockdown. DMD patients containing exon 2 duplications are currently being enrolled in a phase I/II clinical trial aiming to exclude one or both copies of exon 2 from the pre-mRNA. For this, patients will be subjected to intra-venous injections of AAV9 containing small nuclear RNA targeting the intron 1-exon 2 junction (Table 1). The same strategy is ongoing in preclinical trials and aims to generate exon skipping of exons 51 and 53 (Table 1). A gene knockdown strategy is also in preclinical trials for myotonic dystrophy type 1 (DM1) with the aim to increase the muscle targeting not achieved with ASOs as indicated above (Table 1).

5.4. Cell therapy

Myofibers are cells with low division rate and, only after lesion and fiber death, nearby satellite cells will divide to generate myoblasts that will fuse and differentiate into fibers. For this reason, cell transplantation and engraftment is not a feasible therapeutic approach for most myopathies. However, muscle dystrophies where fiber turnover is elevated could be addressed by cell therapy strategies. Several cell therapy trials have been performed in the past providing promising results,

but the stability and myogenic conversion of the transplanted cells need to be improved (Bajek et al., 2015; Torrente et al., 2007). Currently, allogenic transplantation of heart-derived stem cells with multipotent and long-term engraftment capacities completed phase II clinical trials with DMD patients (Table 1). Another phase I/II clinical trials is recruiting DMD patients for allogeneic transplant of stem cells and for autologous transplant of stem cells after *in vitro* modification to restore the defective dystrophin levels (Table 1). It is also planned to transplant myoblasts in a phase I/II trial for DMD (Table 1).

5.5. Small molecules

In addition to directly modify the expression of mutated genes or engraft healthy cells, small molecules targeting cell processes altered in the myopathies may attenuate myopathic signs. Translarma^{TM} (ataluren) is a commercial molecule that enables the ribosome to read through premature stop codons often present in DMD patients and allowing the translation of full-length dystrophin (Berger et al., 2020) (Table 1). Another commercialized molecule for DMD is EMFLAZA® (deflazacort), an anti-inflammatory molecule that attenuates the effects of muscle degeneration (Table 1). Similar anti-inflammatory molecules are currently in clinical trials for DMD and fascioscapulohumeral dystrophy (FSHD) (Table 1). Inhibiting Na^+ channels and thus the Ca^{2+} overload is being clinically tested for DMD and myotonic dystrophy type 1 using remeporide and mexiletine, respectively (Table 1). The anticancer treatment molecule tamoxifen was shown to improve the breathing defects and improved muscle performance of murine model of DMD (Gayi et al., 2018), and also prolonged the survival and motor function of a mouse model for X-linked CNM (Dorchies et al., 2013). Its potential efficiency to treat DMD and X-linked CNM is in phase III and I/II clinical trials (Table 1).

6. GOALS OF MY PhD

My PhD thesis is focused on the study of TAM/STRMK, a clinical continuum encompassing muscle weakness, cramps and myalgia together with multi-systemic phenotypes affecting the stature, eyes, skin, platelets, spleen and the cognitive abilities. It was not until 2013 that *STIM1* was discovered as the first causative gene, and mutations in *ORAI1* and *CASQ1* were found later (Bohm et al., 2017; Bohm et al., 2013; Bohm et al., 2018). GoF mutation in *STIM1* and *ORAI1*, and LoF mutation in *CASQ1* result in over-active SOCE and excessive Ca^{2+} entry via ORAI1. Due to the recent discovery of the causative genes of TAM/STRMK, no animal model described the multi-systemic picture of the disease and, in consequence, little was known on TAM/STRMK physiopathology and no therapeutic proof-of-concept was provided. In order to tackle these bottlenecks, my PhD had the following goals:

- **Goal 1**: To provide a tool to study the physiopathology and treatability of TAM/STRMK, we generated and characterized a mouse model carrying the most common *STIM1* mutation. *Stim1$^{R304W/+}$* mice went through a large phenotypic panel to validate the TAM/STRMK phenotypes affecting the stature, platelets, spleen, skin and skeletal muscle. Additional cells and tissues were studied to find anomalies in the immune system, bones, blood glucose metabolism and liver not reported in patients yet (publication 1).

- **Goal 2**: To determine the negative effects of Ca^{2+} overload in *Stim1$^{R304W/+}$* muscles, we analyzed the transcriptome of *Stim1$^{R304W/+}$* muscles and I performed RT-qPCR, western blot and functional studies to validate the anomalies in Ca^{2+} handling, mitochondrial respiration and ER stress (publication 2). Anomalies in these cell processes can explain the muscle weakness and degeneration observed in *Stim1$^{R304W/+}$* muscles and serve as therapeutic targets to treat TAM/STRMK.

- **Goal 3**: To assess the therapeutic effect of targeting ORAI1 expression and activity, I crossed *Stim1$^{R304W/+}$* mice with *Orai1$^{+/-}$* mice expressing 50% of *Orai1*, and *Orai1$^{R93W/+}$* mice expressing a partially blocked ORAI1 channel. We assessed the disease reversion of the *Stim1$^{R304W/+}$* defects by analyzing the body weight, muscle performance, platelet number, spleen size and histology, and bone morphology of the offspring. The results provided the first therapeutic proof-of-concept for TAM/STRMK that can be translated into shRNA/ASO and small channel inhibitors targeting and reducing ORAI1 expression and activity, respectively (publications 3 and 4).
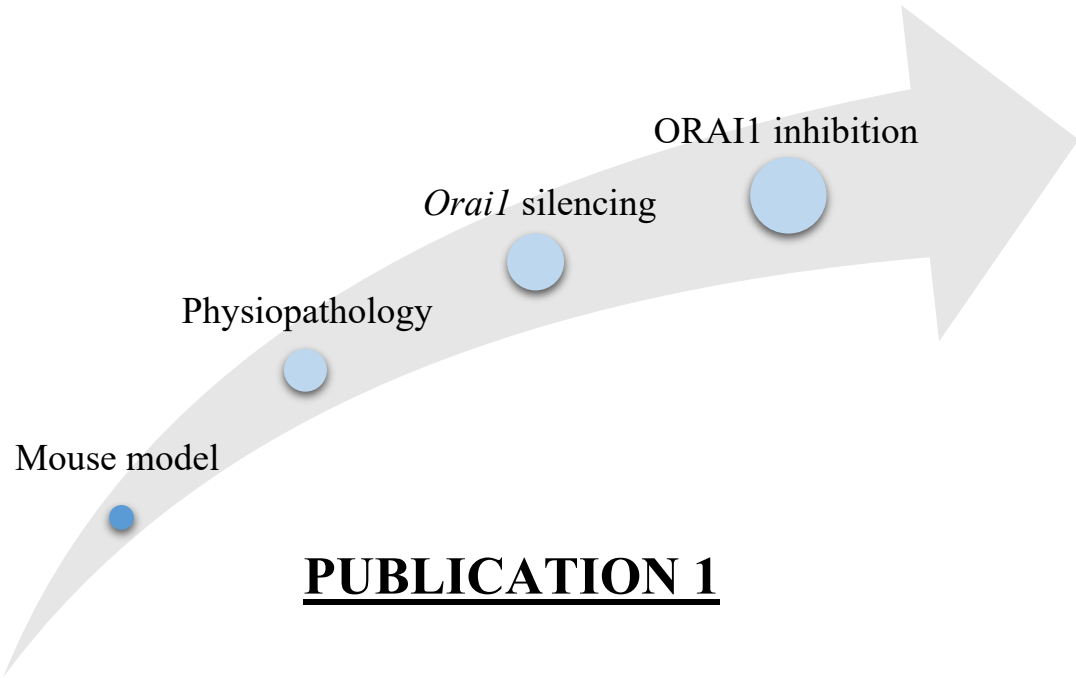
ORAI1 inhibition

Orai1 silencing

Physiopathology

Mouse model

PUBLICATION 1

STIM1 over-activation generates a multi-systemic phenotype affecting the skeletal muscle, spleen, eye, skin, bones and immune system in mice

Roberto Silva-Rojas, Susan Treves, Hugues Jacobs, Pascal Kessler, Nadia Messaddeq, Jocelyn Laporte and Johann Böhm

RESULTS

1. GENERATION AND CHARACTERIZATION OF A MOUSE MODEL FOR TAM/STRMK

1.1. Background

Tubular aggregate myopathy (TAM) and Stormorken syndrome (STRMK) form a clinical continuum characterized by muscle weakness, contractures and myalgia and additional multi-systemic signs including short stature, miosis, ichthyosis, dyslexia, thrombocytopenia and hyposplenia (Bohm and Laporte, 2018; Morin et al., 2020). Most of the TAM/STRMK mutations are GoF mutations in *STIM1* and *ORAI1*, encoding the key players of a mechanism regulating extracellular Ca^{2+} entry known as SOCE (Bohm and Laporte, 2018; Lacruz and Feske, 2015; Morin et al., 2020). STIM1 is a transmembrane protein in the ER/SR with a luminal Ca^{2+}-sensing part a cytosolic part involved in oligomerization and activation of ORAI1 in response to low reticular Ca^{2+} content (Schober et al., 2019; Stathopulos et al., 2008). GoF mutations in *STIM1* constitutively activate STIM1 by promoting oligomerization and GoF mutations in *ORAI1* increase Ca^{2+} permeability of the channel, both ultimately resulting in SOCE over-activation and elevated cytosolic Ca^{2+} levels (Bohm and Laporte, 2018).

1.2. Aim of the study

When I started my PhD in 2017, the three causative TAM/STRMK genes *STIM1*, *ORAI1*, and *CASQ1* were known, and functional studies in the cell had shown that the mutations affect the SOCE pathway and induce excessive extracellular Ca^{2+} entry. However, no faithful animal model recapitulating the multi-systemic picture of TAM/STRMK was described, precluding thorough investigations on the correlation between the cellular alterations and disease development. We thus generated a mouse model carrying the most recurrent TAM/STRMK mutation and performed a broad phenotypical characterization.

1.3. Results

Stim1$^{R304W/+}$ mouse was generated by homologous recombination of exon 7 harboring A>T transversion at position c.910 (p.R304W). Homozygous animals *Stim1$^{R304W/R304W}$* mice died at perinatal stages and heterozygous animals were viable and fertile. When compared to WT littermates, *Stim1$^{R304W/+}$* mice were also smaller, had eye movement anomalies, presented thrombocytopenia and splenomegaly, and displayed anomalies in skin layer disposition. In addition, defects in bone morphology, homeostasis of blood glucose, liver and immune system were reported. *Stim1$^{R304W/+}$* myotubes presented high cytosolic Ca^{2+} and elevated SOCE, skeletal muscle histology revealed muscle degeneration and fiber atrophy, and muscle performance was impacted with reduced force and abnormal contraction and relaxation.

1.4. Conclusion and perspectives

Our Stim1$^{R304W/+}$ mouse model was the first mammalian model recapitulating the main multi-systemic signs of TAM/STRMK. The availability of a faithful animal model allows physiological studies on the pathological effect of Ca^{2+} overload on different affected tissues and organs, and represents a valuable tool to test therapeutic approaches for TAM/STRMK. Moreover, the additional defects involving the bones, liver, immune system and blood glucose metabolism signs observed enlarges the clinical description of TAM/STRMK. If confirmed in patients, this would be of major medical importance for the disease management and clinical follow-up and would help clinicians to guide molecular diagnosis.

1.5. Contribution

I coordinated the breeding and phenotyping of the animals, characterized and analyzed the muscle phenotype of *Stim1$^{R304W/+}$*, and performed SOCE and reticular Ca^{2+} store experiments in *Stim1$^{R304W/+}$* myotubes. *Stim1$^{R304W/+}$* mice were generated and characterized at the Institut Clinique de la Souris (ICS, Strasbourg, France) following International Mouse Phenotyping Consortium protocols. The spleen immune characterization was performed at the external Centre d'Immunophénomique (Ciphe, Marseille, France). Hugues Jacobs from ICS provided valuable

help in the histological characterization of spleen, muscle and bones, Nadia Messaddeq from Institut de Génétique et de Biologie Moléculaire et Cellulaire (IGBMC, Strasbourg, France) prepared and analyzed electron microscopy samples, and Pascal Kessler was a team member that developed an ImageJ plugin to analyze fiber size. Susan Treves was an external collaborator from Basel University Hospital (Basel, Switzerland) who measured the basal Ca^{2+} in $Stim1^{R304W/+}$ myotubes.

OXFORD

GENERAL ARTICLE

STIM1 over-activation generates a multi-systemic phenotype affecting the skeletal muscle, spleen, eye, skin, bones and immune system in mice

Roberto Silva-Rojas[1], Susan Treves[2,3], Hugues Jacobs[1,4], Pascal Kessler[1], Nadia Messaddeq[1], Jocelyn Laporte[1,*] and Johann Böhm[1,*]

[1]Institut de Génétique et de Biologie Moléculaire et Cellulaire (IGBMC), Inserm U1258, CNRS UMR7104, Université de Strasbourg, 67404 Illkirch, France, [2]Departments of Biomedicine and Anaesthesia, Basel University Hospital, Basel University, 4031 Basel, Switzerland, [3]Department of Life Sciences, General Pathology section, University of Ferrara, 44121 Ferrara, Italy and [4]Institut Clinique de la Souris (ICS), 67404 Illkirch, France

*To whom correspondence should be addressed at: Johann Böhm, Email: johann@igbmc.fr and Jocelyn Laporte, IGBMC, 1 Rue Laurent Fries, 67404 Illkirch, France. Tel: +33 (0)3 88 65 34 14; Fax: +33 (0)3 88 65 32 01; Email: jocelyn@igbmc.fr

Abstract

Strict regulation of Ca^{2+} homeostasis is essential for normal cellular physiology. Store-operated Ca^{2+} entry (SOCE) is a major mechanism controlling basal Ca^{2+} levels and intracellular Ca^{2+} store refilling, and abnormal SOCE severely impacts on human health. Overactive SOCE results in excessive extracellular Ca^{2+} entry due to dominant *STIM1* or *ORAI1* mutations and has been associated with tubular aggregate myopathy (TAM) and Stormorken syndrome (STRMK). Both disorders are spectra of the same disease and involve muscle weakness, myalgia and cramps, and additional multi-systemic signs including miosis, bleeding diathesis, hyposplenism, dyslexia, short stature and ichthyosis. To elucidate the physiological consequences of STIM1 over-activation, we generated a murine model harboring the most common TAM/STRMK mutation and characterized the phenotype at the histological, ultrastructural, metabolic, physiological and functional level. In accordance with the clinical picture of TAM/STRMK, the $Stim1^{R304W/+}$ mice manifested muscle weakness, thrombocytopenia, skin and eye anomalies and spleen dysfunction, as well as additional features not yet observed in patients such as abnormal bone architecture and immune system dysregulation. The murine muscles exhibited contraction and relaxation defects as well as dystrophic features, and functional investigations unraveled increased Ca^{2+} influx in myotubes. In conclusion, we provide insight into the pathophysiological effect of the STIM1 R304W mutation in different cells, tissues and organs and thereby significantly contribute to a deeper understanding of the pathomechanisms underlying TAM/STRMK and other human disorders involving aberrant Ca^{2+} homeostasis and affecting muscle, bones, platelets or the immune system.

Introduction

Store-operated Ca^{2+} entry (SOCE) is a conserved and ubiquitous mechanism regulating intracellular Ca^{2+} balance, and small

disturbances can severely impact on the physiology of various cells, tissues and organs (1). Ca^{2+} is mainly stored in the endoplasmic/sarcoplasmic reticulum, and its release to the cytosol

initiates a plethora of cellular pathways and processes including muscle growth and contraction, T-cell differentiation or platelet activation. Ca^{2+} store refill relies on the concerted activity of the reticular Ca^{2+} sensor STIM1 and the plasma membrane Ca^{2+} channel ORAI1. STIM1 senses the luminal Ca^{2+} concentration through EF-hands, and Ca^{2+} store depletion induces a conformational change enabling STIM1 oligomerization. The cytosolic domains of the STIM1 oligomers then activate the Ca^{2+} release-activated Ca^{2+} (CRAC) channel ORAI1 to trigger extracellular Ca^{2+} entry ([2–4]).

Abnormal SOCE has been associated with different human disorders. Recessive *STIM1* and *ORAI1* loss-of-function mutations resulting in insufficient SOCE cause severe immunodeficiency involving recurrent and chronic infections, autoimmunity, ectodermal dysplasia and muscular hypotonia (OMIM #612782 and 612783) ([1,5,6]). In contrast, dominant *STIM1* and *ORAI1* gain-of-function mutations inducing excessive Ca^{2+} entry through SOCE over-activation were found in patients with tubular aggregate myopathy (TAM; OMIM #160565 and #615883) and Stormorken syndrome (STRMK; OMIM #185070) ([7–10]). Both conditions are part of a clinical continuum and are characterized by progressive muscle weakness, cramps and myalgia ([11]), and additional multi-systemic signs including thrombocytopenia, hyposplenism, miosis, ichthyosis, short stature, hypocalcemia and dyslexia ([12–18]). Age of onset, disease severity and occurrence of non-muscle features are heterogeneous and generally correlate with the genotype. The most common gain-of-function mutation R304W, affecting a conserved amino acid in the cytosolic domain of STIM1, was found in 12 unrelated families essentially presenting with the full multi-systemic picture constituting the diagnosis of Stormorken syndrome ([8–10,14,19,20]). Functional studies demonstrated that the R304W mutation induces a helical elongation of the cytosolic domain of STIM1 and thereby promotes the exposure of the ORAI1-interacting SOAR domain, resulting in constitutive ORAI1 channel activation ([21]). Moreover, electrophysiological studies have shown that the R304W mutation suppresses fast Ca^{2+}-dependent channel inactivation of ORAI1, suggesting that R304W also entails prolonged Ca^{2+} influx ([10]).

Mammalian models with abnormal SOCE are rare, impeding a detailed analysis of the long-term consequences of abnormal Ca^{2+} homeostasis on the entire organism and in different tissues and precluding functional investigations on the sequence of events leading to the multi-systemic aberrations observed in severe combined immunodeficiency or TAM/STRMK. *Stim1*$^{-/-}$ and *Orai1*$^{-/-}$ mice showed high neonatal lethality, and surviving animals manifested low body weight and significant hypotonia leading to death within a few weeks ([22–24]). A similar phenotype was observed for *Orai1*$^{R93W/R93W}$ knock-in mice expressing a non-functional Ca^{2+} channel ([25]). Tissue-specific knockout of *Stim1* demonstrated a decrease in number and function of T cells ([26]) and a reduced ability of platelets to switch from a pro-adhesive to a pro-coagulant state ([27]), but provided only a narrow view on the physiological consequences of SOCE suppression. The *Stim1*^{Sax} mouse, generated through random mutagenesis and harboring the same D84G mutation as in a single family with TAM ([7]), displayed spleen enlargement and increased basal Ca^{2+} levels in the platelets resulting in a pre-activation state and elevated platelet consumption ([28]). However, a potential phenotype of muscle, skin or bones was not evaluated.

In order to shed light on the multi-systemic features of TAM/STRMK, we generated a targeted knock-in mouse model harboring the most common *STIM1* gain-of-function mutation R304W. Our exhaustive phenotypic characterization revealed

that the *Stim1*$^{R304W/+}$ mice recapitulate the main clinical features observed in TAM/STRMK patients including muscle weakness, thrombocytopenia, skin and eye anomalies and spleen dysfunction. We also detected increased glucose tolerance, abnormal bone architecture and abnormal immune cell counts, which all might have escaped diagnosis in TAM/STRMK patients to date. Overall, this study highlights the relevance of SOCE in several tissues and organs in normal and pathological conditions and describes a new mouse model as a valuable tool to study the physiopathology and possible therapeutic approaches for TAM/STRMK, as well as for other Ca^{2+}-related disorders involving aberrations of muscle, bones, platelets or the immune system.

Results

To address the physiological impact of SOCE over-activation, we generated a mouse model carrying the most recurrent *STIM1* gain-of-function mutation found in patients with TAM/STRMK ([8–10]). The c.910A>T (p.R304W) point mutation was introduced by homologous recombination targeting exon 7 of *Stim1* in C57BL/6N mouse embryonic stem cells to generate heterozygous *Stim1*$^{R304W/+}$ and homozygous *Stim1*$^{R304W/R304W}$ mice (Supplementary Material, Fig. S1A and B).

Viable homozygous *Stim1*$^{R304W/R304W}$ mice were not obtained at genotyping 7 days after birth, and in breeding cages containing *Stim1*$^{+/+}$ (WT, wild-type) and *Stim1*$^{R304W/+}$ animals, the statistically significant offspring ratio was 59% *Stim1*$^{+/+}$ and 41% *Stim1*$^{R304W/+}$. The absence of homozygous *Stim1*$^{R304W/R304W}$ mice and the decreased birth rate of heterozygous *Stim1*$^{R304W/+}$ animals suggest that the STIM1 R304W mutation causes embryonic or perinatal lethality especially in the homozygous state. The point mutation however did not significantly alter the STIM1 protein level in muscle, as it was comparable in WT and *Stim1*$^{R304W/+}$ tibialis anterior (TA), soleus and gastrocnemius (Supplementary Material, Fig. S1C).

The *Stim1*$^{R304W/+}$ animals underwent thorough phenotypic examinations to investigate the multi-systemic signs and symptoms of TAM/STRMK patients and to potentially uncover anomalies not reported in patients yet. Importantly, the *Stim1*$^{R304W/+}$ mice had a reduced life span with only half of the *Stim1*$^{R304W/+}$ males and females living longer than 9 months (Fig. 1A). Functional and morphological investigations were therefore carried out at 4 and 9 months to assess disease development.

Stim1$^{R304W/+}$ mice are smaller and manifest spleen enlargement

Tracking of body weight and length revealed that the *Stim1*$^{R304W/+}$ mice were smaller and lighter than the WT littermates. At 4 months of age, the body weight was reduced by 21.3% in *Stim1*$^{R304W/+}$ males and by 11.9% in *Stim1*$^{R304W/+}$ females (Fig. 1B), and body length was reduced by 7.7% in *Stim1*$^{R304W/+}$ males and by 7.2% in *Stim1*$^{R304W/+}$ females (Fig. 1C). Accordingly, patients with TAM/STRMK and STIM1 R304W mutation were described with a shorter stature ([8,9,29]). Using quantitative nuclear magnetic resonance (qNMR), we also detected a decreased lean and fat mass rate in *Stim1*$^{R304W/+}$ compared with WT mice, especially in males (Supplementary Material, Fig. S2). To investigate whether the delayed growth results from bone anomalies, we assessed the morphology of the 5th lumbar vertebra, the distal femur and the midshaft tibia by micro-CT. We detected a decreased cellular density, a reduced bone
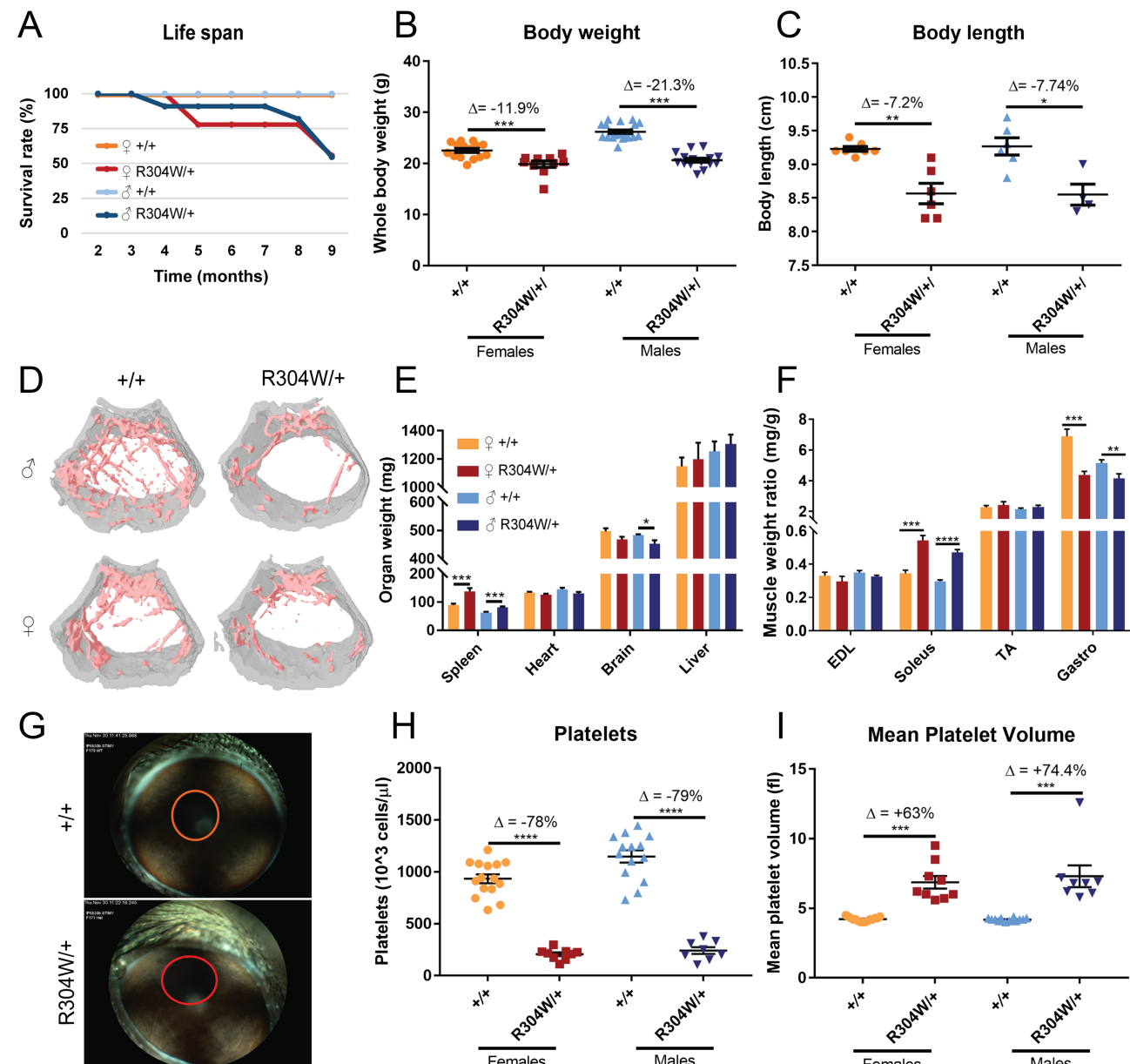
Figure 1. $Stim1^{R304W/+}$ mice manifested a multi-systemic phenotype. **(A)** Survival rate shows a decrease of 50% for $Stim1^{R304W/+}$ mice at 9 months (n = 9–11). **(B and C)** At 4 months, whole-body weight and size of $Stim1^{R304W/+}$ mice were significantly reduced compared with controls. **(D)** 3D representations illustrating the abnormal trabecular microarchitecture (in pink) in the distal femur of 4-month-old $Stim1^{R304W/+}$ mice. **(E)** Spleen enlargement was evident in 4-month-old $Stim1^{R304W/+}$ mice, while heart, brain and liver weight were normal (n = 3–19). **(F)** Relative muscle weight at 4 months revealed hypertrophy of the soleus and hypotrophy of the gastrocnemius from $Stim1^{R304W/+}$ mice, while EDL and TA were comparable to the controls (n = 6–14). **(G)** Representative pupil orientation at 4 months showed upward gaze paresis in $Stim1^{R304W/+}$ mice. **(H and I)** Blood counts revealed a reduced platelet number and an increased mean platelet volume in $Stim1^{R304W/+}$ mice (n = 8 − 15).

marrow area and abnormal mechanical properties with a 10% decrease of polar moment of inertia (MOI), indicating a reduced strength and stiffness of the bones of $Stim1^{R304W/+}$ mice (Fig. 1D; Supplementary Material, Tables S1–S3).

We next weighed various organs, and in agreement with the reduced body size, $Stim1^{R304W/+}$ heart, brain and liver were slightly smaller and lighter or similar compared with WT littermates. We noted a significant spleen enlargement in $Stim1^{R304W/+}$ mice with an increase in spleen weight of 55% in $Stim1^{R304W/+}$ females and 31% in $Stim1^{R304W/+}$ males as compared with wild-type controls (Fig. 1E). The analysis of different lower limb muscles revealed specific weight discrepancies. While the

TA and extensor digitorum longus (EDL) were comparable in $Stim1^{R304W/+}$ and WT littermates, the $Stim1^{R304W/+}$ gastrocnemius was hypotrophic with a 36.6% weight reduction in $Stim1^{R304W/+}$ females and a 19.3% reduction in $Stim1^{R304W/+}$ males, while the soleus was hypertrophic with an increased weight of 57.3% in $Stim1^{R304W/+}$ females and 58.4% in $Stim1^{R304W/+}$ males (Fig. 1F).

$Stim1^{R304W/+}$ mice manifest upward gaze paresis, thrombocytopenia and skin anomalies

We assessed a potential eye phenotype in $Stim1^{R304W/+}$ mice using a slit lamp. Although a miosis was not apparent, we
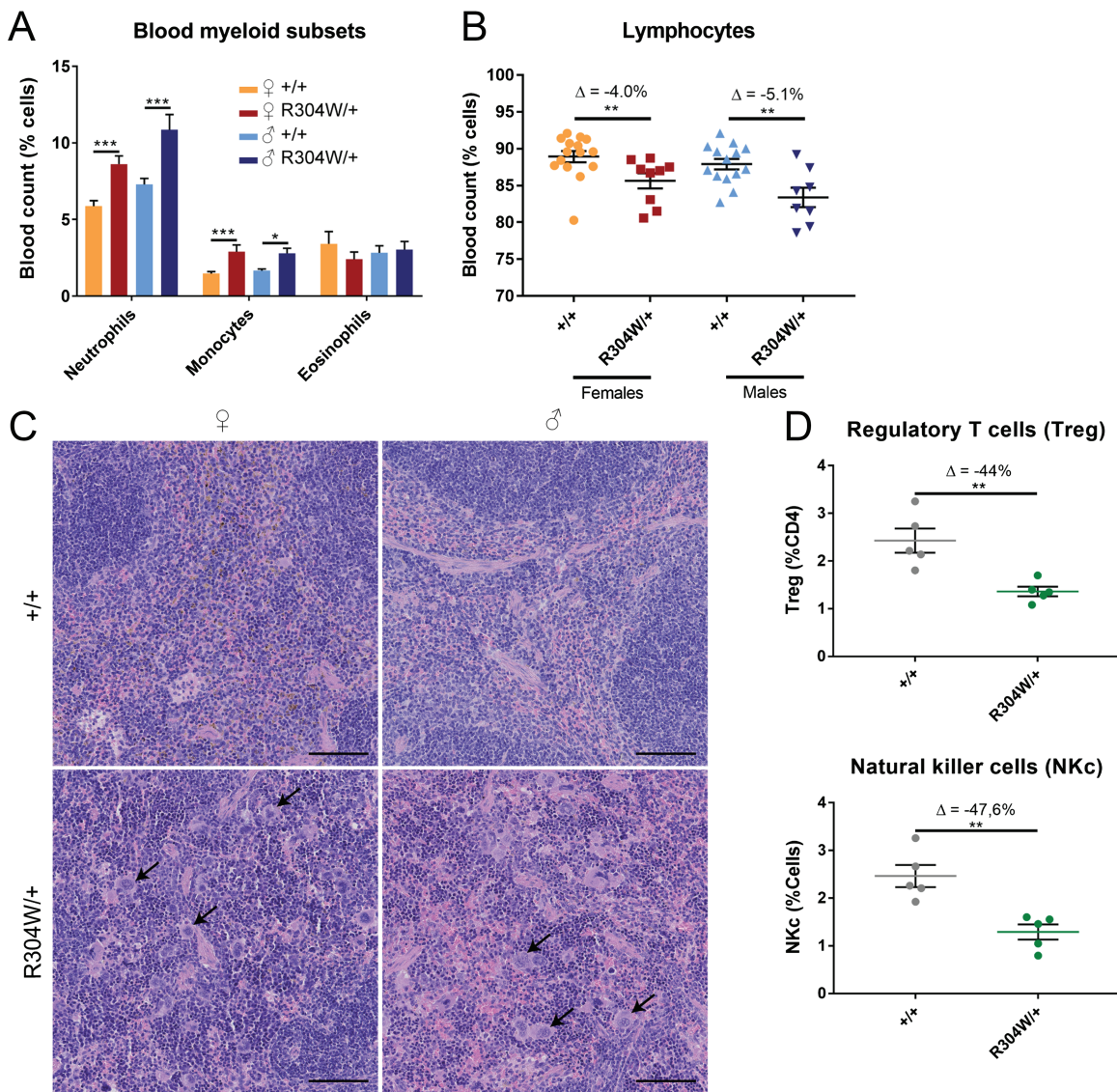
Figure 2. Abnormal immune system in *Stim1*[R304W/+] mice. **(A and B)** Blood counts at 4 months disclosed increased neutrophils and monocytes and decreased lymphocytes in *Stim1*[R304W/+] mice compared with controls (n = 8–15). **(C)** H&E staining on spleen sections revealed megakaryocyte hyperplasia (dark arrows) in *Stim1*[R304W/+] mice at 4 months. **(D)** Compared with controls, Treg and nuclear killer cells (NKcs) were decreased in *Stim1*[R304W/+] spleen at 4 months (n = 5).

noted an upward gaze paresis (Fig. 1G), a limitation of eye movement described in TAM/STRMK patients (7,14). Both *Stim1*[R304W/+] males and females manifested prolonged bleeding times, and blood counts showed a marked reduction of platelets of 78% in *Stim1*[R304W/+] females and 79% in *Stim1*[R304W/+] males compared with control littermates (Fig. 1H). The platelets were significantly bigger in the knock-in animals with an increase of mean platelet volume of 63% in *Stim1*[R304W/+] females and 74.4% in *Stim1*[R304W/+] males. Bleeding diathesis is also commonly seen in TAM/STRMK patients and was shown to result from abnormal platelet structure and function (8,9,14,19).

Patients with TAM/STRMK also often manifest ichthyosis (8,9,19), and accordingly we observed skin irritations in *Stim1*[R304W/+] mice. Histological skin analyses revealed an enlarged dermis and a reduced fat layer compared with the wild-type controls, conforming the qNMR data showing a decreased lean and fat mass rate in *Stim1*[R304W/+] mice (Supplementary Material, Fig. S3) and potentially corresponding to the skin phenotype in TAM/STRMK patients and mice.

The *Stim1*[R304W/+] mice manifest abnormal immune cell counts

SOCE plays a pivotal role in the proliferation and activation of T and B cells, and suppressed Ca^{2+} entry resulting from *STIM1* or *ORAI1* loss-of-function mutations has been associated with life-threatening immunodeficiency (5,6).

To investigate the impact of the STIM1 R304W gain-of-function mutation on the immune system, we quantified the hematopoietic cells in the blood and detected increased numbers of neutrophils and monocytes and decreased numbers of total lymphocytes in *Stim1*[R304W/+] mice compared with WT littermates (Fig. 2A and B), and we obtained similar results in spleen (Supplementary Material, Fig. S4). Histological investigations on *Stim1*[R304W/+] spleen revealed megakaryocyte hyperplasia (Fig. 2C). Of note, further analyses uncovered a significant reduction of regulatory T cells (Treg) and natural killer cells in *Stim1*[R304W/+] spleen (Fig. 2D; Supplementary Material, Fig. S4). Treg modulate the immune system and maintain the

tolerance to self-antigens to prevent auto-immune disorders. Our findings of regulatory T cell reduction might therefore indicate an over-active immune system in *Stim1*[R304W/+] mice.

Stim1[R304W/+] mice exhibit reduced muscle force and delayed muscle relaxation

In the open field test, especially the *Stim1*[R304W/+] females covered less distance and moved with lower pace compared with WT littermates (Fig. 3A). To assess whether this difference results from impaired coordination or abnormal muscle force or fatigue, we performed a series of physiological tests.

Both *Stim1*[R304W/+] and WT littermates performed similarly on the rotarod, indicating that the balance, motor coordination and ability for short-duration exercise are not significantly altered in knock-in animals (Fig. 3B). Plethysmography essentially revealed comparable breathing values between *Stim1*[R304W/+] and WT littermates with exception of an enhanced pause suggesting partial bronchial obstruction in the knock-in animals (Supplementary Material, Table S4). However, grip strength and hanging time were significantly reduced in *Stim1*[R304W/+] mice (Fig. 3C and D). Compared with the WT littermates, the four-paw grip strength was reduced by 18.7% in female *Stim1*[R304W/+] mice and by 27.3% in male *Stim1*[R304W/+] mice. The majority of WT mice successfully accomplished the 60 s hanging test, and all sustained for at least 46 s. In contrast, female *Stim1*[R304W/+] mice fell after 20 s in average, and male *Stim1*[R304W/+] mice after 17 s, which corresponds to a reduction of hanging time of 64.4% and 70.8%, respectively.

To further investigate the muscle phenotype, we quantified the *in situ* muscle force and resistance to fatigue of the TA from 9-month-old *Stim1*[R304W/+] mice using the Aurora force transducer. Following sciatic nerve stimulation, especially *Stim1*[R304W/+] males manifested a significantly reduced maximal and specific force compared with WT littermates. While WT mice developed an average specific force of 14.7 mN/mg, female *Stim1*[R304W/+] mice reached 14.3 mN/mg and male *Stim1*[R304W/+] mice 11.3 mN/mg (−23.7%) (Fig. 3E). We obtained similar results by direct stimulation of the muscle, demonstrating that the nerve-to-muscle signal transmission is not altered (Supplementary Material, Fig. S5).

Noteworthy, we observed a shift in muscle relaxation subsequent to stimulation in *Stim1*[R304W/+] compared with WT TA (Fig. 3E). We therefore applied a continuous stimulation of the sciatic nerve and quantified the decrease of force over time (Fig. 3F). We observed that the specific force of WT mice drops to 50% after 11.6 s in average, and after 17.7 s in case of *Stim1*[R304W/+] mice, representing an increased time to fatigue. We also noted that the *Stim1*[R304W/+] mice developed maximal specific force at lower stimulation frequencies compared with WT mice (Supplementary Material, Fig. S6). Taken together, our force transducer experiments revealed that *Stim1*[R304W/+] TA contracted at lower stimulation frequencies, produced less force at higher stimulation frequencies and relaxed with delay in comparison with WT controls, demonstrating that the STIM1 R304W mutation affects both muscle contraction and muscle relaxation.

Stim1[R304W/+] mice do not show tubular aggregates in muscle fibers

Tubular aggregates represent the main histopathological hallmark in skeletal muscle from TAM/STRMK patients. These central or subsarcolemmal basophilic accumulations appear in red on modified Gomori trichrome staining, and in dark blue on nicotinamide adenine dinucleotide-tetrazolium reductase staining especially in fast-twitch type II fibers (11,30). Additional features as fiber size variability, internalized nuclei, endomysial fibrosis, type I fiber predominance and type II fiber atrophy are consistently seen as well (7,12,13,15,16,19,31–33).

Histological analyses of TA sections from *Stim1*[R304W/+] mice at 4 and 9 months, and of EDL, soleus and gastrocnemius muscles at 4 months revealed a 4–8-fold increase of internalized nuclei, fibrosis and infiltration of inflammatory cells, but tubular aggregates were not detected (Fig. 4A; Supplementary Material, Figs S7–S12). We also noticed an altered fiber-type composition with an increased ratio of slow-twitch type I fibers in all analyzed muscles. To investigate fiber size, we measured the Min-Feret diameter and uncovered a slight reduction in *Stim1*[R304W/+] TA fiber caliber in males compared with WT littermates at 4 months of age (Fig. 4B), while no difference was seen in females (Supplementary Material, Fig. S13A). We also noted a subset of fibers with abnormal shape on the *Stim1*[R304W/+] TA, EDL, soleus, gastrocnemius muscle sections and circularity measurements on TA sections confirmed a tendency of increased rounded fibers in both male and female *Stim1*[R304W/+] mice (Fig. 4C; Supplementary Material, Fig. S13B). Alizarin red staining demonstrated that the 4–7% of rounded fibers contain high amounts of Ca^{2+} (Fig. 4A; Supplementary Material, Figs S7 and S9–S11), indicating that these fibers are damaged.

Ultrastructural analyses on transversal and longitudinal *Stim1*[R304W/+] TA sections uncovered swollen mitochondria at both 4 and 9 months of age in largely intact muscle fibers and confirmed the absence of tubular aggregates (Fig. 4D; Supplementary Material, Fig. S14).

Stim1[R304W/+] mice manifest blood hypocalcemia and increased Ca^{2+} influx in skeletal muscle

In view of the abnormal contraction and relaxation properties of *Stim1*[R304W/+] muscle, and the histological findings of fibers with elevated Ca^{2+} content, we next focused on the Ca^{2+} level in blood and skeletal muscle. This is of particular importance, as TAM/STRMK patients were commonly reported with blood hypocalcemia (8–10,12,13,15,19), and functional investigations demonstrated that the STIM1 gain-of-function mutations induce excessive Ca^{2+} entry in patient myoblasts through SOCE overactivation (7,16).

We measured decreased Ca^{2+} levels and consequently increased phosphate levels in the blood from *Stim1*[R304W/+] mice (Fig. 5A). We also detected a 6–8-fold increase of serum creatine kinase (CK; Supplementary Material, Fig. S15), residing within the range of typical CK elevation in TAM/STRMK patients (7,9,12). In addition, we found altered hepatic enzyme activities (Supplementary Material, Fig. S16A) and increased insulin and decreased glucose levels in accordance with increased glucose tolerance (Supplementary Material, Fig. S16B and C). It has recently been demonstrated that the inhibition of SOCE has an adverse effect and results in impaired insulin secretion from pancreatic islets and systemic glucose intolerance (34,35). Together with our data, it illustrates that tight Ca^{2+} regulation is essential for ß-cell function and that abnormal SOCE directly impacts on insulin secretion and the glucose level in blood.

We next assessed Ca^{2+} homeostasis in cultured myotubes obtained by differentiation of myoblasts from *Stim1*[R304W/+] and WT mice. At physiological 2 mM Ca^{2+} conditions in the medium,
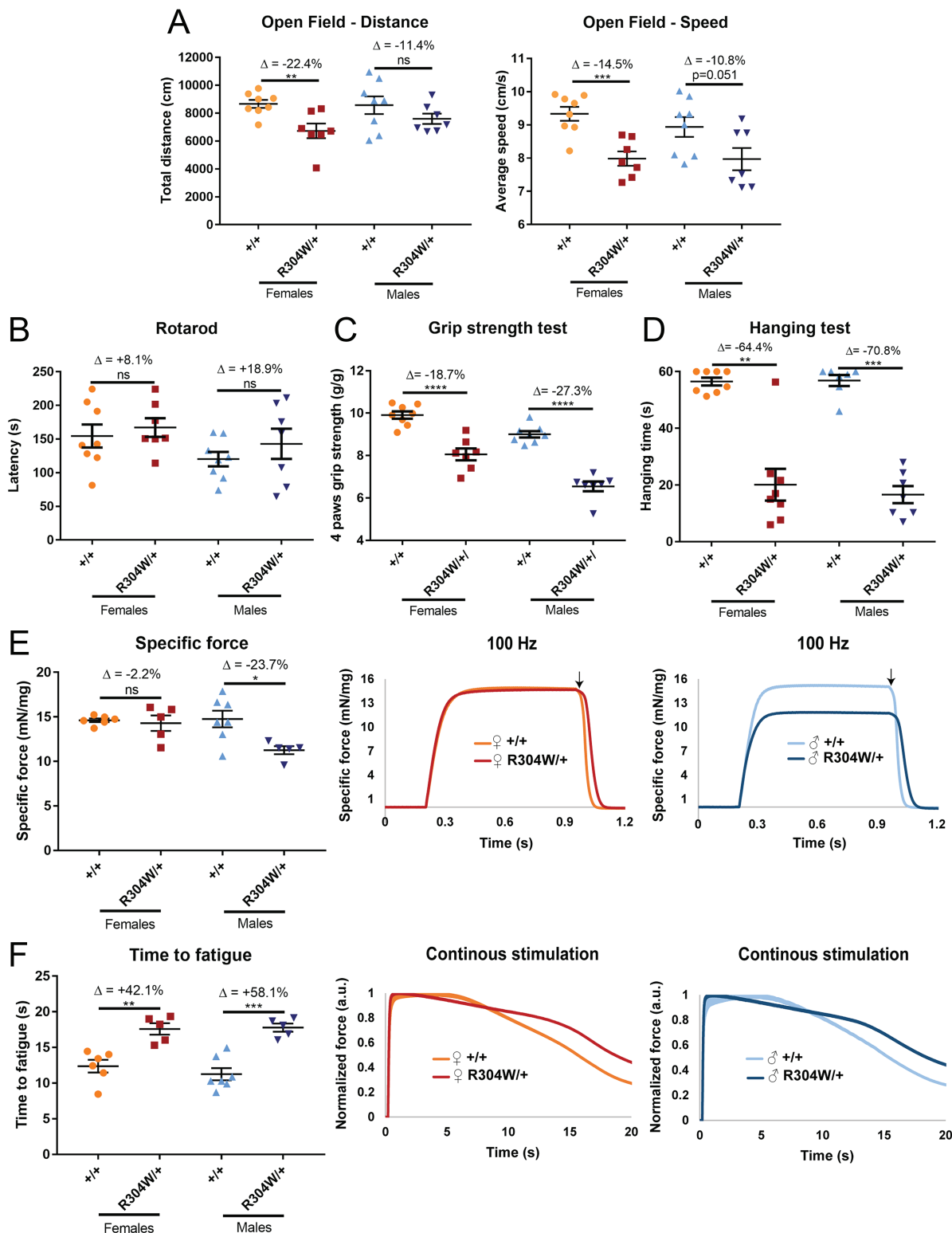
Figure 3. *Stim1*[R304W/+] mice produced less force and exhibited delayed muscle relaxation. **(A)** The open field test at 9 weeks of age revealed a reduction in speed and covered distance for *Stim1*[R304W/+] mice compared with WT controls. **(B)** The Rotarod test at 9 weeks of age did not reveal coordination differences between *Stim1*[R304W/+] and WT mice. **(C and D)** *Stim1*[R304W/+] mice had less grip strength and showed reduced hanging time compared with controls. **(E)** TA force measurements at 9 months (left) and representative traces revealed reduced specific force of *Stim1*[R304W/+] males, while *Stim1*[R304W/+] females were comparable with controls. Both *Stim1*[R304W/+] males and females showed a delay in force decrease subsequent to stimulation (right). **(F)** At 9 months, *Stim1*[R304W/+] TA exhibited an increased time to fatigue upon continuous stimulation (left). Representative traces over 20 s illustrate the slower force decrease of *Stim1*[R304W/+] mice compared with controls (middle and right).
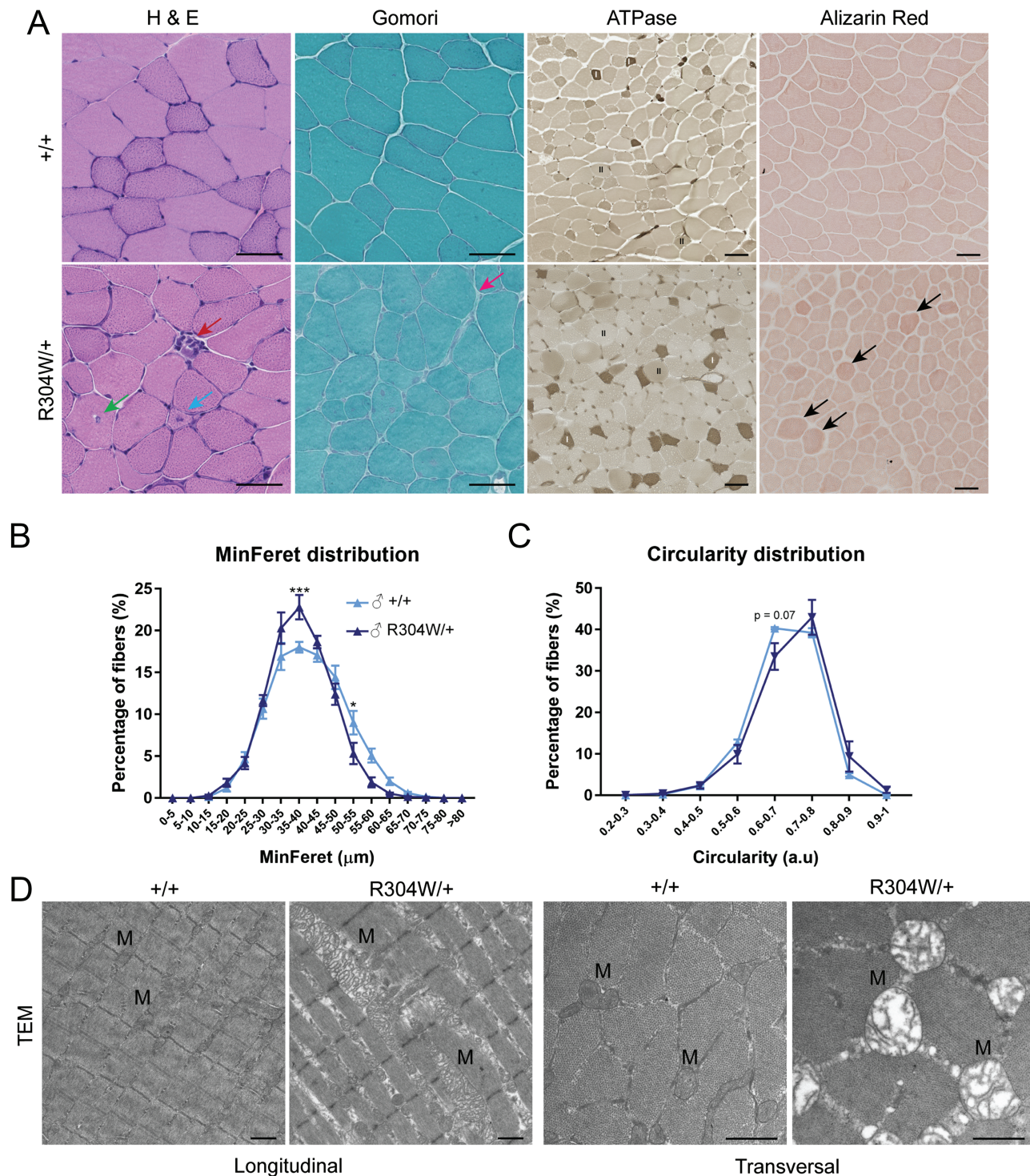
Figure 4. *Stim1*$^{R304W/+}$ muscle histology showed dystrophic features, but no tubular aggregates. **(A)** H&E, Gomori trichrome, ATPase and Alizarin red staining of transverse TA sections at 4 months revealed internalized nuclei (green arrow), regenerating fibers (blue arrow), infiltration of inflammatory cells (red arrow), fibrosis (pink arrow), higher proportion of dark type I fibers and rounded fibers with intense Ca^{2+} signals (black arrows) in *Stim1*$^{R304W/+}$ mice (scale bar = 50 μm). **(B)** MinFeret distribution showed a reduced proportion of large fibers (>50 μm) in *Stim1*$^{R304W/+}$ TA at 4 months (n = 4, 1900 fibers/mice in average). **(C)** Circularity distribution revealed a higher proportion of rounded TA fibers in *Stim1*$^{R304W/+}$ mice at 4 months. Circularity ranges from 0 a.u. (line) to 1 a.u. (circle). **(D)** Electron microscopy on longitudinal (left) and transversal (right) TA sections at 9 months revealed swollen mitochondria in *Stim1*$^{R304W/+}$ mice (scale bar = 2 μm).

the *Stim1*$^{R304W/+}$ myotubes exhibited increased resting Ca^{2+} levels compared with WT myotubes (Fig. 5B). In a second experiment, we kept the myotubes in Ca^{2+}-free media, and administration of 10 mм Ca^{2+} to the medium induced a significantly

more pronounced Ca^{2+} influx in myotubes from *Stim1*$^{R304W/+}$ as compared with the control (Fig. 5C and D). Using a combination of caffeine and thapsigargin to maximally deplete the Ca^{2+} stores, we found that the Ca^{2+} content in the reticulum was
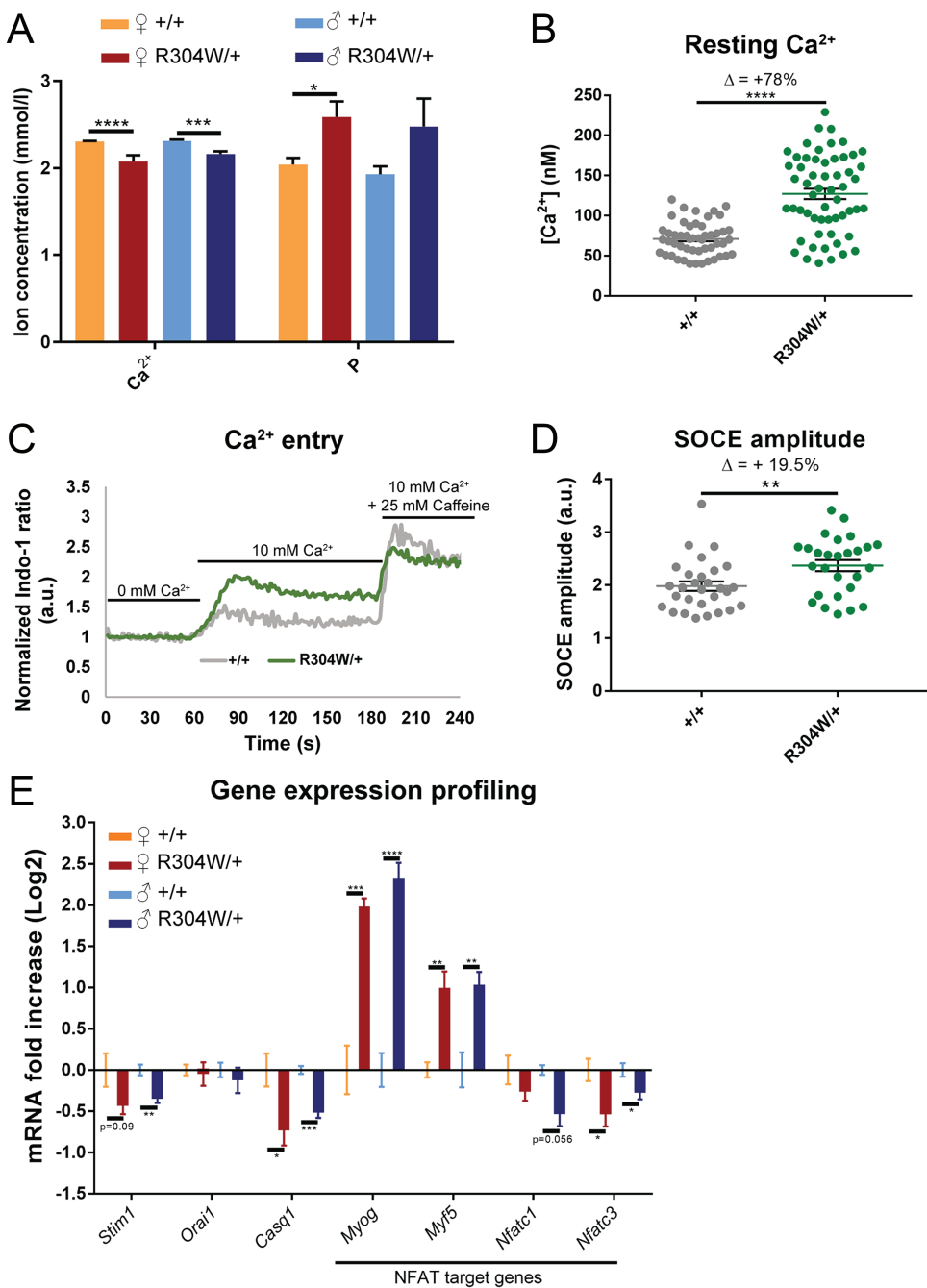
Figure 5. Abnormal Ca^{2+} homeostasis in $Stim1^{R304W/+}$ mice. **(A)** Blood analyses revealed hypocalcemia and hyperphosphatemia in $Stim1^{R304W/+}$ mice at 4 months ($n = 6–15$). **(B)** Ca^{2+} measurements revealed increased resting Ca^{2+} in differentiated myotubes from $Stim1^{R304W/+}$ mice compared with controls (left, $n = 51–57$ from 5 to 6 mice per genotype). **(C)** Mean normalized Indo-1 ratio measurements over time demonstrated an increased extracellular Ca^{2+} entry in $Stim1^{R304W/+}$ myotubes upon addition of 10 mM Ca^{2+} to the medium. Subsequent addition of caffeine confirmed the differentiation state of the myotubes (left, $n = 27–29$ from 5 to 6 mice per genotype). **(D)** SOCE amplitude, representing the maximal Indo-1 ratio following addition of Ca^{2+}, was increased in $Stim1^{R304W/+}$ myotubes compared with WT controls (right, $n = 27–29$ from 5 to 6 mice per genotype). The Indo-1 fluorescence ratio of the $Stim1^{R304W/+}$ myotubes was normalized to the WT baseline to highlight the relative differences in SOCE amplitude. **(E)** Logarithmic illustration of gene expression shows downregulation of the Ca^{2+} regulators $Stim1$ and $Casq1$ and upregulation of the NFAT target genes $Myog$ and $Myf5$ in $Stim1^{R304W/+}$ TA at 4 months compared with controls ($n = 5$).

comparable in WT and $Stim1^{R304W/+}$ myotubes (Supplementary Material, Fig. S17). Taken together, the $Stim1^{R304W/+}$ myotubes exhibited increased resting Ca^{2+} levels and increased extracellular Ca^{2+} influx, while Ca^{2+} storage was not affected.

To investigate the downstream effects of excessive Ca^{2+} influx, we scaled the expression of the SOCE genes $Stim1$

and $Orai1$, as well as of $Casq1$ and selected skeletal muscle genes regulated by the Ca^{2+}-dependent transcription factor NFAT. Quantitative RT(reverse transcription)-qPCR on TA from $Stim1^{R304W/+}$ mice revealed a downregulation of $Stim1$ in males but not in females, of $Nfatc1$ and $Nfatc3$ and an upregulation of the myogenic differentiation markers $Myog$ and $Myf5$ (Fig. 5E).

We also noted a reduced expression of *Casq1* in *Stim1*[R304W/+] TA. *Casq1* is however specifically expressed in type II fibers, and the abnormal composition of the *Stim1*[R304W/+] TA with an increased ratio of type I fibers most probably accounts for the seemingly downregulation of *Casq1*.

Overall, these data demonstrate that the STIM1 R304W mutation induces excessive Ca²⁺ influx in skeletal muscle and leads to partial muscle fiber degeneration involving elevated serum CK levels and the upregulation of muscle differentiation factors, conforming to the dystrophic features observed on muscle sections.

Discussion

Ca²⁺ serves as a second messenger in a variety of biological processes in both excitable and non-excitable cells. SOCE is a primary mechanism regulating extracellular Ca²⁺ entry, and abnormal SOCE leads to severe human disorders. Insufficient SOCE resulting from *STIM1* or *ORAI1* loss-of-function causes immunodeficiency, while overactive SOCE resulting from *STIM1* or *ORAI1* gain-of-function causes TAM/STRMK (1). To elucidate the physiological effect of STIM1 over-activation, we generated a mouse model harboring the most common STIM1 gain-of-function mutation R304W. The *Stim1*[R304W/+] mice phenotypically mimicked TAM/STRMK, and we also discovered additional characteristics of high medical importance that have not been reported for TAM/STRMK patients yet. With a main focus on skeletal muscle, our in-depth investigations on the *Stim1*[R304W/+] mouse provides a first insight into the pathomechanisms resulting from SOCE over-activation and leading to Ca²⁺-related physiological dysfunction.

The *Stim1*[R304W/+] mouse as a tool to study TAM/STRMK and SOCE over-activation

TAM and STRMK are clinically overlapping multi-systemic disorders characterized by muscle weakness, miosis, thrombocytopenia, hyposplenism, short stature, ichthyosis and dyslexia (29). In agreement with the clinical presentation of TAM/STRMK patients, the *Stim1*[R304W/+] mice were smaller than the control littermates and manifested muscle weakness, thrombocytopenia, spleen dysplasia and skin irritations, demonstrating that our mouse model is a suitable and valuable tool to study the physiopathology and the disease development of TAM/STRMK. In line with the reported Ca²⁺ overload and excessive Ca²⁺ influx in myoblasts and myotubes from TAM/STRMK patients (7,16), we measured hypocalcemia in the blood and elevated resting Ca²⁺ levels in *Stim1*[R304W/+] myotubes, as well as SOCE over-activation and excessive extracellular Ca²⁺ entry without prior Ca²⁺ store depletion. This confirms that the muscle dysfunction and most probably also the multi-systemic aberrations of TAM/STRMK are a direct consequence of abnormal Ca²⁺ homeostasis and demonstrates that our *Stim1*[R304W/+] mouse can serve as a model to investigate the consequences and treatment options of overactive SOCE in Ca²⁺-related disorders. Noteworthy, another Stim1[R304W] mouse model has been generated in parallel (36). In contrast to our model, STIM1 was however downregulated in skeletal muscle, Ca²⁺ handling and force production were comparable in Stim1[R304W] and WT muscle fibers, and the authors did not report a multi-systemic phenotype affecting the eye, spleen, skin, bones, or the immune system in heterozygous animals.

Impact of SOCE over-activation on muscle contraction and relaxation

The STIM1 R304W mutation was previously shown to induce excessive extracellular Ca²⁺ entry through a dual pathogenic effect; it induces constitutive STIM1 and SOCE activation and suppresses fast inactivation of the ORAI1 Ca²⁺ entry channel (10,21). Accordingly, we observed higher resting Ca²⁺ levels as well as excessive extracellular Ca²⁺ entry despite replete Ca²⁺ stores in myotubes from *Stim1*[R304W/+] mice. In resting skeletal muscle, cytosolic Ca²⁺ concentrations are low and vary between 30 and 60 nM depending on the fiber type (37), and small Ca²⁺ level changes induce major physiological processes. Ca²⁺ release from the sarcoplasmic reticulum triggers muscle contraction and the generation of force, repeated contractions require the maintenance of high Ca²⁺ gradients and the strict regulation of luminal and cytosolic Ca²⁺ balance and muscle relaxation occurs when Ca²⁺ is removed from the contractile unit (38). The *Stim1*[R304W/+] mice manifested reduced muscle force as well as abnormal muscle contraction and relaxation, all three presumably resulting from aberrant Ca²⁺ homeostasis. The elevated resting cytosolic Ca²⁺ levels in *Stim1*[R304W/+] muscle provoked rapid fiber contraction, diminished the effect of high stimulation frequencies on force production and also extended the relaxation time. The delayed muscle relaxation might thereby explain the muscle cramping phenotype observed in a large number of TAM/STRMK patients (8,10–13,17,19,31,39). The high resting Ca²⁺ levels most probably also account for the swollen mitochondria and the dystrophic features observed in *Stim1*[R304W/+] muscle. Histological analyses revealed rounded and Ca²⁺-rich fibers, typically seen to a larger extent in dystrophies involving major fiber degeneration and regeneration (40). Accordingly, we observed a subset of regenerating fibers in *Stim1*[R304W/+] muscle, increased expression of the myogenic regulatory factors *Myf5* and *Myog* (41), as well as 6–8-fold increased serum CK levels, demonstrating intensified muscle fiber degeneration and myogenesis in *Stim1*[R304W/+] mice.

The role of tubular aggregates in disease development

Histological analyses of muscle biopsies from TAM/STRMK patients typically show basophilic accumulations in the muscle fibers appearing in red on modified Gomori trichrome staining and corresponding to densely packed membrane tubules (7–11). Tubular aggregates also naturally accumulate in normal murine muscle with age and can especially be seen in type II fibers from 10 months in most laboratory mice strains (42).

Surprisingly, analyses of different muscles failed to detect tubular aggregates in the *Stim1*[R304W/+] mice at different time points and up to 9 months. Given the explicit and multi-systemic TAM/STRMK phenotype developed by *Stim1*[R304W/+] mice, we conclude that physiological differences between humans and mice most probably account for the presence or absence of tubular aggregates in pathologic skeletal muscle and that tubular aggregate formation and disease-related muscle dysfunction are not causally linked. This of particular importance for potential therapeutic approaches since tubular aggregates do not represent suitable therapeutic targets and cannot serve as readouts to assess treatment efficacy.

It is conceivable that the abundant tubular aggregates in the muscle fibers of TAM/STRMK patients do not impair muscle function, but rather exert a protective role and prevent fiber degeneration by trapping excessive Ca²⁺. In compliance, signs of dystrophic-like fiber degeneration are more prominent in

muscle from $Stim1^{R304W/+}$ mice compared with muscle from TAM/STRMK patients.

Impact of the STIM1 R304W mutation on coagulation and the immune system

The bleeding diathesis observed in many TAM/STRMK patients results from abnormal platelet number, structure and function. It could be shown that the TAM/STRMK platelets display increased basal Ca^{2+} levels prior to activation, leading to diminished response to stimulation and reduced platelet–platelet adhesion (8,9,14,19). Thrombocytopenia with a reduced platelet number resulting in prolonged bleeding times was also seen in our $Stim1^{R304W/+}$ mice. We additionally observed an increased mean platelet volume, considered as a marker for diverse inflammatory diseases (43–45).

The immune system provides protection against various disease-causing pathogens and is based on a complex interplay between different effector cells with specialized function. T helper 17 cells (Th17) are pro-inflammatory cells recruiting neutrophils to the sites of infection, whereas Treg have an antagonistic effect and inhibit immune response. The balance between Th17 and Treg cells is therefore critical for the development of autoimmune and inflammatory diseases (46). The $Stim1^{R304W/+}$ mice displayed a significant reduction of Treg cells and a simultaneous upregulation of neutrophils and monocytes, suggesting an imbalance of Th17 and Treg, promoting the maintenance of inflammation. Indeed, the $Stim1^{R304W/+}$ mice showed multiple signs of inflammation as infiltration of inflammatory cells in muscle, increased mean platelet volume, spleen hyperplasia, bronchial obstruction, and enlarged dermis. Ichthyosis has often been described in TAM/STRMK patients (8,9,19), but detailed investigations on skin biopsies have not been performed. The $Stim1^{R304W/+}$ mice manifested a skin phenotype as well, and our findings point to an underlying inflammatory disease causing the urticarial eruptions. Noteworthy, the $Stim1^{Sax}$ mouse, harboring another $Stim1$ gain-of-function mutation, similarly displayed spleen enlargement and increased platelet size (28), and additional signs of inflammation might be more discreet due to the milder mutational effect of the Stim1 D84G mutation compared with R304W.

Impact of the STIM1 R304W mutation on growth and lifespan

Here we show that the $Stim1^{R304W/+}$ mice manifest an abnormal architecture of cortical and trabecular bones, resulting in diminished mechanical properties and bone strength. It has previously been reported that mice lacking ORAI1 are smaller than control littermates, which partially results from deficient bone development (47,48). It could be demonstrated that impaired SOCE in precursor cells of both osteoblasts and osteoclasts leads to reduced differentiation and consequently to decreased bone density (47,48). This suggests that normal bone physiology strongly depends on strict SOCE regulation and that bone anomalies resulting from insufficient or overactive SOCE compromise bone stability and growth.

A striking feature of the $Stim1^{R304W/+}$ mouse is the reduced life span. We did not observe any correlation between the overall health status or the physical performances of the $Stim1^{R304W/+}$ mice and the time of death, and we did not note specific behavioral anomalies preceding death. The discrepancy in body weight and size and in motor performances between WT and $Stim1^{R304W/+}$ mice increases with time, and only 50% of the $Stim1^{R304W/+}$ mice live longer than 9 months. We also detected spleen and bone anomalies, indications for an inflammatory disease, and we found evidence for abnormal hepatic function and glucose metabolism. The totality of these signs might reflect an accelerated aging process or might be the result of multi-organ deterioration due to continuous Ca^{2+} stress. Premature mortality and a subset of the multi-systemic murine phenotypes including bone, metabolic or immune system anomalies have not been reported for TAM/Stormorken patients yet, but may currently be unrecognized due to the recent discovery of the causative genes and the respective possibilities of molecular diagnosis. Regular clinical examinations and an extended follow-up of multiple organs and tissues are therefore of major medical importance for TAM/STRMK patients.

SOCE insufficiency and over-activation cause mirror diseases

$STIM1$ and $ORAI1$ mutations have been associated with different human disorders depending on the mutational impact and the mode of inheritance. Recessive $STIM1$ and $ORAI1$ loss-of-function mutations induce severe immunodeficiency characterized by early-onset and recurrent infections, autoimmunity, muscular hypotonia and ectodermal dysplasia (1). Functional investigation demonstrated that the mutations abolished SOCE either through STIM1 or ORAI1 loss, impaired STIM1-ORAI1 interaction or through ORAI1 channel impermeability, and the profound inhibition of Ca^{2+} influx in T cell, B cells and myofibers are the primary cause of the immune system and muscle dysfunction observed in the patients (5,6,49–54). In contrast, dominant $STIM1$ and $ORAI1$ gain-of-function mutations induce TAM/STRMK, and SOCE over-activation is presumably responsible for the multi-systemic phenotype encompassing muscle weakness, miosis, thrombocytopenia, hyposplenism, ichtyosis, short stature and dyslexia (7–10,12–14,17,19).

Despite the opposite mutational impact, SOCE insufficiency or SOCE over-activation involving Ca^{2+} imbalance can have a similar effect on different tissues as shown by platelet dysfunction and prolonged bleeding times, muscle weakness, reduction of Treg and abnormal bone architecture in $Stim1^{-/-}$ (23), $Orai1^{-/-}$ (47,48) or $Stim1^{R304W/+}$ mice (this study).

Concluding remark

In conclusion, the present study significantly contributes to a better understanding of the pathomechanisms leading to TAM/STRMK and our mouse model proved to be a valuable tool to investigate the pathophysiological consequences of SOCE over-activation and aberrant Ca^{2+} homeostasis in various cells, tissues and organs, associated with a plurality of rare and common human disorders.

Materials and Methods

Animal care and generation of the $Stim1^{R304W/+}$ mouse model

Animal care and experimentation was in accordance with French and European legislation and approved by the institutional ethics committee (project numbers 2016031110589922, 2016040511578546 and 2017092717177977). Mice were housed

in ventilated cages with free access to food and water in temperature-controlled rooms with 12 h day light/dark cycles.

The *Stim1*$^{R304W/+}$ (*Stim1*^{tm3Ics}) mutant mouse line was established at the Institut Clinique de la Souris (http://www.ics-mci.fr/en/). In brief, C57BL/6N mouse embryonic stem (ES) cells were electroporated with a targeting vector carrying the A>T transversion at cDNA position 910 (NM_009287.5) and a floxed neomycin resistance cassette with an auto-excision transgene. Following G418 selection, the clones were analyzed by long-range PCR (polymerase chain reaction) and southern blot using an internal neomycin probe and an external 5′ probe. The selected ES clone was karyotyped and micro-injected into BALB/C blastocysts. Resulting male chimeras were bred with WT C57BL/6N females, and germline transmission with direct excision of the selection cassette was achieved in the first litter. Genotyping was performed with the following primers: GCAGGTAGGAGAGTGTACAGGATGCCTT (forward, Ef) and CTTTCCATCCCCACTGCCATTTT (reverse, Er). Sequencing primers were CAGGAGGAGCACCGAACTGTGGAA (forward, Mf) and TTACGCACCGCCCAAGGCAT (reverse, Nr).

Open field, rotarod, grip test and hanging test

The open fields (Panlab, Barcelona, Spain) were placed in a homogeneously illuminated room and virtually divided into central and peripheral areas. Each mouse was placed in the periphery and allowed to freely explore the field for 20 min, with the experimenter out of the animal's sight. The covered distance and the average speed of moving were recorded.

The coordination of the animals was measured using a Rotarod apparatus (Bioseb, Vitrolles, France) with an accelerating scale from 4 to 40 rpm. The four-paw grip strength was assessed with a dynamometer (Bioseb), and for the hanging test, mice were suspended on a cage lid for up to 60 s and the time to fall was recorded.

Pupillary reflex and pupil imaging

The pupillary light reflex was examined on restrained mice using a SL990 slit lamp biomicroscope (CSO, Florence, Italy) at $16\times$ magnification using broad beam illumination and varied back and forth from the minimal to the highest intensity setting. For pupil imaging, mice were anesthetized with isofluorane (2% in a 50/50 mix of air and O_2 at 0.4 ml/min), the corneas were covered with a carbomere ophthalmic gel (TVM, Lempdes, France) and imaged with a Micron III camera equipped with the mouse lens (Phoenix Research Laboratories, Pleasanton, USA).

qNMR and bone morphology

Whole body composition of fat content, lean tissues and free body fluid was assessed with a Minispec+ analyzer (Bruker, Billerica, USA) by Nuclear Magnetic Resonance during light period on conscious fed mice.

Bone morphology was assessed on the 5th lumbar vertebra, the distal femur and the midshaft tibia using the Quantum micro-CT scanner (Perkin Elmer, Waltham, USA). All scans were performed with an isotropic voxel size of 10 μm, 160 μA tube current and 90 kV tube voltage. Gray scale images were preprocessed using the ImageJ software, and morphological 3D measurements were further performed using the CTAn software (Bruker). For the 5th lumbar vertebra and the distal femur, the analysis included bone volume fraction and trabecular thickness, number and separation. For the tibia midshaft, the analysis

included measures of cortical thickness, bone area fraction, total area, bone area, marrow area and polar MOI. Representative images were created by using the CTvol software (Bruker).

Metabolic studies and blood counts

Blood chemistry was assessed following retro-orbital puncture under isoflurane anesthesia to determine glucose, Ca^{2+}, phosphor (P), transaminases (ASAT, ALAT), CK and alkalin phosphatase (ALP) levels using the OLYMPUS AU-400 automated laboratory work station (Beckmann Coulter, Brea, USA) with kits and controls supplied by Beckmann Coulter, Wako Chemical Inc (Richmond, USA) or Randox Laboratories (Crumlin, UK). Insulin was measured on a BioPlex analyzer (BioRad, Hercules, USA) using the Mouse Metabolic Magnetic bead panel kit (Merck, Darmstadt, Germany). Blood counts were performed on the ADVIA 120 system (Siemens, Munich, Germany).

To assess glucose tolerance, glucose was administered by intraperitoneal injection, and blood glucose levels were measured at different time points over 120 min during the light period, and after overnight fasting using the Accu-Chek (Roche Diagnostics, Basel, Switzerland).

Immunology

Mouse spleens were collected in 1 mL sample collection buffer, transferred to a GentleMACS C tube (Miltenyi Biotec, Bergisch Gladbach, Germany) containing enzyme cocktail mix and dissociated with the GentleMACS tissue dissociator (Miltenyi Biotec). Cell suspensions were filtered and diluted 1:100 in Sytox green solution (ThermoFisher Scientific, Waltham, USA) and run on an ATTUNE NxT Flow Cytometer® (ThermoFisher Scientific) with 4×10^6 cells per sample and well. Red blood cells were lysed in 30 μL 1× RBC lysis buffer for 1 min at RT (room temperature), and the reaction was stopped with 250 μL FACS buffer. Fc receptors were then blocked with 100 μL 2.4G2 serum. IMPC1 and IMPC2 immunostaining was performed in 100 μL antibody cocktails and incubated in the dark for 20 min at 4°C. Finally, cell pellets were resuspended in 250 μL HBSS/2% (v/v) FCS with Sytox blue solution (ThermoFisher Scientific) for exclusion of dead cells. Samples were acquired on a SORP® BD LSR2 FORTESSA (BD Biosciences, Franklin Lakes, USA), data were compensated with BD FACS DIVA 8.0.1 software (BD Biosciences) and FCS files were run on R using Flowdensity package for automated supervised gating. Frequencies of populations were calculated as defined in https://www.mousephenotype.org/impress/protocol/174/7. Results per panel were visualized as fold change on a radar plot, frequencies were transformed in asinh and run on the TMEV software for PCA analysis, hierarchical clustering (Euclidian distance, centered linkage) or statistical tests (ANOVA, one-way analysis of variance).

In vivo muscle force and fatigue

The TA is well characterized and suitable for force measurements, and the TA contraction properties were assessed *in situ* using the Complete1300A Mouse Test System (Aurora Scientific, Aurora, Canada). Mice were anesthetized through intraperitoneal injection of domitor/fentanyl mix (2/0.28 mg/Kg), diazepam (8 mg/Kg) and domitor (0.28 mg/Kg). Knees and feet were fixed, and the distal tendon of the TA was excised and attached to the isometric transducer. The sciatic nerve or the muscle was stimulated by pulses of 1–125 Hz to measure maximal force. The specific force corresponds to the maximal force divided by the TA weight. Following a rest period of 5 min,

sciatic nerve or muscle were then stimulated at 50 Hz for 20 s and the time corresponding to a force decrease of 50% was recorded as the time to fatigue.

Histology and electron microscopy

Spleen and skin were fixed in formaldehyde and embedded in paraffin, and 5 μm sections were stained with hematoxylin and eosin (H&E) using routine protocols to assess histological anomalies. TA, EDL, soleus and gastrocnemius muscles were frozen in liquid nitrogen-cooled isopentane, and 8 μm sections were stained with H&E, ATPase (pH 4.3), modified Gomori trichrome and Alizarin red to assess muscle fiber morphology and typing, nuclear positioning, presence of tubular aggregates and Ca^{2+} deposits using the Nanozoomer 2HT slide scanner (Hamamatsu, Japan).

Fiber MinFeret distribution and circularity were determined on 8 μm TA sections stained with Hoechst (Sigma-Aldrich, St Louis, USA) and Wheat Germ Agglutinin, Alexa Fluor™ 647 conjugate (ThermoFisher Scientific) to highlight nuclei and plasma membrane. After 20 min, the sections were mounted using Fluorsave™ Reagent (Merck). The images were recorded using the Nanozoomer 2HT slide scanner (Hamamatsu) and analyzed using a homemade ImageJ plugin.

For electron microscopy, the muscles were fixed in 2.5% glutaraldehyde and 2.5% paraformaldehyde and 50 mM Ca^{2+} in cacodylate buffer (0.1 M, pH 7.4), washed in cacodylate buffer for 30 min, postfixed in 1% osmium tetroxide in 0.1 M cacodylate buffer for 1 h at 4°C and incubated with 5% uranyl acetate for 2 h at 4°C. The samples were dehydrated through graded alcohol (50%, 70%, 90% and 100%) and propylene oxide for 30 min each and embedded in Epon 812. Semithin sections were cut at 2 μm on an Leica Ultracut microtome (Leica, Wetzlar, Germany) and contrasted with toluidine blue, and ultrathin sections were cut at 70 nm and contrasted with uranyl acetate and lead citrate and examined at 70 kv with a Morgagni 268D electron microscope (FEI, Electron Optics, Eindhoven, the Netherlands). Images were captured digitally by Mega View III camera (Soft Imaging System, Münster, Germany).

Protein studies

TA, soleus and gastrocnemius cryosections were lysed in radio immunoprecipitation buffer supplemented with 1 mM PMSF and complete mini EDTA-free protease inhibitor cocktail (Roche). Protein concentrations were determined using DC™ Protein Assay kit (BioRad), and 10 μg of denatured protein samples in 5× Lane Marker Reducing Buffer (ThermoFisher Scientific) were loaded on a 10% SDS-PAGE gel containing 2,2,2-Trichloroethanol (TCE). The gel was then UV-activated for 45 s on a ChemiDoc™ Touch Imaging System (BioRad) and transferred to a nitrocellulose membrane for 7 min at 2.5 A using Transblot® Turbo™ RTA Transfer Kit (BioRad). Membranes were blocked for 1 h in Tris-buffered saline buffer containing 5% non-fat dry milk and 0.1% Tween 20. For immunofluorescence, TA cryosections were fixed and blocked with fetal calf serum. The following primary and secondary antibodies were used: rabbit anti-STIM1 (AB9870, Millipore, Burlington, USA), mouse anti-MHCI (BA-F8, DHSB, Iowa, USA), mouse anti MHCIIa (SC-71, DHSB), peroxidase-coupled goat anti-rabbit (112–036-062, Jackson ImmunoResearch, Ely, UK), Alexa Fluor 488-coupled goat anti-mouse IgG1 (115-485-205, Jackson ImmunoResearch), and Coumarin AMCA-coupled goat anti-mouse IgM (115-156-020, Jackson ImmunoRe-

search). Images were recorded with the Amersham Imager 600 (Amersham, UK) and the DMRXA2 microscope (Leica).

Expression studies

RNA from TA and soleus muscles was extracted with TRI Reagent (Molecular Research Center, Cincinnati, USA), and cDNA synthesis was performed using the SuperScript™ II Transcriptase (ThermoFisher Scientific). For quantitative PCR, the cDNA was amplified with SYBR Green Master Mix I (Roche) and 0.1 μM forward and reverse interexonic primers (Supplementary Material, Table S5), and amplicons were analyzed with a Lightcycler® 480 (Roche). Primers specificity was determined through a melting curve, and PCR products were Sanger-sequenced. Primer sequences for *Rpl27* were obtained from the literature (55).

Ca^{2+} measurements

Primary myoblasts from 5-day-old WT and $Stim1^{R304W/+}$ mice were isolated as described before (56), and non-adherent cells were collected and plated in IMDM supplemented with 20% FCS and 1% CEE (chicken embryo extract) on Matrigel Reduced Factor-coated plates (Corning Life Sciences, Corning, USA). Cells were grown and transferred to laminin-coated ibidi (ibidi GmbH, Martinsried, Germany) or MatTek dishes (MatTek Corporation, Ashland, USA) and differentiated at 70% confluency. Experiments were carried out 4 days post differentiation.

To quantify Ca^{2+} entry and Ca^{2+} store content, myotubes were incubated in Ringer solution containing 2 mM Ca^{2+} and 5 μM Indo-1 or fura-2 for 30 min, washed and incubated in 2 mM Ca^{2+} Ringer solution for another 30 min. The resting Ca^{2+} concentration was assessed in Fura-2 loaded myotubes as previously described (57). For Ca^{2+} entry, the medium was then replaced by Ca^{2+}-free Ringer solution, 10 mM Ca^{2+} was added after 5 min and 25 mM caffeine after additional 2 min. For the Ca^{2+} store content, the medium was replaced by Ca^{2+}-free Ringer solution for 1 min prior to addition of 10 mM caffeine and 1 μM thapsigargin. The Ca^{2+} store content was calculated as the area under the curve between 50 and 300 s. The emission ratio of the Ca^{2+} indicator (405 nm/485 nm) was measured every 1.3 s on a SP8 UV confocal microscope (Leica).

Statistical analyses

Data were verified for normal distribution using the Shapiro–Wilk test and are presented as mean ± SEM. For normally distributed data, significance of changes between WT and $Stim1^{R304W/+}$ mice of same gender was examined using a Student's t-test (with or without Welch's correction). For other data, a Mann–Whitney statistical test was performed. For the circularity and MinFeret distribution of fibers, the significance was assessed by two-way ANOVA followed by *post hoc* Bonferroni. Significant differences are illustrated as $*P < 0.05$, $**P < 0.01$, $***P < 0.001$ and $****P < 0.0001$.

Supplementary Material

Supplementary Material is available at *HMG* online.

Acknowledgements

References

1. Lacruz, R.S. and Feske, S. (2015) Diseases caused by mutations in ORAI1 and STIM1. *Ann. N. Y. Acad. Sci.*, **1356**, 45–79.

2. Park, C.Y., Hoover, P.J., Mullins, F.M., Bachhawat, P., Covington, E.D., Raunser, S., Walz, T., Garcia, K.C., Dolmetsch, R.E. and Lewis, R.S. (2009) STIM1 clusters and activates CRAC channels via direct binding of a cytosolic domain to Orai1. *Cell*, **136**, 876–890.

3. Luik, R.M., Wu, M.M., Buchanan, J. and Lewis, R.S. (2006) The elementary unit of store-operated Ca2+ entry: local activation of CRAC channels by STIM1 at ER-plasma membrane junctions. *J. Cell Biol.*, **174**, 815–825.

4. Stathopulos, P.B., Zheng, L., Li, G.Y., Plevin, M.J. and Ikura, M. (2008) Structural and mechanistic insights into STIM1-mediated initiation of store-operated calcium entry. *Cell*, **135**, 110–122.

5. Feske, S., Gwack, Y., Prakriya, M., Srikanth, S., Puppel, S.H., Tanasa, B., Hogan, P.G., Lewis, R.S., Daly, M. and Rao, A. (2006) A mutation in Orai1 causes immune deficiency by abrogating CRAC channel function. *Nature*, **441**, 179–185.

6. Picard, C., McCarl, C.A., Papolos, A., Khalil, S., Luthy, K., Hivroz, C., LeDeist, F., Rieux-Laucat, F., Rechavi, G., Rao, A. *et al.* (2009) STIM1 mutation associated with a syndrome of immunodeficiency and autoimmunity. *N. Engl. J. Med.*, **360**, 1971–1980.

7. Bohm, J., Chevessier, F., Maues De Paula, A., Koch, C., Attarian, S., Feger, C., Hantai, D., Laforet, P., Ghorab, K., Vallat, J.M. *et al.* (2013) Constitutive activation of the calcium sensor STIM1 causes tubular-aggregate myopathy. *Am. J. Hum. Genet.*, **92**, 271–278.

8. Misceo, D., Holmgren, A., Louch, W.E., Holme, P.A., Mizobuchi, M., Morales, R.J., De Paula, A.M., Stray-Pedersen, A., Lyle, R., Dalhus, B. *et al.* (2014) A dominant STIM1 mutation causes Stormorken syndrome. *Hum. Mutat.*, **35**, 556–564.

9. Morin, G., Bruechle, N.O., Singh, A.R., Knopp, C., Jedraszak, G., Elbracht, M., Bremond-Gignac, D., Hartmann, K., Sevestre, H., Deutz, P. *et al.* (2014) Gain-of-function mutation in STIM1 (P.R304W) is associated with Stormorken syndrome. *Hum. Mutat.*, **35**, 1221–1232.

10. Nesin, V., Wiley, G., Kousi, M., Ong, E.C., Lehmann, T., Nicholl, D.J., Suri, M., Shahrizaila, N., Katsanis, N., Gaffney, P.M. *et al.* (2014) Activating mutations in STIM1 and ORAI1 cause overlapping syndromes of tubular myopathy and congenital miosis. *Proc. Natl. Acad. Sci. U. S. A.*, **111**, 4197–4202.

11. Chevessier, F., Bauche-Godard, S., Leroy, J.P., Koenig, J., Paturneau-Jouas, M., Eymard, B., Hantai, D. and Verdiere-Sahuque, M. (2005) The origin of tubular aggregates in human myopathies. *J. Pathol.*, **207**, 313–323.

12. Bohm, J., Bulla, M., Urquhart, J.E., Malfatti, E., Williams, S.G., O'Sullivan, J., Szlauer, A., Koch, C., Baranello, G., Mora, M. *et al.*

13. (2017) ORAI1 mutations with distinct channel gating defects in tubular aggregate myopathy. *Hum. Mutat.*, **38**, 426–438.

13. Endo, Y., Noguchi, S., Hara, Y., Hayashi, Y.K., Motomura, K., Miyatake, S., Murakami, N., Tanaka, S., Yamashita, S., Kizu, R. *et al.* (2015) Dominant mutations in ORAI1 cause tubular aggregate myopathy with hypocalcemia via constitutive activation of store-operated Ca(2)(+) channels. *Hum. Mol. Genet.*, **24**, 637–648.

14. Markello, T., Chen, D., Kwan, J.Y., Horkayne-Szakaly, I., Morrison, A., Simakova, O., Maric, I., Lozier, J., Cullinane, A.R., Kilo, T. *et al.* (2015) York platelet syndrome is a CRAC channelopathy due to gain-of-function mutations in STIM1. *Mol. Genet. Metab.*, **114**, 474–482.

15. Noury, J.B., Bohm, J., Peche, G.A., Guyant-Marechal, L., Bedat-Millet, A.L., Chiche, L., Carlier, R.Y., Malfatti, E., Romero, N.B. and Stojkovic, T. (2017) Tubular aggregate myopathy with features of Stormorken disease due to a new STIM1 mutation. *Neuromuscul. Disord.*, **27**, 78–82.

16. Walter, M.C., Rossius, M., Zitzelsberger, M., Vorgerd, M., Muller-Felber, W., Ertl-Wagner, B., Zhang, Y., Brinkmeier, H., Senderek, J. and Schoser, B. (2015) 50 years to diagnosis: autosomal dominant tubular aggregate myopathy caused by a novel STIM1 mutation. *Neuromuscul. Disord.*, **25**, 577–584.

17. Garibaldi, M., Fattori, F., Riva, B., Labasse, C., Brochier, G., Ottaviani, P., Sacconi, S., Vizzaccaro, E., Laschena, F., Romero, N.B. *et al.* (2017) A novel gain-of-function mutation in ORAI1 causes late-onset tubular aggregate myopathy and congenital miosis. *Clin. Genet.*, **91**, 780–786.

18. Bohm, J. and Laporte, J. (2018) Gain-of-function mutations in STIM1 and ORAI1 causing tubular aggregate myopathy and Stormorken syndrome. *Cell Calcium*, **76**, 1–9.

19. Harris, E., Burki, U., Marini-Bettolo, C., Neri, M., Scotton, C., Hudson, J., Bertoli, M., Evangelista, T., Vroling, B., Polvikoski, T. *et al.* (2017) Complex phenotypes associated with STIM1 mutations in both coiled coil and EF-hand domains. *Neuromuscul. Disord.*, **27**, 861–872.

20. Alonso-Jimenez, A., Ramon, C., Dols-Icardo, O., Roig, C., Gallardo, E., Clarimon, J., Nunez-Peralta, C. and Diaz-Manera, J. (2018) Corpus callosum agenesis, myopathy and pinpoint pupils: consider Stormorken syndrome. *Eur. J. Neurol.*, **25**, e25–e26.

21. Fahrner, M., Stadlbauer, M., Muik, M., Rathner, P., Stathopulos, P., Ikura, M., Muller, N. and Romanin, C. (2018) A dual mechanism promotes switching of the Stormorken STIM1 R304W mutant into the activated state. *Nat. Commun.*, **9**, 825.

22. Braun, A., Varga-Szabo, D., Kleinschnitz, C., Pleines, I., Bender, M., Austinat, M., Bosl, M., Stoll, G. and Nieswandt, B. (2009) Orai1 (CRACM1) is the platelet SOC channel and essential for pathological thrombus formation. *Blood*, **113**, 2056–2063.

23. Varga-Szabo, D., Braun, A., Kleinschnitz, C., Bender, M., Pleines, I., Pham, M., Renne, T., Stoll, G. and Nieswandt, B. (2008) The calcium sensor STIM1 is an essential mediator of arterial thrombosis and ischemic brain infarction. *J. Exp. Med.*, **205**, 1583–1591.

24. Stiber, J., Hawkins, A., Zhang, Z.S., Wang, S., Burch, J., Graham, V., Ward, C.C., Seth, M., Finch, E., Malouf, N. *et al.* (2008) STIM1 signalling controls store-operated calcium entry required for development and contractile function in skeletal muscle. *Nat. Cell Biol.*, **10**, 688–697.

25. McCarl, C.A., Khalil, S., Ma, J., Oh-hora, M., Yamashita, M., Roether, J., Kawasaki, T., Jairaman, A., Sasaki, Y., Prakriya, M. *et al.* (2010) Store-operated Ca2+ entry through

ORAI1 is critical for T cell-mediated autoimmunity and allograft rejection. *J. Immunol.*, **185**, 5845–5858.

26. Oh-Hora, M., Yamashita, M., Hogan, P.G., Sharma, S., Lamperti, E., Chung, W., Prakriya, M., Feske, S. and Rao, A. (2008) Dual functions for the endoplasmic reticulum calcium sensors STIM1 and STIM2 in T cell activation and tolerance. *Nat. Immunol.*, **9**, 432–443.

27. Ahmad, F., Boulaftali, Y., Greene, T.K., Ouellette, T.D., Poncz, M., Feske, S. and Bergmeier, W. (2011) Relative contributions of stromal interaction molecule 1 and CalDAG-GEFI to calcium-dependent platelet activation and thrombosis. *J. Thromb. Haemost.*, **9**, 2077–2086.

28. Grosse, J., Braun, A., Varga-Szabo, D., Beyersdorf, N., Schneider, B., Zeitlmann, L., Hanke, P., Schropp, P., Muhlstedt, S., Zorn, C. *et al.* (2007) An EF hand mutation in Stim1 causes premature platelet activation and bleeding in mice. *J. Clin. Invest.*, **117**, 3540–3550.

29. Stormorken, H., Sjaastad, O., Langslet, A., Sulg, I., Egge, K. and Diderichsen, J. (1985) A new syndrome: thrombocytopathia, muscle fatigue, asplenia, miosis, migraine, dyslexia and ichthyosis. *Clin. Genet.*, **28**, 367–374.

30. Chevessier, F., Marty, I., Paturneau-Jouas, M., Hantai, D. and Verdiere-Sahuque, M. (2004) Tubular aggregates are from whole sarcoplasmic reticulum origin: alterations in calcium binding protein expression in mouse skeletal muscle during aging. *Neuromuscul. Disord.*, **14**, 208–216.

31. Bohm, J., Chevessier, F., Koch, C., Peche, G.A., Mora, M., Morandi, L., Pasanisi, B., Moroni, I., Tasca, G., Fattori, F. *et al.* (2014) Clinical, histological and genetic characterisation of patients with tubular aggregate myopathy caused by mutations in STIM1. *J. Med. Genet.*, **51**, 824–833.

32. Bohm, J., Lornage, X., Chevessier, F., Birck, C., Zanotti, S., Cudia, P., Bulla, M., Granger, F., Bui, M.T., Sartori, M. *et al.* (2018) CASQ1 mutations impair calsequestrin polymerization and cause tubular aggregate myopathy. *Acta Neuropathol.*, **135**, 149–151.

33. Hedberg, C., Niceta, M., Fattori, F., Lindvall, B., Ciolfi, A., D'Amico, A., Tasca, G., Petrini, S., Tulinius, M., Tartaglia, M. *et al.* (2014) Childhood onset tubular aggregate myopathy associated with de novo STIM1 mutations. *J. Neurol.*, **261**, 870–876.

34. Arruda, A.P., Pers, B.M., Parlakgul, G., Guney, E., Goh, T., Cagampan, E., Lee, G.Y., Goncalves, R.L. and Hotamisligil, G.S. (2017) Defective STIM-mediated store operated Ca(2+) entry in hepatocytes leads to metabolic dysfunction in obesity. *Elife*, **6**. pii: e29968. doi: 10.7554/eLife.29968

35. Kono, T., Tong, X., Taleb, S., Bone, R.N., Iida, H., Lee, C.C., Sohn, P., Gilon, P., Roe, M.W. and Evans-Molina, C. (2018) Impaired store-operated calcium entry and STIM1 loss lead to reduced insulin secretion and increased endoplasmic reticulum stress in the diabetic beta-cell. *Diabetes*, **67**, 2293–2304.

36. Gamage, T.H., Gunnes, G., Lee, R.H., Louch, W.E., Holmgren, A., Bruton, J.D., Lengle, E., Selnes Kolstad, T.R., Revold, T., Amundsen, S.S. *et al.* (2018) STIM1 R304W causes muscle degeneration and impaired platelet activation in mice. *Cell Calcium*, **76**, 87–100.

37. Schiaffino, S. and Reggiani, C. (2011) Fiber types in mammalian skeletal muscles. *Physiol. Rev.*, **91**, 1447–1531.

38. Parekh, A.B. and Penner, R. (1997) Store depletion and calcium influx. *Physiol. Rev.*, **77**, 901–930.

39. Shahrizaila, N., Lowe, J. and Wills, A. (2004) Familial myopathy with tubular aggregates associated with abnormal pupils. *Neurology*, **63**, 1111–1113.

40. Bodensteiner, J.B. and Engel, A.G. (1978) Intracellular calcium accumulation in Duchenne dystrophy and other myopathies: a study of 567,000 muscle fibers in 114 biopsies. *Neurology*, **28**, 439–446.

41. Perry, R.L. and Rudnick, M.A. (2000) Molecular mechanisms regulating myogenic determination and differentiation. *Front. Biosci.*, **5**, D750–D767.

42. Agbulut, O., Destombes, J., Thiesson, D. and Butler-Browne, G. (2000) Age-related appearance of tubular aggregates in the skeletal muscle of almost all male inbred mice. *Histochem. Cell Biol.*, **114**, 477–481.

43. Ekiz, O., Balta, I., Sen, B.B., Rifaioglu, E.N., Ergin, C., Balta, S. and Demirkol, S. (2014) Mean platelet volume in recurrent aphthous stomatitis and Behcet disease. *Angiology*, **65**, 161–165.

44. Soydinc, S., Turkbeyler, I.H., Pehlivan, Y., Soylu, G., Goktepe, M.F., Bilici, M., Zengin, O., Kisacik, B. and Onat, A.M. (2014) Mean platelet volume seems to be a valuable marker in patients with systemic sclerosis. *Inflammation*, **37**, 100–106.

45. Wang, X., Meng, H., Xu, L., Chen, Z., Shi, D. and Lv, D. (2015) Mean platelet volume as an inflammatory marker in patients with severe periodontitis. *Platelets*, **26**, 67–71.

46. Noack, M. and Miossec, P. (2014) Th17 and regulatory T cell balance in autoimmune and inflammatory diseases. *Autoimmun. Rev.*, **13**, 668–677.

47. Hwang, S.Y. and Putney, J.W. (2012) Orai1-mediated calcium entry plays a critical role in osteoclast differentiation and function by regulating activation of the transcription factor NFATc1. *FASEB J.*, **26**, 1484–1492.

48. Robinson, L.J., Mancarella, S., Songsawad, D., Tourkova, I.L., Barnett, J.B., Gill, D.L., Soboloff, J. and Blair, H.C. (2012) Gene disruption of the calcium channel Orai1 results in inhibition of osteoclast and osteoblast differentiation and impairs skeletal development. *Lab. Invest.*, **92**, 1071–1083.

49. Byun, M., Abhyankar, A., Lelarge, V., Plancoulaine, S., Palanduz, A., Telhan, L., Boisson, B., Picard, C., Dewell, S., Zhao, C. *et al.* (2010) Whole-exome sequencing-based discovery of STIM1 deficiency in a child with fatal classic Kaposi sarcoma. *J. Exp. Med.*, **207**, 2307–2312.

50. Fuchs, S., Rensing-Ehl, A., Speckmann, C., Bengsch, B., Schmitt-Graeff, A., Bondzio, I., Maul-Pavicic, A., Bass, T., Vraetz, T., Strahm, B. *et al.* (2012) Antiviral and regulatory T cell immunity in a patient with stromal interaction molecule 1 deficiency. *J. Immunol.*, **188**, 1523–1533.

51. McCarl, C.A., Picard, C., Khalil, S., Kawasaki, T., Rother, J., Papolos, A., Kutok, J., Hivroz, C., Ledeist, F., Plogmann, K. *et al.* (2009) ORAI1 deficiency and lack of store-operated Ca2+ entry cause immunodeficiency, myopathy, and ectodermal dysplasia. *J. Allergy Clin. Immunol.*, **124**, 1311–1318 e1317.

52. Chou, J., Badran, Y.R., Yee, C.S., Bainter, W., Ohsumi, T.K., Al-Hammadi, S., Pai, S.Y., Feske, S. and Geha, R.S. (2015) A novel mutation in ORAI1 presenting with combined immunodeficiency and residual T-cell function. *J. Allergy Clin. Immunol.*, **136** (479–482), e471 10.

53. Schaballie, H., Rodriguez, R., Martin, E., Moens, L., Frans, G., Lenoir, C., Dutre, J., Canioni, D., Bossuyt, X., Fischer, A. *et al.* (2015) A novel hypomorphic mutation in STIM1 results in a late-onset immunodeficiency. *J. Allergy Clin. Immunol.*, **136**, 816–819 e814.

54. Wang, S., Choi, M., Richardson, A.S., Reid, B.M., Seymen, F., Yildirim, M., Tuna, E., Gencay, K., Simmer, J.P. and Hu, J.C. (2014) STIM1 and SLC24A4 are critical for enamel maturation. *J. Dent. Res.*, **93**, 94S–100S.

55. Thomas, K.C., Zheng, X.F., Garces Suarez, F., Raftery, J.M., Quinlan, K.G., Yang, N., North, K.N. and Houweling, P.J. (2014) Evidence based selection of commonly used RT-qPCR reference genes for the analysis of mouse skeletal muscle. *PLoS One*, **9**, e88653 10.

56. De Palma, S., Capitanio, D., Vasso, M., Braghetta, P., Scotton, C., Bonaldo, P., Lochmuller, H., Muntoni, F., Ferlini, A. and Gelfi, C. (2014) Muscle proteomics reveals novel insights into the pathophysiological mechanisms of collagen VI myopathies. *J. Proteome Res.*, **13**, 5022–5030.

57. Bachmann, C., Jungbluth, H., Muntoni, F., Manzur, A.Y., Zorzato, F. and Treves, S. (2017) Cellular, biochemical and molecular changes in muscles from patients with X-linked myotubular myopathy due to MTM1 mutations. *Hum. Mol. Genet.*, **26**, 320–332.

67
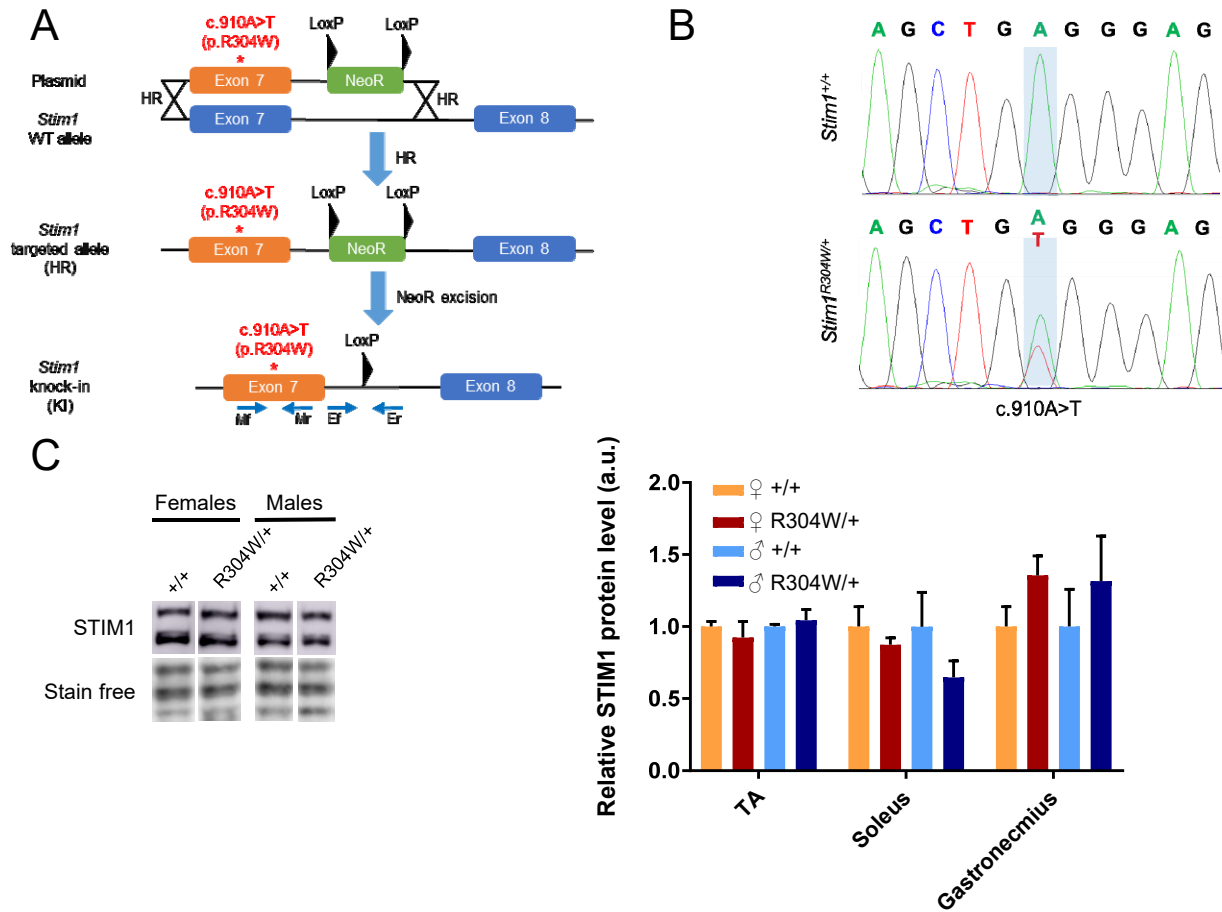
Supplemental Figure S1. Generation of *Stim1^{R304W/+}* mice. (A) The knock-in mouse was generated by homologous recombination with a plasmid containing *Stim1* exon 7 harboring the c.910A>T mutation, neomycin selection of positive ES cells, and subsequent excision of the neomycin cassette. Mf/Mr and Ef/Er = position of sequencing/genotyping primers. (B) Sequencing confirmed the presence of the heterozygous *Stim1* c.910A>T mutation in knock-in mice. (C) Representative western blot of tibialis anterior extracts and protein quantification in TA, soleus, and gastrocnemius revealed comparable STIM1 levels in *Stim1^{R304W/+}* and WT mice. Membrane stain free served as control (n=4-5).
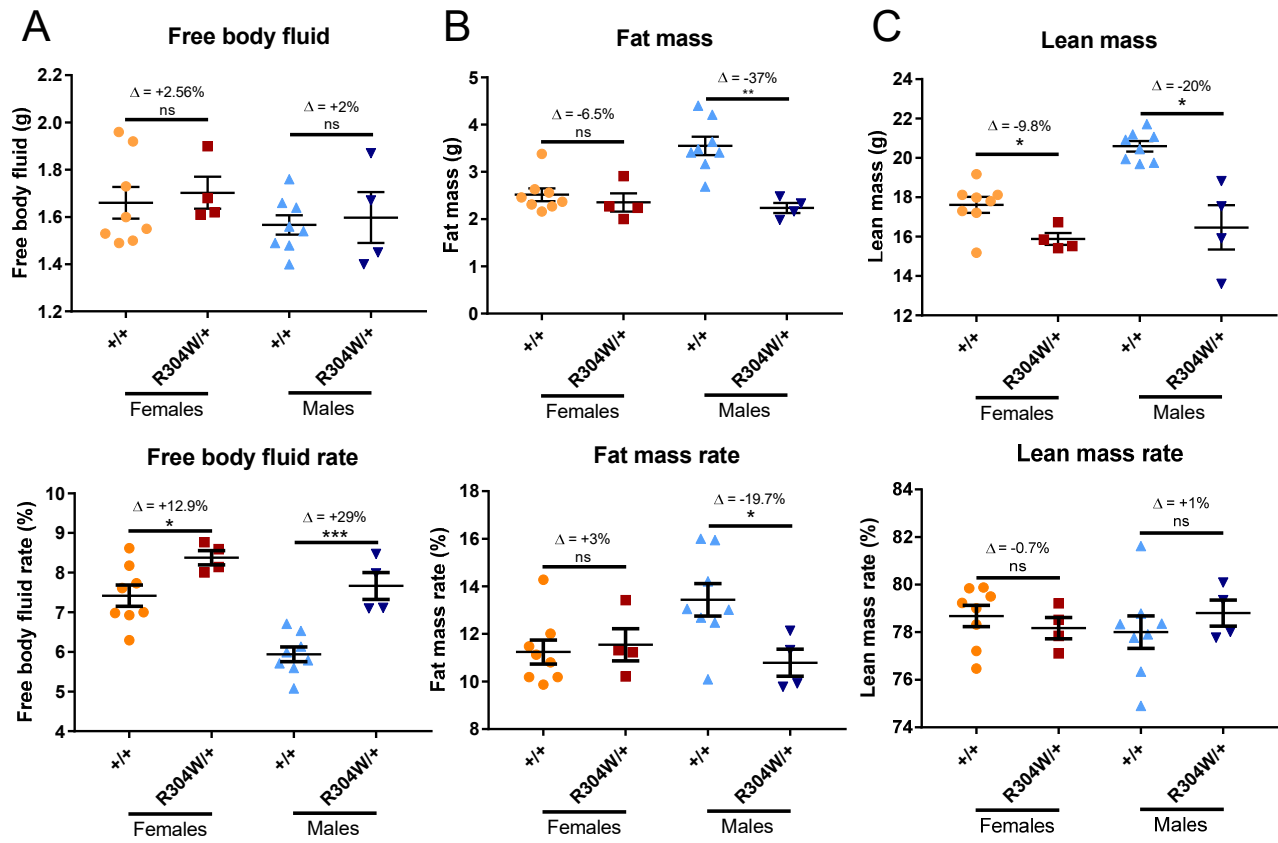
Supplemental Figure S2. Fat and lean mass reduction in *Stim1^{R304W/+}* mice. (A) Analysis of whole body composition at 14 weeks of age demonstrated an increased free body fluid rate in *Stim1^{R304W/+}* mice compared to controls (n=4-8). (B) *Stim1^{R304W/+}* males exhibited a reduction in fat mass and fat mass rate, while *Stim1^{R304W/+}* females were comparable to controls. (C) Lean mass was reduced in *Stim1^{R304W/+}* mice, while lean mass rate was comparable to *Stim1^{+/+}* controls.
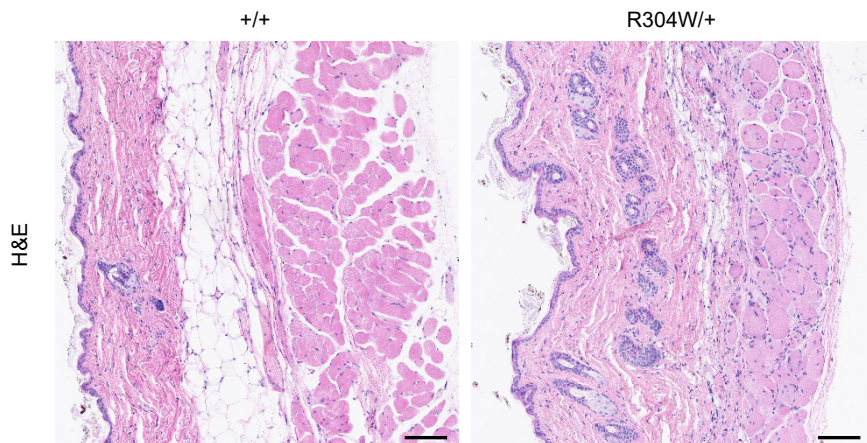
Supplemental Figure S3. Skin anomalies in *Stim1^{R304W/+}* mice. H&E-stained back skin sections at 9 months showed an enlarged dermis and a reduced fat layer in *Stim1^{R304W/+}* males compared to controls (scale bar = 250 μm).
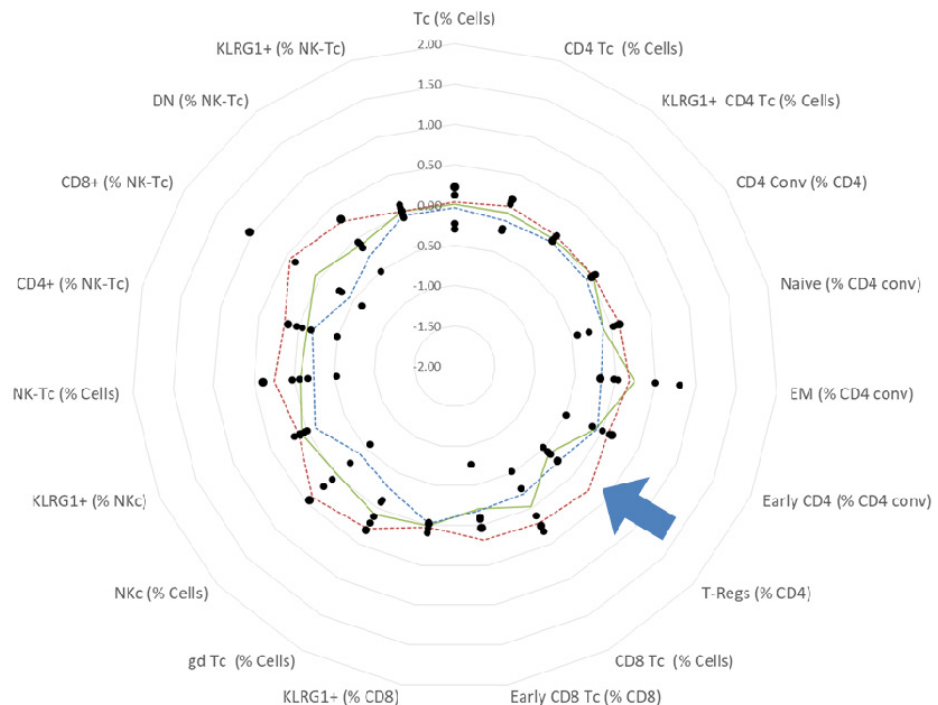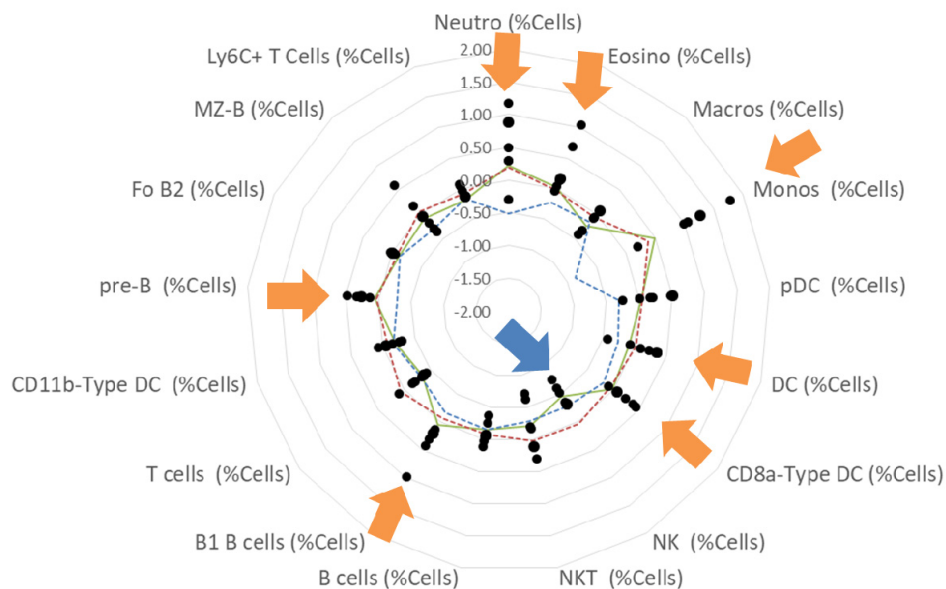
Supplemental Figure S4. Quantitative alterations of different immune cell types in *Stim1^{R304W/+}* mice. (A) Regulatory T cells (Tregs) were reduced in *Stim1^{R304W/+}* spleen (n=5). (B) Decreased nuclear killer cells (NK), and increased neutrophils, eosinophils, monocytes, dendritic cells (DC), DC8-type dendritic cells, B cells, and premature B cells (Pre-B) in *Stim1^{R304W/+}* mice (n=5). Values are normalized to controls.
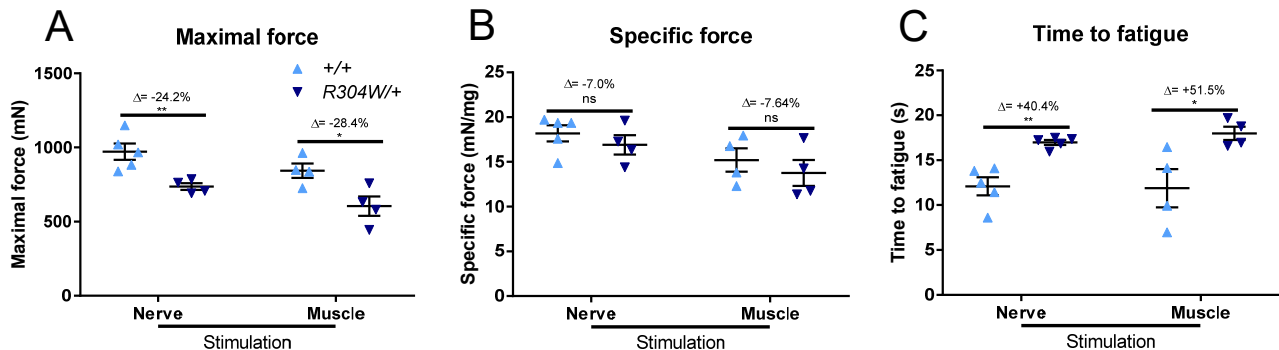
Supplemental Figure S5. Normal nerve-to-muscle signal transmission in *Stim1^{R304W/+}* mice. (A, B) Sciatic nerve or direct tibialis anterior stimulation resulted in similar maximal and specific force reduction in *Stim1^{R304W/+}* males at 4 months compared to controls. (C) Continuous nerve or muscle stimulation of the TA at 4 months resulted in a comparable increase of time to fatigue in *Stim1^{R304W/+}* males compared to controls.
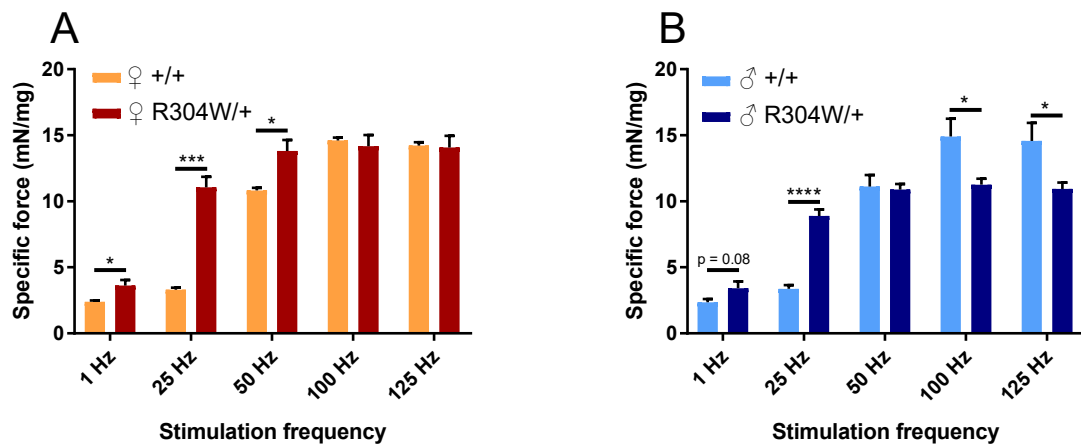
Supplemental Figure S6. High *Stim1^{R304W/+}* muscle force at low stimulation frequencies. (A) Female and (B) male *Stim1^{R304W/+}* tibialis anterior generated more specific force at stimulation frequencies of 1-25 Hz as compared to controls.
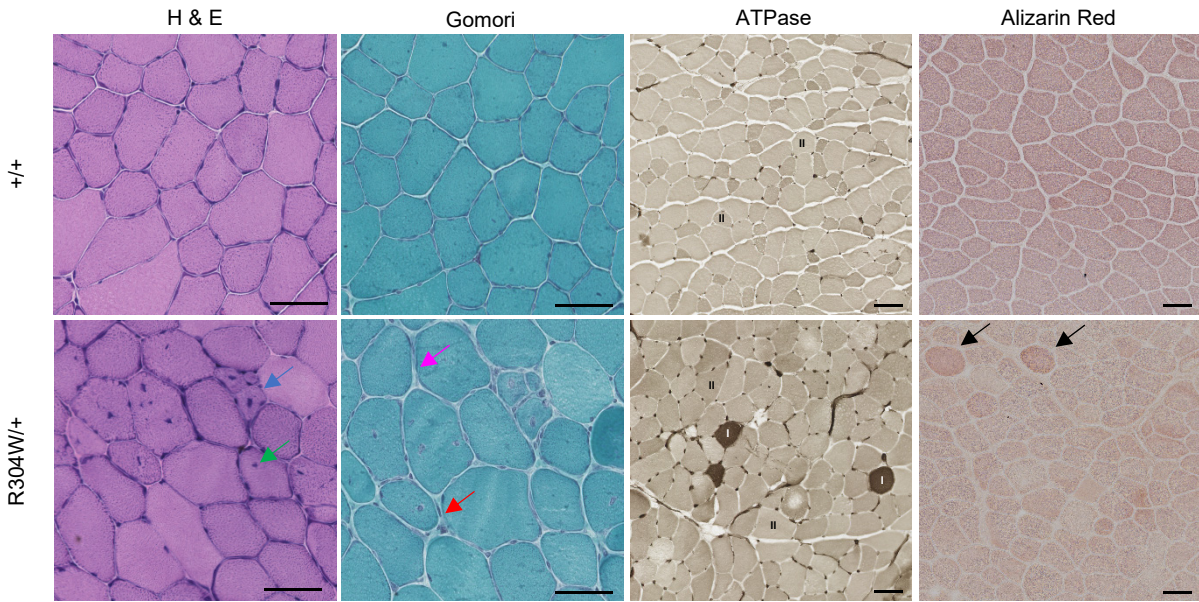
Supplemental Figure S7. Common muscle histopathology in *Stim1^R304W/+* females and males. H&E, Gomori, ATPase pH 4.3, and Alizarin Red staining on tibialis anterior sections from *Stim1^R304W/+* females at 4 months revealed similar pathological features as in *Stim1^R304W/+* males (Figure 3), including internalized nuclei (green arrow), regenerating fibers (blue arrow), infiltration of inflammatory cells (red arrow), fibrosis (pink arrow), increased proportion of type I fibers, and Ca²⁺-rich rounded fibers (black arrows) (n=5, scale bar = 50 µm).
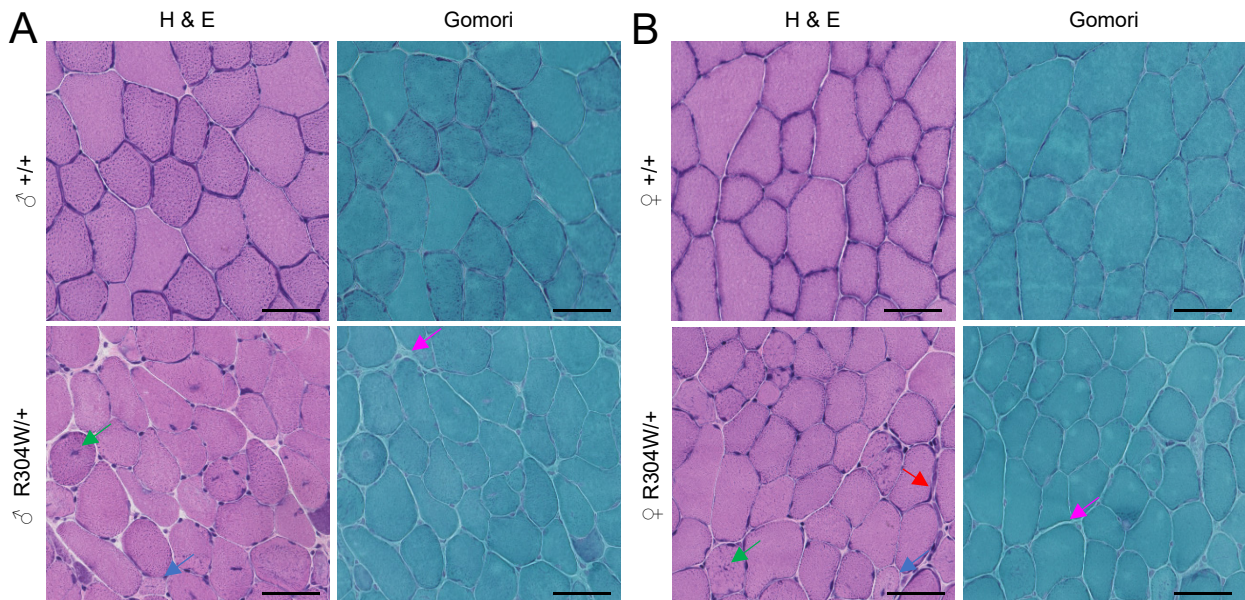
Supplemental Figure S8. Muscle histopathology aggravates over time in *Stim1^R304W/+* mice. (A, B) Internalized nuclei (green arrow), regenerating fibers (blue arrow), infiltration of inflammatory cells (red arrow), and fibrosis (pink arrow) are more pronounced in *Stim1^R304W/+* TA muscle sections at 9 months than at 4 months (scale bar = 50 µm).
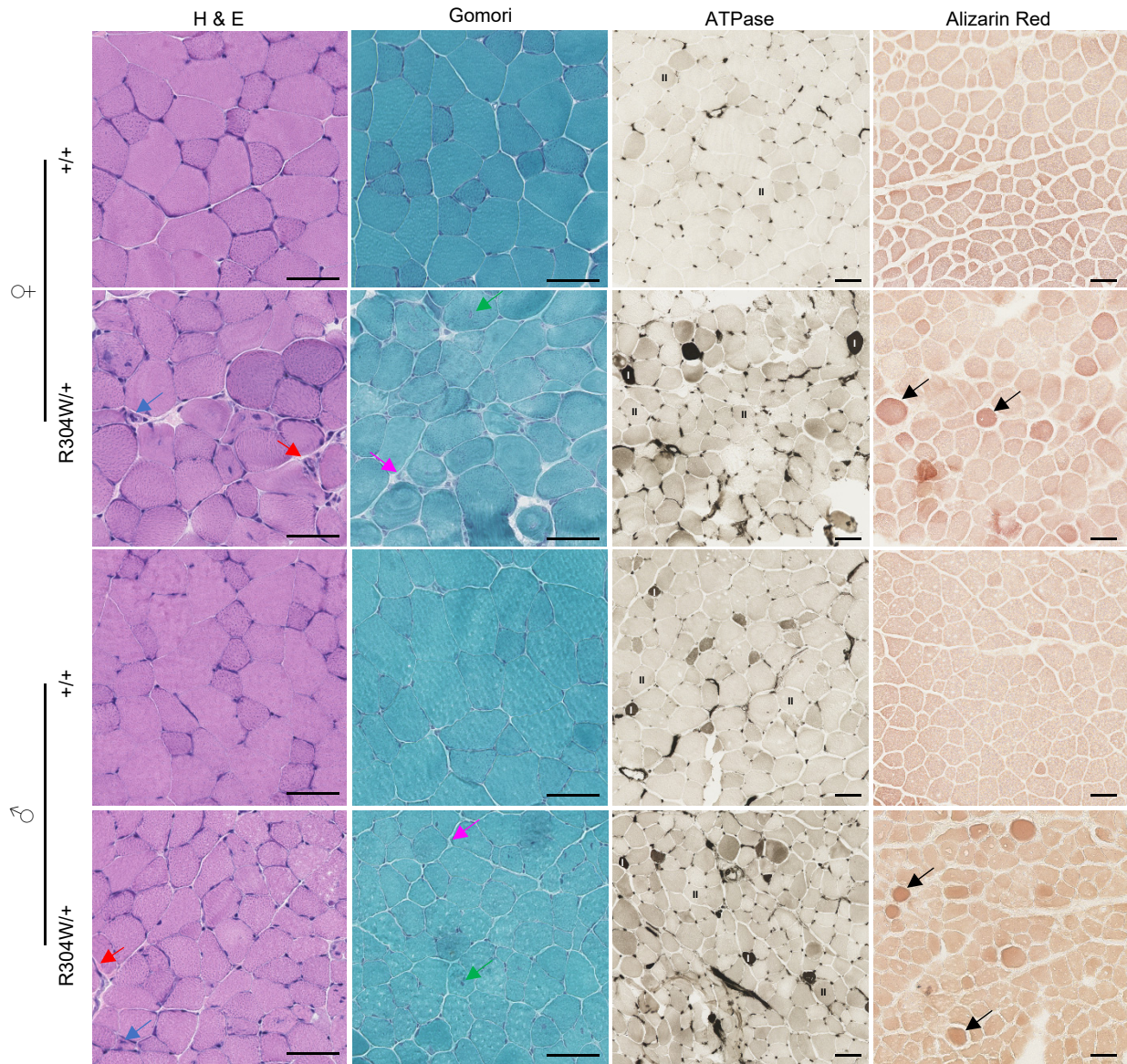
Supplemental Figure S9. *Stim1^{R304W/+}* EDL histopathology. EDL muscle sections from 4 months old *Stim1^{R304W/+}* mice revealed internalized nuclei (green arrows), regenerating fibers (blue arrows), infiltration of inflammatory cells (red arrows), and fibrosis (pink arrows). *Stim1^{R304W/+}* sections also displayed an increased proportion of darker type I fibers, and an increased number of Ca^{2+}-rich rounded fibers (black arrows) compared to the controls (scale bar = 50 μm).
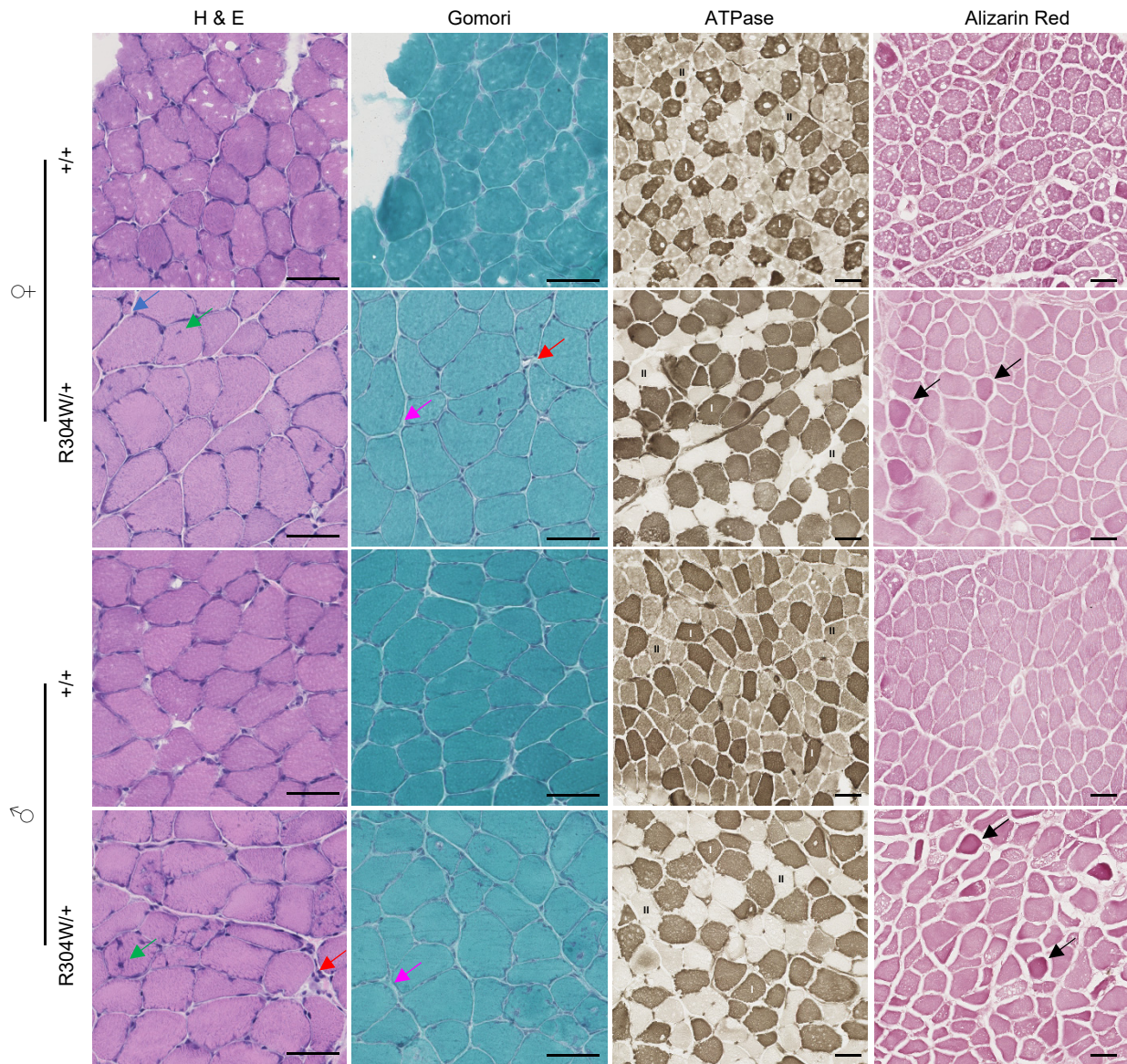
Supplemental Figure S10. *Stim1^{R304W/+}* **soleus histopathology.** Soleus muscle sections from 4 months old *Stim1^{R304W/+}* mice revealed internalized nuclei (green arrows), regenerating fibers (blue arrow), infiltration of inflammatory cells (red arrows), and fibrosis (pink arrows). *Stim1^{R304W/+}* sections also showed more type I fibers compared to the controls and the presence of Ca^{2+}-rich rounded fibers (black arrows) (scale bar = 50 μm).
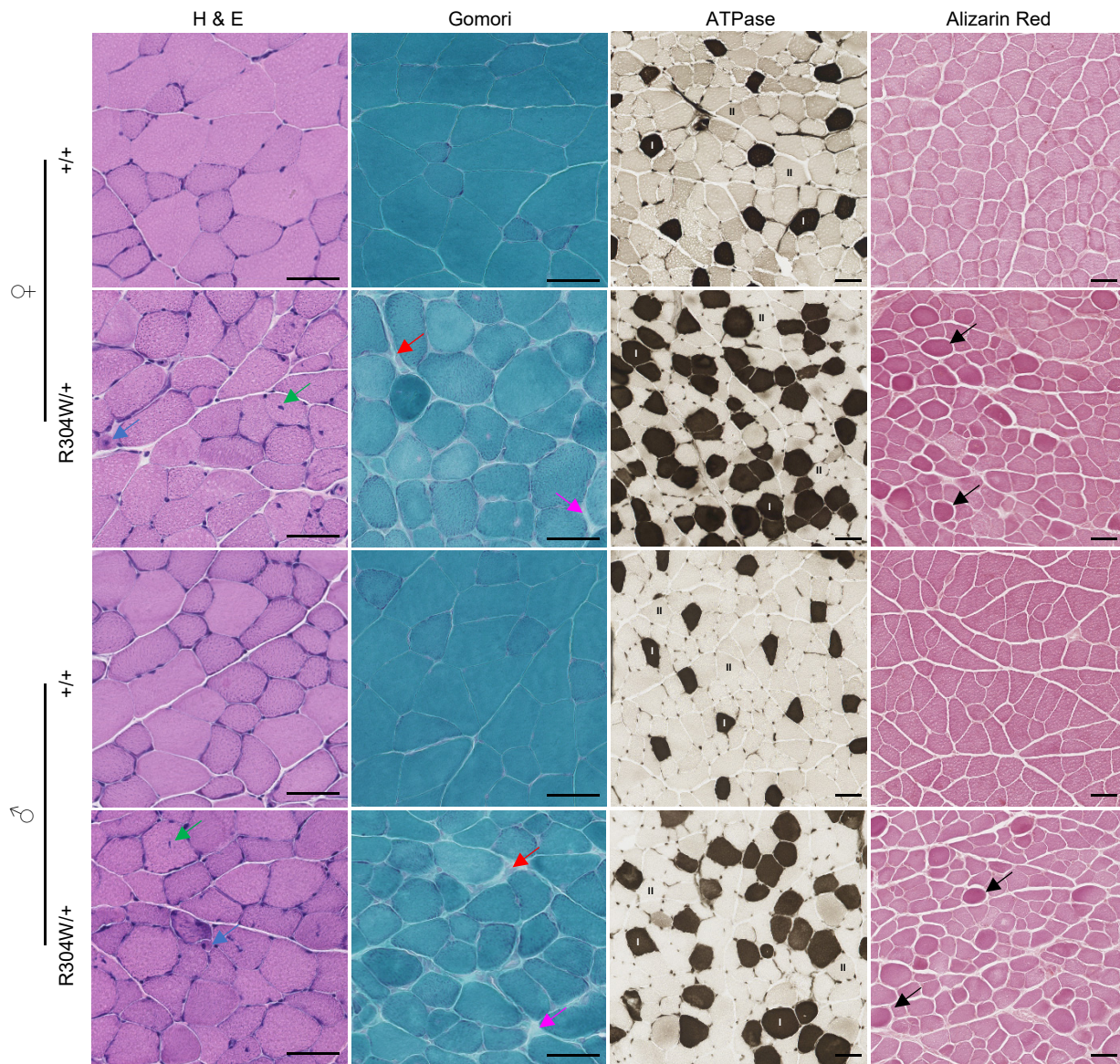
Supplemental Figure S11. *Stim1^{R304W/+}* gastrocnemius histopathology. Gastrocnemius muscle sections from 4 months old *Stim1^{R304W/+}* mice showed internalized nuclei (green arrows), regenerating fibers (blue arrows), infiltration of inflammatory cells (red arrows), fibrosis (pink arrows), an increased ratio of dark type I fibers compared to controls, and the presence of Ca^{2+}-rich rounded fibers (black arrows) (scale bar = 50 μm).
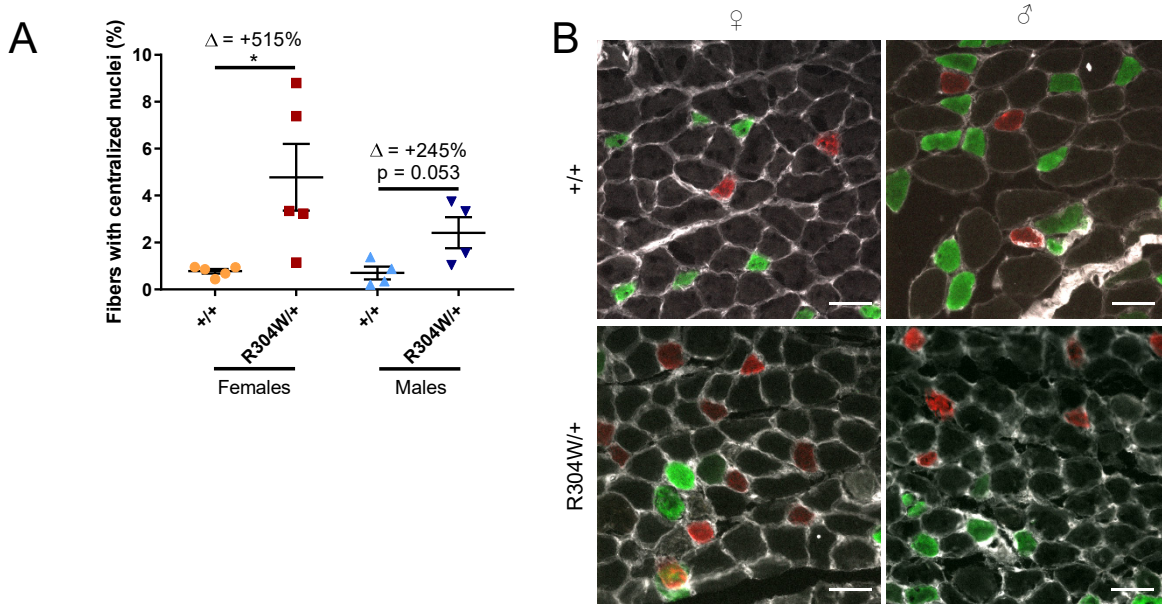
Supplemental Figure S12. Muscle fiber degeneration and regeneration in *Stim1*[R304W/+] mice. (A) At 4 months, tibialis anterior muscle fibers with internalized nuclei were more frequent in *Stim1*[R304W/+] mice than in WT mice (n=4-5 mice, 1700 fibers/mice in average). (B) Immunofluorescence confirm that type I fibers (red) are more frequent in *Stim1*[R304W/+] tibialis anterior (scale bar = 50 µm).
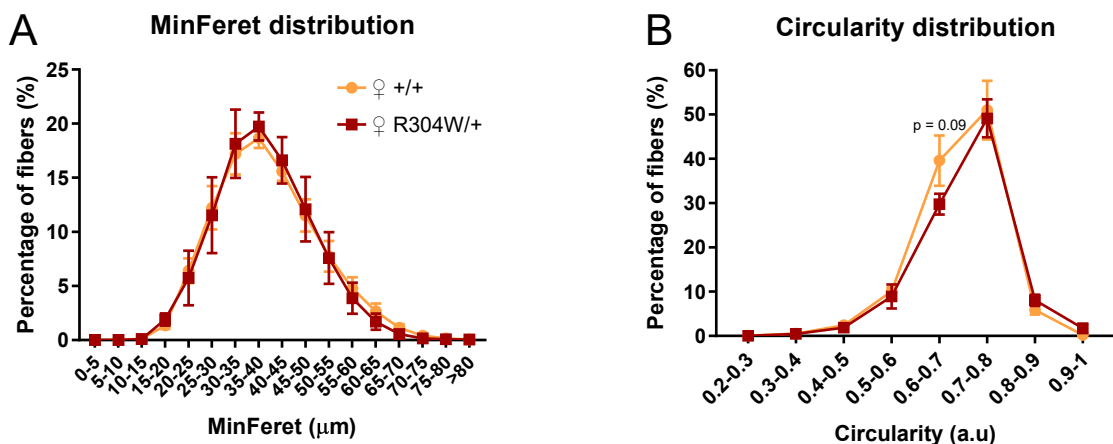
Supplemental Figure S13. Increased muscle fiber circularity in *Stim1*[R304W/+] females. (A) At 4 months, TA fibers from *Stim1*[R304W/+] and *Stim1*^{+/+} females had a comparable MinFeret diameter distribution (n=5 mice, 1900 fibers/mice in average). (B) Circularity measurements showed a tendency to rounded fibers in tibialis anterior from *Stim1*[R304W/+] females (n=5, 1900 fibers/mice in average).
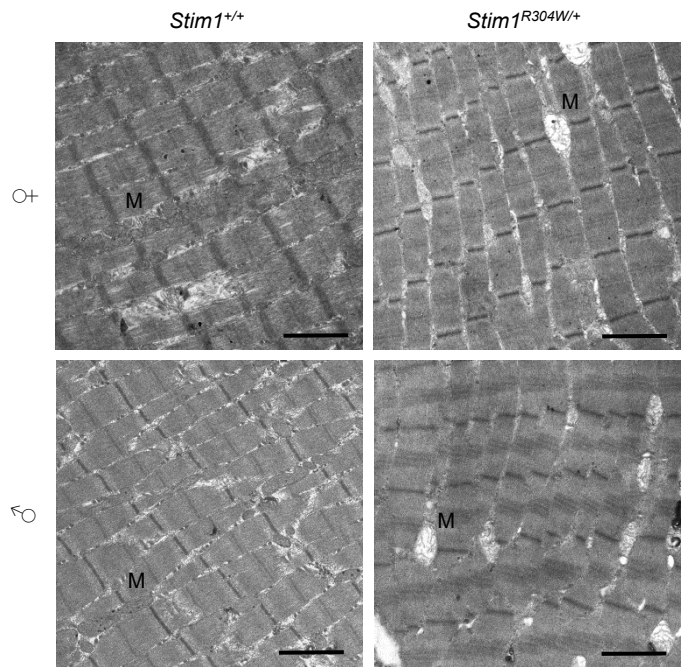
Supplemental Figure S14. Swollen mitochondria in *Stim1^{R304W/+}* mice. Electron micrographs on longitudinal TA sections disclosed swollen mitochondria in both *Stim1^{R304W/+}* males and females at 4 months (scale bar = 2 μm).
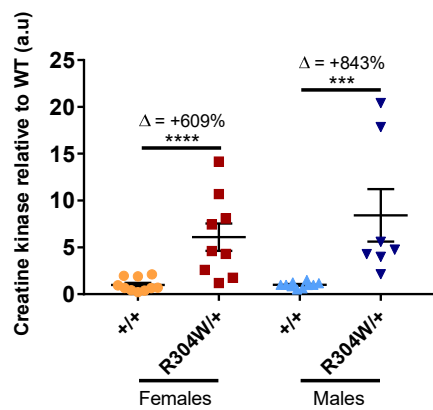
Supplemental Figure S15. Creatine kinase level as a feature of fiber degeneration. Serum creatine kinase levels were 6-8 fold increased in *Stim1^{R304W/+}* mice compared to controls.
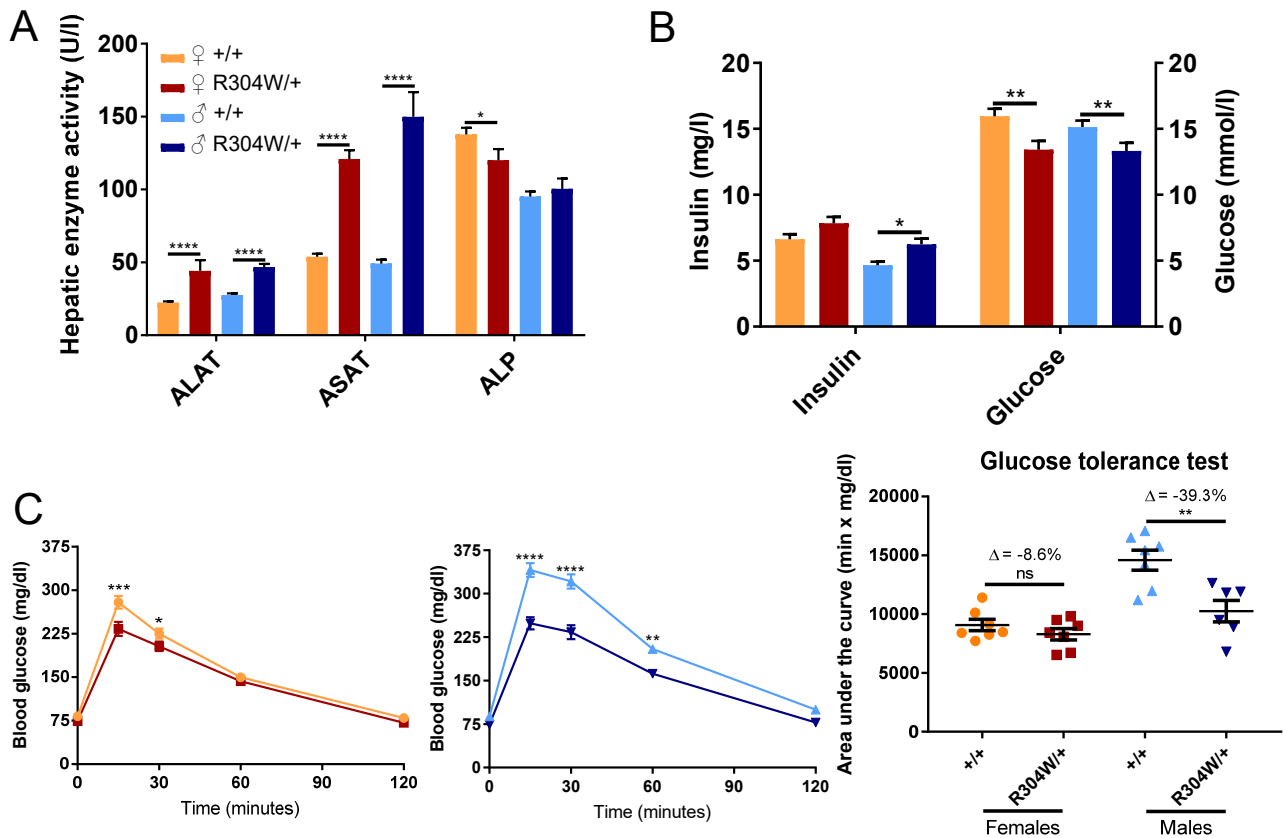
Supplemental Figure S16. Hepatic malfunction and glucose metabolism abnormalities in *Stim1^{R304W/+}* mice. (A) At 4 months, ALAT (alanine transaminase) and ASAT (aspartate transaminase) activities were increased in *Stim1^{R304W/+}* blood, while ALP (alkaline phosphatase) activity was decreased or comparable to controls (n=6-15). (B) Both insulin and glucose concentrations were reduced in *Stim1^{R304W/+}* blood at 4 months compared to controls (n=5-15). (C) Following glucose injection, blood glucose levels were lower in *Stim1^{R304W/+}* mice compared to *Stim1^{+/+}* controls.
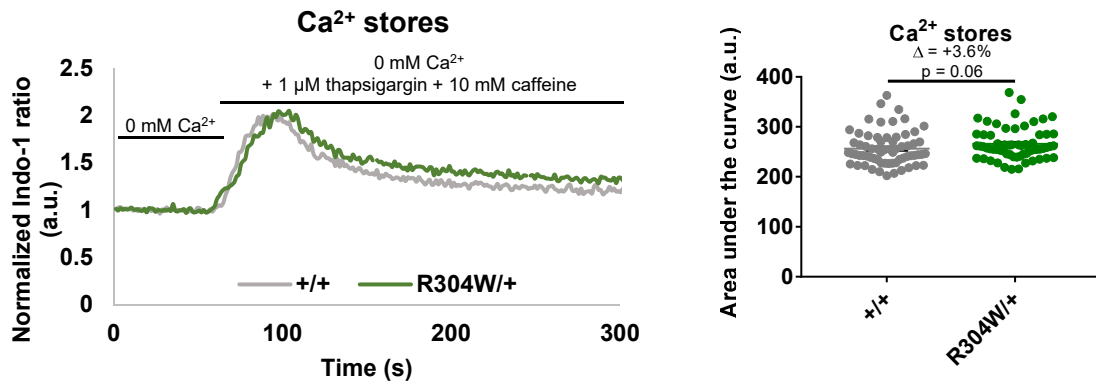
Supplemental Figure S17: Comparable Ca^{2+} content in WT and *Stim1^{R304W/+}* myotubes. Mean normalized Indo-1 ratio measurements over time showed a comparable Ca^{2+} store content in *Stim1^{R304W/+}* and WT myotubes (n=65-62 myotubes from 3-4 mice/genotype).

Supplemental Table S1. Cortical parameters of the midshaft tibia. Ct.Th = cortical thickness, BA/TA = bone area fraction, T.Ar = total area, B.Ar = bone area, M.Ar = marrow area, MOI = polar moment of inertia.

	Ct.Th (mm)	BA/TA (%)	T.Ar(mm^2)	B.Ar (mm^2)	M.Ar (mm^2)	MOI (mm^4)
♀ +/+	0.207 ± 0.004	77.9 ± 0.36	0.757 ± 0.02	0.59 ± 0.01	0.166 ± 0.003	0.1 ± 0.006
♀ R304W/+	0.225 ± 0.007	79.4 ± 0.58	0.719 ± 0.01	0.572 ± 0.01	0.147 ± 0.001	0.08 ± 0.002
Δ (%)	+8.47	+1.93	-4.97	-3.13	-11.47	-17.18
p value	0.066	0.106	0.208	0.487	0.0006	0.071
♂ +/+	0.207 ± 0.003	78.2 ± 0.31	0.743 ± 0.009	0.581 ± 0.009	0.161 ± 0.002	0.09 ± 0.003
♂ R304W/+	0.218 ± 0.003	78.8 ± 0.29	0.686 ± 0.009	0.541 ± 0.009	0.145 ± 0.001	0.07 ± 0.002
Δ (%)	+5.22	+0.71	-7.69	-7.02	-10.08	-22.06
p value	0.04	0.22	0.001	0.008	<0.0001	0.003

Supplemental Table S2. Trabecular parameters of the distal femur. BV/TV = bone volume fraction, Tb.Th = trabecular thickness, Tb.N = trabecular number, Tb.Sp = trabecular separation.

	BV/TV (%)	Tb.Th (μm)	Tb.N (1/mm)	Tb. Sp (μm)
♀ +/+	3.456 ± 0.45	63.19 ± 2.73	0.532 ± 0.07	609.9 ± 44.81
♀ R304W/+	3.231 ± 0.69	64.02 ± 6.49	0.482 ± 0.07	564.4 ± 46.52
Δ (%)	-6.51	+1.31	-9.54	-7.46
p value	0.783	0.898	0.635	>0.999
♂ +/+	5.029 ± 0.47	56.59 ± 2.22	0.855 ± 0.08	302.3 ± 14.75
♂ R304W/+	2.480 ± 0.38	58.95 ± 1.57	0.371 ± 0.06	583.2 ± 47.87
Δ (%)	-50.69	+4.18	-56.59	+92.88
p value	0.007	0.403	0.0035	0.0008

Supplemental Table S3. Trabecular parameters of the 5th lumbar vertebra. BV/TV = bone volume fraction, Tb.Th = trabecular thickness, Tb.N = trabecular number, Tb.Sp = trabecular separation.

	BV/TV (%)	Tb.Th (μm)	Tb.N (1/mm)	Tb. Sp (μm)
♀ +/+	23.93 ± 1.42	64.61 ± 1.35	3.68 ± 0.15	139.2 ± 3.35
♀ R304W/+	18.77 ± 1.58	63.3 ± 2.74	2.89 ± 0.26	148.9 ± 5.53
Δ (%)	-21.55	-2.04	-19.21	+6.97
p value	0.038	0.647	0.034	0.143
♂ +/+	23.75 ± 0.85	61.22 ± 0.83	3.87 ± 0.12	129.6 ± 3.72
♂ R304W/+	19.25 ± 0.93	62.37 ± 1.3	3.09 ± 0.12	158.9 ± 5.8
Δ (%)	-18.94	+1.87	-20.33	+22.64
p value	0.004	0.475	0.0006	0.0016

Supplemental Table S4. Basal breathing values determined by plethysmography.

	Tidal volume (mL)	Breath frequency (bpm)	Enhanced pause (a.u.)
♀ +/+	0.29 ± 0.02	374.7 ± 14.5	0.33 ± 0.03
♀ R304W/+	0.24 ± 0.01	338.7 ± 11.3	0.29 ± 0.0
Δ (%)	-17.5	-9.6	-12.2
p value	>0.05	>0.05	>0.05
♂ +/+	0.29 ± 0.02	381.7 ± 16.3	0.36 ± 0.03
♂ R304W/+	0.27 ± 0.01	357.3 ± 14.4	0.29 ± 0.01
Δ (%)	-6.9	-6.4	-19.45
p value	>0.05	>0.05	<0.05

Supplemental Table S5. List of RT-qPCR primers.

Gene	Forward primer	Reverse primer
Rpl27	AAGCCGTCATCGTGAAGAACA	CTTGATCTTGGATCGCTTGGC
Stim1	CTGAAGGCCCTGGACACA	CAGCCACCCACACCAATAAC
Orai1	GCCAAGCTCAAAGCTTCC	CCTGGTGGGTAGTCATGGTC
Casq1	GAATCCACATTGTCGCCTTT	GTCGGGGTTCTCAGTGTTGT
Myog	CCAACCCAGGAGATCATTTG	ATATCCTCCACCGTGATGCT
Myf5	CTGTCTGGTCCCGAAAGAAC	AAGCAATCCAAGCTGGACAC
Nfatc1	GTCTCACCACAGGGCTCACT	GCGTGAGAGGTTCATTCTCC
Nfatc3	TTGTGAAGCTCCTGGGCTAT	GCACCTGGTAAAATGCATGA
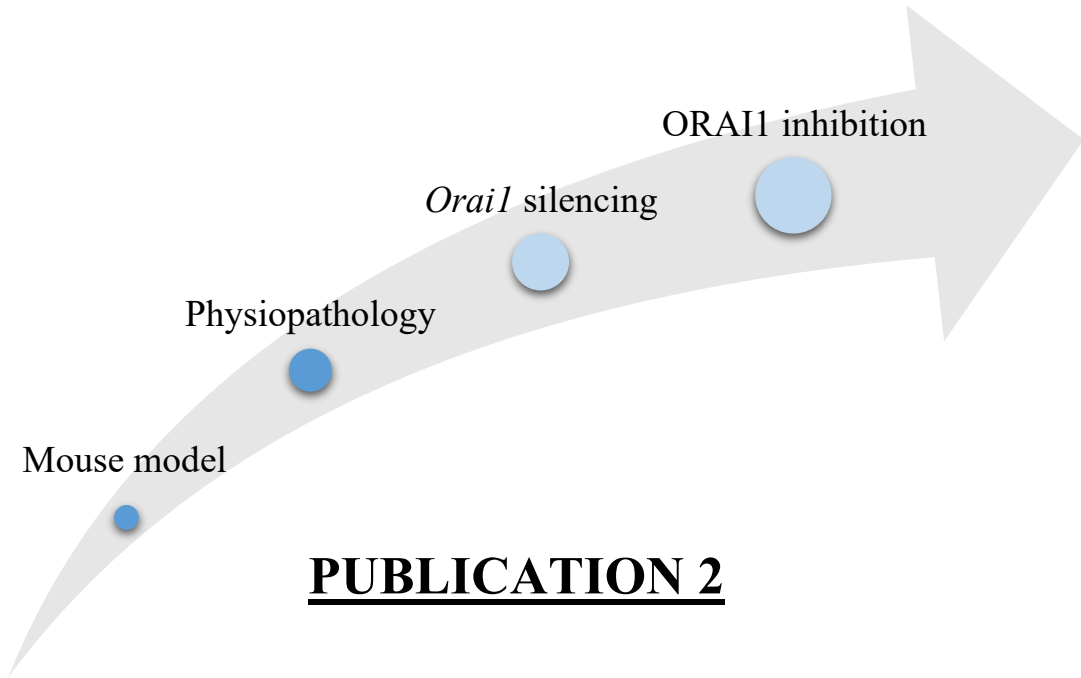
ORAI1 inhibition

Orai1 silencing

Physiopathology

Mouse model

PUBLICATION 2

Pathophysiological effects of overactive STIM1 on murine muscle function and structure

Roberto Silva-Rojas, Anne-Laure Charles, Sarah Djeddi, Bernard Geny, Jocelyn Laporte and Johann Böhm

2. PHYSIOLOGICAL EFFECTS OF CA^{2+} OVERLOAD IN SKELETAL MUSCLE FROM $STIM1^{R304W/+}$ MICE

2.1. Background

In skeletal muscle, Ca^{2+} modulates contraction, cell growth and differentiation (Berridge et al., 2003), and anomalies in Ca^{2+} handling are associated with human diseases (Gattineni, 2014). In particular, Ca^{2+} overload underlies muscle degeneration in muscle dystrophies (Burr and Molkentin, 2015; Vallejo-Illarramendi et al., 2014). High cytosolic Ca^{2+} levels were also observed in myoblast cell lines from TAM/STRMK patients and in myotubes from $Stim1^{R304W/+}$ mice (Bohm et al., 2017; Misceo et al., 2014; Morin et al., 2014; Silva-Rojas et al., 2019). Histological and ultrastructural analyses of $Stim1^{R304W/+}$ muscle samples uncovered dystrophic signs including nuclei internalization, regenerating fibers, and immune cell infiltrations, but the mechanistic link with elevated cytosolic Ca^{2+} levels was not understood.

2.2. Aim of the study

The $Stim1^{R304W/+}$ mouse model represents a valuable tool to study the pathophysiological effects of cytosolic Ca^{2+} overload. In order to determine the sequence of events leading to muscle weakness and myofiber degeneration in $Stim1^{R304W/+}$ mice, we analyzed the transcriptome of $Stim1^{R304W/+}$ muscles complemented by molecular, functional and histological analyses.

2.3. Results

RNAseq on $Stim1^{R304W/+}$ muscles uncovered an altered expression of the main players of excitation-contraction (EC) coupling, sarcoplasmic reticulum (SR) refilling and Ca^{2+} efflux at the plasma membrane, and exhibited delayed muscle contraction and relaxation upon single stimulation. Furthermore, mitochondrial amount was reduced and mitochondrial respiration decreased. $Stim1^{R304W/+}$ muscles displayed sustained ER stress levels that triggered cell death and regeneration. All experiments were performed on tibialis anterior muscle. In order to verify similar effects on two functionally different muscles, we assessed the expression of Ca^{2+} handling genes, mitochondrial function and ER stress in the soleus muscle. This is of particular interest since

tibialis anterior and soleus are functionally opposite muscles and display different Ca^{2+} sensitivities. Overall, similar defects were observed and mitochondrial respiration and amount were more affected in soleus than tibialis anterior.

2.4. Conclusion and perspectives

$Stim1^{R304W/+}$ muscles have reduced EC coupling and SR refilling as evidenced by the gene expression and *in situ* muscle contraction experiments. Mitochondrial amount is reduced and ER stress sustained, resulting in low energy production and the trigger of cell death by apoptosis, respectively. Therefore, EC coupling, SR refilling, mitochondrial biogenesis and ER stress represent drug targets for TAM/STRMK. Of note, small molecules activating EC coupling, SR refilling or reducing ER stress exist and may be beneficial to anticipate or reverse the molecular anomalies in TAM/STRMK myofibers and to counteract muscle weakness. Alternatively, the enhancement of SR refilling by overexpression of SERCA1 or silencing of the SERCA1 inhibitor *Sln* may serve as a therapeutic approach to reduce the cytosolic Ca^{2+} content and improve muscle function in TAM/STRMK.

2.5. Contribution

I performed the *in situ* muscle contraction experiments, immunofluorescence studies, western blots, and extracted RNA for RT-qPCR and RNAseq. As an internal service, RNAseq was performed by the IGBMC Genomeast sequencing platform, and the raw sequence data were processed by Sarah Djeddi. Anne-Laure Charles and Bernard Geny from Centre de Recherche en Biomedecine de Strasbourg (CRBS) performed and analyzed the mitochondrial respirometry studies on dissected mouse muscles in the frame of a scientific collaboration.

Pathophysiological Effects of Overactive STIM1 on Murine Muscle Function and Structure

Roberto Silva-Rojas [1], Anne-Laure Charles [2,3], Sarah Djeddi [1], Bernard Geny [2,3], Jocelyn Laporte [1,*] and Johann Böhm [1,*]

1   IGBMC (Institut de Génétique et de Biologie Moléculaire et Cellulaire), Inserm U1258, CNRS UMR7104, Université de Strasbourg, 67404 Illkirch, France; silvaror@igbmc.fr (R.S.-R.); djeddis@igbmc.fr (S.D.)
2   Fédération de Médecine Translationnelle de Strasbourg, Faculté de Médecine, Institut de Physiologie, Equipe d'Accueil UR3072 "Mitochondrie, Stress Oxydant et Protection Musculaire", Université de Strasbourg, 67000 Strasbourg, France; anne.laure.charles@unistra.fr (A.-L.C.); bernard.geny@chru-strasbourg.fr (B.G.)
3   Service de Physiologie et d'Explorations Fonctionnelles, Pôle de Pathologie Thoracique, Nouvel Hôpital Civil, CHRU de Strasbourg, 67000 Strasbourg, France
*   Correspondence: jocelyn@igbmc.fr (J.L.); johann@igbmc.fr (J.B.); Tel.: +33-3-88-65-34-12 (J.L. & J.B.)

Abstract: Store-operated Ca^{2+} entry (SOCE) is a ubiquitous mechanism regulating extracellular Ca^{2+} entry to control a multitude of Ca^{2+}-dependent signaling pathways and cellular processes. SOCE relies on the concerted activity of the reticular Ca^{2+} sensor STIM1 and the plasma membrane Ca^{2+} channel ORAI1, and dysfunctions of these key factors result in human pathologies. *STIM1* and *ORAI1* gain-of-function (GoF) mutations induce excessive Ca^{2+} influx through SOCE over-activation, and cause tubular aggregate myopathy (TAM) and Stormorken syndrome (STRMK), two overlapping disorders characterized by muscle weakness and additional multi-systemic signs affecting growth, platelets, spleen, skin, and intellectual abilities. In order to investigate the pathophysiological effect of overactive SOCE on muscle function and structure, we combined transcriptomics with morphological and functional studies on a TAM/STRMK mouse model. Muscles from $Stim1^{R304W/+}$ mice displayed aberrant expression profiles of genes implicated in Ca^{2+} handling and excitation-contraction coupling (ECC), and in vivo investigations evidenced delayed muscle contraction and relaxation kinetics. We also identified signs of reticular stress and abnormal mitochondrial activity, and histological and respirometric analyses on muscle samples revealed enhanced myofiber degeneration associated with reduced mitochondrial respiration. Taken together, we uncovered a molecular disease signature and deciphered the pathomechanism underlying the functional and structural muscle anomalies characterizing TAM/STRMK.

Keywords: neuromuscular disorder; congenital myopathy; muscle weakness; York platelet syndrome; calcium; STIM2

1. Introduction

Calcium (Ca^{2+}) is a ubiquitous second messenger implicated in the regulation of fundamental adaptive and developmental processes in all cell types. The activation of Ca^{2+} pumps, Ca^{2+} exchangers, and Ca^{2+} channels in response to stimuli generates transient Ca^{2+} signals, which are decoded through transduction pathways to modulate transcription, induce cell growth and differentiation, and mediate nerve conduction, hormone release, coagulation, and muscle contraction [1]. Consistently, pathologic alterations of Ca^{2+} entry, Ca^{2+} storage, or Ca^{2+} release can severely impact Ca^{2+} signaling and disturb various molecular, physiological, and biochemical functions in the tissues and organs, resulting in human diseases [2].

Tubular aggregate myopathy (TAM) is a progressive muscle disorder caused by abnormal Ca^{2+} homeostasis and characterized by muscle weakness, myalgia, and cramps [3]. Most TAM patients also manifest a varying degree of additional multi-systemic signs such

as thrombocytopenia, hyposplenism, miosis, ichthyosis, short stature, and dyslexia, and the full clinical picture constitutes the diagnosis of Stormorken syndrome (STRMK) [4–7]. TAM/STRMK arises from dominant gain-of-function (GoF) mutations in the Ca^{2+} sensor STIM1 and the Ca^{2+} channel ORAI1, and milder adult-onset cases with exclusive muscle involvement have been associated with mutations in the Ca^{2+} buffer calsequestrin (CASQ1) [8–11]. STIM1 and ORAI1 are key players of store-operated Ca^{2+} entry (SOCE), a ubiquitous mechanism triggering extracellular Ca^{2+} entry to refill the reticular Ca^{2+} stores and counteract the effects of Ca^{2+} deficit [12]. Functional investigations in the cellular model have shown that the *STIM1* and *ORAI1* mutations lead to excessive cytosolic Ca^{2+} levels through SOCE over-activation [9,11,13–19], and a recently reported TAM/STRMK mouse model harboring the most common STIM1 mutation p.Arg304Trp (R304W) was shown to exhibit elevated cytosolic Ca^{2+} levels in skeletal muscle and to recapitulate the main clinical signs of the human disorder including muscle weakness, thrombocytopenia, smaller size, and eye, skin, and spleen anomalies [20]. Histological and ultrastructural analyses of muscle sections from $Stim1^{R304W/+}$ mice confirmed the presence of fibers with Ca^{2+} overload, and additionally revealed increased muscle fiber degeneration and regeneration, as well as the presence of swollen mitochondria [20]. However, the precise molecular and cellular effect of overactive STIM1 and the associated Ca^{2+} excess on muscle function and structure remain elusive.

In order to determine the sequence of events leading to the muscle phenotype in $Stim1^{R304W/+}$ mice, we performed transcriptomic analyses on fast-twitch and slow-twitch muscles, and we identified major dysregulations of genes implicated in intracellular Ca^{2+} handling, excitation-contraction coupling (ECC), unfolded protein response (UPR), and mitochondrial dynamics. We performed complementary functional investigations on muscle contractibility and mitochondrial respiration, and we concluded that the STIM1-mediated elevated cytosolic Ca^{2+} levels interfere with muscle contraction and lead to sustained reticular stress, resulting in increased cell death and muscle fiber turnover, and thereby contribute to the muscle weakness and histological anomalies observed in TAM/STRMK.

2. Materials and Methods

2.1. Animal Care

Animal care and experimentation was in accordance with French and European legislation and approved by the institutional ethics committee (project numbers 2016031110589922 and 2020052817261437). Mice were housed in ventilated cages with free access to food and water in temperature-controlled rooms with 12 h day light/dark cycles. The $Stim1^{R304W/+}$ mouse line was described previously [20]. Sample size was determined based on Sigmastat sample size t-test and analysis of variance (ANOVA) calculator. All mice used in this study were 4 months old males as $Stim1^{R304W/+}$ mice are symptomatic at this age. They are smaller than their littermates, show spleen and eye movement defects, and manifest structural muscle anomalies [20].

2.2. DNA and RNA Studies

For DNA extraction, tibialis anterior and soleus muscle samples were homogenized in lysis buffer supplemented with 0.1 mg/mL protease K (Sigma-Aldrich, St. Louis, MO, USA) and incubated at 55 °C for 3 h. Following precipitation with 5M NaCl, DNA pellets were washed in ethanol and resuspended in H_2O. Skeletal muscle RNA from tibialis anterior and soleus was extracted with TRI Reagent (Molecular Research Center, Cincinnati, OH, USA) and reverse transcribed using the SuperScript[TM] IV Transcriptase (ThermoFisher Scientific, Waltham, MA, USA). For quantitative analyses, DNA and cDNA samples were amplified with the SYBR Green Master Mix I (Roche, Basel, Switzerland) on a LightCycler 480 Real-Time PCR System (Roche) using specific primer sets (Table S1). PCR products were Sanger-sequenced for validation.

For RNAseq, library preparation was performed with the TruSeq Stranded mRNA Sample Preparation Kit (Illumina, San Diego, CA, USA), and samples were single-end sequenced on a HiSeq4000 (Illumina). Raw data were preprocessed using cutadapt version 1.10 (https://doi.org/10.14806/ej.17.1.200), and reads with a Phred quality score above 20 and covering at least 40 nt were mapped onto the mouse genome mm10 assembly using STAR [21]. Gene expression was quantified using htseq-count [22] with annotations from Ensembl version 96 (http://www.ensembl.org/index.html) and union mode, and normalized with DESeq2 [23]. For the establishment of sample-to-sample distances heatmaps, hierarchical clustering was performed using the UPGMA (unweighted pair group method with arithmetic mean) algorithm. Gene ontology analyses were performed with Cluster-Profiler [24] using the overrepresentation test and the Benjamini–Hochberg correction for multiple testing. Enrichments with a corrected *p*-value < 0.05 were considered significant.

2.3. Protein Studies

For western blot, tibialis anterior and soleus muscles were homogenized in RIPA (radio immunoprecipitation) buffer supplemented with 1 mM PMSF and complete mini EDTA-free protease inhibitor cocktail (Roche). Denatured protein samples were loaded on SDS-PAGE, and transferred to a nitrocellulose membrane using the Transblot® TurboTM RTA Transfer Kit (Bio-Rad, Hercules, CA, USA). The following primary and secondary antibodies were used: mouse anti-DHPR (sc-514685, Santa Cruz Biotechnology, Dallas, TX, USA), mouse anti-RyR1 (MA3-925, ThermoFisher Scientific, Waltham, MA, USA), mouse anti-SERCA1 (MA3-911, ThermoFisher Scientific, Waltham, MA, USA), mouse anti-PGC1α (AB3242, Merck Millipore, Burlington, MA, USA), mouse anti-OXPHOS (ab110413, Abcam, Cambridge, UK), rabbit anti-LC3 (NB100-2220, Novus Biologicals, Littleton, CO, USA), mouse anti-P62 (H00008878-M01, Abnova, Taipeh, Taiwan), peroxidase-coupled goat anti-rabbit (112-036-045, Jackson ImmunoResearch, Ely, UK), and peroxidase-coupled goat anti-mouse (115-036-068, Jackson ImmunoResearch, Ely, UK). Immunoblots were revealed with the Supersignal west pico kit (ThermoFisher Scientific, Waltham, MA, USA), and monitored on the Amersham Imager 600 (GE Healthcare Life Sciences, Chicago, IL, USA). Ponceau S staining (Sigma-Aldrich, St. Louis, MO, USA) served as loading control.

For immunohistochemistry, 8 μm muscle sections were incubated with the following antibodies: mouse anti-myosin heavy chain type I (BA-D5, DSHB, Iowa City, IA, USA), mouse anti-myosin heavy chain type IIa (SC-71, DSHB, Iowa City, IA, USA), mouse anti-myosin heavy chain type IIb (BF-F3, DSHB, Iowa City, IA, USA), homemade rabbit anti-cleaved caspase-3, mouse anti-embryonic myosin heavy chain (F1.652, DSHB, Iowa City, IA, USA), Cy3-coupled goat anti-mouse (115-165-207, Jackson ImmunoResearch, West Grove, PA, USA), Cy5-coupled goat anti-mouse (115-545-205, Jackson ImmunoResearch, West Grove, PA, USA), DylightTM 405-coupled goat anti-mouse (115-475-075, Jackson ImmunoResearch, West Grove, PA, USA), and Alexa FluorTM 555-coupled goat anti-rabbit (A21430, ThermoFisher Scientific, Waltham, MA, USA). The sarcolemma was stained with Wheat Germ Agglutinin, Alexa FluorTM 647 conjugate (ThermoFisher Scientific, Waltham, MA, USA). Images were recorded with the Nanozoomer 2HT slide scanner (Hamamatsu Photonics, Hamamatsu, Japan), fiber type percentage was assessed using MuscleJ plug-in [25], and the percentage of regenerating fibers was assessed with cell counter plug-in.

2.4. In Situ Muscle Contraction Measurements

Mice were anesthetized through intraperitoneal injection of a domitor/fentanyl mix (2/0.28 mg/Kg), diazepam (8 mg/Kg), and fentanyl (0.28 mg/Kg). The distal tibialis anterior tendons were excised and attached to the Complete1300A isometric transducer (Aurora Scientific, Aurora, ON, Canada), and the sciatic nerve was stimulated by a single pulse of 1 Hz. Muscle contraction and relaxation speed reflect the time between stimulation and maximal force production, and the time until force decreases by 50%.

2.5. Mitochondrial Respiration

Tibialis anterior and soleus were dissected from anesthetized mice, kept in Krebs-HEPES buffer for preparation, and permeabilized by incubation in buffer S containing saponin (50 µg/mL) as previously described [26,27]. The samples were then placed into the Oxygraph-2k chamber (Oroboros instruments, Innsbruck, Austria) containing buffer R+BSA and a Clark electrode to analyze non-phosphorylating respiration and oxidative phosphorylation using a multiple substrate-uncoupler-inhibitor titration (SUIT) protocol. Complex I-linked substrate state was measured at 37 °C under continuous stirring following the addition of glutamate and malate. Then, ADP was added to activate oxidative phosphorylation through complex I (CI-linked OXPHOS state), and succinate to activate complex II (CI&II-linked OXPHOS state). Oxygen consumption is expressed as pmol/(s*mg) wet weight. H_2O_2 production was assessed simultaneously by adding amplex red and HRP in the Oxygraph-2k chamber, and is expressed as nmol/(s*mg) wet weight.

To measure superoxide anion, muscle fragments were incubated for 30 min in Krebs-HEPES buffer containing DETC and deferoxamin in a thermo-regulated incubator at 37 °C under gas mix (O2: 2.7%, N2: 97.8%) and controlled pressure (20 mmHg; Gas Treatment Chamber BIO-V and Temperature & Gas Controller BIO-III, Noxygen®, Elzach, Germany). Samples were put on ice, and oxidized probe concentrations were measured using the e-scan spectrometer (Bruker Win-EPR®, Elzach, Germany). Finally, muscle fragments were dried for 15 min at 150 °C. The results are expressed in µmol/(min*mg) dry weight.

2.6. Statistical Analyses

All experiments were performed and analyzed in a blinded manner and the investigators were unaware of the genotype of the mice. Data were verified for normal distribution using the Shapiro–Wilk test, and are presented as mean ± SEM. For normally distributed data, statistical differences between wild-type (WT) and *Stim1*$^{R304W/+}$ mice were examined using the Student's t-test (with or without Welch's correction). For other data, a non-parametric Mann–Whitney statistical test was performed.

3. Results

3.1. Transcriptomics Identifies Dysregulated Molecular Networks in Stim$^{R304W/+}$ Tibialis Anterior

Stim1$^{R304W/+}$ mice were previously shown to exhibit abnormal muscle contraction properties, and morphological analyses of muscle sections revealed fiber atrophy and the presence of internalized nuclei, indicating muscle fiber degeneration [20]. This was further supported by an elevated expression of myogenic differentiation markers in muscle samples and by increased serum creatine kinase levels in the blood of the animals [20].

To shed light on the molecular pathways affected by overactive STIM1 and to decipher the sequence of events leading to the muscle phenotype, we generated gene expression profiles through RNAseq on tibialis anterior muscle extracts from *Stim1*$^{R304W/+}$ mice and WT littermates.

Both *Stim1* alleles were expressed at comparable levels in *Stim1*$^{R304W/+}$ muscle (Figure 1A), and hierarchical clustering of the data resulted in separate sample grouping of the *Stim1*$^{R304W/+}$ and WT transcriptomes (Figure 1B). We detected a total of 3346 differentially expressed genes, which were classified into subcategories based on gene ontology (GO) terms. Several groups including the largest category GO:0002274 (myeloid leukocyte activation) were, however, unrelated to skeletal muscle and essentially encompassed genes associated with immune response (Figure S1A). This was expected because myofiber degeneration involves fiber clearance, which is mediated by immune cells [28]. We removed all groups falling under the parental GO:0002376 term immune system process (Figure S1B), and the remaining 2841 differentially expressed genes divided into GO categories associated with myofibril assembly and morphogenesis, Ca^{2+} transport and sarcoplasmic reticulum, or sarcomere organization and contraction, all reflecting essential processes in skeletal muscle development and physiology (Figure 1C).
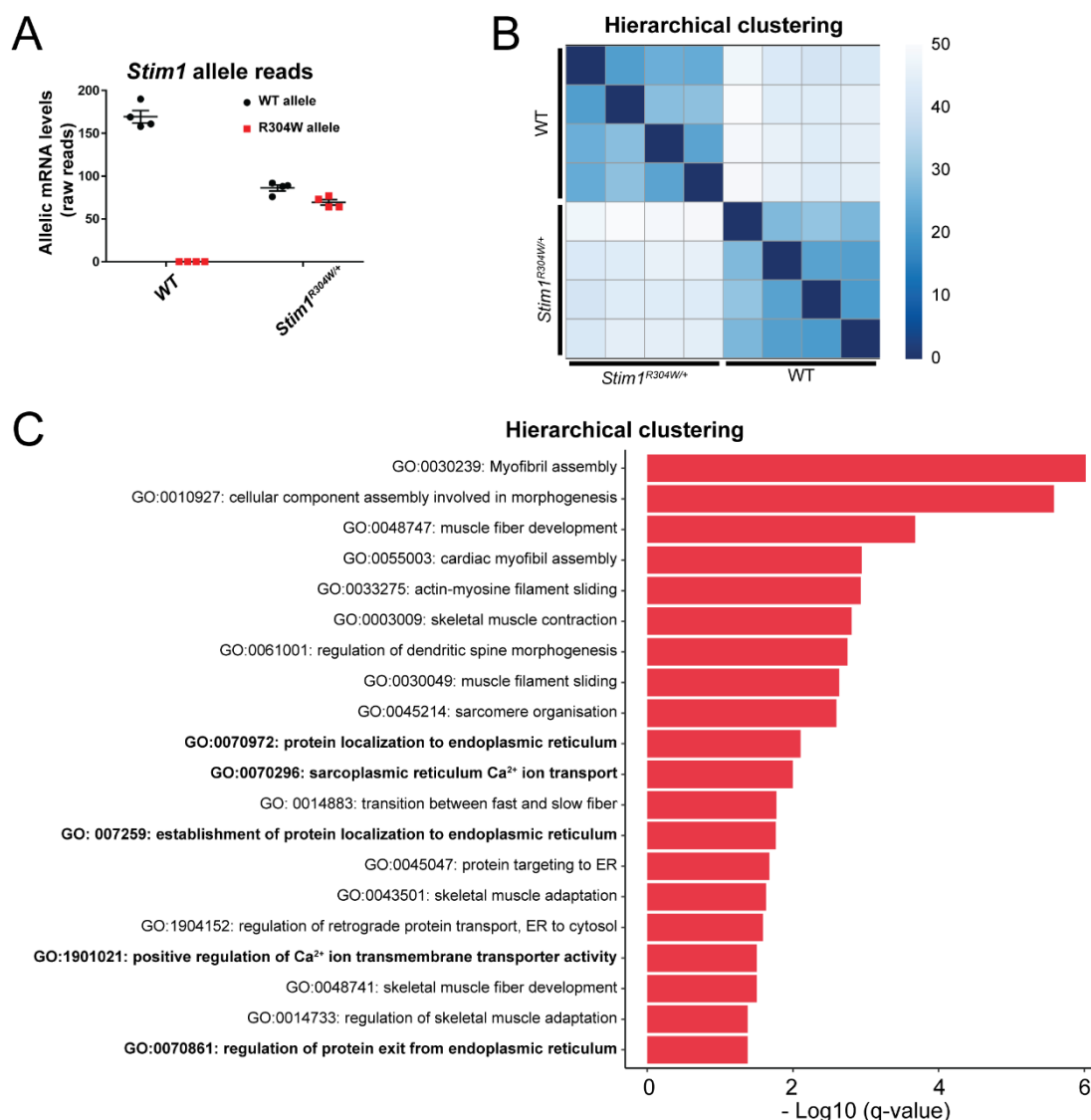
Figure 1. Transcriptomic profile of *Stim1^{R304W/+}* muscle. (**A**) RNAseq on *Stim1^{R304W/+}* tibialis anterior samples revealed a comparable expression of the mutant and WT *Stim1* alleles (*n* = 4). (**B**) Hierarchical clustering of the RNAseq data evidenced distinct sample grouping of WT and *Stim1^{R304W/+}* mice (*n* = 4). (**C**) Classification of abnormally expressed genes in *Stim1^{R304W/+}* tibialis anterior into gene ontology (GO) terms revealed an enrichment of groups associated with myofibril assembly and morphogenesis, Ca^{2+} transport and sarcoplasmic reticulum, and sarcomere organization and contraction. GO categories related to the immune system were removed from the analysis.

3.2. Altered Regulators of Ca^{2+} Handling and Excitation-Contraction Coupling in Stim1^{R304W/+} Tibialis Anterior

In accordance with the assumption that TAM/STRMK is mainly caused by excessive extracellular Ca^{2+} influx [9,11], genes implicated in the Ca^{2+} transport across the sarcolemma (GO:1901021) and the sarcoplasmic reticulum membrane (GO:0070296) were considerably dysregulated in *Stim1^{R304W/+}* muscle. In order to validate the RNAseq data, we determined the relative expression of selected genes and proteins driving intracellular Ca^{2+} handling and Ca^{2+}-related excitation-contraction coupling (ECC) by RT-qPCR and western blot.

Each cell possesses a panel of Ca^{2+} channels, Ca^{2+} pumps, and Ca^{2+} exchangers to control Ca^{2+} flows within the cytosol and between the organelles and orchestrate the complex spatiotemporal interplay of Ca^{2+}-dependent pathways and processes. *Atp2b1* and *Slc8a1*, encoding a plasma membrane Ca^{2+} pump and a Na^+/Ca^{2+} exchanger, respectively, were

significantly downregulated in *Stim1^{R304W/+}* muscles compared with controls (Figure 2A,B). This points to an impaired extrusion of excessive Ca^{2+} from the cytosol, and provides an explanation for the permanently elevated cytosolic Ca^{2+} levels in TAM/STRMK muscle fibers. In agreement, we also measured a decreased expression of *Atp2a1*, encoding the reticular Ca^{2+} pump SERCA1, and a simultaneous upregulation of *Sln*, coding for the SERCA1 inhibitor sarcolipin in the *Stim1^{R304W/+}* muscles (Figure 2A,C,D and Figure S2A).
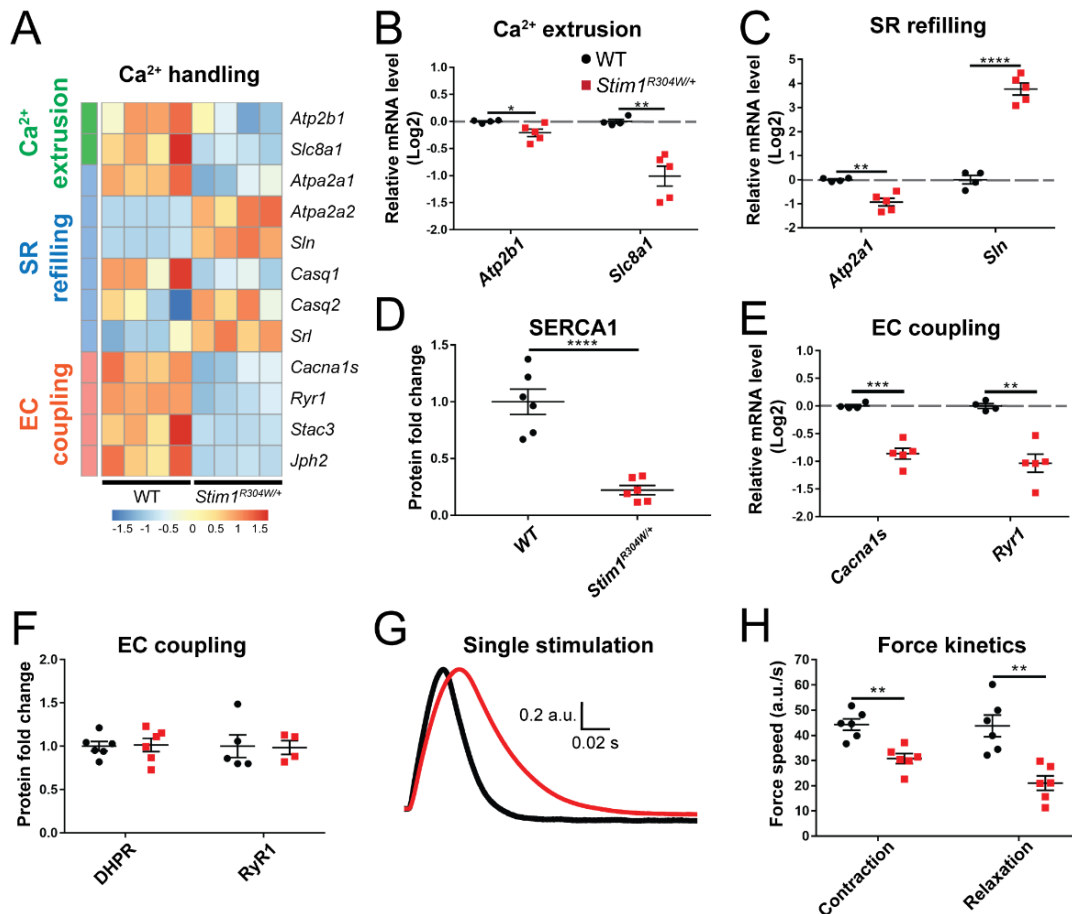
Figure 2. Altered expression of Ca^{2+} handling genes in *Stim1^{R304W/+}* muscle and abnormal contraction and relaxation properties. (**A**) RNAseq heatmap illustrating the relative expression of genes implicated in Ca^{2+} extrusion, sarcoplasmic reticulum (SR) refilling, and excitation-contraction (EC) coupling in *Stim1^{R304W/+}* and wild-type (WT) tibialis anterior (*n* = 4). (**B**) RT-qPCR showing reduced expression of *Atp2b1* (encoding a plasma membrane Ca^{2+} pump) and *Slc8a1* (plasma membrane Na^+/Ca^{2+} exchanger) in *Stim1^{R304W/+}* mice (*n* = 4–5). (**C,D**) SERCA1 gene expression and protein levels are reduced in *Stim1^{R304W/+}* mice, while *Sln* expression is increased (*n* = 4–6). (**E,F**) Downregulation of *Cacna1s* and *Ryr1* in *Stim1^{R304W/+}* tibialis anterior, but normal DHPR and RyR1 protein levels (*n* = 4–6). (**G,H**) Mean normalized force production following a single 1 Hz stimulation showing delayed muscle contraction and relaxation speed in *Stim1^{R304W/+}* mice (*n* = 6). Significant differences are illustrated as * ($p < 0.05$), ** ($p < 0.01$), *** ($p < 0.001$), and **** ($p < 0.0001$).

ECC refers to the generation of muscle force through a multistep process beginning with the electrical stimulation of the voltage-gated Ca^{2+} channel DHPR at the plasma membrane, and concluding with the activation of the reticular Ca^{2+} channel RyR1 and the subsequent release of Ca^{2+} to the cytosol [29]. Cytosolic Ca^{2+} overload is known to interfere with ECC [30,31], and consistently, we observed a reduced expression of *Cacna1s*, encoding the pore-forming subunit of DHPR, and of *Ryr1* and the ECC-regulating genes *Stac3* and *Jph2* in *Stim1^{R304W/+}* muscle samples (Figure 2A,E). We, however, also noted that the DHPR and RyR1 protein levels were similar in TAM/STRMK and WT mice (Figure 2F and Figure S2B,C). As the RT-qPCR and western blot data were not fully conclusive, we investigated the in situ muscle contraction properties of *Stim1^{R304W/+}* and WT tibialis

anterior to determine a possible functional alteration of ECC. Following single-pulse stimulations of the sciatic nerve, *Stim1*$^{R304W/+}$ mice manifested a delay in muscle force production compared with the controls (Figure 2G,H and Figure S2D), reflecting a defective coupling between excitation and contraction. We also observed a delay in muscle relaxation in *Stim1*$^{R304W/+}$ muscles (Figure 2G,H), supposedly resulting from the abundance of Ca^{2+} in the cytosol and at the contractile unit.

Taken together, our data suggest that the Ca^{2+} extrusion systems in *Stim1*$^{R304W/+}$ muscle fibers are impaired and enhance the cytosolic Ca^{2+} surcharge induced by SOCE overactivity, compromising both muscle contraction and relaxation kinetics.

3.3. Less Mitochondria in Stim1$^{R304W/+}$ Tibialis Anterior

Mitochondria were the first intracellular organelles to be associated with an active role in Ca^{2+} homeostasis [32]. They act as Ca^{2+} buffers to rapidly remove Ca^{2+} from the cytosol, and can free large amounts of Ca^{2+} in defined subcellular domains to generate local Ca^{2+} gradients [33]. It is, therefore, possible that the constitutive Ca^{2+} excess in *Stim1*$^{R304W/+}$ muscle fibers overcharges the mitochondria and accounts for the mitochondrial swelling observed by electron microscopy [20]. Comparative analysis of the RNAseq, RT-qPCR, and western blot data revealed a moderately reduced expression of genes implicated in mitochondrial biogenesis (*Ppargc1a*, *Sirt1*, *Nrf1*, *Tfam*) and decreased levels of proteins of the electron transport chain, suggesting a lower number of mitochondria in *Stim1*$^{R304W/+}$ tibialis anterior samples compared with controls (Figure 3A–C and Figure S3A–C). Indeed, quantification of the *mt16S*, *Cox2*, and *Loop* genes, all encoded on the mitochondrial DNA, confirmed a tendency towards a reduced mitochondrial copy number in *Stim1*$^{R304W/+}$ muscle (Figure 3D). We furthermore found a downregulation of genes and proteins driving mitochondrial migration (*Rhot1* and *Trak1*) and fission (*Dnm1l*, *Fis1*), while the expression of genes relevant for mitochondrial fusion (*Opa1* and *Mfn2*) was comparable in *Stim1*$^{R304W/+}$ and WT mice (Figure 3A,E,F). To explore a potential impact of the molecular defects on organelle function, we next determined mitochondrial respiration in dissected *Stim1*$^{R304W/+}$ and WT tibialis anterior muscles.

Respirometric and spectrometric analyses revealed a slight, but not significant reduction of complex I-linked substrate state, complex I-linked OXPHOS state, and complex I/complex II- linked OXPHOS state in *Stim1*$^{R304W/+}$ muscle, and a comparable reactive oxygen species (ROS) production in *Stim1*$^{R304W/+}$ mice and controls (Figure 3G,H and Figure S3D). Overall, our findings suggest that mitochondrial respiration is largely normal in *Stim1*$^{R304W/+}$ muscles. We, however, found evidence of a decreased mitochondrial number, which may contribute to the muscle weakness in TAM/STRMK mice and patients. The swollen mitochondria possibly results from impaired mitochondrial fission.

3.4. ER Stress and Increased Cell Death in Stim1$^{R304W/+}$ Tibialis Anterior

The sarcoplasmic reticulum (SR) is a specialized type of smooth endoplasmic reticulum (ER), represents the primary Ca^{2+} storage organelle in striated muscle cells, and controls intracellular Ca^{2+} cycling through the concerted regulation of Ca^{2+} uptake, Ca^{2+} storage, and Ca^{2+} release [34]. The dysregulation of Ca^{2+} homeostasis in the ER/SR promotes the accumulation of unfolded or misfolded proteins and initiates a protective process known as UPR (unfolded protein response), which interrupts protein translation, degrades unfolded proteins, and activates signaling pathways to produce chaperones [35]. Numerous UPR genes (*Hspa5*, *Hsp90b1*, *Xbp1*, *Ddit3*) were overexpressed in *Stim1*$^{R304W/+}$ muscles compared with WT controls, indicating an important Ca^{2+} stress (Figure 4A,B). We also noticed an upregulation of genes associated with apoptosis (*Bbc3*, *Bmaip1*, *Trib3*), and immunofluorescence experiments confirmed the higher incidence of apoptotic fibers on *Stim1*$^{R304W/+}$ muscle sections (Figure 4A,C and Figure S4). This is in agreement with the notion that continuous Ca^{2+} stress ultimately leads to cell death [35]. Along with the histological signs of muscle fiber degeneration [20], the upregulation of genes involved in muscle fiber regeneration (*Myh3*, *Myh8*), and the occurrence of regenerating fibers in

Stim1^{R304W/+} muscle (Figure 4A,D,E and Figure S4), our data suggest that the STIM1 R304W mutation induces constitutive ER/SR stress and results in increased cycles of muscle fiber degeneration and regeneration.
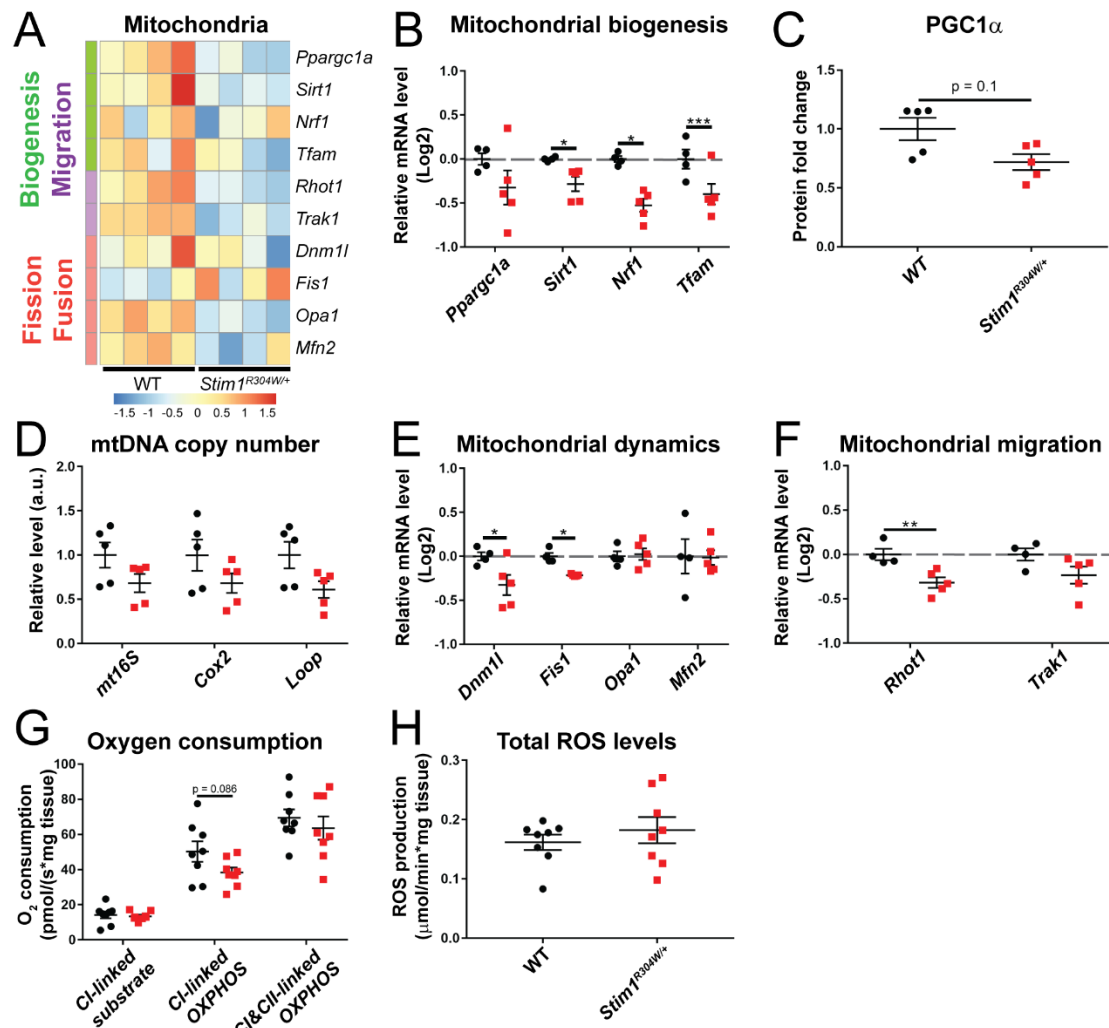
Figure 3. Minor mitochondrial defects in *Stim1^{R304W/+}* muscle. (**A**) RNAseq heatmap showing the relative gene expression of genes involved in mitochondrial biogenesis, migration, fission, and fusion in *Stim1^{R304W/+}* and WT tibialis anterior (*n* = 4). (**B,C**) RT-qPCR confirmed the reduction of the mitochondrial biogenesis genes *Sirt1*, *Nrf1*, and *Tfam* in *Stim1^{R304W/+}* mice, and indicates a decreased PGC1α (*Ppargc1a*) gene expression and protein level (*n* = 4–5). (**D**) The quantities of the mitochondrial copy number maker genes *mt16S*, *Cox2*, and *Loop* tend to be reduced in *Stim1^{R304W/+}* tibialis anterior (*n* = 5). (**E,F**) Mitochondrial fission (*Dnm1l* and *Fis1*) and migration (*Rhot1*) genes are downregulated in *Stim1^{R304W/+}* mice (*n* = 4–5). (**G,H**) Analysis of oxygen consumption shows a comparable mitochondrial non-phosphorylating respiration (CI-linked substrate), oxidative phosphorylation (CI-linked OXPHOS and CI/CII-linked OXPHOS), and ROS production in *Stim1^{R304W/+}* and WT tibialis anterior (*n* = 8). Significant differences are illustrated as * ($p < 0.05$), ** ($p < 0.01$), and *** ($p < 0.001$).
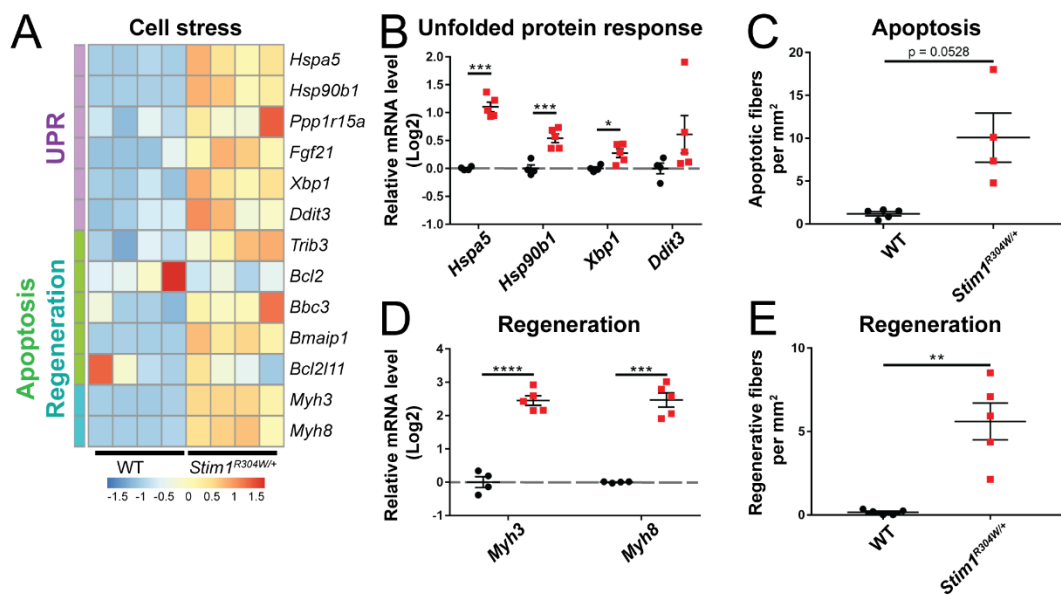
Figure 4. Unsolved reticular stress leading to muscle fiber turnover in *Stim1*$^{R304W/+}$ mice. (**A**) RNAseq heatmap depicting the relative gene expression of genes implicated in unfolded protein response (UPR), apoptosis, and muscle fiber regeneration in *Stim1*$^{R304W/+}$ and WT tibialis anterior (*n* = 4). (**B**) RT-qPCR validates the upregulation of genes encoding chaperones (*Hspa5* and *Hsp90b1*), and the XBP1 transcription factor (*Xbp1*) in *Stim1*$^{R304W/+}$ tibialis anterior (*n* = 4–5). (**C**) Apoptotic fibers tend to be more abundant on *Stim1*$^{R304W/+}$ muscle sections than in controls (*n* = 4–5). (**D**,**E**) Upregulation of the embryonic (*Myh3*) and perinatal (*Myh8*) myosin genes in *Stim1*$^{R304W/+}$ tibialis anterior, and significant increase of regenerating muscle fibers (*n* = 4–5). Significant differences are illustrated as * ($p < 0.05$), ** ($p < 0.01$), *** ($p < 0.001$), and **** ($p < 0.0001$).

3.5. Comparison between Stim1$^{R304W/+}$ Fast-Twitch and Slow-Twitch Muscles

Skeletal muscle is composed of slow-twitch type I and fast-twitch type II fibers, and the ratio and distribution of the individual fiber types characterizes each muscle and its adaptation to either powerful movements or endurance activities [36,37]. The glycolytic tibialis anterior muscle, essentially containing fast type II muscle fibers, was used for the quantification of gene expression and the consecutive functional investigations on *Stim1*$^{R304W/+}$ and WT mice. In order to provide a comparative analysis between fast-twitch and slow-twitch muscles and to explore a potentially diverging effect of overactive STIM1 on slow type I fibers, we assessed the relative expression of selected marker genes in soleus muscle extracts from *Stim1*$^{R304W/+}$ mice and controls. This is of particular interest as type I and type II muscle fibers differ in their SR Ca^{2+} content and cytosolic Ca^{2+} concentration at rest, and feature a different Ca^{2+} sensitivity [38,39].

In analogy to the fast-twitch tibialis anterior, RT-qPCR uncovered a downregulation of *Serca1* and a simultaneous upregulation of the SERCA1 inhibitor *Sln* in the slow-twitch soleus muscle (Figure 5A,B and Figure S5A–C). We, however, noted a normal expression level of *Atp2b1* and *Slc8a1* (Figure 5A), indicating that the extrusion of excessive Ca^{2+} may be less affected in the soleus. Compared with tibialis anterior, the mitochondrial copy number was markedly reduced in *Stim1*$^{R304W/+}$ soleus, and this was substantiated by a significant decrease in mitochondrial non-phosphorylating respiration, oxidative phosphorylation, and ROS production (Figure 5C–F and Figure S6A–D). As type I and type II muscle fibers differ in mitochondrial content and mitochondrial activity, we next explored the fiber type composition in *Stim1*$^{R304W/+}$ soleus. Immunofluorescence experiments on transverse muscle sections evidenced an increased ratio of mitochondria-rich type I muscle fibers in *Stim1*$^{R304W/+}$ mice compared with the WT (Figure S7A), suggesting a fast-to-slow muscle fiber conversion associated with relevant mitochondrial loss in *Stim1*$^{R304W/+}$ soleus, and highlighting a fiber type-specific effect of the STIM1 R304W mutation on mitochondria. Finally, the marker genes for ER/SR stress and myofiber regeneration were overexpressed in the *Stim1*$^{R304W/+}$ soleus compared with the control, and immunofluorescence on muscle

sections provided the evidence for increased apoptosis and muscle fiber regeneration as observed in tibialis anterior (Figure 5G–I and Figure S7B).
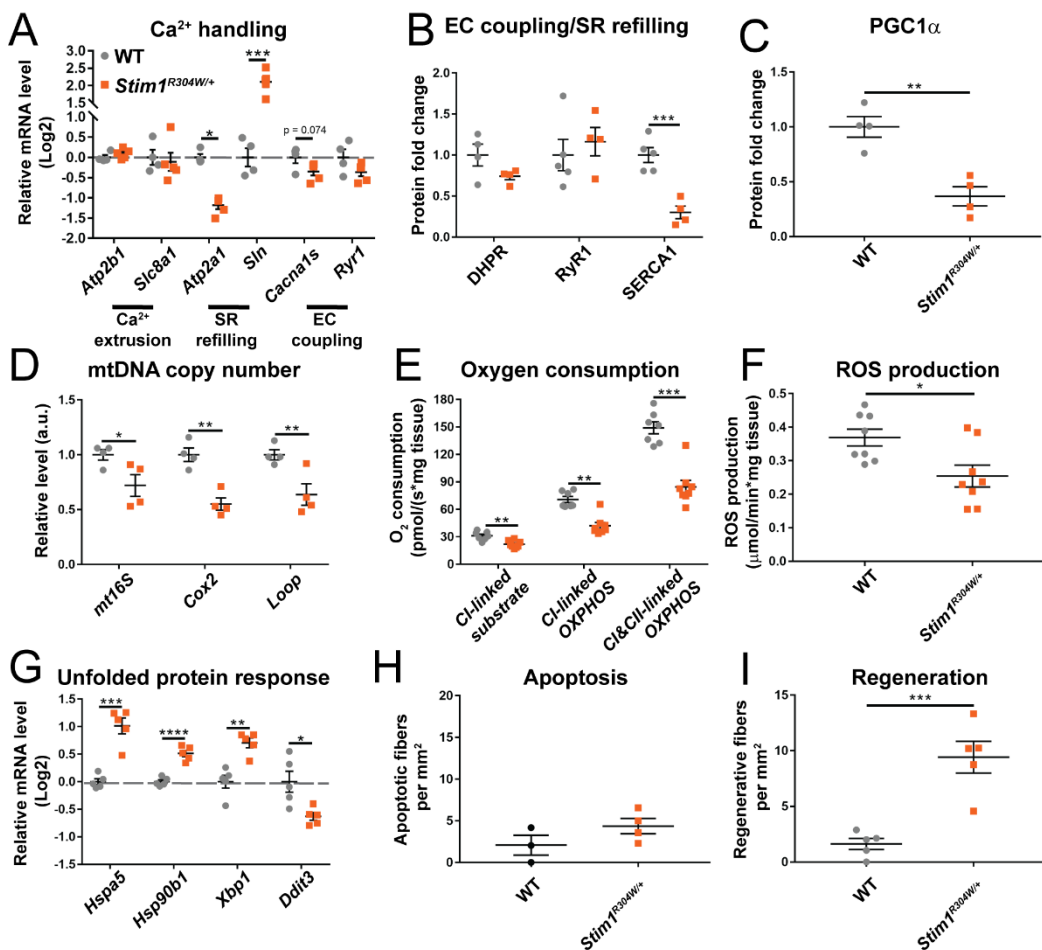
Figure 5. Defective Ca^{2+} handling, reduced mitochondrial copy number, and increased reticular stress in *Stim1*$^{R304W/+}$ slow-twitch muscle. (**A,B**) RT-qPCR on selected genes illustrates a reduction of SERCA1 gene expression and protein level and a simultaneous upregulation of the SERCA1 inhibitor *Sln* in *Stim1*$^{R304W/+}$ soleus, while other genes involved in Ca^{2+} handling are normally expressed (*n* = 4–5). (**C,D**) In agreement with the reduced protein level of the mitochondrial biogenesis regulator PGC1α in *Stim1*$^{R304W/+}$ soleus, the mitochondrial copy number marker genes *mt16s*, *Cox2*, and *Loop* are decreased compared with the WT (*n* = 4). (**E,F**) Oxygen consumption and ROS production are significantly lower in *Stim1*$^{R304W/+}$ compared with WT soleus (*n* = 7–8). (**G**) Increased UPR in *Stim1*$^{R304W/+}$ soleus as illustrated by the upregulation of the stress-regulated genes *Hspa5*, *Hsp90b1*, and *Xbp1* (*n* = 4–5). (**H,I**) *Stim1*$^{R304W/+}$ soleus sections show a tendency of augmented apoptosis and a significant increase of regenerating fibers compared with controls (*n* = 3-5). Significant differences are illustrated as * ($p < 0.05$), ** ($p < 0.01$), *** ($p < 0.001$), and **** ($p < 0.0001$).

In summary, *Stim1*$^{R304W/+}$ tibialis anterior and soleus displayed comparable molecular defects of ECC, reticular Ca^{2+} uptake, and ER physiology, while the deficits in mitochondrial copy number and respiration were more pronounced in the soleus. Apart from the differences in mitochondrial content and activity, our data indicate that the aberrant Ca^{2+} homeostasis in TAM/STRMK affects slow-twitch and fast-twitch muscle fibers to a similar extent, leading to muscle fiber degeneration of both type I and type II fibers.

4. Discussion

4.1. From Constitutive STIM1 Activation to Abnormal Muscle Contraction and Relaxation Kinetics, Muscle Fiber Degeneration, and Mitochondrial Loss

Tubular aggregate myopathy (TAM) and Stormorken syndrome (STRMK) are overlapping disorders principally resulting from abnormal Ca^{2+} balance and affecting skeletal

muscle, platelets, spleen, and skin. *Stim1*$^{R304W/+}$ mice expressing a constitutively active STIM1 mutant feature cytosolic Ca^{2+} overload in the muscle fibers and manifest functional and structural muscle anomalies [20]. Here, we deciphered the sequence of events triggered by overactive STIM1 and leading to the muscle phenotype in the TAM/STRMK mouse model, and we provide transcriptomic, proteomic, and functional data. We demonstrate that the STIM1-mediated abundance of Ca^{2+} impedes accurate muscle contraction and relaxation of tibialis anterior, and induces constitutive reticular stress in both slow-twitch and fast-twitch muscles, ultimately leading to myofiber degeneration and mitochondrial loss.

The coordinated process of muscle contraction is intrinsically linked to the strict regulation of the Ca^{2+} flows between the sarcoplasmic reticulum and the cytosol, hosting the contractile unit. Ca^{2+} triggers the shortening of the sarcomere to generate muscle force, and muscle relaxation occurs when Ca^{2+} is pumped back to the SR [40]. The dysregulation of Ca^{2+} homeostasis can thus interfere with proper excitation-contraction coupling and compromise normal muscle function. In line with the elevated resting Ca^{2+} levels in the cytosol of *Stim1*$^{R304W/+}$ myotubes [20], our in situ force measurement on the murine TAM/STRMK model disclosed extensive ECC perturbations as shown by the aberrant muscle contraction kinetics. The delayed relaxation of *Stim1*$^{R304W/+}$ tibialis anterior following muscle contraction most probably reflects a direct consequence of the inefficient Ca^{2+} removal from the sarcomere, and presumably accounts for the muscle stiffness, cramps, and myalgia observed in TAM/STRMK patients [5]. The Ca^{2+} abundance at the contractile unit primarily comes from the excessive extracellular Ca^{2+} influx through SOCE overactivation, and is exacerbated by the downregulation of the SR Ca^{2+} pump SERCA1 and the reduced expression of plasma membrane Ca^{2+} pumps and Ca^{2+} exchangers, resulting in the inability of the muscle fibers to efficiently clear the Ca^{2+} from the cytosol.

The SERCA1 downregulation and the concurrent upregulation of the SERCA1 inhibitor sarcolipin in both tibialis anterior and soleus possibly represent a protective effort of the *Stim1*$^{R304W/+}$ muscle fibers to limit reticular Ca^{2+} overload and ensure ordered protein synthesis, folding, modification, and transport. Our RNAseq data, however, uncovered a significant overexpression of several UPR marker genes, evidencing distinct reticular Ca^{2+} stress in *Stim1*$^{R304W/+}$ muscle. In accordance with the fact that steady reticular stress ineluctably leads to cell death [35], we detected signs of apoptosis and enhanced muscle fiber degeneration and regeneration cycles in *Stim1*$^{R304W/+}$ mice. Muscle fiber degeneration also involved mitochondrial loss especially in the soleus, which is principally composed of mitochondria-rich type I muscle fibers. Noteworthy, we found an increased ratio of type I fibers in the soleus from *Stim1*$^{R304W/+}$ mice, indicating a conversion from fast to slow myofibers. This is in accordance with previous findings in mice carrying a *Cacna1s* mutation and displaying elevated cytosolic Ca^{2+} levels [41], and a shift towards slow-twitch muscle fibers was also observed in rabbits following muscle fiber degeneration and regeneration [42]. This suggests that the altered myofiber composition in *Stim1*$^{R304W/+}$ soleus is a direct consequence of the Ca^{2+}-induced muscle fiber degeneration.

4.2. Physiological and Structural Similarities in TAM/STRMK and Other Disorders Affecting ECC

Abnormal Ca^{2+} homeostasis interfering with regular muscle contraction and impacting efficient force production is also seen in disorders affecting the key players of the ECC machinery. A large number of mutations in *RYR1* are associated with central core disease (CCD), clinically characterized by childhood-onset hypotonia and proximal muscle weakness [43]. Functional investigations have shown that the mutations either alter the interaction with DHPR, or generate a leaky RyR1 Ca^{2+} channel involving a constitutive cytosolic Ca^{2+} overload [44–46]. In any case, the amount of released Ca^{2+} upon membrane depolarization and DHPR activation is reduced, evidencing an uncoupling of excitation from contraction [47]. In analogy and reflecting significant ECC defects, the *Stim1*$^{R304W/+}$ mice manifested a delay in muscle force production and a downregulation of *RyR1* and *Cacna1s*. Reduced *RYR1* expression levels were also found in differentiated myotubes derived from a TAM/STRMK patient carrying the STIM1 p.Leu96Val (L96V) mutation and

presenting with early-onset lower limb muscle weakness and myalgia [48,49], emphasizing the importance of normal cellular Ca^{2+} balance for effective muscle contraction, and suggesting that the Ca^{2+}-related dysregulation of ECC contributes to the muscle weakness characterizing CCD and TAM/STRMK.

Other *RYR1* mutations render the RyR1 channel hypersensitive to triggering agents in volatile anesthetics and induce excessive Ca^{2+} release from the SR, resulting in malignant hyperthermia (MH) [50,51]. MH is a potentially lethal disorder involving uncontrolled contractures, hyperkalemia, hypermetabolism, and cardiac arrhythmia [52,53]. In a similar way, specific mutations in *CACNA1S*, encoding the alpha-1S subunit of the voltage-gated Ca^{2+} channel DHPR, were shown to increase the sensitivity of RyR1 to activation, resulting in elevated resting Ca^{2+} levels in the cytosol [54,55]. It is noteworthy that muscle biopsies from MH patients display alterations of mitochondrial shape and distribution, indicating abnormal mitochondrial dynamics [56]. This is comparable to the ultrastructural pictures of the mitochondria in muscle samples from the *Stim1$^{R304W/+}$* mice and another TAM/STRMK mouse model carrying the STIM1 I115F mutation [57], and conforms to our RNAseq and RT-qPCR data indicating a reduced expression of genes implicated in mitochondrial fission and migration. Taking into account that cytosolic Ca^{2+} overload is a hallmark of MH and TAM/STRMK, it is conceivable that both disorders share at least partially a common pathomechanism. Although not reported in the literature, TAM/STRMK patients may thus be at risk for MH, and this is supported by the fact that mice lacking the TAM gene *Casq1* exhibit a MH-like phenotype [58]. However, our respirometric experiments provided evidence that mitochondrial respiration is decreased, but functionally normal in *Stim1$^{R304W/+}$* muscle, suggesting that mitochondrial dysfunction is not a contributing factor for TAM/STRMK. In accordance, *Casq1* null mice did not show anomalies of the mitochondrial morphology [58]. The reduced mitochondrial copy number, especially in *Stim1$^{R304W/+}$* slow-twitch muscle fibers, might nevertheless provoke a gap in the required energy production and add to the muscle weakness in TAM/STRMK mice and patients.

4.3. Ca^{2+} Stress in Myopathies and Dystrophies, and Potential Treatment Options

Mice carrying the CCD-related RyR1 mutation p.Ile4895Thr (I4895T) in the pore-forming C-terminus of the channel were reported to manifest increased reticular stress, leading to the activation of UPR in muscle fibers [59], highlighting yet another similarity between *RYR1*-related disorders and TAM/STRMK. This congruence can be explained by the mechanistic interconnection between ECC and SOCE. Indeed, calsequestrin (CASQ1) actively regulates the amount of Ca^{2+} release from the SR in a quaternary complex with RyR1, junction, and triadin [60], and sequesters STIM1 upon Ca^{2+} store depletion, thereby acting as a negative regulator of SOCE [61]. STIM1 was furthermore found to bind DHPR and to suppress depolarization-induced channel opening [62], illustrating a reciprocal regulation of ECC and SOCE.

Of note, treatment of the *Ryr1$^{I4895T/+}$* mice with the chemical chaperone 4-PBA reduced reticular stress and improved skeletal muscle function [59], suggesting that the anticipation of UPR may have a similar therapeutic effect for TAM/STRMK mice and prevent myofiber degeneration. UPR along with a high cytosolic Ca^{2+} content and aberrant ECC was also described in Duchenne muscular dystrophy (DMD), associating progressive muscle loss with dilated cardiomyopathy [63,64], and administration of 4-PBA reduced exercise-induced muscle damage and considerably improved the muscle phenotype in mdx mice, a well-studied murine model for DMD [65]. Moreover, treatment with the ECC effector taurine, overexpression of SERCA, or silencing of the SERCA inhibitor Sarcolipin efficiently decreased the cytosolic Ca^{2+} levels, restored ECC, and alleviated muscle fiber degeneration in mdx mice [66–68], potentially representing additional therapeutic options for TAM/STRMK. Several TAM/STRMK mouse models carrying different STIM1 mutations as D84G [69], I115F [57], or R304W [20,70] exist, and the animals diverge in the occurrence and severity of the muscle and multi-systemic signs. These models thus represent valuable

tools to establish general or mutation-specific treatments and validate their potency to attenuate or revert the muscle, spleen, skin, or platelet phenotypes.

5. Conclusions

The present study revealed a molecular disease signature of TAM/STRMK, and identified abnormal muscle contraction and relaxation kinetics as well as constitutive reticular stress leading to myofiber degeneration as the main cellular pathologies underlying the functional and structural muscle anomalies in $Stim1^{R304W/+}$ mice. The partial overlap with other diseases including malignant hyperthermia, central core disease, and Duchenne muscular dystrophy points to common pathomechanisms and suggests that a unique therapy may efficiently improve the muscular phenotype in different Ca^{2+}-related disorders.

References

1. Berridge, M.J.; Bootman, M.D.; Roderick, H.L. Calcium signalling: Dynamics, homeostasis and remodelling. *Nat. Rev. Mol. Cell Biol.* **2003**, *4*, 517–529. [CrossRef]
2. Gattineni, J. Inherited disorders of calcium and phosphate metabolism. *Curr. Opin. Pediatr.* **2014**, *26*, 215–222. [CrossRef] [PubMed]
3. Chevessier, F.; Bauche-Godard, S.; Leroy, J.P.; Koenig, J.; Paturneau-Jouas, M.; Eymard, B.; Hantai, D.; Verdiere-Sahuque, M. The origin of tubular aggregates in human myopathies. *J. Pathol.* **2005**, *207*, 313–323. [CrossRef] [PubMed]
4. Bohm, J.; Laporte, J. Gain-of-function mutations in STIM1 and ORAI1 causing tubular aggregate myopathy and Stormorken syndrome. *Cell Calcium* **2018**, *76*, 1–9. [CrossRef] [PubMed]
5. Morin, G.; Biancalana, V.; Echaniz-Laguna, A.; Noury, J.B.; Lornage, X.; Moggio, M.; Ripolone, M.; Violano, R.; Marcorelles, P.; Marechal, D.; et al. Tubular aggregate myopathy and Stormorken syndrome: Mutation spectrum and genotype/phenotype correlation. *Hum. Mutat.* **2020**, *41*, 17–37. [CrossRef]
6. Lacruz, R.S.; Feske, S. Diseases caused by mutations in ORAI1 and STIM1. *Ann. N. Y. Acad. Sci.* **2015**, *1356*, 45–79. [CrossRef]
7. Silva-Rojas, R.; Laporte, J.; Bohm, J. STIM1/ORAI1 Loss-of-Function and Gain-of-Function Mutations Inversely Impact on SOCE and Calcium Homeostasis and Cause Multi-Systemic Mirror Diseases. *Front. Physiol.* **2020**, *11*, 604941. [CrossRef]

8. Barone, V.; Del Re, V.; Gamberucci, A.; Polverino, V.; Galli, L.; Rossi, D.; Costanzi, E.; Toniolo, L.; Berti, G.; Malandrini, A.; et al. Identification and characterization of three novel mutations in the CASQ1 gene in four patients with tubular aggregate myopathy. *Hum. Mutat.* **2017**, *38*, 1761–1773. [CrossRef]

9. Bohm, J.; Chevessier, F.; Maues De Paula, A.; Koch, C.; Attarian, S.; Feger, C.; Hantai, D.; Laforet, P.; Ghorab, K.; Vallat, J.M.; et al. Constitutive activation of the calcium sensor STIM1 causes tubular-aggregate myopathy. *Am. J. Hum. Genet.* **2013**, *92*, 271–278. [CrossRef]

10. Bohm, J.; Lornage, X.; Chevessier, F.; Birck, C.; Zanotti, S.; Cudia, P.; Bulla, M.; Granger, F.; Bui, M.T.; Sartori, M.; et al. CASQ1 mutations impair calsequestrin polymerization and cause tubular aggregate myopathy. *Acta Neuropathol.* **2018**, *135*, 149–151. [CrossRef]

11. Nesin, V.; Wiley, G.; Kousi, M.; Ong, E.C.; Lehmann, T.; Nicholl, D.J.; Suri, M.; Shahrizaila, N.; Katsanis, N.; Gaffney, P.M.; et al. Activating mutations in STIM1 and ORAI1 cause overlapping syndromes of tubular myopathy and congenital miosis. *Proc. Natl. Acad. Sci. USA* **2014**, *111*, 4197–4202. [CrossRef] [PubMed]

12. Stathopulos, P.B.; Zheng, L.; Li, G.Y.; Plevin, M.J.; Ikura, M. Structural and mechanistic insights into STIM1-mediated initiation of store-operated calcium entry. *Cell* **2008**, *135*, 110–122. [CrossRef] [PubMed]

13. Bohm, J.; Bulla, M.; Urquhart, J.E.; Malfatti, E.; Williams, S.G.; O'Sullivan, J.; Szlauer, A.; Koch, C.; Baranello, G.; Mora, M.; et al. ORAI1 Mutations with Distinct Channel Gating Defects in Tubular Aggregate Myopathy. *Hum. Mutat.* **2017**, *38*, 426–438. [CrossRef] [PubMed]

14. Endo, Y.; Noguchi, S.; Hara, Y.; Hayashi, Y.K.; Motomura, K.; Miyatake, S.; Murakami, N.; Tanaka, S.; Yamashita, S.; Kizu, R.; et al. Dominant mutations in ORAI1 cause tubular aggregate myopathy with hypocalcemia via constitutive activation of store-operated Ca^{2+} channels. *Hum. Mol. Genet.* **2015**, *24*, 637–648. [CrossRef] [PubMed]

15. Harris, E.; Burki, U.; Marini-Bettolo, C.; Neri, M.; Scotton, C.; Hudson, J.; Bertoli, M.; Evangelista, T.; Vroling, B.; Polvikoski, T.; et al. Complex phenotypes associated with STIM1 mutations in both coiled coil and EF-hand domains. *Neuromuscul. Disord.* **2017**, *27*, 861–872. [CrossRef]

16. Misceo, D.; Holmgren, A.; Louch, W.E.; Holme, P.A.; Mizobuchi, M.; Morales, R.J.; De Paula, A.M.; Stray-Pedersen, A.; Lyle, R.; Dalhus, B.; et al. A dominant STIM1 mutation causes Stormorken syndrome. *Hum. Mutat.* **2014**, *35*, 556–564. [CrossRef]

17. Morin, G.; Bruechle, N.O.; Singh, A.R.; Knopp, C.; Jedraszak, G.; Elbracht, M.; Bremond-Gignac, D.; Hartmann, K.; Sevestre, H.; Deutz, P.; et al. Gain-of-Function Mutation in STIM1 (P.R304W) Is Associated with Stormorken Syndrome. *Hum. Mutat.* **2014**, *35*, 1221–1232. [CrossRef]

18. Noury, J.B.; Bohm, J.; Peche, G.A.; Guyant-Marechal, L.; Bedat-Millet, A.L.; Chiche, L.; Carlier, R.Y.; Malfatti, E.; Romero, N.B.; Stojkovic, T. Tubular aggregate myopathy with features of Stormorken disease due to a new STIM1 mutation. *Neuromuscul. Disord.* **2017**, *27*, 78–82. [CrossRef]

19. Garibaldi, M.; Fattori, F.; Riva, B.; Labasse, C.; Brochier, G.; Ottaviani, P.; Sacconi, S.; Vizzaccaro, E.; Laschena, F.; Romero, N.B.; et al. A novel gain-of-function mutation in ORAI1 causes late-onset tubular aggregate myopathy and congenital miosis. *Clin. Genet.* **2017**, *91*, 780–786. [CrossRef]

20. Silva-Rojas, R.; Treves, S.; Jacobs, H.; Kessler, P.; Messaddeq, N.; Laporte, J.; Bohm, J. STIM1 over-activation generates a multi-systemic phenotype affecting the skeletal muscle, spleen, eye, skin, bones and immune system in mice. *Hum. Mol. Genet.* **2019**, *28*, 1579–1593. [CrossRef]

21. Dobin, A.; Davis, C.A.; Schlesinger, F.; Drenkow, J.; Zaleski, C.; Jha, S.; Batut, P.; Chaisson, M.; Gingeras, T.R. STAR: Ultrafast universal RNA-seq aligner. *Bioinformatics* **2013**, *29*, 15–21. [CrossRef]

22. Anders, S.; Pyl, P.T.; Huber, W. HTSeq—A Python framework to work with high-throughput sequencing data. *Bioinformatics* **2015**, *31*, 166–169. [CrossRef]

23. Love, M.I.; Huber, W.; Anders, S. Moderated estimation of fold change and dispersion for RNA-seq data with DESeq2. *Genome Biol.* **2014**, *15*, 550. [CrossRef]

24. Yu, G.; Wang, L.G.; Han, Y.; He, Q.Y. clusterProfiler: An R package for comparing biological themes among gene clusters. *OMICS* **2012**, *16*, 284–287. [CrossRef]

25. Mayeuf-Louchart, A.; Hardy, D.; Thorel, Q.; Roux, P.; Gueniot, L.; Briand, D.; Mazeraud, A.; Bougle, A.; Shorte, S.L.; Staels, B.; et al. MuscleJ: A high-content analysis method to study skeletal muscle with a new Fiji tool. *Skelet. Muscle* **2018**, *8*, 25. [CrossRef]

26. Duteil, D.; Chambon, C.; Ali, F.; Malivindi, R.; Zoll, J.; Kato, S.; Geny, B.; Chambon, P.; Metzger, D. The transcriptional coregulators TIF2 and SRC-1 regulate energy homeostasis by modulating mitochondrial respiration in skeletal muscles. *Cell Metab.* **2010**, *12*, 496–508. [CrossRef] [PubMed]

27. Mansour, Z.; Bouitbir, J.; Charles, A.L.; Talha, S.; Kindo, M.; Pottecher, J.; Zoll, J.; Geny, B. Remote and local ischemic precondition-ing equivalently protects rat skeletal muscle mitochondrial function during experimental aortic cross-clamping. *J. Vasc. Surg.* **2012**, *55*, 497–505. [CrossRef] [PubMed]

28. Sciorati, C.; Rigamonti, E.; Manfredi, A.A.; Rovere-Querini, P. Cell death, clearance and immunity in the skeletal muscle. *Cell Death Differ.* **2016**, *23*, 927–937. [CrossRef] [PubMed]

29. Schneider, M.F.; Chandler, W.K. Voltage dependent charge movement of skeletal muscle: A possible step in excitation-contraction coupling. *Nature* **1973**, *242*, 244–246. [CrossRef]

30. Lamb, G.D.; Junankar, P.R.; Stephenson, D.G. Raised intracellular [Ca2+] abolishes excitation-contraction coupling in skeletal muscle fibres of rat and toad. *J. Physiol.* **1995**, *489*, 349–362. [CrossRef]

31. Murphy, R.M.; Dutka, T.L.; Horvath, D.; Bell, J.R.; Delbridge, L.M.; Lamb, G.D. Ca2+-dependent proteolysis of junctophilin-1 and junctophilin-2 in skeletal and cardiac muscle. *J. Physiol.* **2013**, *591*, 719–729. [CrossRef]

32. Deluca, H.F.; Engstrom, G.W. Calcium uptake by rat kidney mitochondria. *Proc. Natl. Acad. Sci. USA* **1961**, *47*, 1744–1750. [CrossRef]

33. Rizzuto, R.; De Stefani, D.; Raffaello, A.; Mammucari, C. Mitochondria as sensors and regulators of calcium signalling. *Nat. Rev. Mol. Cell Biol.* **2012**, *13*, 566–578. [CrossRef]

34. Rossi, A.E.; Dirksen, R.T. Sarcoplasmic reticulum: The dynamic calcium governor of muscle. *Muscle Nerve* **2006**, *33*, 715–731. [CrossRef] [PubMed]

35. Bahar, E.; Kim, H.; Yoon, H. ER Stress-Mediated Signaling: Action Potential and Ca^{2+} as Key Players. *Int. J. Mol. Sci.* **2016**, *17*, 1558. [CrossRef]

36. Pullen, A.H. The distribution and relative sized of fibre types in the extensor digitorum longus and soleus muscles of the adult rat. *J. Anat.* **1977**, *123*, 467–486. [PubMed]

37. Pullen, A.H. The distribution and relative sizes of three histochemical fibre types in the rat tibialis anterior muscle. *J. Anat.* **1977**, *123*, 1–19.

38. Lamboley, C.R.; Murphy, R.M.; McKenna, M.J.; Lamb, G.D. Endogenous and maximal sarcoplasmic reticulum calcium content and calsequestrin expression in type I and type II human skeletal muscle fibres. *J. Physiol.* **2013**, *591*, 6053–6068. [CrossRef]

39. Fraysse, B.; Desaphy, J.F.; Pierno, S.; De Luca, A.; Liantonio, A.; Mitolo, C.I.; Camerino, D.C. Decrease in resting calcium and calcium entry associated with slow-to-fast transition in unloaded rat soleus muscle. *FASEB J.* **2003**, *17*, 1916–1918. [CrossRef] [PubMed]

40. Parekh, A.B.; Penner, R. Store depletion and calcium influx. *Physiol. Rev.* **1997**, *77*, 901–930. [CrossRef] [PubMed]

41. Sultana, N.; Dienes, B.; Benedetti, A.; Tuluc, P.; Szentesi, P.; Sztretye, M.; Rainer, J.; Hess, M.W.; Schwarzer, C.; Obermair, G.J.; et al. Restricting calcium currents is required for correct fiber type specification in skeletal muscle. *Development* **2016**, *143*, 1547–1559. [CrossRef] [PubMed]

42. Maier, A.; Gorza, L.; Schiaffino, S.; Pette, D. A combined histochemical and immunohistochemical study on the dynamics of fast-to-slow fiber transformation in chronically stimulated rabbit muscle. *Cell Tissue Res.* **1988**, *254*, 59–68. [CrossRef] [PubMed]

43. Jungbluth, H.; Sewry, C.A.; Muntoni, F. Core myopathies. *Semin. Pediatr. Neurol.* **2011**, *18*, 239–249. [CrossRef] [PubMed]

44. Avila, G.; Dirksen, R.T. Functional effects of central core disease mutations in the cytoplasmic region of the skeletal muscle ryanodine receptor. *J. Gen. Physiol.* **2001**, *118*, 277–290. [CrossRef]

45. Dirksen, R.T.; Avila, G. Altered ryanodine receptor function in central core disease: Leaky or uncoupled Ca^{2+} release channels? *Trends Cardiovasc. Med.* **2002**, *12*, 189–197. [CrossRef]

46. Kraeva, N.; Zvaritch, E.; Rossi, A.E.; Goonasekera, S.A.; Zaid, H.; Frodis, W.; Kraev, A.; Dirksen, R.T.; Maclennan, D.H.; Riazi, S. Novel excitation-contraction uncoupled RYR1 mutations in patients with central core disease. *Neuromuscul. Disord.* **2013**, *23*, 120–132. [CrossRef] [PubMed]

47. Schartner, V.; Laporte, J.; Bohm, J. Abnormal Excitation-Contraction Coupling and Calcium Homeostasis in Myopathies and Cardiomyopathies. *J. Neuromuscul. Dis.* **2019**, *6*, 289–305. [CrossRef]

48. Conte, E.; Pannunzio, A.; Imbrici, P.; Camerino, G.M.; Maggi, L.; Mora, M.; Gibertini, S.; Cappellari, O.; De Luca, A.; Coluccia, M.; et al. Gain-of-Function STIM1 L96V Mutation Causes Myogenesis Alteration in Muscle Cells from a Patient Affected by Tubular Aggregate Myopathy. *Front. Cell Dev. Biol.* **2021**, *9*, 635063. [CrossRef] [PubMed]

49. Bohm, J.; Chevessier, F.; Koch, C.; Peche, G.A.; Mora, M.; Morandi, L.; Pasanisi, B.; Moroni, I.; Tasca, G.; Fattori, F.; et al. Clinical, histological and genetic characterisation of patients with tubular aggregate myopathy caused by mutations in STIM1. *J. Med. Genet.* **2014**, *51*, 824–833. [CrossRef] [PubMed]

50. Manning, B.M.; Quane, K.A.; Ording, H.; Urwyler, A.; Tegazzin, V.; Lehane, M.; O'Halloran, J.; Hartung, E.; Giblin, L.M.; Lynch, P.J.; et al. Identification of novel mutations in the ryanodine-receptor gene (RYR1) in malignant hyperthermia: Genotype-phenotype correlation. *Am. J. Hum. Genet.* **1998**, *62*, 599–609. [CrossRef]

51. Gillard, E.F.; Otsu, K.; Fujii, J.; Khanna, V.K.; de Leon, S.; Derdemezi, J.; Britt, B.A.; Duff, C.L.; Worton, R.G.; MacLennan, D.H. A substitution of cysteine for arginine 614 in the ryanodine receptor is potentially causative of human malignant hyperthermia. *Genomics* **1991**, *11*, 751–755. [CrossRef]

52. Denborough, M.A.; Forster, J.F.; Lovell, R.R.; Maplestone, P.A.; Villiers, J.D. Anaesthetic deaths in a family. *Br. J. Anaesth.* **1962**, *34*, 395–396. [CrossRef] [PubMed]

53. MacLennan, D.H.; Phillips, M.S. Malignant hyperthermia. *Science* **1992**, *256*, 789–794. [CrossRef] [PubMed]

54. Eltit, J.M.; Bannister, R.A.; Moua, O.; Altamirano, F.; Hopkins, P.M.; Pessah, I.N.; Molinski, T.F.; Lopez, J.R.; Beam, K.G.; Allen, P.D. Malignant hyperthermia susceptibility arising from altered resting coupling between the skeletal muscle L-type Ca2+ channel and the type 1 ryanodine receptor. *Proc. Natl. Acad. Sci. USA* **2012**, *109*, 7923–7928. [CrossRef] [PubMed]

55. Weiss, R.G.; O'Connell, K.M.; Flucher, B.E.; Allen, P.D.; Grabner, M.; Dirksen, R.T. Functional analysis of the R1086H malignant hyperthermia mutation in the DHPR reveals an unexpected influence of the III-IV loop on skeletal muscle EC coupling. *Am. J. Physiol. Cell Physiol.* **2004**, *287*, C1094–C1102. [CrossRef]

56. Lavorato, M.; Gupta, P.K.; Hopkins, P.M.; Franzini-Armstrong, C. Skeletal Muscle Microalterations in Patients Carrying Malignant Hyperthermia-Related Mutations of the e-c Coupling Machinery. *Eur. J. Transl. Myol.* **2016**, *26*, 6105. [CrossRef]

57. Cordero-Sanchez, C.; Riva, B.; Reano, S.; Clemente, N.; Zaggia, I.; Ruffinatti, F.A.; Potenzieri, A.; Pirali, T.; Raffa, S.; Sangaletti, S.; et al. A luminal EF-hand mutation in STIM1 in mice causes the clinical hallmarks of tubular aggregate myopathy. *Dis. Models Mech.* **2019**, *13*, dmm041111. [CrossRef]

58. Dainese, M.; Quarta, M.; Lyfenko, A.D.; Paolini, C.; Canato, M.; Reggiani, C.; Dirksen, R.T.; Protasi, F. Anesthetic- and heat-induced sudden death in calsequestrin-1-knockout mice. *FASEB J.* **2009**, *23*, 1710–1720. [CrossRef]

59. Lee, C.S.; Hanna, A.D.; Wang, H.; Dagnino-Acosta, A.; Joshi, A.D.; Knoblauch, M.; Xia, Y.; Georgiou, D.K.; Xu, J.; Long, C.; et al. A chemical chaperone improves muscle function in mice with a RyR1 mutation. *Nat. Commun.* **2017**, *8*, 14659. [CrossRef]

60. Lee, K.W.; Maeng, J.S.; Choi, J.Y.; Lee, Y.R.; Hwang, C.Y.; Park, S.S.; Park, H.K.; Chung, B.H.; Lee, S.G.; Kim, Y.S.; et al. Role of Junctin protein interactions in cellular dynamics of calsequestrin polymer upon calcium perturbation. *J. Biol. Chem.* **2012**, *287*, 1679–1687. [CrossRef]

61. Wang, L.; Zhang, L.; Li, S.; Zheng, Y.; Yan, X.; Chen, M.; Wang, H.; Putney, J.W.; Luo, D. Retrograde regulation of STIM1-Orai1 interaction and store-operated Ca^{2+} entry by calsequestrin. *Sci. Rep.* **2015**, *5*, 11349. [CrossRef]

62. Park, C.Y.; Shcheglovitov, A.; Dolmetsch, R. The CRAC channel activator STIM1 binds and inhibits L-type voltage-gated calcium channels. *Science* **2010**, *330*, 101–105. [CrossRef] [PubMed]

63. Burr, A.R.; Molkentin, J.D. Genetic evidence in the mouse solidifies the calcium hypothesis of myofiber death in muscular dystrophy. *Cell Death Differ.* **2015**, *22*, 1402–1412. [CrossRef] [PubMed]

64. Kargacin, M.E.; Kargacin, G.J. The sarcoplasmic reticulum calcium pump is functionally altered in dystrophic muscle. *Biochim. Biophys. Acta* **1996**, *1290*, 4–8. [CrossRef]

65. Begam, M.; Abro, V.M.; Mueller, A.L.; Roche, J.A. Sodium 4-phenylbutyrate reduces myofiber damage in a mouse model of Duchenne muscular dystrophy. *Appl. Physiol. Nutr. Metab.* **2016**, *41*, 1108–1111. [CrossRef]

66. De Luca, A.; Pierno, S.; Liantonio, A.; Cetrone, M.; Camerino, C.; Simonetti, S.; Papadia, F.; Camerino, D.C. Alteration of excitation-contraction coupling mechanism in extensor digitorum longus muscle fibres of dystrophic mdx mouse and potential efficacy of taurine. *Br. J. Pharmacol.* **2001**, *132*, 1047–1054. [CrossRef] [PubMed]

67. Goonasekera, S.A.; Lam, C.K.; Millay, D.P.; Sargent, M.A.; Hajjar, R.J.; Kranias, E.G.; Molkentin, J.D. Mitigation of muscular dystrophy in mice by SERCA overexpression in skeletal muscle. *J. Clin. Investig.* **2011**, *121*, 1044–1052. [CrossRef] [PubMed]

68. Terrill, J.R.; Pinniger, G.J.; Graves, J.A.; Grounds, M.D.; Arthur, P.G. Increasing taurine intake and taurine synthesis improves skeletal muscle function in the mdx mouse model for Duchenne muscular dystrophy. *J. Physiol.* **2016**, *594*, 3095–3110. [CrossRef]

69. Grosse, J.; Braun, A.; Varga-Szabo, D.; Beyersdorf, N.; Schneider, B.; Zeitlmann, L.; Hanke, P.; Schropp, P.; Muhlstedt, S.; Zorn, C.; et al. An EF hand mutation in Stim1 causes premature platelet activation and bleeding in mice. *J. Clin. Investig.* **2007**, *117*, 3540–3550. [CrossRef]

70. Gamage, T.H.; Gunnes, G.; Lee, R.H.; Louch, W.E.; Holmgren, A.; Bruton, J.D.; Lengle, E.; Kolstad, T.R.S.; Revold, T.; Amundsen, S.S.; et al. STIM1 R304W causes muscle degeneration and impaired platelet activation in mice. *Cell Calcium* **2018**, *76*, 87–100. [CrossRef]

SUPPLEMENTAL MATERIAL

Supplemental Figure S1. Enrichment of immune-related GO-terms. (A) Classification of the dysregulated genes in *Stim1$^{R304W/+}$* tibialis anterior into GO terms reveals an important number of groups associated with the immune response (n=4). (B) RNAseq uncovered a total of 3349 differentially expressed genes (DEG) in *Stim1$^{R304W/+}$* tibialis anterior compared with the WT. Following removal of the immune-related GO terms, 2841 DEG remained.

Supplemental Figure S2. **Reduced expression of SERCA1 in *Stim1$^{R304W/+}$* tibialis anterior.** (A-C) Western blots showing the SERCA1, DHPR and RyR1 protein levels in WT and *Stim1$^{R304W/+}$* tibialis anterior (n=6, corresponding to the graph in Fig. 1D and 1F). Ponceau staining served as loading control.

Supplemental Figure S3. **Decrease of mitochondrial markers in *Stim1$^{R304W/+}$* tibialis anterior.** (A-C) Western blots on muscle extracts showing a decrease of PGC1α protein level (graph in Fig. 2C), and of the mitochondrial electron transport chain proteins ATP5A, UQCRC2, SDHB, and NDUFB8 (n=6). Ponceau staining served as loading control. (D) H_2O_2 production is slightly reduced in *Stim1$^{R304W/+}$* tibialis anterior muscle fibers. Significant differences are illustrated as *($p<0.05$), **($p<0.01$), and ***($p<0.001$).

Supplemental Figure S4. **Increased proportion of apoptotic and regenerating fibers in *Stim1$^{R304W/+}$* tibialis anterior**. Immunofluorescence showing apoptotic fibers on *Stim1$^{R304W/+}$* muscle sections as illustrated by the signal of cleaved caspase-3 (top), and regenerating fibers expressing embryonic myosin (bottom). Wheat germ agglutinin (WGA) outlines the myofibers. Scales correspond to 50 µm.

Supplemental Figure S5. **Decreased SERCA1 levels in** *Stim1^{R304W/+}* **soleus.** (A-C) Western blots showing the SERCA1, DHPR and RyR1 levels in muscle extracts (n=4-5, graph in Fig. 5B). The cross indicates an incorrectly charged lane removed from the analysis. Ponceau staining serves as loading control.

Supplemental Figure S6. **Decreased mitochondrial markers in** *Stim1^{R304W/+}* **soleus**. (A-C) Western blots revealing reduced levels of PGC1α (graph in Fig. 5C) and of ATP5A, UQCRC2, SDHB, and NDUFB8, representing proteins of the mitochondrial electron transport chain complexes V, III, II, and I in *Stim1^{R304W/+}* muscle samples compared with WT. Ponceau staining served as loading control, and crosses indicate incorrectly loaded lanes removed from the analysis. (D) Decreased H_2O_2 production in *Stim1^{R304W/+}* soleus. Significant differences are illustrated as *($p<0.05$).

Supplemental Figure S7. **Increased proportion of type I muscle fibers, apoptosis, and regeneration in** *Stim1^{R304W/+}* **soleus.** (A) Representative muscle cross sections and statistical analysis showing the fiber type pattern and highlighting an increased proportion of type I fibers in *Stim1^{R304W/+}* soleus compared with the control (n=4-5). Type I fibers appear in red, intermediate type IIa fibers in green, and fast type IIb fibers in blue. The remaining fibers are fast IIx. Significant differences are illustrated as **** ($p<0.0001$). (B) Apoptotic fibers in *Stim1^{R304W/+}* soleus staining positive for cleaved caspase-3 (top), and regenerating fibers expressing embryonic myosin (bottom). Wheat germ agglutinin (WGA) outlines the myofibers.

Supplemental Table S1. List of primers and associated sequences used for qPCR and RT-qPCR.
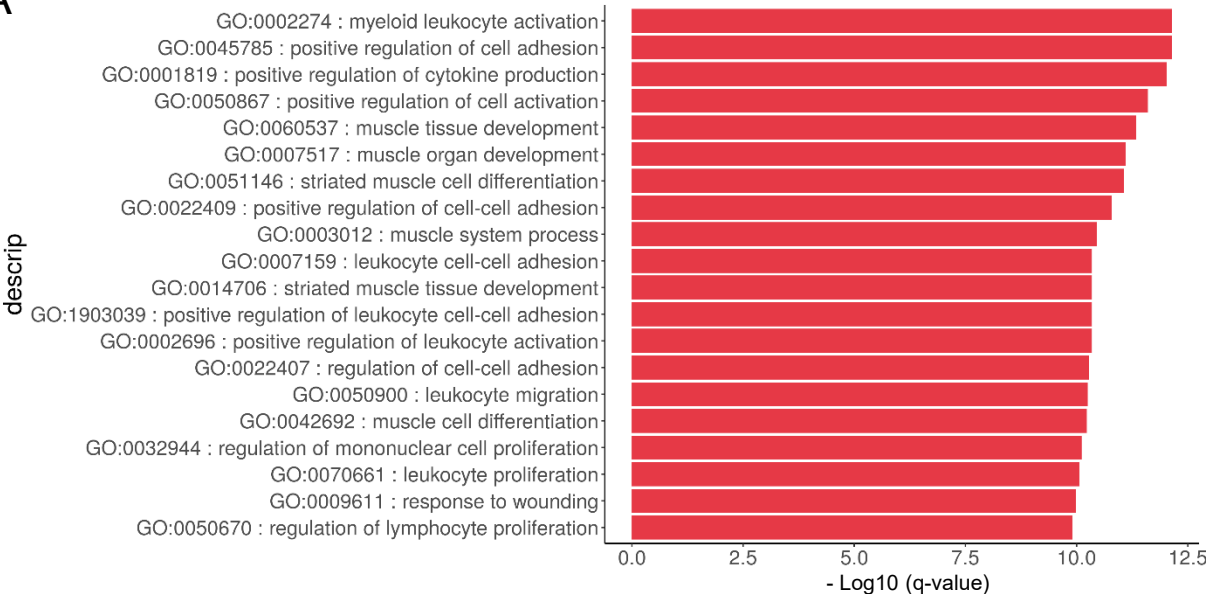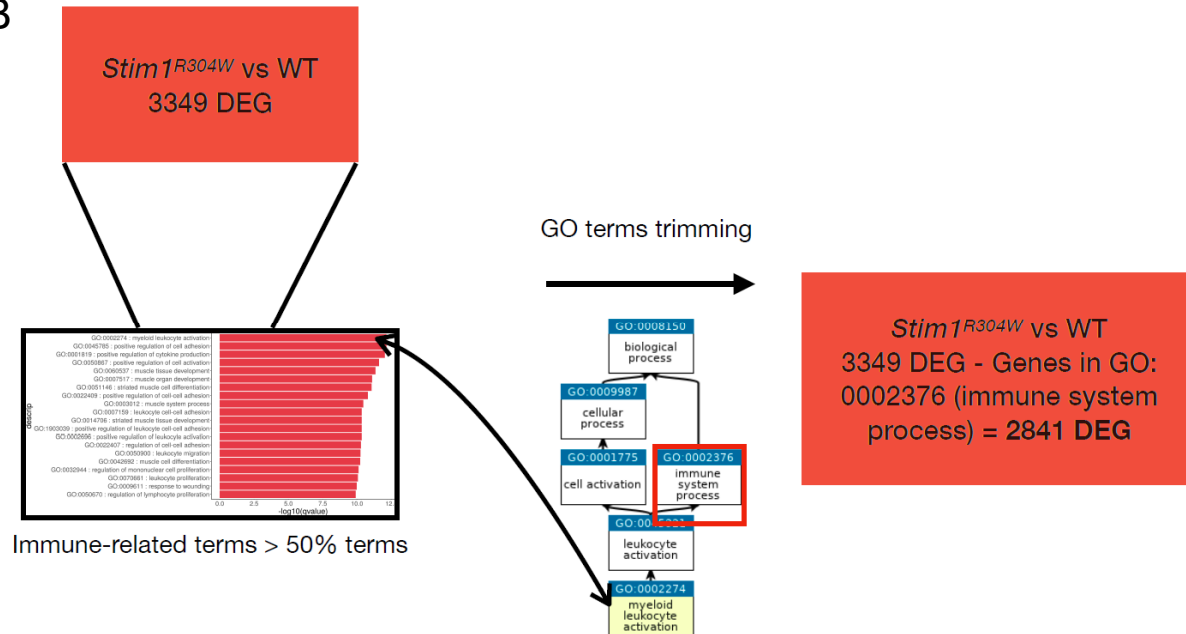
Supplemental Figure S1

Supplemental Figure S2

103

A WT *Stim1^{R304W/+}*

250 kDa
130 kDa
100 kDa
70 kDa

PGC1α

Ponceau

B WT *Stim1^{R304W/+}*

70 kDa
55 kDa
35 kDa
25 kDa
15 kDa
10 kDa

ATP5A (V)
UQCRC2 (III)
SDHB (II)
NDUFB8 (I)

Ponceau

C Oxphos complexes

Protein fold change

1.5
1.0
0.5
0.0

*** ** ** p = 0.07

NDUFB8 (I) SDHB (II) UQCRC2 (III) ATP5A (V)

D H$_2$O$_2$ production

H$_2$O$_2$ production (nmol/(s* mg tissue))

1.0
0.8
0.6
0.4
0.2
0.0

* p = 0.065

CI-linked substrate   CI-linked OXPHOS

Supplemental Figure S3

WT   *Stim1*^{R304W/+}
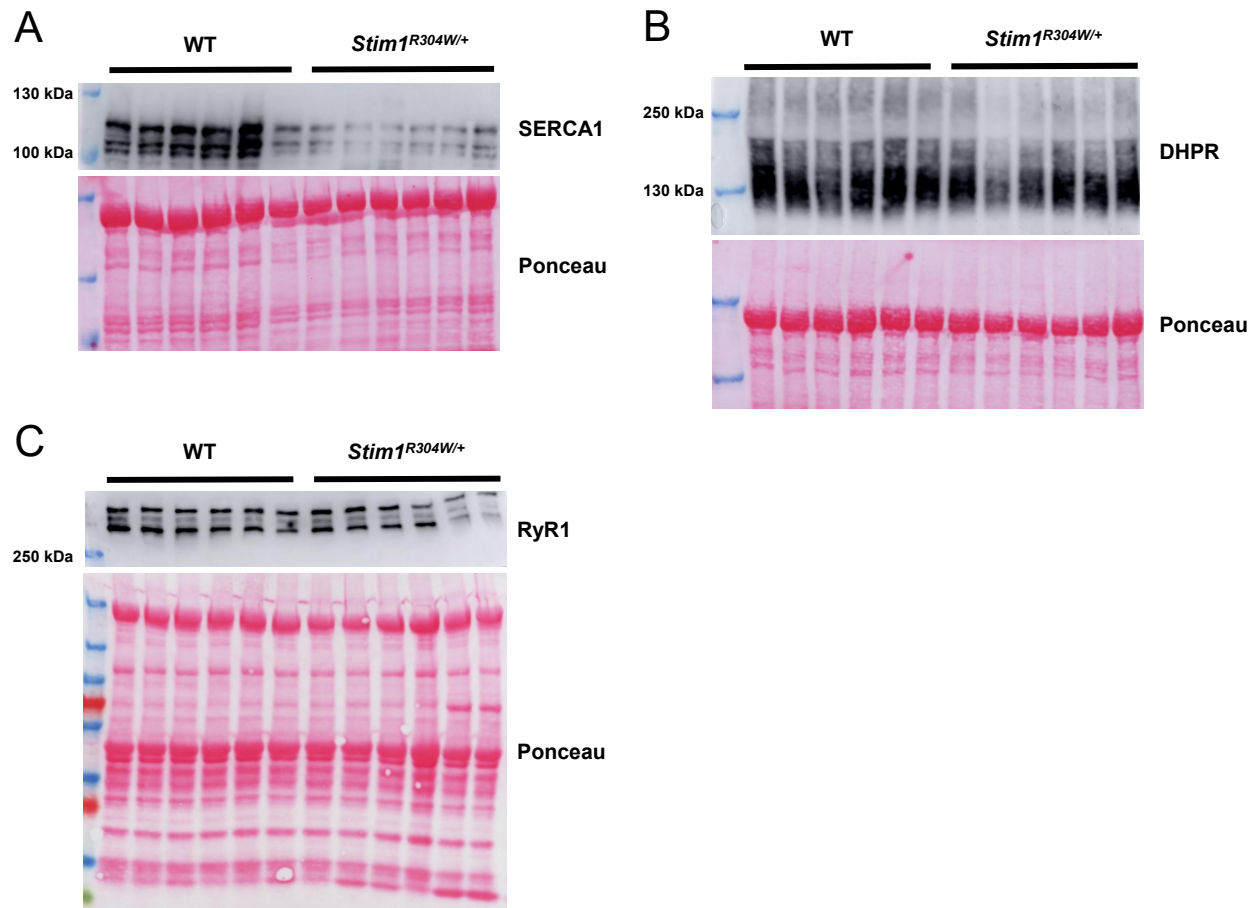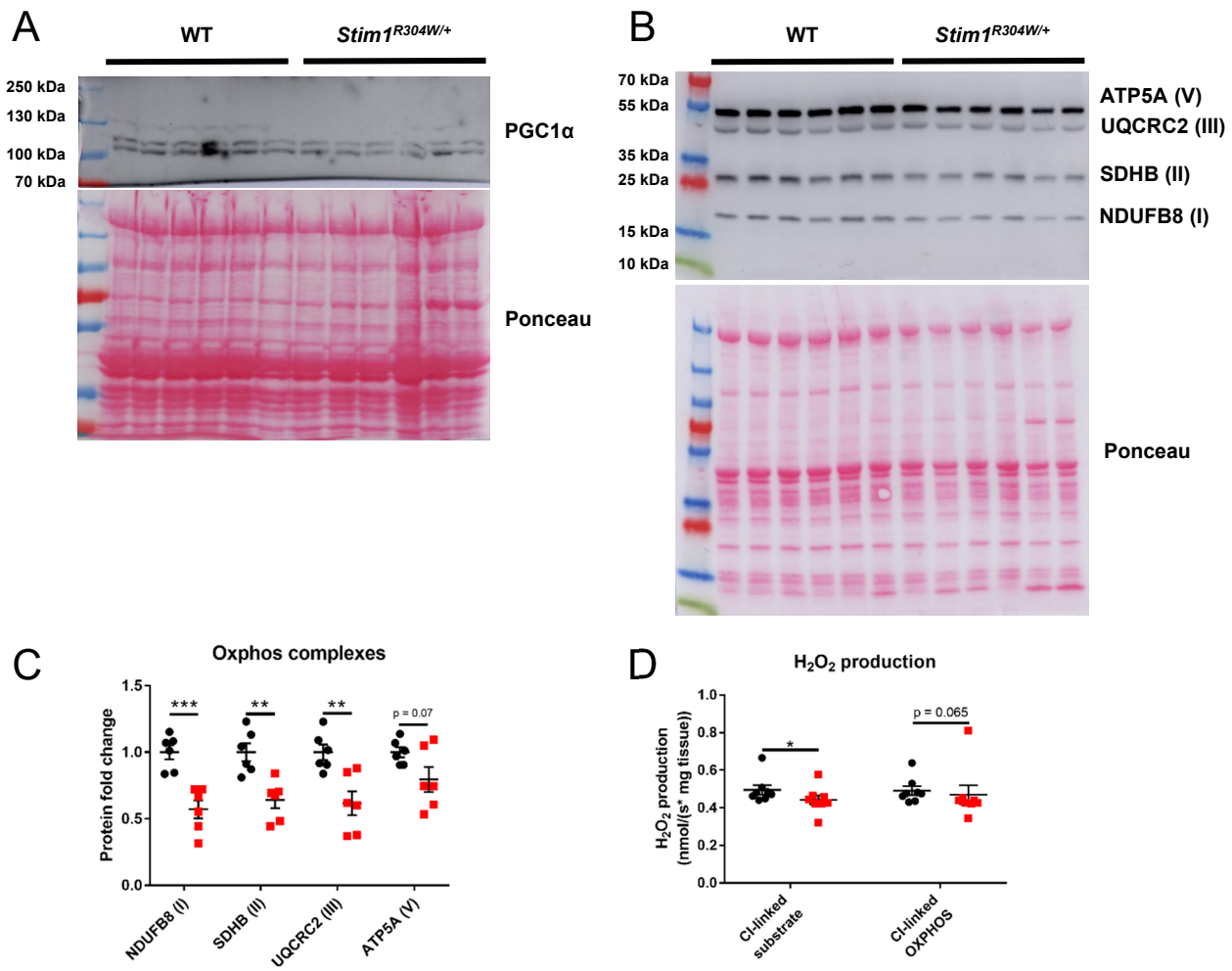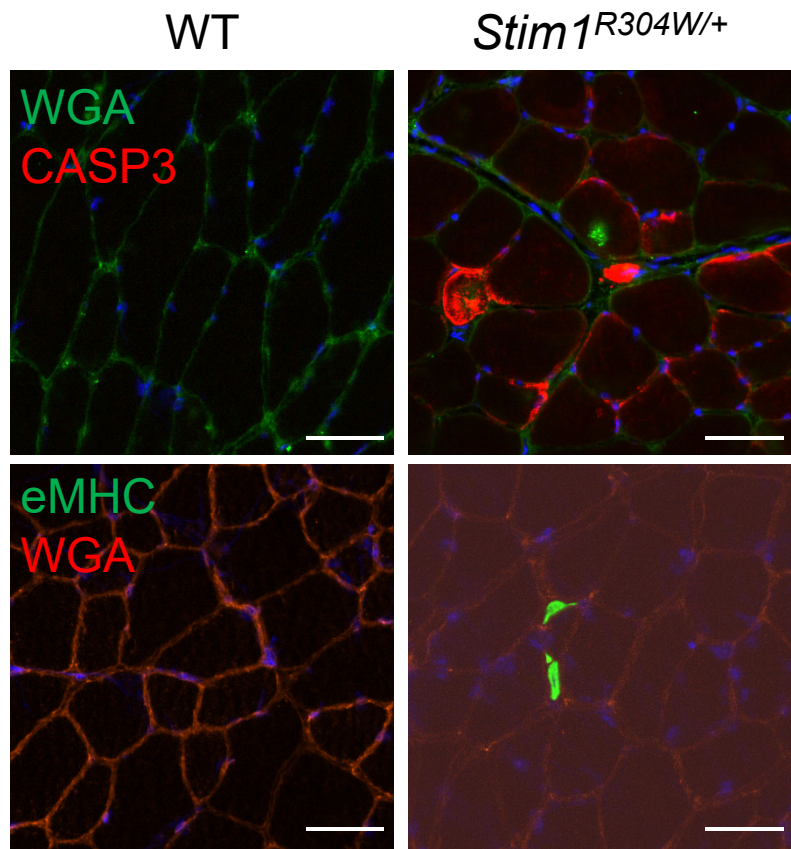
Supplemental Figure S4
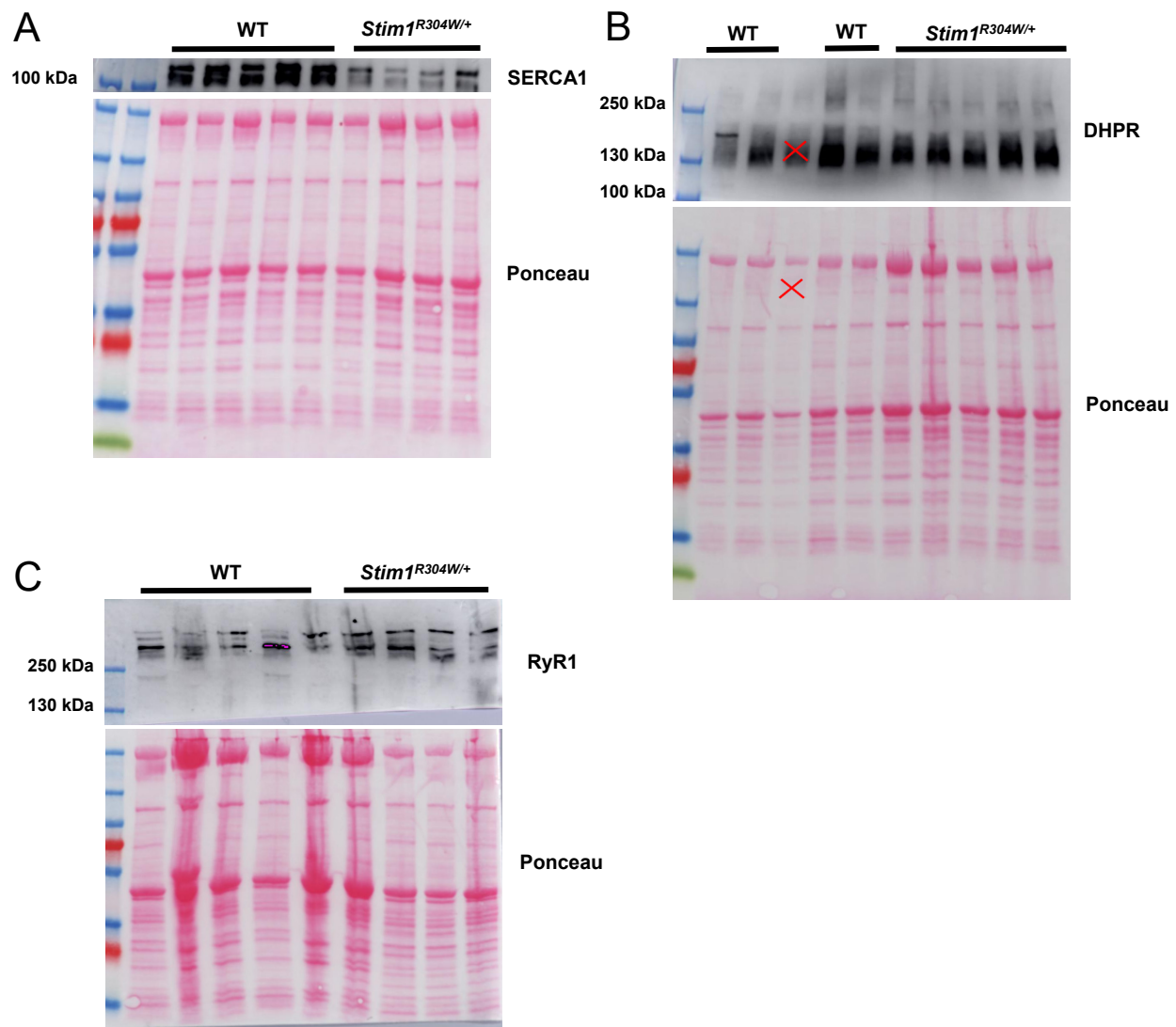
Supplemental Figure S5
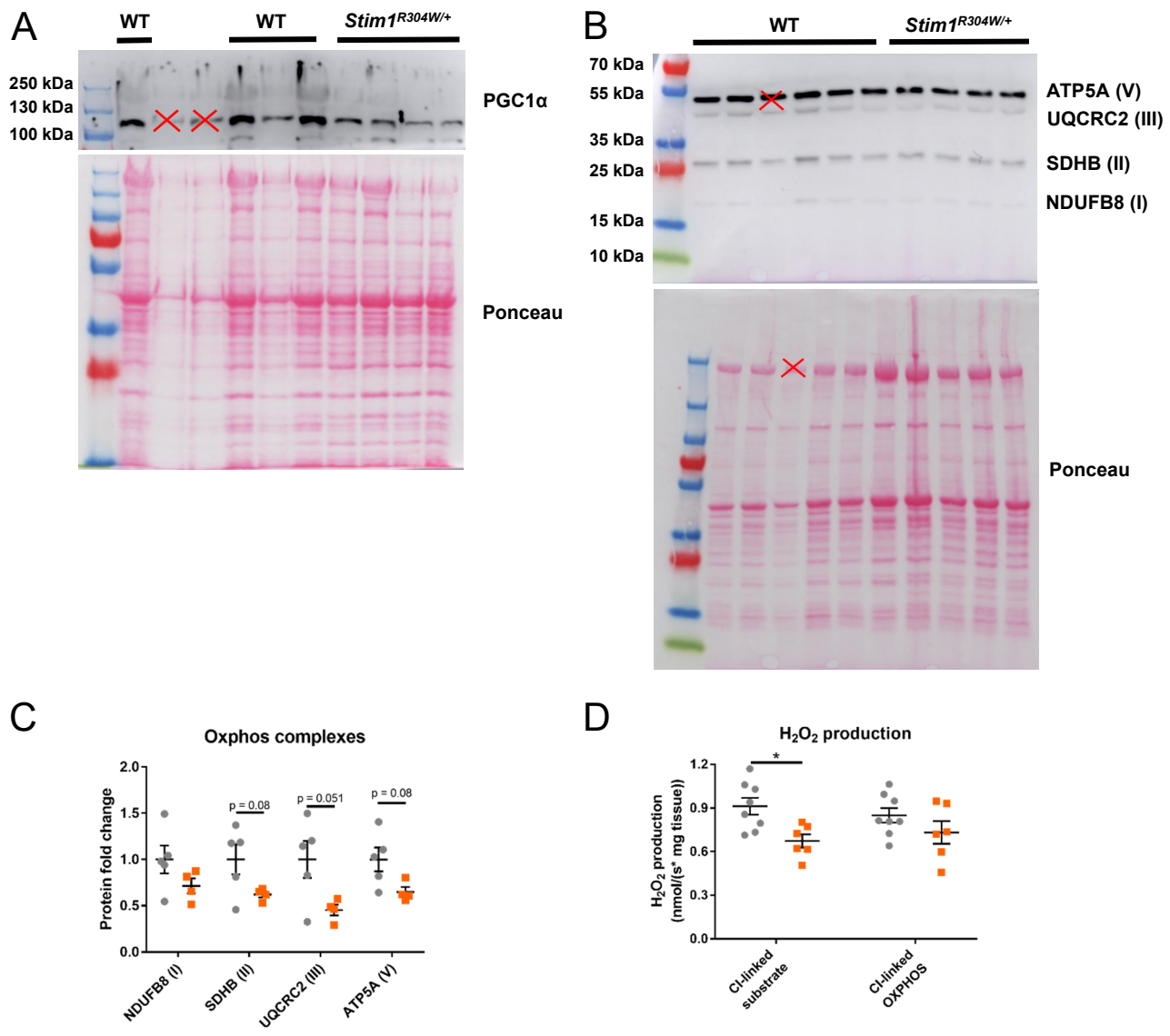
Supplemental Figure S6
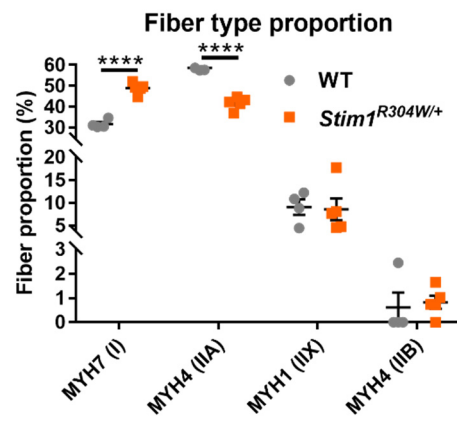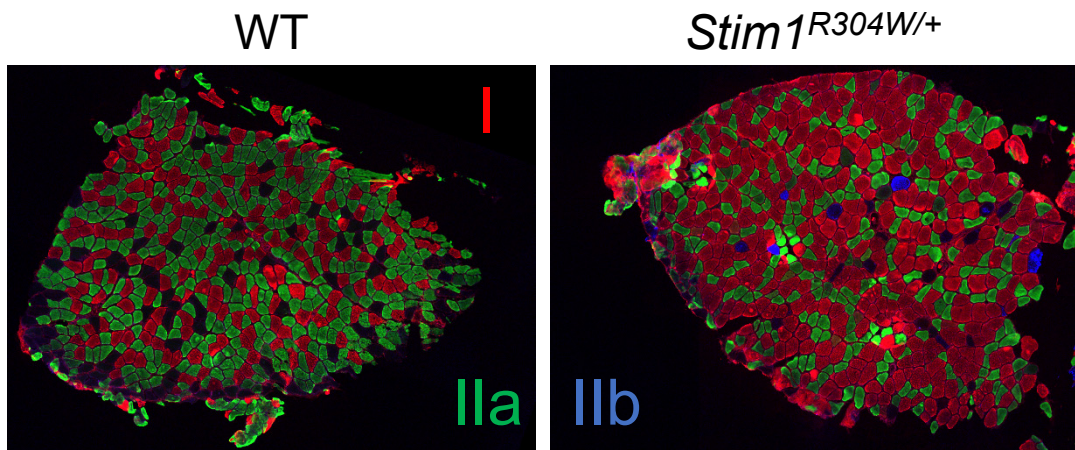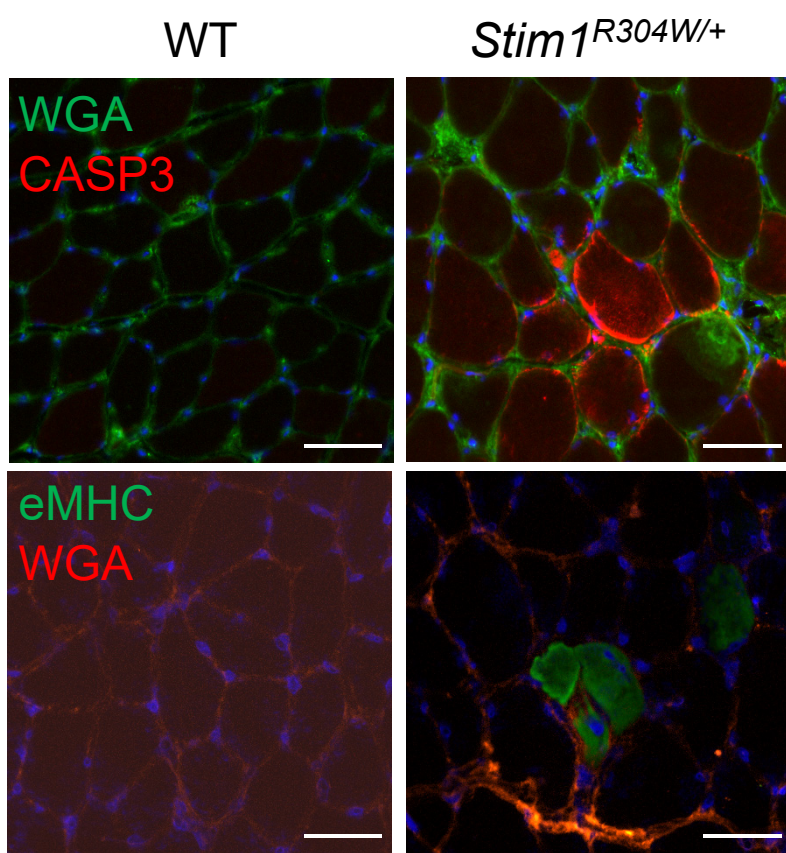
Supplemental Figure S7

Supplemental Table S1.

Pathway	Gene	Forward primer	Reverse primer
Ca²⁺ extrusion	*Atp2b1*	TTATCAACCTCCGGAAGGGGATAAT	GCTCCTTCAATCCACCCCGTTTCT
	Slc8a1	GTTTGTTGCTCTTGGAACCTCGGTG	GTGACATTGCCTATAGACGCATCTG
	Slc8a3	TTTTGTGGCATTCGGCACCTCTGTG	GTGACGTTGCCAATGGAAGCATCTG
SR refilling	*Atp2a1*	CCCTCACCACCAACCAGATGTCAGTT	CAGTGATGGAGAACTCGTTCAGTGAGC
	Sln	TGTCCTCATCACCGTTCTCC	TGGAGTATAGCATGGCCCCT
	Plb	AGTGCAATACCTCACTCGCT	TTCTGACGTGCTTGCTGAGG
EC coupling	*Cana1s*	AACCTGGTGCTGGGTGTCCTG	TCTCTCGGAGCTTTTGGAAGGTTC
	Ryr1	CAGTGGACTACCTCCTGCGGC	GTTTCTCTTTCCCTGTTCCTCGATG
Mitochondrial biogenesis	*Ppargc1a*	GCAGGTCGAACGAAACTGAC	CTTGCTCTTGGTGGAAGCAG
	Sirt1	GGCCGCGGATAGGTCCA	AACAATCTGCCACAGCGTCA
	Nrf1	ATGTCCGCACAGAAGAGCAA	TGTACCAACCTGGATGAGCG
	Tfam	ATAGGCACCGTATTGCGTGA	AGTTTTGCATCTGGGTGTTTAGC
mtDNA copy number	*mt16S*	CTAGAAACCCCGAAACCAAA	CCAGCTATCACCAAGCTCGT
	Cox2	AATTAGCTCCTTAGTCCTCT	CTTGGTCGGTTTGATGTTAC
	Loop	GCGTTATCGCCTCATACGTT	GATTGGGTTTTGCGGACTAA
Mitochondrial transport	*Rhot1*	GGCCATGTACCCGCACG	ATGTGTTTTGGTAGGCCGGT
	Trak1	GTCTCCAGACATCACCCACC	TATCGAGGACCACGTTGCTG
Mitochondrial dynamics	*Dnm1l*	GAGTTGAAGCAGAAGAATGGGG	CGCCTACAGGTACTTTGGTCA
	Fis1	GCAACTACCGGCTCAAGGAAT	GTGAGGCTGCCTTCAGGATT
	Opa1	TGAGGCCCTTCTCTTGTTAGG	TCTTTGTCTGACACCTTCCTGT
	Mfn2	GCTAGAAACTTCTCCTCTGTTCCA	CTTGACGGTGACGATGGAGT
Unfolded protein response	*Hspa5*	CTATTCCTGCGTCGGTGTGT	ATTCCAAGTGCGTCCGATGA
	Hsp90b1	CCACTCAAATCGAACACGGC	AGATTCCGCCTCCTTTCTGC
	Xbp1	AGAAGAGAACCACAAACTCCAGC	ACATAGTCTGAGTGCTGCGG
	Ddit3	CCAGAATAACAGCCGGAACC	ATCCTCATACCAGGCTTCCA
Muscle regeneration	*Myh3*	CTTCACCTCTAGCCGGAATGGT	AATTGTCAGGAGCCACGAAAAT
	Myh8	CAGGAGCAGGAATGATGCTCTGAG	AGTTCCTCAAACTTTCAGCAGCCAA
RT-qPCR control	*Rpl27*	AAGCCGTCATCGTGAAGAACA	CTTGATCTTGGATCGCTTGGC
qPCR control	*B2M*	ATGGGAAGCCGAACATACTG	CAGTCTCAGTGGGGGTGAAT

ORAI1 inhibition

Orai1 silencing

Physiopathology

Mouse model

PUBLICATION 3
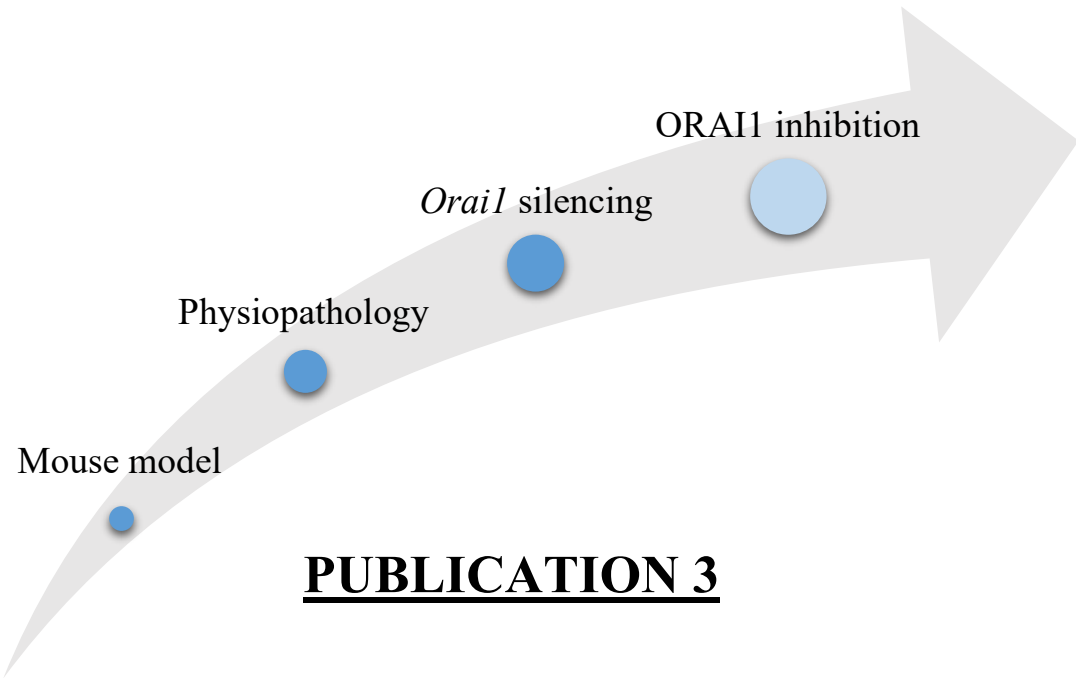
Silencing of the ORAI1 Ca^{2+} channel improves the main clinical signs of Stormorken syndrome in mice

Roberto Silva-Rojas, Emma Lafabrie, David Moulaert, Pascale Koebel, Laura Pérez-Guàrdia, Jocelyn Laporte, Johann Böhm

3. *ORAI1* SILENCING AS THERAPEUTIC APPROACH FOR TAM/STRMK

3.1. Background

TAM/STRMK result from gain-of-function (GoF) mutations in *STIM1* and *ORAI1*, leading to SOCE over activation and excessive extracellular Ca^{2+} entry (Bohm and Laporte, 2018; Silva-Rojas et al., 2021). In contrast, recessive LoF mutations in *STIM1* and *ORAI1* abolish SOCE and cause CRAC channelopathy, characterized by immunodeficiency and autoimmunity, ectodermal dysplasia, mydriasis, autoimmune thrombocytopenia and muscle hypotonia (Lacruz and Feske, 2015). In accordance with the human disease, homozygous *Stim1* or *Orai1* knockout mice die perinatally, highlighting the necessity of SOCE for normal physiology. Of note, heterozygous carriers of CRAC channelopathy mutations and heterozygous *Stim1*$^{+/-}$ or *Orai1*$^{+/-}$ mice are normal and fertile (Baba et al., 2008; Gwack et al., 2008), demonstrating that 50% expression is sufficient to sustain normal physiology.

3.2. Aim of the study

Currently, no therapy is available for TAM/STRMK. ORAI1 represents a suitable target to treat since all TAM/STRMK forms converge in excessive ORAI1 activation. *STIM1* mutations result in constitutive oligomerization and *ORAI1* mutations increase channel permeability. As a first attempt to reduce extracellular Ca^{2+} entry via ORAI1 and to anticipate the multi-systemic phenotypes of TAM/STRMK, I crossed *Stim1*$^{R304W/+}$ and *Orai1*$^{+/-}$ mice and the offspring underwent a broad phenotypical characterization at the macroscopic, histologic and molecular levels. Based on this proof-of-concept, I next aimed to establish a suitable translational approach to downregulate *Orai1* after disease onset in adult mice. To this aim, I locally injected shRNA-containing AAV particles into the tibialis anterior (TA) of adult *Stim1*$^{R304W/+}$ mice and assessed the potential of two shRNA to efficiently reverse the muscle phenotype through cellular, histological and functional analyses.

3.3. Results

The birth ratio of $Stim1^{R304W/+}Orai1^{+/-}$ mice improved compared to $Stim1^{R304W/+}$ mice and was closer to the expected Mendelian ratio, indicating an improved embryonic development. Body weight gain over 4 months also improved, and the increase in bone density accounted for the increase in body length. The anomalies in skin layers previously observed in $Stim1^{R304W/+}$ mice were ameliorated in $Stim1^{R304W/+}Orai1^{+/-}$ mice. Muscle performance was improved with an increase, albeit not significant, in the hanging test abilities, speed and distance travelled in openfield arenas, and *in situ* maximal force of TA. Similar amelioration was noted for contraction defects including force produced at low frequencies of stimulation and contraction and relaxation kinetics. Myofiber size was also improved and probably resulted from improved autophagic flux. However, muscle degeneration was still evident in $Stim1^{R304W/+}Orai1^{+/-}$ muscles and ER stress was unaltered compared to $Stim1^{R304W/+}$ littermates. Also, the anomalies affecting the spleen and the platelets were unchanged and $Stim1^{R304W/+}Orai1^{+/-}$ mice showed splenomegaly and thrombocytopenia. In summary, *Orai1* downregulation had an overall beneficial effect on TAM/STRMK.

The improvement of the TAM/STRMK phenotypes in $Stim1^{R304W/+}Orai1^{+/-}$ mice was obtained by ablation of an *Orai1* allele. In order to downregulate *Orai1* in the perspective of a translational application in TAM/STRMK patients, I designed shRNA targeting different regions of *Orai1* cDNA and validated *Orai1* downregulation *in cellulo* and *in vivo*. shRNAs targeting cDNA at positions 22 (sh22) and 190 (sh190) reduced *Orai1* expression by 80% in $Stim1^{R304W/+}$ TA and improved muscle contraction and relaxation. $Stim1^{R304W/+}$ TA treated with sh22 and sh190 produced less force at low frequencies and the muscle relaxation was improved compared to control $Stim1^{R304W/+}$ TA. However, shRNA treatment did not improve the autophagic flux nor resolved the ER stress and myofiber atrophy and muscle degeneration were still evident in muscle sections from shRNA-treated $Stim1^{R304W/+}$ TA. Taken together, *Orai1* downregulation improved muscle contraction and relaxation but did not reverse the structural defects on TAM/STRMK.

3.4. Conclusion and perspectives

We are the first to show that reducing *Orai1* expression improves some of the TAM/STRMK phenotypes in mice including birth ratio, body weight and size, bone morphology, skin structure, muscle performance and fiber size. Muscle relaxation and degeneration do not improve, probably because higher *Orai1* silencing is needed to attenuate Ca^{2+} entry in the particularly fast and capacitive nature of SOCE in the skeletal muscle. The absence of effects on platelets and spleen suggest implication of other channels in SOCE (e.g. ORAI2 and ORAI3) that may not be affected by *Orai1* downregulation.

Our shRNAs targeting *Orai1* are also the first translational therapeutic approach to reverse TAM/STRMK phenotypes in the skeletal muscle. Treating the TA of adult *Stim1$^{R304W/+}$* mice with sh22 and sh190 improves the muscle contraction and relaxation kinetics thank, probably by the high efficiency of *Orai1* silencing. This is clinically relevant because our shRNA strategy could solve the muscle contraction issues of patients evidenced as incapacitating contractures. Histological defects including small fiber size and muscle degeneration are not improved with the current treatment, indicating that the structural defects established before the age of the injection cannot be reverted.

The excessive extracellular Ca^{2+} entry through ORAI1 also contributes to cytosolic Ca^{2+} overload and muscle degeneration in other muscle diseases including Duchenne's muscular dystrophy (DMD), and the shRNA-mediated *Orai1* downregulation may be beneficial for DMD thus increasing the therapeutic opportunities of *ORAI1* silencing.

3.5. Contribution

I handled the mouse breeding, phenotyping, histology, gene and protein expression, design and cellular and *in vivo* validation of the shRNAs, intramuscular injections, and *in situ* muscle force studies. David Moulaert from the ICS and Laura Pérez-Guàrdia (Master 2/Erasmus student) analyzed bone structure and spleen megakaryocyte hyperplasia, respectively. Emma Lafabrie (Master 1 student) performed he histological and molecular studies of shRNA-treated muscles. The bleeding test was done by Emilie Thiebaut and Ghina About in the ICS facility as an internal service, pAAV plasmids and AAV particles were produced by Pascal Koebel from the Molecular Biology Platform of IGBMC as an internal service, and Raquel Gómez Oca helped in the first stages of the breeding and phenotyping.

Silencing of the ORAI1 Ca^{2+} channel improves the multi-systemic phenotype of tubular aggregate myopathy and Stormorken syndrome in mice

Roberto Silva-Rojas[1], Emma Lafabrie[1], Laura Pérez-Guàrdia[1], David Moulaert[2], Jocelyn Laporte[1], Johann Böhm[1]

[1]IGBMC (Institut de Génétique et de Biologie Moléculaire et Cellulaire), Inserm U1258, CNRS UMR7104, Université de Strasbourg, 67404 Illkirch, France

[2]Institut Clinique de la souris (ICS), 67404, Illkirch, France

*Correspondence: Johann Böhm (johann@igbmc.fr)

Jocelyn Laporte (jocelyn@igbmc.fr)

IGBMC, 1 Rue Laurent Fries, 67404 Illkirch, France

Tel.: +33 (0)3 88 65 34 14

ABSTRACT

Store-operated Ca^{2+} entry (SOCE) is a Ca^{2+} entry mechanism relying on the precise interplay of the reticular Ca^{2+} sensor STIM1 and the plasma membrane Ca^{2+} channel ORAI1. SOCE over-activation has been observed in tubular aggregate myopathy and Stormorken syndrome (TAM/STRMK), a clinical continuum affecting the muscles, eyes, skin, spleen and platelets. A TAM/STRMK mouse model harboring the most common STIM1 mutation R304W has been generated and recapitulates the multi-systemic picture of the patients. However, there is currently no therapy available for TAM/STRMK.

To counterbalance the negative effects of excessive Ca^{2+} entry via ORAI1, we crossed our *Stim1*$^{R304W/+}$ mouse model with mice expressing 50% of *Orai1* (*Orai1*$^{+/-}$) and reduced *Orai1* expression in tibialis anterior muscle with AAVs containing specific shRNAs. Genetic *Orai1* downregulation improved body weight, bone morphology and skin histology while no impact was observed on platelet counts and spleen size. With a particular skeletal muscle, both the genetic and the AAV-related strategies improved muscle performance and contraction. However, while genetic *Orai1* silencing improved fiber size in an autophagy-related manner no improvement was observed in the AAV delivery strategy.

Overall, these results show that the *Orai1* silencing ameliorates several of the main clinical signs of TAM/STRMK, confirms that cellular Ca^{2+} excess is the main pathomechanism underlying the disease, and points to ORAI1 as main therapeutic target. The present study paves the way for the development of translational approaches targeting *Orai1* expression or activity to treat STRMK and potentially other Ca^{2+}-related disorders with over-activated SOCE.

INTRODUCTION

ORAI1, ORAI2, and ORAI3 are broadly expressed and highly selective calcium (Ca^{2+}) channels residing at the plasma membrane. Owing to their primary role as regulators of extracellular Ca^{2+} influx, they were named after the three *horai* Eunomia, Dike, and Eirene, known as the guardians of the gates of Olympus in Greek mythology[1]. Ca^{2+} is a universal second messenger and initiates a wide variety of conserved signaling cascades. It is primarily stored in the endoplasmic/sarcoplasmic reticulum (ER/SR), and the transient increase of cytosolic Ca^{2+} levels modulates transcription and mediates a multitude of biological processes including cell proliferation and motility, exocytosis, nerve conduction, hormone release, coagulation, and muscle contraction[2]. Hence, the precise regulation of Ca^{2+} entry, Ca^{2+} storage, and Ca^{2+} release forms the basis for normal physiology in all cell types. One of the major mechanisms controlling Ca^{2+} homeostasis is store-operated Ca^{2+} entry (SOCE), which essentially relies on the concerted activity of the Ca^{2+} channel ORAI1 and the reticular Ca^{2+} sensor STIM1. Ca^{2+} store depletion from the ER/SR induces a conformational change of STIM1, resulting in protein di- and oligomerization and the interaction with ORAI1 to trigger extracellular Ca^{2+} entry, ensure Ca^{2+} store refill, and maintain high Ca^{2+} gradients enabling oscillatory Ca^{2+} signalling[3; 4].

Pathologic alterations of SOCE impeding or increasing Ca^{2+} influx profoundly compromise proper Ca^{2+} signaling and impact on various molecular, physiological, and biochemical functions in tissues and organs, leading to multi-systemic mirror diseases[5]. Recessive *STIM1* and *ORAI1* loss-of-function (LoF) mutations inhibit SOCE and Ca^{2+} store refill, and cause severe combined immunodeficiency (SCID), characterized by recurrent and chronic infections, autoimmunity, muscular hypotonia, mydriasis, and amelogenesis imperfecta[1; 6; 7]. By contrast, dominant *STIM1* and *ORAI1* gain-of-function (GoF) mutations inducing SOCE overactivity and excessive Ca^{2+} entry give rise to tubular aggregate myopathy (TAM) and Stormorken syndrome (STRMK), two clinically overlapping disorders associating childhood-onset muscle weakness with miosis, ichthyosis, short stature, hyposplenism, thrombocytopenia, and dyslexia[8-14]. In analogy to the human disorders, mice either lacking *Stim1* or *Orai1*, or carrying GoF mutations in these genes recapitulate the main clinical signs of immunodeficiency or TAM/STRMK[15-18] and represent valuable tools to investigate disease progression, uncover the underlying pathomechanisms, and identify therapeutic targets. Most *Orai1*^{-/-} mice die perinatally, and the few surviving pups show

74 defective B-cell and T-cell function and cytokine production, while heterozygous $Orai^{+/-}$ animals

75 are normal and fertile, demonstrating that a remaining *Orai1* expression of 50% is sufficient to

76 ensure vital SOCE activity[18]. $Stim1^{R304W/+}$ mice harboring the most common TAM/STRMK

77 mutation are smaller and weaker than their littermates, and manifest bone, platelet, spleen, and

78 skin anomalies[17]. Histological analyses of $Stim1^{R304W/+}$ muscle sections revealed the presence of

79 fibers with Ca^{2+} overload[17], and functional investigations in animals and on muscle extracts

80 evidenced that the elevated cytosolic Ca^{2+} levels hamper regular muscle contraction and lead to

81 sustained reticular stress, resulting in increased cell death and muscle fiber turnover[19].

82 There is currently no treatment for TAM/STRMK, but SOCE and Ca^{2+} homeostasis are susceptible

83 to manipulation. In order to attenuate extracellular Ca^{2+} entry in the murine TAM/STRMK model,

84 we crossed $Stim1^{R304W/+}$ with $Orai1^{+/-}$ animals, and the offspring underwent systematic

85 phenotyping at the macroscopic and molecular level. The $Stim1^{R304W/+}Orai1^{+/-}$ mice showed

86 improved body size, bone architecture, skin histology, and muscle function and structure compared

87 with their $Stim1^{R304W/+}$ littermates. Based on this proof-of-concept illustrating the therapeutic

88 potential of reduced *Orai1* expression, we next implemented a practical method targeting *Orai1*

89 with the perspective to adapt and translate this approach to TAM/STRMK patients. Local injection

90 of AAVs containing *Orai1*-specific shRNAs resulted in improved muscle contraction and

91 relaxation properties in TAM/STRMK mice. Overall, our data highlight RNA interference as a

92 suitable and potent method to antagonize the multi-systemic TAM/STRMK phenotype, and paves

93 the way for prospective clinical trials.

94

RESULTS

96 Mice harboring the most common TAM/STRMK mutation STIM1 p.Arg304Trp (R304W)

97 recapitulate the main clinical signs of the human disorder and manifest smaller size and lower

98 body weight, muscle weakness, thrombocytopenia, eye movement defects, and skin and spleen

99 anomalies[17]. TAM/STRMK arises from to SOCE overactivity leading to excessive Ca^{2+} entry and

100 high cytosolic Ca^{2+} levels[8; 14], and the availability of a faithful animal model for the disease offers

101 the possibility to establish and validate therapeutic approaches in view of prospective clinical

102 trials. In order to diminish Ca^{2+} influx and antagonize the development of TAM/STRMK, we

103   crossed *Stim1*[R304W/+] mice[17] with *Orai1*^{+/-} animals[18] expressing 50% of the Ca^{2+} channel ORAI1

104   (Fig S1A). The resulting WT, *Orai1*^{+/-}, *Stim1*[R304W/+], and *Stim1*[R304W/+]*Orai1*^{+/-} offspring underwent

105   comparative phenotyping to assess birth ratio, muscle force, platelet number, bone morphology,

106   as well as skin and spleen histology to conclude on the therapeutic potential of *Orai1*

107   downregulation.

Improved birth ratio, body size, and weight gain of *Stim1*[R304W/+]*Orai1*^{+/-} mice

109   We previously reported that the number of *Stim1*[R304W/+] pups is below the expected Mendelian

110   ratio and that the born animals are smaller than their WT littermates throughout life[17]. These

111   observations point to a crucial role of SOCE for prenatal and postnatal development and indicate

112   that Ca^{2+} imbalance can entail embryonic death.

113   Genotyping of almost 300 animals at 7 days after birth revealed a genotype proportion of 23%

114   WT, 31 % *Orai1*^{+/-}, 19% *Stim1*[R304W/+], and 27% *Stim1*[R304W/+]*Orai1*^{+/-} (p = 0.036). Extraction of

115   skeletal muscle RNA and subsequent RT-qPCR evidenced a 50% reduction of *Orai1* expression

116   in *Orai1*^{+/-} and *Stim1*[R304W/+]*Orai1*^{+/-} mice compared with the controls (Fig S1B), while *Orai2* and

117   *Orai3* expression were comparable across the genotypes (Fig S1C-D). We followed body size and

118   weight development of the offspring over 4 months and in accordance with our previous studies[17],

119   the *Stim1*[R304W/+] mice showed a distinct growth deficiency in comparison to the control littermates

120   (Fig 1A and S1E). At every timepoint of measurement, the *Stim1*[R304W/+]*Orai1*^{+/-} mice were

121   significantly bigger and heavier than the *Stim1*[R304W/+] mice with a difference of 75 mm and 5 g at

122   4 months, corresponding to an increase of 23% and 10%, respectively (Fig 1A). Overall, our data

123   confirm the lower birth ratio and weight gain of *Stim1*[R304W/+] mice and the absence of an overt

124   deleterious effect of ORAI1 downregulation in *Orai1*^{+/-} mice. They also suggest that

125   *Stim1*[R304W/+]*Orai1*^{+/-} offspring overcome the risk of prenatal lethality and document a normalized

126   postnatal development of the TAM/STRMK animals with reduced *Orai1* expression.

Improved bone architecture and muscle weight in *Stim1*[R304W/+]*Orai1*^{+/-} mice

128   The continuous growth of organisms from birth to adulthood is intrinsically linked to the

129   elongation of bones, and more precisely to the counterbalance of bone-forming osteoblasts and

130   bone-resorbing osteoclasts[20]. The proliferation and differentiation of both osteoblasts and

131   osteoclasts is Ca^{2+}-dependent, and aberrations of the SOCE pathway involve anomalies of bone

132 architecture[21; 22]. Consistently, *Stim1$^{R304W/+}$* bones were shown to exhibit a decreased cellular

133 density and reduced bone marrow area[17] (Fig 1B), presumably accounting for the short stature of

134 TAM/STRMK patients and mice. Micro-computerized tomography and 3D representations of

135 *Stim1$^{R304W/+}$Orai1$^{+/-}$* bones evidenced an improved cortical and trabecular structure and strength

136 compared with *Stim1$^{R304W/+}$* mice as illustrated by a significant increased moment of inertia (MOI)

137 of 33% and a reduced trabecular separation of 43% of tibia and femur, respectively (Fig 1B and

138 Tables S3-S4).

139 Skeletal muscles are attached to bones to effectuate voluntary movements, and bone growth

140 correlates with the buildup of muscle mass. The ratio of small oxidative type I and large glycolytic

141 type II fibers adapts individual muscles to either powerful movements or endurance activities[23; 24],

142 and the interconversion between type I and type II fibers is Ca^{2+}-dependent[25]. As a result of

143 abnormal Ca^{2+} homeostasis, muscles from *Stim1$^{R304W/+}$* mice showed a fiber type shift associated

144 with hypotrophy of the mixed gastrocnemius, and hypertrophy of the soleus muscle, essentially

145 composed of slow-twitch type I fibers[17; 19]. Dissection of *Stim1$^{R304W/+}$* and *Stim1$^{R304W/+}$Orai1$^{+/-}$*

146 muscles at 4 months of age revealed a similar weight of the gastrocnemius, while the soleus was

147 17% lighter in *Stim1$^{R304W/+}$Orai1$^{+/-}$* mice (Fig S1F-G). Altogether, the analysis of the factors

148 contributing to the ameliorated growth curves of *Stim1$^{R304W/+}$Orai1$^{+/-}$* mice revealed an improved

149 bone structure and a partial normalization of muscle weight.

150 **Improved skin histology, but unchanged spleen and platelet phenotypes in**

151 ***Stim1$^{R304W/+}$Orai1$^{+/-}$* mice**

152 Dermal anomalies including ichthyosis, eczema, or anhidrosis are common features of

153 TAM/STRMK[12]. Histological analyses of patient samples disclosed an obstruction of the eccrine

154 glands, resulting in sweat retention and representing a risk factor for associated skin irritations[26],

155 and *Stim1$^{R304W/+}$* mice displayed an enlarged dermis and a thinning of the subcutaneous fat layer[17].

156 Examinations of skin cross sections from *Stim1$^{R304W/+}$Orai1$^{+/-}$* mice revealed an increase of the fat

157 layer area of 51% compared with *Stim1$^{R304W/+}$* samples (Fig 1C and S1H-I), indicating a direct role

158 of SOCE on dermal composition and highlighting a measurable amelioration of TAM/STRMK

159 skin through *Orai1* downregulation.

160
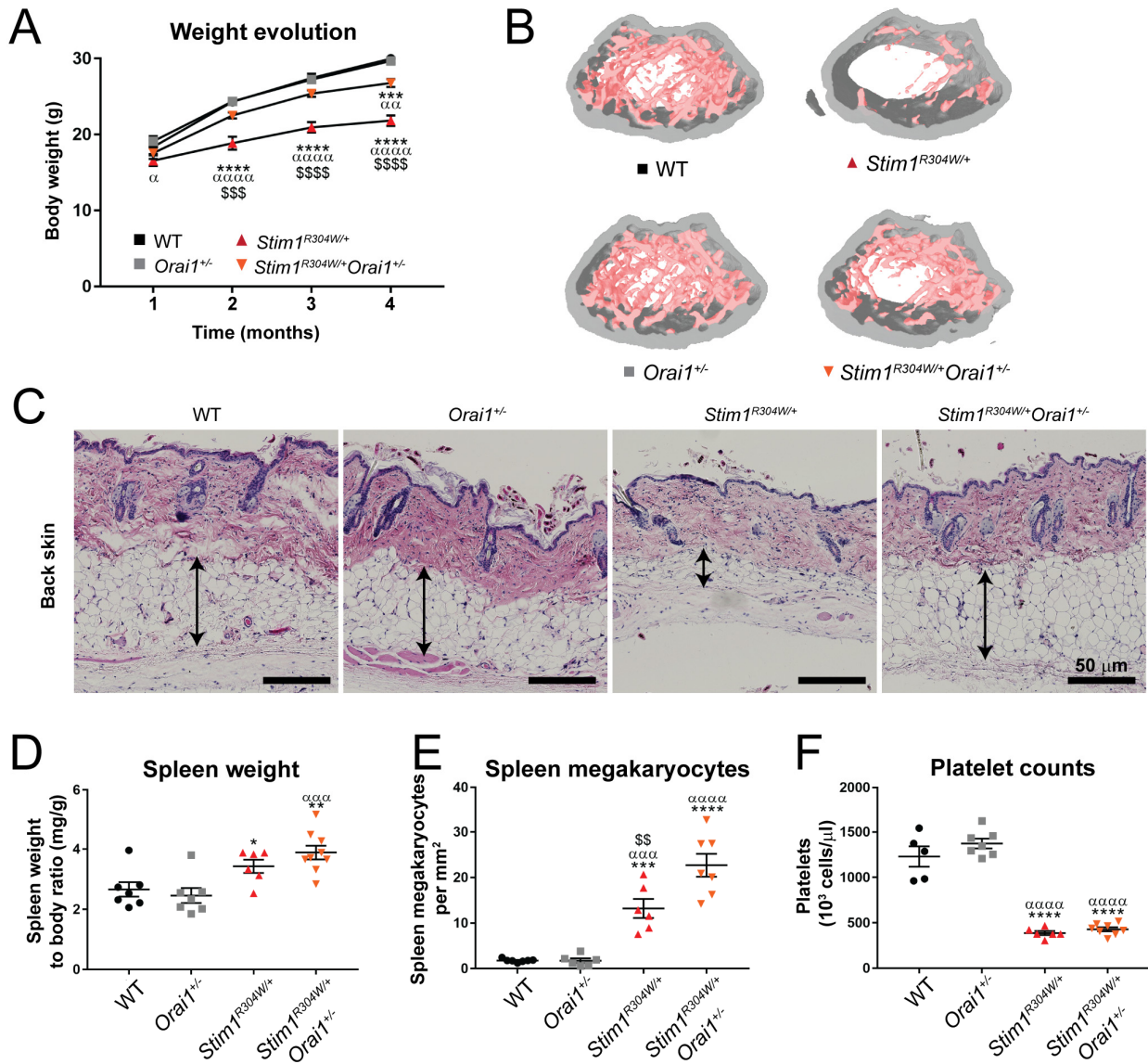
Figure 1. Improved weight gain, bone structure, and skin composition in *Stim1^{R304W/+}Orai1^{+/-}* mice. (A) Body weight evolution was favorable in *Stim1^{R304W/+}Orai1^{+/-}* mice compared with *Stim1^{R304W/+}* littermates over the first months of life (n=11-17). (B) 3D reconstruction of the femur microarchitecture illustrated a similar trabecular density in *Stim1^{R304W/+}Orai1^{+/-}* mice and healthy WT and *Orai1^{+/-}* controls. (C) Histological H&E staining of back skin sections at 8 months evidenced a normalized fat layer thickness (arrows) in *Stim1^{R304W/+}Orai1^{+/-}* mice. (D-F) Relative spleen weight, megakaryocyte numbers, and platelet counts were comparable in *Stim1^{R304W/+}* and *Stim1^{R304W/+}Orai1^{+/-}* mice and significantly differed from the healthy controls (n=5-9). Graphs represent mean ± SEM. Significant differences are indicated as */α/$ P<0.05, **/αα/$$ P<0.01, ***/ααα/$$$ P<0.001, and ****/αααα/$$$$ P<0.0001 with * reflecting the comparison with the WT group, α the comparison with the *Orai1^{+/-}* group, and $ for the comparison with the *Stim1^{R304W/+}Orai1^{+/-}* group.

173   Another hallmark of TAM/STRMK is spleen dysfunction in combination with thrombocytopenia

174   and bleeding diathesis[7; 9; 11; 21; 27]. Alike the human phenotype, *Stim1*[R304W/+] mice showed

175   morphological spleen anomalies and a reduction of the total platelet number by 70%[17], resulting

176   in reduced thrombus formation upon injury and in increased bleeding times. *Stim1*[R304W/+]*Orai1*^{+/-}

177   animals also manifested splenomegaly and hyperplasia of the megakaryocytes, the precursor cells

178   forming and releasing platelets to the bloodstream (Fig 1C-D). In compliance with the uncorrected

179   spleen phenotype, platelet counts were similarly low in *Stim1*[R304W/+] and *Stim1*[R304W/+]*Orai1*^{+/-}

180   animals (Fig 1E), suggesting that the downregulation of *Orai1* by 50% has no major effect on the

181   spleen and platelet anomalies characterizing TAM/STRMK.

Improved muscle performance and contraction properties in *Stim1*[R304W/+]*Orai1*^{+/-} mice

183   Muscle weakness, exercise intolerance, and myalgia are the principal disabling traits of

184   TAM/STRMK[12]. Affected individuals have difficulties climbing stairs, running, or standing up

185   from a squatting position, and consistently, *Stim1*[R304W/+] mice manifested deficiencies in general

186   and specific muscle force[17]. Although still less powerful than the WT and *Orai1*^{+/-} controls at the

187   hanging test, *Stim1*[R304W/+]*Orai1*^{+/-} mice performed better than the *Stim1*[R304W/+] littermates

188   throughout the first 4 months (Fig 2A). They also showed an increased grip strength at 4 months

189   and achieved a higher mean speed and covered distance at open field tests at 3 months (Fig 2B and

190   S2A-B). *In situ* muscle force measurements on tibialis anterior at 8 months of age confirmed the

191   slight but not significant improvement of maximal and specific muscle force of

192   *Stim1*[R304W/+]*Orai1*^{+/-} compared with *Stim1*[R304W/+] mice (Fig 2C and S2C).

193   Muscle contraction is a multistep process initiated by an electrical stimulus and mediated by the

194   release of Ca^{2+} from the SR. The Ca^{2+} ions trigger the shortening of the contractile units to generate

195   force[28], and Ca^{2+} store refill through the ATP-dependent SERCA pumps enables muscle relaxation

196   and maintains high Ca^{2+} gradients across the SR membrane to allow repetitive tetanic stimulations

197   and counteract the effects of fatigue[29; 30]. As a consequence of cytosolic Ca^{2+} overload and the

198   abundance of Ca^{2+} at the contractile units, *Stim1*[R304W/+] mice exhibited an increased force

199   production at low stimulation frequencies together with a delay in muscle contraction/relaxation

200   and abnormal fatigue profiles[17; 19]. In *Stim1*[R304W/+]*Orai1*^{+/-} mice, the force production between

201   1 and 20 Hz shifted towards normal values, just as the muscle contraction and relaxation kinetics

202   following a single impulse (Fig 2D-F and S3A-C). The fatigue curves following repetitive

stimulations remained however identical in *Stim1$^{R304W/+}$Orai1$^{+/-}$* and *Stim1$^{R304W/+}$* mice (Fig S3D-G). In summary, the reduction of *Orai1* expression by half has minor but measurable effects on muscle force and functionality in *Stim1$^{R304W/+}$Orai1$^{+/-}$* mice.
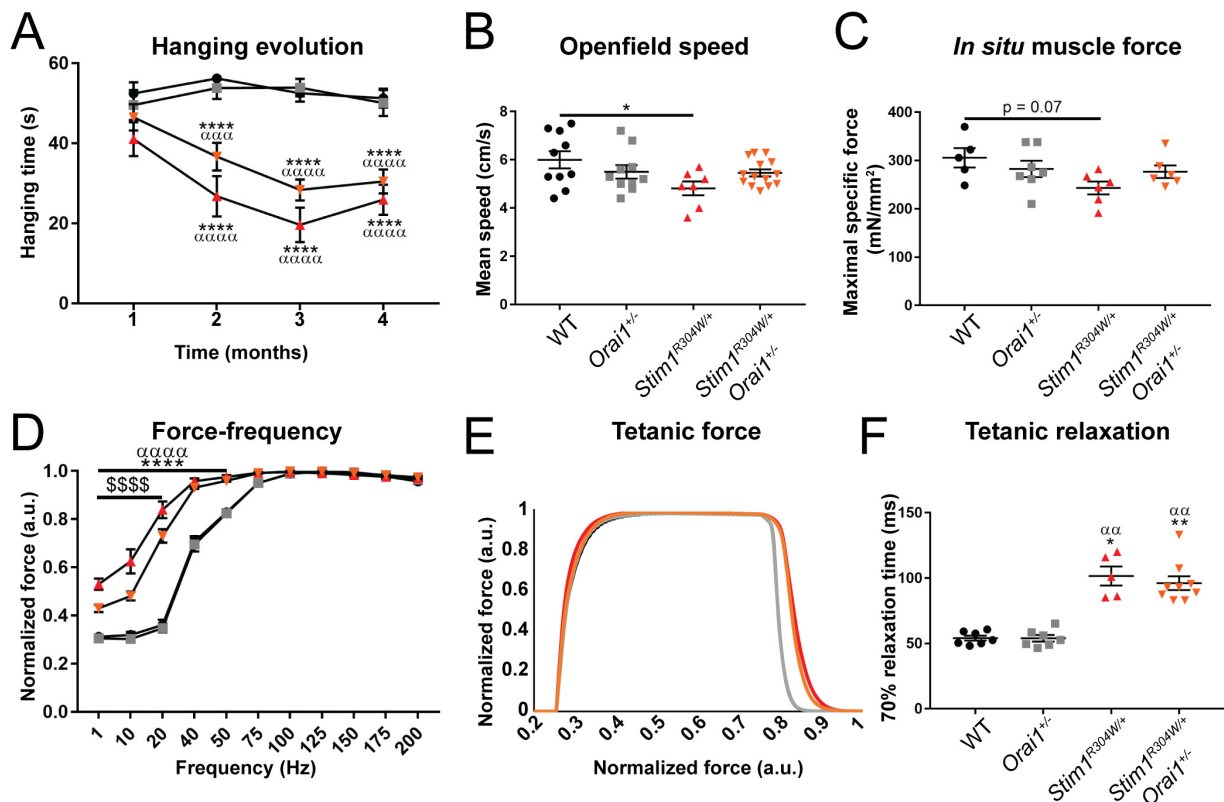
Figure 2. Improved muscle performance of *Stim1$^{R304W/+}$Orai1$^{+/-}$* mice. (A) *Stim1$^{R304W/+}$Orai1$^{+/-}$* mice showed a continuous but not significant tendency of increased hanging times compared with *Stim1$^{R304W/+}$* littermates between 1 and 4 months (n=11-17). (B) The velocity of *Stim1$^{R304W/+}$Orai1$^{+/-}$* mice in the OpenField arena was indistinguishable from WT and *Orai1$^{+/-}$* controls at 10 weeks of age (n=7-14). (C) *In situ* measurements at 2 months revealed a slightly but not significantly elevated muscle force of *Stim1$^{R304W/+}$Orai1$^{+/-}$* mice compared with *Stim1$^{R304W/+}$* littermates (n=5-7). (D-F) Stimulation frequencies of 1-20 Hz evidenced a shift of the *Stim1$^{R304W/+}$Orai1$^{+/-}$* muscle contraction properties towards normal values, while muscle relaxation following tetanic stimulation was similar in *Stim1$^{R304W/+}$* and *Stim1$^{R304W/+}$Orai1$^{+/-}$* mice (n=5-9). Graphs represent mean ± SEM. Significant differences are indicated as */α/$ $P<0.05$, **/αα/$$ $P<0.01$, ***/ααα/$$$ $P<0.001$, and ****/αααα/$$$$ $P<0.0001$ with * reflecting the comparison with the WT group, α the comparison with the *Orai1$^{+/-}$* group, and $ for the comparison with the *Stim1$^{R304W/+}$Orai1$^{+/-}$* group.

Increased muscle fiber size and improved autophagic flux in *Stim1$^{R304W/+}$Orai1$^{+/-}$* mice

Muscle weakness in TAM/STRMK mice is accompanied by structural muscle aberrations including an increased proportion of type I fibers and signs of muscle fiber degeneration and regeneration such as fiber atrophy, nuclear centralization, and infiltration of immune cells[17; 19]. Histological analyses on transverse *Stim1$^{R304W/+}$Orai1$^{+/-}$* tibialis anterior sections revealed an overall enlargement of fiber caliber with 61% of the fibers exceeding a MinFeret diameter of 40 µm compared to 43% in *Stim1$^{R304W/+}$* mice (Fig 3A-C). The number of fibers with central nuclei was however not reduced in *Stim1$^{R304W/+}$Orai1$^{+/-}$* tibialis anterior, indicating that muscle fiber degeneration was not fully resolved despite the increase of fiber size (Fig 3D).

Muscle fiber degeneration in *Stim1$^{R304W/+}$* mice results from Ca^{2+}-induced reticular stress and the activation of unfolded protein response (UPR) and apoptosis pathways[19]. RT-qPCR on selected UPR markers revealed a comparable upregulation of the chaperones *Hsp5* and *Hsp90b1* in the tibialis anterior of both *Stim1$^{R304W/+}$* and *Stim1$^{R304W/+}$Orai1$^{+/-}$* animals (Fig 3E-F), suggesting that reticular stress is not resolved in *Stim1$^{R304W/+}$Orai1$^{+/-}$* muscle and accounts for the observed muscle fiber degeneration. To explore the pathomechanisms underlying the increase of myofiber diameter in *Stim1$^{R304W/+}$Orai1$^{+/-}$* mice, we next addressed autophagy, an organelle recycling pathway implicated in the regulation of muscle mass[31]. We detected a decreased expression of the main autophagy genes *Map1lc3a*, *Map1lc3a*, and *Sqstm1* in *Stim1$^{R304W/+}$* mice compared with the WT (Fig S4A), while western blots on muscle extracts revealed an increased level of the autophagosome components LC3 II and p62 (Fig 3G and Fig S4B-C), indicating enhanced autophagosome formation or impaired fusion with the lysosome and suggesting a bock of late-stage autophagy. Noteworthy, the LC3 II and p62 levels were significantly reduced in *Stim1$^{R304W/+}$Orai1$^{+/-}$* tibialis anterior compared with *Stim1$^{R304W/+}$* mice (Fig 3H-I and S4D), indicating a recovery of the autophagic flux through *Orai1* downregulation and providing a potential explanation for the increase in muscle fiber diameter despite continued UPR and myofiber degeneration.
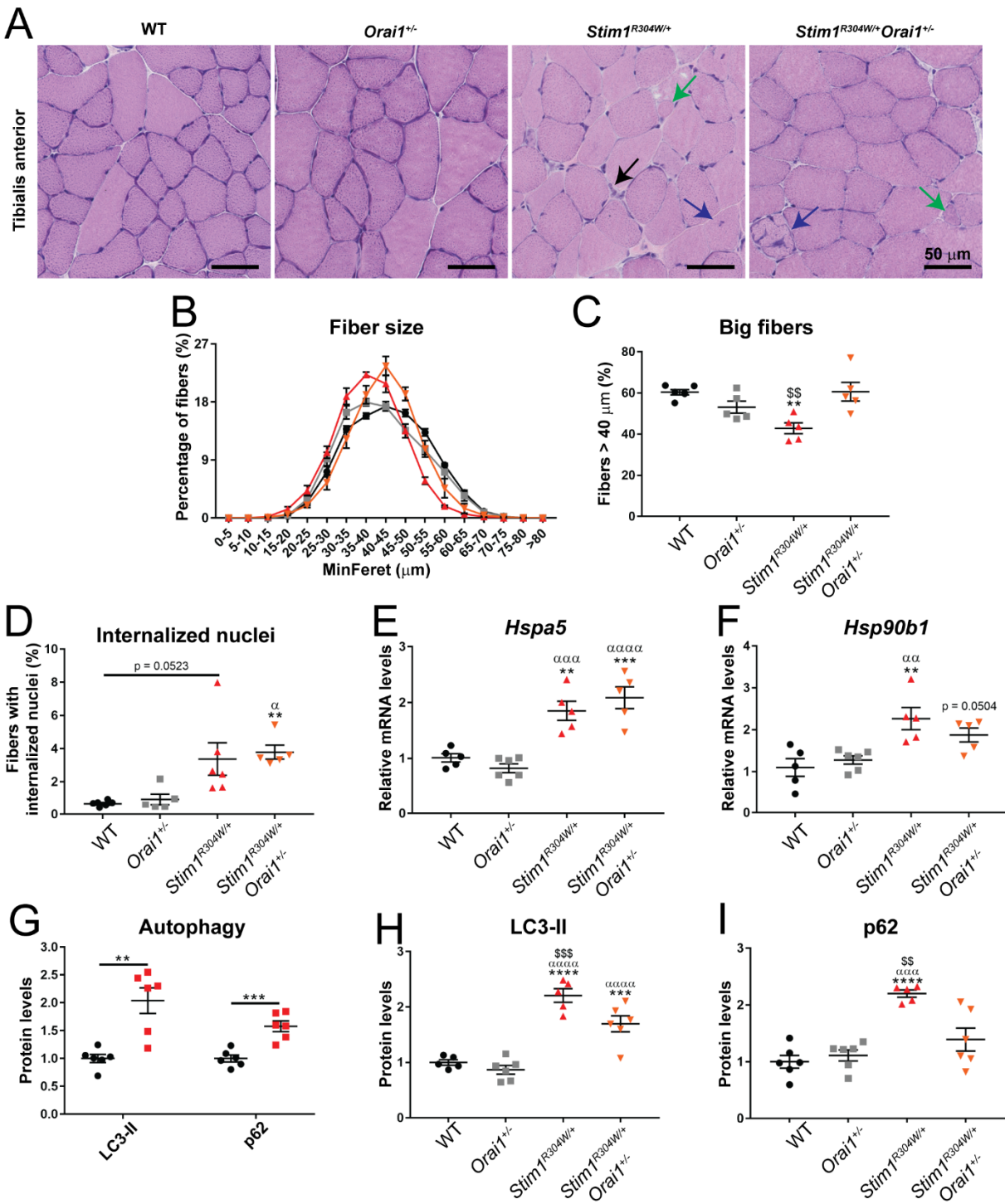
Figure 3. Increased myofiber size and improved autophagic flux in *Stim1R304W/+Orai1+/-* mice. (A) H&E staining on muscle sections from both *Stim1R304W/+* and *Stim1R304W/+Orai1+/-* mice at 4 months revealed signs of muscle fiber degeneration such as centralized nuclei (blue arrows), regenerating fibers (green arrow) and immune cell infiltrations (black arrows). (B-C) Different fiber size distribution in *Stim1R304W/+* and *Stim1R304W/+Orai1+/-* mice and significant increase of fibers with a MinFeret diameter of >40 μm in *Stim1R304W/+Orai1+/-* muscle at 4 months (n=5). (D-F)

259

shRNA-driven *Orai1* silencing partially reverses the muscle phenotype of *Stim1^{R304W/+}* mice

The crossing experiments on our TAM/STRMK mouse model and the survey of birth ratio, growth, and bone, skin, spleen, platelet, and muscle phenotypes of the *Stim1^{R304W/+}Orai1^{+/-}* offspring and control littermates provided the proof-of-concept that decreased *Orai1* expression efficiently anticipates full disease development. In order to establish an appropriate and applicable procedure to specifically downregulate *Orai1* in postnatal tissues, we used RNA interference.

We aligned the mouse *Orai1* sequence with its paralogues *Orai2* and *Orai3*, and we designed four shRNAs targeting stretches of 19 to 22 *Orai1*-specific nucleotides also conserved in humans (Fig S5A). Transfection of murine C2C12 myoblasts and subsequent RNA extraction and RT-qPCR demonstrated an *Orai1* downregulation of least 50% through shRNAs sh22, sh190 and sh760 compared with untransfected controls or cells expressing scramble shRNAs (Fig S5A). To validate *Orai1* silencing *in vivo*, we generated AAVs containing the shRNAs and injected the tibialis anterior of 1-month-old WT mice. Four weeks post-injection, sh22 and sh190 yielded an *Orai1* downregulation of more than 80% as compared to NaCl-injected control muscles, while sh760 was less efficient and therefore discarded (Fig S5A).

To determine the ability of the selected shRNAs to reverse the muscle defects of TAM/STRMK, we proceeded with the intramuscular AAV injection of WT and *Stim1^{R304W/+}* mice at 2 months of age, and we investigated muscle function, structure, and physiology 8 weeks post injection. *Orai1* downregulation ranged from 50% to 80% (Fig 4A), whereas the expression levels of *Orai2* and *Orai3* were comparable in the injected, non-injected, and scramble-injected muscles (Fig S6A-D), demonstrating high specificity of the shRNAs. *In situ* measurements on anesthetized animals showed a positive effect of both sh22 and sh190 on the force production at low stimulation

282 frequencies of *Stim1^{R304W/+}* mice compared with the scramble shRNAs, while the muscle

283 contraction properties did not vary between shRNA-injected and control WT mice, ruling out a

284 negative impact of the shRNAs on normal muscle function (Fig 4B). We also observed an

285 improvement of the muscle relaxation kinetics with reduced relaxation times in *Stim1^{R304W/+}*

286 tibialis anterior injected with sh22 and sh190 following single and tetanic stimulations (Fig 4C-E).

287 Histological examination of the dissected *Stim1^{R304W/+}* tibialis anterior failed to disclose significant

288 ameliorations of shRNA delivery on the muscle structure. The proportion of fibers with a MinFeret

289 diameter of > 55µM and the number of fibers with centralized nuclei were comparable in shRNA

290 and scramble-injected *Stim1^{R304W/+}* muscles (Fig S7A-D). In agreement with the morphological

291 findings, there was no difference in the expression levels of UPR and autophagy markers in

292 *Stim1^{R304W/+}* tibialis anterior treated with sh22, sh190, or scramble shRNAs (Fig S8A-D and S9A).

293 Overall, the shRNA-mediated downregulation of ORAI1 did not resolve reticular Ca^{2+} stress and

294 autophagy block, but significantly improved muscle contraction and relaxation properties in the

295 murine TAM/STRMK model.

296

297
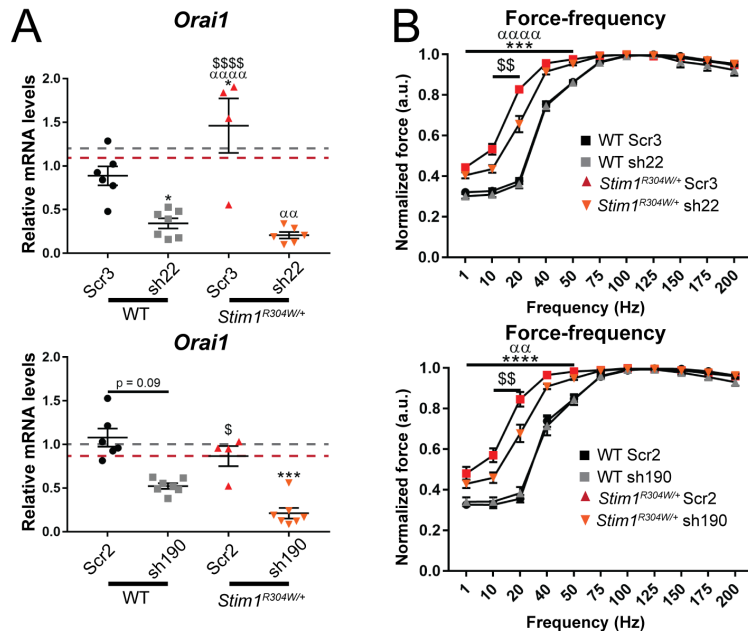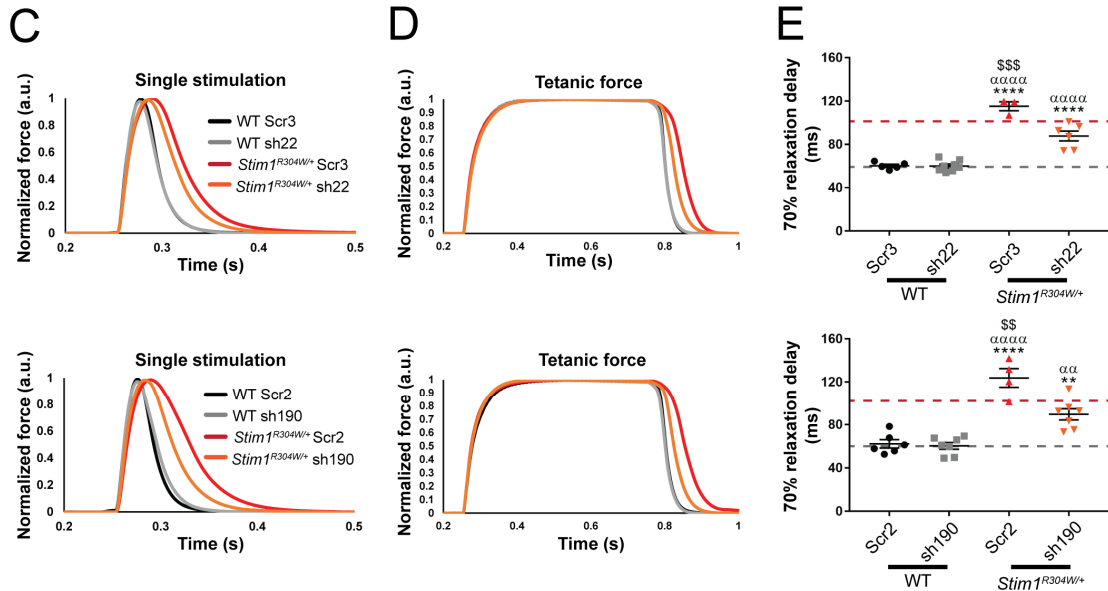
Figure 4. Improved muscle contraction and relaxation properties in TAM/STRMK mice through *Orai1* **silencing 8 weeks post shRNA injection.** (A) sh22 (top) and sh190 (bottom) yielded 80% decrease of *Orai1* expression in *Stim1^{R304W/+}* muscle compared to scramble-injected WT, NaCl-injected WT (black dashed line), and NaCl-injected *Stim1^{R304W/+}* (red dashed line) controls (n=4-6). (B) Shifted force production towards normal values at low stimulation frequencies in *Stim1^{R304W/+}* tibialis anterior treated with sh22 (top) and sh190 (bottom) compared with scramble-injected controls (n=4-8). (C-D) Improved muscle relaxation after single and tetanic stimulation of *Stim1^{R304W/+}* tibialis anterior injected with sh22 (top) and sh190 (bottom) compared with scramble-injected controls (n=3-8). (E) The time required for a muscle relaxation of 70% is significantly reduced in *Stim1^{R304W/+}* tibialis anterior injected with sh22 (top) and sh190 (bottom) compared with scramble-injected controls (n=3-8). Graphs represent mean ± SEM. Significant differences are indicated as */α/$ $P<0.05$, **/αα/$$ $P<0.01$, ***/ααα/$$$ $P<0.001$ and ****/αααα/$$$$ $P<0.0001$ with * reflecting the comparison with the scramble-injected WT group, α the comparison with the shRNA-injected WT sh group, and $ for the comparison with the scramble-injected *Stim1^{R304W/+}* group.

DISCUSSION

Tubular aggregate myopathy (TAM) and Stormorken syndrome (STRMK) are spectra of the same multi-systemic disease affecting muscle, bones, skin, muscles, spleen, and skin[9]. They are caused by gain-of-function mutations in *STIM1* and *ORAI1*, encoding key components of the ubiquitous store-operated Ca^{2+} entry (SOCE) mechanism[12]. There is currently no treatment for TAM/STRMK, and here we provide the proof-of-concept that the genetic downregulation of the Ca^{2+} entry channel ORAI1 significantly and stably improves the multi-systemic phenotype in a faithful mouse model of the disorder. In addition, we specifically targeted *Orai1* expression through AAV-mediated delivery of shRNAs in murine TAM/STRMK muscle to attenuate Ca^{2+} influx, and thus furnished a suitable method for a potential application in humans.

ORAI1 as the principal target to treat the multi-systemic TAM/STRMK phenotype

Store-operated Ca^{2+} entry (SOCE) is an essential mechanism controlling Ca^{2+} influx in all tissues and organs to regulate countless Ca^{2+}-dependent metabolic processes, signaling pathways, and cellular functions. By way of example, SOCE drives osteoblastogenesis and osteoclastogenesis and thereby governs the dynamic balance of bone deposition and bone resorption required for growth[22; 32; 33]. SOCE also activates blood clotting following injury through Ca^{2+}-dependent secretion of alpha granules from platelets to induce thrombus formation[34; 35], directs the differentiation and migration of keratinocytes in the epidermis[36; 37], and triggers the opening of a Ca^{2+}-activated chloride channel for sweat production[38]. Furthermore, efficient muscle contraction is predicated on the precise control of Ca^{2+} flows between the SR and the cytosol, and the SOCE-mediated Ca^{2+} store refill counteracts the effects of fatigue[29; 30]. As a consequence, the dysfunction of SOCE and its principal elements STIM1 and ORAI1 severely interferes with Ca^{2+} homeostasis and compromises normal physiology in multiple tissues[39].

Considering that TAM/STRMK arises from excessive extracellular Ca^{2+} entry, the reduction of Ca^{2+} influx through ORAI1 appears as the most straightforward approach to attenuate or reverse the multi-systemic anomalies of bones, skin, spleen, platelets, and muscle. Moreover, ORAI1 acts downstream of the other known TAM/STRMK genes, and hence represents the most appropriate target for a common therapy of all disease forms. Indeed, the overall reduction of available ORAI1 monomers to shape functional channels hexamers will at least partially repeal the effects of *ORAI1*

342   mutations generating a leaky channel[40], of *STIM1* mutations inducing constitutive ORAI1

343   opening[8; 11; 13; 14], and of *CASQ1* mutations interfering with STIM1 retention and the negative

344   regulation of SOCE[41; 42]. This is supported by a previous study showing that the dystrophic

345   phenotype of transgenic mice overexpressing WT STIM1 is improved by a dominant-negative

346   ORAI1 mutant[43].

Downregulation of *Orai1* improves the majority, but not all multi-systemic TAM/STRMK phenotypes

349   The $Stim1^{R304W/+}$ mouse replicates the multi-systemic phenotype of the human disorder[17], and

350   represents an adequate model to assess preclinical therapies. Here we crossed our $Stim1^{R304W/+}$

351   model with $Orai1^{+/-}$ mice to obtain $Stim1^{R304W/+}Orai1^{+/-}$ offspring carrying the most common

352   TAM/STRMK mutation and expressing only 50% of the Ca^{2+} entry channel ORAI1. Of note, the

353   total knockout of *Orai1* in mice is lethal[18], and the tissue-specific deletion of *Orai1* or the

354   generation of chimeras through transplantation of hematopoietic $Orai1^{-/-}$ stem cells results in

355   defective T cell activation in response to antigens[18; 44], reduced platelet activation and thrombus

356   formation[45], anhidrosis[38], amelogenesis imperfecta[18], and muscle weakness[46]. Accordingly,

357   patients carrying homozygous *ORAI1* LoF mutations abolishing SOCE manifest severe combined

358   immunodeficiency (SCID) associated with skin anomalies, ectodermal dysplasia, and muscular

359   hypotonia[1], emphasizing the importance of operative SOCE for normal development and physical

360   integrity. However, heterozygous carriers of SCID mutations are healthy, and mice deprived of a

361   single *Orai1* allele do not show any apparent pathology, demonstrating that the remaining *Orai1*

362   expression of 50% is sufficient to preserve the necessary SOCE activity in immune, skin, blood,

363   ectoderm, and muscle cells.

364   Phenotyping of the $Stim1^{R304W/+}Orai1^{+/-}$ mice from birth to the age of 4 months revealed a rescue

365   of the birth ratio, and a significant improvement of growth and weight development, bone

366   architecture, skin histology, and muscle function and structure compared with $Stim1^{R304W/+}$ mice

367   fully expressing *Orai1*. However, the spleen phenotype was not relieved, and $Stim1^{R304W/+}Orai1^{+/-}$

368   mice displayed the same thrombocytopenia and coagulation defects as their TAM/STRMK

369   littermates. This is possibly due to the disparate Ca^{2+} sensitivity and Ca^{2+} balance of the different

370   cell types forming an organism. Lymphocytes, macrophages, megakaryocytes, or platelets might

371   be more responsive to subtle changes of intracellular Ca^{2+} concentrations than osteoblasts,

372 fibroblasts, or muscle fibers, and require a more stringent reduction of Ca^{2+} influx for the

373 normalization of SOCE-dependent pathways. Alternatively, the ORAI1 paralogues ORAI2 and

374 ORAI3 or other Ca^{2+} channels as the TRPCs may adopt a leading role in the regulation of SOCE

375 in spleen and platelets, and thereby dilute the effect of *Orai1* downregulation.

shRNA-mediated silencing of *Orai1* as a promising therapeutic approach

377 The rescue of birth ratio and the improvement of postnatal development of *Stim1^{R304W/+}Orai1^{+/-}*

378 offspring as exemplified by growth, bone structure, skin composition, open field activity, muscle

379 force and muscle contraction properties illustrate the strong therapeutic potential of *Orai1*

380 reduction for TAM/STRMK. Based on this proof-of-concept and in view of a prospective

381 treatment of TAM/STRMK patients, we aimed to establish a practical method to downregulate

382 *Orai1* in our murine *Stim1^{R304W/+}* model and assess the reversal of the TAM/STRMK phenotype

383 in postnatal muscle. We designed *Orai1*-specific shRNAs with homology to the human *ORAI1*

384 sequence, validated their effectiveness in cells, and delivered the most capable shRNAs via local

385 AAV injections into the tibialis anterior of WT and *Stim1^{R304W/+}* mice. We noticed significant

386 improvements of the muscle contraction and relaxation kinetics in transduced *Stim1^{R304W/+}* animals

387 without achieving complete normalization despite the reduction of *Orai1* expression of more than

388 50 %. This may be related to the structure and physiology of skeletal muscle. Myofibers are

389 syncytia emerging from the fusion of hundreds and thousands of mononuclear myoblasts[47] and

390 require an important transduction efficacy of the AAVs. Here, we used AAV particles with the

391 serotype 9 capsid, which has been shown to satisfactorily but not profusely infect skeletal muscle[48]

392 and is commonly used in preclinical and clinical trials for neuromuscular disorders such as

393 centronuclear myopathy (CNM) or Duchenne's muscular dystrophy (DMD)[49-51]. Other adeno-

394 associated viruses as AAV2 and AAV8 target skeletal muscle as well and potentially more

395 efficiently[48; 52], and may represent notable alternatives.

396 Another important characteristic feature of skeletal muscle is its longevity. Indeed, myofibers have

397 a comparatively low turnover by contrast with monocytes or intestinal epithelial cells for

398 instance[53; 54]. The full therapeutic effect of the selected shRNA may therefore be visible several

399 weeks following AAV injection and possibly beyond the incubation period of 2 months. However,

400 Ca^{2+} stress-induced UPR and structural muscle anomalies such as internalized nuclei were neither

401 rescued in shRNA-treated *Stim1^{R304W/+}* tibialis anterior nor in *Stim1^{R304W/+}Orai1^{+/-}* mice,

402   suggesting that other limiting factors than myofiber turnover and AAV transduction are

403   accountable for the absence of rescuing effects on reticular stress and myofiber degeneration. At

404   least the blockage of autophagic flux appeared to be resolved $Stim1^{R304W/+}Orai1^{+/-}$ mice and

405   provides a potential explanation for the increased number of larger fibers and the gain of muscle

406   mass compared with $Stim1^{R304W/+}$ mice. It also suggests that the treatment with activators of

407   autophagy such as trans-resveratrol, spermidine, or AICAR and mTORC1 inhibitors

408   (RAD001/AZD8055) may be beneficial for TAM/STRMK patients to increase muscle force.

409   Indeed, the administration of these compounds has previously been shown to restore the autophagy

410   defects in murine models of DMD, collagen VI-related muscular dystrophies, and X-linked

411   centronuclear myopathy (XLCNM)[55-57]. In a similar way, treatment with the chemical chaperone

412   4-PBA may overcome UPR and thereby anticipate the effects of Ca^{2+} stress and raise myofiber

413   survival. This approach was proved to be effective in mouse models for DMD[58] and central core

414   disease (CCD)[59], another muscle disorders involving cytosolic Ca^{2+} overload and reticular stress[60-

415   62]. Taken together, the pharmacological treatment with autophagy activators and chaperones may

416   complement shRNA-mediated *Orai1* downregulation for a synergistic therapeutic outcome.

417   **Concluding remarks**

418   Overall, our data on $Stim1^{R304W/+}Orai1^{+/-}$ mice highlight and evidence a physiological benefit of

419   constitutive *Orai1* downregulation on the majority of the multi-systemic phenotypes

420   characterizing TAM/STRMK with a measurable effect on body size and weight development, bone

421   architecture, skin composition, and muscle function. We also established a translational approach

422   using AAV-mediated delivery of shRNAs specifically and efficiently reducing *Orai1* expression,

423   and we observed significant ameliorations of muscle contraction properties in treated $Stim1^{R304W/+}$

424   mice. The effective and durable knockdown of target genes through AAV-encapsulated shRNAs

425   was previously achieved in murine models for XLCNM and myotonic dystrophy (DM1) and

426   resulted in distinct disease reversal[50; 63], further emphasizing the therapeutic potential of this

427   approach. The downregulation of ORAI1 may not only prove useful for TAM/STRMK patients,

428   but might also be of medical interest for other Ca^{2+}-related diseases.

429

430

MATERIALS AND METHODS

Animals

Animal care and experimentation was in accordance with French and European legislation and approved by the institutional ethics committee (project numbers 2019062813376603, 2020052517411298, 2019103108289018 and 2020012813132770). Mice were housed in ventilated cages with 12h day/night cycles and access to food and water *ad libitum*. $Stim1^{R304W/+}$ and $Orai1^{+/-}$ mice were described previously[17; 64], and the $Orai1^{+/-}$ mice were a kind gift of Paul F. Worley (Johns Hopkins University, Baltimore, USA). Crossing of both mouse lines resulted in four genotypes: WT, $Orai1^{+/-}$, $Stim1^{R304W/+}$, and $Stim1^{R304W/+}Orai1^{+/-}$. Following primers were used for genotyping: GCAGGTAGGAGAGTGTACAGGATGCCTT (forward) and CTTTCCATCCCCACTGCCATTTT (reverse) for *Stim1*, and ATGCCTACTGCCAAAATTGAC (forward) and AAATACTGAGCCATCTCTCCTG (reverse) for *Orai1*.

Hanging, grip, and open field tests

To assess general muscle force, mice were suspended upside down to a cage grid for a maximum of 60 s, and the hanging time was recorded. The four-paw grip strength was measured using a dynamometer (Bioseb, Vitrolles, France) and normalized to body weight. Both hanging and grip tests were performed in triplicate with a 5-10 min rest interval. Hanging time was determined monthly and grip strength once at 4 months of age.

The open field test was performed on 2 months old mice in a homogenously illuminated arena (Bioseb) in a noise-isolated room. Covered distance, speed, and rearing were assessed during 30 min.

In situ muscle force

To determine maximal and specific muscle force, 4 and 8 months old mice were anesthetized with intraperitoneal injections of domitor/fentanyl mix (2/0.28 mg/Kg), diazepam (8mg/Kg) and fentanyl (0.28 mg/Kg). The tibialis anterior (TA) was partially excised and the tendon was attached to the isometric transducer of the *in situ* whole animal system 1305A (Aurora Scientific, Aurora, Canada). Maximal force was determined by sciatic nerve stimulations of 2-200 Hz pulses with an interval of 30 s, and fatigue by 80 stimulations of 40 Hz spaced by 2 s. Specific muscle force was

459 assessed by dividing the maximal force with the TA cross sectional area calculated as wet muscle

460 weight (mg) / optimal muscle length (mm) X mammalian muscle density (1.06 mg/mm^3).

Micro-computerized bone tomography (µCT)

462 Trabecular and cortical bone morphology and structure were assessed on femur and tibia using the

463 Quantum µCT scanner (Perkin Elmer, Waltham, USA). Scans were performed with an isotropic

464 voxel size of 10 µm, 160 µA tube current, and 90 kV tube voltage. Gray scale images were pre-

465 processed using the ImageJ software, and morphological 3D measurements were executed with

466 the CTAn software (Bruker, Billerica, USA). Representative images were generated using the

467 CTvol software (Bruker).

Bleeding test and blood counts

469 Mice were anesthetized by inhalation of isoflurane through masks. A distal 10-mm segment of the

470 tail was amputated with a scalpel, and the tail was immediately immersed in 0.9% isotonic PBS

471 solution at 37°C. The bleeding time was defined as the time required until bleeding ceased. The

472 blood-PBS solution underwent OD analysis to determine overall blood loss.

473 Blood counts were performed on the ADVIA 120 system (Siemens, Munich, Germany) following

474 submandibular puncture under isoflurane anesthesia of 4 and 8 months old mice to determine total

475 platelet, erythrocyte, and leukocyte numbers, and to quantify hemoglobin and hematocrit levels.

Muscle, spleen, and skin histology

477 TA muscles were frozen in liquid nitrogen-cooled isopentane and transverse 8 µm sections were

478 stained with hematoxylin and eosin (H&E), and the Cellpose algorithm[65] was used to segment and

479 delineate the individual myofibers. The MinFeret diameter was calculated using ImageJ, and the

480 number of fibers with internal nuclei was determined through the Cell Counter ImageJ plugin. The

481 spleen and a dorsal skin fragment were fixed in 4% paraformaldehyde for 24 h, embedded in

482 paraffin, and 5 µm sections were stained with H&E. The megakaryocyte number was determined

483 on random images covering 12.3 mm^2 per spleen using the ImageJ Cell Counter plugin, and the

484 thickness and relative proportion of the subcutaneous fat layer was determined on a 5 mm^2 skin

485 sample area using the NDP Viewer software (Hamamatsu, Hamamatsu, Japan). All muscle, spleen,

486 and skin section were imaged with the Nanozoomer 2HT slide scanner (Hamamatsu).

Gene expression and protein studies

Total RNA was extracted from TA samples with TRI Reagent (Molecular Research Center, Cincinnati, USA) and reverse transcribed using the SuperScriptTM IV Transcriptase (ThermoFisher Scientific, Waltham, USA). For quantitative PCR, the cDNA was amplified using the SYBR Green Master Mix I (Roche Diagnostics, Basel, Switzerland) on a LightCycler 480 Real-Time PCR System (Roche) with forward and reverse primers (Table S1). Primer specificity was determined through melting curve products followed by Sanger sequencing of the amplicons. *Rpl27* was used as reference gene[66].

For protein studies, TA cryosections were lysed in RIPA (radio immunoprecipitation) buffer supplemented with 1 mM PMSF, 1 mM DTT and complete mini EDTA-free protease inhibitor cocktail (Roche). The denatured samples were loaded on 10% or 15% SDS-PAGE gels and transferred onto nitrocellulose membranes using the Transblot® TurboTM RTA Transfer Kit (Biorad, Hercules, USA). Ponceau S staining (Sigma-Aldrich, St Louis, USA) served as loading control. Following primary and secondary antibodies were used: mouse anti-P62 (1/5000; H00008878-M01, Abnova, Taipeh, Taiwan), rabbit anti-LC3 (1/1000; NB100-2220, Novus Biologicals, Littleton, USA), peroxidase-coupled goat anti-mouse (1/10000; 115-036-068, Jackson ImmunoResearch), and peroxidase-coupled goat anti-rabbit (1/10000; 112-036-045, Jackson ImmunoResearch, Ely, UK). Signal intensity was recorded with the Amersham Imager 600 (Amersham, UK).

shRNA cloning and AAV production

shRNA sequences were designed to target *Orai1* regions conserved in human and mice and diverging from *Orai2* and *Orai3*. For each *Orai1* shRNA, scramble shRNAs were calculated using a specific design software (https://www.invivogen.com/sirnawizard/scrambled.php). The shRNAs (Table S2) were subcloned into pENTR1A and cloned into the pAAV plasmid under the control of the U6 promoter and flanked by serotype 2 inverted terminal repeats using the Gateway system (ThermoFisher Scientific). sh190 targets the same 19 nucleotides as the SYL116011 siRNA, developed by Sylentis to treat ocular allergies and conjunctivitis[67; 68]

AAV particles were produced by triple transfection of the HEK293T cell line with pAAV, the helper plasmid, and pXR1 containing rep and cap genes of AAV serotype 9. Cell lysates were

treated with 50 U/mL Benzonase (Sigma-Aldrich) for 30 min at 37°C and clarified by centrifugation. Viral particles were purified by iodixanol gradient ultracentrifugation using Amicon Ultra-15 Centrifucal Filters (Merck, Darmstadt, Germany) and followed by dialysis. Particle quantity was determined by real-time PCR using TACGGTAAACTGCCCACTTG (forward) and AGGAAAGTCCCATAAGGTCA (reverse) primers. Titers are expressed as viral genomes per mL (vg/mL).

shRNA screening and intramuscular AAV injection

For the cellular shRNA screening, pENTR1A plasmids were transfected into C2C12 myoblasts using Lipofectamine 3000 (Invitrogen, Waltham, USA). Cells were harvested after 48 h to extract RNA and quantify *Orai1* expression. For *in vivo* validation, 1 month old WT mice were anesthetized by intraperitoneal injection of ketamine 100 µg/g and xylazine 5 µg/g of body weight. TAs were injected with 1.2×10^{10} viral genomes/TA or 20 µL of NaCl 0.9% as control. At 2 months of age, the animals were euthanized, and *Orai1* silencing in TA samples was assessed by RT-qPCR.

To evaluate the therapeutic potential of the shRNAs, 2 months old WT and *Stim1$^{R304W/+}$* mice were anesthetized and randomly injected with 1.5×10^{10} viral genomes/TA or 25 µL of NaCl 0.9% as control. At 4 months of age, the mice underwent *in situ* muscle force measurements, and the TAs were dissected for subsequent morphological and gene expression analyses.

Study randomization and statistical analysis

All experiments were performed and analyzed in a blinded manner and the investigators were unaware of the genotype of the mice. The normal distribution of the data was assessed using the Shapiro-Wilk test and presented as mean ± standard error of the mean (SEM). For normally distributed data, the significance of changes was examined by two-tailed Student's t-test with or without Welch's correction for comparison of 2 groups or by one-way ANOVA followed by Tukey's post hoc test for comparison of more than 2 groups. In case of not-normally distributed data, Mann-Whitney test was used to compare 2 groups and Kruskal-Wallis followed by Dunn's multiple comparison test to compare more than 2 groups. The statistical significance of birth ratio was assessed by chi-square test.

AUTHOR CONTRIBUTIONS

RSR, EL, DM, PK, and LPG performed the experiments, RSR, EL, DM, JL, and JB analyzed the data, JL and JB designed and coordinated the study, RSR and JB drafted the manuscript.

DATA AVAILABILITY STATEMENT

The authors confirm that the data supporting the findings of this study are available within the article and its supplementary materials.

CONFLICTS OF INTEREST

None of the authors declares conflict of interest.

REFERENCES

1. Feske, S., Gwack, Y., Prakriya, M., Srikanth, S., Puppel, S.H., Tanasa, B., Hogan, P.G., Lewis, R.S., Daly, M., and Rao, A. (2006). A mutation in Orai1 causes immune deficiency by abrogating CRAC channel function. Nature 441, 179-185.

2. Berridge, M.J., Bootman, M.D., and Roderick, H.L. (2003). Calcium signalling: dynamics, homeostasis and remodelling. Nat Rev Mol Cell Biol 4, 517-529.

3. Stathopulos, P.B., Zheng, L., Li, G.Y., Plevin, M.J., and Ikura, M. (2008). Structural and mechanistic insights into STIM1-mediated initiation of store-operated calcium entry. Cell 135, 110-122.

4. Zhang, S.L., Yu, Y., Roos, J., Kozak, J.A., Deerinck, T.J., Ellisman, M.H., Stauderman, K.A., and Cahalan, M.D. (2005). STIM1 is a Ca2+ sensor that activates CRAC channels and migrates from the Ca2+ store to the plasma membrane. Nature 437, 902-905.

5. Gattineni, J. (2014). Inherited disorders of calcium and phosphate metabolism. Curr Opin Pediatr 26, 215-222.

6. Picard, C., McCarl, C.A., Papolos, A., Khalil, S., Luthy, K., Hivroz, C., LeDeist, F., Rieux-Laucat, F., Rechavi, G., Rao, A., et al. (2009). STIM1 mutation associated with a syndrome of immunodeficiency and autoimmunity. N Engl J Med 360, 1971-1980.

7. Lacruz, R.S., and Feske, S. (2015). Diseases caused by mutations in ORAI1 and STIM1. Ann N Y Acad Sci 1356, 45-79.

8. Bohm, J., Chevessier, F., Maues De Paula, A., Koch, C., Attarian, S., Feger, C., Hantai, D., Laforet, P., Ghorab, K., Vallat, J.M., et al. (2013). Constitutive activation of the calcium sensor STIM1 causes tubular-aggregate myopathy. Am J Hum Genet 92, 271-278.

9. Bohm, J., and Laporte, J. (2018). Gain-of-function mutations in STIM1 and ORAI1 causing tubular aggregate myopathy and Stormorken syndrome. Cell Calcium 76, 1-9.

10. Endo, Y., Noguchi, S., Hara, Y., Hayashi, Y.K., Motomura, K., Miyatake, S., Murakami, N., Tanaka, S., Yamashita, S., Kizu, R., et al. (2015). Dominant mutations in ORAI1 cause tubular aggregate myopathy with hypocalcemia via constitutive activation of store-operated Ca(2)(+) channels. Hum Mol Genet 24, 637-648.

11. Misceo, D., Holmgren, A., Louch, W.E., Holme, P.A., Mizobuchi, M., Morales, R.J., De Paula, A.M., Stray-Pedersen, A., Lyle, R., Dalhus, B., et al. (2014). A dominant STIM1 mutation causes Stormorken syndrome. Hum Mutat 35, 556-564.

12. Morin, G., Biancalana, V., Echaniz-Laguna, A., Noury, J.B., Lornage, X., Moggio, M., Ripolone, M., Violano, R., Marcorelles, P., Marechal, D., et al. (2020). Tubular aggregate myopathy and Stormorken syndrome: Mutation spectrum and genotype/phenotype correlation. Hum Mutat 41, 17-37.

13. Morin, G., Bruechle, N.O., Singh, A.R., Knopp, C., Jedraszak, G., Elbracht, M., Bremond-Gignac, D., Hartmann, K., Sevestre, H., Deutz, P., et al. (2014). Gain-of-Function Mutation in STIM1 (P.R304W) Is Associated with Stormorken Syndrome. Hum Mutat 35, 1221-1232.

14. Nesin, V., Wiley, G., Kousi, M., Ong, E.C., Lehmann, T., Nicholl, D.J., Suri, M., Shahrizaila, N., Katsanis, N., Gaffney, P.M., et al. (2014). Activating mutations in STIM1 and ORAI1 cause overlapping syndromes of tubular myopathy and congenital miosis. Proc Natl Acad Sci U S A 111, 4197-4202.

15. Cordero-Sanchez, C., Riva, B., Reano, S., Clemente, N., Zaggia, I., Ruffinatti, F.A., Potenzieri, A., Pirali, T., Raffa, S., Sangaletti, S., et al. (2019). A luminal EF-hand mutation in STIM1 in mice causes the clinical hallmarks of tubular aggregate myopathy. Dis Model Mech 13.

16. Oh-Hora, M., Yamashita, M., Hogan, P.G., Sharma, S., Lamperti, E., Chung, W., Prakriya, M., Feske, S., and Rao, A. (2008). Dual functions for the endoplasmic reticulum calcium sensors STIM1 and STIM2 in T cell activation and tolerance. Nat Immunol 9, 432-443.

609 17. Silva-Rojas, R., Treves, S., Jacobs, H., Kessler, P., Messaddeq, N., Laporte, J., and Bohm, J. (2019). STIM1
610   over-activation generates a multi-systemic phenotype affecting the skeletal muscle, spleen, eye,
611   skin, bones and immune system in mice. Hum Mol Genet 28, 1579-1593.
612 18. Gwack, Y., Srikanth, S., Oh-Hora, M., Hogan, P.G., Lamperti, E.D., Yamashita, M., Gelinas, C., Neems,
613   D.S., Sasaki, Y., Feske, S., et al. (2008). Hair loss and defective T- and B-cell function in mice lacking
614   ORAI1. Mol Cell Biol 28, 5209-5222.
615 19. Silva-Rojas, R., Charles, A.L., Djeddi, S., Geny, B., Laporte, J., and Bohm, J. (2021). Pathophysiological
616   Effects of Overactive STIM1 on Murine Muscle Function and Structure. Cells 10.
617 20. Florencio-Silva, R., Sasso, G.R., Sasso-Cerri, E., Simoes, M.J., and Cerri, P.S. (2015). Biology of Bone
618   Tissue: Structure, Function, and Factors That Influence Bone Cells. Biomed Res Int 2015, 421746.
619 21. Silva-Rojas, R., Laporte, J., and Bohm, J. (2020). STIM1/ORAI1 Loss-of-Function and Gain-of-Function
620   Mutations Inversely Impact on SOCE and Calcium Homeostasis and Cause Multi-Systemic Mirror
621   Diseases. Front Physiol 11, 604941.
622 22. Chen, Y., Ramachandran, A., Zhang, Y., Koshy, R., and George, A. (2018). The ER Ca(2+) sensor STIM1
623   can activate osteoblast and odontoblast differentiation in mineralized tissues. Connect Tissue Res
624   59, 6-12.
625 23. Pullen, A.H. (1977). The distribution and relative sized of fibre types in the extensor digitorum longus
626   and soleus muscles of the adult rat. J Anat 123, 467-486.
627 24. Pullen, A.H. (1977). The distribution and relative sizes of three histochemical fibre types in the rat
628   tibialis anterior muscle. J Anat 123, 1-19.
629 25. Schiaffino, S., and Reggiani, C. (2011). Fiber types in mammalian skeletal muscles. Physiol Rev 91, 1447-
630   1531.
631 26. Ishitsuka, Y., Inoue, S., Furuta, J., Koguchi-Yoshioka, H., Nakamura, Y., Watanabe, R., Okiyama, N.,
632   Fujisawa, Y., Enokizono, T., Fukushima, H., et al. (2019). Sweat retention anhidrosis associated
633   with tubular aggregate myopathy. Br J Dermatol 181, 1104-1106.
634 27. Markello, T., Chen, D., Kwan, J.Y., Horkayne-Szakaly, I., Morrison, A., Simakova, O., Maric, I., Lozier, J.,
635   Cullinane, A.R., Kilo, T., et al. (2015). York platelet syndrome is a CRAC channelopathy due to gain-
636   of-function mutations in STIM1. Mol Genet Metab 114, 474-482.
637 28. Schneider, M.F., and Chandler, W.K. (1973). Voltage dependent charge movement of skeletal muscle:
638   a possible step in excitation-contraction coupling. Nature 242, 244-246.
639 29. Pan, Z., Yang, D., Nagaraj, R.Y., Nosek, T.A., Nishi, M., Takeshima, H., Cheng, H., and Ma, J. (2002).
640   Dysfunction of store-operated calcium channel in muscle cells lacking mg29. Nat Cell Biol 4, 379-
641   383.
642 30. Zhao, X., Yoshida, M., Brotto, L., Takeshima, H., Weisleder, N., Hirata, Y., Nosek, T.M., Ma, J., and
643   Brotto, M. (2005). Enhanced resistance to fatigue and altered calcium handling properties of
644   sarcalumenin knockout mice. Physiol Genomics 23, 72-78.
645 31. Neel, B.A., Lin, Y., and Pessin, J.E. (2013). Skeletal muscle autophagy: a new metabolic regulator.
646   Trends Endocrinol Metab 24, 635-643.
647 32. Blair, H.C., Robinson, L.J., Huang, C.L., Sun, L., Friedman, P.A., Schlesinger, P.H., and Zaidi, M. (2011).
648   Calcium and bone disease. Biofactors 37, 159-167.
649 33. Eapen, A., Sundivakkam, P., Song, Y., Ravindran, S., Ramachandran, A., Tiruppathi, C., and George, A.
650   (2010). Calcium-mediated stress kinase activation by DMP1 promotes osteoblast differentiation.
651   J Biol Chem 285, 36339-36351.
652 34. van der Meijden, P.E.J., and Heemskerk, J.W.M. (2019). Platelet biology and functions: new concepts
653   and clinical perspectives. Nat Rev Cardiol 16, 166-179.
654 35. Berna-Erro, A., Jardin, I., Smani, T., and Rosado, J.A. (2016). Regulation of Platelet Function by Orai,
655   STIM and TRP. Adv Exp Med Biol 898, 157-181.

656   36. Numaga-Tomita, T., and Putney, J.W. (2013). Role of STIM1- and Orai1-mediated Ca2+ entry in Ca2+-
657   induced epidermal keratinocyte differentiation. J Cell Sci 126, 605-612.
658   37. Vandenberghe, M., Raphael, M., Lehen'kyi, V., Gordienko, D., Hastie, R., Oddos, T., Rao, A., Hogan,
659   P.G., Skryma, R., and Prevarskaya, N. (2013). ORAI1 calcium channel orchestrates skin
660   homeostasis. Proc Natl Acad Sci U S A 110, E4839-4848.
661   38. Concepcion, A.R., Vaeth, M., Wagner, L.E., 2nd, Eckstein, M., Hecht, L., Yang, J., Crottes, D., Seidl, M.,
662   Shin, H.P., Weidinger, C., et al. (2016). Store-operated Ca2+ entry regulates Ca2+-activated
663   chloride channels and eccrine sweat gland function. J Clin Invest 126, 4303-4318.
664   39. Peacock, M. (2010). Calcium metabolism in health and disease. Clin J Am Soc Nephrol 5 Suppl 1, S23-
665   30.
666   40. Bohm, J., Bulla, M., Urquhart, J.E., Malfatti, E., Williams, S.G., O'Sullivan, J., Szlauer, A., Koch, C.,
667   Baranello, G., Mora, M., et al. (2017). ORAI1 Mutations with Distinct Channel Gating Defects in
668   Tubular Aggregate Myopathy. Hum Mutat 38, 426-438.
669   41. Barone, V., Del Re, V., Gamberucci, A., Polverino, V., Galli, L., Rossi, D., Costanzi, E., Toniolo, L., Berti,
670   G., Malandrini, A., et al. (2017). Identification and characterization of three novel mutations in the
671   CASQ1 gene in four patients with tubular aggregate myopathy. Hum Mutat 38, 1761-1773.
672   42. Bohm, J., Lornage, X., Chevessier, F., Birck, C., Zanotti, S., Cudia, P., Bulla, M., Granger, F., Bui, M.T.,
673   Sartori, M., et al. (2018). CASQ1 mutations impair calsequestrin polymerization and cause tubular
674   aggregate myopathy. Acta Neuropathol 135, 149-151.
675   43. Goonasekera, S.A., Davis, J., Kwong, J.Q., Accornero, F., Wei-LaPierre, L., Sargent, M.A., Dirksen, R.T.,
676   and Molkentin, J.D. (2014). Enhanced Ca(2)(+) influx from STIM1-Orai1 induces muscle pathology
677   in mouse models of muscular dystrophy. Hum Mol Genet 23, 3706-3715.
678   44. McCarl, C.A., Khalil, S., Ma, J., Oh-hora, M., Yamashita, M., Roether, J., Kawasaki, T., Jairaman, A.,
679   Sasaki, Y., Prakriya, M., et al. (2010). Store-operated Ca2+ entry through ORAI1 is critical for T cell-
680   mediated autoimmunity and allograft rejection. J Immunol 185, 5845-5858.
681   45. Braun, A., Varga-Szabo, D., Kleinschnitz, C., Pleines, I., Bender, M., Austinat, M., Bosl, M., Stoll, G., and
682   Nieswandt, B. (2009). Orai1 (CRACM1) is the platelet SOC channel and essential for pathological
683   thrombus formation. Blood 113, 2056-2063.
684   46. Carrell, E.M., Coppola, A.R., McBride, H.J., and Dirksen, R.T. (2016). Orai1 enhances muscle endurance
685   by promoting fatigue-resistant type I fiber content but not through acute store-operated Ca2+
686   entry. FASEB J 30, 4109-4119.
687   47. Snijders, T., Nederveen, J.P., McKay, B.R., Joanisse, S., Verdijk, L.B., van Loon, L.J., and Parise, G. (2015).
688   Satellite cells in human skeletal muscle plasticity. Front Physiol 6, 283.
689   48. Colon-Thillet, R., Jerome, K.R., and Stone, D. (2021). Optimization of AAV vectors to target persistent
690   viral reservoirs. Virol J 18, 85.
691   49. Koo, T., Malerba, A., Athanasopoulos, T., Trollet, C., Boldrin, L., Ferry, A., Popplewell, L., Foster, H.,
692   Foster, K., and Dickson, G. (2011). Delivery of AAV2/9-microdystrophin genes incorporating helix
693   1 of the coiled-coil motif in the C-terminal domain of dystrophin improves muscle pathology and
694   restores the level of alpha1-syntrophin and alpha-dystrobrevin in skeletal muscles of mdx mice.
695   Hum Gene Ther 22, 1379-1388.
696   50. Tasfaout, H., Lionello, V.M., Kretz, C., Koebel, P., Messaddeq, N., Bitz, D., Laporte, J., and Cowling, B.S.
697   (2018). Single Intramuscular Injection of AAV-shRNA Reduces DNM2 and Prevents Myotubular
698   Myopathy in Mice. Mol Ther 26, 1082-1092.
699   51. Yang, Q., Tang, Y., Imbrogno, K., Lu, A., Proto, J.D., Chen, A., Guo, F., Fu, F.H., Huard, J., and Wang, B.
700   (2012). AAV-based shRNA silencing of NF-kappaB ameliorates muscle pathologies in mdx mice.
701   Gene Ther 19, 1196-1204.
702   52. Wang, D., Tai, P.W.L., and Gao, G. (2019). Adeno-associated virus vector as a platform for gene therapy
703   delivery. Nat Rev Drug Discov 18, 358-378.

704 53. Seim, I., Ma, S., and Gladyshev, V.N. (2016). Gene expression signatures of human cell and tissue
705   longevity. NPJ Aging Mech Dis 2, 16014.
706 54. Sender, R., and Milo, R. (2021). The distribution of cellular turnover in the human body. Nat Med 27,
707   45-48.
708 55. Castets, P., Frank, S., Sinnreich, M., and Ruegg, M.A. (2016). "Get the Balance Right": Pathological
709   Significance of Autophagy Perturbation in Neuromuscular Disorders. J Neuromuscul Dis 3, 127-
710   155.
711 56. Fetalvero, K.M., Yu, Y., Goetschkes, M., Liang, G., Valdez, R.A., Gould, T., Triantafellow, E., Bergling, S.,
712   Loureiro, J., Eash, J., et al. (2013). Defective autophagy and mTORC1 signaling in myotubularin null
713   mice. Mol Cell Biol 33, 98-110.
714 57. Kuno, A., Hosoda, R., Sebori, R., Hayashi, T., Sakuragi, H., Tanabe, M., and Horio, Y. (2018). Resveratrol
715   Ameliorates Mitophagy Disturbance and Improves Cardiac Pathophysiology of Dystrophin-
716   deficient mdx Mice. Sci Rep 8, 15555.
717 58. Begam, M., Abro, V.M., Mueller, A.L., and Roche, J.A. (2016). Sodium 4-phenylbutyrate reduces
718   myofiber damage in a mouse model of Duchenne muscular dystrophy. Appl Physiol Nutr Metab
719   41, 1108-1111.
720 59. Lee, C.S., Hanna, A.D., Wang, H., Dagnino-Acosta, A., Joshi, A.D., Knoblauch, M., Xia, Y., Georgiou, D.K.,
721   Xu, J., Long, C., et al. (2017). A chemical chaperone improves muscle function in mice with a RyR1
722   mutation. Nat Commun 8, 14659.
723 60. Avila, G., and Dirksen, R.T. (2001). Functional effects of central core disease mutations in the
724   cytoplasmic region of the skeletal muscle ryanodine receptor. J Gen Physiol 118, 277-290.
725 61. Dirksen, R.T., and Avila, G. (2002). Altered ryanodine receptor function in central core disease: leaky
726   or uncoupled Ca(2+) release channels? Trends Cardiovasc Med 12, 189-197.
727 62. Kraeva, N., Zvaritch, E., Rossi, A.E., Goonasekera, S.A., Zaid, H., Frodis, W., Kraev, A., Dirksen, R.T.,
728   Maclennan, D.H., and Riazi, S. (2013). Novel excitation-contraction uncoupled RYR1 mutations in
729   patients with central core disease. Neuromuscul Disord 23, 120-132.
730 63. Bisset, D.R., Stepniak-Konieczna, E.A., Zavaljevski, M., Wei, J., Carter, G.T., Weiss, M.D., and
731   Chamberlain, J.R. (2015). Therapeutic impact of systemic AAV-mediated RNA interference in a
732   mouse model of myotonic dystrophy. Hum Mol Genet 24, 4971-4983.
733 64. Ahuja, M., Schwartz, D.M., Tandon, M., Son, A., Zeng, M., Swaim, W., Eckhaus, M., Hoffman, V., Cui,
734   Y., Xiao, B., et al. (2017). Orai1-Mediated Antimicrobial Secretion from Pancreatic Acini Shapes
735   the Gut Microbiome and Regulates Gut Innate Immunity. Cell Metab 25, 635-646.
736 65. Stringer, C., Wang, T., Michaelos, M., and Pachitariu, M. (2021). Cellpose: a generalist algorithm for
737   cellular segmentation. Nat Methods 18, 100-106.
738 66. Thomas, K.C., Zheng, X.F., Garces Suarez, F., Raftery, J.M., Quinlan, K.G., Yang, N., North, K.N., and
739   Houweling, P.J. (2014). Evidence based selection of commonly used RT-qPCR reference genes for
740   the analysis of mouse skeletal muscle. PLoS One 9, e88653.
741 67. Gonzalez, V., Paneda, C., Martinez, T., Guerra, A., Monteiro, S., Vargas, B., Bleau, A.M., Ruz, V., and
742   Jimenez, A.I. (2018). Development of a RNAi therapeutic for the treatment of allergic
743   conjunctivitis. Invest Ophth Vis Sci 59.
744 68. Jimenez, A.I., Martinez, T., Gonzalez, V., Martinez-Garcia, C., and Paneda, C. (2015). Development of a
745   RNAi therapeutic for the treatment of allergic conjunctivitis. Invest Ophth Vis Sci 56.

746

747

748
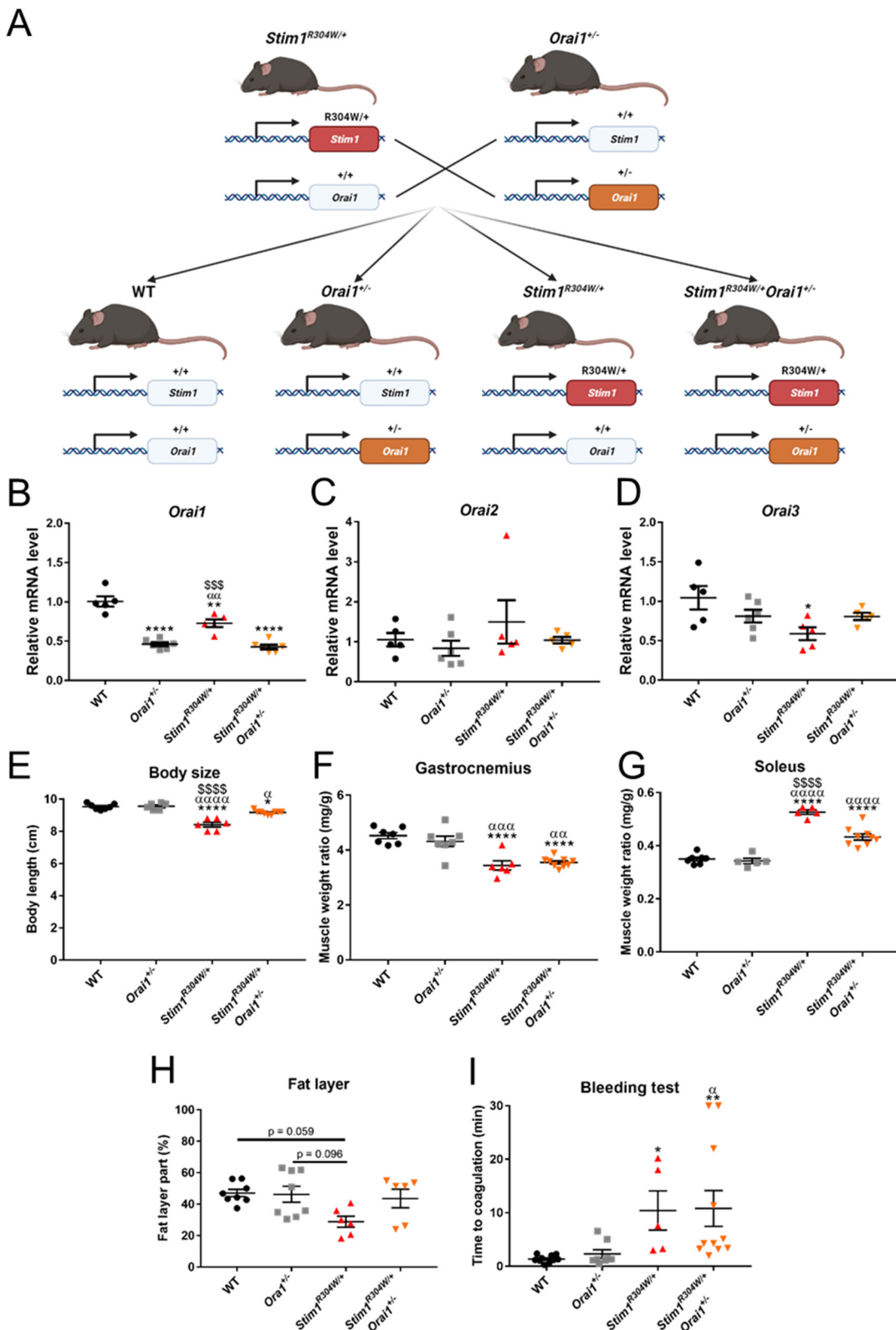
751 **Supplemental Figure S1. Normal *Orai2* and *Orai3* expression, increased body length, and improved skin**
752 **morphology in *Stim1^{R304W/+}Orai1^{+/-}* mice.** (A) Crossing of *Stim1^{R304W/+}* and *Orai1^{+/-}* mice resulted in four genotypes:
753 WT, *Orai1^{+/-}*, *Stim1^{R304W/+}*, and *Stim1^{R304W/+}Orai1^{+/-}*. (B-D) *Orai1* expression was reduced by half in
754 *Stim1^{R304W/+}Orai1^{+/-}* offspring, while *Orai2* and *Orai3* expression was unaffected (n=4-6). (E) *Stim1^{R304W/+}Orai1^{+/-}*
755 mice were larger than the *Stim1^{R304W/+}* littermates at 4 months (n=5-9). (F-G) The gastrocnemius was hyotrophic in
756 both *Stim1^{R304W/+}* and *Stim1^{R304W/+}Orai1^{+/-}* mice, while the soleus hypertrophy was partially rescued in
757 *Stim1^{R304W/+}Orai1^{+/-}* mice at 4 months. (H) Normalized fat layer part of the back skin in *Stim1^{R304W/+}Orai1^{+/-}* mice at
758 4-8 months of age (n=6-11). (I) Increased coagulation time in *Stim1^{R304W/+}* and *Stim1^{R304W/+}Orai1^{+/-}* mice at 2 months
759 compared to healthy controls (n=6-11). Graphs represent mean ± SEM. Significant differences are indicated as */α/$
760 $P<0.05$, **/αα/$$ $P<0.01$, ***/ααα/$$$ $P<0.001$, and ****/αααα/$$$$ $P<0.0001$ with * reflecting the comparison
761 with the WT group, α the comparison with the *Orai1^{+/-}* group, and $ for the comparison with the *Stim1^{R304W/+}Orai1^{+/-}*
762 group.
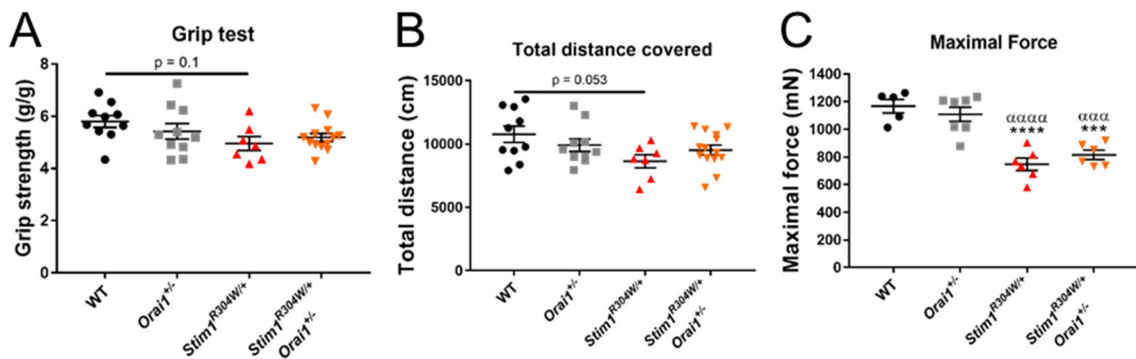
763

764 **Supplemental Figure S2. Grip strength, OpenField test, and muscle force of *Stim1^{R304W/+}Orai1^{+/-}* mice.** (A-C)
765 Non-significant tendencies of increased of 4-paw grip strength, covered distance in the OpenField arena, and maximal
766 muscle force of *Stim1^{R304W/+}Orai1^{+/-}* mice compared with *Stim1^{R304W/+}* controls at 4 months and 10 weeks of age (n=5-
767 14). (C) Graphs represent mean ± SEM. Significant differences are indicated as ***/ααα $P<0.001$, and ****/αααα
768 $P<0.0001$ with * reflecting the comparison with the WT group and α the comparison with the *Orai1^{+/-}* group.

142

769
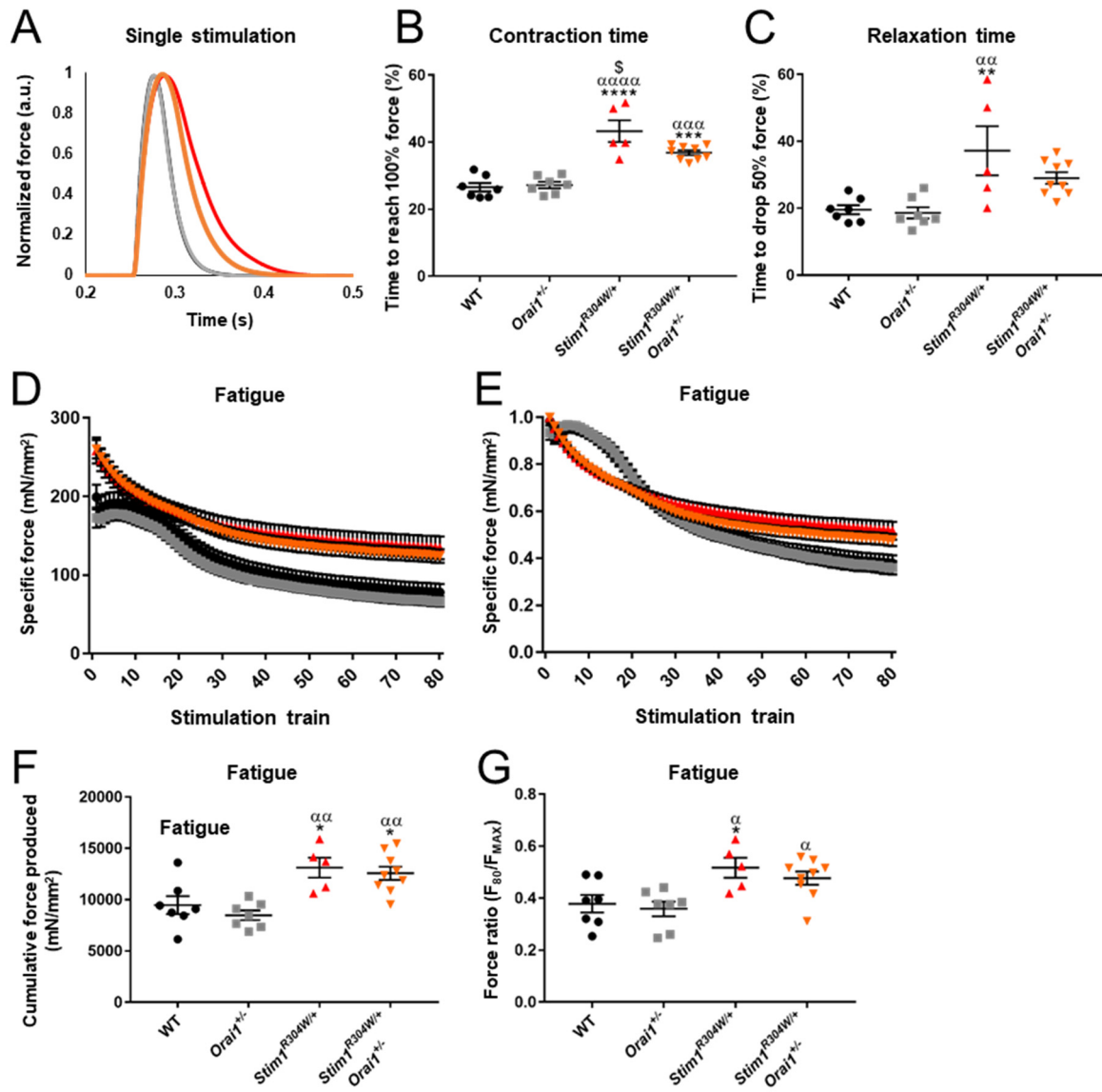
Supplemental Figure S3. Improved muscle contraction and relaxation properties in *Stim1^{R304W/+}Orai1^{+/-}* mice. (A-C) Tendency of faster muscle contraction and relaxation following single stimulations in *Stim1^{R304W/+}Orai1^{+/-}* compared with *Stim1^{R304W/+}* mice at 4 months (n=5-9). (D-E) Specific and normalized force produced across 80 stimulation trains of 40 Hz illustrate different fatigue curves of *Stim1^{R304W/+}* and *Stim1^{R304W/+}Orai1^{+/-}* muscle compared with healthy controls at 4 months (n=5-9). (F) Quantification of fatigue as the cumulation of force following 80 stimulations (n=5-9). (G) Quantification of fatigue as the ratio between the last and the highest force level within the stimulation train (n=5-9). Graphs represent mean ± SEM. Significant differences are indicated as */α/$ P<0.05, **/αα/$$ P<0.01, ***/ααα/$$$ P<0.001, and ****/αααα/$$$$ P<0.0001 with * reflecting the comparison with the WT group, α the comparison with the *Orai1^{+/-}* group, and $ for the comparison with the *Stim1^{R304W/+}Orai1^{+/-}* group.
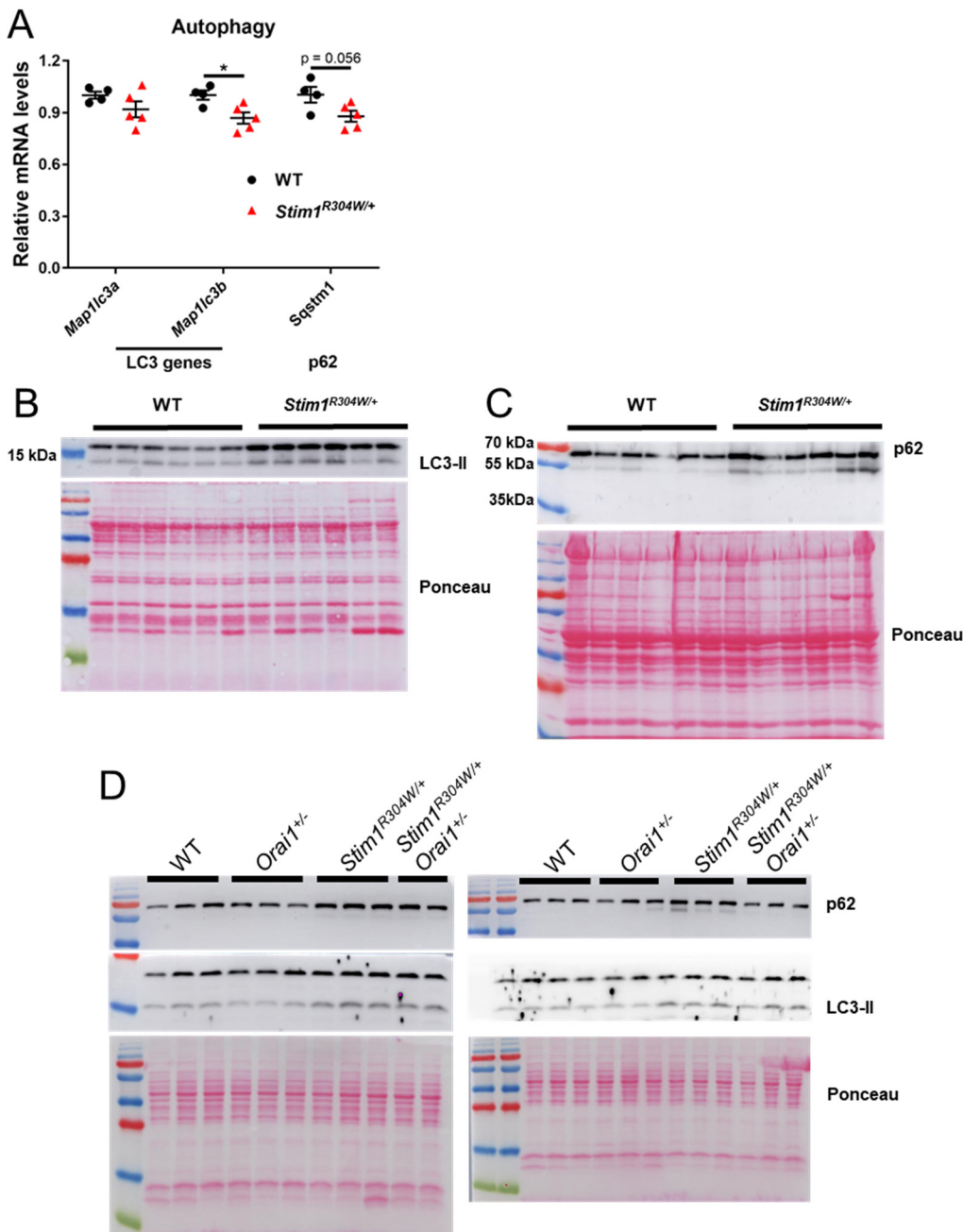
Supplemental Figure S4. Partially resolved autophagy defects in *Stim1^{R304W/+}Orai1^{+/-}* muscle. (A) Slight decrease of *Map1lc3a*, *Map1lc3b* (both encoding LC3-II), and *Sqstm1* (p62) expression in *Stim1^{R304W/+}* muscle compared with the WT at 4 months (n=4-5). (B-D) Western blots on muscle extracts evidences intense LC3-II and p62 signals in *Stim1^{R304W/+}* muscle and partial normalization in *Stim1^{R304W/+}Orai1^{+/-}* muscle (n=5-6). Ponceau S staining served as loading control. Graph represents mean ± SEM. Significant differences are indicated as * P<0.05, with * reflecting the comparison with the WT group.

786
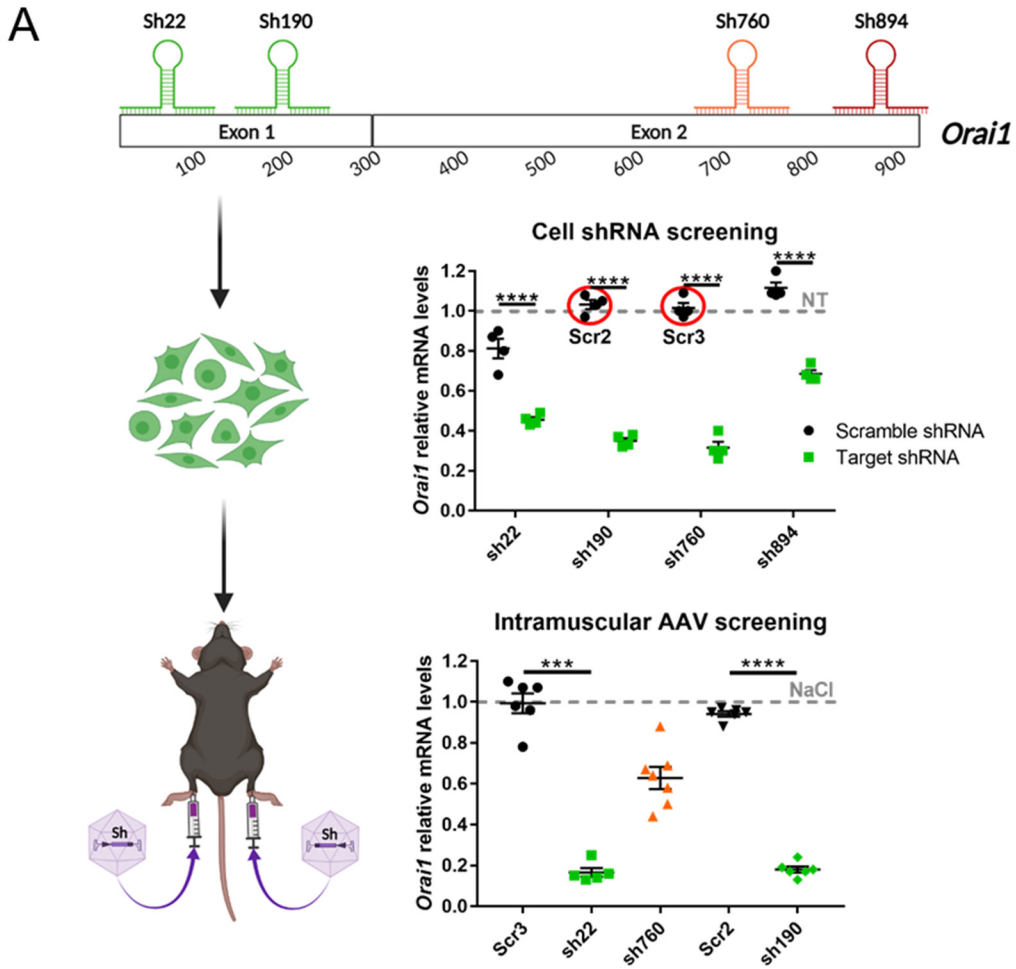
Supplemental Figure S5. *In cellulo* and *in vivo* validation of shRNAs. Schematic representation of *Orai1* mRNA and positions targeted by the shRNAs. sh22, sh190 and sh760 efficiently reduced *Orai1* expression in transfected C2C12 cells, while scrambles 2 and 3 (Scr2, Scr3) had no effect (n=4). The dashed line reflects the *Orai1* expression level in untreated cells. AAVs containing the shRNAs were injected into the tibialis anterior of 1-month old mice. sh22 and sh190 yielded a reduction of *Orai1* expression of 80% compared with scramble shRNAs and NaCl treatment (dashed line) 4 weeks pots injection (n=6-7). Graphs represent mean ± SEM. Significant differences are indicated as *** $P<0.001$ and **** $P<0.0001$ with * reflecting the comparison with the scramble-injected group.
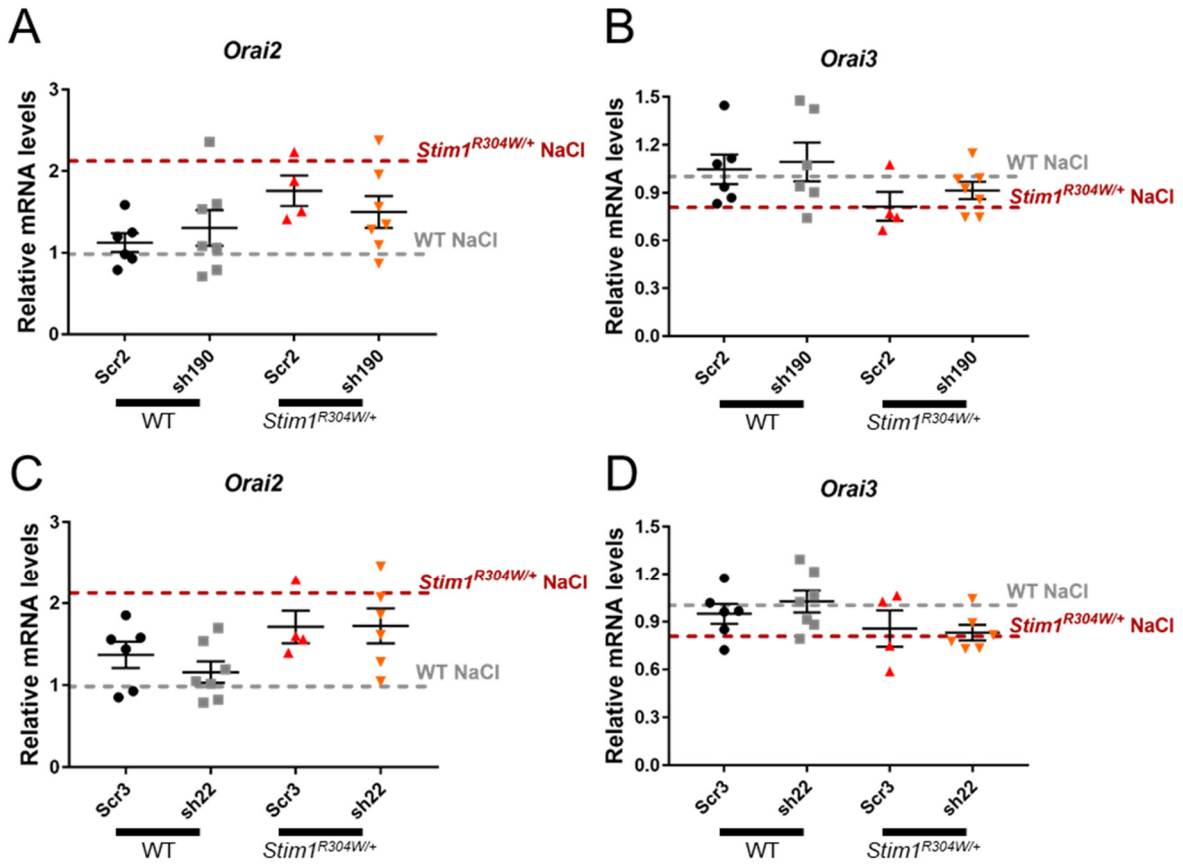
Supplemental Figure S6. Normal *Orai2* and *Orai3* expression following shRNA treatment. (A-D) Comparable *Orai2* and *Orai3* expression levels in *Stim1*$^{R304W/+}$ muscle treated with *Orai1*-specific shRNAs, scramble shRNAs or NaCl 8 weeks post injection (n=4-7). Graphs represent mean ± SEM.
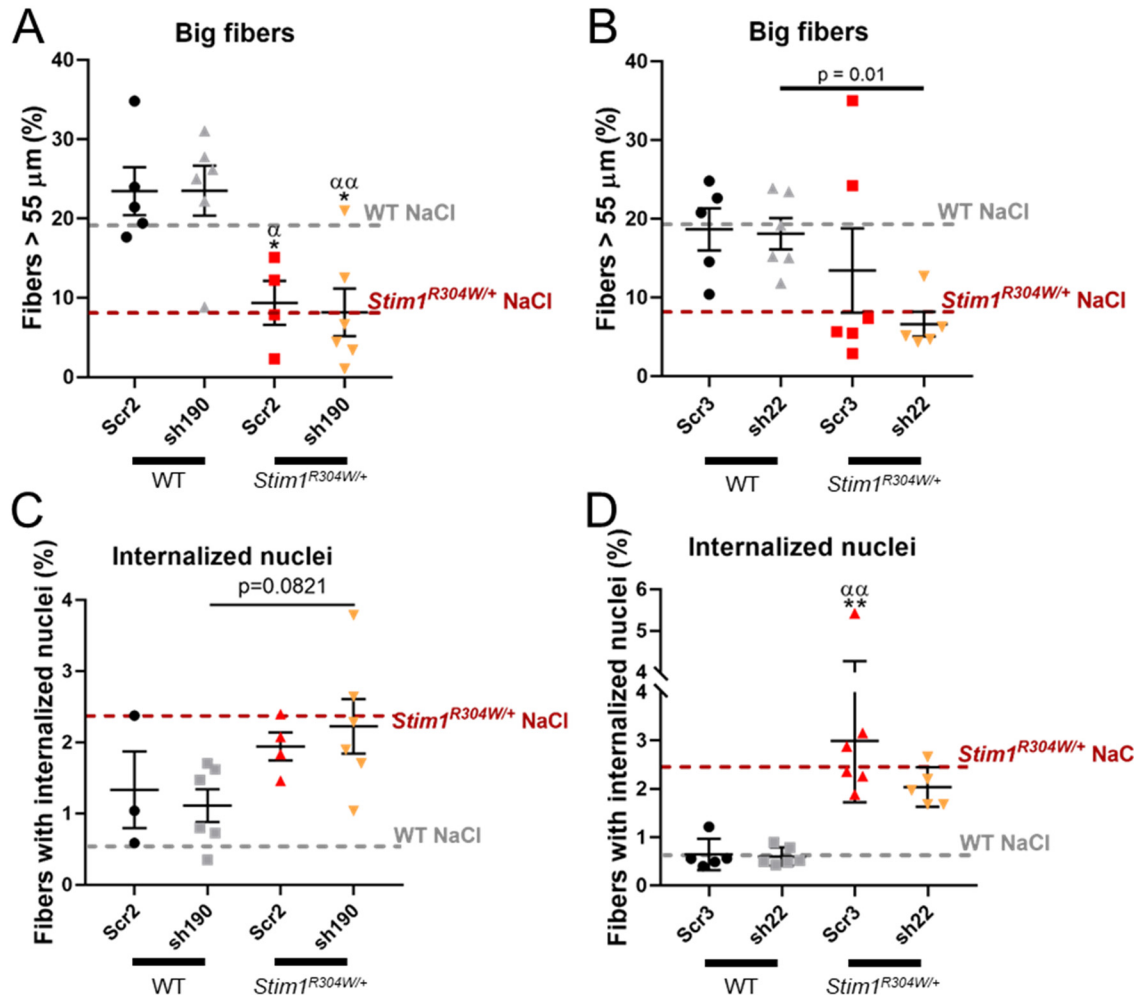
Supplemental Figure S7. No effect of sh22 and sh190 on fiber size and muscle degeneration. (A-D) The low percentage of big fibers and the increased proportion of myofibers with central nuclei in $Stim1^{R304W/+}$ muscle was not rescued by shRNA treatment 8 weeks post injection (n=3-7). Graphs represent mean ± SEM. Significant differences are indicated as */α P<0.05 and **/αα P<0.01 with * reflecting the comparison with the scramble-injected WT group and α the comparison with the shRNA-injected WT group.

804
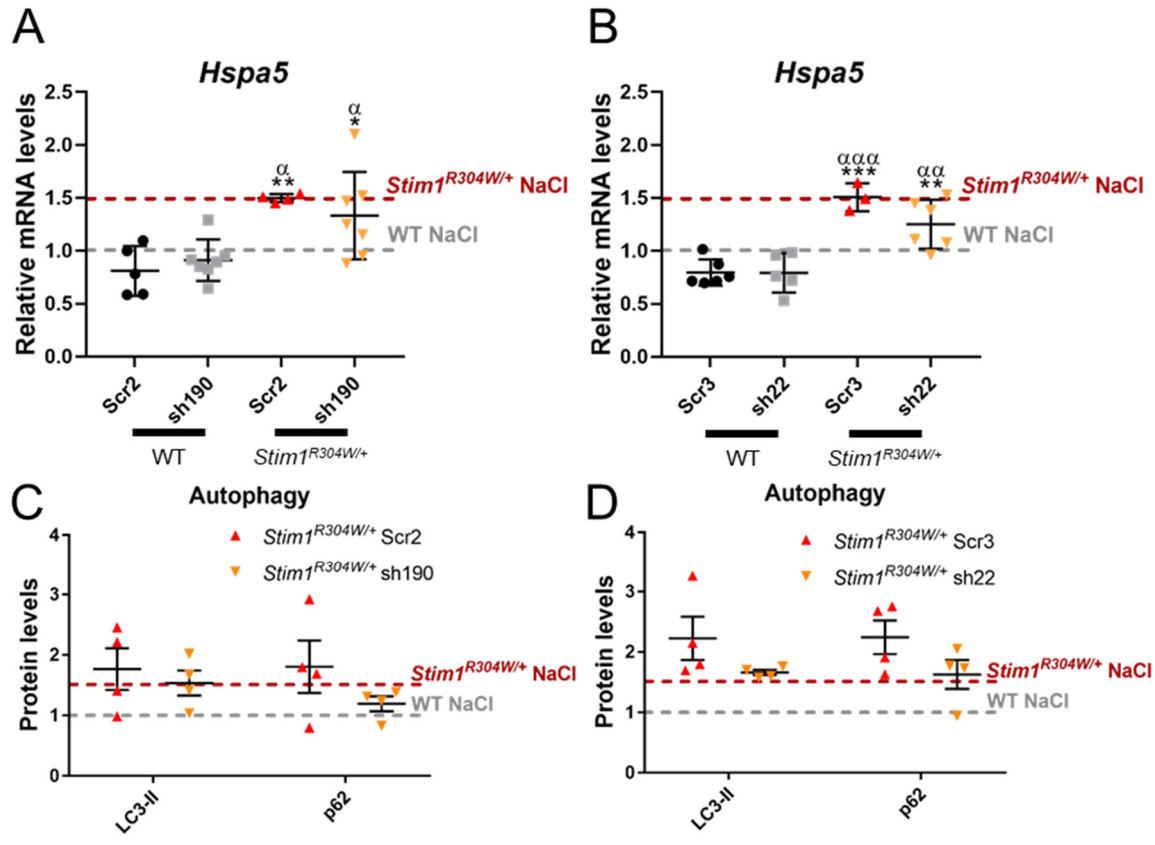
Supplemental Figure S8. No effect of sh22 and sh190 on UPR and autophagosome accumulation. (A-B) Comparable expression of the UPR marker *Hsp5* in treated and untreated *Stim1^{R304W/+}* muscle 8 weeks post injection (n=3-7). (C-D) Comparable protein levels of lipidated LC3 (LC3-II) and p62 in treated and untreated *Stim1^{R304W/+}* muscle 8 weeks post injection (n=4). Graphs represent mean ± SEM. Significant differences are indicated as */α P<0.05, **/αα P<0.01, and ***/ααα/$$$ P<0.0001 with * reflecting the comparison with the scramble-injected WT group and α the comparison with the shRNA-injected WT group.

Supplemental Figure S9. LC3-II and p62 protein levels. Western blots indicated comparable LC3-II and p62 signal intensities in extracts from treated and untreated $Stim1^{R304W/+}$ muscles 8 weeks post injection (n=4). Ponceau S staining served as loading control.

Supplemental Table S1. List of primers used for RT-qPCR.

Gene	Forward primer	Reverse primer
Rpl27	AAGCCGTCATCGTGAAGAACA	CTTGATCTTGGATCGCTTGGC
Orai1	GCCAAGCTCAAAGCTTCC	CCTGGTGGGTAGTCATGGTC
Orai2	GCAGCTACCTGGAACTCGTCACG	GAGGGTACTGGTACTTGGTCTCCA
Orai3	GGGCCAGTCAGCACTCTC	AGTGGTGCAGGCACTAAATG
Hspa5	CTATTCCTGCGTCGGTGTGT	ATTCCAAGTGCGTCCGATGA
Hspb90b1	CCACTCAAATCGAACACGGC	AGATTCCGCCTCCTTTCTGC
Map1lc3a	CTATGAACAGGAGAAGGATGAAG	ACTCAGAAGCCGAAGGTT
Map1lc3b	CGTCCTGGACAAGACCAAGT	ATTGCTGTCCCGAATGTCTC
Sqstm1	CCTTGCCCTACAGCTGAGTC	CACACTCTCCCCCACATTCT

| 817 | **Supplemental Table S2. Oligonucleotides used for shRNA cloning.** Underlined sequences indicate the shRNA |
| 818 | backbone hybridizing to the *Orai1* mRNA. |

Oligo name	Sequence
Scr1_Fw	AGCTTTGTTTACGACGTCACGGCAGCGATCACTTCAAGAGAGTGATCGCTGCCGTGACGTCGTCTTTTTA
Scr1_Rv	GATCTAAAAAGACGACGTCACGGCAGCGATCACTCTCTTGAAGTGATCGCTGCCGTGACGTCGTAAACAA
Sh22_Fw	AGCTTTGTTT**G**CCCGAGTCACAGCAATCCGGATTCAAGAGA<u>TCCGGATTGCTGTGACTCGGG</u>**C**CTTTTTA
Sh22_Rv	GATCTAAAAA**G**CCCGAGTCACAGCAATCCGGATCTCTTGAA<u>TCCGGATTGCTGTGACTCGGG</u>**C**AAACAA
Scr19_Fw	AGCTTTGTTTTAGGCGCGTCACGAAGAACTTCAAGAGAGTTCTTCGTGACGCGCCTACTTTTTA
Scr19_Fw	GATCTAAAAAGTAGGCGCGTCACGAAGAACTCTCTTGAAGTTCTTCGTGACGCGCCTAAAACAA
Sh190_Fw	AGCTTTGTTT**GG**ATGAGCCTCAACGAGCATTCAAGAGA<u>TGCTCGTTGAGGCTCATC</u>**C**CTTTTTA
Sh190_Rv	GATCTAAAAA**GG**ATGAGCCTCAACGAGCATCTCTTGAA<u>TGCTCGTTGAGGCTCATC</u>**C**AAACAA
Scr22_Fw	AGCTTTGTTTTCTTATGCGGTATTCTCTCTTCTTCAAGAGAGAAGAGAGAATACCGCATAAGACTTTTTA
Scr22_Rv	GATCTAAAAAGTCTTATGCGGTATTCTCTCTTCTCTCTTGAAGAAGAGAGAATACCGCATAAGAAAACAA
Sh760_Fw	AGCTTTGTTT<u>ATCGTCTTTGCTGTTCACTTC</u>TTTCAAGAGA<u>AGAAGTGAACAGCAAAGACGAT</u>CTTTTTA
Sh760_Rv	GATCTAAAAA<u>GATCGTCTTTGCTGTTCACTTC</u>TTCTCTTGAA<u>AGAAGTGAACAGCAAAGACGAT</u>AAACAA
Scr4_Fw	AGCTTTGTTTGACCACACAGTCGCGCTATACCTTCAAGAGAGGTATAGCGCGACTGTGTGGTCCTTTTTA
Scr4_Rv	GATCTAAAAAGGACCACACAGTCGCGCTATACCTCTCTTGAAGGTATAGCGCGACTGTGTGGTCAAACAA
Sh894_Fw	AGCTTTGTTT<u>ACCGGGCACCCACTATGCCTAA</u>TTCAAGAGA<u>TTAGGCATAGTGGGTGCCCGGT</u>CTTTTTA
Sh894_Rv	GATCTAAAAA<u>GACCGGGCACCCACTATGCCTAA</u>TCTCTTGAA<u>TTAGGCATAGTGGGTGCCCGGT</u>AAACAA

819

820	**Supplemental Table S3. Trabecular bone parameters of femur.** BV/TV, bone volume fraction; Tb.Th, trabecular
821	thickness; Tb.N, trabecular number; Tb.Sp, trabecular separation. P values refer to the comparison of *Stim1*[R304W/+] and
822	*Stim1*[R304W/+]*Orai1*^{+/-} by Tukey's post hoc test one-way ANOVA of all groups (n=6-7).

	BV/TV (%)	Tb.Th (μm)	Tb.N (1/mm)	Tb.Sp (μm)
WT	7.61 ± 1.36	68.71 ± 3.01	1.08 ± 0.15	377.60 ± 40.76
Orai1^{+/-}	4.74 ± 1.21	60.93 ± 4.54	0.73 ± 0.14	390.86 ± 22.18
Stim1[R304W/+]	0.72 ± 0.25	51.60 ± 3.46	0.13 ± 0.04	781.76 ± 24.58
Stim1[R304W/+]*Orai1*^{+/-}	3.60 ± 0.79	62.07 ± 2.96	0.55 ± 0.10	520.74 ± 36.42
p value disease vs therapy	0.1883	0.4805	0.0645	<0.0001

823

824	**Supplemental Table S4. Cortical bone parameters of midshaft tibia.** Ct.Th, cortical thickness; T.Ar, total area;
825	B.Ar, bone area; BA/TA, bone area fraction; M.Ar, marrow area; MOI, polar moment of inertia. P values refer to the
826	comparison of $Stim1^{R304W/+}$ and $Stim1^{R304W/+}Orai1^{+/-}$ by Tukey's post hoc test one-way ANOVA of all groups (n=5-
827	7).

	Ct.Th (mm)	T.Ar (mm^2)	B.Ar (mm^2)	BA/TA (%)	M.Ar (mm^2)	MOI (mm^4)
WT	0.25 ± 0.01	0.91 ± 0.03	0.74 ± 0.03	81.09 ± 0.47	0.17 ± 0.00	0.15 ± 0.01
$Orai1^{+/-}$	0.23 ± 0.01	0.84 ± 0.04	0.67 ± 0.04	79.48 ± 0.56	0.17 ± 0.00	0.13 ± 0.01
$Stim1^{R304W/+}$	0.22 ± 0.01	0.73 ± 0.03	0.57 ± 0.03	78.64 ± 0.83	0.15 ± 0.00	0.09 ± 0.00
$Stim1^{R304W/+}Orai1^{+/-}$	0.25 ± 0.01	0.84 ± 0.02	0.68 ± 0.02	80.98 ± 0.32	0.16 ± 0.00	0.12 ± 0.00
p value disease vs therapy	0.0348	0.0640	0.0575	0.0304	>0.9999	0.1488

828

PUBLICATION 4

Inhibition of the ORAI1 Ca^{2+} channel reverses the main clinical signs of tubular aggregate myopathy (TAM) and Stormorken syndrome (STRMK) in mice

Roberto Silva-Rojas, Laura Pérez-Guàrdia, Alix Simon, Sarah Djeddi, Jocelyn Laporte, Johann Böhm

4. ORAI1 INHIBITION AS THERAPEUTIC APPROACH FOR TAM/STRMK

4.1. Background

As an alternative approach to shRNA-mediated downregulation of *Orai1*, the physical inhibition of ORAI1 may represent another treatment option for TAM/STRMK. ORAI1 assembles as hexamers with the first transmembrane domains of each monomer forming the channel pore and regulating channel permeability (Hou et al., 2012). The Arg91 residue located at the narrowest part of the ion conduction pathways, and a homozygous missense mutation involving the substitution of arginine by the bulky amino acid tryptophan (R91W) and resulting in channel blockage was found in CRAC channelopathy patients (Feske et al., 2006). Accordingly, knock-in mice carrying the corresponding R93W mutation at the homozygous state die shortly after birth (McCarl et al., 2010). Humans and mice harboring the R91W/R93W at the heterozygous state are however normal and fertile, demonstrating that amino acid change allows sufficient Ca^{2+} flow through the ORAI1 hexamers to ensure normal physiology.

4.2. Aim of the study

SOCE is susceptible to manipulation, and the reduction of extracellular Ca^{2+} entry through ORAI1 inhibition appears as a suitable therapeutic approach for TAM/STRMK. To this aim, I crossed the *Stim1$^{R304W/+}$* mice with *Orai1$^{R93W/+}$* mice and we monitored the disease progression of the offspring up to 4 months. At this time point, we assessed body weight, femur bone density, spleen weigh and histology, platelet counts, muscle performance and contraction/relaxation kinetics, and muscle histology. In addition, we also analyzed the transcriptome of dissected muscles in order to assess and quantify a potential molecular improvement of pathways implicated in muscle function.

4.3. Results

The birth ratio of *Stim1$^{R304W/+}$Orai1$^{R93W/+}$* mice improved compared to *Stim1$^{R304W/+}$* mice and was closer to the expected Mendelian ratio, indicating ameliorated embryonic development. Body weight gain over 4 months was improved, as so did the body length and femur bone density at 4 months. Spleen weight was normalized and platelet counts, albeit not significant, doubled the

levels of $Stim1^{R304W/+}$ littermates. Performance in hanging test and openfield arenas was improved in $Stim1^{R304W/+}Orai1^{R93W/+}$ mice, and muscle contraction/relaxation defects were restored. The sings of muscle degeneration that included nuclei internalization, infiltration of immune cells and regenerating fibers were not present in $Stim1^{R304W/+}Orai1^{R93W/+}$ muscle sections. In the same line, the expression of ER stress-triggered genes was normalized in $Stim1^{R304W/+}Orai1^{R93W/+}$ muscles, evidencing alleviation of ER stress. Overall, ORAI1 inhibition restored or improved all the TAM/STRMK phenotypes affecting the size, bones, spleen, platelets and the skeletal muscle.

In contrast to $Stim1^{R304W/+}Orai1^{+/-}$ mice, $Stim1^{R304W/+}Orai1^{R93W/+}$ mice showed an additional improvement of spleen size, platelet counts, hanging performance, muscle relaxation and muscle histology. The comparative transcriptomics also revealed molecular pathways differentially restored and highlighted the alleviation of ER stress as the main effector of muscle improvement in $Stim1^{R304W/+}Orai1^{R93W/+}$ mice. In summary, ORAI1 inhibition was more efficient than $Orai1$ silencing to treat TAM/STRMK in mice.

4.4. Conclusion and perspectives

$Stim1^{R304W/+}Orai1^{R93W/+}$ mice had a great phenotypic improvement when compared to $Stim1^{R304W/+}$ littermates. They were bigger and heavier, had increased bone density, smaller spleen, higher blood platelet levels, contracted and relaxed more properly, and displayed less signs of ER stress and muscle degeneration. In comparison with $Stim1^{R304W/+}Orai1^{+/-}$ mice, $Stim1^{R304W/+}Orai1^{R93W/+}$ mice yielded higher improvement of the muscle performance, contraction kinetics, histology and ER stress. The higher therapeutic efficiency of ORAI1 inhibition can be explained by the ORAI1 stoichiometry and the effect of STIM1 R304W mutant on ORAI1 channels. In contrast to $Orai1$ silencing where $Orai1$ levels decrease but ORAI1 hexamers remain fully active, expression of ORAI1 R93W mutant difficult channel permeability in all hexamers and block Ca^{2+} entry. In addition, ORAI1 forms hexamers with ORAI2 and ORAI3 in cells where they are more expressed than in skeletal muscle. For this reason, it is expected that ORAI1 R93W mutant would intercede with channel permeability of ORAI1/2/3 hexameric channels and explain the improvement of spleen and platelet phenotypes in $Stim1^{R304W/+}Orai1^{R93W/+}$ mice.

Small molecules that specifically inhibit ORAI1 activity exist and include Auxora/CM4620, RP4010 or RP3128, which currently undergo clinical trials for pancreatitis, pneumonia, asthma

and lymphoma. In view of our result demonstrating a measurable therapeutic effect of ORAI1 blocking on the multi-systemic phenotype of $Stim1^{R304W/+}Orai1^{R93W/+}$ mice, Auxora/CM4620, RP4010 and RP3128 may also prove beneficial for the treatment of TAM/STRMK patients and potentially other disorders caused by abundant cytosolic Ca^{2+} levels as DMD. Future preclinical trials using these molecules on murine TAM/STRMK and DMD models may be useful and potentially pave the way for a common therapeutic approach.

4.5. Contribution

I handled mouse breeding, organized and conducted the phenotyping experiments, and performed the histological and molecular analysis of muscle and spleen together with Laura Pérez-Guàrdia (Master 2/Erasmus student). As an internal IGBMC service, the Genomeast sequencing platform performed RNA sequencing, and the data were conjointly processed by Alix Simon and Sarah Djeddi (M2/PhD students in the team). Aurelie Auburtin and Marie-France Champy from the ICS analyzed the blood and plasma samples, and David Moulart analyzed the femur bone structure.

1   **Inhibition of the ORAI1 Ca^{2+} channel reverses the main clinical signs of**

2   **tubular aggregate myopathy (TAM) and Stormorken syndrome (STRMK) in**

3   **mice**

4

5   **Roberto Silva-Rojas[1], Laura Pérez-Guàrdia[1], Alix Simon[1], Sarah Djeddi[1], Jocelyn Laporte[1],**

6   **Johann Böhm[1]**

7

8   [1]IGBMC (Institut de Génétique et de Biologie Moléculaire et Cellulaire), Inserm U1258, CNRS

9   UMR7104, Université de Strasbourg, 67404 Illkirch, France

10

11

12   *Correspondence: Johann Böhm (johann@igbmc.fr)

13   IGBMC, 1 Rue Laurent Fries, 67404 Illkirch, France

14   Tel.: +33 (0)3 88 65 34 14

15

16

17

18

19 **ABSTRACT**

20 Tubular Aggregate Myopathy (TAM) and Stormorken Syndrome (STRMK) are clinically

21 overlapping disorders and involve defects of skeletal muscle, platelets, spleen, skin, bones, and

22 eyes. TAM/STRMK is caused by gain-of-function mutations in STIM1 and ORAI1, encoding

23 key players of store-operated Ca^{2+} entry (SOCE), and result in abnormal Ca^{2+} homeostasis and

24 cytosolic Ca^{2+} overload. Currently, no therapy is available for TAM/STRMK although we

25 recently showed that targeting *Orai1* expression was beneficial in our *Stim1$^{R304W/+}$* mouse

26 model. Here, we crossed the *Stim1$^{R304W/+}$* mice with *Orai1$^{R93W/+}$* mice, harbouring a mutation

27 partially blocking the pore of the ORAI1 Ca^{2+} channel. The *Stim1$^{R304W/+}$ Orai1$^{R93W/+}$* offspring

28 underwent phenotypic characterization at the macroscopic, histologic, and molecular levels.

29 Compared to the TAM/STRMK controls, the *Stim1$^{R304W/+}$Orai1$^{R93W/+}$* mice presented a higher

30 body weight and size, an increase in platelet counts, normalized spleen weight and histology,

31 and improved muscle performance and structure. Moreover, the phenotypical and transcriptomic

32 comparison of this approach reducing ORAI1 permeability with the cohort reducing *Orai1*

33 expression highlighted ORAI1 inhibition as the most efficient therapeutic approach for

34 TAM/STRMK and paves the way for prospective treatments for TAM/STRMK and other Ca^{2+}-

35 related disorders.

36

37

38

39

INTRODUCTION

Store-operated Ca^{2+} entry (SOCE) is a major mechanism regulating cytosolic Ca^{2+} homeostasis in all cells and tissues and STIM1 and ORAI1 are the main effectors. STIM1 is located in the endoplasmic/sarcoplasmic reticulum (ER/SR) and has a Ca^{2+} sensing luminal part and a cytosolic part mediating STIM1 oligomerization and contact with ORAI1 Ca^{2+} channel in the plasma membrane[1; 2]. Following ER/SR Ca^{2+} depletion, the luminal EF-hands of STIM1 detach from Ca^{2+} and initiate a conformational change of its cytosolic part facilitating ORAI1 activation and the extracellular Ca^{2+} entry[3].

Loss-of-function (LoF) and gain-of-function (GoF) mutations in *STIM1* and *ORAI1* cause multi-systemic disorders where similar organ and tissues are affected[4]. Recessive LoF mutations in *STIM1* and *ORAI1* negatively impact stability or function and cause CRAC channelopathy, a multisystemic disorder characterized by severe-combined immune deficiency and recurrent infections, autoimmunity, splenomegaly, ectodermal dysplasia and anhydrosis, mydriassis and muscle hypotonia[5]. In contrast, autosomal dominant GoF mutations increase STIM1 oligomerization or increase ORAI1 channel permeability and cause tubular aggregate myopathy and Stormorken syndrome (TAM/STRMK), a clinical continuum encompassing short size, dyslexia, thrombocytopenia, hyposplenia, ichthyosis, miosis and muscle weakness, cramps and myalgia[6; 7].

Mouse models carrying recessive LoF mutations in *Stim1* or *Orai1* result in SOCE abolishment and mice die perinatally[8; 9]. Tissue-specific deletion of *Stim1* and *Orai1* or the generation of fetal chimeras validated the defects in immune system, ectodermic tissues (skin, sweat glands and teeth) and muscle defects observed in CRAC channelopathy patients[4]. Mice carrying heterozygous GoF

62 mutations in *Stim1* are viable and fertile and display anomalies affecting the size, the bones, the

63 spleen, the platelets, the skin and the skeletal muscle[10-12]. As CRAC channelopathy and

64 TAM/STRMK syndrome are mirror diseases caused by inverted SOCE capacities[4], we previously

65 assessed the therapeutic efficiency *Orai1* silencing in *Stim1$^{R304W/+}$* TAM/STRMK mouse model

66 and showed improved size, bone morphology, skin histology and muscle performance and

67 morphology while platelet counts and spleen size were not ameliorated (unpublished).

68 The therapeutic effects of *Orai1* silencing provided the first clues for a potential target to treat

69 TAM/STRMK but the therapeutic effects remains limited. In order to further inhibit ORAI1

70 function, we crossed the *Stim1$^{R304W/+}$* mice with *Orai1$^{R93W/+}$* mice, expressing a dominant negative

71 ORAI1 mutant[13-15], and followed disease progression of the offspring at the phenotypical,

72 histological and molecular level. *Stim1$^{R304W/+}$Orai1$^{R93W/+}$* displayed improved body weight and

73 size, bone structure, spleen size, platelet counts, muscle performance and histology when

74 compared to *Stim1$^{R304W/+}$* mice. As the improvement of all the phenotypes was higher when ORAI1

75 was inhibited, we compared the transcriptomes of tibialis anterior (TA) from this cohort and the

76 previous cohort reducing *Orai1* expression and found that the expression of a vast majority of the

77 dysregulated genes in *Stim1$^{R304W/+}$* TA was restored in *Stim1$^{R304W/+}$Orai1$^{R93W/+}$* TA. Overall, we

78 show that ORAI1 inhibition improves all the signs of TAM/STRMK in mice and transcriptomics

79 of tibialis anterior confirms this strategy as more efficient than *Orai1* silencing.

80

81

82

83

RESULTS

Non-muscle phenotypes of TAM/STRMK are improved in *Stim1^{R304W/+}Orai1^{R93W/+}* mice

Stim1^{R304W/+} mouse was the first described mouse model for TAM/STRMK recapitulating most of the multi-systemic phenotypes observed in patients[12]. *Stim1^{R304W/+}* mice were smaller than the control littermates, had bone and spleen anomalies, presented thrombocytopenia and displayed altered muscle performance and hostology[12]. Reducing *Orai1* expression improved some of the phenotypes and pointed to ORAI1 as a therapeutic target for TAM/STRMK but the therapeutic effects were limited (unpublished). In order to inhibit ORAI1 activity, we crossed *Stim1^{R304W/+}* mice with *Orai1^{R93W/+}* mice, carrying a mutation in ORAI1 (p.R93W) that difficults channel permeability and acts as dominant negative ORAI1 mutant[13-15] (Fig. S1A). The resulting offspring revealed a slight increase in birth ratio of *Stim1^{R304W/+}Orai1^{R93W/+}* mice compared to *Stim1^{R304W/+}* littermates (33.5% WT, 22.3% *Orai1^{R93W/+}*, 19.5% *Stim1^{R304W/+}* and 24.7% *Stim1^{R304W/+}Orai1^{R93W/+}*, n=215, p value =0.025). Gene and protein expression of ORAI1 were assessed in TA and, while no effect was observed on *Orai1* mRNA, ORAI1 was upregulated in *Stim1^{R304W/+}* TA and normalized in *Stim1^{R304W/+}Orai1^{R93W/+}* TA (Fig. S1B-D). This suggests an accumulation of ORAI1 due to the STIM1 over-activation resolved by interference of ORAI1 R93W mutant in STIM1/ORAI1 interaction[16].

Body weight was recorded monthly and bones, spleen, platelets and muscle studied at 4 months of age. The weight of *Stim1^{R304W/+}Orai1^{R93W/+}* was significantly improved compared to *Stim1^{R304W/+}* mice at all ages studied with an increase of 17% in body weight and 4% in body length at 4 months (Fig, 1A and S2A).

Figure 1. Improved weight, bone structure, spleen weight and platelet levels in *Stim1$^{R304W/+}$Orai1$^{R93W/+}$* mice. (A) Body weight increased in *Stim1$^{R304W/+}$Orai1$^{R93W/+}$* mice compared with *Stim1$^{R304W/+}$* littermates at all ages studied (n=11-14). (B) 3D reconstruction of the femur microarchitecture illustrated a similar trabecular density in *Stim1$^{R304W/+}$Orai1$^{R93W/+}$* mice and healthy WT and *Orai1$^{R93W/+}$* controls at 4 months. (C-E) Spleen to body weight ratio and spleen megakaryocyte numbers in *Stim1$^{R304W/+}$Orai1$^{R93W/+}$* mice were similar to WT and *Orai1$^{R93W/+}$* controls, and platelet counts slightly doubled compared to *Stim1$^{R304W/+}$* mice at 4 months (n=6-14). (F) Histological H&E staining of spleen sections at 4 months evidenced the increased rate of megakaryocytes (black arrows) in *Stim1$^{R304W/+}$* mice and their normal distribution in WT, *Stim1$^{R304W/+}$Orai1$^{R93W/+}$, Stim1$^{R304W/+}$Orai1$^{R93W/+}$* mice at 4 months. Scale bar = 250 µm. Graphs represent mean ± SEM. Significant differences are indicated as */α/$ P<0.05, **/αα/$$ P<0.01,
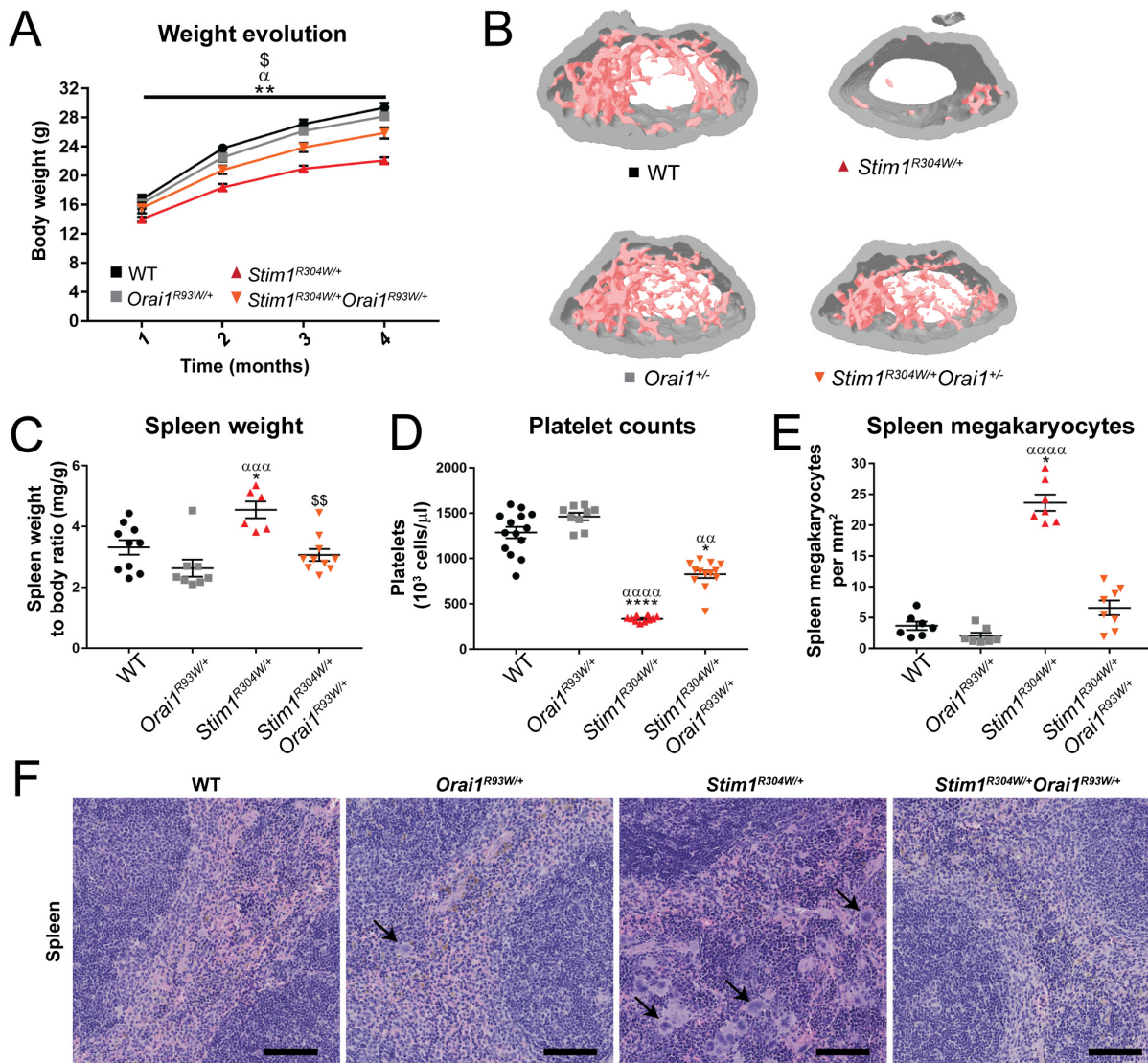
/ααα/$$$ P<0.001, and */αααα/$$$$ P<0.0001 with * reflecting the comparison with the WT group, α the

116 comparison with the *Orai1$^{R93W/+}$* group, and $ for the comparison between *Stim1$^{R304W/+}$* and *Stim1$^{R304W/+}$Orai1$^{R93W/+}$*

117 group.

118

119 In line with the improvement in size, *Stim1$^{R304W/+}$Orai1$^{R93W/+}$* femurs were analyzed and trabecular

120 architecture imaged by micro-computerized tomography revealing increased trabecular thickness

121 (+35%) and number (+640%), and reduced trabecular separation (-28%) when compared to

122 *Stim1$^{R304W/+}$* littermates (Fig. 1B and Table S2). Muscle weight can also contribute to the

123 improvement in body weight and the analysis of gastrocnemius and soleus revealed an

124 improvement of the gastrocnemius atrophy and soleus the hypertrophy in *Stim1$^{R304W/+}$Orai1$^{R93W/+}$*

125 mice compared to *Stim1$^{R304W/+}$* littermates (Fig. S2B-C).

126 In contrast to the commonly reported hyposplenia from TAM/STRMK patients, the available

127 mouse models displayed spleen enlargement[10-12], probably arising from human/mouse

128 physiological divergences[17]. The splenomegaly observed in *Stim1$^{R304W/+}$* mice was reversed in

129 *Stim1$^{R304W/+}$Orai1$^{R93W/+}$* mice (Fig. 1C). Low platelet numbers in peripheral blood are commonly

130 seen in TAM/STRMK patients and mice[7; 10-12; 18-20], and result from platelet pre-activation and

131 increased platelet turnover as a consequence of over-activated SOCE[11; 12]. Blood platelet counts

132 are 2.5 times higher in *Stim1$^{R304W/+}$Orai1$^{R93W/+}$* mice when compared to *Stim1$^{R304W/+}$* mice while

133 still differing from control groups, indicating a partial effect of ORAI1 inhibition on platelet

134 turnover (Fig. 1D). In the same line, counting of spleen megakaryocytes, the platelet precursors,

135 revealed normalized levels in *Stim1$^{R304W/+}$Orai1$^{R93W/+}$* compared to *Stim1$^{R304W/+}$* mice (Fig. 1E-F).

136

137

138 *Stim1^{R304W/+}Orai1^{R93W/+}* **mice have improved muscle performance and morphology**

139 The performance in hanging test was reduced in *Stim1$^{R304W/+}$* mice compared to control groups at

140 2, 3 and 4 months, and *Stim1$^{R304W/+}$Orai1$^{R93W/+}$* mice fell 20s later in average than *Stim1$^{R304W/+}$*

141 littermates at 4 months (Fig. 2A). Similarly, grip strength assessed at 2 months showed a tendency

142 to increase in *Stim1$^{R304W/+}$Orai1$^{R93W/+}$* compared to *Stim1$^{R304W/+}$* littermates (Fig. S2D), and

143 *Stim1$^{R304W/+}$Orai1$^{R93W/+}$* mice travelled 17% more distance and faster than *Stim1$^{R304W/+}$* littermates

144 in the open field arenas at 10 weeks of age (Fig. S2E-F). The muscle weakness of *Stim1$^{R304W/+}$*

145 mice may underlie abnormal muscle contraction and relaxation resulting from Ca^{2+} handling

146 anomalies[12; 21]. *In situ* muscle force produced at low frequencies (1-50 Hz) was reduced in

147 *Stim1$^{R304W/+}$Orai1$^{R93W/+}$* TA compared to *Stim1$^{R304W/+}$*, and contraction and relaxation time was

148 also reduced by 10 ms and 7 ms, respectively (Fig. 2C-E). In the same line, the time to reach 50%

149 relaxation after tetanic stimulation (100 Hz) was reduced by 33 ms in *Stim1$^{R304W/+}$Orai1$^{R93W/+}$* mice

150 compared to *Stim1$^{R304W/+}$* TA and didn't differ significantly from WT and *Orai1$^{R93W/+}$* (Fig. 2F-

151 G). Resistance to fatigue was assessed *in situ* by a train of 80 repetitive 40 Hz stimulations

152 revealing increased resistance to fatigue in *Stim1$^{R304W/+}$* mice as previously reported[12], and no

153 major improvement was observed in *Stim1$^{R304W/+}$Orai1$^{R93W/+}$* mice (Fig. S2G-H).

154

Figure 2. Improved muscle performance and contraction in *Stim1^{R304W/+}Orai1^{R93W/+}* mice. (A-B) The performance of *Stim1^{R304W/+}Orai1^{R93W/+}* mice in the hanging test improved over time and significantly differed from *Stim1^{R304W/+}* mice at 4 months (n=11-14). (B) *In situ* muscle force production at low frequency stimulations (1-50 Hz) was reduced in *Stim1^{R304W/+}Orai1^{R93W/+}* reaching the levels of healthy controls (n=5-7). (C-E) Following a single stimulation, *Stim1^{R304W/+}Orai1^{R93W/+}* TA had a non-significant tendency of faster contraction and the time to relax was significantly reduced when compared to *Stim1^{R304W/+}* TA at 4 months (n=5-7). (F-G) Upon tetanic stimulation (100 Hz), the muscle relaxation of *Stim1^{R304W/+}Orai1^{R93W/+}* TA was similar to WT and *Orai1^{R93W/+}* healthy controls at 4 months (n=5-7). Graphs represent mean ± SEM. Significant differences are indicated as */α/$ P<0.05, **/αα/$$ P<0.01, ***/ααα/$$$
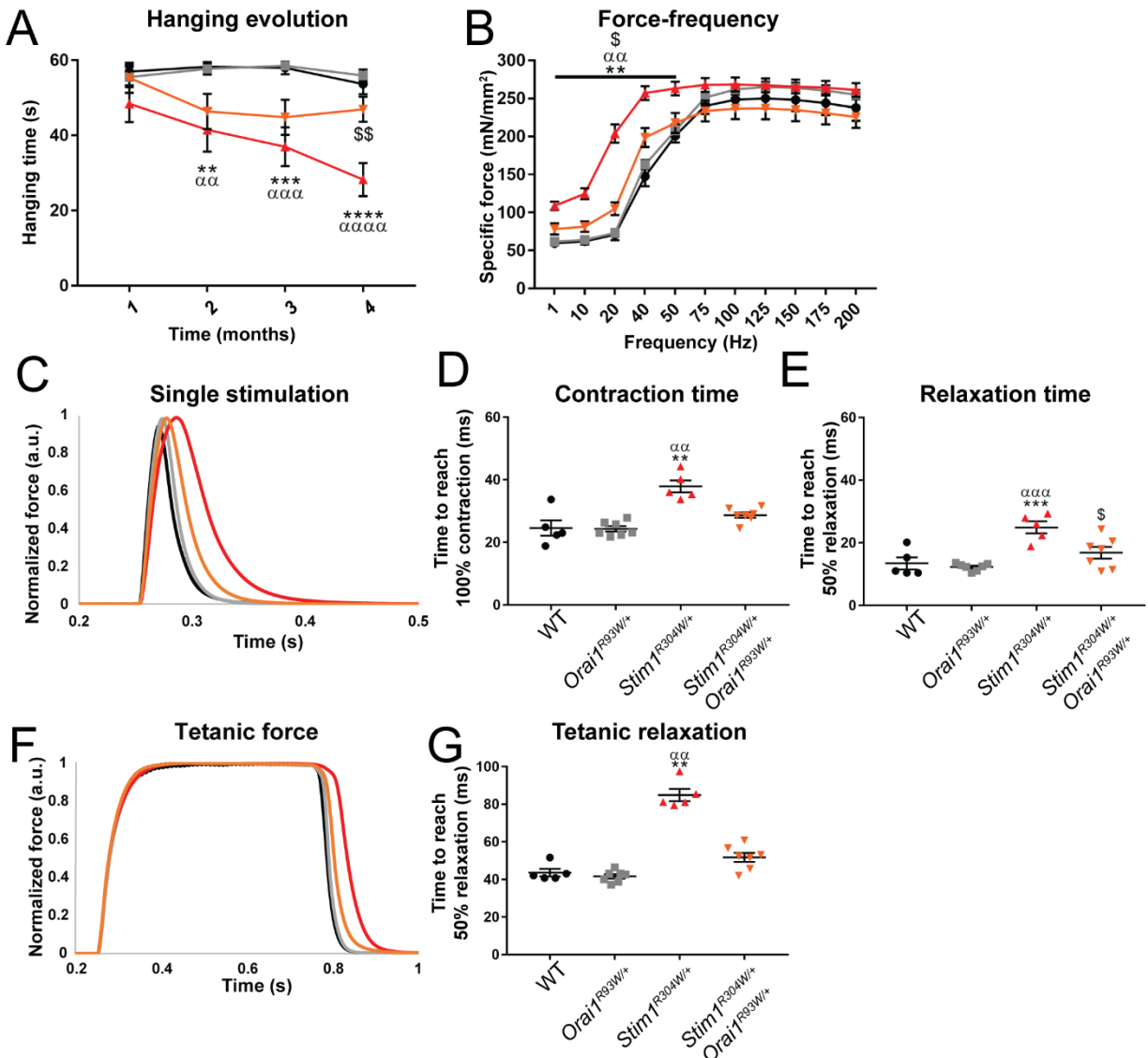
164

165

166   Discrete signs of muscle degeneration are observed in *Stim1*^{R304W/+} mice such as the presence of

167   fibers with internalized nuclei, immune cell infiltration or small fibers in regeneration[12; 21].

168   Counting of fibers with internalized nuclei in TA and gastrocnemius from *Stim1*^{R304W/+}*Orai1*^{R93W/+}

169   mice revealed a similar rate to WT and *Orai1*^{R93W/+} control muscles (0.2-0.4%) and a reduction

170   compared to *Stim1*^{R304W/+} mice (1-1.1%) (Fig. 3A-B and S.3A-B). Moreover, the rate of

171   regenerative fibers was assessed by immunofluorescence of embryonic myosin heavy chain and

172   blood circulating creatine kinase were measured, both showing a decrease in

173   *Stim1*^{R304W/+}*Orai1*^{R93W/+} mice compared to *Stim1*^{R304W/+} littermates (Fig. 3A and 3C and S.3C).

174   Muscle degeneration in *Stim1*^{R304W/+} mice results from unresolved ER stress and was evidenced

175   by the increased expression of reticular chaperones implicated in unfolded protein response in

176   *Stim1*^{R304W/+} muscles[21]. These ER chaperones (*Hspa5* and *Hsp90b1*) displayed reduced expression

177   in *Stim1*^{R304W/+}*Orai1*^{R93W/+} TA compared to *Stim1*^{R304W/+} TA (Fig. 3D), indicating that the ORAI1

178   inhibition is sufficient to attenuate ER stress and to reduce muscle turnover in

179   *Stim1*^{R304W/+}*Orai1*^{R93W/+} mice.
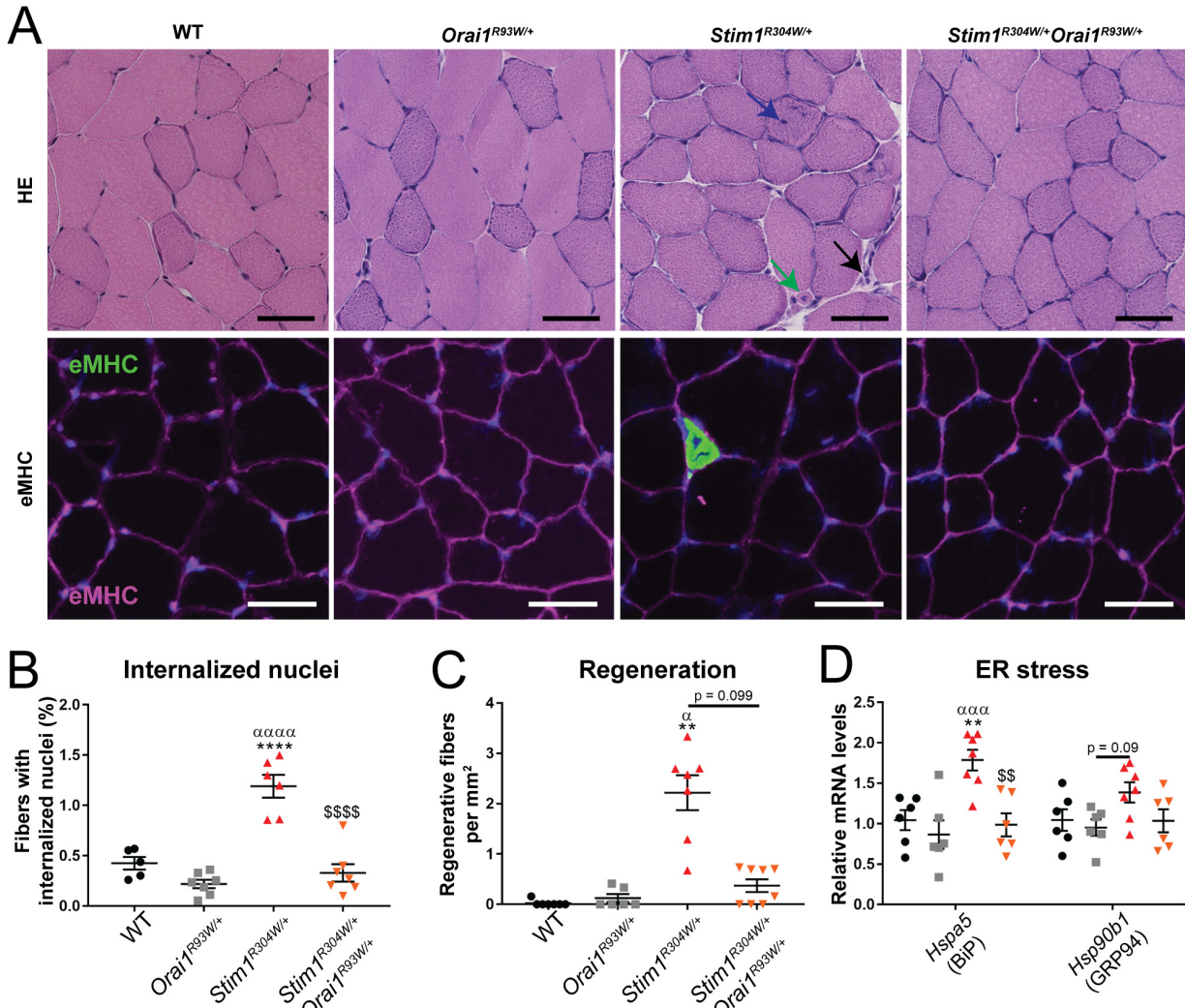
Figure 3. Rescued muscle degeneration and resolved ER stress in *Stim1^{R304W/+}Orai1^{R93W/+}* mice. (A) H&E staining on muscle sections from both *Stim1^{R304W/+}* revealed fibers with internalized nuclei (blue arrow), regenerating fibers (green arrow) and infiltration of immune cells (black arrow), and immunofluorescence showed regenerative fibers expressing embryonic myosin. Scale bar = 50 μm. (B-C) The rate of fibers with internalized nuclei and regenerating fibers were reduced in *Stim1^{R304W/+}Orai1^{R93W/+}* compared to *Stim1^{R304W/+}* mice (n=5-8). (D) The expression of the UPR markers were significantly reduced (*Hspa5*) was had a non-significant tendency to decrease (*Hsp90b1*) in *Stim1^{R304W/+}Orai1^{R93W/+}* muscles compared to *Stim1^{R304W/+}* mice (n=6). Graphs represent mean ± SEM. Significant differences are indicated as */α/\$ P<0.05, **/αα/\$\$ P<0.01, ***/ααα/\$\$\$ P<0.001, and ****/αααα/\$\$\$\$ P<0.0001 with * reflecting the comparison with the WT group, α the comparison with the *Orai1^{R93W/+}* group, and \$ for the comparison between *Stim1^{R304W/+}* and *Stim1^{R304W/+}Orai1^{R93W/+}* group.

ORAI1 inhibition has higher transcriptional impact than *Orai1* silencing

We previously showed that targeting *Orai1* expression improves several of the phenotypes observed in *Stim1$^{R304W/+}$* mice including size, bone structure, skin histology, and muscle contraction and histology. However, platelet counts and spleen size were not improved in *Stim1$^{R304W/+}$Orai1$^{+/-}$* mice (unpublished). Here, we performed a comparative analysis of the phenotypical improvement the *Orai1* silencing cohort and the ORAI1 inhibition cohort described here. After normalizing all phenotypical parameters to their WT (100% rescue) and *Stim1$^{R304W/+}$* littermates (0% rescue), *Stim1$^{R304W/+}$Orai1$^{R93W/+}$* displayed normalized spleen size and improved platelet counts, both not achieved in *Stim1$^{R304W/+}$Orai1$^{+/-}$* mice (Fig.4A). Regarding the skeletal muscle, hanging time and muscle relaxation defects were fully restored in *Stim1$^{R304W/+}$Orai1$^{R93W/+}$* mice while just a slight improvement was observed in *Stim1$^{R304W/+}$Orai1$^{+/-}$* mice (Fig. 4A). *Orai1* silencing didn't improve the rate of fibers with internalized nuclei (muscle histology) while ORAI1 inhibition in *Stim1$^{R304W/+}$Orai1$^{R93W/+}$* mice normalized this defect and the high levels of ER stress, suggesting the alleviation in protein folding stress drove the restauration of normal muscle histology (Fig. 4A). The phenotypical comparison of *Orai1* silencing and ORAI1 inhibition pointed the later approach as the most efficient therapeutic strategy for TAM/STRMK.

To determine the common and specific signature of *Orai1* silencing and ORAI1 inhibition at the molecular level, we performed RNA sequencing (RNA-seq) for transcriptomic analysis in TA from 16 weeks old mice. Hierarchical clustering of the data revealed clear sample grouping in the *Orai1* silencing cohort where *Stim1$^{R304W/+}$* and *Stim1$^{R304W/+}$Orai1$^{+/-}$* displayed similar transcriptomic patterns, while the ORAI1 inhibition cohort showed a difference between *Stim1$^{R304W/+}$* and the rest of the groups including *Stim1$^{R304W/+}$Orai1$^{R93W/+}$* (Fig. 1B).

A

Orai1 silencing

ORAI1 inhibition

■ Rescued
■ Not rescued

B

■ WT   ■ *Stim1^{R304W/+}*
■ *Orai1^{+/-}*   ■ *Stim1^{R304W/+}Orai1^{+/-}*

■ WT   ■ *Stim1^{R304W/+}*
■ *Orai1^{R93W/+}*   ■ *Stim1^{R304W/+}Orai1^{R93W/+}*

C

Venn's diagram of rescued genes

Orai1 silencing — 109 — 113 — 1127 — ORAI1 inhibition

D

Gene expression improvement

Gene status
■ Rescued
■ Partially rescued
■ Not rescued

213

168
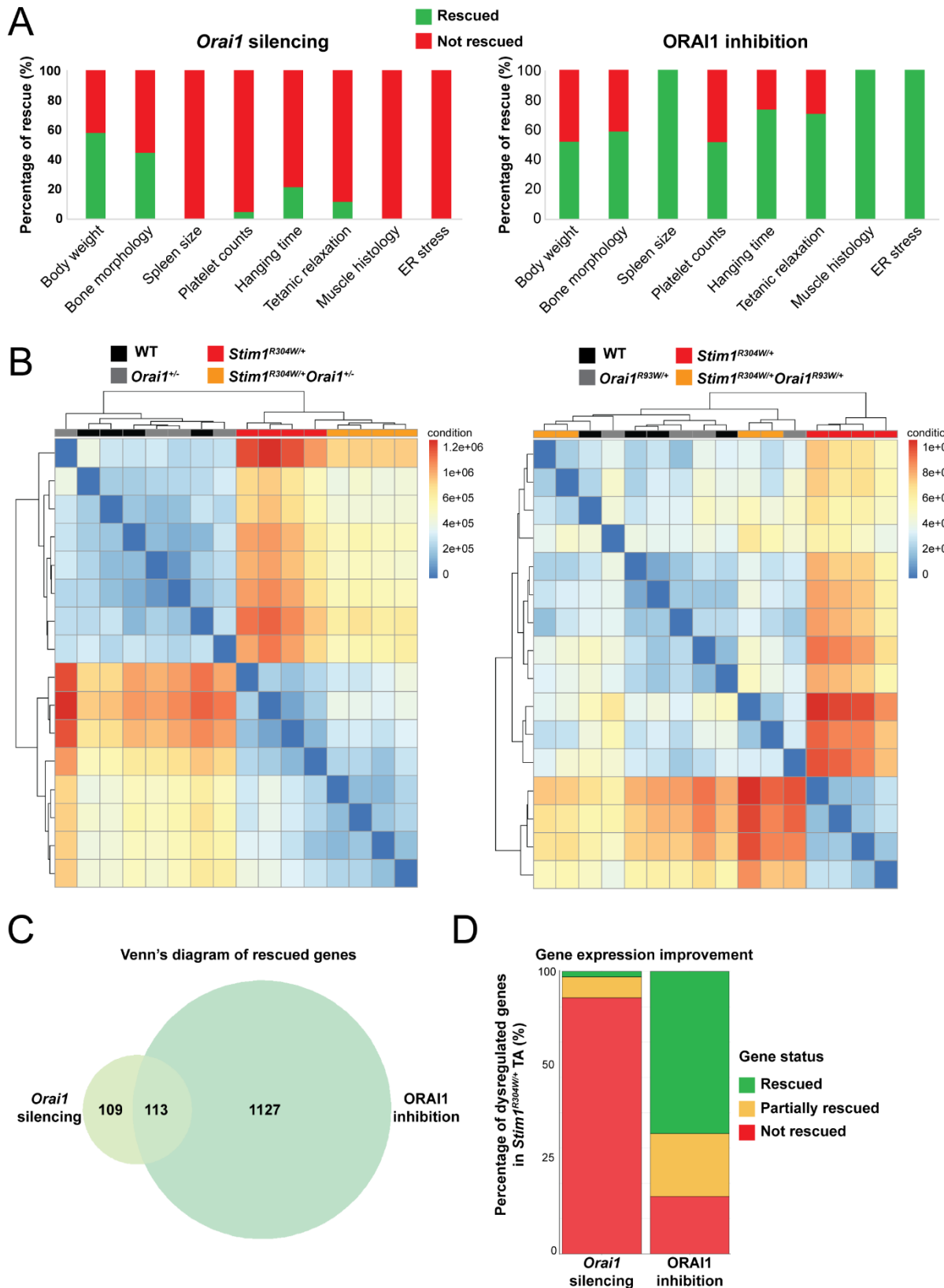
Figure 4. ORAI1 inhibition yielded larger phenotype reversion and transcriptomic changes than *Orai1* silencing

(A) Phenotype reversion of different *Stim1$^{R304W/+}$* phenotypes was normalized with WT (100% rescue) and *Stim1$^{R304W/+}$* values (0% rescue). *Stim1$^{R304W/+}$Orai1$^{R93W/+}$* mice (ORAI1 inhibition) showed a larger phenotype improvement compared to the disease of *Stim1$^{R304W/+}$Orai1$^{+/-}$* mice (*Orai1* silencing) and particularly in spleen, platelets and skeletal muscle readouts. Bone morphology referred to the femur bone trabecular number, spleen size to spleen to body weight ratio, tetanic relaxation to the tetanic relaxation time, muscle histology to the rate of the fibers with internalized nuclei, and ER stress to the relative mRNA levels of *Hspa5*. (B) Hierarchical clustering of the RNAseq depicted a sample grouping of *Stim1$^{R304W/+}$* and *Stim1$^{R304W/+}$Orai1$^{+/-}$* mice visually different from healthy WT and *Orai1$^{+/-}$* controls, while *Stim1$^{R304W/+}$Orai1$^{R93W/+}$* mice grouped with healthy controls WT and *Orai1$^{R93W/+}$* muscles and differed from *Stim1$^{R304W/+}$* mice (n=4). (C-D) Venn diagram illustrating the shared and specific genes with improved expression in *Stim1$^{R304W/+}$Orai1$^{+/-}$* (*Orai1* silencing) and *Stim1$^{R304W/+}$Orai1$^{R93W/+}$* (ORAI1 inhibition) mice and the percentage of genes with improved or rescued expression were more abundant in the ORAI1 inhibition cohort.

We analyzed the gene ontology (GO) enrichment of the genes improved in the therapeutic group of both cohorts. This analysis revealed a shared GO enrichment in genes associated to muscle contraction and differentiation (5 out of 20) (Fig. S4). The major difference appeared in the ORAI1 inhibition cohort where several immune-related terms appeared (12 out of 20) in the ORAI1 inhibition (Fig. S4B). We previously showed that *Stim1$^{R304W/+}$* mice have increased rate of fiber degeneration with the consequent resolving inflammation and regeneration[21]. As *Stim1$^{R304W/+}$Orai1$^{R93W/+}$* TA display improved muscle histology compared to *Stim1$^{R304W/+}$* TA (Fig. 3), it was expected that *Stim1$^{R304W/+}$Orai1$^{R93W/+}$* TA had reduced expression of immune-related genes. However, the most enriched GO term in the ORAI1 inhibition cohort was the response to endoplasmic reticulum stress (GO:0034976) (Fig. S4B), confirming that the reduced degeneration and inflammation observed by ORAI1 inhibition is mainly driven by reducing the ER stress levels.

239   Regarding the number dysregulated genes in $Stim1^{R304W/+}$ TA, $Orai1$ silencing and ORAI1

240   inhibition improved the expression of 222 and 1240 genes respectively and shared a common

241   improvement in the expression of 109 genes (Fig. 4C). When assessing if the gene expression

242   reached WT levels (rescue), we realized that $Orai1$ silencing only rescued 1.8% and improved

243   7.5% of the genes while ORAI1 inhibition rescued 57.3% and improved 22.2% of the genes (Fig.

244   4D). Overall, ORAI1 inhibition has a more extended impact on TAM/STRMK than $Orai1$

245   silencing and improved or rescued muscle defects of TAM/STRMK mice at the performance,

246   histological and molecular level.

247   **DISCUSSION**

248   GoF mutations in $STIM1$ and $ORAI1$ are associated with TAM/STRMK, a clinical continuum

249   characterized by anomalies affecting the skin, the eyes, the platelets, the spleen and the skeletal

250   muscle[6; 7]. $STIM1$ and $ORAI1$ mutations result in SOCE over-activation and excessive extracellular

251   Ca^{2+} entry via ORAI1[18; 22; 23]. We previously showed that $Orai1$ silencing in $Stim1^{R304W/+}$ mice, a

252   TAM/STRMK mouse model, improved several phenotypes including the size, bone structure, skin

253   histology and skeletal muscle contraction and histology while platelet and spleen defects were not

254   improved (unpublished). To determine whether ORAI1 inhibition is more efficient than $Orai1$

255   silencing, we crossed the $Stim1^{R304W/+}$ mice with mice carrying an $Orai1$ mutation partially

256   blocking the channel ($Orai1^{R93W/+}$)[13]. $Stim1^{R304W/+}Orai1^{R93W/+}$ mice restored body size and weight,

257   improved trabecular bone structure, restored spleen size, improved platelet counts, and restored

258   muscle performance and histology. In addition, we compared the transcriptional impact of

259   silencing $Orai1$ and ORAI1 inhibition, and concluded that the later yield higher therapeutic effects

260   at the molecular level.

TAM/STRMK developmental defects are improved by targeting ORAI1

SOCE-dependent Ca^{2+} entry is required for egg fertilization and controls the first steps of development[24; 25]. SOCE deficiency also has consequences in later developmental stages and tissues derived from the ectoderm are affected in CRAC channelopathy patients, carrying recessive LoF mutations in *STIM1* or *ORAI1*[5]. The implication of SOCE in development is more important in mice where constitutive *Stim1* or *Orai1* deletion in mice results in perinatal lethality[8; 9]. SOCE over-activation also alters embryonic development where *Stim1*^{R304W/R304W} mice die perinatally and *Stim1*^{R304W/+} has reduced birth ratio[12]. In line with the birth ratio anomalies, SOCE over-activation may also delay embryonic development and partially explain the decreased stature observed in TAM/STRMK patients and mice[7; 10; 12]. Another explanation would rely on anomalies of bone formation and resorption where SOCE has shown to play a crucial role[26-29]. Indeed, *Stim1*^{R304W/+} mice present abnormal structure of both cortical and trabecular bones[12]. *Orai1* silencing (unpublished) and ORAI1 inhibition improve the birth ratio, the femur trabecular structure and consequently the body weight and size. These results suggest that modulating ORAI1 expression or activity are sufficient to improve bone turnover and therefore improve body size in TAM/STRMK.

ORAI1 inhibition improves spleen and platelet defects

The spleen is the largest lymphoid organ acting as niche of innate and immune cells and filtering blood to remove circulating dead cells including platelet and white and red cells[30; 31]. TAM/STRMK patients usually present hyposplenia or asplenia and Howell-Jolly bodies, a blood marker of abnormal splenic function, are also commonly found in the blood of several patients[7; 18; 19; 32; 33]. In contrast to patients, three TAM/STRMK mouse models with GoF mutations in *Stim1*

283   are characterized by increased spleen size[10-12], possibly due to different requirements of spleen for

284   hematopoiesis during adulthood[17; 34]. Another inter-species difference relies on the platelet

285   production niches where human platelets are mostly produced in bone marrow in adults, and the

286   contribution to platelet production in mice is shared between the bone marrow and the spleen[35].

287   TAM/STRMK patients present thrombocytopenia and increased bleeding tendency[7; 18-20; 22; 36] as

288   a result of aberrant platelet function and increased clearance while platelet production remains

289   normal[11; 20; 36]. *Stim1$^{R304W/+}$* mice have reduced platelet counts and the spleen has a compensating

290   increase of platelet precursors in the spleen (megakaryocytes)[12]. *Orai1* silencing did not improve

291   the platelet counts and the compensating increased presence of megakaryocytes in the spleen while

292   ORAI1 inhibition improved the thrombocytopenia and restored the amount of platelet precursors

293   in spleen. This partial effect on platelet counts may arise from different Ca^{2+} sensitivity, Ca^{2+}

294   balance and ORAI1 relevance in different cells and tissues. Indeed, ORAI1 and its homologues

295   ORAI2 and ORAI3 have partially overlapping expression patterns, interact with STIM1 and form

296   heteromeric channels in platelets[37; 38]. Therefore, it is expected that the presence of R93W

297   modification in ORAI1 would have a partial effect on the heteromeric channels present in the

298   platelets [38] compared to higher effect in tissues like the skeletal muscle where the expression of

299   ORAI1 is more pronounced than ORAI2 and ORAI3 paralogues.

300   **ORAI1 inhibition fully restores muscle performance, contraction and histology**

301   The muscle defects in TAM/STRMK arise from excessive extracellular Ca^{2+}, inducing a

302   dysregulation of muscle contraction, and resulting in muscle weakness, cramps and myalgia[6]. At

303   the histological level, TAM/STRMK is characterized by the presence of tubular aggregates and

304   discrete signs of muscle degeneration with the subsequent increase in circulating creatine kinase

305   levels[4; 6; 7; 18; 19; 22; 23; 39]. *Stim1$^{R304W/+}$* mice recapitulated the defects in muscle performance and

306 contraction[12]. At the histological level, tubular aggregates were not found while degeneration is

307 more abundant than observed in patients, and we further pointed to endoplasmic reticulum stress

308 as the main molecular driver of myofiber death in $Stim1^{R304W/+}$ mice[21]. Tubular aggregates may act

309 as intracellular Ca^{2+} buffering systems to control the elevated cytosolic Ca^{2+} in patient, protecting

310 patient myofibers from degeneration.

311 Muscle performance and histology were improved in $Stim1^{R304W/+}Orai1^{R93W/+}$ mice to a higher

312 extent than previously observed in $Stim1^{R304W/+}Orai1^{+/-}$ mice. Indeed, reducing $Orai1$ expression

313 by 50% would impact the total pool of ORAI1 molecules but STIM1 R304W mutant is predicted

314 to constitutively active them. In contrast, the heterozygous expression of the dominant negative

315 ORAI1 R93W mutant would impact the channel permeability of all ORAI1 hexamers[14; 15]. In

316 addition to the permeability inhibition, ORAI1 R91W mutant (R93W in mice) was shown to

317 reduce the interaction with STIM1[16], an effect that would reduce the sequestration of ORAI1 in

318 the TAM/STRMK scenario and would further attenuate the pathological effects of STIM1 R304W

319 mutant. In this line, expression of ORAI1 R93W mutant improved or restored the expression of

320 nearly 80% of the genes dysregulated in $Stim1^{R304W/+}$ mice, a transcriptional effect almost 8 times

321 higher than the reduction in $Orai1$ expression. Response to endoplasmic reticulum was the most

322 enriched biological process and leaded the improvement of muscle degeneration in

323 $Stim1^{R304W/+}Orai1^{R93W/+}$ mice. Other muscle diseases with Ca^{2+} handling anomalies like central

324 core disease or Duchenne's muscle dystrophy also develop sustained ER stress and fiber

325 degeneration in mice, and the treatment with sodium 4-phenylbutyrate (4-PBA) improved or

326 restored the muscle performance and histology[40; 41]. 4-PBA is a FDA-approved compound

327 commonly used to treat urea cycle disorders. Assessing it efficiency to improve $Stim1^{R304W/+}$

328 phenotypes would be a practical strategy to shorten the clinical validation period and speed the

329 access of TAM/STRMK patients to a therapy.

330 **Targeting ORAI1 in other Ca^{2+}-related diseases**

331 STIM1/ORAI1 over-activation with the subsequent effect on Ca^{2+} entry is also reported in other

332 muscle disorders[42]. *Mdx* mice, a dystrophin-deficient murine model of Duchenne muscular

333 dystrophy (DMD), has increased expression of *Orai1* and SOCE over-activation [43]. Indeed, co-

334 expression with dominant-negative ORAI1, similar to our present study with *Stim1$^{R304W/+}$* mice,

335 improved the dystrophic histological anomalies[44; 45], indicating that SOCE-dependent Ca^{2+} entry

336 participates in the muscle degeneration of *mdx* mice. Malignant hyperthermia is a muscle disorder

337 characterized by a life-threatening sensitivity to halogenated anesthetics such as halothane or

338 isoflurane. It is mainly caused by *RYR1* and *CACNA1S* mutations rendering the channel highly

339 reactive to these compounds and triggering SR Ca^{2+} leakage[46]. It has been proposed that SR store

340 leak triggers sustained SOCE activation and contributes to disease severity[47]. In this line, treating

341 the murine MH model *Ryr1$^{R163C/+}$* with ORAI1 inhibitors like BTP-2, Gd^{3+} and GsMTx-4, or co-

342 expressing the same dominant-negative ORAI1 cited above, reduced SR leakage and elevation of

343 cytoplasmic Ca^{2+} levels[48].

344 ORAI1 is also commonly reported as a target for other disease conditions where inflammation is

345 implicated (e.g. pancreatitis, COVID-19 pneumonia, psoriasis, conjunctivitis, rheumatoid arthritis,

346 asthma) or cancer[49-51]. Several specific ORAI1 inhibitors exist[52-56] and some are currently been

347 tested in clinical trials for acute pancreatitis (Auxora/CM4620, phase II, NCT03709342,

348 NCT04681066 and NCT03401190), COVID-19 pneumonia (Auxora/CM4620, phase II,

349 NCT04661540 and NCT04345614), asthma (RP3128, phase I, NCT02958982), and relapsed or

350   refractory lymphomas (RP4010, phase II, NCT03119467). Carboxyamidotriazole, a non-selective

351   SOCE inhibitor is currently been tested to attenuate tumor progression in different types of cancer

352   (phase II, NCT00006486, NCT00019461, NCT00005045, NCT00004146; phase III;

353   NCT00003869). In addition to the ORAI1 inhibitors, the interest to specifically target ORAI1

354   increased in the last years and results show that monoclonal antibodies targeting ORAI1 reduce

355   autoimmune responses in mice and patient T cells *ex vivo*[57-60]. In the same line, allergic

356   conjunctivitis is been targeted in preclinical trials with SYL116011, an *Orai1/ORAI1*-specific

357   interference RNA[61; 62]. Thus, the clinical interest of targeting ORAI1 goes beyond TAM/STRMK

358   and the dedicated efforts to treat other ORAI1-related diseases would positively revert into

359   TAM/STRMK patients in the future.

360   **Concluding remark**

361   In conclusion, the present study assess ORAI1 inhibition as a therapeutic approach to treat

362   TAM/STRMK in mice and shows higher therapeutic efficiency at the phenotypical and molecular

363   level compared to *Orai1* silencing. Small molecules inhibiting ORAI1 are currently going through

364   clinical trials for other SOCE-related diseases and their future assessment in $Stim1^{R304W/+}$ mice

365   might provide the first adaptable approach to treat TAM/STRMK patients.

366

367

368

369

370

MATERIALS AND METHODS

Animals

Animal care and experimentation was in accordance with French and European legislation and approved by the institutional ethics committee (project numbers 2019062813376603 and 2020052517411298). Mice were housed in ventilated cages with 12h day/night cycles and access to food *ad libitum*. *Stim1*$^{R304W/+}$ and *Orai1*$^{R93W/+}$ mice were described previously[12; 13]. Mice expressing 50% of mutated *Orai1* (*Orai1*$^{R93W/+}$) were crossed with *Stim1*$^{R304W/+}$ mice to generate the four groups studied here: WT, *Orai1*$^{R93W/+}$, *Stim1*$^{R304W/+}$ and *Stim1*$^{R304W/+}$ *Orai1*$^{R93W/+}$. Genotyping was performed using the following primers: GCAGGTAGGAGAGTGTACAGGATGCCTT (forward) and CTTTCCATCCCCACTGCCATTTT (reverse) for *Stim1*; and ATTTCCCAATACGTTCCACCTCCC (forward) and TCGTACCACCTTCTTGGGACTTGA (reverse) for *Orai1*.

Hanging, grip and open field tests

Mice hanging ability was assessed by suspending the mice on a cage lid for a maximum of 60 seconds and the time to fall was recorded. Four-paw grip strength was measured using a dynamometer and normalized to body weight (Bioseb, Vitrolles, France). Both hanging and grip test were repeated 3 times with a 5-10 minutes rest interval. Hanging time was assessed monthly and grip strength only in 2 months mice.

The open field test was performed on a homogenously-illuminated (100 lux at arena level) and noise-isolated room. 10 weeks-old mice were placed in the arena (Bioseb) and distance, speed and rearing were assessed during 30 minutes.

In situ muscle force

4 months old mice were anesthetized with intraperitoneal injections of domitor/fentanyl mix (2/0.28 mg/Kg), diazepam (8mg/Kg) and fentanyl (0.28 mg/Kg). Tibialis anterior (TA) was partially excised and the tendon attached to the isometric transducer using suture thread. TA contraction properties were assessed using the *in situ* whole animal system 1305A (Aurora Scientific, Aurora, Canada). The sciatic nerve was stimulated by pulses of 1-200 Hz spaced by 30 seconds to measure maximal force. Following a 3 minutes resting period, fatigue was assessed by applying 80 stimulations of 40 Hz spaced by 2 seconds. Specific force was determined by dividing the maximal force with muscle cross sectional area calculated as wet muscle (mg) / optimal muscle length (mm) X mammalian muscle density (1.06 mg/mm3). Single stimulation contraction and relaxation time were calculated as the time to reach 100% or decrease to 50% force production, respectively. Tetanic relaxation time was calculated as the time to decrease 50% the force after stimulation ceased.

Micro-computerized bone tomography (μCT)

Trabecular bone morphology and structure were imaged on femur from 4 months old mice using the Quantum μCT scanner (Perkin Elmer, Whaltham, USA). All scans were performed with an isotropic voxel size of μm, 160 μA tube current and 90 kV tube voltage. Gray scale images were pre-processed using the ImageJ software, and morphological 3D measurements were further performed using the CTAn software (Bruker, Billerica, USA). Representative images were creating using the CTvol software (Bruker).

Blood counting and plasma studies

Blood counting was assessed following submandibular puncture of 4 months mice. Blood counts were determined on ADVIA 120 system (Siemens, Munich, Germany). Plasma was obtained using heparin-coated tubes (20.1345.100, SARSTEDT, Darmstadt, Germany) and creatine kinase levels (CK) were determined using the OLYMPUS AU-480 automated laboratory work station (Beckman Coulter, Brea, USA) with kits and controls supplied by Beckman Coulter.

Histology, imaging and analysis

Spleen were fixed in 4% paraformaldehyde for 24 hours, embedded in paraffin, and 5 μm sections were stained with hematoxylin and eosin (H&E). TA and gastrocnemius muscles were frozen in liquid nitrogen-cooled isopentane and 8 μm sections were stained with H&E to assess fiber morphology and nuclei internalization. All sections were imaged using Nanozoomer 2HT slide scanner (Hamamatsu, Japan).

To assess megakaryocyte number, random images were selected representing 12.3 mm^2 per spleen and megakaryocytes counted using ImageJ Cell Counter plugin. Myofiber segmentation was performed using Cellpose segmentation algorithm[63] and MinFeret diameter calculated using ImageJ. Fibers with internalized nuclei were counted using Cell Counter ImageJ plugin.

For immunofluorescence, 8 μm TA sections were incubated with 1/50 mouse anti-embryonic myosin heavy chain (F1.652, DHSB, Iowa City, USA), 1/250 Cy3-coupled goat anti-mouse (115-545-205), and nuclei and sarcolemma were stained with 1/2000 DAPI and 1/250 Wheat Germ Agglutinin, Alexa Fluor^{TM} 647 conjugate (ThermoFisher Scientific, Waltham, USA). Images were recorded using Zeiss Axioserver microscope (Zeiss, Oberkochen, Germany) and regenerative fibers were counted using Cell Counter ImageJ plugin.

Gene expression studies

RNA from TA was extracted using TRI Reagent (Molecular Research Center, Cincinnati, USA) and diluted in ultrapure water. For quantitative PCR (RT-qPCR), cDNA synthesis was performed with SuperScriptTM IV Transcriptase (ThermoFisher Scientific, Waltham, USA) and amplified using SYBR Green Master Mix I (Roche Diagnostics, Basel, Switzerland) and 0.1 µM forward and reverse primers (Table S1). Primers specificity was determined through melting curve products and Sanger-sequencing of PCR products. *Rpl27* gene was used as reference gene[64].

For RNAseq, library preparation was performed with the TruSeq Stranded mRNA Sample Preparation Kit (Illumina, San Diego, USA), and samples were single-end sequenced on a HiSeq4000 (Illumina). Raw data were preprocessed using cutadapt (https://doi.org/10.14806/ej.17.1.200), and reads with a Phred quality score above 20 and covering at least 40 nucleotides were mapped onto the mouse genome mm10 assembly using STAR[65]. Gene expression was quantified using htseq-count[66] with annotations from Ensembl (http://www.ensembl.org/index.html) and union mode, and normalized with DESeq2[67]. For the establishment of sample-to-sample distances heatmaps, hierarchical clustering was performed using the complete linkage algorithm. GO analysis were performed with ClusterProfiler[68] using the overrepresentation analysis and the Benjamini–Hochberg correction for multiple testing. Enrichments with a corrected p-value < 0.05 were considered significant[68].

Protein expression studies

TA cryosections were lysed in radio immunoprecipitation (RIPA) buffer supplemented with 1 mM PMSF, 1 mM DTT and complete mini EDTA-free protease inhibitor cocktail (Roche). 10 µg of denaturated proteins in 5X Lane Marker Reducing buffer (ThermoFischer Scientific) were loaded

459 in 10% or 15% SDS-PAGE gel. Gel was run and transferred to nitrocellulose membrane using

460 Transblot® TurboTM RTA Transfert Kit (Biorad, Hercules, USA) and protein loading controlled

461 using Ponceau S staining (Sigma-Aldrich, St Louis, USA). Membranes were blocked for 1h in

462 Tris-buffered saline buffer containing 5% of non-fat milk and 0.1% of Tween 20. 1/1000 mouse

463 anti-ORAI1 (sc-377281, Santa Cruz Biotechnology, Dallas, USA) and 1/10000 peroxidase-

464 coupled goat anti-mouse (115-036-068, Jackson ImmunoResearch) were used as primary and

465 secondary antibodies, respectively. Images were recorded with the Amersham Imager 600

466 (Amersham, UK).

467 **Statistical analysis**

468 All experiments were performed and analyzed in a blinded manner and the investigators were

469 unaware of the genotype of the mice. The significance of the birth ratio differences was assessed

470 by chi-square test. The normal distribution of the data was assessed using the Shapiro-Wilk test

471 and presented as mean ± standard error of the mean (SEM). For normally distributed data by one-

472 way ANOVA followed by Tukey's post hoc test. In case of not-normally distributed data, Kruskal-

473 Wallis followed by Dunn's multiple comparison test was used. The significant difference of birth

474 ratio was assessed by chi-square test. Two-way ANOVA followed by Tukey's post hoc test was

475 used for body weight and hanging time evolution, and force-frequency studies. Significant

476 differences are illustrated as *P<0.05, **P<0.01, ***P<0.001 and ****P<0.0001. * for

477 comparisons with WT group, α for comparisons with *Orai1$^{R93W/+}$* group and $ for comparisons

478 with *Stim1$^{R304W/+}$* group.

479

480

AUTHOR CONTRIBUTIONS

RSR, and LPG performed the experiments, RSR, SD, AS, LPG, JL, and JB analyzed the data, RSR, SD, JL and JB designed and coordinated the study, RSR and JB drafted the manuscript.

DATA AVAILABILITY STATEMENT

The authors confirm that the data supporting the findings of this study are available within the article and its supplementary materials.

CONFLICTS OF INTEREST

None of the authors declares conflict of interest.

REFERENCES

1. Stathopulos, P.B., and Ikura, M. (2017). Store operated calcium entry: From concept to structural mechanisms. Cell Calcium 63, 3-7.
2. Stathopulos, P.B., Zheng, L., Li, G.Y., Plevin, M.J., and Ikura, M. (2008). Structural and mechanistic insights into STIM1-mediated initiation of store-operated calcium entry. Cell 135, 110-122.
3. Prakriya, M., and Lewis, R.S. (2015). Store-Operated Calcium Channels. Physiol Rev 95, 1383-1436.
4. Silva-Rojas, R., Laporte, J., and Bohm, J. (2020). STIM1/ORAI1 Loss-of-Function and Gain-of-Function Mutations Inversely Impact on SOCE and Calcium Homeostasis and Cause Multi-Systemic Mirror Diseases. Front Physiol 11, 604941.
5. Lacruz, R.S., and Feske, S. (2015). Diseases caused by mutations in ORAI1 and STIM1. Ann N Y Acad Sci 1356, 45-79.
6. Bohm, J., and Laporte, J. (2018). Gain-of-function mutations in STIM1 and ORAI1 causing tubular aggregate myopathy and Stormorken syndrome. Cell Calcium 76, 1-9.
7. Morin, G., Biancalana, V., Echaniz-Laguna, A., Noury, J.B., Lornage, X., Moggio, M., Ripolone, M., Violano, R., Marcorelles, P., Marechal, D., et al. (2020). Tubular aggregate myopathy and Stormorken syndrome: Mutation spectrum and genotype/phenotype correlation. Hum Mutat 41, 17-37.
8. Baba, Y., Nishida, K., Fujii, Y., Hirano, T., Hikida, M., and Kurosaki, T. (2008). Essential function for the calcium sensor STIM1 in mast cell activation and anaphylactic responses. Nat Immunol 9, 81-88.
9. Oh-Hora, M., Yamashita, M., Hogan, P.G., Sharma, S., Lamperti, E., Chung, W., Prakriya, M., Feske, S., and Rao, A. (2008). Dual functions for the endoplasmic reticulum calcium sensors STIM1 and STIM2 in T cell activation and tolerance. Nat Immunol 9, 432-443.
10. Cordero-Sanchez, C., Riva, B., Reano, S., Clemente, N., Zaggia, I., Ruffinatti, F.A., Potenzieri, A., Pirali, T., Raffa, S., Sangaletti, S., et al. (2019). A luminal EF-hand mutation in STIM1 in mice causes the clinical hallmarks of tubular aggregate myopathy. Dis Model Mech 13.
11. Grosse, J., Braun, A., Varga-Szabo, D., Beyersdorf, N., Schneider, B., Zeitlmann, L., Hanke, P., Schropp, P., Muhlstedt, S., Zorn, C., et al. (2007). An EF hand mutation in Stim1 causes premature platelet activation and bleeding in mice. J Clin Invest 117, 3540-3550.
12. Silva-Rojas, R., Treves, S., Jacobs, H., Kessler, P., Messaddeq, N., Laporte, J., and Bohm, J. (2019). STIM1 over-activation generates a multi-systemic phenotype affecting the skeletal muscle, spleen, eye, skin, bones and immune system in mice. Hum Mol Genet 28, 1579-1593.
13. Bergmeier, W., Oh-Hora, M., McCarl, C.A., Roden, R.C., Bray, P.F., and Feske, S. (2009). R93W mutation in Orai1 causes impaired calcium influx in platelets. Blood 113, 675-678.
14. Hou, X., Pedi, L., Diver, M.M., and Long, S.B. (2012). Crystal structure of the calcium release-activated calcium channel Orai. Science 338, 1308-1313.
15. McCarl, C.A., Khalil, S., Ma, J., Oh-hora, M., Yamashita, M., Roether, J., Kawasaki, T., Jairaman, A., Sasaki, Y., Prakriya, M., et al. (2010). Store-operated Ca2+ entry through ORAI1 is critical for T cell-mediated autoimmunity and allograft rejection. J Immunol 185, 5845-5858.
16. Muik, M., Fahrner, M., Schindl, R., Stathopulos, P., Frischauf, I., Derler, I., Plenk, P., Lackner, B., Groschner, K., Ikura, M., et al. (2011). STIM1 couples to ORAI1 via an intramolecular transition into an extended conformation. EMBO J 30, 1678-1689.
17. Bronte, V., and Pittet, M.J. (2013). The spleen in local and systemic regulation of immunity. Immunity 39, 806-818.
18. Misceo, D., Holmgren, A., Louch, W.E., Holme, P.A., Mizobuchi, M., Morales, R.J., De Paula, A.M., Stray-Pedersen, A., Lyle, R., Dalhus, B., et al. (2014). A dominant STIM1 mutation causes Stormorken syndrome. Hum Mutat 35, 556-564.

548 19. Morin, G., Bruechle, N.O., Singh, A.R., Knopp, C., Jedraszak, G., Elbracht, M., Bremond-Gignac, D.,
549 Hartmann, K., Sevestre, H., Deutz, P., et al. (2014). Gain-of-Function Mutation in STIM1
550 (P.R304W) Is Associated with Stormorken Syndrome. Hum Mutat 35, 1221-1232.
551 20. Nesin, V., Wiley, G., Kousi, M., Ong, E.C., Lehmann, T., Nicholl, D.J., Suri, M., Shahrizaila, N.,
552 Katsanis, N., Gaffney, P.M., et al. (2014). Activating mutations in STIM1 and ORAI1 cause
553 overlapping syndromes of tubular myopathy and congenital miosis. Proc Natl Acad Sci U S A 111,
554 4197-4202.
555 21. Silva-Rojas, R., Charles, A.-L., Djeddi, S., Geny, B., Laporte, J., and Böhm, J. (2021).
556 Pathophysiological Effects of Overactive STIM1 on Murine Muscle Function and Structure. Cells
557 10, 1730.
558 22. Bohm, J., Bulla, M., Urquhart, J.E., Malfatti, E., Williams, S.G., O'Sullivan, J., Szlauer, A., Koch, C.,
559 Baranello, G., Mora, M., et al. (2017). ORAI1 Mutations with Distinct Channel Gating Defects in
560 Tubular Aggregate Myopathy. Hum Mutat 38, 426-438.
561 23. Bohm, J., Chevessier, F., Maues De Paula, A., Koch, C., Attarian, S., Feger, C., Hantai, D., Laforet, P.,
562 Ghorab, K., Vallat, J.M., et al. (2013). Constitutive activation of the calcium sensor STIM1 causes
563 tubular-aggregate myopathy. Am J Hum Genet 92, 271-278.
564 24. Lee, B., Palermo, G., and Machaca, K. (2013). Downregulation of store-operated Ca2+ entry during
565 mammalian meiosis is required for the egg-to-embryo transition. J Cell Sci 126, 1672-1681.
566 25. Wakai, T., Vanderheyden, V., and Fissore, R.A. (2011). Ca2+ signaling during mammalian fertilization:
567 requirements, players, and adaptations. Cold Spring Harb Perspect Biol 3.
568 26. Blair, H.C., Robinson, L.J., Huang, C.L., Sun, L., Friedman, P.A., Schlesinger, P.H., and Zaidi, M.
569 (2011). Calcium and bone disease. Biofactors 37, 159-167.
570 27. Chen, Y., Ramachandran, A., Zhang, Y., Koshy, R., and George, A. (2018). The ER Ca(2+) sensor
571 STIM1 can activate osteoblast and odontoblast differentiation in mineralized tissues. Connect
572 Tissue Res 59, 6-12.
573 28. Eapen, A., Sundivakkam, P., Song, Y., Ravindran, S., Ramachandran, A., Tiruppathi, C., and George,
574 A. (2010). Calcium-mediated stress kinase activation by DMP1 promotes osteoblast differentiation.
575 J Biol Chem 285, 36339-36351.
576 29. Florencio-Silva, R., Sasso, G.R., Sasso-Cerri, E., Simoes, M.J., and Cerri, P.S. (2015). Biology of Bone
577 Tissue: Structure, Function, and Factors That Influence Bone Cells. Biomed Res Int 2015, 421746.
578 30. de Porto, A.P., Lammers, A.J., Bennink, R.J., ten Berge, I.J., Speelman, P., and Hoekstra, J.B. (2010).
579 Assessment of splenic function. Eur J Clin Microbiol Infect Dis 29, 1465-1473.
580 31. Lewis, S.M., Williams, A., and Eisenbarth, S.C. (2019). Structure and function of the immune system
581 in the spleen. Sci Immunol 4.
582 32. Harris, E., Burki, U., Marini-Bettolo, C., Neri, M., Scotton, C., Hudson, J., Bertoli, M., Evangelista, T.,
583 Vroling, B., Polvikoski, T., et al. (2017). Complex phenotypes associated with STIM1 mutations
584 in both coiled coil and EF-hand domains. Neuromuscul Disord 27, 861-872.
585 33. Noury, J.B., Bohm, J., Peche, G.A., Guyant-Marechal, L., Bedat-Millet, A.L., Chiche, L., Carlier, R.Y.,
586 Malfatti, E., Romero, N.B., and Stojkovic, T. (2017). Tubular aggregate myopathy with features of
587 Stormorken disease due to a new STIM1 mutation. Neuromuscul Disord 27, 78-82.
588 34. Parekh, C., and Crooks, G.M. (2013). Critical differences in hematopoiesis and lymphoid development
589 between humans and mice. J Clin Immunol 33, 711-715.
590 35. Schmitt, A., Guichard, J., Masse, J.M., Debili, N., and Cramer, E.M. (2001). Of mice and men:
591 comparison of the ultrastructure of megakaryocytes and platelets. Exp Hematol 29, 1295-1302.
592 36. Markello, T., Chen, D., Kwan, J.Y., Horkayne-Szakaly, I., Morrison, A., Simakova, O., Maric, I.,
593 Lozier, J., Cullinane, A.R., Kilo, T., et al. (2015). York platelet syndrome is a CRAC channelopathy
594 due to gain-of-function mutations in STIM1. Mol Genet Metab 114, 474-482.
595 37. Alansary, D., Bogeski, I., and Niemeyer, B.A. (2015). Facilitation of Orai3 targeting and store-operated
596 function by Orai1. Biochim Biophys Acta 1853, 1541-1550.

597 38. Berna-Erro, A., Galan, C., Dionisio, N., Gomez, L.J., Salido, G.M., and Rosado, J.A. (2012).
598   Capacitative and non-capacitative signaling complexes in human platelets. Biochim Biophys Acta
599   1823, 1242-1251.
600 39. Bohm, J., Chevessier, F., Koch, C., Peche, G.A., Mora, M., Morandi, L., Pasanisi, B., Moroni, I., Tasca,
601   G., Fattori, F., et al. (2014). Clinical, histological and genetic characterisation of patients with
602   tubular aggregate myopathy caused by mutations in STIM1. J Med Genet 51, 824-833.
603 40. Begam, M., Abro, V.M., Mueller, A.L., and Roche, J.A. (2016). Sodium 4-phenylbutyrate reduces
604   myofiber damage in a mouse model of Duchenne muscular dystrophy. Appl Physiol Nutr Metab
605   41, 1108-1111.
606 41. Lee, C.S., Hanna, A.D., Wang, H., Dagnino-Acosta, A., Joshi, A.D., Knoblauch, M., Xia, Y., Georgiou,
607   D.K., Xu, J., Long, C., et al. (2017). A chemical chaperone improves muscle function in mice with
608   a RyR1 mutation. Nat Commun 8, 14659.
609 42. Michelucci, A., Garcia-Castaneda, M., Boncompagni, S., and Dirksen, R.T. (2018). Role of
610   STIM1/ORAI1-mediated store-operated Ca(2+) entry in skeletal muscle physiology and disease.
611   Cell Calcium 76, 101-115.
612 43. Zhao, X., Moloughney, J.G., Zhang, S., Komazaki, S., and Weisleder, N. (2012). Orai1 mediates
613   exacerbated Ca(2+) entry in dystrophic skeletal muscle. PLoS One 7, e49862.
614 44. Goonasekera, S.A., Davis, J., Kwong, J.Q., Accornero, F., Wei-LaPierre, L., Sargent, M.A., Dirksen,
615   R.T., and Molkentin, J.D. (2014). Enhanced Ca(2)(+) influx from STIM1-Orai1 induces muscle
616   pathology in mouse models of muscular dystrophy. Hum Mol Genet 23, 3706-3715.
617 45. Wei-Lapierre, L., Carrell, E.M., Boncompagni, S., Protasi, F., and Dirksen, R.T. (2013). Orai1-
618   dependent calcium entry promotes skeletal muscle growth and limits fatigue. Nat Commun 4, 2805.
619 46. Yang, L., Tautz, T., Zhang, S., Fomina, A., and Liu, H. (2019). The current status of malignant
620   hyperthermia. J Biomed Res 34, 75-85.
621 47. Yarotskyy, V., Protasi, F., and Dirksen, R.T. (2013). Accelerated activation of SOCE current in
622   myotubes from two mouse models of anesthetic- and heat-induced sudden death. PLoS One 8,
623   e77633.
624 48. Eltit, J.M., Ding, X., Pessah, I.N., Allen, P.D., and Lopez, J.R. (2013). Nonspecific sarcolemmal cation
625   channels are critical for the pathogenesis of malignant hyperthermia. FASEB J 27, 991-1000.
626 49. Bakowski, D., Murray, F., and Parekh, A.B. (2021). Store-Operated Ca(2+) Channels: Mechanism,
627   Function, Pharmacology, and Therapeutic Targets. Annu Rev Pharmacol Toxicol 61, 629-654.
628 50. Bonnefond, M.L., Florent, R., Lenoir, S., Lambert, B., Abeilard, E., Giffard, F., Louis, M.H., Elie, N.,
629   Briand, M., Vivien, D., et al. (2018). Inhibition of store-operated channels by carboxyamidotriazole
630   sensitizes ovarian carcinoma cells to anti-BclxL strategies through Mcl-1 down-regulation.
631   Oncotarget 9, 33896-33911.
632 51. Miller, J., Bruen, C., Schnaus, M., Zhang, J., Ali, S., Lind, A., Stoecker, Z., Stauderman, K., and Hebbar,
633   S. (2020). Auxora versus standard of care for the treatment of severe or critical COVID-19
634   pneumonia: results from a randomized controlled trial. Crit Care 24, 502.
635 52. Bartoli, F., Bailey, M.A., Rode, B., Mateo, P., Antigny, F., Bedouet, K., Gerbaud, P., Gosain, R., Plante,
636   J., Norman, K., et al. (2020). Orai1 Channel Inhibition Preserves Left Ventricular Systolic Function
637   and Normal Ca(2+) Handling After Pressure Overload. Circulation 141, 199-216.
638 53. Di Sabatino, A., Rovedatti, L., Kaur, R., Spencer, J.P., Brown, J.T., Morisset, V.D., Biancheri, P.,
639   Leakey, N.A., Wilde, J.I., Scott, L., et al. (2009). Targeting gut T cell Ca2+ release-activated Ca2+
640   channels inhibits T cell cytokine production and T-box transcription factor T-bet in inflammatory
641   bowel disease. J Immunol 183, 3454-3462.
642 54. Ramos, S., Grigoryev, S., Rogers, E., Roos, J., Whitten, J., Stauderman, K., and Velicelebi, G. (2012).
643   CM3457, a potent and selective oral CRAC channel inhibitor, suppresses T and mast cell function
644   and is efficacious in rat models of arthritis and asthma. Journal of Immunology 188.
645 55. Riva, B., Griglio, A., Serafini, M., Cordero-Sanchez, C., Aprile, S., Di Paola, R., Gugliandolo, E.,
646   Alansary, D., Biocotino, I., Lim, D., et al. (2018). Pyrtriazoles, a Novel Class of Store-Operated

647   Calcium Entry Modulators: Discovery, Biological Profiling, and in Vivo Proof-of-Concept
648   Efficacy in Acute Pancreatitis. J Med Chem 61, 9756-9783.
649 56. Shawer, H., Norman, K., Cheng, C.W., Foster, R., Beech, D.J., and Bailey, M.A. (2021). ORAI1 Ca(2+)
650   Channel as a Therapeutic Target in Pathological Vascular Remodelling. Front Cell Dev Biol 9,
651   653812.
652 57. Cox, J.H., Hussell, S., Sondergaard, H., Roepstorff, K., Bui, J.V., Deer, J.R., Zhang, J., Li, Z.G.,
653   Lamberth, K., Kvist, P.H., et al. (2013). Antibody-mediated targeting of the Orai1 calcium channel
654   inhibits T cell function. PLoS One 8, e82944.
655 58. Gaida, K., Salimi-Moosavi, H., Subramanian, R., Almon, V., Knize, A., Zhang, M., Lin, F.F., Nguyen,
656   H.Q., Zhou, L., Sullivan, J.K., et al. (2015). Inhibition of CRAC with a human anti-ORAI1
657   monoclonal antibody inhibits T-cell-derived cytokine production but fails to inhibit a T-cell-
658   dependent antibody response in the cynomolgus monkey. J Immunotoxicol 12, 164-173.
659 59. Lin, F.F., Elliott, R., Colombero, A., Gaida, K., Kelley, L., Moksa, A., Ho, S.Y., Bykova, E., Wong,
660   M., Rathanaswami, P., et al. (2013). Generation and characterization of fully human monoclonal
661   antibodies against human Orai1 for autoimmune disease. J Pharmacol Exp Ther 345, 225-238.
662 60. Liu, S., Hasegawa, H., Takemasa, E., Suzuki, Y., Oka, K., Kiyoi, T., Takeda, H., Ogasawara, T.,
663   Sawasaki, T., Yasukawa, M., et al. (2017). Efficiency and Safety of CRAC Inhibitors in Human
664   Rheumatoid Arthritis Xenograft Models. J Immunol 199, 1584-1595.
665 61. Gonzalez, V., Paneda, C., Martinez, T., Guerra, A., Monteiro, S., Vargas, B., Bleau, A.M., Ruz, V., and
666   Jimenez, A.I. (2018). Development of a RNAi therapeutic for the treatment of allergic
667   conjunctivitis. Invest Ophth Vis Sci 59.
668 62. Jimenez, A.I., Martinez, T., Gonzalez, V., Martinez-Garcia, C., and Paneda, C. (2015). Development
669   of a RNAi therapeutic for the treatment of allergic conjunctivitis. Invest Ophth Vis Sci 56.
670 63. Stringer, C., Wang, T., Michaelos, M., and Pachitariu, M. (2021). Cellpose: a generalist algorithm for
671   cellular segmentation. Nat Methods 18, 100-106.
672 64. Thomas, K.C., Zheng, X.F., Garces Suarez, F., Raftery, J.M., Quinlan, K.G., Yang, N., North, K.N.,
673   and Houweling, P.J. (2014). Evidence based selection of commonly used RT-qPCR reference genes
674   for the analysis of mouse skeletal muscle. PLoS One 9, e88653.
675 65. Dobin, A., Davis, C.A., Schlesinger, F., Drenkow, J., Zaleski, C., Jha, S., Batut, P., Chaisson, M., and
676   Gingeras, T.R. (2013). STAR: ultrafast universal RNA-seq aligner. Bioinformatics 29, 15-21.
677 66. Anders, S., Pyl, P.T., and Huber, W. (2015). HTSeq--a Python framework to work with high-throughput
678   sequencing data. Bioinformatics 31, 166-169.
679 67. Love, M.I., Huber, W., and Anders, S. (2014). Moderated estimation of fold change and dispersion for
680   RNA-seq data with DESeq2. Genome Biol 15, 550.
681 68. Yu, G., Wang, L.G., Han, Y., and He, Q.Y. (2012). clusterProfiler: an R package for comparing
682   biological themes among gene clusters. OMICS 16, 284-287.
683
684
685
686
687

A

$Stim1^{R304W/+}$ $Orai1^{R93W/+}$

WT $Orai1^{R93W/+}$ $Stim1^{R304W/+}$ $Stim1^{R304W/+}Orai1^{R93W/+}$

B *Orai1*

C ORAI1

D
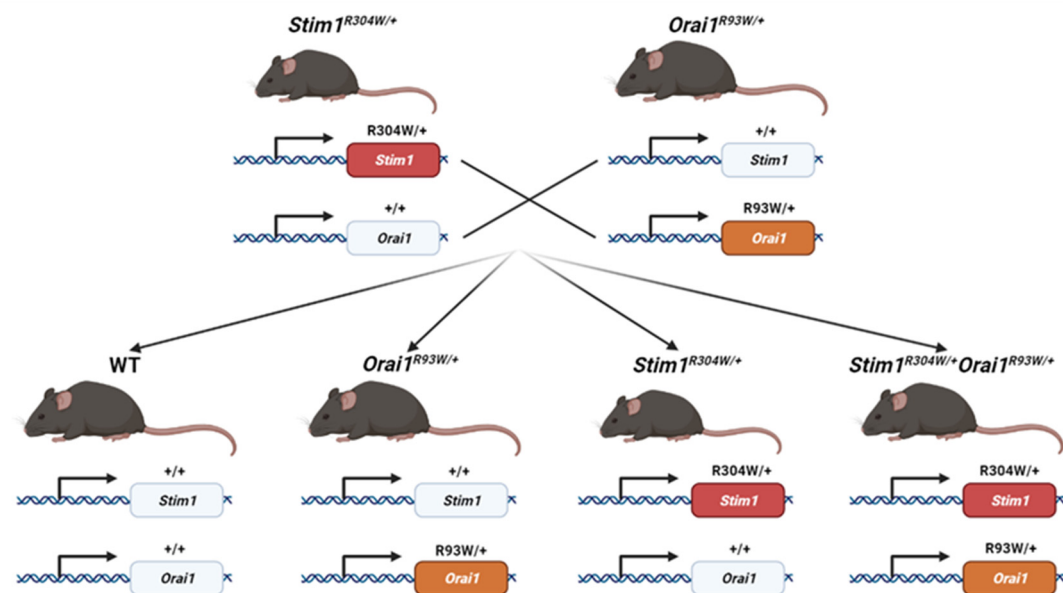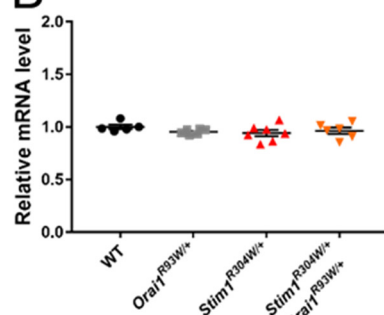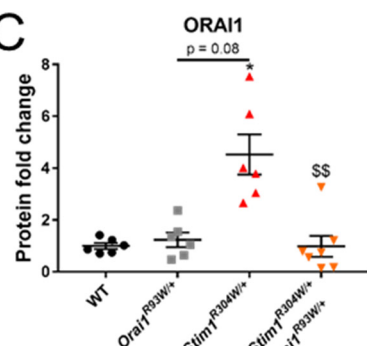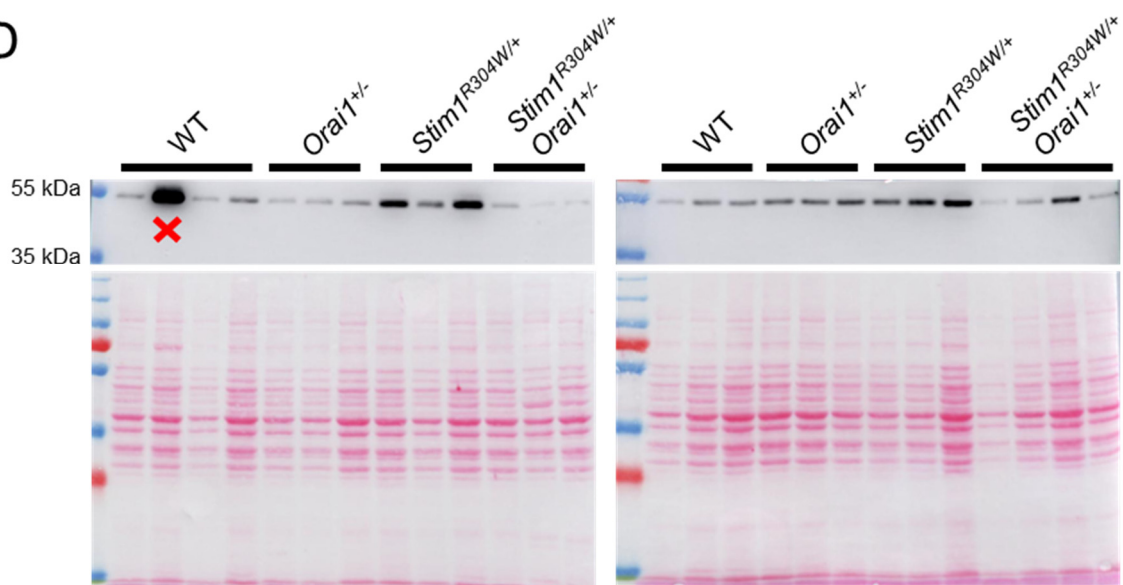
Supplemental Figure S1. ORAI1 R91W mutant reduced ORAI1 accumulation. (A) Crossing of $Stim1^{R304W/+}$ and $Orai1^{R93W/+}$ mice resulted in four genotypes: WT, $Orai1^{R93W/+}$, $Stim1^{R304W/+}$, and $Stim1^{R304W/+}Orai1^{R93/W+}$. (B-C) Orai1 expression was unaltered in the four groups while ORAI1 protein accumulated in $Stim1^{R304W/+}$ muscle extracts and was normalized in $Stim1^{R304W/+}Orai1^{R93/W+}$ mice at 4 months (n=6-7). (D) Western blots of ORAI1 on muscle extracts from the 4 groups and Ponceau S staining as loading control. The lane marked with a red cross was considered as an outlier and removed from the statistical study. Graphs represent mean ± SEM. Significant differences are indicated as */α/\$ $P<0.05$, **/αα/\$\$ $P<0.01$, ***/ααα/\$\$\$ $P<0.001$, and ****/αααα/\$\$\$\$ $P<0.0001$ with * reflecting the comparison with the WT group, α the comparison with the $Orai1^{R93W/+}$ group, and \$ for the comparison between $Stim1^{R304W/+}$ and $Stim1^{R304W/+}Orai1^{R93W/+}$ group.
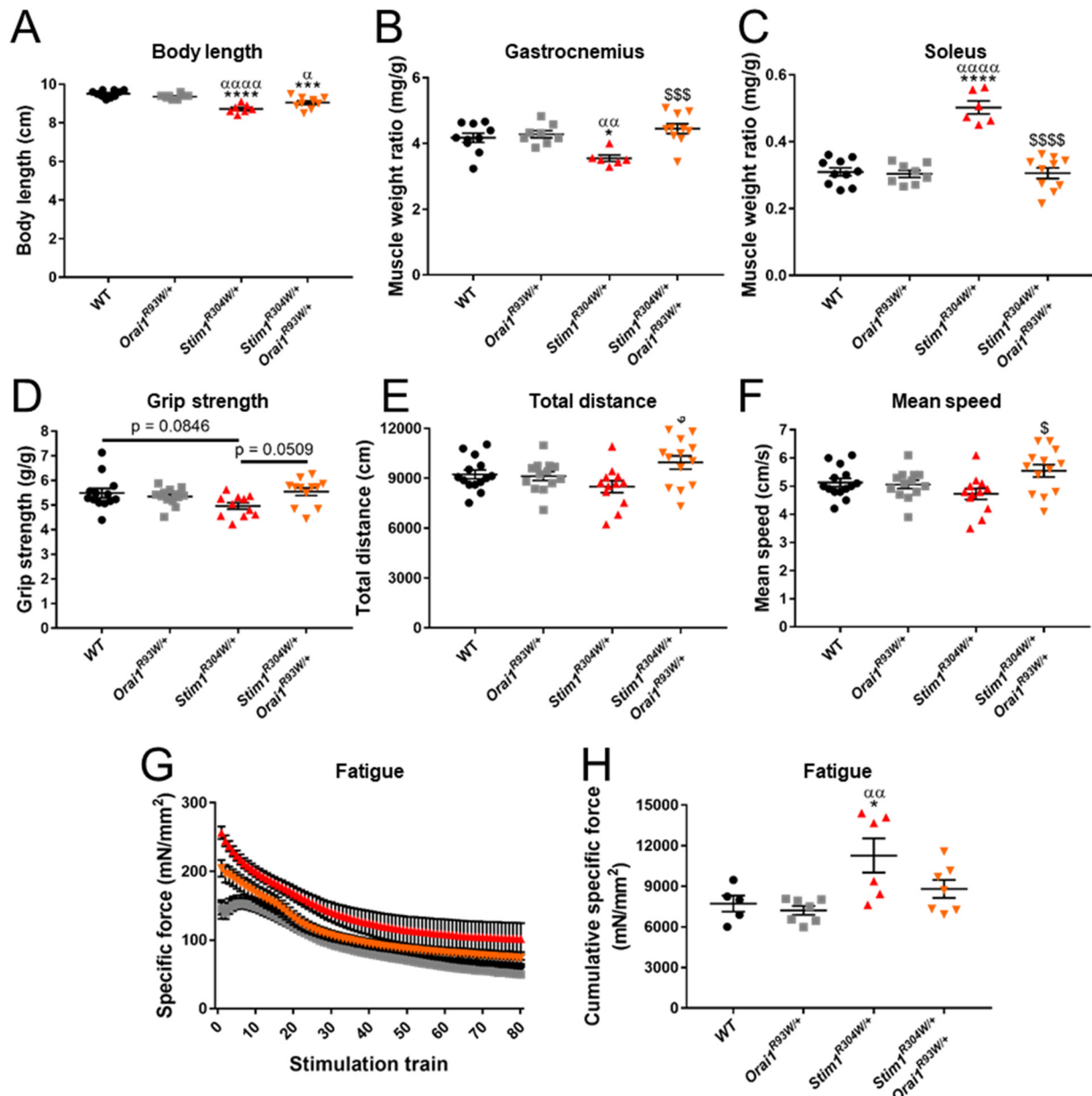
Supplemental Figure S2. Body length and muscle weight and performance were improved in *Stim1^{R304W/+}Orai1^{R93W/+}* mice. (A-C) Body length was bigger and muscle to weight ratio of gastrocnemius and soleus were restored in *Stim1^{R304W/+}Orai1^{R93W/+}* mice compared to *Stim1^{R304W/+}Orai1^{R93W/+}* littermates at 4 months (n=6-10). (D-F) Grip strength at 2 months had a tendency to increase and distance covered and speed were increased in *Stim1^{R304W/+}Orai1^{R93W/+}* mice compared to *Stim1^{R304W/+}* mice at 10 weeks (n=11-14). (G-H) Force produced during 80 consecutive 40 Hz stimulations and its addition showed a different mean curve and a tendency to decrease in *Stim1^{R304W/+}Orai1^{R93W/+}* mice compared to *Stim1^{R304W/+}* mice, respectively (n=5-7). Graphs represent mean ± SEM.
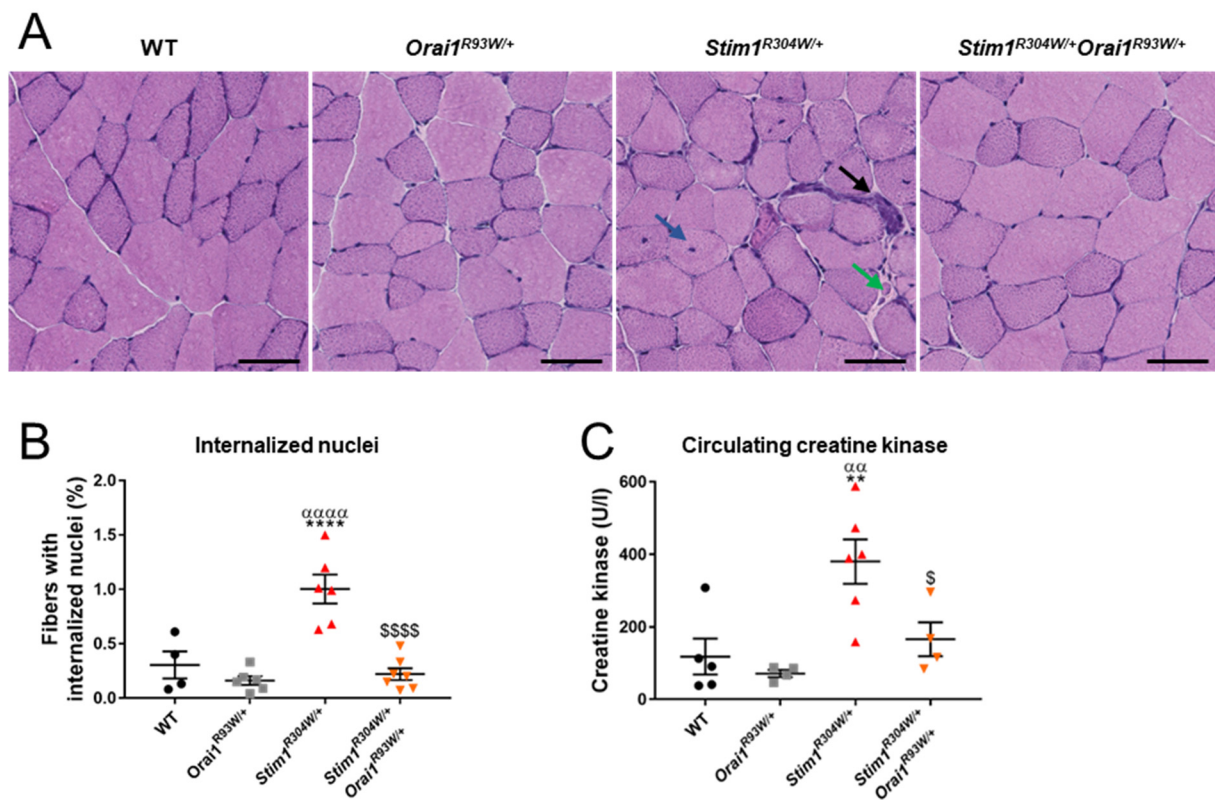
710

Supplemental Figure S3. Rescued muscle degeneration in *Stim1$^{R304W/+}$Orai1$^{R93W/+}$* mice. (A) H&E staining on gastrocnemius sections from both *Stim1$^{R304W/+}$* revealed fibers with internalized nuclei (blue arrow), regenerating fibers (green arrow) and infiltration of immune cells (black arrow). Scale bar = 50 μm. (B-C) The rate of fibers with internalized nuclei in gastrocnemius sections and the circulating blood creatine kinase were reduced in *Stim1$^{R304W/+}$Orai1$^{R93W/+}$* compared to *Stim1$^{R304W/+}$* mice (n=4-6). Graphs represent mean ± SEM. Significant differences are indicated as */α/$ P<0.05, **/αα/$$ P<0.01, ***/ααα/$$$ P<0.001, and ****/αααα/$$$$ P<0.0001 with * reflecting the comparison with the WT group, α the comparison with the *Orai1$^{R93W/+}$* group, and $ for the comparison between *Stim1$^{R304W/+}$* and *Stim1$^{R304W/+}$Orai1$^{R93W/+}$* group.
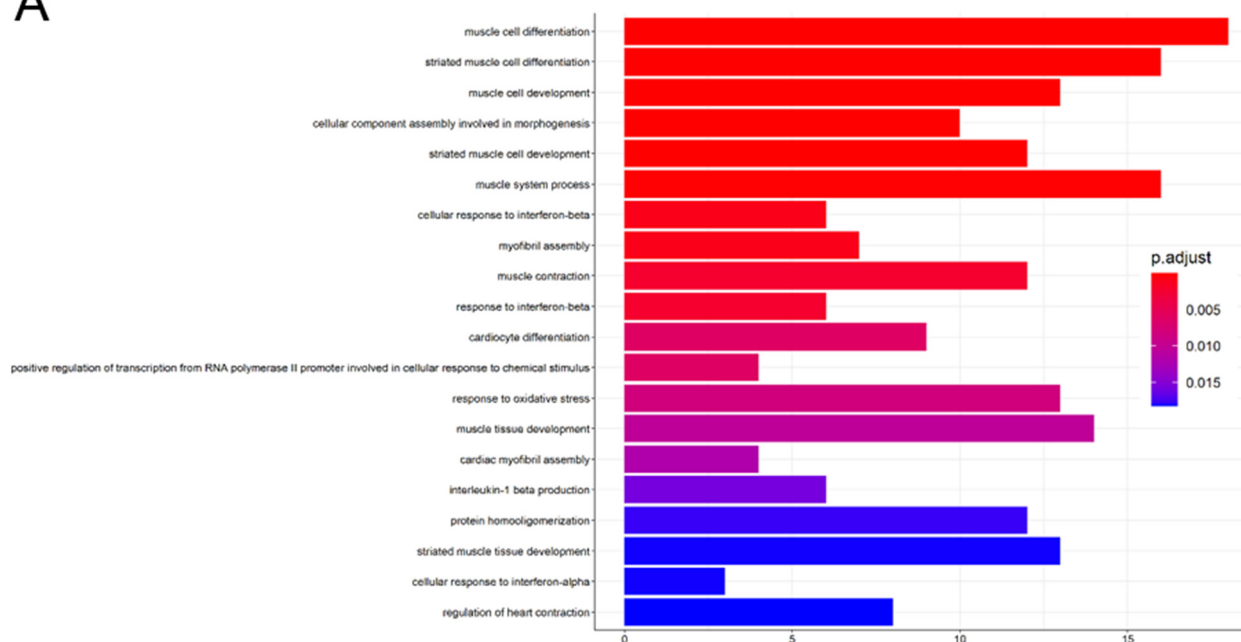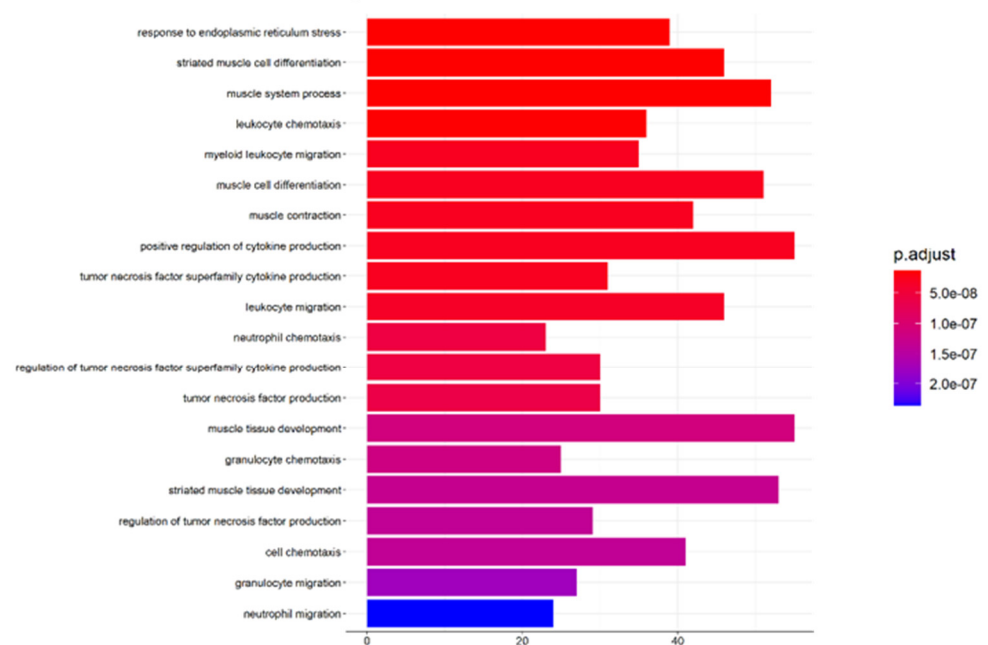
Supplemental Figure S4. GO enrichments of *Orai1* silencing and ORAI1 inhibition. (A-B) Classification of the dysregulated genes in *Stim1$^{R304W/+}$* mice with improved expression in *Stim1$^{R304W/+}$Orai1$^{+/-}$* mice (*Orai1* silencing) and *Stim1$^{R304W/+}$Orai1$^{R93W/+}$* mice (ORAI1 inhibition) into GO terms revealed a common implication of genes associated

723 | to muscle contraction and differentiation, while ORAI1 inhibition was characterized by improved expression of

724 | immune-related terms and the response to endoplasmic reticulum stress (n=4).

725

726 | **Supplemental Table S1. List of primers used for RT-qPCR**

Gene	Forward primer	Reverse primer
Rpl27	AAGCCGTCATCGTGAAGAACA	CTTGATCTTGGATCGCTTGGC
Orai1	GCCAAGCTCAAAGCTTCC	CCTGGTGGGTAGTCATGGTC
Hspa5	CTATTCCTGCGTCGGTGTGT	ATTCCAAGTGCGTCCGATGA
Hspb90b1	CCACTCAAATCGAACACGGC	AGATTCCGCCTCCTTTCTGC

727

728 | **Supplemental Table S2. Trabecular bone parameters of femur.**

	BV/TV (%)	Tb.Th (μm)	Tb.N (1/mm)	Tb.Sp (μm)
WT	5.48 ± 1.03	66.08 ± 3.70	0.80 ± 0.13	455.13 ± 29.63
Orai1$^{R93W/+}$	3.44 ± 0.44	63.39 ± 2.20	0.54 ± 0.06	538.69 ± 37.32
Stim1$^{R304W/+}$	0.40 ± 0.10	49.66 ± 2.25	0.08 ± 0.02	770.95 ± 11.96
Stim1$^{R304W/+}$Orai1$^{R93W/+}$	3.55 ± 0.78	66.95 ± 2.99	0.51 ± 0.10	555.80 ± 43.69
p value disease vs therapy	0.0257	0.0012	0.0564	0.0393

729

730

DISCUSSION AND PERSPECTIVES

During my PhD, I contributed to a better understanding of TAM/STRMK pathophysiology by characterizing a new **mouse model for TAM/STRMK** carrying the STIM1 p.R304W mutation (Results Part 1) (Silva-Rojas et al., 2019), and I further studied the **negative effects of elevated cytosolic Ca^{2+}** on the muscle physiology of $Stim1^{R304W/+}$ mice (Results Part 2) (Silva-Rojas et al., 2021). The second part of my PhD aimed to test **ORAI1 as a therapeutic target for TAM/STRMK**. I crossed $Stim1^{R304W/+}$ with mice expressing 50% of $Orai1$ and observed an amelioration of the overall TAM/STRMK phenotype. To generate a translational approach I performed intramuscular injections of AAVs containing shRNAs targeting and reducing $Orai1$ expression by up to 80%, and I noted improved muscle contraction and relaxation properties of $Stim1^{R304W/+}$ muscles (Results Part 3). Finally, the crossing of $Stim1^{R304W/+}$ with heterozygous mice harboring a ORAI1 channel blocking mutation revealed an even more important rescue degree and evidenced ORAI1 inhibition as the most efficient approach to treat TAM/STRMK (Results Part 4).

1. AVAILABLE TAM/STRMK MOUSE MODELS

TAM/STRMK forms a clinical continuum encompassing muscle weakness, cramps and myalgia, short stature, thrombocytopenia, hyposplenism, ichthyosis and miosis (Bohm and Laporte, 2018; Borsani et al., 2018; Morin et al., 2020). Muscle sections from TAM/STRMK patients display characteristic red aggregates in Gomori staining referred as tubular aggregates by their honeycomb-link structure of packed and parallel arrangement of tubules derived from sarcoplasmic reticulum (SR) (Bohm and Laporte, 2018; Chevessier et al., 2005). These structures are also reported in aging male mice and they possibly act as Ca^{2+} buffer to compensate cytosolic Ca^{2+} overload in TAM/STRMK and continuous Ca^{2+} stress in aging mice (more details in appendix TUBULAR AGGREGATES IN AGING AND DISEASE section) (Salviati et al., 1985; Silva-Rojas et al., 2020). Discrete signs of muscle degeneration are also reported in patients such as fibers with internalized nuclei in muscle histology and a moderate elevation in serum creatine kinase (Bohm et al., 2017; Bohm et al., 2013; Chevessier et al., 2005; Endo et al., 2015; Salviati

et al., 1985). TAM/STRMK is caused by GoF mutations in *STIM1* and *ORAI1* that result in excessive extracellular Ca^{2+} entry via ORAI1.

The STIM1 exons encoding the EF-hand domain represent a mutation hotspot. These mutations directly or indirectly impair Ca^{2+} sensing and lead to constitutive STIM1 oligomerization and ORAI1 activation (Schober et al., 2019). The STIM1 Arg304 residue locates in the cytosolic CC1 domain and the amino acid change to tryptophan is the most recurrent TAM/STRMK mutation. The mutation destabilizes the CC1-CC3 interaction in the resting state facilitating the STIM1 elongation, oligomerization and constitutive ORAI1 activation (Fahrner et al., 2018). Genotype/phenotype correlation studies showed that EF-hand mutations primarily impacted the skeletal muscle while p.R304W had bigger impact on platelets and spleen than skeletal muscle (Bohm and Laporte, 2018; Morin et al., 2020). This difference could not be explained by different degree of ORAI1 activation and Ca^{2+} entry (Peche et al., 2020), and may rather be explained by a pathogenic effect of p.R304W mutation on the interaction with other STIM1 partners in the affected tissues. *ORAI1* missense mutations are found in all four transmembrane domains (TM) of ORAI1. While mutations affecting the pore-forming TM1 generate a leaky channel with constant Ca^{2+} influx, mutations affecting the TM2-TM4 are less severe since they render the channel over-active upon stimulation through STIM1 (Bohm and Laporte, 2018; Morin et al., 2020).

Recently, several TAM/STRMK mouse models have been generated and extensively characterized to correlate the cellular defects with disease development, better understand the physiopathology underlying the multisystemic phenotype, and provide a tool for prospective preclinical trials of therapeutic approaches.

1.1. Mouse models with STIM1 luminal mutations

The first TAM/STRMK mouse model was generated by random mutagenesis using N-ethyl-N-nitrosourea with the aim of finding genes implicated in coagulation, and where a mouse line harboring the luminal STIM1 D84G mutation was identified. Homozygous mice died perinatally and heterozygous *Stim1*^(D84G/+) animals presented reduced platelet counts and increased bleeding time. *Stim1*^(D84G/+) platelets had a higher mean volume, indicating increased platelet removal and

possibly contributing to the reduced life span. Although platelet activation markers were abnormally increased at the basal condition, thrombus formation was impaired, indicating that *Stim1^{D84G/+}* platelets were pre-activated and dysfunctional. This, together with the reduced platelet number, would account for the increased bleeding tendency observed in *Stim1^{D84G/+}* mice. *Stim1^{D84G/+}* mice further presented with splenomegaly, and splenectomy only slightly improved the average platelet half time, suggesting that platelet death directly results from platelet pre-activation and does not reflect premature aging (Grosse et al., 2007). Other potential phenotypes affecting the stature, eyes, skin or the skeletal muscle were not assessed in *Stim1^{D84G/+}* mice (Table 3).

Another TAM/STRMK mouse model, carrying a luminal STIM1 I115F mutation (c.343A>T), was recently generated and characterized through a broad panel of phenotypical tests. *Stim1^{I115F/+}* mice were lighter and weaker than their WT littermates, and the analysis of muscle sections revealed swollen mitochondria and dystrophic signs such as immune cell infiltrations, fibers with internalized nuclei and increased presence of endomysial tissue. Tubular aggregates, the main histological hallmark in TAM/STRMK patients, were however absent in *Stim1^{I115F/+}* muscles. Moreover, *Stim1^{I115F/+}* mice manifested thrombocytopenia and increased bleeding times, and blood analysis revealed anomalies in monocyte differentiation and reduced nuclear killer cell counts. The mice also showed an increased spleen size (Cordero-Sanchez et al., 2019), which contrasts with the hyposplenism in TAM/STRMK patients and may be associated with physiological or functional divergences between humans and mice (Bronte and Pittet, 2013). Eye and skin anomalies were not assessed in *Stim1^{I115F/+}* mice (Table 3).

An unpublished *Stim1^{H109Q/+}* mice was presented at the 24th International Annual Congress of the World Muscle Society in Copenhagen (https://doi.org/10.1016/j.nmd.2019.06.168), and reportedly exhibited muscle weakness and atrophy with reduced fiber size and the presence of dystrophic signs including internalized nuclei, endomysial fibrosis and elevated serum creatine kinase levels. Tubular aggregates were not present, and potential platelets, spleen, skin and body size defects were not referred (Table 3).

Table 3. Comparison of clinical signs of TAM/STRMK patients and mouse models.

Tissue	Patients	$Stim1^{D84G/+}$	$Stim1^{H109Q/+}$	$Stim1^{I115F/+}$	$Stim1^{R304W/+}$	$Orai1^{G100S/+}$
Stature	Smaller	-	-	Smaller	Smaller	-
Eye	Miosis Gaze paresis	-	-	-	Gaze paresis	-
Skin	Ichthyosis	-	-	-	Reduced fat layer	-
Spleen	Hyposplenia	Splenomegaly	-	Splenomegaly	Splenomegaly	-
Platelets	↓	-	-	↓	↓	-
Serum CK	↑	-	↑	↑	↑	Normal
Muscle degeneration	Discrete	-	YES	YES	YES	NO
Tubular aggregates	YES	-	NO	NO	NO	YES

1.2. Mouse models with STIM1 cytosolic mutations

The vast majority of the STIM1 mutations affect amino acids in the Ca^{2+}-sensing EF hand domains, and most were found in individual families. Outside the luminal segment of STIM1, only a single mutation spot has been reported to date, but the R304Q and especially R304W account for half of the TAM/STRMK cases (Bohm and Laporte, 2018; Morin et al., 2020). As a general rule, patients harboring the most common R304W mutation present the full clinical STRMK picture, while patients with EF-hand mutations are milder and essentially present with muscle weakness and less multi-systemic signs (Jiang et al., 2021; Morin et al., 2020; Silva-Rojas et al., 2020; Ticci et al., 2021). We generated $Stim1^{R304W/+}$ mice, and phenotypic characterization showed that the animals recapitulate the main clinical signs observed in patients. $Stim1^{R304W/+}$ mice were smaller and lighter than their WT littermates, developed skin layer anomalies and gaze paresis, and showed thrombocytopenia and splenomegaly. At the muscular level, $Stim1^{R304W/+}$ mice manifested muscle weakness associated with moderate muscle fiber degeneration and elevated circulating levels of creatine kinase. Tubular aggregates were absent and the mitochondria were swollen as in $Stim1^{I115F}$ mice (Cordero-Sanchez et al., 2019; Silva-Rojas et al., 2019) (Table 3). Our broad phenotypical

panel permitted the discovery of clinical signs not previously reported or assessed in patients. Bone structure and morphology were abnormal with reduced cellular density, potentially involving bone fragility. Circulating immune cell counts were altered with increased levels of neutrophils, monocytes, and reduced lymphocytes. Furthermore, spleen cell counts evidenced reduced numbers of nuclear killer cells and regulatory T cells. Blood plasma analyses revealed reduced levels of glucose resulting from elevated insulin, and elevated levels of liver transaminases as an indication of abnormal liver function (Silva-Rojas et al., 2019). Overall, $Stim1^{R304W/+}$ mice are a faithful model for TAM/STRMK, and our thorough phenotypic characterization of the animals uncovered additional anomalies of potential medical interest for patients.

In parallel to our $Stim1^{R304W/+}$ mouse model, another team published a mouse model carrying the same R304W mutation with a significantly weaker phenotype The $Stim1^{R304W/+}$ mice from the other team manifested signs of muscle degeneration in quadriceps. However, body size, muscle performance and platelet anomalies were indistinguishable from WT littermates and Ca^{2+} levels in skeletal muscle, fibroblasts and platelets did not differ or were even reduced compared to the unaffected controls. This is possible due to the technical approach used to generate this mouse model which may have impacted $Stim1$ transcription or translation as evidenced by the reduced levels of STIM1 in fibroblasts, platelets and skeletal muscle from this mouse model (Gamage et al., 2018).

1.3. Mouse models with ORAI1 mutations

A mouse model carrying a knock-in mutation in the first transmembrane domain (TM1) of ORAI1 ($Orai1^{G100S/+}$) was also presented in the 24th International Annual Congress of the World Muscle Society in Copenhagen (https://doi.org/10.1016/j.nmd.2019.06.168). Similarly to patients with the equivalent mutation in ORAI1 (G98S), $Orai1^{G100S/+}$ had muscle weakness, blood hypocalcemia and tubular aggregates in histology. However, muscle degeneration were absent in $Orai1^{G100S/+}$ mice with normal blood creatine kinase levels and no fibrosis or nuclei internalization in muscle histology. Compared to other TAM/STRMK mouse models, $Orai1^{G100S/+}$ mice shared the muscle weakness phenotype but lacked the presence of muscle degeneration signs and additionally presented tubular aggregates. Of note, tubular aggregates are Ca^{2+} rich structures and are suggested

as a protective mechanism to face cytosolic Ca^{2+} overload in the muscle (Salviati et al., 1985). This suggests that the presence of tubular aggregates in $Orai1^{G100S/+}$ mice exert a protective role as a Ca^{2+} buffer to avoid cytosolic Ca^{2+} overload and muscle degeneration. Other potential phenotypes affecting the stature, eyes, skin spleen or platelets were not reported in $Orai1^{G100S/+}$ mice (Table 3).

2. PATHOLOGICAL EFFECTS OF HIGH CA^{2+} CONTENT

In skeletal muscle, Ca^{2+} plays pivotal role in muscle contraction, growth and differentiation of muscle cells. Its homeostasis needs to be tightly regulated and several Ca^{2+} handling mechanisms regulate cytosolic Ca^{2+}: extracellular Ca^{2+} entry, Ca^{2+} release from the reticular store, Ca^{2+} store refill, and Ca^{2+} extrusion from the cell. Anomalies of Ca^{2+} handling result in cellular stress affecting mitochondrial energetics, triggering accumulation of misfolded protein and organelles, and can ultimately lead to cell death. $Stim1^{R304W/+}$ myotubes displayed elevated basal Ca^{2+} levels than healthy controls (Silva-Rojas et al., 2019). Investigations with $Stim1^{R304W/+}$ muscles evidenced anomalies in Ca^{2+} handling, mitochondrial respiration, autophagic flux and sustained ER stress, and thereby provided insights into the physiopathological effect of Ca^{2+} overload in $Stim1^{R304W/+}$ mice (Silva-Rojas et al., 2021). My studies uncovered a number of dysregulated pathways that partially overlap with other myopathies and may present suitable common therapeutic targets.

2.1. Ca^{2+} handling

TAM/STRMK arises from SOCE over-activation and elevated cytosolic Ca^{2+} displayed in patients and mice (Bohm et al., 2017; Misceo et al., 2014; Morin et al., 2014; Silva-Rojas et al., 2019). It has previously seen that dysregulation of extracellular Ca^{2+} entry alters the protein expression of pumps and channels required for reticular Ca^{2+} store refill and efflux to the extracellular matrix (Abell et al., 2011). Accordingly, the *Atp2b1* and *Slc8a1* genes encoding the plasma membrane pumps PMCA and NCX3 were slightly downregulated in $Stim1^{R304W/+}$ TA, suggesting reduced Ca^{2+} efflux abilities in $Stim1^{R304W/+}$ muscle fibers. In the same line, SERCA1 protein levels were

reduced and *Sln* gene, encoding for SERCA1 inhibitor sarcolipin, was upregulated in *Stim1$^{R304W/+}$* muscles, indicating defective reticular Ca^{2+} store refilling (Silva-Rojas et al., 2021). Thus, the excessive Ca^{2+} entry via SOCE, together with the reduced abilities to extrude the surplus of Ca^{2+} from the cytosol towards the extracellular matrix or the reticulum collectively account for the elevated basal Ca^{2+} levels in *Stim1$^{R304W/+}$* muscles (Silva-Rojas et al., 2021; Silva-Rojas et al., 2019) (Figure 11). Alterations of Ca^{2+} handling are also observed in myoblasts from a TAM/STRMK patient carrying the STIM1 L96V mutation, and in murine cells overexpressing human STIM1 R304Q as evidenced by reduced *Atp2a1* (SERCA1) expression and smaller reticular Ca^{2+} store, indicating that expression of TAM/STRMK mutants negatively impacts the reticular Ca^{2+} store refilling abilities of the cell (Conte et al., 2021; Park et al., 2021). *Stim1$^{R304W/+}$* mice displayed relaxation anomalies with delayed relaxation speed upon single stimulation and myotonia after tetanic stimulation (Silva-Rojas et al., 2019). These relaxation anomalies may result from the excessive Ca^{2+} entry and impaired reorientation of Ca^{2+} to the extracellular matrix and reticulum, and probably account for the myotonia and cramps observed in TAM/STRMK patients (Morin et al., 2020; Silva-Rojas et al., 2021; Silva-Rojas et al., 2019) (Figure 11).

It has been previously reported that prolonged cytosolic Ca^{2+} overload disrupt the EC coupling and the interaction between DHPR and RyR1 in the triads, membrane contact sites between sarcolemma invaginations (T-tubule) and sarcoplasmic reticulum (Lamb et al., 1995). Later, it was shown that Ca^{2+} stress triggered the proteolysis of junctophylin 1 and 2, which tethered the T-tubules and the sarcoplasmic reticulum, resulting in disrupted EC coupling (Murphy et al., 2013). Functional investigations with murine cells overexpressing human STIM1 R304Q revealed higher basal Ca^{2+} than controls and reduced EC coupling, suggesting that the sustained high levels of cytosolic Ca^{2+} negatively affect EC coupling (Park et al., 2021). In the same line, contraction upon single stimulation in *Stim1$^{R304W/+}$* muscles was delayed consistent with reduced EC coupling that may contribute to the muscle weakness in *Stim1$^{R304W/+}$* mice and TAM/STRMK patients (Silva-Rojas et al., 2021) (Figure 11).

2.2. Mitochondria

In conditions of exercise, cytosolic Ca^{2+} rises and is incorporated into mitochondria by the mitochondrial Ca^{2+} uniporter (MCU), elevating the matrix Ca^{2+} content and thus the activity of NADH dehydrogenases. The rise in matrix NADH content fuels the electron transport chain and energy production to sustain muscle contraction (Finkel et al., 2015). Cytosolic Ca^{2+} also defines the mitochondrial content by regulating the expression of PGC1α, the master regulator of mitochondrial biogenesis, as evidenced by reduced PGC1α expression in calcineurin knockout mice (Roberts-Wilson et al., 2010). Mitochondrial respiration was reduced in our $Stim1^{R304W/+}$ muscles, as so did the expression of PGC1α and the mitochondrial content. The expected reduction in energy production would thus contribute to the muscle weakness in $Stim1^{R304W/+}$ mice (Silva-Rojas et al., 2019) (Figure 11).

In conditions of sustained cytosolic Ca^{2+} stress, the incorporation of Ca^{2+} into the mitochondria via MCU triggering the opening of mitochondrial permeability transition pore (mPTP) and the release of mitochondrial content including cytochrome c, which ultimately activates cell death by apoptosis (Finkel et al., 2015). Constitutive SOCE over-activation and extracellular Ca^{2+} entry contributes to the elevated resting Ca^{2+} in our $Stim1^{R304W/+}$ mouse model and in a STIM1 transgenic mice. Both mouse models displayed swollen mitochondria and the latest displayed higher amounts of matrix Ca^{2+} compared to WT mice, which may trigger mitochondrial rupture and cell death (Goonasekera et al., 2014; Silva-Rojas et al., 2019). Mitochondrial fission and fusion are dynamic processes regulating mitochondrial number and mainly controlled by fission dynamin 1-like protein (*Dnm1l*) and mitochondrial fission 1 protein (*Fis1*), and fusion dynamin-like 120 kDa protein (*Opa1*) and mitofusin 2 (*Mfn2*) (Yu et al., 2020). $Stim1^{R304W/+}$ muscles showed reduced *Dnm1l* and *Fis1* expression and comparable *Opa1* and *Mfn2* expression to WT littermates, indicating that the swollen pattern of mitochondria could be facilitated by reduced expression of fission markers (Silva-Rojas et al., 2021). Defects in mitochondrial fission were also reported recently on murine cells overexpressing human STIM1-R304Q construct where mitochondria display an elongated pattern (Park et al., 2021). Similar elongated mitochondria are also reported in patient myoblasts carrying STIM1 L96V mutation where genes implicated in electron transport chain were also downregulated (Conte et al., 2021). While both studies did not assess

mitochondrial amount by qPCR or western blot, the implication of TAM/STRMK mutations in mitochondrial function is evident and would likely impact energy production and fiber death, contributing to the muscle weakness and degeneration observed in TAM/STRMK patients and mouse models (Cordero-Sanchez et al., 2019; Morin et al., 2020; Silva-Rojas et al., 2021; Silva-Rojas et al., 2019) (Figure 11).

2.3. Autophagy

Autophagy is a recycling pathway consisting on the engulfment of cellular material into vesicles (autophagosomes) for the final fusion with lysosomes forming the autolysosomes where the material is degradated by lysosomal hydrolases. During the initial steps of material engulfment, LC3 is lipidated and anchored to the membrane of the nascent autophagosome (phagophore) and will recruit p62 coupled to the ubiquitninated proteins (cargo) (Marino et al., 2014). Autophagy plays a crucial role regulating muscle mass and LoF mutations in genes implicated in autolyosome formation and function cause congenital myopathies (Dowling et al., 2021; Neel et al., 2013). $Stim1^{R304W/+}$ mice displayed normal RNA levels of $Map1lc3a$, $Map1lc3b$ and $Sqstm1$, encoding the LC3 and p62 proteins, suggesting no transcriptional upregulation of autophagy. However, the protein levels of lipidated LC3 (LC3 II) were increased, which could indicate increased autophagosome formation or decreased degradation in autolysosomes. The additional accumulation of p62, normally degraded in autolysosomes, suggests a defect in autophagosome-lysosome fusion and autolysosome function (Results Part 3). Indeed, genes encoding lysosomal proteins and proteins driving autophagosome-lysosome fusion are downregulated in $Stim1^{R304W/+}$ TA while ubiquitinated proteins accumulate (data not shown), further supporting the hypothesis of autophagy block at later stages in $Stim1^{R304W/+}$ mice. A link between $STIM1$ mutations and autophagy has also been investigated by others. Overexpression of luminal STIM1 TAM/STRMK mutants in HEK-293T cells increased the Ca^{2+} entry, the nuclear translocation of transcriptional factors inducing autophagy, and the increased presence of autophagosomes (Sallinger et al., 2020). However, the expression of genes encoding LC3, p62 and lysosome markers was not assessed, and autophagic flux studies would be required to conclude on the step affected. For example, treating these cells with bafilomycin A1, a molecule blocking autophagosome-lysosome fusion, would

determine if anomalies in this step account for the autophagosome accumulation (Galluzzi et al., 2017).

Overall, SOCE-dependent Ca^{2+} entry regulates autophagy and we showed with *Stim1$^{R304W/+}$* muscles a potential block of autophagy in later stages. *Orai1* downregulation in *Stim1$^{R304W/+}$ Orai1$^{+/-}$* mice increased muscle fiber size and reduced the accumulation of lipidated LC3 and p62, suggesting an improvement in autophagic flux and increase in fiber size ([Results Part 3](#)). A better characterization of the autophagy step affected is needed to select the most appropriate molecules to use in TAM/STRMK. While autophagosome-lysosome fusion seem to be the affected step, there are no molecules improving the fusion or the lysosome function in clinics (Bonam et al., 2019). Initial autophagy steps may be compromised too and molecules targeting these initial steps exist (Galluzzi et al., 2017). In order to determine a potential anomaly in early autophagy, treatment of *Stim1$^{R304W/+}$* primary myoblasts with rapamycin would activate the first steps of autophagy and determine any alteration in this part of the process whose treatment would be translated into clinics using activators of the first steps of autophagy (Galluzzi et al., 2017) (Figure 11).

2.4. ER stress and cell death

It is known that altered energy production and anomalies in cytosolic Ca^{2+} homeostasis are associated with protein misfolding, aggregation and ER stress, triggering the activation of unfolded protein response (UPR) in order to restore normal ER function. However, in situations with sustained ER stress, cell death by apoptosis can be activated (Bahar et al., 2016; Krebs et al., 2015; Ruiz et al., 2010). As *Stim1$^{R304W/+}$* muscles presented cell stresses that could activate UPR, I scaled the expression of UPR-activated genes *Hspa5*, *Hsp90b1* and *Xbp1* in *Stim1$^{R304W/+}$* muscles and showed higher levels than WT control muscles. The sustained ER stress resulted in fiber death by apoptosis and regeneration in *Stim1$^{R304W/+}$* mice (Silva-Rojas et al., 2021). Similarly, muscle biopsies from TAM patients showed an increased protein expression of UPR-related GRP78 and GRP94, which were also found inside the tubular aggregates (Ikezoe et al., 2003). ORAI1 inhibition in *Stim1$^{R304W/+}$Orai1$^{R93W/+}$* mice yielded a full rescue of the muscle degeneration signs observed in *Stim1$^{R304W/+}$* mice including fibers with internalized nuclei, immune cell infiltrations and the amount of regenerative fibers. Moreover, transcriptomic analysis of

$Stim1^{R304W/+}Orai1^{R93W/+}$ muscles showed the resolution of ER stress as the main contributor to the improved muscle function in $Stim1^{R304W/+}Orai1^{R93W/+}$ mice as evidenced by the restored expression of genes implicated in the response to endoplasmic reticulum stress ([Results Part 4](#)) (Figure 11).

2.5. Therapeutic options to counteract the negative effects of Ca^{2+} overload

Cytosolic Ca^{2+} overload is a major physiopathological feature in TAM/STRMK, and is also found in mouse models for other myopathies including *mdx* mice for Duchenne's muscular dystrophy (DMD) and δ sarcoglycan-deficient mice ($Sgcd^{-/-}$) for limb girdle muscle dystrophy type 2E (LGMD2E) (Goonasekera et al., 2014; Goonasekera et al., 2011). In accordance with the downstream effects of Ca^{2+} overload observed in $Stim1^{R304W/+}$ mice, anomalies in the Ca^{2+} handling, mitochondria, autophagy and ER stress are also reported in *mdx* mice. The Ca^{2+} overload in *mdx* and also $Sgcd^{-/-}$ mice was shown to arise from excessive Ca^{2+} entry that resulted from a combination of membrane fragility and SOCE over-activation (Edwards et al., 2010a; Goonasekera et al., 2014; Millay et al., 2009; Zhao et al., 2012). Reduced SERCA1 expression and upregulation of its inhibitor sarcolipin were also observed in *mdx* mice and indicated deficient capacities to refill reticular Ca^{2+} store (Divet and Huchet-Cadiou, 2002; Goonasekera et al., 2011; Kargacin and Kargacin, 1996). Similar observations were done in muscles from $Sgcd^{-/-}$ mice, and the overexpression of SERCA1 improved the skeletal muscle defects of both *mdx* and $Sgcd^{-/-}$ mice, while the knockdown of the gene encoding sarcolipin (*Sln*) also improved skeletal and cardiac muscle defects of *mdx* mice (Goonasekera et al., 2011; Voit et al., 2017). The *mdx* mice also manifested reduced EC coupling, and treatment with the EC coupling activator taurine improved muscle contraction in *mdx* mice (De Luca et al., 2001; Woods et al., 2004). It is therefore conceivable that over-expressing SERCA1, downregulating *Sln* and treatment with taurine may similarly reduce cytosolic Ca^{2+} and facilitate contraction in TAM/STRMK mice and patients improving muscle function (Figure 11).
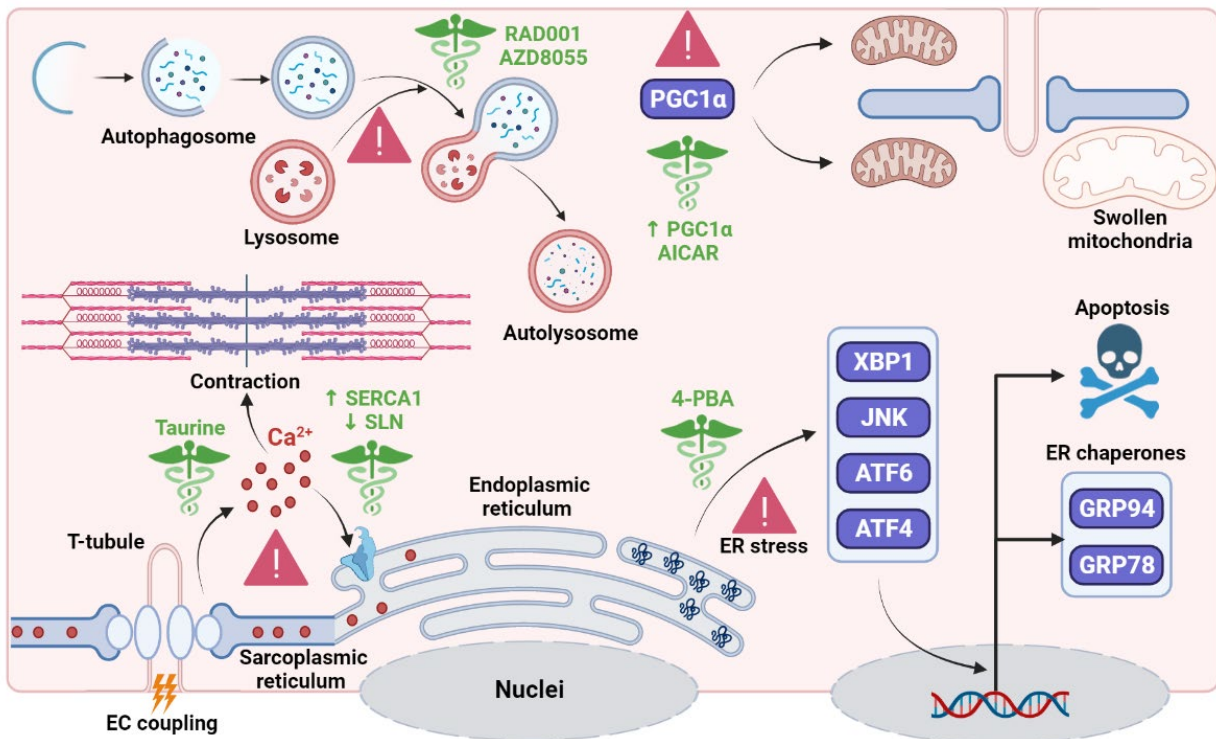
Figure 11. Pathophysiological effects of SOCE over-activation on $Stim1^{R304W/+}$ muscle function and therapeutic options.

$Stim1^{R304W/+}$ muscles displayed reduced expression of genes encoding EC coupling and SR refilling players, resulting in abnormal muscle contraction and relaxation. Treatment with the EC coupling activator taurine, or SERCA1 overexpression / sarcolipin knockdown would improve EC coupling and SR refilling rates (bottom left). Mitochondrial content due reduced expression of PGC1α and swollen mitochondria were also evident. Overexpression of PGC1α or treatment with AICAR might restore the mitochondrial amount and improve cell energetics (top right). Autophagosome components accumulated by a potential reduction in autophagosome-lysosome fusion. RAD001 and AZD8055 molecules activate this fusion step and would be beneficial to potentiate autophagic flux (top left). ER stress triggers unfolded protein response (UPR), involving the internalization of transcription factor and the expression of ER chaperones. Sustained ER stress results in cell death by apoptosis and the treatment with the chemical chaperone 4-PBA would resolve ER stress and fiber death in $Stim1^{R304W/+}$ muscles (bottom right). This image was created with BioRender (https://biorender.com/).

Ca^{2+} overload also affected mitochondrial function in *mdx* mice, and the stimulation of mitochondrial biogenesis by PGC1α overexpression increased mitochondrial activity and attenuated apoptosis (Godin et al., 2012). Treatment with 5-aminoimidazole-4-carboxamide-1-b-D-ribofuranoside (AICAR), an AMPK activator molecule, increased mitochondrial biogenesis and rescued muscle defects of a mouse model of mitochondrial myopathy (Peralta et al., 2016). The same molecule activated autophagy in *mdx* mice and improved diaphragm performance and histology (Pauly et al., 2012). Autophagy is also blocked in a mouse model for X-linked centronuclear myopathy (*Mtm1$^{-/y}$*) and collagen VI-related myopathy (*Col6a1$^{-/-}$*), and the treatment with autophagy activators (trans-resveratrol, spermidine, AICAR and mTORC1 inhibitors (RAD001/AZD8055)) restored autophagy flux and improved skeletal muscle function (Castets et al., 2016; Fetalvero et al., 2013; Kuno et al., 2018). A better characterization of the autophagy defects in TAM/STRMK would determine the most appropriate molecules to guarantee normal autophagic flux and improve the fiber atrophy observed in *Stim1$^{R304W/+}$* mice (Figure 11).

We hypothesize that steady and unresolved ER stress is the main driver of apoptosis in *Stim1$^{R304W/+}$* mice (Silva-Rojas et al., 2021). Other murine models manifesting abnormal Ca^{2+} handling through reduced RyR1 activity (*RyR1$^{I4898T/+}$*) or sarcolemmal instability and SOCE over-activation (*mdx*) also presented sustained ER stress, and the treatment with the chemical chaperone sodium 4-phenylbutyrate (4-PBA) improved their muscle phenotype (Begam et al., 2016; Lee et al., 2017) (Figure 11). Apoptosis and regeneration are present in *Stim1$^{R304W/+}$* mice and, while less prominent than in muscle dystrophies, muscle degeneration contributes to muscle weakness in *Stim1$^{R304W/+}$* mice (Silva-Rojas et al., 2021; Silva-Rojas et al., 2019). Treatments to interfere with the apoptosis signaling exist and were assessed in congenital muscle dystrophies with positive results (Dominov et al., 2005; Girgenrath et al., 2004). Myofiber death and regeneration generates a pro-inflammatory microenvironment that contributes to muscle degeneration in *mdx* and *Stim1$^{R304W/+}$* mice, and the direct attenuation of myofiber death would positively impact muscle morphology and function.

In summary, *Stim1$^{R304W/+}$* mice share common pathomechanisms with other myopathy mouse models for which the treatment with clinically approved molecules targeting EC coupling, mitochondrial biogenesis, autophagy and ER stress have shown to improve the muscle performance and histology of *mdx*, *Sgcd$^{-/-}$*, *Mtm1$^{-/y}$*, *Col6a1$^{-/-}$*, and *RyR1$^{I4898T/+}$* mice. These

molecules represent a potential opportunity to reverse the molecular effects of Ca^{2+} overload and improve the muscle function of TAM/STRMK mice and patients.

3. ORAI1 AS A THERAPEUTIC TARGET FOR TAM/STRMK

SOCE is a ubiquitous mechanism regulating Ca^{2+} entry and plays a crucial role in different cell processes. In bones, it is required for osteoclast and osteoblast growth and differentiation, and the abnormal bone morphology in $Stim1^{R304W/+}$ mice would be a direct consequence of SOCE over-activation, and presumably contributes to the short stature of TAM/STRM mice and patients (Blair et al., 2011; Chen et al., 2018; Eapen et al., 2010; Silva-Rojas et al., 2019). Following injury of the blood vessels, SOCE also plays a crucial role in platelet activation and thrombus formation through phosphatidylserine exposure and the secretion of α granules (Berna-Erro et al., 2016; van der Meijden and Heemskerk, 2019). As a result of SOCE over-activation, TAM/STRMK platelets are in a pre-activated state, fail to form a thrombus, and are prematurely removed from the blood flow, resulting in thrombocytopenia and bleeding diathesis in patients and mice (Cordero-Sanchez et al., 2019; Grosse et al., 2007; Markello et al., 2015; Misceo et al., 2014; Silva-Rojas et al., 2019). In skeletal muscle, SOCE activates following depletion of reticular Ca^{2+} store by EC coupling and provide the Ca^{2+} necessary to refill the reticular Ca^{2+} store and to sustain muscle contraction during repetitive stimulations (Edwards et al., 2010b; Launikonis et al., 2009; Wei-Lapierre et al., 2013; Zhao et al., 2005). SOCE over-activation in $Stim1^{R304W/+}$ mice increases the resting Ca^{2+} and negatively interferes with muscle contraction and relaxation. It also negatively impacts mitochondrial function, autophagy and ER stress, ultimately leading to myofiber death (Silva-Rojas et al., 2021; Silva-Rojas et al., 2019). Overexpression of STIM1 in skeletal muscle also triggers muscle degeneration and the co-expression with a dominant negative ORAI1 mutant restored the histological phenotypes (Goonasekera et al., 2014). The co-expression of the same dominant negative ORAI1 mutant in mdx and $Sgcd^{-/-}$ mouse models resulted in improved muscle histology, indicating that ORAI1 activity contributes to muscle degeneration in DMD and LGMD2E (Goonasekera et al., 2014).

Similarly to DMD and LGMD2E, all forms of TAM/STRMK arise from ORAI1 over-activation. *STIM1* mutations either trigger unfolding of the luminal part of STIM1 or elongate cytosolic part

of STIM1 resulting in constitutive oligomerization and ORAI1 over-activation (Fahrner et al., 2018; Sallinger et al., 2020; Schober et al., 2019). *ORAI1* mutations affecting the pore-forming transmembrane domain 1 increase channel permeability while mutations in the concentric channel rings result in STIM1-dependent ORAI1 over-activation (Bohm et al., 2017; Endo et al., 2015; Nesin et al., 2014). The reticular Ca^{2+} buffer calsequestrin (CASQ1) polymerizes with rising reticular Ca^{2+} concentrations and depolymerizes upon Ca^{2+} store depletion. Monomeric calsequestrin sequesters STIM1 and thereby negatively regulates SOCE. The *CASQ1* mutations were shown to compromise the polymerization/depolymerization dynamics of calsequestrin, and the reduced amount of monomeric calsequestrin leads to increased ORAI1 activity (Barone et al., 2017; Bohm et al., 2017). As a result, SOCE over-activation in all forms of TAM/STRMK results from ORAI1 over-activation (Figure 12).
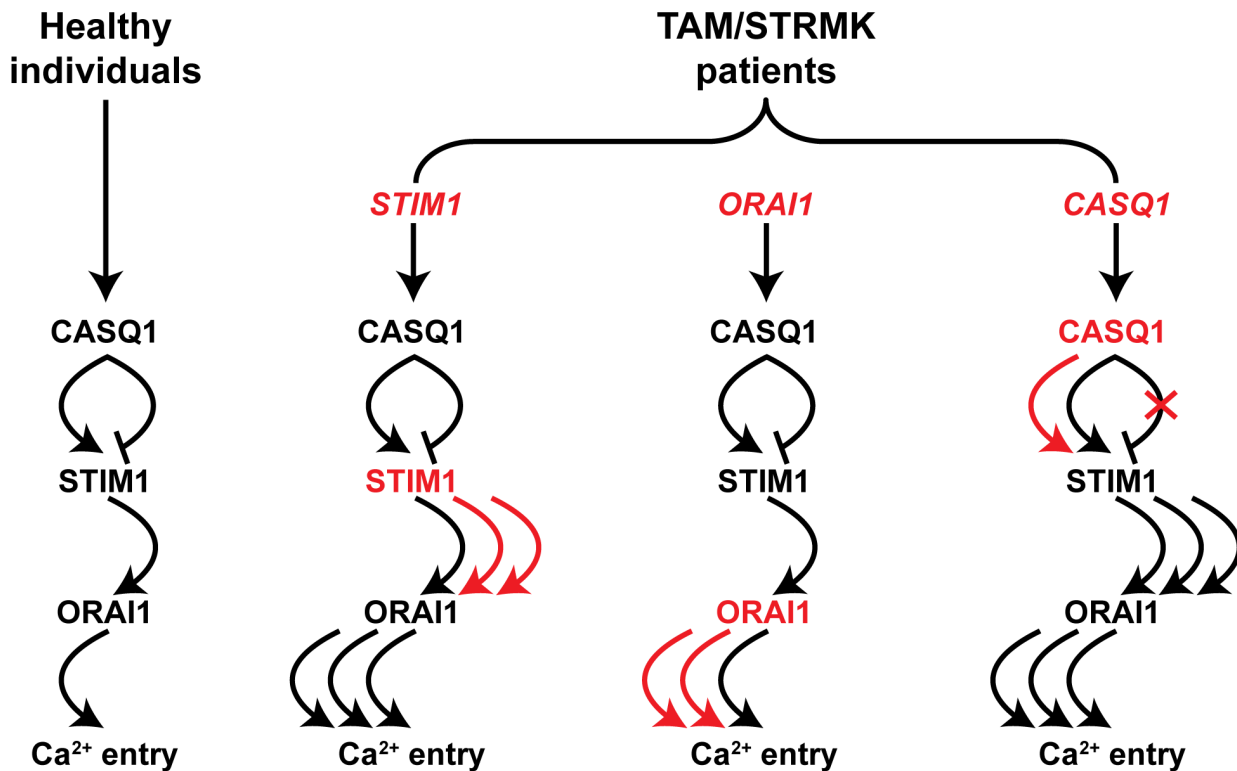
Figure 12. Protein activity in all forms of TAM/STRMK.

In normal conditions, CASQ1 monomers bind STIM1 to prevent ORAI1 activation. In TAM/STRMK patients carrying STIM1 mutations, STIM1 constitutively activates ORAI1. ORAI1 mutations generate leaky channels or increase the sensitivity to STIM1. CASQ1 mutations alter depolymerization and the role of CASQ1 monomers as negative SOCE regulators. Any case results in excessive extracellular Ca^{2+} entry through ORAI1.

3.1. *Proof-of-concept of Orai1* silencing

CRAC channelopathy is a multi-systemic disorder characterized by immunodeficiency and autoimmunity, ectodermal dysplasia, mydriasis, autoimmune thrombocytopenia and muscle hypotonia. It is caused by recessive LoF mutations in *STIM1* and *ORAI1* that result in total loss of STIM1 or ORAI1 protein, interfere the STIM1-ORAI1 interaction, or generate a blocked ORAI1 channel (R91W) (Lacruz and Feske, 2015; Silva-Rojas et al., 2020). In accordance with the severity of ORAI1 loss in patients, *Orai1*$^{-/-}$ mice develop a severe phenotype and die perinatally. Heterozygous *Orai1*$^{+/-}$ mice are normal and fertile and no phenotypical defect has been reported (Gwack et al., 2008). This is in line with CRAC channelopathy carriers where no clinical sign has been reported to date, indicating that 50% expression of *ORAI1* is sufficient to maintain normal functioning of immune system, ectoderm-derived tissues, pupil contraction, coagulation and skeletal muscle.

In order to reduce *Orai1* expression to tolerable levels in the TAM/STRMK scenario, we bred the *Stim1*$^{R304W/+}$ and *Orai1*$^{+/-}$ mice and the resulting *Stim1*$^{R304W/+}$*Orai1*$^{+/-}$ mice had a 50% reduction in *Orai1* expression in the skeletal muscle. This approach improved the TAM/STRMK phenotypes related to body weight, bone structure, skin composition and muscle performance (Results Part 3). Yet the *Orai1* silencing achieved by genetic crossing was not sufficient to improve some of the TAM/STRMK phenotypes the defects in muscle contraction and the histological signs of muscle degeneration. This can be related to following reasons:

a) A compensation in expression of the *Orai1* paralogues *Orai2* and *Orai3* that would compensate the *Orai1* downregulation and sustain elevated SOCE. However, *Orai2* and *Orai3* expression were unaltered in *Stim1*$^{R304W/+}$*Orai1*$^{+/-}$ muscles revealing no compensating effect on *Orai1* paralogues.

b) A compensating expression of genes encoding TRPC channels expressed in skeletal muscle that would participate to SOCE and attenuate the effect of *Orai1* silencing. I assessed *Trpc1, Trpc2, Trpc3* and *Trpc4* expression and it was not altered in *Stim1*$^{R304W/+}$*Orai1*$^{+/-}$ mice, indicating no compensation by TRPC channels (data not shown).

c) 50% reduction in *Orai1* expression is not enough to counterbalance the SOCE over-activation observed in *Stim1*$^{R304W/+}$ mice. In order to reach higher *Orai1* silencing and

propose a translational approach targeting *Orai1* expression, we produced AAV containing shRNA targeting *Orai1*. Adult WT and *Stim1$^{R304W/+}$* mice were injected intramuscularly and muscle contraction and histology was assessed 2 months post-injection.

3.2. Translational approach of *Orai1* silencing: shRNA

Two shRNAs targeting *Orai1* at cDNA position 22 (sh22) and 190 (sh190) yielded reduction in *Orai1* expression by 80% in *Stim1$^{R304W/+}$* TA. The more efficient *Orai1* silencing achieved by *Orai1* shRNAs improved contraction and relaxation kinetics to a higher extent than previously reported when *Orai1* was reduced to 50% by genetic cross, and confirms *Orai1* silencing as a potential therapeutic approach for TAM/STRMK and other Ca^{2+}-related myopathies with muscle contraction anomalies. ORAI1 activity contributes to the cytosolic Ca^{2+} overload in *mdx* and *Sgcd$^{-/-}$* mice that ultimately lead to cell death (Edwards et al., 2010a; Goonasekera et al., 2014; Zhao et al., 2012). Co-expression of a dominant negative ORAI1 mutant reversed the histological defects, showing ORAI1 as an efficient therapeutic target in DMD and LGMD2E (Goonasekera et al., 2014). A poster presented in the 63rd Annual meeting of Biophysical Society in Baltimore by an American team showed that tamoxifen-induced knockout of *Orai1* reduced Ca^{2+} entry and membrane fragility in adult *mdx* mice (https://doi.org/10.1016/j.bpj.2018.11.2817). Based on the high *Orai1* silencing efficiency of our shRNAs, injecting *mdx* with our AAV would represent the translational approach of to treat the muscle defects of DMD and TAM/STRMK.

TAM/STRMK displays a multi-systemic phenotype and ubiquitous dissemination of *Orai1* shRNA by AAV systemic injection would provide higher therapeutic interest. However, only the intramuscular injection of AAV yielded sufficient *Orai1* reduction to improve the muscle contraction phenotypes. Indeed, we also tested the intraperitoneal injection of AAV containing *Orai1* shRNA in newborn mice but the *Orai1* reduction in TA at 4 months was only reduced by 40% in the case of sh190 shRNA without any significant improvement in hanging test, openfield or histology (data not shown). The major advantage of AAV is their life-long therapeutic effect but can turn in a disadvantage if more than one injection is needed to reach enough *ORAI1* silencing. Indeed, AAV cannot be injected twice because they would be recognized by the host immune system and would be neutralized (more details in Introduction Adeno-associated viruses

section). Instead, antisense oligonucleotides (ASOs) targeting *ORAI1* can be designed to reduce *ORAI1* expression, and injected several times to reach a therapeutic reduction of *ORAI1* levels. Regarding the antisense oligonucleotide chemistry, gapmer ASO using cET or MOE chemistry would be the ideal option in order to activate RNAse H activity and reduce murine *Orai1* expression (see more details in Introduction [Antisense oligonucleotides](#) section). I designed ASO sequences specific to *Orai1*, checked the presence of motifs increasing ASO efficiency (Matveeva et al., 2000)*,* and tested their efficiency to bind *Orai1* mRNA *in silico* (Table 4). These ASOs and our shRNAs may provide a common therapeutic approach for TAM/STRMK and other muscle dystrophies including DMD.

Table 4. ASOs targeting *Orai1 in silico*.

ASO enhancing motifs: CCAC, TCCC, ACTC, GCCA and CTCT.
ASO inactivating motifs: GGGG, ACTG, AAA and TAA.

ASO #	*Orai1* cDNA position	ASO sequence	*Orai1* specificity	Enhancing motifs	Binding disruption energy (kcal/mol)
1	27	GCTCCGGATTGCTGTGACTC	YES	YES	12.7
2	28	AGCTCCGGATTGCTGTGACT	YES	NO	11.6
3	482	GGTGACTCTTTGACCGAGTT	NO	YES	5.6
4	483	GGGTGACTCTTTGACCGAGT	NO	YES	6.4
5	664	TGTGGTTGGCGACGATGACT	YES	NO	19
6	665	CTGTGGTTGGCGACGATGAC	YES	NO	18.3
7	890	TGGGTGCCCGGTGTTAGAGA	YES	NO	12.1
8	892	AGTGGGTGCCCGGTGTTAGA	YES	NO	11.5
9	893	TAGTGGGTGCCCGGTGTTAG	YES	NO	11.7

Moreover, TAM/STRMK patients present pupil contraction and eye movement anomalies (gaze paresis) that may underlie contraction defects of ocular muscles. [Sylentis](#) is one of the world's leading companies using siRNAs. The company developed siRNA targeting *ORAI1* to treat ocular allergies and conjunctivitis, and the SYL116011 siRNA currently undergoes preclinical trials (Patent ref: US20160304880A1) (Gonzalez et al., 2018; Jimenez et al., 2015). This siRNA shares the 19 nucleotide sequence used in our sh190 shRNA. The promising results obtained on our *Stim1*[R304W/+] mice where sh190 treatment improved the muscle contraction properties suggests that, in case that local ocular treatment with SYL116011 siRNA penetrates into the ocular muscles,

TAM/STRMK patients may benefit from this compound to restore the miosis and gaze paresis and restore their vision anomalies.

3.3. ORAI1 inhibition proof of concept

Orai1 silencing improved several but not all the phenotypical aspects of TAM/STRMK in mice (Results Part 3). It is expected that the *Orai1* downregulation would reduce the amount of ORAI1 molecules but ORAI1 hexamers would be constitutively activated by STIM1 R304W mutant. Another therapeutic strategy would be to directly inactivate the channel using channel blocking mutations that would incorporate in all ORAI1 hexamers. Autosomal dominant mutations in ORAI1 exist and the murine ORAI1 E108Q mutant (human ORAI1 E106Q) was an artificial mutation that associated and inhibited ORAI1 activity to a level even higher than *Stim1* knockdown (Vig et al., 2006a; Wei-Lapierre et al., 2013; Yarotskyy and Dirksen, 2012). The co-expression of ORAI1 E108Q mutant in STIM1 transgenic mice normalized the Ca^{2+} entry and restored the muscle degeneration (Goonasekera et al., 2014). In a similar strategy, I crossed the $Stim1^{R304W/+}$ mice with $Orai1^{R93W/+}$ mice carrying a channel blocking mutation in murine ORAI1 (R93W) whose human equivalent (R91W) causes CRAC channelopathy in the homozygous state but has no clinical impact in the heterozygous state (Feske et al., 2006). We performed a phenotypic characterization of the offspring and observed that $Stim1^{R304W/+}Orai1^{R93W/+}$ mice showed body size, spleen weight, platelet counts, and muscle performance and histology similar to healthy controls. Compared to *Orai1* silencing, the ORAI1 inhibition was a more effective treatment for TAM/STRMK and transcriptomic analysis re the resolution of ER stress was the major driver of the muscle improvement (Results Part 4).

SOCE over-activation is also reported in *mdx* and $Sgcd^{-/-}$ mice and the excessive, and the co-expression with the ORAI1 E108Q mutant restored the muscle degeneration defects (Edwards et al., 2010a; Goonasekera et al., 2014; Millay et al., 2009; Zhao et al., 2012). The combination of the therapeutic effect of ORAI1 inhibition in mouse models for TAM/STRMK, DMD and LGMD2E suggests that small compounds specifically inhibiting ORAI1 activity would be the common translational approach to attenuate Ca^{2+} overload, reduce muscle degeneration and improve muscle performance in these diseases.

3.4. ORAI1 inhibition translational approach: molecules

Specific ORAI1 inhibitors exist and some are currently been clinically tested in the context of inflammation and immune system anomalies (pancreatitis, pneumonia, asthma, lymphoma) (Table 5) (Shawer et al., 2021). CalciMedica and Rhizen Pharmaceuticals AG are the 2 leading companies developing ORAI1 inhibitors while other smaller startups like ChemiCare emerged recently. Monoclonal antibodies targeting ORAI1 were developed and successfully tested *in vivo* for autoimmune disorders but clinical trials are not reported so far (Haustrate et al., 2019). The relevance ORAI1 in the context of inflammation and cancer, and the establishment of dedicated companies created a scenario that may benefit TAM/STRMK patients in the future. The outcome of clinical trials testing ORAI1 inactivation in other diseases is expected to shorten the delay to test these molecules in TAM/STRMK patients.

Table 5. Clinical trials with ORAI1 inhibitors.

Compound	Potential use	Clinical trial type	Clinial trial ref	Company
Auxora/CM4620	Acute pancreatitis	II	NCT03709342 NCT04681066 NCT03401190	CalciMedica
Auxora/CM4620	COVID-19	II	NCT04661540 NCT04345614	CalciMedica
RP4010	Lymphoma	I terminated	NCT03119467	Rhizen Pharmaceuticals AG
RP3128	Asthma	I finished	NCT02958982	Rhizen Pharmaceuticals AG

The above mentioned compounds are exclusively produced and protected by their manufacturing companies and their adaptation for the treatment of a rare condition like TAM/STRMK is likely to increase their cost and reduce the access for patients, particularly in countries without a public social insurance system. Another solution would be the drug repurposing of compounds approved by American and European medicament agencies (FDA and EMA) as a quick and safe strategy to provide a treatment for TAM/STRMK in the short future. As an immediate future prospective of ORAI1 inhibition in TAM/STRMK, we are currently performing a middle throughput cell drug

screening to find molecules reducing Ca^{2+} entry. This drug screening is a collaboration between the team of Jocelyn Laporte and the IBiSA-labelled screening platform of Strasbourg (https://pharmacie.unistra.fr/pcbis/), and I participated during my PhD to the establishment and miniaturization of cell readouts for TAM/STRMK. The screening consist on measuring Ca^{2+} entry on doxycycline-inducible HEK-293T cells over-expressing mCherry-tagged STIM1 R304W or mKO-tagged ORAI1 V108M mutants and using Fluo-4 as cytosolic Ca^{2+} indicator of the Ca^{2+} entry (Figure 13). A first screening with 10 µM concentration of the molecules already started and aim to find the best hits upon a library with more than 1500 molecules including the FDA and EMA-approved molecules and a list of 15 molecules with proven efficacy to reduce SOCE (Table 6).

Table 6. SOCE inhibitors added to the screen and described Ca^{2+} handling off targets.

SOCE inhibitor	Ca^{2+} off targets	Reference
Synta66	None	(Shawer et al., 2021)
2-APB	ORAI2, ORAI3, IP$_3$R, SERCA and TRPCs	(Shawer et al., 2021)
DPB162-AE	ER Ca^{2+} leak	(Shawer et al., 2021)
SKF-96365	TRPCs, voltage channel, SERCA	(Shawer et al., 2021)
BTP2/ YM-58483	TRPM4 and TRPCs	(Shawer et al., 2021)
5J 4	Unknown	(Kim et al., 2014)
GSK-7875A	ORAI2, CaV, TRPV6	(Shawer et al., 2021)
GSK-5503A	ORAI3	(Jairaman and Prakriya, 2013)
AnCoA4	Unknown	(Shawer et al., 2021)
RO2959	Voltage Ca^{2+} channels	(Shawer et al., 2021)
Gadolinium chloride	TRP channels and voltage channels	(Shawer et al., 2021)
Diethylstilbestrol	Voltage channels, TRPCs and mitochondrial channels	(Liang et al., 2021)ref
Carboxyamoditriazole	Non-voltage Ca^{2+} channels	(Shawer et al., 2021)
Mibefradil	ORAI2 and ORAI3	(Liang et al., 2021)
Trans-resveratrol	Voltage Ca^{2+} channels	(Casas-Rua et al., 2013)

The best hits will be then tested at two different concentrations and will be validated on dose-response studies. The shortened list of molecules that will pass these 3 screening steps on Ca^{2+} entry will be additionally confirmed using the NFAT translocation readout. NFAT is a transcription factor with Ca^{2+}-dependent translocation into the nucleus and this readout consist on measuring the effect of molecules on the excessive NFAT nuclear translocation that result from SOCE/ORAI1 over-activation in cells overexpressing STIM1 R304W and ORAI1 V107M mutants (Peche et al., 2020; Sallinger et al., 2020; Schober et al., 2019) (Figure 13). In order to determine if the molecules act at the level of STIM1 clustering or ORAI1 permeability, a final test will measure the potential reversion of STIM1 R304W clustering by the molecules (Bohm et al., 2014; Bohm et al., 2013; Peche et al., 2020; Sallinger et al., 2020; Schober et al., 2019) (Figure 13). The best 3-5 molecules that reduced Ca^{2+} entry and NFAT translocation will be tested in our *Stim1^{R304W/+}* mice and also in *Stim1^{I115F/+}* mice to validate the effects of these molecules on different mouse models of TAM/STRMK (Cordero-Sanchez et al., 2019; Silva-Rojas et al., 2019). It is expected that, within 3 years from now, a subset of molecules will have been tested *in vivo*, paving the way for the development of therapeutic approaches to treat TAM/STRMK.
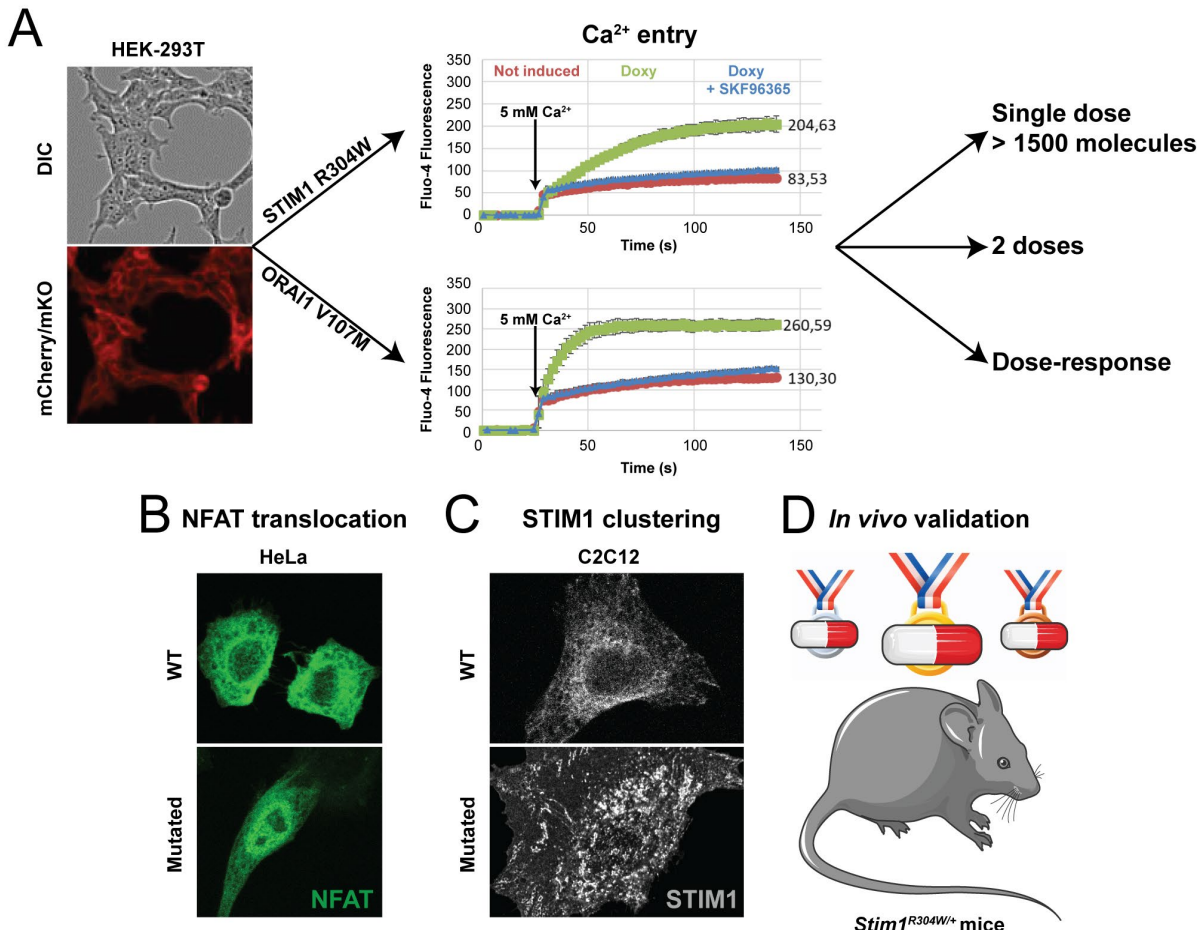
Figure 13. TAM/STRMK cell readouts used for drug screening.

(A) HEK-293T cells with doxycycline-inducible mCherry-STIM1 R304W and mKO-ORAI1 V107M over-expression show higher Ca^{2+} entry (green line) than not induced cells (red line), and treatment with SKF96365 restores the Ca^{2+} entry (blue line). A first round of screening will test one single concentration (10 µM) of more than 1500 FDA/EMA-approved compounds and it is expected to provide a list of best hits that will be subsequently characterized using two doses and dose-response studies. (B) The best hits will be confirmed by measuring the effect of these molecules on the enhanced NFAT translocation observed when expressing STIM1 and ORAI1. (C) The best hits obtained in Ca^{2+} entry and NFAT translocation readouts will pass through an additional screening step to determine a potential effect of those molecules on constitutive clustering of STIM1 R304W mutant. (D) The molecules that best reduced Ca^{2+} entry and NFAT translocation in cells will be assessed in vivo using our Stim1$^{R304W/+}$ mouse model. Adapted from Peche et al., 2020.

GENERAL CONCLUSION

TAM/STRMK is multi-systemic disorder encompassing muscle weakness, cramps and myalgia together with multi-systemic phenotypes affecting the stature, eyes, skin, platelets, spleen and the cognitive abilities. At the start of my PhD, it was known that mutations in *STIM1* and *ORAI1* resulted in excessive Ca^{2+} entry. However, animal models with extensive characterization were lacking and, in consequence little was known on TAM/STRMK physiopathology and no therapeutic strategy was proposed. In order to address these bottlenecks, my PhD goals aimed to:

1. **Generate and characterize a mouse model for TAM/STRMK.** The *Stim1^{R304W/+}* mice presented most of the clinical sigs observed in patients and manifested reduced size, thrombocytopenia, splenomegaly, anomalies in skin layers, and defects in muscle performance and histology. In addition, I also discovered additional phenotypes not yet reported in TAM/STRMK patients including anomalies of the bone structure, glucose metabolism, liver, and immune system. Overall, the *Stim1^{R304W/+}* model represents a faithful model for the human disorder, and the discovery of additional TAM/STRMK signs may be of importance for the disease management and the clinical follow-up of the patients.

2. **Study the physiopathology of STIM1 over-activation in skeletal muscle.** The availability of a faithful animal model for TAM/STRMK also represents an excellent opportunity to study the pathological effects of SOCE over-activation and excessive extracellular Ca^{2+} entry in different cells and tissues. Through physiological, histological, ultrastructural, and molecular studies on *Stim1^{R304W/+}* muscle sections and samples, I found reduced expression of genes implicated in the mobilization of Ca^{2+} for contraction and relaxation, and *Stim1^{R304W/+}* muscles showed delayed muscle contraction and relaxation. Cytosolic Ca^{2+} overload was accompanied by reduced mitochondrial biogenesis, autophagy flux block and sustained ER stress. These defects would cause reduced energy production and accentuate muscle weakness, alter protein removal and cause fiber atrophy, and trigger cell death by apoptosis, all contributing to the muscle defects observed in TAM/STRMK. Taken together, I revealed cellular processes altered in TAM/STRMK that explain the muscle phenotypes, and represent potential therapeutic targets.

3. **Provide therapeutic proof-of-concepts for TAM/STRMK.** ORAI1 is the main Ca^{2+} entry channel of SOCE and channel gating is triggered and controlled by STIM1. Functional studies in the cell model have shown that the STIM1 mutations induce constitutive oligomerization, while the ORAI1 mutations generate increased channel permeability. In any case, TAM/STRMK is caused by excessive extracellular Ca^{2+} entry through ORAI1, making ORAI1 the principal target for therapeutic approaches. In order to downregulate *Orai1*, I crossed *Stim1$^{R304W/+}$* mice with *Orai1$^{+/-}$* mice expressing 50% of *Orai1* and the offspring was evaluated phenotypically at the macroscopic, histologic and molecular levels. *Stim1$^{R304W/+}$Orai1$^{+/-}$* mice had improved birth ratio, body weight and size, skin structure, bone morphology, and muscle performance and fiber size. However, other phenotypes affecting the platelets counts, spleen size or muscle relaxation and degeneration were not improved. *Orai1* downregulation by genetic cross improved some of the TAM/STRMK phenotypes and confirmed ORAI1 as a therapeutic target for TAM/STRMK. As a translational application of *Orai1* downregulation, I designed shRNAs targeting *Orai1* cDNA at position 22 (sh22) and 190 (sh190). I injected shRNA-containing AAVs intramuscularly into the tibialis anterior of adult *Stim1$^{R304W/+}$* mice and assessed muscle phenotype reversion two months later. Muscle relaxation and contraction were greatly improved by sh22 and sh190 treatment in *Stim1$^{R304W/+}$* muscles while muscle degeneration signs were still evident.

As an alternative strategy, I tested ORAI1 inhibition as a therapeutic strategy by crossing *Stim1$^{R304W/+}$* mice with *Orai1$^{R93W/+}$* mice, expressing a mutation partially blocking the channel. In contrast to *Stim1$^{R304W/+}$Orai1$^{+/-}$* mice, *Stim1$^{R304W/+}$Orai1$^{R93W/+}$* showed broader improvement in all phenotypes assessed at 4 months of age including body weight and size, bone morphology, spleen size, platelet counts, hanging time, muscle relaxation and muscle degeneration. Transcriptomic analysis of tibialis anterior showed that ORAI1 inhibition better restored the molecular pathways altered in TAM/STRMK compared to *Orai1* silencing. ER stress was greatly resolved in *Stim1$^{R304W/+}$Orai1$^{R93W/+}$* muscles, indicating that the alleviation of protein misfolding probably accounts for the resolved muscle degeneration. In conclusion, ORAI1 is a suitable target to treat TAM/STRMK and ORAI1 inhibition provides more potent and extensive effects compared to *Orai1* silencing. ORAI1 inhibitors will be tested in the future and may provide a common therapy for TAM/STRMK and other diseases with SOCE over-activation including DMD.

Overall, my PhD work contributed to a better understanding of the pathomecanisms underlying TAM/STRMK and the negative effects of SOCE over-activation in different cells and tissues. My studies revealed additional anomalies in TAM/STRMK that, if confirmed in patients, would improve patient's healthcare and management. I also identified therapeutic targets that could improve the muscle function of TAM/STRMK mice and patients. By targeting *Orai1* expression with genetic cross or with a translational shRNA strategy I provided the first therapeutic proof-of-concept and translational approach for TAM/STRMK. In a second therapeutic proof-of-concept, I proved ORAI1 inhibition as a more efficient therapeutic approach to revert disease progression, paving the way for the trials with ORAI1 inhibitors as a translational application to inhibit the negative effects of SOCE over-activation. Noteworthy, SOCE over-activation is also seen in other diseases including Duchenne's muscular dystrophy (DMD), limb girdle muscle dystrophy type 2E (LGMD2E) and malignant hyperthermia (MH). The development and preclinical validation of therapeutic approaches for TAM/STRMK may therefore benefit all these conditions with a common therapy.

APPENDIX

1. TUBULAR AGGREGATES IN AGING AND DISEASE

1.1. Tubular aggregates in humans

Tubular aggregates are structures composed of ordered membrane tubules and were firstly identified in patients with hypo and hyperkalemic periodic paralysis, later associated to mutations in potassium and sodium channels (Engel et al., 1970; Luan et al., 2009; Plaster et al., 2001) (Table A1). Tubular aggregates also appear in patients with deficient proline and creatine synthesis, and cholesterol trafficking and glycolysis (Edvardson et al., 2010; Fleury et al., 2007; Oh et al., 2006; Salameh et al., 2013; Valtonen et al., 1996; Wedatilake et al., 2015) (Table A1). The presence of tubular aggregates as the major histopathological hallmark on muscle biopsies from patients with childhood or adolescence-onset muscle weakness coined the descriptive term "tubular aggregate myopathy" (TAM). In contrast to other muscle conditions with tubular aggregates, tubular aggregates from TAM patients affect both slow and fast fibers (Barone et al., 2017; Bohm et al., 2017; Bohm et al., 2014; Bohm et al., 2013; Bohm et al., 2018; Endo et al., 2015; Misceo et al., 2014; Morin et al., 2020; Schiaffino and Reggiani, 2011) (Table A1). The majority of TAM patients show additional multi-systemic sing including short stature, miosis, ichthyosis, dyslexia, thrombocytopenia and hyposplenia, and the full clinical presentation is referred as Stormorne syndrome (STRMK) (Bohm and Laporte, 2018). TAM/STRMK is caused by GoF mutations in *STIM1* and *ORAI1*. Missense mutations in the muscle-specific *CASQ1* are reported in TAM patients with late onset muscle weakness and myalgia. In any case, all TAM/STRMK mutations alter cellular Ca^{2+} homeostasis and affect cytosolic Ca^{2+} levels in the skeletal muscle (Silva-Rojas et al., 2020). Accordingly, glycosylation of STIM1 and ORAI1 regulate SOCE and mutations in glycosiltransferases DPAGT1, GFPT1 and ALG2 cause congenital myasthenic syndrome with tubular aggregates (Belaya et al., 2012; Cordts et al., 2016; Cossins et al., 2013; Huh et al., 2012; Selcen et al., 2014) (Table A1.) Tubular aggregates are Ca^{2+}-rich and presumably originate from the sarcoplasmic reticulum (more details in Sarcoplasmic reticulum origin of tubular aggregates section below) (Salviati et al., 1985; Schiaffino, 2012).

Table A1. Human diseases with aggregates.

Disease	Gene	Protein function	Location	Common defects	Reference
Dyskalemic periodic paralysis	-	-	II fibers	Muscle weakness	(Engel et al., 1970)
Andersen Tawil syndrome	*KCNJ2*	K^+ channel	-	Muscle weakness	(Plaster et al., 2001)
Hypokalemic periodic paralysis type 2	*SNC4A*	Na^+ channel	II fibers	Muscle weakness	(Luan et al., 2009)
Gyrate atrophy of choroid and retina and hyperorthinemia	*OAT*	Proline biosynthesis	II fibers	Muscle weakness	(Fleury et al., 2007; Valtonen et al., 1996)
Mitochondrial encephalopathy	*SERAC1*	Cholesteol trafficking	-	Muscle weakness	(Wedatilake et al., 2015)
Cerebral creatine deficiency syndrome type 3	*GATM*	Brain creatine synthesis	-	Muscle weakness, hyperCKemia	(Edvardson et al., 2010)
Glycogen storage disease	*PGAM2*	Glycolysis	II fibers	Muscle weakness, cramps, hyperCKemia	(Oh et al., 2006; Salameh et al., 2013)
Congenital myasthenic syndrome	*DPAGT1*	Glycosyltransferase	-	Muscle weakness, contractures, hyperCKemia	(Belaya et al., 2012; Selcen et al., 2014)
Congenital myasthenic syndrome	*GFPT1*	Glycosyltransferase	II fibers	Muscle weakness, contractures, hyperCKemia	(Huh et al., 2012)
Congenital myasthenic syndrome	*ALG2*	Glycosyltransferase	-	Muscle weakness, contractures, hyperCKemia	(Cossins et al., 2013)
Autoimmune myasthenic syndrome	-	-	II fibers	Muscle weakness, hyperCKemia	(Cordts et al., 2016)
TAM/STRMK	*STIM1*	Reticular Ca^{2+} sensor	I and II fibers	Muscle weakness, cramps, hyperCKemia, myalgia	(Bohm et al., 2014; Bohm et al., 2013; Misceo et al., 2014; Morin et al., 2014)
TAM/STRMK	*ORAI1*	Ca^{2+} channel	I and II fibers	Muscle weakness, cramps, hyperCKemia, myalgia	(Bohm et al., 2017; Endo et al., 2015)
TAM	*CASQ1*	Ca^{2+} buffer	I and II fibers	Muscle weakness, cramps, hyperCKemia, myalgia	(Barone et al., 2017; Bohm et al., 2018)

Tubular aggregates were not only associated with various congenital, metabolic, and mitochondrial myopathies and in myasthenic human syndromes, they were also found to accumulate in muscle in several murine models. A knockin mouse model for *Scn4a* recapitulated the defect in muscle excitability characteristic of hypokalemic periodic paralysis and tubular aggregates were also found in muscle sections (Wu et al., 2011) (Table A2). Muscle-specific knockout of *Gfpt1* recapitulated the defects of neurotransmission observed in congenital myasthenic syndrome and tubular aggregates were found on muscle sections (Issop et al., 2018). Besides, tubular aggregates are also found in heterozygous *Lama2*$^{+/-}$ dystrophic mice, in mice deficient in creatine kinase, in mice deficient in caveolin 1 or caveolin 2, and in myostatin deficient mice (Amthor et al., 2007; Craig and Allen, 1980; Schubert et al., 2007; Steeghs et al., 1997) (Table A2). As referred in the AVAILABLE TAM/STRMK MOUSE MODELS section in the Discussion, *Orai1*$^{G100S/+}$ is currently the only TAM/STRMK mouse model accumulating tubular aggregates in the muscle fibers. Noteworthy, the *Orai1*$^{G100S/+}$ mice show significantly less signs of myofiber degeneration than *Stim1*$^{H109Q/+}$ mice (https://doi.org/10.1016/j.nmd.2019.06.168), emphasizing the inverse correlation between tubular aggregates and muscle fiber degeneration/regeneration cycles, and supporting the idea that tubular aggregates may serve as a Ca^{2+} sink to protect the muscle from deleterious Ca^{2+} stress.

Tubular aggregates are not exclusively associated to muscle disorders in mice, but also accumulate in normal muscles with age. The formation of tubular aggregates depends on different factors as gender, type of muscle and age, and can occur as early as 5 months in the C57BL/6 inbred strain and only affecting the males (Agbulut et al., 2000; Chevessier et al., 2004; Kuncl et al., 1989) (Table A2). Tubular aggregates are not described in aged human probably because most myopathies involve biopsies at young age and since healthy elder people are rarely biopsied. Nevertheless, the correlation of tubular aggregates with aging was further supported by their premature apparition in mouse models with accelerated senescence and in mice deficient in serum response factor with faster aging (Lahoute et al., 2008; Nishikawa et al., 2000) (Table A2).

Table A2. Mouse models with tubular aggregates.

Human condition	Mouse model	Location	Reference
Limb girdle muscle dystrophy, congenital muscle dystrophy	*Lama2$^{Dy/+}$* mice	II fibers	(Craig and Allen, 1980)
Dilated cardiomyopathy	*Ckm$^{-/-}$* deficient mice	-	(Steeghs et al., 1997)
Lypodystrophy, pulmonary hypertension	*Cav1$^{-/-}$* and *Cav2$^{-/-}$* mice	-	(Schubert et al., 2007)
Muscle hypertrophy	*Mstn$^{-/-}$* mice	IIb fibers	(Amthor et al., 2007)
Hypokalemic periodic paralysis	*Scn4A* KI mice	-	(Wu et al., 2011)
Congenital myasthenic syndrome	*Gfpt1$^{-/-}$* mice	II fibers	(Issop et al., 2018)
TAM/STRMK	*Orai1$^{G100S/+}$* mice	-	(https://doi.org/10.1016/j.nmd.2019.06.168)
Aging	Aged mice	II fibers	(Agbulut et al., 2000; Chevessier et al., 2004; Kuncl et al., 1989)
Aging	Senescence-accelerated aging	II fibers	(Nishikawa et al., 2000)
Aging	Serum response factor deficient mice	-	(Lahoute et al., 2008)

1.3. Sarcoplasmic reticulum origin of tubular aggregates

Tubular aggregates are essentially composed of sarcoplasmic reticulum proteins as evidenced by immunofluorescence. Endoplasmic/sarcoplasmic reticulum (ER/SR) resident proteins including CASQ1, SERCA1, triadin, sarcalumenin, STIM1 and RyR1 accumulated in the tubular aggregates from TAM/STRMK patients, congenital myasthenic syndrome patients and aging mice (Bohm et al., 2017; Bohm et al., 2014; Bohm et al., 2013; Bohm et al., 2018; Boncompagni et al., 2012; Brady et al., 2016; Chevessier et al., 2005; Chevessier et al., 2004; Endo et al., 2015; Funk et al., 2013). Proteins residing in sarcolemma or in the T-tubules like DHPR and ORAI1 were detected within the tubular aggregates in several but not all studies (Bohm et al., 2018; Boncompagni et al., 2020; Chevessier et al., 2005; Morin et al., 2014), nuclear emerin protein was also reported inside the tubular aggregates in two single studies (Chevessier et al., 2005; Funk et al., 2013), and

mitochondrial accumulation was shown in the vicinity of tubular aggregates in one study (Chevessier et al., 2005). This indicates either different compositions of tubular aggregates depending on the condition, or technical reasons account for this discrepancy. Indeed, immunofluoresnce and immunohistochemistry are biased studies and an unbiased approach is needed to conclude. For this, the dissection of tubular aggregates using laser dissection microscopes, and their analysis by mass spectrometry would determine the exact protein composition of tubular aggregates. Other sarcoplasmic components of the myofibers are absent in tubular aggregates including myofilaments and sarcolemma as evidenced by their negative staining of myosins, desmin, spectrin, tubulin and dystrophin, indicating no major effect of tubular aggregates on muscle contraction and contractile units (Brady et al., 2016; Chevessier et al., 2005; Chevessier et al., 2004; Funk et al., 2013; Ikezoe et al., 2003).

Although it is widely assumed and accepted that tubular aggregates originate from the SR, the mechanisms underlying their formation are not understood. It was suggested that tubular aggregates may originate from protein aggregation within the ER/SR (Schiaffino, 2012). Over-expression of ER resident proteins including HMG-CoA reductase (3-hydroxy-3-methyl-glutaryl-coenzyme A reductase), cytochrome b5 and Inositol trisphosphate receptor (IP_3R) in CHO and COS cells induced the elongation of ER into tubule arrays similar resembling tubular aggregates (Chin et al., 1982; Snapp et al., 2003; Takei et al., 1994). Moreover, rat skeletal muscle fibers subjected to anoxia, a stress that induces protein misfolding and aggregation (Diaz-Bulnes et al., 2019), triggered the formation of tubular aggregates within 3 hours (Schiaffino et al., 1977). Interestingly, markers of unfolded protein response including GRP78 and GRP94 were shown to accumulate inside tubular aggregates of TAM/STRMK patients, indicating protein misfolding and protein aggregation (Funk et al., 2013; Ikezoe et al., 2003). If tubular aggregate originate from protein misfolding and aggregation, CASQ1 would be a relevant player in the process since it is one of the most abundant proteins in the ER/SR and can form high-order oligomeric structures that would serve as matrix for the formation of tubules (Wang and Michalak, 2020). In this line, deletion of *Casq1* in mice reduced the age-related SR dilatation and the formation of tubular aggregates, confirming a central role of CASQ1 in the formation of tubular aggregates (Boncompagni et al., 2012).

1.4. Conditions altering tubular aggregate formation in mice

The formation of tubular aggregates may represent a protective mechanism of skeletal muscle to face elevated cytosolic Ca^{2+} levels in TAM/STRMK and cumulative Ca^{2+} stress in aging muscle. Indeed, tubular aggregates are absent from murine TAM/STRMK muscles, but dystrophic signs including nuclei internalization and infiltration of immune cells associated with enhanced myofiber degeneration and regeneration are more prominent on murine muscle sections compared to TAM/STRMK patients, suggesting a causal link between tubular aggregates and myofiber degeneration (Silva-Rojas et al., 2020). As for old WT mice, tubular aggregates only appear in type II fibers (Table A2), which are known to be more sensitive to Ca^{2+}, are more prone membrane damage by mechanical stretch, and display higher SR content than slow fibers (Barthel et al., 2021; Schiaffino, 2012; Schiaffino and Reggiani, 2011; Webster et al., 1988). Altogether, tubular aggregates appear likely to form when Ca^{2+} stress is sustained and protein misfolding and aggregation could enhance SR elongation.

The absence of tubular aggregates in aged female mice is intriguing and indicate a potential role of sex hormones. This is supported by the observation that castrated male mice displayed significantly less tubular aggregates in the gastrocnemius muscle at 6 months than uncastrated animals (Kuncl et al., 1989). Estrogens are known to protect muscle membrane from contraction-induced membrane damage and would thus reduce the membrane permeability to Ca^{2+} and other ions (Koot et al., 1991). The association of tubular aggregates with aging was further supported by the correlation with senescence. Mice with accelerated senescence develop tubular aggregates prematurely while mice with retarded senescence did not show tubular aggregates in histology (Nishikawa et al., 2000) (Table A2).

Another contributing factor in the formation of tubular aggregates is mitochondrial function. Indeed, mitochondrial energetics and redox state seem to impact ER stress and the formation of tubular aggregates. This is supported by reduced ER stress and tubular aggregate formation in transgenic mice over-expressing PGC1α, the master regulator of mitochondrial biogenesis. In contrast, PGC1α deficient mice showed higher percentage of fibers with tubular aggregates compared to WT controls at 24 months (Gill et al., 2019). In accordance, the diet supplementation of trans-resveratrol, an antioxidant polyphenol that activates PGC1α via Sirtuin 1, reduced the

percentage of fibers with tubular aggregates in 18 months old mice treated over the last 6 months (Toniolo et al., 2018). Resveratrol is also known to inhibit STIM1 activity by reducing its ERK1/2-mediated phosphorylation, negatively impacting STIM1 oligomerization and inducing a potential decrease of SOCE activity (Casas-Rua et al., 2013). The combined activity of resveratrol in mitochondrial biogenesis and SOCE possibly accounts for the reduced tubular aggregate formation.

CASQ1 is an ER/SR resident protein acting as a Ca^{2+} buffer and polymerizes with increasing luminal Ca^{2+} concentration (Wang and Michalak, 2020). Upon sustained Ca^{2+} stress in TAM/STRMK or cumulative Ca^{2+} stress in the process of aging, CASQ1 supposedly forms higher-order polymers to absorb the surplus Ca^{2+} in the reticulum and may thereby act as a pillar in the formation of tubular aggregates (Chevessier et al., 2005; Chevessier et al., 2004). Accordingly, the deletion of *Casq1* in murine muscles reduced the SR Ca^{2+} content and tubular aggregates did not properly form (Boncompagni et al., 2012; Murphy et al., 2009).

Ca^{2+} entry units (CEUs) are intracellular junctions between the longitudinal SR and the T-tubule and are formed during acute exercise to permit stable STIM1-ORAI1 interactions within I band of the sarcomeres (Protasi et al., 2021). CEUs are known to facilitate SOCE and enhance the resistance to fatigue (Boncompagni et al., 2017; Michelucci et al., 2019; Michelucci et al., 2020). Similarly, murine deletion of *Casq1* avoided tubular aggregate formation but also generated constant CEUs in the absence of exercise, and *Casq1*^{-/-} mice showed enhanced resistance to fatigue accordingly (Michelucci et al., 2020). Similar structures were seen in aged trained mice subjected to regular training on wheel cages. The regular exercise improved the SOCE-dependent resistance to fatigue and tubular aggregates in muscle histology were less abundant in aged mice compared with untrained littermates (Boncompagni et al., 2020). The authors hypothesized that a part of the STIM1 pool was sequestered within the tubular aggregates of untrained mice, while regular exercise requires a large number of STIM1 molecules to allow the formation of the CEUs. As STIM1 is a transmembrane protein connecting membrane structures, the authors measured the distance between membrane contact sites where STIM1 could be located and found a similar distance pattern of 8 nm. These membrane contacts sites were: 1) SR vesicles in adult mice, 2) T-tubules and longitudinal SR in the CEUs, 3) transversal tubules of tubular aggregates, 4) and ER-plasma membrane junctions in HEK cells over-expressing YFP-STIM1 (Boncompagni et al.,

2020; Orci et al., 2009) (Figure A1). Taken together, tubular aggregates in aged mice seem to be correlated with sustained cytosolic Ca^{2+} stress and require CASQ1 as pillar to form. However, while STIM1 was hypothesized recently as a linker of the SR tubules within the tubular aggregates, additional experiments are needed to conclude on the process for tubular aggregate formation.
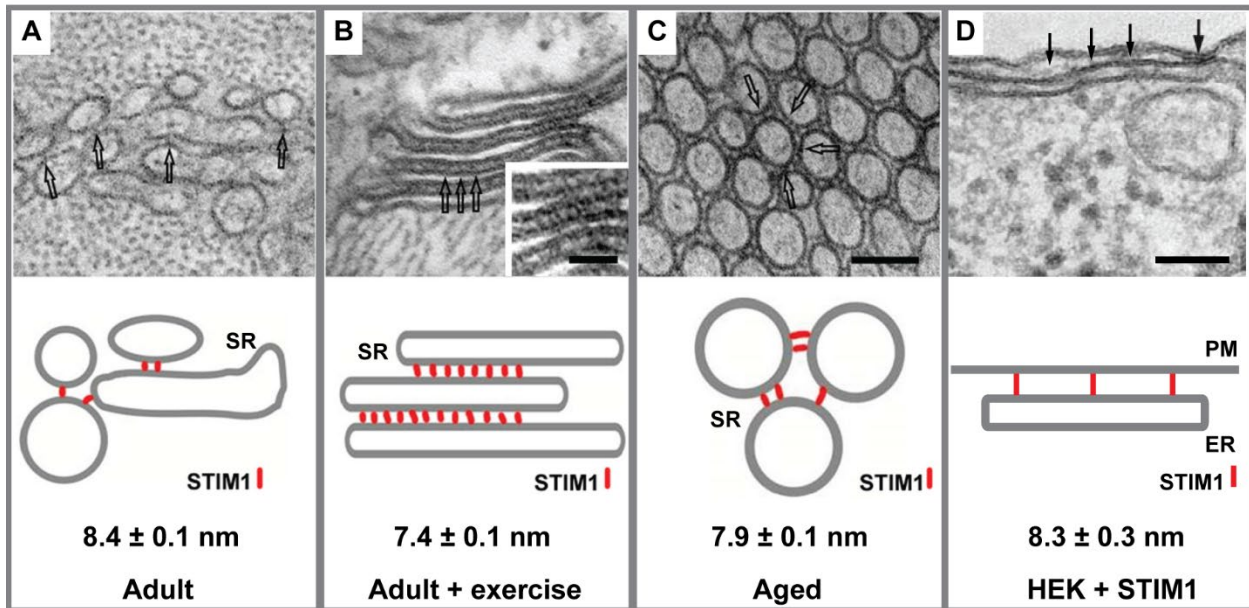
Figure A1. **Membrane contacts between where STIM1 can be involved.**

(A-D) Representative EM images and corresponding cartoons of (A) SR/tubules contacts within I band of adult muscle, (B) SR stacks in Ca^{2+} entry units (CEUs) of exercised adult muscle, (C) tubular aggregates, and (D) endoplasmic reticulum-plasma membrane (ER-PM) contact sites in HEK cells over-expressing YFP-STIM1. STIM1 linkers are represented as arrows in EM images and red lines in cartoons, and the size of membrane linkers are shown as mean ± SEM. Scale bar dezoomed regions= 100 nm and scale bar zoomed region (B) = 50 nm. Adapted from Boncompagni et al., 2020 and Orci et al., 2009).

1.5. *Stim1* knockdown impedes tubular aggregate formation in mice

In order to determine the requirement of STIM1 for tubular aggregate formation and the potential effects of *Stim1* knockdown, I generated heterozygous $Stim1^{+/-}$ males and assessed a potential muscle phenotype until late adulthood, and the presence of tubular aggregates in aged animals. The homozygous deletion of *Stim1* in mice is lethal but heterozygous animals are viable and fertile (Baba et al., 2008; Oh-Hora et al., 2008). Here, I crossed $Stim1^{L2/+}$ mice with heterozygous Cre deleter mice and obtained $Stim1^{+/+}$ and $Stim1^{+/-}$ mice with the expected birth ratio (47% $Stim1^{+/+}$ and 53% $Stim1^{+/-}$; n=126, p value =0.27). Western blot analysis confirmed the 50% reduction of STIM1 expression in $Stim1^{+/-}$ males compared to $Stim1^{+/+}$ controls at 4 and 18 months (Fig, A2A). $Stim1^{+/-}$ and $Stim1^{+/+}$ mice were followed over 4 months and no major difference was observed in weight gain and general muscle performance as evidenced by the hanging tests (Fig A2B). However, despite normal values of maximal specific force were reached by $Stim1^{+/-}$ mice, *in situ* muscle contraction and relaxation upon single stimulation was delayed and increased force decay was observed when subjected to continuous stimulation at 40 Hz frequency (Fig. A2D-G). No major histological anomalies were reported and fiber size of tibialis anterior fibers from $Stim1^{+/-}$ mice was comparable to $Stim1^{+/-}$ controls (data not shown). Overall, the genetic reduction of *Stim1* did not have any major negative impact on muscle performance or morphology and only minor anomalies in contraction/relaxation and resistance to fatigue were noted in aged $Stim1^{+/-}$ animals.

Tubular aggregates were more abundant in gastrocnemius than tibialis anterior from $Stim1^{+/+}$ littermates and were completely absent in the soleus (data not shown), confirming that they principally appear in type II fiber-rich muscles. In contrast, $Stim1^{+/-}$ gastrocnemius and tibialis anterior did not display tubular aggregates, further supporting the hypothesis of STIM1 as a potential brick in the formation of tubular aggregates (Fig. A2H). Altogether, the absence of tubular aggregates in $Stim1^{+/-}$ mice associated with minor muscle performance anomalies, thus confirming STIM1 as a stabilizing factor for the formation of tubular aggregates, and showing that 50% reduction of STIM1 impacts muscle relaxation and resistance to fatigue. This indicates that heterozygous carriers with CRAC channelopathy mutations in *STIM1* may have minor muscle pathologies while a targeted reduction of STIM1 would represent a potential therapy to counteract the overactive STIM1 in TAM/STRMK.
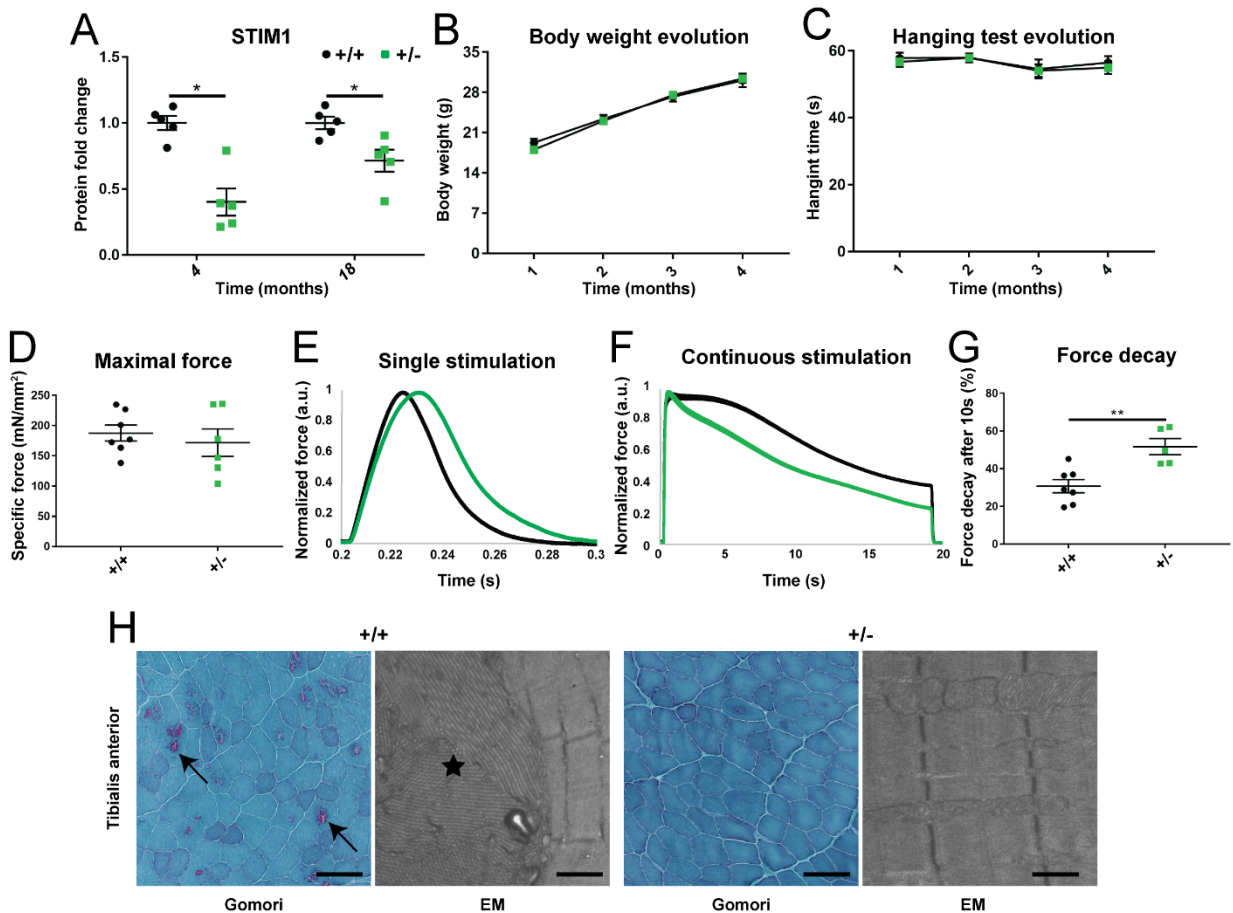
Figure A2. Absence of tubular aggregates and anomalies in contraction and resistance to fatigue in aged *Stim1*⁺/⁻ mice

*(A) STIM1 protein levels were decreased by half in tibialis anterior extracts from Stim1⁺/⁻ mice compared with Stim1⁺/⁺ littermates at 4 and 18 months of age (n=4-5). (B-C) Body weight gain and hanging test abilities were comparable in Stim1⁺/⁻ mice and Stim1⁺/⁺ controls (n=13-18). (D-E) The maximal specific force produced by tibialis anterior from Stim1⁺/⁻ mice was comparable to Stim1⁺/⁺ controls, while contraction and relaxation were delayed following single stimulation (n=6). (F-G) Upon continuous stimulation of 40 Hz, the force decay was more pronounced in Stim1⁺/⁻ mice compared with controls (n=5-7). (H) Tubular aggregates were only detected in the tibialis anterior from Stim1⁺/⁺ (arrows and asterisk) and not in Stim1⁺/⁻ mice (n=5). Gomori scale bar = 100 μm and EM scale bar = 1 μm. Graphs illustrate the mean ± SEM. Significant differences are indicated as *p<0.05, **p<0.01, ***p<0.001 and ****p<0.0001.*

1.6. Additional material and methods

This additional material and methods section refers to the results displayed in Appendix 1.

Mouse lines

Animals were maintained at room temperature with 12h day/12h night light cycles and access to food and water *ab libidum*. Animal experimentation was in accordance with French and European legislations and all experiments were approved by ethical committees (project numbers 2016031110589922, 2020052516535988 and 2019062813376603). The *Stim1^{L2/+}* mouse line was a king gift from Prof. Anjana Rao (La Jolla Institute, La Jolla, California, USA) (Oh-Hora et al., 2008), the Gt(ROSA)26 Cre deleter mouse line was provided by the ICS (Birling et al., 2012), and the *Orai1^{+/-}* mouse line was a kind gift from Prof. Paul F. Worley (John Hopkins University School of Medecine, Baltimore, Maryland, USA) (Ahuja et al., 2017). All mice had a C57BL/6 background. Genotyping primers were: AACGTCTTGCAGTTGCTGTAGGC (forward) and GGCTCTGCTGACCTGGAACTATAGTG (reverse) for *Stim1*; GAACCTGATGGACATGTTCAGG (forward) and AGTGCGTTCGAACGCTAGAGCCTGT (reverse) for Cre; and ATGCCTACTGCCAAAATTGAC (forward) and AAATACTGAGCCATCTCTCCTG (reverse) for *Orai1*.

Mouse phenotyping and in situ force measurements

Body weight was assessed weekly and hanging ability was determined by suspending the mice on a cage lid for a maximum time of 60 seconds. The time to fall was recorded with 3 repetitions and an interval resting time of 5 minutes.

To assess *in situ* muscle force of tibialis anterior, 18 months old mice were anesthetized with intraperitoneal injection of domitor/fentanyl 2/0.28 mg/Kg), diazepam (8 mg/Kg) and fentanyl (0.28 mg/Kg). The tibialis anterior was partially excised and attached to the isometric force transducer. To assess maximal force, increasing stimulation frequencies were applied to the sciatic nerve (1, 25, 50, 100 and 125 Hz) and the maximal force was retained. For the force decay studies, the nerve was continuously stimulated with 50 Hz frequency for 20 seconds. The contraction and relaxation time after single stimulations were calculated as the time to reach 100% of the force or decrease by 50%. The specific maximal force was calculated as the maximal force produced

divided by the cross sectional area calculated as the muscle mass (mg)/ optimal length (mm) X mammalian muscle density (1.06 mg/mm^3). Force ratio was calculated as the percentage of force drop after 10 seconds of stimulation.

Muscle histology and electron microscopy

For morphological analyses, tibialis anterior, gastrocnemius and soleus from 18 month old mice were frozen in liquid nitrogen-cooled isopentane, and 8 µm sections were stained with modified Gomori trichrome staining and imaged the using Nanozoomer 2HT slide scanner (Hamamatsu, Japan).

For electron microscopy, TA sections were fixed in 2.5% glutaraldehyde, 2.5% paraformaldehyde, 50 mM Ca^{2+} in cacodylate buffer (0.1M, pH 7.4). For inclusion, samples were washed in cacodylate buffer for 30 minutes, postfixed in 1% osmium tetroxide in 0.1M cacodylate for 1 h at 4°C. Samples were dehydrated through graded alcohol (50%, 70%, 90% and 100%) and propylene oxide for 30 minutes each and embedded in Epon 812. Ultrathin sections of 70 nm were cut on a Leica Ultracut microtome (Leica, Wetzlar, Germany), contrasted with uranyl acetate and lead citrate, and examined at 70kv with a Morgagni 268D electron microscope (FEI, Electron Optics, Eindhoven, Netherlands). Images were captured digitally by a Mega View III Camera (Soft Imaging System, Münster, Germany).

Protein expression studies

For protein expression studies, tibialis anterior cryosections were lysed in radio immunoprecipitation (RIPA) buffer supplemented with 1 mM PMSF, 1 mM DTT and complete mini EDTA-free protease inhibitor cocktail (Roche). 10 µg of denaturated protein were loaded on a 10 % SDS-PAGE gel, run and transferred to nitrocellulose membranes using the Transblot® TurboTM RTA Transfert Kit (Biorad, Hercules, USA). Ponceau S staining served a loading control (Sigma-Aldrich, St Louis, USA). Membranes were blocked 1 h in Tris-buffered saline containing 5% of non-fat milk and 0.1% Tween 20. Following primary and secondary antibodies were used: rabbit anti-STIM1 (1/2000; AB9870, Millipore, Burlington, USA) and peroxidase-coated goat anti rabbit (1/10000; 111-036-045, Jackson ImmunoResearch, Ely, UK). Images were recorded with the Amesham Imager 600 (Amersham, UK).

All experiments were performed and analyzed in a blinded manner and the investigators were unaware of the genotype of the mice. Difference in birth ratio were assessed by chi-square test. The normal distribution of the data was assessed using the Shapiro-Wilk test and presented as mean ± standard error of the mean (SEM). For normally distributed data, the groups were examined using a Student's t test (with or without Welch's correction). For other data, Mann-Whitney statistical test was used. Significant differences are illustrated as $*p<0.05$, $**p<0.01$, $***p<0.001$ and $****p<0.0001$.

2. SECONDARY PUBLICATIONS (chronological order)

2.1. Mice with muscle-specific deletion of Bin1 recapitulate centronuclear myopathy and acute downregulation of dynamin 2 improves their phenotypes.
Molecular Therapy (2021).

Authors: <u>Roberto Silva-Rojas</u>*, Vasugi Nattarayan*, Francisco Jaque-Fernandez, Raquel Gomez-Oca, Alexia Menuet, David Reiss, Marie Goret, Nadia Messaddeq, Valentina M. Lionello, Christine Kretz, Belinda S. Cowling, Vincent Jacquemond and Jocelyn Laporte. * Equal contribution.

My contribution: I performed the *in situ* muscle force experiments and histological analysis of the *Bin1^{mck-/-}* cohort treated with ASO targeting *Dnm2*. I also collected and analyzed the data, drafted the article with Jocelyn Laporte, and performed the required experiments in the revision process.

2.2. Selective loss of a LAP1 isoform causes a muscle-specific nuclear envelopathy.
Neurogenetics (2021).

Authors: Xavière Lornage, Martial Mallaret, <u>Roberto Silva-Rojas</u>, Valérie Biancalana, Diane Giovannini, Klaus Dieterich, Safaa Saker, Jean-François Deleuze, Bernard Wuyam, Jocelyn Laporte and Johann Böhm.

My contribution: I extracted RNA and protein from the patient cell line and performed RT-qPCR and western blot to show the impact of the *TOR1AIP1* patient mutations on the expression of the different isoforms.

2.3. Functional analyses of STIM1 mutations reveal a common pathomechanism for tubular aggregate myopathy and Stormorken syndrome.
Neuropathology (2020).

Authors: Georges Arielle Peche, Coralie Spiegelhalter*, <u>Roberto Silva-Rojas</u>*, Jocelyn Laporte and Johann Böhm. * Equal contribution.

My contribution: I measured the basal Ca^{2+} level in cells transfected with STIM1 TAM/STRMK mutants, collected and analyzed the data, and designed the figures.

Authors: Xènia Massana-Muñoz, Christine Kretz, <u>Roberto Silva-Rojas</u>, Julien Ochala, Alexia Menuet, Norma B. Romero, Belinda S. Cowling, and Jocelyn Laporte.

My contribution: I performed the *in situ* muscle force measurements in $Dnm2^{S619L/+}$ mice with or without treatment of ASO targeting *Dnm2*.

REFERENCES

Abell, E., Ahrends, R., Bandara, S., Park, B.O., and Teruel, M.N. (2011). Parallel adaptive feedback enhances reliability of the Ca2+ signaling system. P Natl Acad Sci USA *108*, 14485-14490.

Agbulut, O., Destombes, J., Thiesson, D., and Butler-Browne, G. (2000). Age-related appearance of tubular aggregates in the skeletal muscle of almost all male inbred mice. Histochem Cell Biol *114*, 477-481.

Ahuja, M., Schwartz, D.M., Tandon, M., Son, A., Zeng, M., Swaim, W., Eckhaus, M., Hoffman, V., Cui, Y., Xiao, B.*, et al.* (2017). Orai1-Mediated Antimicrobial Secretion from Pancreatic Acini Shapes the Gut Microbiome and Regulates Gut Innate Immunity. Cell Metab *25*, 635-646.

Al-Qusairi, L., and Laporte, J. (2011). T-tubule biogenesis and triad formation in skeletal muscle and implication in human diseases. Skelet Muscle *1*, 26.

Amthor, H., Macharia, R., Navarrete, R., Schuelke, M., Brown, S.C., Otto, A., Voit, T., Muntoni, F., Vrbova, G., Partridge, T.*, et al.* (2007). Lack of myostatin results in excessive muscle growth but impaired force generation. Proc Natl Acad Sci U S A *104*, 1835-1840.

Annunziato, L., Secondo, A., Pignataro, G., Scorziello, A., and Molinaro, P. (2020). New perspectives for selective NCX activators in neurodegenerative diseases. Cell Calcium *87*, 102170.

Antigny, F., Sabourin, J., Sauc, S., Bernheim, L., Koenig, S., and Frieden, M. (2017). TRPC1 and TRPC4 channels functionally interact with STIM1L to promote myogenesis and maintain fast repetitive Ca(2+) release in human myotubes. Biochim Biophys Acta Mol Cell Res *1864*, 806-813.

Augusto, V., Padovani, C., and Campos, G. (2004). Augusto V, Padovani CR, Campos GR. Braz J Morphol Sci *21*, 89-94.

Ayuso, E., Mingozzi, F., and Bosch, F. (2010). Production, purification and characterization of adeno-associated vectors. Curr Gene Ther *10*, 423-436.

Baba, Y., Nishida, K., Fujii, Y., Hirano, T., Hikida, M., and Kurosaki, T. (2008). Essential function for the calcium sensor STIM1 in mast cell activation and anaphylactic responses. Nat Immunol *9*, 81-88.

Bahar, E., Kim, H., and Yoon, H. (2016). ER Stress-Mediated Signaling: Action Potential and Ca(2+) as Key Players. Int J Mol Sci *17*.

Bajek, A., Porowinska, D., Kloskowski, T., Brzoska, E., Ciemerych, M.A., and Drewa, T. (2015). Cell Therapy in Duchenne Muscular Dystrophy Treatment: Clinical Trials Overview. Crit Rev Eukar Gene *25*, 1-11.

Bal, N.C., Jena, N., Chakravarty, H., Kumar, A., Chi, M., Balaraju, T., Rawale, S.V., Rawale, J.S., Sharon, A., and Periasamy, M. (2015). The C-Terminal Calcium-Sensitive Disordered Motifs Regulate Isoform-Specific Polymerization Characteristics of Calsequestrin. Biopolymers *103*, 15-22.

Barone, V., Del Re, V., Gamberucci, A., Polverino, V., Galli, L., Rossi, D., Costanzi, E., Toniolo, L., Berti, G., Malandrini, A.*, et al.* (2017). Identification and characterization of three novel mutations in the CASQ1 gene in four patients with tubular aggregate myopathy. Hum Mutat *38*, 1761-1773.

Barthel, B.L., Cox, D., Barbieri, M., Ziemba, M., Straub, V., Hoffman, E.P., and Russell, A.J. (2021). Elevation of fast but not slow troponin I in the circulation of patients with Becker and Duchenne muscular dystrophy. Muscle Nerve *64*, 43-49.

Begam, M., Abro, V.M., Mueller, A.L., and Roche, J.A. (2016). Sodium 4-phenylbutyrate reduces myofiber damage in a mouse model of Duchenne muscular dystrophy. Appl Physiol Nutr Metab *41*, 1108-1111.

Belaya, K., Finlayson, S., Slater, C.R., Cossins, J., Liu, W.W., Maxwell, S., McGowan, S.J., Maslau, S., Twigg, S.R., Walls, T.J.*, et al.* (2012). Mutations in DPAGT1 cause a limb-girdle congenital myasthenic syndrome with tubular aggregates. Am J Hum Genet *91*, 193-201.

Berger, J., Li, M., Berger, S., Meilak, M., Rientjes, J., and Currie, P.D. (2020). Effect of Ataluren on dystrophin mutations. J Cell Mol Med *24*, 6680-6689.

Berna-Erro, A., Jardin, I., Smani, T., and Rosado, J.A. (2016). Regulation of Platelet Function by Orai, STIM and TRP. Adv Exp Med Biol *898*, 157-181.

Berridge, M.J., Bootman, M.D., and Roderick, H.L. (2003). Calcium signalling: dynamics, homeostasis and remodelling. Nat Rev Mol Cell Biol *4*, 517-529.

Birling, M.C., Dierich, A., Jacquot, S., Herault, Y., and Pavlovic, G. (2012). Highly-efficient, fluorescent, locus directed cre and FlpO deleter mice on a pure C57BL/6N genetic background. Genesis *50*, 482-489.

Biscans, A., Caiazzi, J., McHugh, N., Hariharan, V., Muhuri, M., and Khvorova, A. (2021). Docosanoic acid conjugation to siRNA enables functional and safe delivery to skeletal and cardiac muscles. Mol Ther *29*, 1382-1394.

Blair, H.C., Robinson, L.J., Huang, C.L., Sun, L., Friedman, P.A., Schlesinger, P.H., and Zaidi, M. (2011). Calcium and bone disease. Biofactors *37*, 159-167.

Boczek, T., Sobolczyk, M., Mackiewicz, J., Lisek, M., Ferenc, B., Guo, F., and Zylinska, L. (2021). Crosstalk among Calcium ATPases: PMCA, SERCA and SPCA in Mental Diseases. Int J Mol Sci *22*.

Bohm, J., Bulla, M., Urquhart, J.E., Malfatti, E., Williams, S.G., O'Sullivan, J., Szlauer, A., Koch, C., Baranello, G., Mora, M.*, et al.* (2017). ORAI1 Mutations with Distinct Channel Gating Defects in Tubular Aggregate Myopathy. Hum Mutat *38*, 426-438.

Bohm, J., Chevessier, F., Koch, C., Peche, G.A., Mora, M., Morandi, L., Pasanisi, B., Moroni, I., Tasca, G., Fattori, F.*, et al.* (2014). Clinical, histological and genetic characterisation of patients with tubular aggregate myopathy caused by mutations in STIM1. J Med Genet *51*, 824-833.

Bohm, J., Chevessier, F., Maues De Paula, A., Koch, C., Attarian, S., Feger, C., Hantai, D., Laforet, P., Ghorab, K., Vallat, J.M.*, et al.* (2013). Constitutive activation of the calcium sensor STIM1 causes tubular-aggregate myopathy. Am J Hum Genet *92*, 271-278.

Bohm, J., and Laporte, J. (2018). Gain-of-function mutations in STIM1 and ORAI1 causing tubular aggregate myopathy and Stormorken syndrome. Cell Calcium *76*, 1-9.

Bohm, J., Lornage, X., Chevessier, F., Birck, C., Zanotti, S., Cudia, P., Bulla, M., Granger, F., Bui, M.T., Sartori, M.*, et al.* (2018). CASQ1 mutations impair calsequestrin polymerization and cause tubular aggregate myopathy. Acta Neuropathol *135*, 149-151.

Bonam, S.R., Wang, F.J., and Muller, S. (2019). Lysosomes as a therapeutic target. Nature Reviews Drug Discovery *18*, 923-948.

Boncompagni, S., Michelucci, A., Pietrangelo, L., Dirksen, R.T., and Protasi, F. (2017). Exercise-dependent formation of new junctions that promote STIM1-Orai1 assembly in skeletal muscle. Sci Rep *7*, 14286.

Boncompagni, S., Pecorai, C., Michelucci, A., Pietrangelo, L., and Protasi, F. (2020). Long-Term Exercise Reduces Formation of Tubular Aggregates and Promotes Maintenance of Ca(2+) Entry Units in Aged Muscle. Front Physiol *11*, 601057.

Boncompagni, S., Protasi, F., and Franzini-Armstrong, C. (2012). Sequential stages in the age-dependent gradual formation and accumulation of tubular aggregates in fast twitch muscle fibers: SERCA and calsequestrin involvement. Age (Dordr) *34*, 27-41.

Borsani, O., Piga, D., Costa, S., Govoni, A., Magri, F., Artoni, A., Cinnante, C.M., Fagiolari, G., Ciscato, P., Moggio, M.*, et al.* (2018). Stormorken Syndrome Caused by a p.R304W STIM1 Mutation: The First Italian Patient and a Review of the Literature. Front Neurol *9*, 859.

Brady, S., Healy, E.G., Gang, Q., Parton, M., Quinlivan, R., Jacob, S., Curtis, E., Al-Sarraj, S., Sewry, C.A., Hanna, M.G.*, et al.* (2016). Tubular Aggregates and Cylindrical Spirals Have Distinct Immunohistochemical Signatures. J Neuropathol Exp Neurol *75*, 1171-1178.

Brini, M., and Carafoli, E. (2011). The plasma membrane Ca(2)+ ATPase and the plasma membrane sodium calcium exchanger cooperate in the regulation of cell calcium. Cold Spring Harb Perspect Biol *3*.

Bronte, V., and Pittet, M.J. (2013). The spleen in local and systemic regulation of immunity. Immunity *39*, 806-818.

Burr, A.R., and Molkentin, J.D. (2015). Genetic evidence in the mouse solidifies the calcium hypothesis of myofiber death in muscular dystrophy. Cell Death Differ *22*, 1402-1412.

Carreras-Sureda, A., Abrami, L., Kim, J.-H., Frieden, M., Didier, M., Van der Goot, F.G., and Demaurex, N. (2021). S-acylation targets ORAI1 channels to lipid rafts for efficient Ca2+ signaling by T cell receptors at the immune synapse. bioRxiv, 2021.2002.2003.429577.

Casas-Rua, V., Alvarez, I.S., Pozo-Guisado, E., and Martin-Romero, F.J. (2013). Inhibition of STIM1 phosphorylation underlies resveratrol-induced inhibition of store-operated calcium entry. Biochem Pharmacol *86*, 1555-1563.

Castets, P., Frank, S., Sinnreich, M., and Ruegg, M.A. (2016). "Get the Balance Right": Pathological Significance of Autophagy Perturbation in Neuromuscular Disorders. J Neuromuscul Dis *3*, 127-155.

Catterall, W.A. (2011). Voltage-gated calcium channels. Cold Spring Harb Perspect Biol *3*, a003947.

Chen, Y., Ramachandran, A., Zhang, Y., Koshy, R., and George, A. (2018). The ER Ca(2+) sensor STIM1 can activate osteoblast and odontoblast differentiation in mineralized tissues. Connect Tissue Res *59*, 6-12.

Chen, Y.J., Quintanilla, C.G., and Liou, J. (2019). Recent insights into mammalian ER-PM junctions. Curr Opin Cell Biol *57*, 99-105.

Chevessier, F., Bauche-Godard, S., Leroy, J.P., Koenig, J., Paturneau-Jouas, M., Eymard, B., Hantai, D., and Verdiere-Sahuque, M. (2005). The origin of tubular aggregates in human myopathies. J Pathol *207*, 313-323.

Chevessier, F., Marty, I., Paturneau-Jouas, M., Hantai, D., and Verdiere-Sahuque, M. (2004). Tubular aggregates are from whole sarcoplasmic reticulum origin: alterations in calcium binding protein expression in mouse skeletal muscle during aging. Neuromuscul Disord *14*, 208-216.

Chin, D.J., Luskey, K.L., Anderson, R.G., Faust, J.R., Goldstein, J.L., and Brown, M.S. (1982). Appearance of crystalloid endoplasmic reticulum in compactin-resistant Chinese hamster cells with a 500-fold increase in 3-hydroxy-3-methylglutaryl-coenzyme A reductase. Proc Natl Acad Sci U S A *79*, 1185-1189.

Choi, J.H., Jeong, S.Y., Oh, M.R., Allen, P.D., and Lee, E.H. (2020). TRPCs: Influential Mediators in Skeletal Muscle. Cells *9*.

Choi, Y.J., Zhao, Y., Bhattacharya, M., and Stathopulos, P.B. (2017). Structural perturbations induced by Asn131 and Asn171 glycosylation converge within the EFSAM core and enhance stromal interaction molecule-1 mediated store operated calcium entry. Biochim Biophys Acta Mol Cell Res *1864*, 1054-1063.

Collins, S.R., and Meyer, T. (2011). Evolutionary origins of STIM1 and STIM2 within ancient Ca2+ signaling systems. Trends Cell Biol *21*, 202-211.

Colon-Thillet, R., Jerome, K.R., and Stone, D. (2021). Optimization of AAV vectors to target persistent viral reservoirs. Virol J *18*, 85.

Conte, E., Pannunzio, A., Imbrici, P., Camerino, G.M., Maggi, L., Mora, M., Gibertini, S., Cappellari, O., De Luca, A., Coluccia, M.*, et al.* (2021). Gain-of-Function STIM1 L96V Mutation Causes Myogenesis Alteration in Muscle Cells From a Patient Affected by Tubular Aggregate Myopathy. Front Cell Dev Biol *9*, 635063.

Cordero-Sanchez, C., Riva, B., Reano, S., Clemente, N., Zaggia, I., Ruffinatti, F.A., Potenzieri, A., Pirali, T., Raffa, S., Sangaletti, S.*, et al.* (2019). A luminal EF-hand mutation in STIM1 in mice causes the clinical hallmarks of tubular aggregate myopathy. Dis Model Mech *13*.

Cordts, I., Funk, F., Schulz, J.B., Weis, J., and Claeys, K.G. (2016). Tubular aggregates in autoimmune Lambert-Eaton myasthenic syndrome. Neuromuscul Disord *26*, 880-884.

Cossins, J., Belaya, K., Hicks, D., Salih, M.A., Finlayson, S., Carboni, N., Liu, W.W., Maxwell, S., Zoltowska, K., Farsani, G.T.*, et al.* (2013). Congenital myasthenic syndromes due to mutations in ALG2 and ALG14. Brain *136*, 944-956.

Craig, I.D., and Allen, I.V. (1980). Tubular aggregates in murine dystrophy heterozygotes. Muscle Nerve *3*, 134-140.

Darbellay, B., Arnaudeau, S., Bader, C.R., Konig, S., and Bernheim, L. (2011). STIM1L is a new actin-binding splice variant involved in fast repetitive Ca2+ release. J Cell Biol *194*, 335-346.

Darbellay, B., Arnaudeau, S., Konig, S., Jousset, H., Bader, C., Demaurex, N., and Bernheim, L. (2009). STIM1- and Orai1-dependent store-operated calcium entry regulates human myoblast differentiation. J Biol Chem *284*, 5370-5380.

Dayal, A., Schrotter, K., Pan, Y., Fohr, K., Melzer, W., and Grabner, M. (2017). The Ca2+ influx through the mammalian skeletal muscle dihydropyridine receptor is irrelevant for muscle performance. Nature Communications *8*.

De Luca, A., Pierno, S., Liantonio, A., Cetrone, M., Camerino, C., Simonetti, S., Papadia, F., and Camerino, D.C. (2001). Alteration of excitation-contraction coupling mechanism in extensor digitorum longus muscle fibres of dystrophic mdx mouse and potential efficacy of taurine. Br J Pharmacol *132*, 1047-1054.

Diaz-Bulnes, P., Saiz, M.L., Lopez-Larrea, C., and Rodriguez, R.M. (2019). Crosstalk Between Hypoxia and ER Stress Response: A Key Regulator of Macrophage Polarization. Front Immunol *10*, 2951.

Divet, A., and Huchet-Cadiou, C. (2002). Sarcoplasmic reticulum function in slow- and fast-twitch skeletal muscles from mdx mice. Pflugers Arch *444*, 634-643.

Dominov, J.A., Kravetz, A.J., Ardelt, M., Kostek, C.A., Beermann, M.L., and Miller, J.B. (2005). Muscle-specific BCL2 expression ameliorates muscle disease in laminin {alpha}2-deficient, but not in dystrophin-deficient, mice. Hum Mol Genet *14*, 1029-1040.

Dorchies, O.M., Reutenauer-Patte, J., Dahmane, E., Ismail, H.M., Petermann, O., Patthey- Vuadens, O., Comyn, S.A., Gayi, E., Piacenza, T., Handa, R.J.*, et al.* (2013). The anticancer drug tamoxifen counteracts the pathology in a mouse model of duchenne muscular dystrophy. Am J Pathol *182*, 485-504.

Dorr, K., Kilch, T., Kappel, S., Alansary, D., Schwar, G., Niemeyer, B.A., and Peinelt, C. (2016). Cell type-specific glycosylation of Orai1 modulates store-operated Ca2+ entry. Science Signaling *9*.

Dowling, J.J., Gonorazky, H.D., Cohn, R.D., and Campbell, C. (2018). Treating pediatric neuromuscular disorders: The future is now. American Journal of Medical Genetics Part A *176*, 804-841.

Dowling, J.J., Weihl, C.C., and Spencer, M.J. (2021). Molecular and cellular basis of genetically inherited skeletal muscle disorders. Nat Rev Mol Cell Biol.

Dyrda, A., Koenig, S., and Frieden, M. (2020). STIM1 long and STIM1 gate differently TRPC1 during store-operated calcium entry. Cell Calcium *86*, 102134.

Eapen, A., Sundivakkam, P., Song, Y., Ravindran, S., Ramachandran, A., Tiruppathi, C., and George, A. (2010). Calcium-mediated stress kinase activation by DMP1 promotes osteoblast differentiation. J Biol Chem *285*, 36339-36351.

Edvardson, S., Korman, S.H., Livne, A., Shaag, A., Saada, A., Nalbandian, R., Allouche-Arnon, H., Gomori, J.M., and Katz-Brull, R. (2010). l-arginine:glycine amidinotransferase (AGAT) deficiency: clinical presentation and response to treatment in two patients with a novel mutation. Mol Genet Metab *101*, 228-232.

Edwards, J.N., Friedrich, O., Cully, T.R., von Wegner, F., Murphy, R.M., and Launikonis, B.S. (2010a). Upregulation of store-operated Ca2+ entry in dystrophic mdx mouse muscle. Am J Physiol Cell Physiol *299*, C42-50.

Edwards, J.N., Murphy, R.M., Cully, T.R., von Wegner, F., Friedrich, O., and Launikonis, B.S. (2010b). Ultra-rapid activation and deactivation of store-operated Ca(2+) entry in skeletal muscle. Cell Calcium *47*, 458-467.

Endo, Y., Noguchi, S., Hara, Y., Hayashi, Y.K., Motomura, K., Miyatake, S., Murakami, N., Tanaka, S., Yamashita, S., Kizu, R., *et al.* (2015). Dominant mutations in ORAI1 cause tubular aggregate myopathy with hypocalcemia via constitutive activation of store-operated Ca(2)(+) channels. Hum Mol Genet *24*, 637-648.

Engel, W.K., Bishop, D.W., and Cunningham, G.G. (1970). Tubular aggregates in type II muscle fibers: ultrastructural and histochemical correlation. J Ultrastruct Res *31*, 507-525.

Fahrner, M., Stadlbauer, M., Muik, M., Rathner, P., Stathopulos, P., Ikura, M., Muller, N., and Romanin, C. (2018). A dual mechanism promotes switching of the Stormorken STIM1 R304W mutant into the activated state. Nat Commun *9*, 825.

Feske, S., Gwack, Y., Prakriya, M., Srikanth, S., Puppel, S.H., Tanasa, B., Hogan, P.G., Lewis, R.S., Daly, M., and Rao, A. (2006). A mutation in Orai1 causes immune deficiency by abrogating CRAC channel function. Nature *441*, 179-185.

Fetalvero, K.M., Yu, Y., Goetschkes, M., Liang, G., Valdez, R.A., Gould, T., Triantafellow, E., Bergling, S., Loureiro, J., Eash, J., *et al.* (2013). Defective autophagy and mTORC1 signaling in myotubularin null mice. Mol Cell Biol *33*, 98-110.

Finkel, T., Menazza, S., Holmstrom, K.M., Parks, R.J., Liu, J., Sun, J., Liu, J., Pan, X., and Murphy, E. (2015). The ins and outs of mitochondrial calcium. Circ Res *116*, 1810-1819.

Fleury, M., Barbier, R., Ziegler, F., Mohr, M., Caron, O., Dollfus, H., Tranchant, C., and Warter, J.M. (2007). Myopathy with tubular aggregates and gyrate atrophy of the choroid and retina due to hyperornithinaemia. J Neurol Neurosurg Psychiatry *78*, 656-657.

Fraysse, B., Rouaud, T., Millour, M., Fontaine-Perus, J., Gardahaut, M.F., and Levitsky, D.O. (2001). Expression of the Na(+)/Ca(2+) exchanger in skeletal muscle. Am J Physiol Cell Physiol *280*, C146-154.

Frontera, W.R., and Ochala, J. (2015). Skeletal muscle: a brief review of structure and function. Calcif Tissue Int *96*, 183-195.

Funk, F., Ceuterick-de Groote, C., Martin, J.J., Meinhardt, A., Taratuto, A.L., De Bleecker, J., Van Coster, R., De Paepe, B., Schara, U., Vorgerd, M., *et al.* (2013). Morphological spectrum and clinical features of myopathies with tubular aggregates. Histol Histopathol *28*, 1041-1054.

Gailly, P. (2012). TRP channels in normal and dystrophic skeletal muscle. Curr Opin Pharmacol *12*, 326-334.

Galluzzi, L., Bravo-San Pedro, J.M., Levine, B., Green, D.R., and Kroemer, G. (2017). Pharmacological modulation of autophagy: therapeutic potential and persisting obstacles. Nat Rev Drug Discov *16*, 487-511.

Gamage, T.H., Gunnes, G., Lee, R.H., Louch, W.E., Holmgren, A., Bruton, J.D., Lengle, E., Kolstad, T.R.S., Revold, T., Amundsen, S.S., *et al.* (2018). STIM1 R304W causes muscle degeneration and impaired platelet activation in mice. Cell Calcium *76*, 87-100.

Gattineni, J. (2014). Inherited disorders of calcium and phosphate metabolism. Curr Opin Pediatr *26*, 215-222.

Gayi, E., Neff, L.A., Massana Munoz, X., Ismail, H.M., Sierra, M., Mercier, T., Decosterd, L.A., Laporte, J., Cowling, B.S., Dorchies, O.M.*, et al.* (2018). Tamoxifen prolongs survival and alleviates symptoms in mice with fatal X-linked myotubular myopathy. Nat Commun *9*, 4848.

Gill, J.F., Delezie, J., Santos, G., McGuirk, S., Schnyder, S., Frank, S., Rausch, M., St-Pierre, J., and Handschin, C. (2019). Peroxisome proliferator-activated receptor gamma coactivator 1alpha regulates mitochondrial calcium homeostasis, sarcoplasmic reticulum stress, and cell death to mitigate skeletal muscle aging. Aging Cell *18*, e12993.

Girgenrath, M., Dominov, J.A., Kostek, C.A., and Miller, J.B. (2004). Inhibition of apoptosis improves outcome in a model of congenital muscular dystrophy. J Clin Invest *114*, 1635-1639.

Godin, R., Daussin, F., Matecki, S., Li, T., Petrof, B.J., and Burelle, Y. (2012). Peroxisome proliferator-activated receptor gamma coactivator1- gene alpha transfer restores mitochondrial biomass and improves mitochondrial calcium handling in post-necrotic mdx mouse skeletal muscle. J Physiol *590*, 5487-5502.

Goncalves, M.A. (2005). Adeno-associated virus: from defective virus to effective vector. Virol J *2*, 43.

Gonzalez, V., Paneda, C., Martinez, T., Guerra, A., Monteiro, S., Vargas, B., Bleau, A.M., Ruz, V., and Jimenez, A.I. (2018). Development of a RNAi therapeutic for the treatment of allergic conjunctivitis. Invest Ophth Vis Sci *59*.

Goonasekera, S.A., Davis, J., Kwong, J.Q., Accornero, F., Wei-LaPierre, L., Sargent, M.A., Dirksen, R.T., and Molkentin, J.D. (2014). Enhanced Ca(2)(+) influx from STIM1-Orai1 induces muscle pathology in mouse models of muscular dystrophy. Hum Mol Genet *23*, 3706-3715.

Goonasekera, S.A., Lam, C.K., Millay, D.P., Sargent, M.A., Hajjar, R.J., Kranias, E.G., and Molkentin, J.D. (2011). Mitigation of muscular dystrophy in mice by SERCA overexpression in skeletal muscle. J Clin Invest *121*, 1044-1052.

Goyenvalle, A., Leumann, C., and Garcia, L. (2016). Therapeutic Potential of Tricyclo-DNA antisense oligonucleotides. J Neuromuscul Dis *3*, 157-167.

Grosse, J., Braun, A., Varga-Szabo, D., Beyersdorf, N., Schneider, B., Zeitlmann, L., Hanke, P., Schropp, P., Muhlstedt, S., Zorn, C.*, et al.* (2007). An EF hand mutation in Stim1 causes premature platelet activation and bleeding in mice. J Clin Invest *117*, 3540-3550.

Gwack, Y., Srikanth, S., Oh-Hora, M., Hogan, P.G., Lamperti, E.D., Yamashita, M., Gelinas, C., Neems, D.S., Sasaki, Y., Feske, S.*, et al.* (2008). Hair loss and defective T- and B-cell function in mice lacking ORAI1. Mol Cell Biol *28*, 5209-5222.

Haustrate, A., Hantute-Ghesquier, A., Prevarskaya, N., and Lehen'kyi, V. (2019). Monoclonal Antibodies Targeting Ion Channels and Their Therapeutic Potential. Front Pharmacol *10*, 606.

Horinouchi, T., Higashi, T., Higa, T., Terada, K., Mai, Y., Aoyagi, H., Hatate, C., Nepal, P., Horiguchi, M., Harada, T.*, et al.* (2012). Different binding property of STIM1 and its novel splice variant STIM1L to Orai1, TRPC3, and TRPC6 channels. Biochem Bioph Res Co *428*, 252-258.

Hou, X., Pedi, L., Diver, M.M., and Long, S.B. (2012). Crystal structure of the calcium release-activated calcium channel Orai. Science *338*, 1308-1313.

Huh, S.Y., Kim, H.S., Jang, H.J., Park, Y.E., and Kim, D.S. (2012). Limb-girdle myasthenia with tubular aggregates associated with novel GFPT1 mutations. Muscle Nerve *46*, 600-604.

Ikezoe, K., Furuya, H., Ohyagi, Y., Osoegawa, M., Nishino, I., Nonaka, I., and Kira, J. (2003). Dysferlin expression in tubular aggregates: their possible relationship to endoplasmic reticulum stress. Acta Neuropathol *105*, 603-609.

Issop, Y., Hathazi, D., Khan, M.M., Rudolf, R., Weis, J., Spendiff, S., Slater, C.R., Roos, A., and Lochmuller, H. (2018). GFPT1 deficiency in muscle leads to myasthenia and myopathy in mice. Hum Mol Genet *27*, 3218-3232.

Jairaman, A., and Prakriya, M. (2013). Molecular pharmacology of store-operated CRAC channels. Channels (Austin) *7*, 402-414.

Jiang, L.J., Zhao, X., Dou, Z.Y., Su, Q.X., and Rong, Z.H. (2021). Stormorken Syndrome Caused by a Novel STIM1 Mutation: A Case Report. Front Neurol *12*, 522513.

Jimenez, A.I., Martinez, T., Gonzalez, V., Martinez-Garcia, C., and Paneda, C. (2015). Development of a RNAi therapeutic for the treatment of allergic conjunctivitis. Invest Ophth Vis Sci *56*.

Kargacin, M.E., and Kargacin, G.J. (1996). The sarcoplasmic reticulum calcium pump is functionally altered in dystrophic muscle. Biochim Biophys Acta *1290*, 4-8.

Kawasaki, T., Ueyama, T., Lange, I., Feske, S., and Saito, N. (2010). Protein kinase C-induced phosphorylation of Orai1 regulates the intracellular Ca2+ level via the store-operated Ca2+ channel. J Biol Chem *285*, 25720-25730.

Kilch, T., Alansary, D., Peglow, M., Dorr, K., Rychkov, G., Rieger, H., Peinelt, C., and Niemeyer, B.A. (2013). Mutations of the Ca2+-sensing stromal interaction molecule STIM1 regulate Ca2+ influx by altered oligomerization of STIM1 and by destabilization of the Ca2+ channel Orai1. J Biol Chem *288*, 1653-1664.

Kim, K.D., Srikanth, S., Tan, Y.V., Yee, M.K., Jew, M., Damoiseaux, R., Jung, M.E., Shimizu, S., An, D.S., Ribalet, B.*, et al.* (2014). Calcium signaling via Orai1 is essential for induction of the nuclear orphan receptor pathway to drive Th17 differentiation. J Immunol *192*, 110-122.

Knapp, M.L., Förderer, K., Alansary, D., Jung, M., Schwarz, Y., Lis, A., and Niemeyer, B.A. (2020). Alternative splicing switches STIM1 targeting to specialized membrane contact sites and modifies SOCE. bioRxiv, 2020.2003.2025.005199.

Koot, R.W., Amelink, G.J., Blankenstein, M.A., and Bar, P.R. (1991). Tamoxifen and oestrogen both protect the rat muscle against physiological damage. J Steroid Biochem Mol Biol *40*, 689-695.

Krebs, J., Agellon, L.B., and Michalak, M. (2015). Ca(2+) homeostasis and endoplasmic reticulum (ER) stress: An integrated view of calcium signaling. Biochem Biophys Res Commun *460*, 114-121.

Kuncl, R.W., Pestronk, A., Lane, J., and Alexander, E. (1989). The MRL +/+ mouse: a new model of tubular aggregates which are gender- and age-related. Acta Neuropathol *78*, 615-620.

Kuno, A., Hosoda, R., Sebori, R., Hayashi, T., Sakuragi, H., Tanabe, M., and Horio, Y. (2018). Resveratrol Ameliorates Mitophagy Disturbance and Improves Cardiac Pathophysiology of Dystrophin-deficient mdx Mice. Sci Rep *8*, 15555.

Lacruz, R.S., and Feske, S. (2015). Diseases caused by mutations in ORAI1 and STIM1. Ann N Y Acad Sci *1356*, 45-79.

Lahoute, C., Sotiropoulos, A., Favier, M., Guillet-Deniau, I., Charvet, C., Ferry, A., Butler-Browne, G., Metzger, D., Tuil, D., and Daegelen, D. (2008). Premature aging in skeletal muscle lacking serum response factor. PLoS One *3*, e3910.

Lamb, G.D. (2000). Excitation-contraction coupling in skeletal muscle: Comparisons with cardiac muscle. Clin Exp Pharmacol P *27*, 216-224.

Lamb, G.D., Junankar, P.R., and Stephenson, D.G. (1995). Raised intracellular [Ca2+] abolishes excitation-contraction coupling in skeletal muscle fibres of rat and toad. J Physiol *489 (Pt 2)*, 349-362.

Launikonis, B.S., Stephenson, D.G., and Friedrich, O. (2009). Rapid Ca2+ flux through the transverse tubular membrane, activated by individual action potentials in mammalian skeletal muscle. J Physiol *587*, 2299-2312.

Lee, C.S., Hanna, A.D., Wang, H., Dagnino-Acosta, A., Joshi, A.D., Knoblauch, M., Xia, Y., Georgiou, D.K., Xu, J., Long, C.*, et al.* (2017). A chemical chaperone improves muscle function in mice with a RyR1 mutation. Nat Commun *8*, 14659.

Lewis, R.S. (2011). Store-operated calcium channels: new perspectives on mechanism and function. Cold Spring Harb Perspect Biol *3*.

Liang, X., Zhang, N., Pan, H., Xie, J., and Han, W. (2021). Development of Store-Operated Calcium Entry-Targeted Compounds in Cancer. Front Pharmacol *12*, 688244.

Liou, J., Kim, M.L., Heo, W.D., Jones, J.T., Myers, J.W., Ferrell, J.E., and Meyer, T. (2005). STIM is a Ca2+ sensor essential for Ca2+-store-depletion-triggered Ca2+ influx. Current Biology *15*, 1235-1241.

Lipskaia, L., Chemaly, E.R., Hadri, L., Lompre, A.M., and Hajjar, R.J. (2010). Sarcoplasmic reticulum Ca(2+) ATPase as a therapeutic target for heart failure. Expert Opin Biol Ther *10*, 29-41.

Lopez, E., Jardin, I., Berna-Erro, A., Bermejo, N., Salido, G.M., Sage, S.O., Rosado, J.A., and Redondo, P.C. (2012). STIM1 tyrosine-phosphorylation is required for STIM1-Orai1 association in human platelets. Cell Signal *24*, 1315-1322.

Lopez, J.J., Jardin, I., Sanchez-Collado, J., Salido, G.M., Smani, T., and Rosado, J.A. (2020). TRPC Channels in the SOCE Scenario. Cells *9*.

Luan, X., Chen, B., Liu, Y., Zheng, R., Zhang, W., and Yuan, Y. (2009). Tubular aggregates in paralysis periodica paramyotonica with T704M mutation of SCN4A. Neuropathology *29*, 579-584.

Lunz, V., Romanin, C., and Frischauf, I. (2019). STIM1 activation of Orai1. Cell Calcium *77*, 29-38.

Lyon, A.R., Babalis, D., Morley-Smith, A.C., Hedger, M., Suarez Barrientos, A., Foldes, G., Couch, L.S., Chowdhury, R.A., Tzortzis, K.N., Peters, N.S.*, et al.* (2020). Investigation of the safety and feasibility of AAV1/SERCA2a gene transfer in patients with chronic heart failure supported with a left ventricular assist device - the SERCA-LVAD TRIAL. Gene Ther *27*, 579-590.

Lytton, J., Westlin, M., Burk, S.E., Shull, G.E., and Maclennan, D.H. (1992). Functional Comparisons between Isoforms of the Sarcoplasmic or Endoplasmic-Reticulum Family of Calcium Pumps. Journal of Biological Chemistry *267*, 14483-14489.

Ma, G., Wei, M., He, L., Liu, C., Wu, B., Zhang, S.L., Jing, J., Liang, X., Senes, A., Tan, P.*, et al.* (2015). Inside-out Ca(2+) signalling prompted by STIM1 conformational switch. Nat Commun *6*, 7826.

Ma, G., Zheng, S., Ke, Y., Zhou, L., He, L., Huang, Y., Wang, Y., and Zhou, Y. (2017). Molecular Determinants for STIM1 Activation During Store- Operated Ca2+ Entry. Curr Mol Med *17*, 60-69.

Manjarres, I.M., Rodriguez-Garcia, A., Alonso, M.T., and Garcia-Sancho, J. (2010). The sarco/endoplasmic reticulum Ca2+ ATPase (SERCA) is the third element in capacitative calcium entry. Cell Calcium *47*, 412-418.

Marino, G., Niso-Santano, M., Baehrecke, E.H., and Kroemer, G. (2014). Self-consumption: the interplay of autophagy and apoptosis. Nat Rev Mol Cell Biol *15*, 81-94.

Markello, T., Chen, D., Kwan, J.Y., Horkayne-Szakaly, I., Morrison, A., Simakova, O., Maric, I., Lozier, J., Cullinane, A.R., Kilo, T.*, et al.* (2015). York platelet syndrome is a CRAC channelopathy due to gain-of-function mutations in STIM1. Mol Genet Metab *114*, 474-482.

Matveeva, O.V., Tsodikov, A.D., Giddings, M., Freier, S.M., Wyatt, J.R., Spiridonov, A.N., Shabalina, S.A., Gesteland, R.F., and Atkins, J.F. (2000). Identification of sequence motifs in oligonucleotides whose presence is correlated with antisense activity. Nucleic Acids Res *28*, 2862-2865.

McCarl, C.A., Khalil, S., Ma, J., Oh-hora, M., Yamashita, M., Roether, J., Kawasaki, T., Jairaman, A., Sasaki, Y., Prakriya, M.*, et al.* (2010). Store-operated Ca2+ entry through ORAI1 is critical for T cell-mediated autoimmunity and allograft rejection. J Immunol *185*, 5845-5858.

Michelucci, A., Boncompagni, S., Pietrangelo, L., Garcia-Castaneda, M., Takano, T., Malik, S., Dirksen, R.T., and Protasi, F. (2019). Transverse tubule remodeling enhances Orai1-dependent Ca(2+) entry in skeletal muscle. Elife *8*.

Michelucci, A., Boncompagni, S., Pietrangelo, L., Takano, T., Protasi, F., and Dirksen, R.T. (2020). Pre-assembled Ca2+ entry units and constitutively active Ca2+ entry in skeletal muscle of calsequestrin-1 knockout mice. J Gen Physiol *152*.

Michelucci, A., Garcia-Castaneda, M., Boncompagni, S., and Dirksen, R.T. (2018). Role of STIM1/ORAI1-mediated store-operated Ca(2+) entry in skeletal muscle physiology and disease. Cell Calcium *76*, 101-115.

Miederer, A.M., Alansary, D., Schwar, G., Lee, P.H., Jung, M., Helms, V., and Niemeyer, B.A. (2015). A STIM2 splice variant negatively regulates store-operated calcium entry. Nat Commun *6*, 6899.

Millay, D.P., Goonasekera, S.A., Sargent, M.A., Maillet, M., Aronow, B.J., and Molkentin, J.D. (2009). Calcium influx is sufficient to induce muscular dystrophy through a TRPC-dependent mechanism. Proc Natl Acad Sci U S A *106*, 19023-19028.

Misceo, D., Holmgren, A., Louch, W.E., Holme, P.A., Mizobuchi, M., Morales, R.J., De Paula, A.M., Stray-Pedersen, A., Lyle, R., Dalhus, B.*, et al.* (2014). A dominant STIM1 mutation causes Stormorken syndrome. Hum Mutat *35*, 556-564.

Morin, G., Biancalana, V., Echaniz-Laguna, A., Noury, J.B., Lornage, X., Moggio, M., Ripolone, M., Violano, R., Marcorelles, P., Marechal, D.*, et al.* (2020). Tubular aggregate myopathy and Stormorken syndrome: Mutation spectrum and genotype/phenotype correlation. Hum Mutat *41*, 17-37.

Morin, G., Bruechle, N.O., Singh, A.R., Knopp, C., Jedraszak, G., Elbracht, M., Bremond-Gignac, D., Hartmann, K., Sevestre, H., Deutz, P.*, et al.* (2014). Gain-of-Function Mutation in STIM1 (P.R304W) Is Associated with Stormorken Syndrome. Hum Mutat *35*, 1221-1232.

Murphy, R.M., Dutka, T.L., Horvath, D., Bell, J.R., Delbridge, L.M., and Lamb, G.D. (2013). Ca2+-dependent proteolysis of junctophilin-1 and junctophilin-2 in skeletal and cardiac muscle. J Physiol *591*, 719-729.

Murphy, R.M., Larkins, N.T., Mollica, J.P., Beard, N.A., and Lamb, G.D. (2009). Calsequestrin content and SERCA determine normal and maximal Ca2+ storage levels in sarcoplasmic reticulum of fast- and slow-twitch fibres of rat. J Physiol *587*, 443-460.

Neel, B.A., Lin, Y., and Pessin, J.E. (2013). Skeletal muscle autophagy: a new metabolic regulator. Trends Endocrinol Metab *24*, 635-643.

Nesin, V., Wiley, G., Kousi, M., Ong, E.C., Lehmann, T., Nicholl, D.J., Suri, M., Shahrizaila, N., Katsanis, N., Gaffney, P.M.*, et al.* (2014). Activating mutations in STIM1 and ORAI1 cause overlapping syndromes of tubular myopathy and congenital miosis. Proc Natl Acad Sci U S A *111*, 4197-4202.

Neufeld, E.F. (2006). Enzyme replacement therapy - a brief history. In Fabry Disease: Perspectives from 5 Years of FOS, A. Mehta, M. Beck, and G. Sunder-Plassmann, eds. (Oxford).

Nicoll, D.A., Sawaya, M.R., Kwon, S., Cascio, D., Philipson, K.D., and Abramson, J. (2006). The crystal structure of the primary Ca2+ sensor of the Na+/Ca2+ exchanger reveals a novel Ca2+ binding motif. J Biol Chem *281*, 21577-21581.

Nishikawa, T., Takahashi, J.A., Matsushita, T., Ohnishi, K., Higuchi, K., Hashimoto, N., and Hosokawa, M. (2000). Tubular aggregates in the skeletal muscle of the senescence-accelerated mouse; SAM. Mech Ageing Dev *114*, 89-99.

Novello, M.J., Zhu, J., Feng, Q., Ikura, M., and Stathopulos, P.B. (2018). Structural elements of stromal interaction molecule function. Cell Calcium *73*, 88-94.

Oh-Hora, M., Yamashita, M., Hogan, P.G., Sharma, S., Lamperti, E., Chung, W., Prakriya, M., Feske, S., and Rao, A. (2008). Dual functions for the endoplasmic reticulum calcium sensors STIM1 and STIM2 in T cell activation and tolerance. Nat Immunol *9*, 432-443.

Oh, S.J., Park, K.S., Ryan, H.F., Jr., Danon, M.J., Lu, J., Naini, A.B., and DiMauro, S. (2006). Exercise-induced cramp, myoglobinuria, and tubular aggregates in phosphoglycerate mutase deficiency. Muscle Nerve *34*, 572-576.

Orci, L., Ravazzola, M., Le Coadic, M., Shen, W.W., Demaurex, N., and Cosson, P. (2009). From the Cover: STIM1-induced precortical and cortical subdomains of the endoplasmic reticulum. Proc Natl Acad Sci U S A *106*, 19358-19362.

Park, C.Y., Hoover, P.J., Mullins, F.M., Bachhawat, P., Covington, E.D., Raunser, S., Walz, T., Garcia, K.C., Dolmetsch, R.E., and Lewis, R.S. (2009). STIM1 Clusters and Activates CRAC Channels via Direct Binding of a Cytosolic Domain to Orai1. Cell *136*, 876-890.

Park, J.H., Jeong, S.Y., Choi, J.H., and Lee, E.H. (2021). Pathological Mechanism of a Constitutively Active Form of Stromal Interaction Molecule 1 in Skeletal Muscle. Biomolecules *11*, 1064.

Pauly, M., Daussin, F., Burelle, Y., Li, T., Godin, R., Fauconnier, J., Koechlin-Ramonatxo, C., Hugon, G., Lacampagne, A., Coisy-Quivy, M.*, et al.* (2012). AMPK activation stimulates autophagy and ameliorates muscular dystrophy in the mdx mouse diaphragm. Am J Pathol *181*, 583-592.

Peche, G.A., Spiegelhalter, C., Silva-Rojas, R., Laporte, J., and Bohm, J. (2020). Functional analyses of STIM1 mutations reveal a common pathomechanism for tubular aggregate myopathy and Stormorken syndrome. Neuropathology *40*, 559-569.

Peralta, S., Garcia, S., Yin, H.Y., Arguello, T., Diaz, F., and Moraes, C.T. (2016). Sustained AMPK activation improves muscle function in a mitochondrial myopathy mouse model by promoting muscle fiber regeneration. Hum Mol Genet *25*, 3178-3191.

Periasamy, M., and Kalyanasundaram, A. (2007). SERCA pump isoforms: their role in calcium transport and disease. Muscle Nerve *35*, 430-442.

Plaster, N.M., Tawil, R., Tristani-Firouzi, M., Canun, S., Bendahhou, S., Tsunoda, A., Donaldson, M.R., Iannaccone, S.T., Brunt, E., Barohn, R.*, et al.* (2001). Mutations in Kir2.1 cause the developmental and episodic electrical phenotypes of Andersen's syndrome. Cell *105*, 511-519.

Pozo-Guisado, E., Campbell, D.G., Deak, M., Alvarez-Barrientos, A., Morrice, N.A., Alvarez, I.S., Alessi, D.R., and Martin-Romero, F.J. (2010). Phosphorylation of STIM1 at ERK1/2 target sites modulates store-operated calcium entry. J Cell Sci *123*, 3084-3093.

Prakriya, M., Feske, S., Gwack, Y., Srikanth, S., Rao, A., and Hogan, P.G. (2006). Orai1 is an essential pore subunit of the CRAC channel. Nature *443*, 230-233.

Prakriya, M., and Lewis, R.S. (2015). Store-Operated Calcium Channels. Physiol Rev *95*, 1383-1436.

Protasi, F., Pietrangelo, L., and Boncompagni, S. (2021). Calcium entry units (CEUs): perspectives in skeletal muscle function and disease. J Muscle Res Cell Motil *42*, 233-249.

Putney, J.W., Jr. (1986). A model for receptor-regulated calcium entry. Cell Calcium *7*, 1-12.

Ramesh, G., Jarzembowski, L., Schwarz, Y., Poth, V., Konrad, M., Knapp, M.L., Schwar, G., Lauer, A.A., Grimm, M.O.W., Alansary, D.*, et al.* (2021). A short isoform of STIM1 confers frequency-dependent synaptic enhancement. Cell Rep *34*, 108844.

Roberts-Wilson, T.K., Reddy, R.N., Bailey, J.L., Zheng, B., Ordas, R., Gooch, J.L., and Price, S.R. (2010). Calcineurin signaling and PGC-1alpha expression are suppressed during muscle atrophy due to diabetes. Biochim Biophys Acta *1803*, 960-967.

Roos, J., DiGregorio, P.J., Yeromin, A.V., Ohlsen, K., Lioudyno, M., Zhang, S., Safrina, O., Kozak, J.A., Wagner, S.L., Cahalan, M.D.*, et al.* (2005). STIM1, an essential and conserved component of store-operated Ca2+ channel function. J Cell Biol *169*, 435-445.

Rosado, J.A., Diez, R., Smani, T., and Jardin, I. (2015). STIM and Orai1 Variants in Store-Operated Calcium Entry. Front Pharmacol *6*, 325.

Ruiz-Perez, V.L., Carter, S.A., Healy, E., Todd, C., Rees, J.L., Steijlen, P.M., Carmichael, A.J., Lewis, H.M., Hohl, D., Itin, P.*, et al.* (1999). ATP2A2 mutations in Darier's disease: variant cutaneous phenotypes are associated with missense mutations, but neuropsychiatric features are independent of mutation class. Hum Mol Genet *8*, 1621-1630.

Ruiz, A., Matute, C., and Alberdi, E. (2010). Intracellular Ca2+ release through ryanodine receptors contributes to AMPA receptor-mediated mitochondrial dysfunction and ER stress in oligodendrocytes. Cell Death Dis *1*, e54.

Sacchetto, R., Margreth, A., Pelosi, M., and Carafoli, E. (1996). Colocalization of the dihydropyridine receptor, the plasma-membrane calcium ATPase isoform 1 and the sodium/calcium exchanger to the junctional-membrane domain of transverse tubules of rabbit skeletal muscle. Eur J Biochem *237*, 483-488.

Salameh, J., Goyal, N., Choudry, R., Camelo-Piragua, S., and Chong, P.S. (2013). Phosphoglycerate mutase deficiency with tubular aggregates in a patient from Panama. Muscle Nerve *47*, 138-140.

Sallinger, M., Tiffner, A., Schmidt, T., Bonhenry, D., Waldherr, L., Frischauf, I., Lunz, V., Derler, I., Schober, R., and Schindl, R. (2020). Luminal STIM1 Mutants that Cause Tubular Aggregate Myopathy Promote Autophagic Processes. Int J Mol Sci *21*.

Salviati, G., Pierobon-Bormioli, S., Betto, R., Damiani, E., Angelini, C., Ringel, S.P., Salvatori, S., and Margreth, A. (1985). Tubular aggregates: sarcoplasmic reticulum origin, calcium storage ability, and functional implications. Muscle Nerve *8*, 299-306.

Saw, P.E., and Song, E.W. (2020). siRNA therapeutics: a clinical reality. Sci China Life Sci *63*, 485-500.

Schartner, V., Laporte, J., and Bohm, J. (2019). Abnormal Excitation-Contraction Coupling and Calcium Homeostasis in Myopathies and Cardiomyopathies. J Neuromuscul Dis *6*, 289-305.

Schiaffino, S. (2012). Tubular aggregates in skeletal muscle: just a special type of protein aggregates? Neuromuscul Disord *22*, 199-207.

Schiaffino, S., and Reggiani, C. (2011). Fiber types in mammalian skeletal muscles. Physiol Rev *91*, 1447-1531.

Schiaffino, S., Severin, E., Cantini, M., and Sartore, S. (1977). Tubular aggregates induced by anoxia in isolated rat skeletal muscle. Lab Invest *37*, 223-228.

Schober, R., Bonhenry, D., Lunz, V., Zhu, J., Krizova, A., Frischauf, I., Fahrner, M., Zhang, M., Waldherr, L., Schmidt, T.*, et al.* (2019). Sequential activation of STIM1 links Ca(2+) with luminal domain unfolding. Sci Signal *12*.

Schubert, W., Sotgia, F., Cohen, A.W., Capozza, F., Bonuccelli, G., Bruno, C., Minetti, C., Bonilla, E., Dimauro, S., and Lisanti, M.P. (2007). Caveolin-1(-/-)- and caveolin-2(-/-)-deficient mice both display numerous skeletal muscle abnormalities, with tubular aggregate formation. Am J Pathol *170*, 316-333.

Scoles, D.R., Minikel, E.V., and Pulst, S.M. (2019). Antisense oligonucleotides: A primer. Neurol Genet *5*, e323.

Selcen, D., Shen, X.M., Brengman, J., Li, Y., Stans, A.A., Wieben, E., and Engel, A.G. (2014). DPAGT1 myasthenia and myopathy: genetic, phenotypic, and expression studies. Neurology *82*, 1822-1830.

Shawer, H., Norman, K., Cheng, C.W., Foster, R., Beech, D.J., and Bailey, M.A. (2021). ORAI1 Ca(2+) Channel as a Therapeutic Target in Pathological Vascular Remodelling. Front Cell Dev Biol *9*, 653812.

Sheng, P., Flood, K.A., and Xie, M. (2020). Short Hairpin RNAs for Strand-Specific Small Interfering RNA Production. Front Bioeng Biotechnol *8*, 940.

Silva-Rojas, R., Charles, A.L., Djeddi, S., Geny, B., Laporte, J., and Bohm, J. (2021). Pathophysiological Effects of Overactive STIM1 on Murine Muscle Function and Structure. Cells *10*.

Silva-Rojas, R., Laporte, J., and Bohm, J. (2020). STIM1/ORAI1 Loss-of-Function and Gain-of-Function Mutations Inversely Impact on SOCE and Calcium Homeostasis and Cause Multi-Systemic Mirror Diseases. Front Physiol *11*, 604941.

Silva-Rojas, R., Treves, S., Jacobs, H., Kessler, P., Messaddeq, N., Laporte, J., and Bohm, J. (2019). STIM1 over-activation generates a multi-systemic phenotype affecting the skeletal muscle, spleen, eye, skin, bones and immune system in mice. Hum Mol Genet *28*, 1579-1593.

Smyth, J.T., Petranka, J.G., Boyles, R.R., DeHaven, W.I., Fukushima, M., Johnson, K.L., Williams, J.G., and Putney, J.W., Jr. (2009). Phosphorylation of STIM1 underlies suppression of store-operated calcium entry during mitosis. Nat Cell Biol *11*, 1465-1472.

Snapp, E.L., Hegde, R.S., Francolini, M., Lombardo, F., Colombo, S., Pedrazzini, E., Borgese, N., and Lippincott-Schwartz, J. (2003). Formation of stacked ER cisternae by low affinity protein interactions. J Cell Biol *163*, 257-269.

Stafford, N., Wilson, C., Oceandy, D., Neyses, L., and Cartwright, E.J. (2017). The Plasma Membrane Calcium ATPases and Their Role as Major New Players in Human Disease. Physiol Rev *97*, 1089-1125.

Stathopulos, P.B., Zheng, L., Li, G.Y., Plevin, M.J., and Ikura, M. (2008). Structural and mechanistic insights into STIM1-mediated initiation of store-operated calcium entry. Cell *135*, 110-122.

Steeghs, K., Benders, A., Oerlemans, F., de Haan, A., Heerschap, A., Ruitenbeek, W., Jost, C., van Deursen, J., Perryman, B., Pette, D., *et al.* (1997). Altered Ca2+ responses in muscles with combined mitochondrial and cytosolic creatine kinase deficiencies. Cell *89*, 93-103.

Sweeney, H.L., and Hammers, D.W. (2018). Muscle Contraction. Cold Spring Harb Perspect Biol *10*.

Takei, K., Mignery, G.A., Mugnaini, E., Sudhof, T.C., and De Camilli, P. (1994). Inositol 1,4,5-trisphosphate receptor causes formation of ER cisternal stacks in transfected fibroblasts and in cerebellar Purkinje cells. Neuron *12*, 327-342.

Ticci, C., Cassandrini, D., Rubegni, A., Riva, B., Vattemi, G., Mata, S., Ricci, G., Baldacci, J., Guglielmi, V., Di Muzio, A., *et al.* (2021). Expanding the clinical and genetic spectrum of pathogenic variants in STIM1. Muscle Nerve *64*, 567-575.

Tiffner, A., Schober, R., Hoglinger, C., Bonhenry, D., Pandey, S., Lunz, V., Sallinger, M., Frischauf, I., Fahrner, M., Lindinger, S., *et al.* (2021). CRAC channel opening is determined by a series of Orai1 gating checkpoints in the transmembrane and cytosolic regions. J Biol Chem *296*, 100224.

Toniolo, L., Fusco, P., Formoso, L., Mazzi, A., Canato, M., Reggiani, C., and Giacomello, E. (2018). Resveratrol treatment reduces the appearance of tubular aggregates and improves the resistance to fatigue in aging mice skeletal muscles. Exp Gerontol *111*, 170-179.

Torrente, Y., Belicchi, M., Marchesi, C., D'Antona, G., Cogiamanian, F., Pisati, F., Gavina, M., Giordano, R., Tonlorenzi, R., Fagiolari, G.*, et al.* (2007). Autologous transplantation of muscle-derived CD133+ stem cells in Duchenne muscle patients. Cell Transplant *16*, 563-577.

Vaeth, M., Yang, J., Yamashita, M., Zee, I., Eckstein, M., Knosp, C., Kaufmann, U., Karoly Jani, P., Lacruz, R.S., Flockerzi, V.*, et al.* (2017). ORAI2 modulates store-operated calcium entry and T cell-mediated immunity. Nat Commun *8*, 14714.

Vallejo-Illarramendi, A., Toral-Ojeda, I., Aldanondo, G., and Lopez de Munain, A. (2014). Dysregulation of calcium homeostasis in muscular dystrophies. Expert Rev Mol Med *16*, e16.

Valtonen, M., Nanto-Salonen, K., Heinanen, K., Alanen, A., Kalimo, H., and Simell, O. (1996). Skeletal muscle of patients with gyrate atrophy of the choroid and retina and hyperornithinaemia in ultralow-field magnetic resonance imaging and computed tomography. J Inherit Metab Dis *19*, 729-734.

van der Meijden, P.E.J., and Heemskerk, J.W.M. (2019). Platelet biology and functions: new concepts and clinical perspectives. Nat Rev Cardiol *16*, 166-179.

Vangheluwe, P., Schuermans, M., Zador, E., Waelkens, E., Raeymaekers, L., and Wuytack, F. (2005). Sarcolipin and phospholamban mRNA and protein expression in cardiac and skeletal muscle of different species. Biochem J *389*, 151-159.

Vattemi, G., Gualandi, F., Oosterhof, A., Marini, M., Tonin, P., Rimessi, P., Neri, M., Guglielmi, V., Russignan, A., Poli, C.*, et al.* (2010). Brody disease: insights into biochemical features of SERCA1 and identification of a novel mutation. J Neuropathol Exp Neurol *69*, 246-252.

Vig, M., Beck, A., Billingsley, J.M., Lis, A., Parvez, S., Peinelt, C., Koomoa, D.L., Soboloff, J., Gill, D.L., Fleig, A.*, et al.* (2006a). CRACM1 multimers form the ion-selective pore of the CRAC channel. Curr Biol *16*, 2073-2079.

Vig, M., Peinelt, C., Beck, A., Koomoa, D.L., Rabah, D., Koblan-Huberson, M., Kraft, S., Turner, H., Fleig, A., Penner, R.*, et al.* (2006b). CRACM1 is a plasma membrane protein essential for store-operated Ca2+ entry. Science *312*, 1220-1223.

Voit, A., Patel, V., Pachon, R., Shah, V., Bakhutma, M., Kohlbrenner, E., McArdle, J.J., Dell'Italia, L.J., Mendell, J.R., Xie, L.H.*, et al.* (2017). Reducing sarcolipin expression mitigates Duchenne muscular dystrophy and associated cardiomyopathy in mice. Nat Commun *8*, 1068.

Wan, W.B., and Seth, P.P. (2016). The Medicinal Chemistry of Therapeutic Oligonucleotides. J Med Chem *59*, 9645-9667.

Wang, D., Tai, P.W.L., and Gao, G. (2019). Adeno-associated virus vector as a platform for gene therapy delivery. Nat Rev Drug Discov *18*, 358-378.

Wang, Q., and Michalak, M. (2020). Calsequestrin. Structure, function, and evolution. Cell Calcium *90*, 102242.

Watts, J.K., and Corey, D.R. (2012). Silencing disease genes in the laboratory and the clinic. J Pathol *226*, 365-379.

Webster, C., Silberstein, L., Hays, A.P., and Blau, H.M. (1988). Fast muscle fibers are preferentially affected in Duchenne muscular dystrophy. Cell *52*, 503-513.

Wedatilake, Y., Plagnol, V., Anderson, G., Paine, S.M., Clayton, P.T., Jacques, T.S., and Rahman, S. (2015). Tubular aggregates caused by serine active site containing 1 (SERAC1) mutations in a patient with a mitochondrial encephalopathy. Neuropathol Appl Neurobiol *41*, 399-402.

Wei-Lapierre, L., Carrell, E.M., Boncompagni, S., Protasi, F., and Dirksen, R.T. (2013). Orai1-dependent calcium entry promotes skeletal muscle growth and limits fatigue. Nat Commun *4*, 2805.

West, S.J., Kodakandla, G., Wang, Q., Tewari, R., Zhu, M.X., Boehning, D., and Akimzhanov, A.M. (2022). S-acylation of Orai1 regulates store-operated Ca2+ entry. J Cell Sci *135*.

Wirth, K.J., and Scheibenbogen, C. (2021). Pathophysiology of skeletal muscle disturbances in Myalgic Encephalomyelitis/Chronic Fatigue Syndrome (ME/CFS). J Transl Med *19*, 162.

Woods, C.E., Novo, D., DiFranco, M., and Vergara, J.L. (2004). The action potential-evoked sarcoplasmic reticulum calcium release is impaired in mdx mouse muscle fibres. J Physiol *557*, 59-75.

Wu, F., Mi, W., Burns, D.K., Fu, Y., Gray, H.F., Struyk, A.F., and Cannon, S.C. (2011). A sodium channel knockin mutant (NaV1.4-R669H) mouse model of hypokalemic periodic paralysis. J Clin Invest *121*, 4082-4094.

Xu, R., Jia, Y., Zygmunt, D.A., and Martin, P.T. (2019). rAAVrh74.MCK.GALGT2 Protects against Loss of Hemodynamic Function in the Aging mdx Mouse Heart. Mol Ther *27*, 636-649.

Yarotskyy, V., and Dirksen, R.T. (2012). Temperature and RyR1 regulate the activation rate of store-operated Ca(2)+ entry current in myotubes. Biophys J *103*, 202-211.

Yazbeck, P., Tauseef, M., Kruse, K., Amin, M.R., Sheikh, R., Feske, S., Komarova, Y., and Mehta, D. (2017). STIM1 Phosphorylation at Y361 Recruits Orai1 to STIM1 Puncta and Induces Ca(2+) Entry. Sci Rep *7*, 42758.

Yen, M., and Lewis, R.S. (2019). Numbers count: How STIM and Orai stoichiometry affect store-operated calcium entry. Cell Calcium *79*, 35-43.

Yla-Herttuala, S. (2012). Endgame: Glybera Finally Recommended for Approval as the First Gene Therapy Drug in the European Union. Molecular Therapy *20*, 1831-1832.

Yu, R., Lendahl, U., Nister, M., and Zhao, J. (2020). Regulation of Mammalian Mitochondrial Dynamics: Opportunities and Challenges. Front Endocrinol (Lausanne) *11*, 374.

Zhang, S.L., Yeromin, A.V., Zhang, X.H.F., Yu, Y., Safrina, O., Penna, A., Roos, J., Stauderman, K.A., and Cahalan, M.D. (2006). Genome-wide RNAi screen of Ca2+ influx identifies genes that regulate Ca2+ release-activated Ca2+ channel activity. P Natl Acad Sci USA *103*, 9357-9362.

Zhang, X., Pathak, T., Yoast, R., Emrich, S., Xin, P., Nwokonko, R.M., Johnson, M., Wu, S., Delierneux, C., Gueguinou, M.*, et al.* (2019). A calcium/cAMP signaling loop at the ORAI1 mouth drives channel inactivation to shape NFAT induction. Nat Commun *10*, 1971.

Zhao, X., Moloughney, J.G., Zhang, S., Komazaki, S., and Weisleder, N. (2012). Orai1 mediates exacerbated Ca(2+) entry in dystrophic skeletal muscle. PLoS One *7*, e49862.

Zhao, X., Yoshida, M., Brotto, L., Takeshima, H., Weisleder, N., Hirata, Y., Nosek, T.M., Ma, J., and Brotto, M. (2005). Enhanced resistance to fatigue and altered calcium handling properties of sarcalumenin knockout mice. Physiol Genomics *23*, 72-78.

FRENCH SUMMARY

Titre de thèse

"Physiopathology of Tubular Aggregate Myopathy and Therapeutic Approaches"

Introduction

La myopathie à agrégats tubulaires (TAM) et le syndrome de Stormorken (STRMK) forment un continuum clinique rare caractérisé par de la faiblesse musculaire, crampes et myalgie, et accompagnée par des défauts des yeux, de la peau, des plaquettes, de la rate, de la croissance et des capacités cognitives. TAM/STRMK est une maladie génique due à des mutations de gain de fonction dans les gènes *STIM1* et *ORAI1* qui codent pour les acteurs principaux du « store-operated Ca^{2+} entry » (SOCE), une voie essentielle régulant l'homéostasie calcique dans tout type de cellule. STIM1 est une protéine qui agit en tant que senseur de Ca^{2+} dans le réticulum endoplasmique et son interaction avec ORAI1 régule l'entrée de Ca^{2+} extracellulaire. Les mutations des patients TAM/STRMK déclenchent une sur-activation du SOCE avec le conséquent excès d'entrée de Ca^{2+} extracellulaire. Pour mieux comprendre les effets de cet excès d'entrée calcique mon projet de thèse s'est divisé en trois étapes :

- **Caractérisation d'un modèle murin pour TAM/STRMK** portant la mutation la plus fréquente touchant STIM1 (p.R304W).

- Étude sur les **effets toxiques de la sur-activation du SOCE** dans les muscles de la souris *Stim1*$^{R304W/+}$.

- Génération de la première **preuve de concept thérapeutique pour TAM/STRMK** en visant ORAI1 comme cible thérapeutique.

Méthodologie

Afin d'étudier le développement de TAM/STRMK, un modèle souris a été généré en incorporant, par recombinaison homologue, la mutation TAM/STRMK la plus fréquente sur *STIM1* (murine c.910A>T, p.R304W). Les souris hétérozygotes ont complété une étude phénotypique approfondie afin de déterminer la présence des défauts caractéristiques de la maladie et conclure sur la fiabilité

du modèle. Pour l'étude des effets toxiques de la sur-activation du SOCE dans le muscle, des études transcriptomiques, morphologiques et fonctionnelles ont été faits dans des muscles rapides et lents. Enfin, la validation d'ORAI1 comme cible thérapeutique pour TAM/STRMK a été évaluée grâce à des croissements géniques de la souris *Stim1*^*R304W/+* avec des souris présentant 50% d'expression d'*Orai1* (*Orai1*^*+/-*) ou 50% d'ORAI1 dysfonctionnel (*Orai1*^*R93W/+*). Une approche translationnelle a été proposée via diminution de l'expression d'*Orai1* par injection intramusculaire de virus adéno-associé (AAV) contenant des shRNA ciblant *Orai1*.

Résultats

Caractérisation d'un modèle murin pour TAM/STRMK

Pour mieux comprendre TAM/STRMK et pouvoir développer des thérapies, un modèle animal récapitulant les défauts décrits pour les différents organes et tissus est requis. À cette fin, nous avons généré et caractérisé un modèle souris portant la mutation p.R304W (c.910A>T dans la souris) dans STIM1. Les souris en état homozygote ne sont pas viables et les hétérozygotes présentent un léger taux de mortalité prénatale mais les souris *Stim1*^*R304W/+* nées sont viables et fertiles. Les souris *Stim1*^*R304W/+* ont passé un large panel de phénotypage afin de déterminer la présence des phénotypes observés dans TAM/STRMK :

- Taille : Les souris *Stim1*^*R304W/+* sont plus petites et plus légères tout au long de leur vie comparée aux WT.

- Peau : À 8 mois, les mâles *Stim1*^*R304W/+* présentent des anomalies de la peau avec un élargissement de la dermis et une réduction de la couche graisseuse sous-cutanée.

- Yeux : Un défaut du mouvement oculaire, souvent observé dans des patients, a également été remarqué.

- Plaquettes : Une thrombocytopenie a été observé dans les souris *Stim1*^*R304W/+*.

- Rate : Les souris *Stim1*^*R304W/+* présentent une anomalie de la taille de la rate où, contrairement à l'hyposplénie typique des patients, une splénomégalie a été observée.

- Muscle : Les souris *Stim1^{R304W/+}* ont de la faiblesse musculaire probablement associée à des défauts de contraction et relaxation également observés.

D'autres organes et tissus ont été étudiés en détail et des anomalies ont été observées touchant : 1) le système immunitaire avec des anomalies du comptage de certains types cellulaires dans le sang et aussi du pourcentage de cellules T régulatrices et des cellules NK dans la rate, ce qui pourrait amener à une possible anomalie auto-immunitaire pas encore décrite chez les patients ; 2) les os avec des défauts morphologiques et structurales du fémur et tibia, probablement à l'origine des défauts de taille de la souris *Stim1^{R304W/+}*, et pouvant impliquer de la fragilité osseuse ; 3) le foie avec des taux élevés de transaminases dans le sang des souris *Stim1^{R304W/+}*; et 4) la régulation de la glycémie avec un taux élevé d'insuline et un taux diminué de glucose dans le sang des souris *Stim1^{R304W/+}*. En résumé, la souris *Stim1^{R304W/+}* est un modèle animal fidèle de TAM/STRMK et présente aussi des défauts pas encore décrits chez les patients. *Stim1^{R304W/+}* est le seul modèle présentant des défauts multi-systémiques, permettant ainsi l'étude du pathomechanisme de TAM/STRMK et la sur-activation du SOCE dans différents tissus. Par ailleurs, la découverte de défauts pas encore décrits dans TAM/STRMK permettra un meilleur suivi des patients de cette maladie.

Effets toxiques de la sur-activation du SOCE

La disponibilité d'un modèle murin fidèle pour TAM/STRMK permet d'étudier en détail les causes moléculaires de la maladie. Pour cela, je me suis focalisé sur le muscle squelettique afin de décrypter les effets moléculaires de l'excès de Ca^{2+} qui amènent à la dégénérescence musculaire, et j'ai combiné des analyses transcriptomiques par RNAseq avec des analyses morphologiques et fonctionnelles. Parmi les 2841 gènes différentiellement exprimés dans les muscles *Stim1^{R304W/+}*, un enrichissement est remarqué pour des gènes impliqués dans le transport du Ca^{2+} réticulaire, de la dynamique mitochondriale et du stress lié au réticulum. Concernant le transport de Ca^{2+} réticulaire, une diminution dans l'expression des gènes impliqués dans le couplage d'excitation-contraction a été observée, ainsi que la diminution d'expression protéique de la pompe calcique SERCA1, ce qui pourrait expliquer le ralentissement dans la contraction et relaxation du muscle. La biogenèse mitochondriale est réduite avec la conséquente réduction de la quantité de mitochondries et de la respiration qui pourrait entrainer une perte énergétique, contribuant ainsi à

la faiblesse musculaire. Le stress lié au réticulum, observé par la surexpression des gènes codant des chaperones réticulaires (*Hspa5* et *Hsp90b1*), pourrait être la cause majeure de l'apoptose observé en histologie.

Cette étude montre les effets négatifs de la sur-activation du SOCE dans le muscle squelettique au niveau transcriptionnel, morphologique et fonctionnel et suggère des pistes thérapeutiques pour TAM/STRMK en agissant au niveau du transport de Ca^{2+} réticulaire, la biogenèse de mitochondries et le stress du réticulum

Preuve de concept thérapeutique pour TAM/STRMK

TAM/STRMK est dû à des mutations de gain de fonction dans les gènes *STIM1* et *ORAI1*, qui codent pour les acteurs principaux du SOCE, une voie ubiquitaire d'entrée de Ca^{2+} extracellulaire. STIM1 agit en amont d'ORAI1 et leur interaction permet l'ouverture du canal ORAI1. ORAI1 représente donc une cible thérapeutique majeure pour diminuer l'entrée excessive de Ca^{2+} caractéristique de TAM/STRMK. Pour cela nous avons testé 2 stratégies :

- Diminuer *Orai1*. Les souris *Stim1$^{R304W/+}$* ont été croisées avec des souris exprimant 50% d'*Orai1* (*Orai1$^{+/-}$*). Les souris obtenues de ce croissement ont été évaluées phénotypiquement au niveau macroscopique, histologique et moléculaire. Les souris *Stim1$^{R304W/+}$Orai1$^{+/-}$* présentent une amélioration du poids et taille, de la morphologie osseuse et de la peau, et de la performance musculaire. Par contre, ni les taux plaquettaire dans le sang ni le poids de la rate sont améliorés dans les souris *Stim1$^{R304W/+}$Orai1$^{+/-}$* comparés aux *Stim1$^{R304W/+}$*. L'histologie musculaire révèle que la taille des fibres est partiellement normalisée mais le pourcentage de fibres avec noyaux internalisés reste élevé ainsi que le taux de stress du réticulum déterminé par RT-qPCR des gènes *Hspa5* et *Hps90b1*. Suite aux résultats prometteurs obtenus avec la preuve de concept par croissement génique, nous avons décidé de proposer une approche translationnelle. Pour ceci, nous avons produit des AAV contenant shRNAs spécifiques contre *Orai1*, puis testés *in cellulo* et *in vivo*. Les AAV les plus efficaces, avec un taux de diminution de 80%, ont été injectés dans des souris *Stim1$^{R304W/+}$* avec 8 semaines d'âge afin de tester leur effet thérapeutique. J'ai démontré que ces shRNA diminuent l'expression d'*Orai1* jusqu'à 80% et ont des effets plus positifs sur la contraction et relaxation des muscles *Stim1$^{R304W/+}$* que ceux observés dans l'approche de croissement génique.

- Inhiber ORAI1. L'inhibition du canal a été testée par croissement des souris $Stim1^{R304W/+}$ avec des souris qui expriment 50% d'ORAI1 portent une mutation qui réduit le flux calcique du canal ($Orai1^{R93W/+}$). Les souris $Stim1^{R304W/+}Orai1^{R93W/+}$ montrent une amélioration dans leur poids et taille, la morphologie osseuse, le taux de plaquettes dans le sang, la taille de la rate et la performance et morphologie musculaire. Un traitement pharmacologique visant le flux Ca^{2+} d'ORAI1 serait donc une approche translationelle pour TAM avec un grand potentiel.

Dans l'ensemble, nos expériences valident ORAI1 comme cible thérapeutique et ouvre la voie du traitement de TAM/STRMK par deux stratégies alternatives.

Conclusion

Dans cette thèse un modèle murin pour TAM/STRMK a été généré et caractérisé. Par phénotypage détaillé, j'ai montré sa fidélité comme modèle pour cette maladie multi systémique. Ceci a permis de mieux comprendre la maladie et découvrir des nouveaux signes cliniques maintenant en cours d'évaluation chez les patients. Par ailleurs, la souris $Stim1^{R304W/+}$ a permis d'étudier les effets d'une sur-activation du SOCE et la séquence d'évènements qui amènent à la dégénérescence musculaire. ORAI1 a été testé comme cible et des croisements géniques pour cibler son expression ou activité ont été menés, résultant dans une amélioration des signes majeurs de la maladie. Afin de générer une approche translationnelle, des AAV contenant shRNA ciblant $Orai1$ ont été générés et leur injection intra-musculaire dans la souris $Stim1^{R304W/+}$ améliore les défauts de contraction.

RESULTATS MAJEURS

1. GÉNÉRATION ET CARACTÉRISATION D'UN MODÈLE DE SOURIS POUR TAM/STRMK

1.1. Contexte

La myopathie des agrégats tubulaires (TAM) et le syndrome de Stormorken (STRMK) forment un continuum clinique caractérisé par une faiblesse musculaire, des contractures et des myalgies, ainsi que des signes multi-systémiques supplémentaires, notamment une petite taille, un myosis, une ichtyose, une dyslexie, une thrombocytopénie et une hyposplénie (Bohm et Laporte, 2018 ; Morin et al., 2020). La plupart des mutations TAM/STRMK sont des mutations GoF dans *STIM1* et *ORAI1*, codant les acteurs clés d'un mécanisme de régulation de l'entrée du Ca^{2+} extracellulaire connu sous le nom de SOCE (Bohm et Laporte, 2018 ; Lacruz et Feske, 2015 ; Morin et al., 2020). STIM1 est une protéine transmembranaire du RE/RS avec une partie luminale détectant le Ca^{2+} réticulaire et une partie cytosolique impliquée dans l'oligomérisation et l'activation d'ORAI1 en réponse à une faible teneur en Ca^{2+} réticulaire (Schober et al., 2019 ; Stathopulos et al., 2008). Les mutations GoF dans STIM1 activent constitutivement STIM1 en favorisant l'oligomérisation et les mutations GoF dans ORAI1 augmentent la perméabilité au Ca^{2+} du canal, les deux aboutissant finalement à une sur-activation de SOCE et à des niveaux élevés de Ca^{2+} cytosolique (Bohm et Laporte, 2018).

1.2. Objectif de l'étude

Lorsque j'ai commencé mon doctorat en 2017, les trois gènes TAM/STRMK responsables *STIM1*, *ORAI1* et *CASQ1* étaient connus, et des études fonctionnelles dans la cellule avaient montré que les mutations affectent la voie SOCE et induisent une entrée excessive de Ca^{2+} extracellulaire. Cependant, aucun modèle animal fidèle récapitulant le tableau multi-systémique du TAM/STRMK n'a été décrit, ce qui a empêché des investigations approfondies sur la corrélation entre les altérations cellulaires et le développement de la maladie. Nous avons donc généré un modèle de souris portant la mutation la plus récurrente du TAM/STRMK et réalisé une large caractérisation phénotypique.

1.3. Résultats

La souris *Stim1^{R304W/+}* a été générée par recombinaison homologue de l'exon 7 portant la mutation missense A>T en position c.910 (p.R304W). Les animaux homozygotes *Stim1^{R304W/R304W}* sont morts aux stades périnataux et les animaux hétérozygotes étaient viables et fertiles. Par rapport à leurs congénères WT, les souris *Stim1^{R304W/+}* étaient également plus petites, présentaient des anomalies des mouvements oculaires, une thrombocytopénie et une splénomégalie, ainsi que des anomalies dans la disposition des couches de la peau. En outre, des anomalies de la morphologie osseuse, de l'homéostasie du glucose sanguin, du foie et du système immunitaire ont été signalées. Les myotubes *Stim1^{R304W/+}* ont présenté un taux élevé de Ca^{2+} cytosolique et un SOCE élevé, l'histologie des muscles squelettiques a révélé une dégénérescence musculaire et une atrophie des fibres, et les performances musculaires ont été affectées par une force réduite et des anomalies de contraction et de relaxation.

1.4. Conclusion et perspectives

Notre modèle de souris Stim1R304W/+ a été le premier modèle mammifère récapitulant les principaux signes multi-systémiques de TAM/STRMK. La disponibilité d'un modèle animal fidèle permet des études physiologiques sur l'effet pathologique de la surcharge en Ca2+ sur les différents tissus et organes affectés, et représente un outil précieux pour tester les approches thérapeutiques du TAM/STRMK. De plus, les défauts supplémentaires impliquant les os, le foie, le système immunitaire et les signes du métabolisme du glucose sanguin observés élargissent la description clinique du TAM/STRMK. S'il est confirmé chez les patients, cela aurait une importance médicale majeure pour la gestion de la maladie et le suivi clinique et aiderait les cliniciens à orienter le diagnostic moléculaire.

1.5. Contribution

J'ai coordonné l'élevage et le phénotypage des animaux, caractérisé et analysé le phénotype musculaire de *Stim1^{R304W/+}*, et réalisé des expériences de SOCE et de stockage réticulaire de Ca^{2+}

dans les myotubes de *Stim1*[R304W/+]. Les souris *Stim1*[R304W/+] ont été générées et caractérisées à l'Institut Clinique de la Souris (ICS, Strasbourg, France) selon les protocoles de l'International Mouse Phenotyping Consortium (IMPC). La caractérisation immunitaire de la rate a été réalisée au Centre externe d'Immunophénomique (Ciphe, Marseille, France). Hugues JACOBS de l'ICS a fourni une aide précieuse dans la caractérisation histologique de la rate, des muscles et des os, Nadia MESSADDEQ de l'Institut de Génétique et de Biologie Moléculaire et Cellulaire (IGBMC, Strasbourg, France) a préparé et analysé les échantillons de microscopie électronique, et Pascal KESSLER était un membre de l'équipe qui a développé un plugin ImageJ pour analyser la taille des fibres. Susan TREVES était une collaboratrice externe de l'hôpital universitaire de Bâle (Bâle, Suisse) qui a mesuré le Ca^{2+} basal dans les myotubes *Stim1*[R304W/+].

2. EFFETS PHYSIOLOGIQUES D'UNE SURCHARGE EN Ca²⁺ DANS LE MUSCLE SQUELETTIQUE DE SOURIS *STIM1^{R304W/+}*.

2.1. Contexte

Dans le muscle squelettique, le Ca^{2+} module la contraction, la croissance cellulaire et la différenciation (Berridge et al., 2003), et des anomalies dans la manipulation du Ca^{2+} sont associées à des maladies humaines (Gattineni, 2014). En particulier, la surcharge en Ca^{2+} cause la dégénérescence musculaire dans les dystrophies musculaires (Burr et Molkentin, 2015 ; Vallejo-Illarramendi et al., 2014). Des niveaux élevés de Ca^{2+} cytosolique ont également été observés dans des lignées cellulaires de myoblastes provenant de patients TAM/STRMK et dans des myotubes de souris *Stim1^{R304W/+}* (Bohm et al., 2017 ; Misceo et al., 2014 ; Morin et al., 2014 ; Silva-Rojas et al., 2019). Les analyses histologiques et ultra-structurales à partir d'échantillons de muscles *Stim1^{R304W/+}* ont mis en évidence des signes dystrophiques, notamment l'internalisation des noyaux, des fibres en régénération et des infiltrations de cellules immunitaires, mais le lien mécanistique avec les niveaux élevés de Ca^{2+} cytosolique n'était pas compris.

2.2. Objectif de l'étude

Le modèle de souris *Stim1^{R304W/+}* représente un outil précieux pour étudier les effets physiopathologiques de la surcharge en Ca^{2+} cytosolique. Afin de déterminer la séquence d'événements conduisant à la faiblesse musculaire et à la dégénérescence des myofibres chez les souris *Stim1^{R304W/+}*, nous avons analysé le transcriptome des muscles *Stim1^{R304W/+}* et complété par des analyses moléculaires, fonctionnelles et histologiques.

2.3. Résultats

L'analyse du seuquençage d'ARN des muscles *Stim1^{R304W/+}* a révélé une altération de l'expression des principaux acteurs du couplage excitation-contraction (EC), du remplissage du réticulum sarcoplasmique (RS) et de l'efflux de Ca^{2+} au niveau de la membrane plasmique, ainsi qu'un retard dans la contraction et la relaxation musculaire lors d'une stimulation unique. En outre, la quantité de mitochondries était réduite et la respiration mitochondriale diminuée. Les muscles *Stim1^{R304W/+}*

présentaient des niveaux de stress réticulaire soutenus qui déclenchaient la mort et la régénération des cellules musculaires. Toutes les expériences ont été réalisées sur le muscle tibialis anterior. Afin de vérifier des effets similaires sur deux muscles fonctionnellement différents, nous avons évalué l'expression des gènes de manipulation du Ca^{2+}, la fonction mitochondriale et le stress du réticulum dans le muscle soléaire. Ceci est particulièrement intéressant car le tibialis anterior et le muscle soléaire sont des muscles fonctionnellement opposés et présentent des sensibilités différentes au Ca^{2+}. Dans l'ensemble, des défauts similaires ont été observés et la respiration et la quantité de mitochondries étaient plus affectées dans le muscle soléaire que dans le tibialis anterior.

2.4. Conclusion et perspectives

Les muscles $Stim1^{R304W/+}$ présentent une réduction du couplage EC et du remplissage du RS, comme le montrent les expériences d'expression génique et de contraction musculaire faites *in situ*. La quantité de mitochondries est réduite et le stress du réticulum est soutenu, ce qui entraîne une faible production d'énergie et le déclenchement de la mort cellulaire par apoptose, respectivement. Par conséquent, le couplage EC, le remplissage SR, la biogenèse mitochondriale et le stress réticulaire représentent des cibles médicamenteuses pour TAM/STRMK. Il est à noter que de petites molécules activant le couplage EC, le remplissage du RS ou réduisant le stress du réticulum existent et pourraient être bénéfiques pour anticiper ou inverser les anomalies moléculaires dans les myofibres TAM/STRMK et contrer la faiblesse musculaire. Par ailleurs, l'amélioration du remplissage du RS par la surexpression de SERCA1 ou la sous-expression de l'inhibiteur de SERCA1, *Sln*, pourrait constituer une approche thérapeutique pour réduire la teneur en Ca^{2+} cytosolique et améliorer la fonction musculaire chez les patients TAM/STRMK.

2.5. Contribution

J'ai réalisé les expériences de contraction musculaire in situ, les études d'immunofluorescence, les western blots, et j'ai extrait l'ARN pour la RT-qPCR et le séquençage d'ARN. En tant que service interne, le séquençage d'ARN a été réalisé par la plateforme de séquençage Genomeast de l'IGBMC, et les données brutes de séquence ont été traitées par Sarah DJEDDI. Anne-Laure CHARLES et Bernard GENY du Centre de Recherche en Biomédecine de Strasbourg (CRBS) ont

réalisé et analysé les études de respirométrie mitochondriale sur des muscles de souris disséqués dans le cadre d'une collaboration scientifique.

3. LE SILENCING D'ORAI1 COMME APPROCHE THÉRAPEUTIQUE POUR TAM/STRMK

3.1. Contexte

Les TAM/STRMK résultent de mutations à gain de fonction (GoF) dans *STIM1* et *ORAI1*, entraînant une sur-activation de SOCE et une entrée excessive de Ca^{2+} extracellulaire (Bohm et Laporte, 2018 ; Silva-Rojas et al., 2021). En revanche, les mutations LoF récessives de *STIM1* et *ORAI1* abolissent SOCE et provoquent la canalopathie CRAC, caractérisée par une immunodéficience et une auto-immunité, une dysplasie ectodermique, une mydriase, une thrombocytopénie auto-immune et une hypotonie musculaire (Lacruz et Feske, 2015). Conformément à la maladie humaine, les souris knock-out homozygotes *Stim1* ou *Orai1* meurent à des étapes périnatales, ce qui souligne la nécessité de la SOCE pour une physiologie normale. Il convient de noter que les porteurs hétérozygotes de mutations de la canalopathie de CRAC et les souris hétérozygotes *Stim1*$^{+/-}$ ou *Orai1*$^{+/-}$ sont normaux et fertiles (Baba et al., 2008 ; Gwack et al., 2008), ce qui démontre que l'expression de 50 % est suffisante pour maintenir une physiologie normale.

3.2. Objectif de l'étude

Actuellement, aucune thérapie n'est disponible pour le TAM/STRMK. ORAI1 représente une cible appropriée à traiter puisque toutes les formes de TAM/STRMK convergent vers une activation excessive d'ORAI1. Les mutations de STIM1 entraînent une oligomérisation constitutive et les mutations d'ORAI1 augmentent la perméabilité des canaux. Comme première tentative pour réduire l'entrée extracellulaire de Ca^{2+} via ORAI1 et pour anticiper les phénotypes multi-systémiques de TAM/STRMK, j'ai croisé des souris *Stim1*$^{R304W/+}$ et *Orai1*$^{+/-}$ et la progéniture a subi une large caractérisation phénotypique aux niveaux macroscopique, histologique et moléculaire. Sur la base de cette preuve de concept, j'ai ensuite cherché à établir une approche translationnelle appropriée pour déréguler *Orai1* après l'apparition de la maladie chez les souris adultes. À cette fin, j'ai injecté localement des particules AAV contenant un shRNA dans le tibialis anterior (TA) de souris adultes *Stim1*$^{R304W/+}$ et j'ai évalué le potentiel de deux shRNA pour inverser

efficacement le phénotype musculaire par le biais d'analyses cellulaires, histologiques et fonctionnelles.

3.3. Résultats

Le ratio de naissance des souris $Stim1^{R304W/+}Orai1^{+/-}$ s'est amélioré par rapport aux souris $Stim1^{R304W/+}$ et était plus proche du ratio mendélien attendu, ce qui indique un meilleur développement embryonnaire. Le gain de poids corporel sur 4 mois s'est également amélioré, et l'augmentation de la densité osseuse explique l'augmentation de la longueur du corps. Les anomalies des couches cutanées précédemment observées chez les souris $Stim1^{R304W/+}$ ont été améliorées chez les souris $Stim1^{R304W/+}Orai1^{+/-}$. Les performances musculaires ont été améliorées avec une augmentation, bien que non significative, des capacités du test de suspension, de la vitesse et de la distance parcourue dans les arènes en champ libre, et de la force maximale in situ du TA. Une amélioration similaire a été constatée pour les défauts de contraction, notamment la force produite à de faibles fréquences de stimulation et les cinétiques de contraction et de relaxation. La taille des myofibres a également été améliorée et résulte probablement d'un meilleur flux autophagique. Cependant, la dégénérescence musculaire était toujours évidente dans les muscles $Stim1^{R304W/+}Orai1^{+/-}$ et le stress du réticulum n'a pas été modifié par rapport aux homologues $Stim1^{R304W/+}$. De même, les anomalies affectant la rate et les plaquettes sont restées inchangées et les souris $Stim1^{R304W/+}Orai1^{+/-}$ ont présenté une splénomégalie et une thrombocytopénie. En résumé, la régulation négative d'$Orai1$ a eu un effet bénéfique global sur le TAM/STRMK.

L'amélioration des phénotypes TAM/STRMK chez les souris $Stim1^{R304W/+}Orai1^{+/-}$ a été obtenue par l'ablation d'un allèle $Orai1$. Afin de déréguler $Orai1$ dans la perspective d'une application translationnelle chez les patients TAM/STRMK, j'ai conçu des shRNA ciblant différentes régions de l'ADNc d'$Orai1$ et validé la dérégulation de $Orai1$ in cellulo et in vivo. Les shRNA ciblant l'ADNc aux positions 22 (sh22) et 190 (sh190) ont réduit l'expression de $Orai1$ de 80% chez les muscles $Stim1^{R304W/+}$ et ont amélioré la contraction et la relaxation musculaire. Le TA $Stim1^{R304W/+}$ traitée avec sh22 et sh190 a produit moins de force à basse fréquence et la relaxation musculaire a été améliorée par rapport au TA $Stim1^{R304W/+}$ témoin. Cependant, le traitement par shRNA n'a pas amélioré le flux autophagique ni résolu le stress du reticulum et l'atrophie des myofibres et la dégénérescence musculaire étaient toujours évidentes dans les sections musculaires du TA

Stim1$^{R304W/+}$ traitée par shRNA. Dans l'ensemble, la régulation négative d'*Orai1* a amélioré la contraction et la relaxation musculaire mais n'a pas inversé les défauts structuraux de TAM/STRMK.

3.4.   Conclusion et perspectives

Nous sommes les premiers à montrer que la réduction de l'expression de *Orai1* améliore certains des phénotypes TAM/STRMK chez la souris, notamment le ratio de naissance, le poids et la taille du corps, la morphologie osseuse, la structure de la peau, la performance musculaire et la taille des fibres. La relaxation et la dégénérescence musculaires ne s'améliorent pas, probablement parce qu'une plus grande atténuation d'Orai1 est nécessaire pour atténuer l'entrée de Ca^{2+} dans la nature particulièrement rapide et capacitive de la SOCE dans le muscle squelettique. L'absence d'effets sur les plaquettes et la rate suggère l'implication d'autres canaux dans la SOCE (par exemple ORAI2 et ORAI3) qui pourraient ne pas être affectés par la dérégulation d'*Orai1*.

Nos shRNA ciblant *Orai1* constituent également la première approche thérapeutique translationnelle visant à inverser les phénotypes TAM/STRMK dans le muscle squelettique. Le traitement du TA des souris adultes *Stim1$^{R304W/+}$* avec sh22 et sh190 améliore la cinétique de contraction et de relaxation du muscleprobablement grâce à la grande efficacité de la sous-expression d'*Orai1*. Ceci est cliniquement pertinent car notre stratégie shRNA pourrait résoudre les problèmes de contraction musculaire des patients qui se manifestent par des contractures invalidantes. Les défauts histologiques, notamment la petite taille des fibres et la dégénérescence musculaire, ne sont pas améliorés par le traitement actuel, ce qui indique que les défauts structuraux établis avant l'âge de l'injection ne peuvent être inversés.

L'entrée excessive de Ca^{2+} extracellulaire par ORAI1 contribue également à la surcharge de Ca^{2+} cytosolique et à la dégénérescence musculaire dans d'autres maladies musculaires, notamment la dystrophie musculaire de Duchenne (DMD), et la dérégulation d'*Orai1* par shRNA peut être bénéfique pour la DMD, ce qui accroît les possibilités thérapeutiques du blocage d'ORAI1.

3.5.   Contribution

Je me suis occupé de l'élevage des souris, du phénotypage, de l'histologie, de l'expression des gènes et des protéines, de la conception et de la validation cellulaire et in vivo des shRNA, des injections intramusculaires et des études de la force musculaire in situ. David MOULAERT de l'ICS et Laura PEREZ-GUARDIA (étudiante en Master 2/Erasmus) ont analysé respectivement la structure osseuse et l'hyperplasie des mégacaryocytes de la rate. Emma LAFABRIE (étudiante en Master 1) a réalisé les études histologiques et moléculaires des muscles traités par shRNA. Le test de saignement a été réalisé par Emilie THIEBAUT et Ghina ABOUT dans les installations de l'ICS en tant que service interne, les plasmides pAAV et les particules AAV ont été produits par Pascal KOEBEL de la Plateforme de Biologie Moléculaire de l'IGBMC en tant que service interne, et Raquel GOMEZ OCA a aidé aux premières étapes de l'élevage et du phénotypage.

4. L'INHIBITION D'ORAI1 COMME APPROCHE THÉRAPEUTIQUE POUR TAM/STRMK

4.1. Contexte

En tant qu'approche alternative à la dérégulation d'*Orai1* médiée par shRNA, l'inhibition physique d'ORAI1 peut représenter une autre option thérapeutique pour TAM/STRMK. ORAI1 s'assemble sous forme d'hexamères, les premiers domaines transmembranaires de chaque monomère formant le pore du canal et régulant la perméabilité du canal (Hou et al., 2012). Le résidu Arg91 est situé à la partie la plus étroite des voies de conduction ionique, et une mutation homozygote faux-sens impliquant la substitution de l'arginine par l'acide aminé volumineux tryptophane (R91W) et entraînant le blocage du canal a été trouvée chez les patients atteints de canalopathie CRAC (Feske et al., 2006). En conséquence, les souris knock-in portant la mutation R93W correspondante à l'état homozygote meurent peu après la naissance (McCarl et al., 2010). Les humains et les souris portant la mutation R91W/R93W à l'état hétérozygote sont cependant normaux et fertiles, ce qui démontre que le changement d'acide aminé permet un flux de Ca^{2+} suffisant à travers les hexamères d'ORAI1 pour assurer une physiologie normale.

4.2. Objectif de l'étude

Le SOCE est susceptible d'être manipulé, et la réduction de l'entrée extracellulaire de Ca^{2+} par l'inhibition d'ORAI1 apparaît comme une approche thérapeutique adaptée au TAM/STRMK. Dans ce but, j'ai croisé les souris $Stim1^{R304W/+}$ avec des souris $Orai1^{R93W/+}$ et nous avons suivi la progression de la maladie de la descendance jusqu'à 4 mois. À ce stade, nous avons évalué le poids corporel, la densité osseuse du fémur, le poids et l'histologie de la rate, le nombre de plaquettes, la performance musculaire et la cinétique de contraction/relaxation, ainsi que l'histologie musculaire. En outre, nous avons également analysé le transcriptome des muscles disséqués afin d'évaluer et de quantifier une éventuelle amélioration moléculaire des voies impliquées dans la fonction musculaire.

4.3. Résultats

Le rapport de naissance des souris $Stim1^{R304W/+}Orai1^{R93W/+}$ s'est amélioré par rapport à celui des souris $Stim1^{R304W/+}$ et était plus proche du rapport mendélien attendu, ce qui indique une amélioration du développement embryonnaire. Le gain de poids corporel sur 4 mois a été amélioré, de même que la longueur du corps et la densité osseuse du fémur à 4 mois. Le poids de la rate a été normalisé et le nombre de plaquettes, bien que non significatif, a doublé par rapport à celui des compagnons de la portée $Stim1^{R304W/+}$. Les performances dans les arènes de test de suspension et dans le text « Openfield » ont été améliorées chez les souris $Stim1^{R304W/+}Orai1^{R93W/+}$, et les défauts de contraction/relaxation musculaire ont été restaurés. Les signes de dégénérescence musculaire comprenant l'internalisation des noyaux, l'infiltration de cellules immunitaires et la régénération des fibres n'étaient pas présents dans les sections de muscle $Stim1^{R304W/+}Orai1^{R93W/+}$. Dans le même sens, l'expression des gènes déclenchant le stress du réticulum était normalisée dans les muscles $Stim1^{R304W/+}Orai1^{R93W/+}$, ce qui témoigne de l'atténuation du stress du réticulum. Dans l'ensemble, l'inhibition d'ORAI1 a restauré ou amélioré tous les phénotypes TAM/STRMK affectant la taille, les os, la rate, les plaquettes et le muscle squelettique.

Contrairement aux souris $Stim1^{R304W/+}Orai1^{+/-}$, les souris $Stim1^{R304W/+}Orai1^{R93W/+}$ ont montré une amélioration supplémentaire de la taille de la rate, du nombre de plaquettes, des performances de suspension, de la relaxation musculaire et de l'histologie musculaire. La transcriptomique comparative a également révélé des voies moléculaires restaurées de manière différentielle et a mis en évidence l'atténuation du stress du reticulum comme principal facteur d'amélioration des muscles chez les souris $Stim1^{R304W/+}Orai1^{R93W/+}$. En résumé, l'inhibition d'ORAI1 s'est avérée plus efficace que l'atténuation d'$Orai1$ pour traiter le TAM/STRMK chez les souris.

4.4. Conclusion et perspectives

Les souris $Stim1^{R304W/+}Orai1^{R93W/+}$ ont présenté une grande amélioration phénotypique par rapport à leurs congénères $Stim1^{R304W/+}$. Ils étaient plus grands et plus lourds, avaient une densité osseuse accrue, une rate plus petite, des taux de plaquettes sanguines plus élevés, se contractaient et se détendaient plus correctement, et présentaient moins de signes de stress du réticulum et dégénérescence musculaire. Par rapport aux souris $Stim1^{R304W/+}Orai1^{+/-}$, les souris

Stim1$^{R304W/+}$Orai1$^{R93W/+}$ ont présenté une amélioration plus importante de la performance musculaire, de la cinétique de contraction, de l'histologie et du stress du réticulum. L'efficacité thérapeutique supérieure de l'inhibition d'ORAI1 peut s'expliquer par la stœchiométrie d'ORAI1 et l'effet du mutant STIM1 R304W sur les canaux ORAI1. Contrairement à la sous-expression d'*Orai1* où les niveaux d'*Orai1* diminuent mais où les hexamères d'ORAI1 restent pleinement actifs, l'expression du mutant ORAI1 R93W rend difficile la perméabilité des canaux dans tous les hexamères et bloque l'entrée de Ca^{2+}. En outre, ORAI1 forme des hexamères avec ORAI2 et ORAI3 dans les cellules où ils sont plus exprimés que dans le muscle squelettique. Pour cette raison, on s'attend à ce que le mutant ORAI1 R93W intervienne dans la perméabilité des canaux hexamériques ORAI1/2/3 et explique l'amélioration des phénotypes de la rate et des plaquettes chez les souris *Stim1$^{R304W/+}$Orai1$^{R93W/+}$*.

Il existe des petites molécules qui inhibent spécifiquement l'activité d'ORAI1, notamment Auxora/CM4620, RP4010 ou RP3128, qui font actuellement l'objet d'essais cliniques pour la pancréatite, la pneumonie, l'asthme et le lymphome. Au vu de notre résultat démontrant un effet thérapeutique mesurable du blocage d'ORAI1 sur le phénotype multisystémique des souris *Stim1$^{R304W/+}$Orai1$^{R93W/+}$*, Auxora/CM4620, RP4010 et RP3128 pourraient également s'avérer bénéfiques pour le traitement des patients atteints de TAM/STRMK et potentiellement d'autres troubles causés par des niveaux abondants de Ca^{2+} cytosolique comme la DMD. Les futurs essais précliniques utilisant ces molécules sur des modèles murins de TAM/STRMK et de DMD pourraient être utiles et ouvrir la voie à une approche thérapeutique commune.

4.5. Contribution

Je me suis occupé de l'élevage des souris, j'ai organisé et réalisé les expériences de phénotypage et j'ai effectué l'analyse histologique et moléculaire des muscles et de la rate avec Laura PEREZ-GUARDIA (Master 2/étudiante Erasmus). En tant que service interne de l'IGBMC, la plateforme de séquençage Genomeast a réalisé le séquençage des ARN, et les données ont été traitées conjointement par Alix SIMON et Sarah DJEDDI (étudiantes M2/PhD dans l'équipe). Aurélie AUBURTIN et Marie-France CHAMPY de l'ICS ont analysé les échantillons de sang et de plasma, et David MOULAERT a analysé la structure osseuse du fémur.

Roberto SILVA ROJAS

Physiopathology of Tubular Aggregate Myopathy (TAM) and Therapeutic Approaches

Résumé

La myopathie à agrégats tubulaires (TAM) et le syndrome de Stormorken (STRMK) forment un spectre clinique dû à des mutations de gain de fonction dans les gènes *STIM1* et *ORAI1* menant à l'entrée excessive de Ca^{2+} extracellulaire. Les mécanismes pathologiques menant aux défauts multi-systémiques restent à élucider et aucune thérapie n'est disponible. Afin d'éclairer les effets pathologiques de la sur-activation de STIM1, nous avons généré un modèle murin portant la mutation TAM/STRMK la plus commune, et les souris *Stim1$^{R304W/+}$* ont récapitulé les signes majeurs de la maladie. J'ai également montré que la surcharge de Ca^{2+} cellulaire interfère avec la contraction et relaxation musculaire, induit du stress réticulaire et de la dégénérescence musculaire. Enfin, j'ai exploré des approches thérapeutiques visant à traiter TAM/STRMK.

Mots clés : Myopathie à agrégats tubulaires, syndrome de Stormorken, calcium, STIM1, ORAI1

Résumé en anglais

Tubular aggregate myopathy (TAM) and Stormorken syndrome (STRMK) are clinically overlapping disorders caused by gain-of-function mutations in *STIM1* and *ORAI1* inducing excessive extracellular Ca^{2+} entry. The precise molecular pathomechanisms leading to the multi-systemic clinical picture remain however unknown, and no therapy is currently available. In order to identify the pathological effects of STIM1 over-activation, we generated a mouse model carrying the most common TAM/STRMK mutation, and *Stim1$^{R304W/+}$* mice recapitulated the main signs of the disease. I also showed that cellular Ca^{2+} overload interferes with proper muscle contraction and relaxation, and induces sustained reticular stress and muscle fiber degeneration. Finally, I explored therapeutic approaches to treat TAM/STRMK.

Keywords: Tubular aggregate myopathy, Stormorken syndrome, calcium, STIM1, ORAI1